



Universidade Estadual de Campinas
Faculdade de Engenharia Química
Laboratório de Equilíbrio de Fases



ÁREA DE CONCENTRAÇÃO
DESENVOLVIMENTO DE PROCESSOS QUÍMICOS

Termodinâmica e Aplicações de Líquidos Iônicos

Aluno: Víctor Hugo Álvarez Álvarez

Orientador: Prof. Dr. Martín Aznar

Co-orientador: Prof. Dr. Rubens Maciel Filho

Tese de Doutorado apresentada à Faculdade de Engenharia Química da Universidade Estadual de Campinas como parte dos requisitos necessários para a obtenção do Título de Doutor em Engenharia Química.

Campinas - São Paulo

Setembro – 2010

FICHA CATALOGRÁFICA ELABORADA PELA
BIBLIOTECA DA ÁREA DE ENGENHARIA E ARQUITETURA - BAE - UNICAMP

AL86t Álvarez Álvarez, Víctor Hugo
Termodinâmica e aplicações de líquidos iônicos /
Víctor Hugo Álvarez Álvarez. --Campinas, SP: [s.n.],
2010.

Orientadores: Martín Aznar, Rubens Maciel Filho.
Tese de Doutorado - Universidade Estadual de
Campinas, Faculdade de Engenharia Química.

1. Líquidos iônicos. 2. Equilíbrio líquido-vapor. 3.
Modelagem. 4. Equação de estado. I. Aznar, Martín. II.
Maciel Filho, Rubens. III. Universidade Estadual de
Campinas. Faculdade de Engenharia Química. IV.
Título.

Título em Inglês: Thermodynamic and applications of ionic liquids
Palavras-chave em Inglês: Ionic liquids, Vapor-liquid equilibrium, Modeling,
Equation of state

Área de concentração: Desenvolvimento de Processos Químicos

Titulação: Doutor em Engenharia Química

Banca examinadora: Silvana Mattedi e Silva, Roberta Ceriani, Maria Alvina
Krähenbühl, Ricardo Belchior Torres

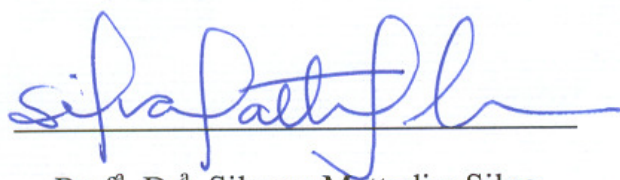
Data da defesa: 28/09/2010

Programa de Pós Graduação: Engenharia Química

Tese de doutorado defendida por Víctor Hugo Álvarez Álvarez e aprovada em 28 de setembro de 2010 pela banca examinadora constituída pelos doutores:



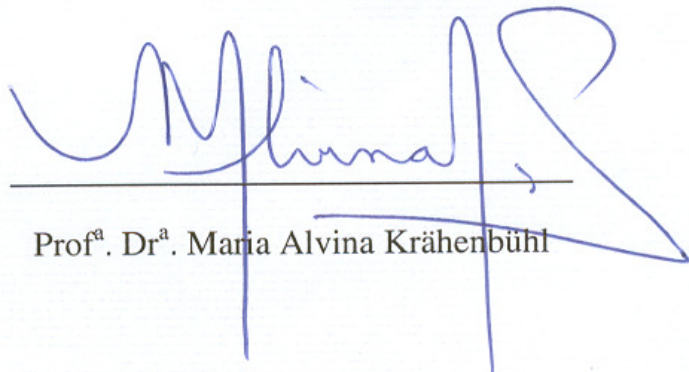
Prof. Dr. Martin Aznar



Prof^a. Dr^a. Silvana Mattedi e Silva



Prof^a. Dr^a. Roberta Ceriani



Prof^a. Dr^a. Maria Alvina Krähenbühl



Prof. Dr. Ricardo Belchior Torres

Este exemplar corresponde à versão final da Tese de Doutorado em Engenharia
Química



Prof. Dr. Martin Aznar

*Grato a Deus pela força,
saúde e esclarecimento de mente
para enfrentar o dia a dia.*

Dedicado a meus pais e irmãos.

*No início da humanidade, usávamos energia natural.
Agora, temos que nos vincular novamente à ela
e deixar que ela também alimente e multiplique nossos processos.*

AGRADECIMENTOS

Meu sincero agradecimento para quem depositou em mim a sua confiança e me permitiu amadurecer cientificamente para finalizar este trabalho de pesquisa, o Prof. Dr. Martin Aznar, pela sua direção e apoio.

Meu sincero agradecimento à Prof^a. Dr^a. Silvana Mattedi, pela direção e apoio na realização deste projeto.

O presente estudo foi realizado na Faculdade de Engenharia Química da Universidade de Campinas no período 2007-2010. Parte do trabalho foi realizada no Laboratório de Termodinâmica Aplicada (Universidade Federal da Bahia, Brasil) durante 5 meses em 2007, e no Laboratório de Propriedades Físicas e de Transporte (Universidade de Santiago de Compostela, Espanha) durante 6 meses em 2009. Agradeço aos coordenadores desses laboratórios, Prof^a. Dr^a. Silvana Mattedi e Prof. Dr. Miguel Iglesias, por me permitir utilizar as suas instalações.

À minha família pelo apoio constante na distância.

À família Simonete Alves da Silva, pela amizade e carinho.

Aos amigos da Faculdade, especialmente a Nádson, Elmer, Edson, Mario e Melvin.

Aos amigos de laboratório Leonardo, Diego, Julio e Mariana.

Aos amigos pela amizade e alegria dos momentos, especialmente Roger, Juan, Lady, David, Richard, Eulalia, e Hernán.

À FAPESP pelo apoio financeiro, sem o qual este trabalho não poderia ter sido feito.

RESUMO

AUTOR: Víctor Hugo Álvarez Álvarez.

TITULO: Termodinâmica e Aplicações de Líquidos Iônicos.

ORIENTADOR: Prof. Dr. Martín Aznar., CO-ORIENTADOR: Prof. Dr. Rubens Maciel Filho

Laboratório de Equilíbrio de Fases, DPQ-FEQ, UNICAMP

Os líquidos iônicos são uma interessante alternativa para aperfeiçoar processos com objetivos econômicos e ecológicos. Esta pesquisa tem como objetivo estudar propriedades físico-químicas de líquidos iônicos, próticos e apróticos, puros ou em misturas binárias com ésteres e aldeídos, tais como densidade, velocidade do som, viscosidade aparente, índice de refração e temperatura de decomposição térmica. Além disso, é estudado o comportamento termodinâmico de algumas aplicações dos líquidos iônicos, como equilíbrio líquido-vapor, absorção de gases e equilíbrio líquido-líquido. Inicialmente, foram sintetizados onze líquidos iônicos próticos usando moléculas de hidroxiaminas no cátion e moléculas de ácido orgânico com cadeias alquílicas de diferentes tamanhos no ânion. As propriedades físico-químicas dos líquidos iônicos, no estado puro e em misturas, indicam a formação de agregados nos líquidos iônicos próticos com mais de dois carbonos no ânion, e que o líquido iônico prático contendo o ânion formiato é instável, formando um éster com o passar do tempo. Nos líquidos iônicos puros, a densidade diminui com o crescer da temperatura ou a cadeia alquílica do ânion; além disso, a viscosidade diminui com o crescer da temperatura, mas aumenta com o crescer da cadeia alquílica do ânion. Nos resultados das misturas binárias de líquidos iônicos com aldeídos ou ésteres, mostra-se que os líquidos iônicos baseados no cátion amônio são parcialmente insolúveis em aldeídos, ocorrendo o contrário para o líquido iônico baseado no cátion imidazólio, embora sejam insolúveis em ésteres. No equilíbrio líquido-vapor a baixas pressões de sistemas binários, observa-se o aumento da temperatura de ebulição do aldeído ou éster influenciado pela concentração do líquido iônico, e a mudança do ponto azeotrópico na mistura etanol-água. No equilíbrio líquido-vapor a altas pressões, o CO₂ é mais absorvido nos líquidos iônicos próticos do que nos líquidos iônicos apróticos, especialmente naqueles que contêm o ânion acetato, mostrando quimisorção nesse grupo funcional. No equilíbrio líquido-líquido do sistema ternário líquido iônico + dibenzotiofeno + n-dodecano, observa-se que os líquidos iônicos baseados no cátion amônio conseguem extrair dibenzotiofeno do n-dodecano, tanto quanto um líquido iônico baseado no cátion imidazólio de estrutura mais complexa. Nos estudos de absorção desde uma corrente de CO₂ em dois líquidos iônicos próticos a pressão ambiente, a temperatura e o fluxo de gás foram as variáveis limitantes da absorção. Os dados do equilíbrio líquido-vapor e densidade das misturas binárias foram correlacionados através da equação de estado de Peng-Robinson acoplada com a regra de mistura Wong-Sandler/GE. Para o cálculo de GE, foram implementados os modelos termodinâmicos de NRTL, UNIQUAC e COSMO-SAC. Para o equilíbrio líquido-vapor, os desvios na predição foram menores que 2,5% e na correlação menores que 1,5%. Para a densidade da solução, os desvios na predição foram menores que 2,7%. Assim, os líquidos iônicos e as aplicações estudadas demonstram que estes novos compostos podem ser usados para produzir novos processos e os modelos termodinâmicos disponíveis na literatura podem representar esses processos com precisão.

Palavras Chave: síntese de líquidos iônicos, equilíbrio líquido-vapor, modelagem, equação de estado.

ABSTRACT

AUTHOR : Víctor Hugo Álvarez Álvarez.

TITLE : Thermodynamic and Applications of Ionic Liquids.

TUTOR : Prof. Dr. Martín Aznar, CO-TUTOR: Prof. Dr. Rubens Maciel Filho

Laboratory of Phase Equilibria, DPQ-FEQ, UNICAMP

The ionic liquids are an interesting alternative to improve processes with ecological and economic goals. This research aims to study the physicochemical properties of aprotic and protic ionic liquids, pure or in binary mixtures with esters and aldehydes, such as density, sound velocity, viscosity, refractive index and thermal decomposition temperature. Furthermore, it is analyzed the thermodynamic behavior of some applications of ionic liquids as vapor-liquid equilibrium, gas absorption, and liquid-liquid equilibrium. Initially, eleven protic ionic liquids were synthesized using hydroxylethylamine molecules in the cation and organic acid molecules with alkyl chains of different sizes in the anion. The physicochemical properties in pure and in mixtures of ionic liquids indicate the formation of aggregates with more than two carbons in the anion. The protic ionic liquid containing the formate anion is unstable, forming an ester over time. In pure ionic liquids, the density decreases with increasing temperature or alkyl chain of the anion, the viscosity decreases with increasing temperature, but increases with increasing alkyl chain anion. In the results of binary mixtures of ionic liquids with aldehydes and esters, it is shown that ionic liquids based on ammonium cation are partly insoluble in aldehydes and soluble in esters, but for the ionic liquid based on imidazolium was the opposite. In the vapor-liquid equilibrium at low pressures of binary systems, there is an increase of the boiling point of the aldehyde or ester influenced by the concentration of ionic liquid. It changes the azeotropic point of ethanol-water mixture. In the vapor and liquid at high pressures, more CO_2 is absorbed in the protic ionic liquids than in aprotic ionic liquids. This is especially shown in those containing acetate anion, indicating quimisorption with this functional group. In liquid-liquid equilibrium of ternary system ionic liquid + dibenzothiophene + n-dodecane, it is observed that the ionic liquids based on ammonium cation can be extracted dibenzothiophene from n-dodecane. Both as an ionic liquid based on imidazolium cation of more complex structure. In studies of absorption from a CO_2 flow in two protic ionic liquids at ambient pressure, the variables limiting the absorption were the temperature and flow rate. Data from the vapor-liquid equilibrium and density of binary mixtures were correlated using the equation of state of Peng-Robinson with the mixing rule of Wong-Sandler/ G^E . For the calculation of G^E , it was implemented thermodynamic models as NRTL, UNIQUAC and COSMO-SAC. For the vapor-liquid equilibrium, the deviations in the prediction and correlation were lower than 2.5% and 1.5%, respectively. For the mixture density, the deviations in the prediction were lower than 2.7%. Therefore, the ionic liquids and the applications studied demonstrate that these new compounds are reliable to yield new processes and the current thermodynamic models can represent these processes with accuracy.

Keywords: synthesis of ionic liquids, liquid-vapor equilibrium, modeling, equation of state

SUMÁRIO

RESUMO	vii
ABSTRACT	viii
LISTA DE FIGURAS	xii
LISTA DE TABELAS	xiv
NOMENCLATURA	xv
LISTA DE ARTIGOS APRESENTADOS	xvii
1. INTRODUÇÃO E OBJETIVOS	1
1.1. INTRODUÇÃO	1
1.2. JUSTIFICATIVA E OBJETIVOS	4
1.3. ORGANIZAÇÃO DA TESE	5
2. REVISÃO BIBLIOGRÁFICA	11
2.1. ESTADO DA ARTE DOS LÍQUIDOS IÔNICOS	11
2.1.1. CLASSIFICAÇÃO.....	13
2.1.2. ESTRUTURA	16
2.1.2.1 Cátions	17
2.1.2.2 Ânions.....	18
2.1.2.3 Organização estrutural dos líquidos iônicos puros	18
2.1.2.4 Organização estrutural em solução.....	20
2.1.2.5 Propriedades de cristal líquido	20
2.1.2.6 Propriedades físico-químicas.....	21
2.1.3. PRODUÇÃO E CONSUMO DOS LÍQUIDOS IÔNICOS	25
2.1.3.1 Reações de metátese (Welton, 1999).....	26
2.1.3.2 Reações de neutralização ácido-base (Welton, 1999; Álvarez et al., 2010).....	26
2.1.3.3 Combinação direta de sal e metal	26
2.1.3.4 Manuseio dos líquidos iônicos	26
2.1.4. QUÍMICA VERDE E OS LÍQUIDOS IÔNICOS	27
2.1.4.1 Síntese.....	28
2.1.4.2 Reciclagem	29
2.1.4.3 Toxicologia.....	29
2.2. MODELAGEM	32
2.2.1 Equilíbrio Líquido-vapor a baixas pressões	35
2.2.2 Equilíbrio líquido-vapor a altas pressões	37
2.2.3 Equilíbrio líquido-líquido.....	39
2.3. PRINCIPAIS APLICAÇÕES DOS LÍQUIDOS IÔNICOS	39
2.3.1 Catalisadores homogêneos e heterogêneos	40
2.3.2 Processos biocatalíticos.....	40
2.3.3 Remoção de íons metálicos	40
2.3.4 Purificação de gases	40
2.3.5 Degradação fotolítica de compostos orgânicos em líquidos iônicos.....	40
2.3.6 Projeto de líquidos iônicos para aplicações específicas	41
3. MATERIAIS E MÉTODOS	43
3.1. OBJETIVOS.....	43
3.2. MATERIAIS	43
3.2.1. REAGENTES.....	43
3.2.2. APARELHOS UTILIZADOS.....	45

3.3.	SINTESE DE LÍQUIDOS IÔNICOS E CARATERIZAÇÃO	49
3.3.1	SÍNTESE DE LÍQUIDOS IÔNICOS	49
3.3.2	DESIDRATAÇÃO DE LÍQUIDOS IÔNICOS	51
3.3.3	MANUSEIO DOS LÍQUIDOS IÔNICOS PUROS E SUAS MISTURAS	52
3.3.4	CARATERIZAÇÃO	53
3.3.4.1	Ressonância Magnética Nuclear.....	53
3.3.4.2	Propriedades físicas	54
3.3.4.3	Calorimetria diferencial exploratória.....	54
3.3.4.4	Propriedades volumétricas.....	56
3.4.	SOLUÇÕES CONTENDO LÍQUIDOS IÔNICOS	57
3.4.1.	PROPRIEDADES FÍSICO-QUÍMICAS	57
3.4.2.	EQUILÍBRIO DE FASES.....	59
3.4.2.1.	Equilíbrio líquido-vapor a baixas pressões	59
a)	Validação do Procedimento Experimental.....	59
b)	Metodologia	60
c)	Procedimento experimental no ebulíometro	60
d)	Síntese e purificação dos líquidos iônicos	62
e)	Testes de solubilidade	62
f)	ELV dos sistemas binários aldeído ou éster + líquido iônico	62
3.4.2.2.	Equilíbrio líquido-vapor a altas pressões	63
3.4.2.3.	Equilíbrio líquido-líquido	63
3.5.	ALGUMAS APLICAÇÕES DOS LÍQUIDOS IÔNICOS	65
3.5.1	SEPARAÇÃO DO AZEÓTROPO ETANOL + ÁGUA.....	65
3.5.2	ABSORÇÃO DE CO ₂ EM UM FLUXO DE GÁS.....	66
3.5.3	DESSULFURIZAÇÃO DO PETRÓLEO.....	69
3.6.	EQUAÇÕES UTILIZADAS	71
3.6.1.	MODELAGEM DAS CARACTERÍSTICAS DE SOLVATAÇÃO	72
3.6.2.	MODELAGEM USANDO O COEFICIENTE DE FUGACIDADE	73
3.6.3.	MODELAGEM UTILIZANDO O COEFICIENTE DE ATIVIDADE	74
3.6.4.	MODELOS PARA A ENERGIA LIVRE DE GIBBS EM EXCESSO	75
a)	Correlação dos dados	75
b)	Predição dos dados.....	77
3.6.5.	PREDIÇÃO DA DENSIDADE	79
3.6.6.	ESTIMAÇÃO DOS PARÂMETROS	80
4.	RESULTADOS E DISCUSSÃO	81
4.1.	SÍNTESE DE LÍQUIDOS IÔNICOS E CARATERIZAÇÃO	81
4.1.1	DESIDRATAÇÃO DOS LÍQUIDOS IÔNICOS.....	81
4.1.2	CALORIMETRIA DIFERENCIAL EXPLORATÓRIA.....	82
4.1.3	DIFRAÇÃO DE RAIOS X	84
4.1.4	DEGRADAÇÃO DE ALGUMS LÍQUIDOS IÔNICOS.....	86
4.2.	MISTURAS CONTENDO LÍQUIDOS IÔNICOS	107
4.2.1.	PROPRIEDADES FÍSICO-QUÍMICAS	107
4.2.2.	EQUILÍBRIO DE FASES.....	142
4.2.2.1	Testes de solubilidade para os sistemas binários e equilíbrio líquido-vapor a baixas pressões	142
4.2.2.2	Equilíbrio líquido-vapor a baixa pressão.....	143
4.2.2.3	Equilíbrio líquido-vapor a altas pressões.....	220

4.2.2.4 Equilíbrio líquido-líquido	295
4.3. ALGUMAS APLICAÇÕES DOS LÍQUIDOS IÔNICOS	306
4.3.1 Separação do azeótropo etanol + água	306
4.3.2 Absorção de gases usando líquidos iônicos	326
4.3.3 Dessulfurização do petróleo	342
5. CONCLUSÕES E SUGESTÕES FUTURAS	345
5.1. CONCLUSÕES	345
5.2. PROPOSTAS DE PESQUISAS FUTURAS	349
REFERÊNCIAS	351
ANEXO	363
A. Estrutura de alguns líquidos iônicos citados na tese	363
B. Os 12 princípios da química verde (Anastas e Warner, 2000)	364
C. Literatura produzida nesta pesquisa	365

LISTA DE FIGURAS

Figura 1.1. Patentes (Δ) e estudos na literatura aberta (Θ) dos líquidos iônicos durante os últimos anos. Fonte: Web of Science (2010).....	3
Figura 1.2. Diagrama de Fluxo da pesquisa desenvolvida.....	9
Figura 2.1. Diagrama do ponto de fusão (linha) e temperatura de clareamento (pontos) do líquido iônico $[c_n\text{-mim}]^+[\text{PF}_6]^-$. Fonte: Gordon et al., 1998.....	17
Figura 2.2. Modelo simplificado bidimensional das características estruturais de líquidos iônicos 1,3 dialquilimidazólio. Fonte: Dupont (2004).	20
Figura 2.3. Diagrama de fases para o sistema CO_2 supercrítico $[\text{bmim}]^+[\text{PF}_6]^-$ a 313 K.....	38
Figura 2.4. Algumas aplicações dos líquidos iônicos até o momento.....	39
Figura 3.1. Destilador e coluna de troca iônica para purificação da água.....	45
Figura 3.2. Foto do analizador de densidade e velocidade do som, modelo DSA 5000.....	46
Figura 3.3. Foto do Refratômetro Mettler-Toledo, modelo RE 40D.	46
Figura 3.4. Foto do reômetro Visco Elite, modelo L.	47
Figura 3.5. Foto do Titulador de Karl-Fisher, modelo DL31.....	47
Figura 3.6. Foto do eboliômetro Fisher Labodest, modelo VLE-602.	48
Figura 3.7. Célula de equilíbrio, vista lateral e superior. Unidades em mm. Fonte: Stragevitch, 1997.....	49
Figura 3.8. Célula em repouso para obter duas fases límpidas.	49
Figura 3.9. Foto da montagem utilizada para a síntese dos líquidos iônicos.	50
Figura 3.10. Balão (a) e sistema de vácuo (b) projetado para a desidratação e armazenamento do líquido iônico.	52
Figura 3.11. Caixa de acrílico para obter uma atmosfera seca.....	53
Figura 3.12. Esquema de um DSC.	55
Figura 3.13. Foto do Eboliômetro tipo Othmer.....	66
Figura 3.14. Foto dos aparelhos utilizados para medir a absorção de CO_2 nos líquidos iônicos... 68	68
Figura 3.15. Foto de três células em série para determinar o ELL, com mistura sob agitação.....	71
Figura 4.1. Perfil da desidratação em batelada do líquido iônico etilsulfato de 1-etyl-3-metilimidazólio vs. tempo. No tempo zero é medida a umidade inicial. (□) armazenagem em ar, (○) armazenagem em nitrogênio.	81
Figura 4.2. Perfil da desidratação em batelada do líquido iônico hexanoato de N-metil-2-hidroxietilamônio vs. Tempo, com armazenagem em nitrogênio.....	82
Figura 4.3. Fluxo de calor contra a temperatura, para m-2-HEAA (—), m-2-HEAB(···) e m-2-HEAH (—).....	84
Figura 4.4. Gráficos clássicos de difração de raios X. (a) Intensidade contra o ângulo de medição, 2theta, (b) Intensidade contra distâncias intramoleculares.	85
Figura 4.5. Produtos possíveis pela degradação de formiato de N-metil-2-hidroxietilamônio.....	86
Figura 4.6. Espectros de hidrogenio para o m-2-HEAF. (a) Após uma semana de ter sido sintetizado. Fonte: CACTUS-USC, (b) após dois meses de ter sido sintetizado. Fonte: Prof. Coutinho.....	87
Figura 4.7: Densidade em função da temperatura a pressão ambiente para líquidos iônicos puros: m-2-HEAA (□), m-2-HEAB (○), m-2-HEAH (◊), 2-HE2AB (x) e N-(2-HE)edAB (+).....	88

Figura 4.8: Temperatura contra. composição do sistema binario ester + líquido iônico: Acetato de metila, (○); acetato de etila, (□); e acetato de propila, (Δ). Os símbolos fechados é o ELV com m-2-HEAB, os simbolos avertos é o ELV co m-2-HEAH e o simbolo X é o ELV com N-(2-HE)edAB.....	144
Figura 4.9: Temperatura contra. composição de sistemas binario etanol + líquido iônico: [emim][EtSO ₄], (Δ); 2-HE2AB, (○); N-(2-HE)edAB, (□).....	144
Figura 4.10. Distribuição do DBT entre o líquido iônico e o n-dodecano a 298,15 K. Utilizando, m-2-HEAB (■); m-2-HEAH (□); [emim] ⁺ [EtSO ₄] ⁻ (♦), [emim] ⁺ [DEtPO ₄] ⁻ (▲); linhas calculadas pelo modelo NRTL.....	342
Figura 4.11. Seletividade do líquido iônico a 298,15 K. Utilizando-se, m-2-HEAB (■); m-2-HEAH (□); [emim] ⁺ [EtSO ₄] ⁻ (♦), [emim] ⁺ [DEtPO ₄] ⁻ (▲); linhas calculadas pelo modelo NRTL	343
Figura 4.12. Porcentagem do DBT removido do óleo modelo, a 298,15 K. Utilizando-se, m-2-HEAB (■); m-2-HEAH (□); [emim] ⁺ [EtSO ₄] ⁻ (♦), [emim] ⁺ [DEtPO ₄] ⁻ (▲).	343
Figura 4.13. Porcentagem do DBT removido do óleo modelo, a 298,15 K. Utilizando-se, m-2-HEAB (■); 2-HE2AB (□); N-(2-HE)edAB (◀).....	344

LISTA DE TABELAS

Tabela 2.1. Produção das principais indústrias e o fator Sheldon E	14
Tabela 2.2. Estruturas de cátions e ânions comumente utilizados em líquidos iônicos. R representa cadeias alquilaicas.....	16
Tabela 3.1. Densidades a 298,15 K.....	44
Tabela 4.1. Temperatura de degradação (T_d) de líquidos iônicos sintetizados	83
Tabela 4.2: Densidade experimental para líquidos iônicos puros com umidade inferior a 1000 ppm.	88
Tabela 4.3. Solubilidade de misturas binárias de líquido iônico + solvente a 298,15 K.	143
Tabela 4.4. Solubilidade de misturas binárias de líquido iônico + solvente a 323,15 K.	143
Tabela 4.5. Dados experimentais do ELV para os sistemas binários contendo etanol.	145
Tabela 4.6. Indice de refração a 20 °C para os sistemas binários contendo etanol ou acetato de metila.....	146
Tabela 4.7. Funções termodinâmicas da solvatação do CO ₂ nos líquidos iônicos estudados.....	221

NOMENCLATURA

Símbolos

a_c	Constante da EdE para o componente puro
$a_i, a_j, b_i, b_j, d_i, d_j$	Constantes da EdE para componentes puros
a_m, b_m, d_m	Constantes da EdE para misturas
a_{ij}, b_{ij}, d_{ij}	Constantes da EdE entre o componente “i” e “j” na mistura
A^E_∞	Energia livre de Helmholtz em excesso a pressão infinita
f_2^L	Fugacidade do componente 2 na fase líquida
f_2^V	Fugacidade do componente 2 na fase vapor
F_i^E	Parâmetro na função $\alpha(Tr, \omega)$
g^E	energia livre de Gibbs em excesso molar
G^E	Energia livre de Gibbs em excesso
k_{ij}	Parâmetro de interação binário para a constante de força da EdE PR
M	Massa molar
N	Número de compostos
P	Pressão
P_{ci}	Pressão crítica do componente “i”
P^π	Pressão na fase π
q	Parâmetro de área na equação UNIQUAC
r	Parâmetro de volume na equação UNIQUAC
R	Constante dos gases
s	Entropia molar
T	Temperatura
T^π	Temperatura na fase π
T_{ci}	Temperatura crítica do componente “i”
T_r	Temperatura reduzida
v	Volume molar
V	Volume total
x, y	Fração molar da fase líquida e fase vapor
x_i, x_j	Fração molar na fase líquida do componente “i” ou “j”
y_i, y_j	Fração molar na fase vapor do componente “i” ou “j”
Z	Fator de compressibilidade
Z_c	Fator de compressibilidade crítico

Abreviaturas

atm	atmosferas
COSMO	Conductor-like screening model
COSMO-SAC	COSMO Segment Activity Coefficient
$\Delta P(\%)$	Desvio relativo porcentual da pressão
<i>EdE</i>	Equação de estado
<i>ELV</i>	Equilíbrio líquido vapor
<i>MPa</i>	Mega Pascal
<i>NP</i>	Número de pontos no sistema
<i>NRTL</i>	Modelo “Non-Random-TwoLiquid” para G^E
<i>PR</i>	Equação de estado de Peng-Robinson
<i>RK</i>	Equação de estado de Redlich-Kwong

<i>SRK</i>	Equação de estado de Soave-Redlich-Kwong
<i>TPa</i>	Tera Pascal
<i>UNIQUAC</i>	Modelo “UNIversal-QUAsiChemical” para G^{ex}
<i>vdW</i>	van der Waals
<i>WS</i>	Regra de Mistura de Wong-Sandler
Letras Gregas	
$\alpha(T)$	Função da temperatura na EdE
α	Parâmetro da equação NRTL
β_i ,	Parâmetro de interação para a constante de volume
Δ	Desvio
ϕ_2^L	Coeficiente de fugacidade para o componente 2 na fase líquida
ϕ_2^V	Coeficiente de fugacidade para o componente 2 na fase vapor
γ	Coeficiente de atividade
π	Representação da fase
ω	Fator acêntrico
\mathcal{Q}	Constante na regra de mistura com energia livre de G^E
Superescritos	
<i>E</i>	Propriedade em excesso
<i>Exp</i>	Experimental
<i>Cal</i>	Calculado
<i>L</i>	Fase líquida
<i>R</i>	Propriedade residual
<i>Sat</i>	Saturação
<i>V</i>	Fase vapor
Subscritos	
<i>i</i>	Composto i
∞	Infinito

LISTA DE ARTIGOS APRESENTADOS

Artigo 4.1: Brønsted ionic liquids for sustainable processes: Synthesis and physical properties..	90
Artigo 4.2: Synthesis and thermophysical properties of two new protic long-chain ionic liquids with the oleate anion	98
Artigo 4.3: Thermophysical properties of binary mixtures of ionic liquid 2-hydroxy ethylammonium acetate + (water, methanol or ethanol)	108
Artigo 4.4: Isobaric vaporliquid equilibria of 1-ethyl-3-methylimidazolium ethylsulfate plus (propionaldehyde or valeraldehyde): experimental data and prediction.....	147
Artigo 4.5: Density, Refractive Index and Vapor-Liquid Equilibria of N-Methyl-2-Hydroxyethylammonium Butyrate plus (Methyl Acetate or Ethyl Acetate or Propyl Acetate) at Several Temperatures.....	170
Artigo 4.6: Density, Refractive Index and Vapor-Liquid Equilibria of N-Methyl-2-Hydroxyethylammonium Hexanoate plus (Methyl Acetate or Ethyl Acetate or Propyl Acetate) at Several Temperatures	195
Artigo 4.7: Application of a thermodynamic consistency test to binary mixtures containing an ionic liquid	223
Artigo 4.8: An efficient approach to optimal interpolation of experimental data	237
Artigo 4.9: High pressure phase behavior of carbon dioxide in 1-alkyl-3-methylimidazolium bis(trifluoromethylsulfonyl)imide ionic liquids.....	243
Artigo 4.10: High pressure phase behavior of carbon dioxide in 1-butyl-3-methylimidazolium bis(trifluoromethylsulfonyl)imide and 1-butyl-3-methylimidazolium dicyanamide ionic liquids.....	252
Artigo 4.11: Specific solvation interactions of CO ₂ on acetate and trifluoroacetate imidazolium based ionic liquids at high pressures.....	259
Artigo 4.12: High carbon dioxide solubilities in trihexyltetradecylphosphonium-based ionic liquids.....	269
Artigo 4.13: High Pressure CO ₂ Solubility in N-methyl-2-hydroxyethylammonium Protic Ionic Liquids	277
Artigo 4.14: Liquid-liquid equilibrium for n-dodecane + DBT + n-methyl-2-hydroxyethylammonium butyrate at 25°C and 95 kPa	296
Artigo 4.15: Use of ionic liquid 2-hydroxy ethylammonium formate as entrainer for anhydrous ethanol production	307
Artigo 4.16: Production of Anhydrous Ethanol by Extractive Distillation of Diluted Alcoholic Solutions with Ionic Liquids	315
Artigo 4.17: An Evaluation and Industrial Application of Ionic Liquid as Separation Agent for Separation of Diluted Ethanol-Water Mixtures	321
Artigo 4.18: CO ₂ absorption into amine-based ionic liquids	327

1. INTRODUÇÃO E OBJETIVOS

PREFÁCIO

Este capítulo apresenta as motivações, objetivos e contribuições vinculadas ao desenvolvimento desta tese. Inicialmente, busca-se ressaltar as vantagens do uso dos princípios da química verde e a importância dos líquidos iônicos. Em seguida, parte-se para a apresentação das pesquisas que marcaram importantes abordagens sobre a síntese dos líquidos iônicos e aplicação nos processos industriais. O capítulo é, posteriormente, finalizado com a apresentação dos objetivos e do conteúdo dos demais capítulos.

1.1. INTRODUÇÃO

A química verde é definida pela IUPAC como “A invenção, desenvolvimento e aplicação de produtos e processos químicos para reduzir ou eliminar o uso e a geração de substâncias perigosas” (Tundo et al., 2000). Nessa definição, o termo “perigoso” deve ser entendido como substâncias nocivas de algum modo à saúde humana ou ao meio ambiente. Assim, a química verde é uma abordagem altamente eficaz para a prevenção da poluição porque aplica inovadoras soluções científicas para situações ambientais do mundo real. Os 12 princípios da química verde, originalmente desenvolvidos por Anastas e Warner (2000), fornecem uma direção para os pesquisadores implementá-la. A química verde inclui a redução de rejeitos, de materiais e energia, do risco, da periculosidade e do custo de processos químicos. Alguns exemplos de pesquisa em química verde são: desenvolvimento de catalisadores; eliminação ou substituição de solventes; uso de matérias-primas renováveis; substituição de produtos tóxicos por outros ambientalmente aceitáveis; monitoramento, controle e a intensificação de processos; uso eficiente de energia; melhoria nos processos de separação; reagentes e reações intrinsecamente mais seguras.

Desde que foi observada a hidrofobicidade de alguns líquidos iônicos, propriedade que lhes permitem substituir clássicos solventes orgânicos voláteis em diversos processos, como na extração líquido-líquido (Huddleston et al., 1998) e na extração supercrítica (Blanchard et al., 1999), a comunidade científica e a indústria estão entusiasmadas com a nova revolução da química verde baseada nos líquidos iônicos. Estes poderiam reduzir o uso de solventes poluentes

e perigosos. A importância crescente dos líquidos iônicos é evidenciada pela velocidade de crescimento dos artigos publicados.

A Figura 1.1 mostra o avanço das pesquisas, sendo patentes ou literatura aberta, sobre líquidos iônicos, que até o ano 1990 se manteve com uma tendência estável no número de publicações. Nessa figura, também pode ser observado que a indústria sempre notou o alto potencial dos sais fundios à temperatura ambiente, verificado na maior quantidade de patentes do que artigos na literatura aberta. Após os anos 90, a pesquisa na literatura aberta cresceu como consequência da possibilidade de projetar sais fundidos à temperatura ambiente estáveis em água e ar (Christie et al., 1991; Wilkes e Zaworotko, 1992), que permitiu novas aplicações como a extração e isolamento de solutos (Tian e Hughbanks, 1995); em 1996, Suarez et al. projetaram sais fundidos à temperatura ambiente de baixa tendência higroscópica. Em 1997, Seddon propõe o termo líquidos iônicos para estes compostos e descreve qualidades interessantes destes para síntese e processos catalíticos. A primeira modelagem do equilíbrio líquido-vapor (ELV) de misturas contendo líquidos iônicos foi apresentada por Shariati e Peters (2003). Entre 1993 e 2000, as pesquisas na literatura aberta e as patentes apresentavam quantidades similares, mostrando o crescente interesse da comunidade científica nos líquidos iônicos. Este novo interesse permitiu a patente de novos processos industriais.

Os termos: líquido iônico a temperatura ambiente, líquido iônico não aquoso, sal fundido a temperatura ambiente, sal orgânico líquido e sal fundido são usados para descrever sais em fase líquida (Welton, 1999). Em contraposição às altas temperaturas de fusão que são comumente associadas aos sais fundidos, (1073,95 K para o cloreto de sódio e 878,15 K para cloreto de lítio), o qual limita seu uso como solventes em muitas aplicações (Yang e Dionysiou, 2004), os líquidos iônicos são sais líquidos a baixas temperaturas, compostos unicamente por íons (Davis e Fox, 2003).

Inicialmente, os líquidos iônicos foram considerados pouco comuns, mas agora sabe-se que muitos sais permanecem líquidos à temperatura ambiente. Os líquidos iônicos são sempre sais orgânicos ou misturas contendo ao menos um componente orgânico, com ponto de fusão menor que 100 °C (Johnson, 2007). A composição e as propriedades associadas dos líquidos iônicos dependem da união do cátion e ânion, pelo qual existiriam mais de 10^9 diferentes estruturas de líquidos iônicos.

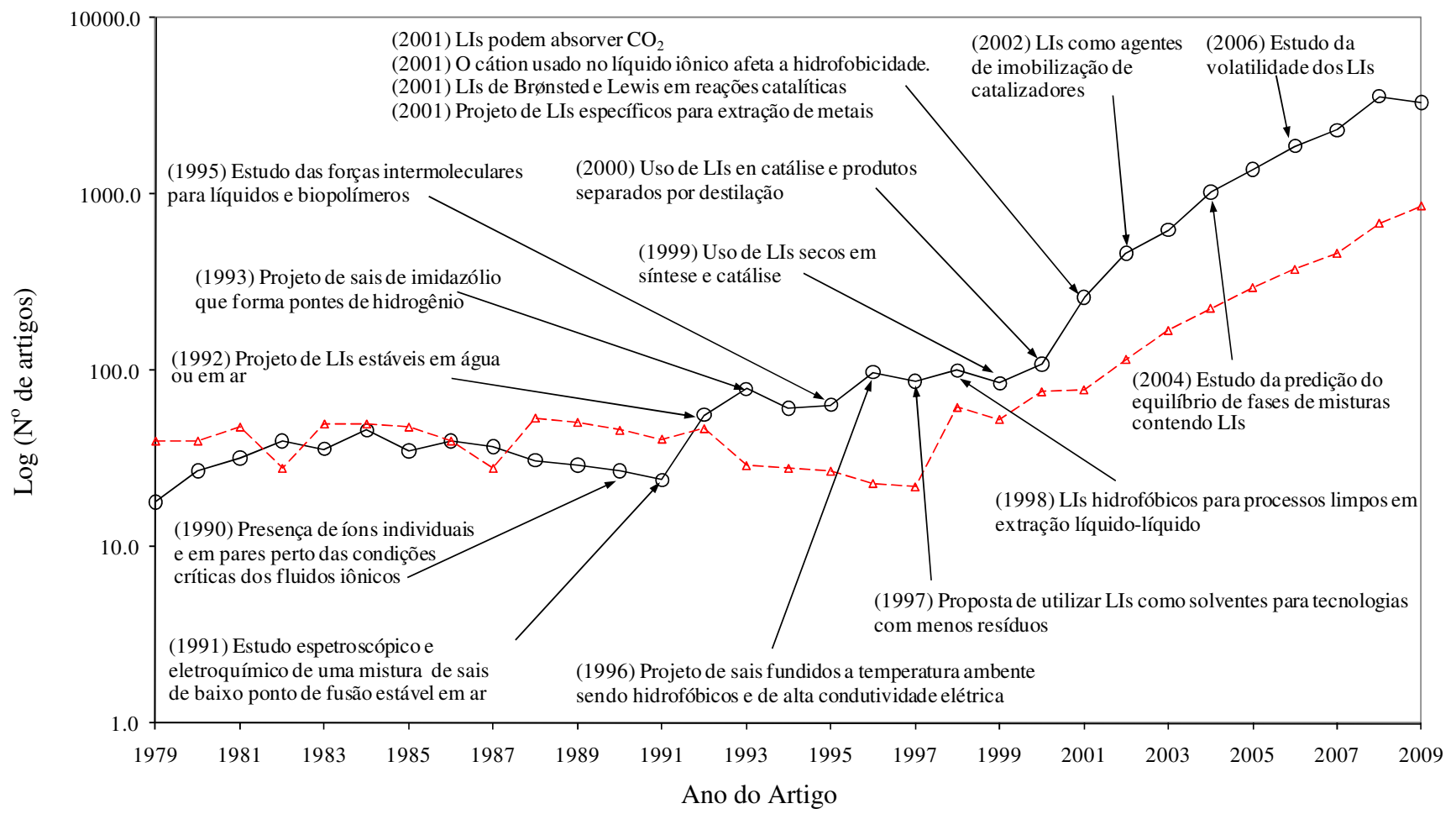


Figura 1.1. Patentes (Δ) e estudos na literatura aberta (Θ) dos líquidos iônicos durante os últimos anos. Fonte: Web of Science (2010).

1.2. JUSTIFICATIVA E OBJETIVOS

Em anos recentes tem-se dado muita importância aos líquidos iônicos baseados no cátion imidazólio e pouca àqueles com cátion de amônio. Em busca de dados de um determinado sistema contendo líquidos iônicos, logo percebe-se que alguns dos conjuntos de dados experimentais são dados a uma única temperatura, e muitas vezes não são estudadas as misturas a diferentes concentrações. Uma revisão crítica dos dados disponíveis para alguns líquidos iônicos contendo amônio revela que as propriedades físicas, como densidade e viscosidade, são frequentemente relatadas (Greaves et al. 2006), mas dificilmente dados de equilíbrio de líquido-vapor ou líquido-líquido podem ser encontrados. Por outro lado, a pesquisa sobre líquidos iônicos é muito dinâmica e seu crescimento divulga novas publicações diariamente. No entanto, grandes discrepâncias entre os diferentes autores podem ainda ser observadas. Os dados disponíveis sobre propriedades físico-químicas de componentes puros ou misturas ainda são escassos; além disso, as medições foram realizadas sobretudo, até recentemente, usando compostos de baixa pureza.

Na atualidade existem três problemas clássicos na indústria para os quais os líquidos iônicos podem fornecer soluções inovativas: o rompimento de azeótropo, a remoção de CO₂ de um efluente gasoso, e a remoção de compostos sulfurosos do petróleo. O presente trabalho estudou a aplicação de líquidos iônicos nessas áreas industriais, através de um extenso estudo para caracterizar os líquidos iônicos puros e suas misturas e finalmente aplicá-los. Assim, o presente trabalho pretende fornecer uma nova direção nos estudos futuros. A estrutura da tese pretende organizar a pesquisa realizada, já que os resultados experimentais, colocados como artigos, ao parecerem dispersos, enlaçem e justifiquem mais de um caso de estudo. Assim, neste trabalho, propriedades físico-químicas de solventes hidroxílicos (água, etanol, metanol), aldeídos (propanal, pentanal, hexanal) ou ésteres (acetato de metila, acetato de etila, acetato de propila) e líquidos iônicos (formiato de n-metil-2-hidroxietilamônio, m-2-HEAF; acetato de n-metil-2-hidroxietilamônio, m-2-HEAA; propionato de n-metil-2-hidroxietilamônio, m-2-HEAP; butirato de n-metil-2-hidroxietilamônio, m-2-HEAB; isobutirato de n-metil-2-hidroxietilamônio, m-2-HEAiB; pentanoato de n-metil-2-hidroxietilamônio, m-2-HEAP; hexanoato de n-metil-2-hidroxietilamônio, m-2-HEAH; dibutirato de N-(2-hidroxietil)etilendiamônio, N-(2-HE)edAB; butirato de bis(2-hidroxietil)amônio, 2-HE₂AB; etilsulfato de 1-etil-3-metilimidazolio, [emim]⁺[EtSO₄]⁻; metilsulfato de 1-butil-3-

metilimidazolio), $[bmim]^+[MeSO_4]^-$; como a densidade, velocidade do som, viscosidade, índice de refração e suas respectivas funções termodinâmicas, foram estudadas em um amplo intervalo de temperatura (288 a 323 K) e em todo o intervalo de composição nas soluções. Assim, foram estudadas as propriedades físico-químicas com respeito ao tamanho da cadeia alquilica do ânion e à variação do cátion para um tipo de ânion. Também foi realizado um estudo do equilíbrio líquido-vapor e/ou líquido-líquido nas misturas binárias com solventes hidroxílicos, aldeídos ou ésteres; a modelagem termodinâmica destes dados foi feita utilizando a equação de estado de Peng-Robinson (1976).

1.3. ORGANIZAÇÃO DA TESE

Esta tese consta de cinco capítulos. Os capítulos 1 e 2, referentes à Introdução e Revisão Bibliográfica, respectivamente, destinam-se a inserir o leitor no tema central desta tese, dando o embasamento teórico para a metodologia experimental e para os estudos desenvolvidos que são apresentados no capítulo 3. Já, os resultados experimentais ou de simulação obtidos durante a pesquisa são apresentados no capítulo 4, na forma de artigos científicos que, individualmente, abrangem cada um dos objetivos estabelecidos, podendo ser lidos independentemente dos demais. A fim de manter a característica original dos artigos, estes não foram traduzidos quando inseridos na tese. O capítulo 4 foi estruturado em três subcapítulos sendo: síntese e caraterização de líquidos iônicos, propriedades físico-químicas e equilíbrio de fases de misturas contendo líquidos iônicos e algumas aplicações dos líquidos iônicos. Baseado nesses objetivos gerais, os objetivos específicos deste trabalho são:

1-Síntese de novos líquidos iônicos variando o tamanho da cadeia alquílica do ânion.

2-Estudo do efeito de solventes hidroxílicos sobre a estrutura dos líquidos iônicos.

3-Estudo do equilíbrio líquido-vapor em sistemas binários contendo aldeídos ou ésteres.

4-Estudo do equilíbrio líquido-líquido em sistemas ternários contendo dibenzotiofeno e n-dodecano.

5-Estudo do rompimento da mistura azeotrópica etanol-água.

6. Estudo da absorção de CO₂ nos líquidos iônicos.

7. Extração de compostos sulfurados de um composto semelhante ao petróleo.

O capítulo de resultados foi desenvolvido com os artigos resultantes da pesquisa. Assim, os dados experimentais no conteúdo desta tese não foram repetidos e podem ser obtidos dos respectivos artigos listados.

O item “Síntese e caracterização de líquidos iônicos”, no capítulo 4, apresenta os artigos:

- *Brønsted ionic liquids for sustainable processes: Synthesis and physical properties, Journal of Chemical & Engineering Data, v.55, p. 625–632, 2010.*
- *Synthesis and thermophysical properties of new protic long-chain ionic liquids with oleate anion, Fluid Phase Equilibria, submetido, 2010.*

Esses artigos reportam a síntese de oito novos líquidos iônicos baseados em cátions do tipo hidroxiamina. Estudos de RMN (*Ressonância Magnética Nuclear*), densidade, velocidade do som, viscosidade e índice de refração foram utilizados para caracterizá-los.

O item “Propriedades físico-químicas e equilíbrio de fases de misturas contendo líquidos iônicos”, no capítulo 4, apresenta estudos das misturas binárias de solventes e líquidos iônicos, o equilíbrio líquido-vapor a baixas e altas pressões, e o equilíbrio líquido-líquido com compostos sulfurosos:

- *Thermophysical properties of binary mixtures of ionic liquid 2-hydroxy ethylammonium acetate + (water, methanol or ethanol), Journal of Chemical Thermodynamics, submetido, 2010.*
- *Isobaric vapor-liquid equilibria for n-methyl-2-hydroxyethylammonium butyrate + ester (methyl acetate, ethyl acetate, propyl acetate) + at 100 kPa: Experimental data and predictive modeling, aceito no XVIII Congresso Brasileiro de Engenharia Química, COBEQ 2010, Foz do Iguaçu, 2010.*
- *Density, refractive index and vapor-liquid equilibria of n-methyl-2-hydroxyethylammonium butyrate plus (methyl acetate or ethyl acetate or propyl acetate): Experimental data and predictive modeling, em preparação.*

- Density, refractive index and vapor-liquid equilibria of *n*-methyl-2-hydroxyethylammonium hexanoate plus (methyl acetate or ethyl acetate or propyl acetate): Experimental data and predictive modeling, em preparação.
- Isobaric vapor-liquid equilibria of 1-ethyl-3-methylimidazolium ethylsulfate plus (propionaldehyde or valeraldehyde): Experimental data and prediction, *The Journal of Chemical Thermodynamics*, submetido, 2010.
- Application of a thermodynamic consistency test to binary mixtures containing an ionic liquid, *The Open Thermodynamics Journal*, v. 2, p. 25-38, 2008.
- An efficient approach to optimal interpolation of experimental data, *Journal of the Taiwan Institute of Chemical Engineers*, v. 41, p. 184-189, 2010.
- High pressure phase behavior of carbon dioxide in 1-alkyl-3-methylimidazolium bis(trifluoromethylsulfonyl)imide ionic liquids, *Journal of Supercritical Fluids*, v. 48, p. 99–107, 2009.
- High pressure phase behavior of carbon dioxide in 1-butyl-3-methylimidazolium bis(trifluoromethylsulfonyl)imide and 1-butyl-3-methylimidazolium dicyanamide ionic liquids, *Journal of Supercritical Fluids*, v. 50, p. 105–111, 2009.
- Specific solvation interactions of CO₂ on acetate and trifluoroacetate imidazolium based ionic liquids at high pressures, *Journal of Physical Chemistry B*, v. 113, p. 6803-6812, 2009.
- High carbon dioxide solubilities in trihexyltetradecylphosphonium-based ionic liquids, the journal of supercritical fluids, *Journal of Supercritical Fluids*, v.52, p. 258–265, 2010.
- High Pressure CO₂ Solubility in *N*-methyl-2-hydroxyethylammonium Protic Ionic Liquids, *Journal of Supercritical Fluids*, submetido, 2010.
- Liquid-liquid equilibrium for *n*-dodecane + DBT + *n*-methyl-2-hydroxyethylammonium butyrate at 25°C and 95 kPa, aceito no XVIII Congresso Brasileiro de Engenharia Química, COBEQ 2010, Foz do Iguaçu, 2010.

Estes artigos estudam o comportamento molecular dos líquidos iônicos na mistura com solventes hidroxílicos (água, metanol, etanol), ésteres (acetato de metila, acetato de etila, acetato de propila), e aldeídos (propanal e pentanal). No equilíbrio líquido-vapor a 101,3 kPa são estudados sistemas binários com ésteres ou aldeídos; no equilíbrio líquido-vapor a altas pressões são estudado sistemas supercríticos contendo CO₂; e no equilíbrio líquido-líquido são estudados sistemas ternários com n-dodecano e dibenzotiofeno.

O item “Algumas aplicações dos líquidos iônicos”, no capítulo 4, apresenta três casos de aplicações dos líquidos iônicos sintetizados. O rompimento do azeótropo etanol-água, absorção de CO₂ de um efluente gasoso e dessulfurização do petróleo. Nesse item, são apresentados os artigos:

- *Use of ionic liquid 2-hydroxy ethylammonium formate as entrainer for anhydrous ethanol production, XVII Congresso Brasileiro de Engenharia Química, COBEQ 2008, Recife, 2008.*
- *Use of ionic liquid as entrainer for production of anhydrous ethanol by extractive distillation, 18th International Congress of Chemical And Process Engineering - CHISA2008, 2008, Praga, 2008.*
- *Production of anhydrous ethanol by extractive distillation of diluted alcoholic solutions with ionic liquids, 10th International Symposium on Process Systems Engineering, Elsevier, v. 27, p. 1137-1142, 2009.*
- *An evaluation and industrial application of ionic liquid as separation agent for separation of diluted ethanol-water mixtures, Fenomenos de Transferencia, v4, p. 8-12, 2008.*
- *CO₂ absorption into amine-based ionic liquids, Brazilian Journal of Chemical Engineering, submetido, 2010.*
- *Liquid-liquid equilibrium for n-dodecane + DBT + protic ionic liquid at 25°C and 95 kPa, The Journal of Physical Chemistry B, submetido, 2010.*

O Capítulo 5, referente às Considerações Finais e Conclusões, apresenta as principais conclusões dos resultados obtidos nos artigos desenvolvidos nesta tese. Em seguida, articulam-se propostas de perspectivas futuras para a síntese e aplicação de líquidos iônicos.

Como anteriormente explicado, ainda que a organização da tese seja extensa pelos diversos trabalhos feitos, a pesquisa foi ampla nas principais áreas atingidas. Entretanto, é apresentada a Figura 1.2 para uma melhor visualização dos itens estudados. Nesta figura, observa-se três eixos principais: o estudo dos líquidos iônicos puros, suas misturas com solventes e três aplicações.

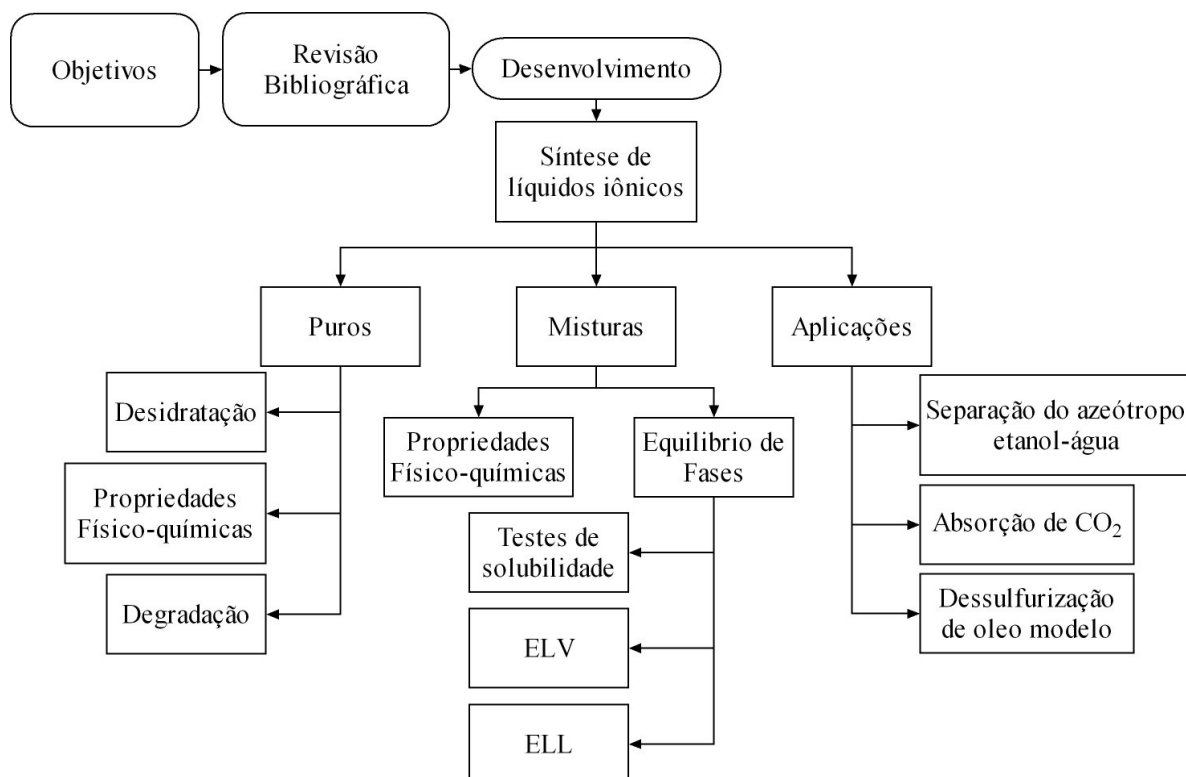


Figura 1.2. Diagrama de Fluxo da pesquisa desenvolvida.

Finalmente, são apresentados anexos para complementar a explicação de alguns itens. O anexo apresenta informações adicionais a respeito da estrutura molecular dos líquidos iônicos utilizados, química verde e produção científica da tese.

2. REVISÃO BIBLIOGRÁFICA

PREFÁCIO

Neste capítulo, é apresentada uma visão geral do desenvolvimento de pesquisas na síntese e aplicações dos líquidos iônicos. Além disso, é destacada a abordagem de tópicos específicos da estrutura e modelagem de sistemas em equilíbrio, mais especificamente o equilíbrio líquido-vapor e líquido-líquido, para aplicação de modelos em processos.

2.1. ESTADO DA ARTE DOS LÍQUIDOS IÔNICOS

Os líquidos iônicos não são novos; alguns deles são conhecidos há muitos anos, com o nome de sais fundidos. Por exemplo, o nitrato de 2-hidroxietilamônio (ponto de fusão 52-55 °C) foi relatado em 1888 por Gabriel e Weiner (1888); um dos primeiros líquidos iônicos à temperatura ambiente foi o nitrato de etilamônio (ponto de fusão 12 °C), sintetizado em 1914 por Walden (1914). Entre os sais de imidazólio, o primeiro sintetizado foi um composto obtido pela mistura de cloreto de 1-etil-3-metilimidazólio com tricloreto de alumínio, em 1951. Porém, estes líquidos iônicos com íons organoaluminatos são instáveis ao ar e água, e não são inertes na mistura com vários compostos orgânicos, o que limita suas aplicações (Dupont, 2004).

Apenas na década de 1990 apareceram os primeiros relatórios sobre a síntese de líquidos iônicos estáveis em ar e água (Wilkes e Zawarotko, 1992), sendo solúveis ou insolúveis em água, o tetrafluoroborato de 1-n-butil-3-metilimidazólio ($[bmim]^+[BF_4]^-$) ou hexafluorofosfato de 1-n-butil-3-metilimidazólio ($[bmim]^+[PF_6]^-$) e seus análogos (Holbrey e Seddon, 1999; Huddleston et al., 2001). Assim, na década de 1990 foi iniciado um renascimento da química em sais fundidos, que continua crescendo (Dupont, 2004). Os líquidos iônicos mais utilizados são os sais de imidazólio. Informes da base de dados da ISI Web of Knowledge (2010) confirmam esta idéia. Por exemplo, de 8525 artigos publicados dos últimos 5 anos estudando líquidos iônicos, 4159 utilizam sais de imidazólio.

A atual tendência para a comercialização de líquidos iônicos cria oportunidades para novos pesquisadores trabalharem com materiais de pureza conhecida (o que é uma preocupação fundamental). Coincidente com esta evolução, existe uma crescente percepção de que existe uma

infinidade de sais de baixo ponto de fusão, nunca antes explorados como sais fundidos, oferecendo novas oportunidades para a exploração e descoberta. Não há então nenhuma dúvida de que a investigação sobre o uso de líquidos iônicos como solventes, reagentes, catalisadores e materiais continuará a crescer (Davis e Fox, 2003).

Existe um amplo grau de variedade das ofertas comerciais dos imidazólios oferecidos. Esta diversidade surge quase totalmente do emparelhamento de um número muito pequeno de cátions, principalmente aqueles imidazólio, com qualquer ânion. Os ânions mais utilizados nos líquidos iônicos são espécies inorgânicas poliatômicas. O mais comum entre estes é o $[PF_6]^-$, obtido do trabalho de Wilkes e Zaworotko (1992), os quais o emparelharam com o cátion imidazólio, sendo estável em ar e água, com características hidrofóbicas. Assim, o íon $[PF_6]^-$ e o íon $[BF_4]^-$ são provavelmente os ânions mais utilizados na investigação dos líquidos iônicos.

Em resposta a preocupações de segurança e de custos, alguns fabricantes, como a Solvent Innovations em 2005 e a Sachem em 2003, introduziram novos líquidos iônicos com ânions livres de flúor. As ofertas principais são líquidos iônicos com ânions de sulfatos de alquilo, como ECOENG 212 e ECOENG 500; do mesmo modo, a Sachem lançou recentemente a linha Terrasail, que consiste em líquidos iônicos com base no ânion “docusato” (nome genérico de um surfactante).

A Cytec despertou para o fato de que muitos halogenetos fosfônicos que foram oferecidos durante anos para aplicativos de transferência de massa são líquidos iônicos, e apresentou recentemente um relatório sobre a sua preparação industrial. A Sachem também produz sais que foram desenvolvidos como catalisadores de transferência de massa, mas que são funcionalmente líquidos iônicos.

Atualmente, as ofertas comerciais de sais explicitamente descritos como líquidos iônicos estão, na maioria, baseadas no cátion imidazólio. Notavelmente, a BASF, como pioneira, divulgou o envolvimento de um líquido iônico tipo imidazólio em um processo comercial, para produção de fosfinas de fenil alcóxi (Seddon, 2003). Recentemente, a dessulfurização do petróleo tem tido muita pesquisa com resultados ainda preliminares; embora as patentes sejam simples aplicação dos líquidos iônicos (Likhanova et al., 2009), o processo completo está perto de ser obtido.

2.1.1. CLASSIFICAÇÃO

Os processos químicos são dominados pelo estudo das espécies em solução. Uma solução é uma mistura homogênea de duas ou mais substâncias em que uma ou mais destas substâncias (sólido) é dissolvida em outra substância (solvente). Um soluto pode ser um gás, sólido ou líquido. Uma substância é solúvel em outra quando misturadas, formam uma solução, um sistema homogêneo. A solubilidade é uma propriedade específica de uma substância e depende do solvente ao qual é misturada. A miscibilidade é o termo usado para compostos que formam soluções em toda a faixa de composições. A solubilidade é o termo utilizado para misturas homogêneas formadas por sólidos ou gases mais líquidos.

A quantidade do soluto em relação ao solvente em uma solução é a concentração da solução. A maior concentração possível de um soluto em um solvente é a solubilidade de uma solução. Quando o solvente contém mais soluto do que pode conter, a solução é dita saturada, e se ele tem menos soluto do que ele pode conter, a solução é definida como insaturada.

Apesar de qualquer líquido poder ser usado como um solvente, relativamente poucos são de uso geral. No entanto, como a introdução de tecnologias mais limpas tem se tornado uma grande preocupação em toda a indústria e universidades, a busca de alternativas aos solventes mais prejudiciais se tornou uma prioridade. Os solventes estão no topo da lista de produtos químicos prejudiciais, por duas razões simples:

-Eles são usados em grandes quantidades

-Eles são normalmente líquidos voláteis (VOCs, do inglês *Volatile Organic Solvents*) difíceis de estocar.

Considerando a grande quantidade de compostos orgânicos voláteis utilizados pela indústria, Sheldon (2007) propõe o fator Sheldon E para avaliar a indústria. Esse fator mede, em base mássica, subprodutos do processo em proporção à produção. Segundo a análise desse fator, indústrias geralmente consideradas como anti-ecológicas, como as indústrias do petróleo, produtos químicos ou produtos químicos a granel, são extremamente conscientes na produção de resíduos. Por outro lado, a química fina e as empresas farmacêuticas estão usando

ineficientemente os solventes, com processos contaminantes, embora em menor quantidade, como é observado na Tabela 2.1.

Tabela 2.1. Produção das principais indústrias e o fator Sheldon E.

Indústria	Produção (ton/ano)	Fator E
Refinaria do petróleo	10^6 - 10^8	0.1
Produtos químicos a granel	10^4 - 10^6	1-5
Química fina	10^2 - 10^4	5-50
Farmacêutica	10^1 - 10^3	25-100

Fonte: Sheldon (2007).

Na mistura, as substâncias em solução podem interagir umas com as outras de maneiras específicas. A solvatação descreve essas interações. Quando um soluto se dissolve, as moléculas do solvente se organizam em torno das moléculas do soluto. O calor da mistura está envolvido, e a entropia aumenta, tornando a solução termodinamicamente mais estável do que o soluto sozinho. Essa organização é medida pelas propriedades químicas do solvente e soluto, como ligações de hidrogênio, momento do dipolo e polarizabilidade (Lowry e Richardson, 1987).

A constante dielétrica (ϵ) do solvente fornece uma medida aproximada da polaridade de um solvente e permite classificar os solventes em duas categorias: polares e não polares. A constante dielétrica dá apenas uma aproximação grosseira das propriedades dos solventes, e não se correlaciona bem com os efeitos medidos dos solventes nas taxas de reação. Solventes com constante dielétrica menor que 15 geralmente são considerados apolares (Lowry e Richardson, 1987). Em termos comuns, a constante dielétrica do solvente pode ser pensada como a capacidade de reduzir a carga interna do soluto.

A constante dielétrica não é a única medida de polaridade. Já que os solventes são utilizados pela química para realizar reações químicas ou observar os fenômenos químicos e biológicos, medidas mais específicas de polaridade foram propostas. Por exemplo, Gutmann (1976) propõe o número doador ou número receptor na escala de polaridade, medido em termos de como um solvente interage com substâncias específicas, como ácido de Lewis forte ou base de Lewis forte. A polaridade, momento de dipolo, polarizabilidade e ligações de hidrogênio determinam que tipo de compostos, o solvente é capaz de dissolver e em quais solventes ou compostos líquidos, ele é miscível.

As ligações de hidrogênio provavelmente têm uma maior influência sobre as interações solvente-soluto do que qualquer outra propriedade no solvente. Solventes que têm ligações O-H ou N-H são doadores de prótons, e capazes de formar ligações de hidrogênio, enquanto a maioria dos hidrogênios ligados ao carbono é muito fracamente ácida para formar ligações de hidrogênio. Qualquer sítio com elétrons não compartilhados é um potencial receptor de ligações de hidrogênio (Lowry e Richardson, 1987). Solventes com uma constante dielétrica superior a 15 podem ser divididos em próticos e apróticos, classificando como solventes próticos aqueles que são bons doadores de prótons e formam ligação de hidrogênio e como solventes apróticos aqueles que não o são. Note que os solventes apróticos podem conter ligações de hidrogênio. Por exemplo, a água é um solvente prótico e solventes apróticos, tais como acetona ou diclorometano tendem a ter grandes momentos dipolares (separação das cargas parcialmente positivas e as parcialmente negativas dentro da mesma molécula) e são positivamente carregados através do seu dipolo negativo.

Deste modo, os líquidos iônicos, sendo solventes, podem ser também classificados em dois tipos: líquidos iônicos apróticos (AILs, do inglês *aprotic ionic liquids*) e líquidos iônicos próticos (PILs, do inglês *protic ionic liquids*).

Algumas propriedades simples dos líquidos iônicos à temperatura ambiente, que os tornam interessantes como potenciais solventes em diversos processos, são as seguintes:

1. São bons solventes para um vasto leque de materiais orgânicos e inorgânicos. Assim, misturas de reagentes podem ser trazidas para uma mesma fase.
2. Frequentemente são compostos por íons de coordenação fraca, então eles têm o potencial de ser altamente polares, ainda sendo solventes não coordenados.
3. São imiscíveis com uma série de solventes orgânicos, oferecendo a oportunidade de formar uma fase polar não aquosa para obter sistemas de duas fases. Líquidos iônicos hidrofóbicos também podem ser utilizados como a fase polar imiscível em água.
4. Têm volatilidade muito baixa, portanto podem ser usados em sistemas de alto vácuo e eliminar muitos problemas de armazenamento.

Uma das vantagens mais destacadas dos líquidos iônicos, que tem sido a justificativa para a sua caracterização como “solventes ecológicos”, é a sua volatilidade insignificante. Portanto, têm menos chances de serem inflamáveis ou explosivos, pela distribuição aérea de seus vapores. Esta característica os mostra com uma grande vantagem e como promissores substitutos para os VOCs. Além disso, dependendo do processo, muitos líquidos iônicos podem ser reciclados e reutilizados repetidamente (Renner, 2001; Visser et al. 2002).

2.1.2. ESTRUTURA

A combinação de diferentes cátions e ânions pode resultar em sais com pontos de fusão baixos; exemplos de algumas dessas estruturas que podem resultar em um líquido iônico são apresentadas na Tabela 2.2.

Tabela 2.2. Estruturas de cátions e ânions comumente utilizados em líquidos iônicos. R representa cadeias alquílicas.

Íon	Estrutura
Cátions	
Ânions	

Assim, para fazer um líquido iônico, os pesquisadores podem escolher entre dezenas de ânions pequenos, como hexafluorofosphato ($[PF_6^-]$) e tetrafluoroborato ($[BF_4^-]$), e centenas de milhares de cátions grandes, como 1-hexil-3-metilimidazólio ou 1-butil-3-metilimidazólio, obtendo diferentes propriedades fisico-químicas da estrutura final do líquido iônico. Estes tipos de variações que ocorrem nas propriedades pela diferença de íons deu origem à descrição dos líquidos iônicos como “solventes projetados”. Deste modo, é possível escolher entre diferentes íons para fazer um líquido iônico que se adapte para uma necessidade específica, como dissolver certas substâncias químicas em uma reação ou extração de moléculas específicas desde uma solução (Huddleston et al., 1998).

O baixo ponto de fusão é o resultado da composição dos líquidos iônicos, os quais contêm um cátion comprido e assimétrico comparado aos sais inorgânicos. Esta assimetria diminui a energia

de coesão na rede e, portanto, o ponto de fusão, obtendo como resultado um meio iônico fraco. Frequentemente, o ânion é relativamente comprido e influencia no baixo ponto de fusão (Yang e Dionysiou, 2004).

Os líquidos iônicos próticos são interessantes porque têm um próton de alta mobilidade, além das propriedades clássicas anteriormente citadas. PILs são produzidos através da transferência de prótons de um ácido de Brønsted a uma base de Brønsted. Neste contexto, Bicak (2005) sintetizou um líquido iônico a partir da neutralização de monoetanolamina com ácido fórmico. Greaves et al. (2006) propuseram diferentes PILs de aminas primárias e ácidos inorgânicos. Iglesias e colaboradores (Álvarez et al., 2010; Iglesias et al.; 2008) sintetizaram uma família de PILs, modificando a cadeia alifática dos ácidos orgânicos e/ou utilizando hidroxiaminas secundárias e terciárias. Estes autores enfatizam o baixo custo e a simplicidade de síntese desta nova família de líquidos iônicos. Além disso, a toxicidade muito baixa deste tipo de líquidos iônicos foi verificada (Sierra et al., 2008; Couling et al., 2006).

2.1.2.1 Cátions

A mudança do cátion tem um profundo efeito sobre as propriedades físicas, como ponto de fusão, viscosidade e densidade (Gordon et al., 1998; Seddon et al., 2002). Isso pode ser facilmente visto através do exame dos diagramas de fase para os sais de hexafluorofosfato (ver Figura 2.1), onde o ponto de fusão mostra uma dependência do comprimento da cadeia alquílica.

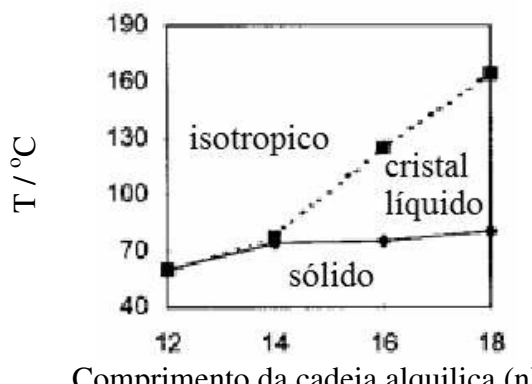


Figura 2.1. Diagrama do ponto de fusão (linha) e temperatura de clareamento (pontos) do líquido iônico $[C_n\text{-mim}]^+[\text{PF}_6]^-$. Fonte: Gordon et al., 1998.

Na Figura 2.1, observa-se que sais com cadeias alquílicas com menos de 14 carbonos não mostraram comportamento mesomorfo, quer no aquecimento ou resfriamento, enquanto todos os

outros exibem mesofases enantiotrópicas. Os pontos de fusão dos sais aumentaram ligeiramente com o aumento do comprimento da cadeia alquílica, enquanto o ponto de clareamento aumentou acentuadamente. Dando um intervalo de temperatura na mesofase maior que 353 K no sal de octadecil. Assim, o intervalo de cristal líquido aumentou consideravelmente com o aumento do comprimento da cadeia alquila.

2.1.2.2 Ânions

A mudança do ânion afeta de maneira drástica o comportamento químico e a estabilidade do líquido iônico (Swatloski et al., 2002; Suarez et al., 1996; Davis e Fox, 2003). Os ânions mais utilizados são espécies poliatômicas inorgânicas e podem ser classificados como fluorados ($[PF_6]^-$, $[BF_4]^-$, $[CF_3SO_3]^-$, $[(CF_3SO_3)_2N]^-$), não-fluorados e não-convencionais.

O $[PF_6]^-$ e o $[BF_4]^-$ são provavelmente os ânions mais utilizados na pesquisa dos líquidos iônicos. Embora possa esperar-se pouca variação nas propriedades entre os sais do mesmo cátion, as diferenças reais podem ser extremas. Por exemplo, o $[bmim]^+[PF_6]^-$ é imiscível em água (parcialmente miscível), enquanto que o $[bmim]^+[BF_4]^-$ é completamente solúvel em água (totalmente miscível). Apesar de sua ampla utilização, os líquidos iônicos com ânions de $[PF_6]^-$ e $[BF_4]^-$ foram descritos como sensíveis ao aquecimento na presença de água, liberando HF (Trulove e Mantz, 2002). Esses inconvenientes levaram a introduzir outros ânions, embora muitos deles ainda sejam materiais fluorados. Por exemplo, o flúor ligado ao carbono, C-F, ligação inerte à hidrólise, produz líquidos iônicos baseados em $[CF_3SO_3]^-$ ou $[(CF_3SO_3)_2N]^-$, mas eles ainda são de alto custo de síntese.

Em resposta a preocupações de segurança e custo, novos líquidos iônicos com ânions não fluorados foram introduzidos. Entre os mais interessantes estão os sais derivados dos ânions de produtos químicos baratos. Os ânions baseados em sulfatos de alquila são razoavelmente não-tóxicos e biodegradáveis. O líquido iônico, ECOENG 500 (PEG-5 Metossulfato cocomonium) foi o primeiro comercialmente disponível com dados toxicológicos completos.

2.1.2.3 Organização estrutural dos líquidos iônicos puros

O estudo estrutural dos líquidos iônicos diferencia principalmente os sais prólicos e apróticos. Dupont (2004) fez um estudo da estrutura de AILs baseados no cátion imidazólio. Esses resultados revelaram que os líquidos iônicos 1,3 dialquilimidazólio puros são melhores descritos

como supramoléculas poliméricas de ligações de hidrogênio do tipo $([(DAI)_x (X)_{x-n}]^{n+} [(DAI)_{x-n} (X)_x]^{n-}$, onde DAI é o cátion 1,3-dialquilimidazólio e X o ânion. Este padrão estrutural é uma tendência geral para a fase sólida e mantém-se em grande medida na fase líquida e até mesmo na fase gasosa. A introdução de outras moléculas e macromoléculas ocorre com um rompimento da rede de ligação de hidrogênio e, em alguns casos, pode gerar nano-estruturas com regiões polares e não-polares, onde compostos podem ser introduzidos (Dupont, 2004). Estudos de raios X notificados nos últimos anos sobre a estrutura do sais de 1,3- dialquilimidazólio revelam uma tendência típica: eles formam no estado sólido uma rede alargada de cátions e ânions ligados entre si por ligações de hidrogênio. A unidade monomérica é sempre constituída pelo cátion imidazólio cercado ao menos por três ânions, onde cada ânion está cercado por pelo menos três cátions imidazólio (Figura 2.2). Embora o número de ânions que cercam o cátion (e vice-versa) possa mudar, dependendo do tamanho e do tipo de ânion do substituintes N-alquil imidazólio, esse padrão estrutural é uma tendência geral em sais imidazólio (Dupont, 2004). Do mesmo modo, líquidos iônicos de cadeia longa têm atraído algum interesse devido às propriedades de líquido cristalino (LC).

Como indicado anteriormente, os líquidos iônicos contendo ligações O-H ou N-H formam o grupos dos PILs. Esse grupo consegue ter diferenças estruturais ao utilizar os dois grupos ou um deles no mesmo líquido iônico. Angell e colaboradores têm estudado amplamente a estrutura e propriedades desses interessantes líquidos iônicos (Angell et al., 2007; Belieres e Angell, 2007) e confirmam uma ampla rede de ligações de hidrogênio na estrutura do líquido iônico, com uma interessante alta mobilidade do próton, ainda sem misturas aquosas. Líquidos iônicos baseados no cátion imidazólio/pirrolidinio e ânion de carboxilato formam PILs, nos quais o comprimento da cadeia alquílica com mais de 5 carbonos no ânion origina estruturas agregadas (Anouti et al., 2009). Líquidos iônicos contendo grupos O-H e N-H no cátion conseguem formas estruturas agregadas com cadeias alquílicas a partir de dois carbonos no ânion e mantêm a alta mobilidade no próton (Álvarez et al., 2010a).

Finalmente, a fase gasosa sobre um líquido iônico aprótico $[A]^+[X]^-$ consiste de pares de íons neutros, $[AX]$, sem íons livres ou agregados maiores, enquanto que a fase gasosa sobre um líquido iônico prótico $[BH]^+[X]^-$ é composta por moléculas neutras isoladas, B e HX (Leal et al., 2007). Assim, essas duas classes de líquidos iônicos são conceitual e empiricamente diferentes, e

uma distinção importante para futuros trabalhos nesta área, tendo em conta que ambos os tipos já estão sendo utilizados em processos industriais.

2.1.2.4 Organização estrutural em solução

Segundo a seção anterior, os líquidos iônicos "puros" em fases sólidas e líquidas são estruturas poliméricas supramoleculares com ligações de hidrogênio bem organizadas. Além disso, a introdução de outras moléculas ou macromoléculas ocorre com um rompimento da rede de ligação de hidrogênio e, em alguns casos, geração de nano-estruturas com regiões não-polares e polares, onde a inclusão de compostos pode ser feita (Dupont, 2004; Anouti et al., 2009).

Quando eles são infinitamente diluídos em outras moléculas, podem formar pares de íons separados do solvente; ao aumentar a concentração do líquido iônico, eles colapsam para formar pares de íons de contato, e um novo aumento da concentração do líquido iônico leva a obter íons triplos, até formar agregados (Figura 2.2). Esse comportamento é explicado através de ligações de hidrogênio envolvendo o cátion e ânion (Dupont, 2004; Álvarez et al., 2010a).

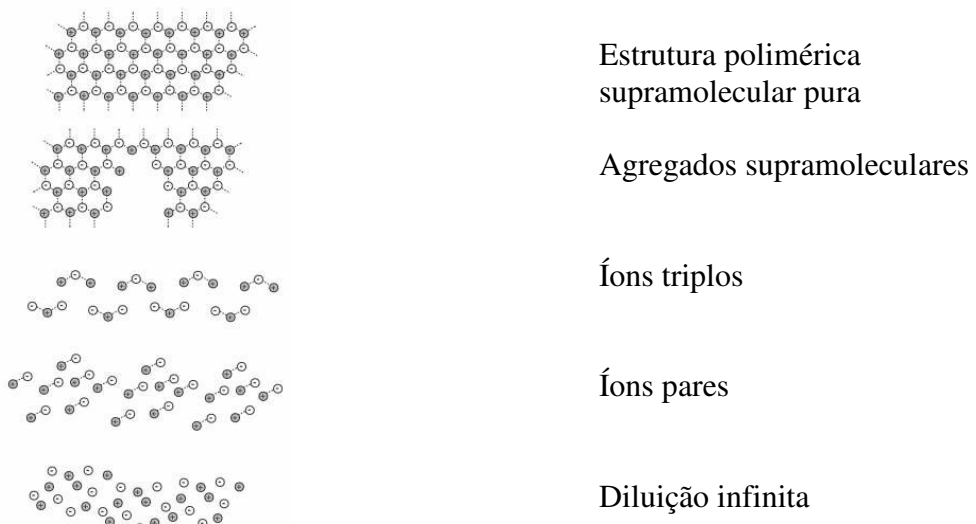


Figura 2.2. Modelo simplificado bidimensional das características estruturais de líquidos iônicos 1,3 dialquilimidazólio. Fonte: Dupont (2004).

2.1.2.5 Propriedades de cristal líquido

No estado líquido cristalino ou mesomórfico, os materiais apresentam simultaneamente propriedades de fluidez como um líquido e forte anisotropia em algumas de suas propriedades físicas, isto é, suas moléculas estão orientadas como cristais (Chandrasekhar, 1994). Estes

materiais são em geral constituídos por moléculas orgânicas anisométricas. Estas moléculas têm uma das suas dimensões muito maior do que as restantes (ex.: podem ter uma forma alongada ou a forma de discos). Até pouco tempo, os líquidos cristalinos conhecidos eram formados por moléculas neutras. Entretanto, o estudo em líquidos iônicos sugere que alguns deles apresentam o estado cristalino e tem condutividade iônica. O estudo tem-se baseado em líquidos iônicos com longas cadeias alquílicas em cátions de imidazólio, piridínio e amônio e mostra a necessidade de novos estudos com variações estruturais no ânion (Binnemans, 2005).

2.1.2.6 Propriedades físico-químicas

Uma das primeiras propriedades dos líquidos iônicos que interessou a indústria foi sua condutividade elétrica; posteriormente a baixa pressão de vapor seduziu os cientistas com a possibilidade de criar processos com nenhuma poluição de orgânicos voláteis. Além disso, podem existir como líquidos em um intervalo amplo de temperatura, de até 300 °C, permitindo controlar reações químicas e uma grande facilidade de separação das moléculas orgânicas por destilação, sem perda do líquido iônico.

Até agora, muitos líquidos iônicos têm sido baseados no cátion imidazólio e, em menor proporção, em piridínios alquila ou trialquilaminas (Marsh et al., 2004). Ao alterar o ânion ou o comprimento da cadeia alquílica no cátion, um vasto leque de propriedades, tais como hidrofobicidade, viscosidade, densidade e poder de solvatação podem ser modulados abrindo as possibilidades para o líquido iônico adaptar-se a projetos específicos. Desta forma, Bicak (2005) sintetizou um líquido iônico formado a partir da neutralização de monoetanolamina com ácido fórmico. Greaves et al. (2006) sintetizaram diferentes líquidos iônicos próticos a partir de aminas primárias e ácidos inorgânicos. Iglesias e colaboradores (Cota et al., 2007, Álvarez et al., 2010a) sintetizaram uma família desses líquidos iônicos, modificando a cadeia alifática dos ácidos orgânicos e/ou utilizando hidroxiaminas secundárias e terciárias. Estes autores explicam o baixo custo e simplicidade de síntese. Além disso, a baixa toxicidade e degradabilidade desse tipo de líquidos iônicos foi verificada (Sierra et al., 2008; Peric et al., 2010).

Como estudado nas seções anteriores, os líquidos iônicos possuem um único conjunto de propriedades físico-químicas que os tornam adequados em numerosas aplicações específicas, nos quais os solventes convencionais não são aplicáveis ou não são suficientemente eficazes.

Adicionalmente, um estudo sobre algumas propriedades gerais dos líquidos iônicos puros ou em mistura são descritas:

Alta estabilidade à luz UV

A sensibilidade à luz UV é um problema para vários compostos e também para alguns líquidos iônicos de cadeia longa nos sais de imidazólio com uma exposição maior que 90 horas (Stepnowski e Zaleska, 2005; Yang e Dionysiou, 2004). Entretanto, podem ser sintetizados líquidos iônicos de alta estabilidade à luz UV. Assim, Tindale e Ragogna (2009) sintetizaram uma nova classe de líquidos iônicos de fosfônios fluorados e comparações do espectro ^1H NMR, antes e depois de aplicações de radiação UV durante 90 h, não detectaram a destruição ou qualquer outra alteração da estrutura molecular ou ligação.

Alta condutividade elétrica

O início dos líquidos iônicos foi caracterizado pelo estudo e aplicação como eletrólitos em baterias, com o primeiro líquido iônico com o ânion de cloroaluminato tendo sido patenteado em 1948 (Hurley, 1948). Ao que parece, seria este o início da era moderna para os líquidos iônicos, porque pela primeira vez um público mais vasto de químicos começou a se interessar por estes solventes iônicos não aquosos (Chum et al., 1975; Wilkes e Zaworotko, 1992; Wilkes, 2002). Principalmente para os líquidos iônicos baseados no alquilimidazólio, o cátion tende a ser o responsável pelas propriedades de transporte. Assim, aparentemente a estrutura do cátion é o mais influente íon, nos dados de difusão e condutividade elétrica (Trulove e Mantz, 2002).

Estabilidade química

Na maioria destas aplicações, a estabilidade dos líquidos iônicos, pelo menos em certa medida, é crucial para o desempenho do processo ideal. Vários estudos têm indicado que, embora não sejam totalmente inertes, determinados líquidos iônicos incorporando cátions 1,3-dialquil imidazólio geralmente são mais resistentes do que os solventes tradicionais sob determinadas condições de processo, como as que ocorrem na oxidação, fotólise e processos de radiação (Yang e Dionysiou, 2004; Tindale e Ragogna, 2009).

Cor

Líquidos iônicos de alta qualidade incorporando cátions $[bmim]^+$ e uma variedade de ânions, tais como $[PF_6]^-$, $[BF_4]^-$, $[CF_3SO_3]^-$, $[CF_3CO_2]^-$ e $[(CF_3SO_2)_2N]^-$ foram relatados incolores, embora eles não sejam totalmente puros. A cor dos líquidos iônicos menos puros geralmente varia de amarelo para laranja. A formação da cor tem sido atribuída ao uso de matérias-primas com cor ou aquecimento excessivo durante a síntese de sal imidazólio (Yang e Dionysiou, 2004). A síntese de líquidos iônicos próticos utilizando o cátion amônio é sensível à temperatura, sendo que uma síntese a baixa temperatura com uma boa mistura dos compostos produz líquidos iônicos incolores. O posterior aquecimento para sua purificação os torna de uma cor levemente amarela. Isto mostra, provavelmente, que pequenas impurezas são originadas pela degradação do cátion amônio. Embora a concentração das impurezas não possa ser detectada pelo espectro de RMN, as impurezas podem ser observadas pela mudança de cor no líquido iônico (Álvarez et al., 2010a).

Higroscopicidade

Os líquidos iônicos, normalmente compostos de cátions orgânicos (por exemplo, alquil-substituídos fosfônio $^+$, piridínio $^+$, imidazólio $^+$) e ânions hidrofóbicos (por exemplo, $[PF_6]^-$, $[(CF_3SO_2)_2N]^-$), geralmente não se misturam com água, ou seja, grande parte deles é hidrofóbica. No entanto, mesmo sendo hidrofóbicos, muitos deles são higroscópicos e podem conter uma quantidade significativa de água, com o caráter hidrofílico do ânion e com o comprimento decrescente dos substituintes alquílicos sobre o cátion (Chaumont et al., 2005). É bem conhecido que as propriedades físicas dos líquidos iônicos são grandemente influenciadas pelo teor de água (Carvalho et al., 2009a, 2009b).

Hidrofobicidade

Como já relatado, o ânion tem uma grande influência sobre as propriedades do líquido iônico e podem-se obter líquidos iônicos hidrofóbicos com anions tipo $[bmim]^+[PF_6]^-$ (Davis e Fox, 2003). Além disso, o grau de polaridade pode ser variado, adaptando o comprimento do grupo alquílico no cátion ou ânion.

Reciclagem

Em comparação com amostras de líquidos iônicos obtidos de fabricantes, a degradação do líquido iônico depende das impurezas contidas. A estabilidade térmica, química e à luz UV originam

uma propriedade adicional aos líquidos iônicos: a de poderem ser reciclados mantendo suas propriedades. Esta propriedade é explorada pelas aplicações tecnológicas que podem ser impostas à diferentes líquidos iônicos (Yang e Dionysiou, 2004).

Propriedades termofísicas

O conhecimento básico das propriedades termofísicas dos líquidos iônicos é vital para o seu projeto e avaliação. As propriedades termodinâmicas permitem observar as diferenças em relação aos solventes tradicionais e as aplicações estudadas permitem avaliar sua possível utilização na indústria. Por exemplo, pontos de fusão, temperatura de transição vítreia, e temperaturas de decomposição térmica são necessários para definir a temperatura possível e o alcance operacional de um fluido. A densidade (em função da temperatura) é necessária para o dimensionamento do equipamento, capacidade calorífica é necessária para estimar o aquecimento e arrefecimento, bem como os requisitos para a capacidade de armazenamento de calor.

Desde a síntese e investigação de líquidos iônicos estáveis em água, relativamente recente, as informações sobre propriedades físicas do componente puro é um pouco limitada ou incompleta. Por exemplo, para os sais de imidazólio, têm-se muito mais dados da densidade a uma dada temperatura do que como uma função da temperatura.

Pontos de fusão e temperatura de transição vítreia para líquidos iônicos são medidos por calorimetria diferencial exploratória (DSC), e a temperatura de decomposição térmica medida pela análise termogravimétrica (TGA). Há evidências de que a presença de uma atmosfera oxidante (O_2), ou inerte (N_2), não tem um efeito significativo sobre a temperatura de decomposição de sais de imidazólio (Ngo et al., 2000). No entanto, há também evidências de que alguns sais de imidazólio decompõem em baixas temperaturas, na presença de O_2 (Awad et al., 2004). Estes dados para sais de imidazólio são mais disponíveis; entretanto, em contraste, dados de capacidade calorífica são muito escassos, (Magee, 2002; Holbrey et al., 2003; Fredlake et al., 2004).

Propriedades em misturas

O conhecimento das propriedades termodinâmicas de misturas é de interesse prático, pois a partir desses dados é possível obter parâmetros de interação binária que podem ser usados para

modelar, desenvolver e aperfeiçoar processos. Atualmente é considerado que misturas contendo líquidos iônicos continuam absorvendo umidade do ambiente (Cuadrado-Prado et al. 2009). Os líquidos iônicos são geralmente muito higroscópicos, mesmo sendo hidrofóbicos (Chaumont et al., 2005; Cuadrado-Prado et al. 2009). Assim, suas misturas são sensíveis à umidade do ar, sendo que pequenas quantidades de água podem afetar significativamente as suas propriedades. Considerando isto, os grupos de pesquisa têm utilizado meios que permitam uma atmosfera o mais seca possível para evitar a contaminação por água nas misturas (Welton, 1999).

2.1.3. PRODUÇÃO E CONSUMO DOS LÍQUIDOS IÔNICOS

Sais de 1,3-dialquíl imidazólio são os líquidos iônicos mais populares e investigados. Grande parte do foco em sais de imidazólio é devido à utilidade que demonstraram possuir nas pesquisas iniciais (Seddon, 1997). O mais significativo no uso de sais imidazólio foi a estabilidade em água, e sua relativa facilidade de síntese, e agora são comercialmente disponíveis. Numa pesquisa no catálogo da Sigma-Aldrich, comercializadora de produtos químicos, descobre-se mais de cento e vinte sais disponíveis comercialmente chamados líquidos iônicos e mais de cento e trinta sais (sem a denominação de líquido iônico) com ponto de fusão entre 0 e 100 °C. Estes dados sugerem que muitos líquidos iônicos novos poderiam ser facilmente criados pela combinação de um cátion desejado de um sal com um ânion diferente. Assim, podem-se conseguir novos líquidos iônicos, observando pontos de aplicação pré-existentes para usos potenciais de líquidos iônicos substituindo os compostos tradicionais, sais ou derivados clássicos (Davis e Fox, 2003). Desta forma, o uso de aminoácidos na síntese de líquidos iônicos é um exemplo interessante (Ohno e Fukumoto, 2007).

A preparação dos líquidos iônicos, mesmo em grandes quantidades, não apresenta grandes dificuldades. Desde que sejam de pureza satisfatória (>95% em massa), a maioria dos líquidos iônicos podem ser armazenados sem decomposição por longos períodos, embora alguns sejam relativamente higroscópicos (Welton, 1999). Um caso particular são os líquidos iônicos próticos que contém íons pequenos como o formiato; a literatura e experiências em um de nossos testes tem mostrado a decomposição no tempo em ésteres e Greaves et al. (2006) informam a decomposição no tempo em amidas.

Existem dois métodos básicos para a preparação de líquidos iônicos: metátese de um sal de halóide e reações de neutralização ácido-base; um terceiro seria a combinação direta de um sal de halóide com um metal halóide.

2.1.3.1 Reações de metátese (Welton, 1999)

Muitos alquilamônios de halóides estão disponíveis comercialmente ou podem ser preparados pela reação do halogênio-alcano adequado e aminas. A preparação de sais de piridínio e halogênio-imidazólio pode ser feita de forma semelhante. Para halogênio-alcanos voláteis, a preparação precisa de um tubo fechado para a reação, como na síntese de $[\text{emim}]^+[\text{Cl}]^-$ (onde $[\text{emim}]^+$ é o cátion 1-etil-3-metilimidazólio). Entretanto, sais com substituintes de cadeia mais longa, como $[\text{bmim}]^+[\text{Cl}]^-$ (onde $[\text{bmim}]^+$ é o cátion 1-butil-3-metilimidazólio), podem ser preparadas em recipientes de vidro convencional por aquecimento sob refluxo.

2.1.3.2 Reações de neutralização ácido-base (Welton, 1999; Alvarez et al., 2010)

Sais baseados em monoalquilamônio são mais bem preparados pela neutralização de aminas com ácidos. Logo, os líquidos iônicos são isolados, removendo o excesso de água no vácuo. Em uma reação similar, sulfonatos de tetraalquilamônio são preparados pela mistura de quantidades equimolares de ácido sulfônico e hidróxido de tetraalquilamônio. Novamente, o excesso de água é removido sob vácuo. Para garantir a pureza dos líquidos iônicos, estes são dissolvidos em acetonitrila ou tetrahidrofurano e tratados com carvão ativado, pelo menos, 24 h, e, finalmente, o solvente orgânico é removido sob vácuo. A preparação é feita em recipientes de vidro convencional sob resfriamento.

2.1.3.3 Combinação direta de sal e metal

O método final para a síntese de líquidos iônicos é a combinação direta de um sal de haleto com um halogeneto de metal. É desta maneira que líquidos iônicos de halogênio-aluminato (III) e cloreto de cobre (I) são preparados.

2.1.3.4 Manuseio dos líquidos iônicos

Na maioria das aplicações, a estabilidade dos líquidos iônicos, pelo menos em certa medida, é crucial para o ótimo desempenho do processo. É amplamente conhecido que muitos dos novos

líquidos iônicos são estáveis ao ar e umidade, alguns são até mesmo hidrofóbicos. Embora seja verdade que os novos líquidos iônicos estão livres de muitos dos problemas que tornam a hidrólise dos halogenoaluminatos (III) tão difícil de lidar, sais de amônio e imidazólio são higroscópicos e se são usados em recipientes abertos, a hidratação certamente ocorre, mesmo sendo hidrofóbicos. Também é importante conhecer a temperatura de degradação; por exemplo, líquidos iônicos contendo o ânion $[PF_6]^-$ ou $[BF_4]^-$ se decompõem quando aquecidos na presença de água, desprendendo HF (Trulove e Mantz, 2002).

O grau em que as impurezas ou temperatura constituem um problema vai depender do uso para o qual o líquido iônico está sendo preparado e do soluto que vai ser usado. Por exemplo, uma pequena quantidade de catalisador pode ser desativada por quantidades mínimas de água. Assim, é recomendável a manipulação dos líquidos iônicos sob atmosfera inerte e seca.

Entre os líquidos iônicos a temperatura ambiente que tem recebido maior atenção, os nitratos e percloratos orgânicos, os quais são potencialmente explosivos, quando secos. Embora não foram relatados problemas, muito cuidado deve ser considerado em todos os momentos em que se manipulem líquidos iônicos (Welton, 1999).

2.1.4. QUÍMICA VERDE E OS LÍQUIDOS IÔNICOS

Assim que foi aprovada a Lei de Prevenção da Poluição de 1990 (*Pollution Prevention Act*) nos Estados Unidos, a qual prescrevia uma nova atitude de crescimento industrial, o Instituto de Prevenção à Poluição e Tóxicos (*Pollution Prevention and Toxics, OPPT*) explorou a idéia de desenvolver novos produtos químicos e processos, ou melhorar os existentes, para torná-los menos perigosos para o ambiente e a saúde humana.

Em 1991, o OPPT lançou um novo programa de pesquisa chamado “Caminhos Alternativos de Síntese para a Prevenção da Poluição” (*Alternative Synthetic Pathways for Pollution Prevention*). Esse programa proporcionou bolsas para projetos de pesquisa sem precedentes, que incluíram a prevenção da poluição na concepção e síntese de produtos químicos. Desde então, este programa tem construído muitas colaborações com universidades, indústrias, agências governamentais e organizações não-governamentais para promover o uso da química para a prevenção da poluição.

Logo, foi acunhado (?) o termo “Química Verde” no mundo. Assim, a química verde é o uso da química para a prevenção da poluição. Mais especificamente, a química verde é o projeto de produtos e processos químicos que reduzam ou eliminem o uso e a geração de substâncias perigosas.

Desde 1990 até hoje, a química verde mostrou ser uma filosofia altamente eficaz para a prevenção da poluição, pois aplica soluções científicas inovadoras para situações reais do ambiente. Os 12 princípios da química verde (ver no apêndice), originalmente desenvolvidos por Anastas e Warner (2000), fornecem um roteiro aos pesquisadores para implementar a química verde.

Os princípios da química verde abrangem uma nova atitude para com as práticas industriais e síntese química em que os resíduos ou compostos perigosos são eliminados antes de ser trazidos ao meio ambiente (Visser et al., 2002). Assim, o potencial dos líquidos iônicos para fornecer um sistema com solventes não-voláteis tornou-se um alvo prático para reduzir o desperdício e eliminar os riscos dos tradicionais solventes orgânicos voláteis. Mas isso não é suficiente para a segurança das indústrias químicas.

Apesar do entusiasmo, os químicos são cautelosos sobre as características ecológicas dos líquidos iônicos (Renner, 2001). A principal confusão está no sentido de serem chamados solventes verdes por sua baixa volatilidade, embora não tenha sido observado todo o ciclo de vida do líquido iônico, desde sua síntese até sua disposição final no meio ambiente. Assim, novos estudos sobre a síntese, reciclagem e toxicidade estão mostrando novas tendências às características de novos líquidos iônicos.

2.1.4.1 Síntese

Na realidade, os líquidos iônicos em si são feitos a partir de espécies que, antes de sua combinação são compostos orgânicos voláteis, e logo os VOCs são utilizados para a purificação desses líquidos iônicos. Este é um problema importante; entretanto, poucos grupos de pesquisa têm dado a devida consideração. No entanto, já em 2001 houve avanços na síntese de líquidos iônicos; por exemplo, Namboodiri e Varma (2002) prepararam halogenetos do 1-alquil-3-metilimidazólio, sem solventes em recipientes abertos, no forno de microondas. Incentivando a

não aplicação de solventes adicionais, Iglesias e colaboradores têm sintetizado novos líquidos iônicos tipo Brønsted sem o acréscimo de solventes adicionais à síntese (Cota et al. 2007; Álvarez et al., 2010a).

2.1.4.2 Reciclagem

A purificação dos líquidos iônicos pode produzir resíduos secundários, pela lavagem com água ou VOCs, eliminando os benefícios ecológicos dos líquidos iônicos (Renner, 2002). Assim, os grupos de pesquisa estão procurando melhores processos com reciclagem dos líquidos iônicos, como por exemplo, o uso de CO₂ supercrítico para remover compostos orgânicos do seio do líquido iônico (Blanchard et al, 1999) e a extração de compostos sulfurados de líquidos combustíveis (Jiang et al., 2008).

2.1.4.3 Toxicologia

Embora as informações sobre a física, termodinâmica, cinética ou de engenharia dos líquidos iônicos venham sendo ampliadas continuamente, poucos dados quanto à toxicidade e ecotoxicidade se encontram disponíveis. Mesmo que os líquidos iônicos não contribuam para a poluição atmosférica, a maioria é solúvel em água e podem entrar no ambiente por esta via. Até agora não sabemos exatamente quais são as consequências para esses casos; embora, no geral, existam duas aproximações para o estudo das propriedades de toxicidade, metabolismo e degradação dos compostos:

- Considerando-se a estrutura química e utilizando o conhecimento sobre a relação estrutura-atividade (SAR, do inglês *Structure-Activity-Relationships*) e a correlação estrutura-propriedade (SPC, do inglês *Structure-Property-Correlations*). Ambos os métodos utilizam técnicas estatísticas para correlacionar propriedades com a estrutura da molécula.
- Métodos experimentais toxicológicos (Couling et al., 2006) são utilizados para corroborar a hipótese dos trabalhos teóricos das estruturas e para obter informações sobre os efeitos potenciais de novas substâncias em sistemas complexos que só podem ser previstos com grande incerteza.

Assim, o contínuo trabalho conjunto entre as duas abordagens leva a resultados mais exatos, como pode ser observado na seguinte listagem dos trabalhos feitos na literatura sobre os líquidos iônicos.

- Referindo-se a sua estrutura química, Trulove e Mantz (2002) assinalaram que líquidos iônicos contendo ânions de halogênios tem fraca estabilidade em água, e espécies tóxicas e corrosivas, como HCl ou HF podem ser liberadas. Por isso, eles sugerem a utilização de ânions livres de halogênio com hidrólise relativamente estável, como os compostos de octilsulfato.
- Pernak et al. (2003) fizeram ensaios da atividade antimicrobiana de uma série de sais de 3-alcoximetil-1-metilimidazólio contendo Cl^- , $[\text{BF}_4]^-$ e $[\text{PF}_6]^-$ sobre diferentes bactérias e fungos. Os resultados mostraram que o aumento no comprimento da cadeia substituinte no alcoximetil aumenta a atividade antimicrobiana. Esta atividade não foi afetada pelo tipo de ânion utilizado.
- Gathergood e Scammells (2002) sintetizaram líquidos iônicos com cadeias laterais contendo diversos grupos funcionais. Essas modificações permitiram a hidrólise enzimática do líquido iônico no ensaio tipo “Closed Bottle Test” e o acréscimo de sua biodegradabilidade foi demonstrado.
- Stock et al. (2004) apresentam os resultados iniciais sobre a toxicidade de líquidos iônicos baseados em imidazólio, piridínio e fosfônio utilizando o ensaio da inibição da enzima acetilcolinesterase, obtida do peixe *Electrophorus Electricus*. Os resultados mostram a seguinte ordem de toxicidade: imidazólio > piridínio > fosfônio, mostrando que líquidos iônicos contendo nitrogênio carregado positivamente são mais tóxicos, e que um grupo alquil maior no segundo nitrogênio do imidazólio eleva a toxicidade. O ânion não tem influência na toxicidade nesses líquidos iônicos.
- Ranke et al. (2004) fizeram estudos de inibição de luminescência na bactéria marina *Vibrio Fischeri* e da viabilidade de células de mamíferos (IPC 81, Leukemia cells; C6, Glioma cells) influenciada por diferentes concentrações de sais de R1-alquil-R2-alquil-imidazólio contendo $[\text{BF}_4]^-$, $[\text{PF}_6]^-$, o Cl^- e Br. Os resultados mostram similar toxicidade utilizando os dois

métodos, onde o comprimento da cadeia alquílica na posição R2 aumenta a toxicidade do líquido iônico na bactéria e nas células. O tipo de ânion não mostrou influência na toxicidade dos líquidos iônicos.

- Couling et al. (2006) fizeram estudos no crustáceo dáfnia (*Daphnia Magna*), o qual é a base da cadeia alimentícia em rios. Os autores estudaram os efeitos de líquidos iônicos baseados em cátions de imidazólio, piridínio e amônio quaternário. Os resultados mostram que os líquidos iônicos contendo átomos de nitrogênio com ligações duplas são tóxicos, tanto quanto o fenol. Entretanto, os líquidos iônicos contendo o cátion amônio quaternário são relativamente não tóxicos, sendo a ordem de toxicidade crescente: imidazólio com cadeias alquílicas longas > imidazólio com cadeias alquílicas curtas > piridínio > amônio quaternário. Átomos com carga negativa no cátion diminuem a toxicidade e átomos com carga positiva no ânion a aumentam. Com um modelo tipo SAR foi predito que o triazolio é o cátion mais tóxico.
- Sierra et al. (2008) e Couling et al. (2006) explicaram o baixo custo, simplicidade de síntese, e as diferentes aplicações do líquidos iônicos obtidos da síntese do etanolamina. Além disso, a baixa toxicidade e degradabilidade desses líquidos iônicos pelas bactérias do solo foi verificada.

Esses resultados permitem que pesquisadores sejam otimistas ao futuro dos líquidos iônicos; pois dados de propriedades toxicológicas permitem projetar estruturas biodegradáveis e não tóxicas de líquidos iônicos, iniciando o projeto dos líquidos iônicos por meio da avaliação teórica da possível atividade biológica com a ajuda de métodos SAR ou SPC antes de síntese.

Toxicidade e biodegradabilidade

O aspecto toxicológico e a biodegradabilidade dos líquidos iônicos devem ser cuidadosamente investigados devido à formação de produtos de decomposição, sua estabilidade no ecossistema e sua influência direta no corpo humano. Nos estudos das muitas aplicações dos líquidos iônicos, não é analisado o seu perigo potencial destes nos sistemas biológicos. Estudos pioneiros sobre a biodegradação de líquidos iônicos, a quantifica através da produção de CO₂ com o método de Sturm (Gathergood and Scammells, 2002). Atualmente, por meio de estudos nos sistemas biológicos, sabe-se que existem líquidos iônicos com baixo e alto potencial de risco na ecologia,

dependendo fortemente da estrutura molecular do líquido iônico (Docherty et al., 2007). Como observado anteriormente, a toxicidade é, em sua maioria, influenciada pelo cátion no líquido iônico e tem a seguinte ordem crescente: amônio < fosfônio < piridínio < imidazolio e os ânions mais tóxicos são aqueles que contêm fósforo em sua estrutura, na seguinte ordem crescente: Cl^- < $[\text{C}_8\text{H}_{17}\text{SO}_3]^-$ < $[\text{CF}_3\text{SO}_3]^-$ < $[\text{BF}_4]^-$ < $[\text{PF}_6]^-$ < $[\text{SbF}_6]^-$. A toxicidade dos líquidos iônicos é predominantemente determinada pelas cadeias alquílicas contidas no cátion. Pham et al. (2010) mostram que em grupos hidroxila, amônio, ésteres, e o aumento de átomos de carbono nas cadeias alquílicas ($>\text{C}_5$) nos cátions imidazólio, piridínio e dimetilamino, acrescentam a biodegradabilidade, embora grupos alquílicos de cadeia longa aumentem a toxicidade. Quanto às questões regulamentares e legislativas, a persistência de um composto no ecossistema é um parâmetro chave para a autorização de uso do mesmo em processos industriais. Em consequência, a utilização de líquidos iônicos persistentes no ecossistema ficaria muito restrita. Assim, o projeto estrutural de líquidos iônicos deve visar a sua biodegradabilidade e baixa toxicidade, sendo que é uma necessidade essencial com vista à sua utilização industrial. Nesse contexto, o presente trabalho acredita que os líquidos iônicos contendo o cátion amônio são os mais adequados para garantir baixa toxicidade e alta biodegradabilidade.

2.2. MODELAGEM

Os líquidos iônicos, com sua combinação ilimitada de cátions e ânions, podem oferecer o solvente ideal para uma finalidade específica. Mas nem todos os estudos experimentais são possíveis, uma vez que os experimentos são caros e demorados. Uma seleção criteriosa das várias estruturas moleculares dos líquidos iônicos possíveis é necessária, visando selecionar o solvente adequado. Nesse sentido, um método de triagem deve ser proposto para o projeto molecular de líquidos iônicos, com o objetivo de reduzir de forma eficiente os esforços experimentais necessários. Logo, é necessário desenvolver modelos para prever as propriedades termodinâmicas de fluidos para vários sistemas, incluindo líquidos iônicos, tais como solubilidade e equilíbrio de fases. Assim, existem três abordagens para a modelagem: a primeira utiliza os coeficientes de fugacidade para sistemas em alta ou baixa pressão; a segunda utiliza o coeficiente de atividade para sistemas a baixas pressões; e a última utiliza os coeficientes segundo conveniência da fase a modelar.

Os coeficientes de fugacidade são calculados com as equações de estado, que cumprem um importante papel na engenharia química e no estudo do equilíbrio de fases dos fluidos. Originalmente, estas foram usadas para componentes puros. Quando foram aplicadas a misturas, foram usadas somente para misturas não-polares (Soave, 1972; Peng e Robinson, 1976) e fracamente polares (Huron et al., 1978; Asselineau et al., 1978; Graboski e Daubert, 1978). A vantagem das equações de estado é sua grande escala de aplicabilidade na temperatura e na pressão, desde gases leves até líquidos densos. Podem ser usadas para modelar o equilíbrio líquido-vapor e equilíbrio líquido-líquido, abrangendo os fluidos supercríticos.

Os modelos de coeficiente de atividade centram-se na descrição da energia livre de Gibbs em excesso de um fluido, geralmente um líquido incompressível, a partir do qual o coeficiente de atividade das espécies é facilmente obtido. Estes modelos, como NRTL (Renon e Prausnitz, 1968), Wilson (Wilson, 1964), e UNIQUAC (Abrams e Prausnitz, 1975), são precisos para misturas de líquidos, mas não são aplicáveis na fase vapor. Nesse contexto, para misturas altamente não ideais, esforços têm sido feitos para desenvolver avançadas regras de mistura para uso de equações de estado. Com o desenvolvimento de regras de mistura mais sofisticadas, as equações de estado tornaram-se rapidamente úteis para o cálculo do equilíbrio de fases em misturas não-polares e polares.

Wong e Sandler (1992) propuseram um novo tipo de regra de mistura que garante a forma quadrática do segundo coeficiente virial em todo o intervalo de pressões, mantendo a idéia original de que uma equação de estado se comporta como um modelo de coeficiente de atividade no limite da alta pressão. Para esta regra de mistura, pode-se usar como uma boa aproximação $A_{\infty}^E \approx A_o^E \approx G_o^E$. A energia livre de Gibbs em excesso a baixa pressão, G_o^E , é calculada utilizando qualquer modelo clássico apropriado para a fase líquida. Na literatura, se utilizam geralmente os modelos clássicos UNIQUAC e NRTL.

Os modelos UNIQUAC e NRTL foram desenvolvidos para correlacionar dados experimentais e logo calcular propriedades da mistura. Mas dados de equilíbrio para sistemas que envolvem novos compostos, como os líquidos iônicos, são escassos. Assim, modelos preditivos, que não requerem ajuste de parâmetros baseados em dados experimentais, são de crucial importância. Nesse sentido, a simulação molecular pode ser muito útil para predizer as propriedades PVT de novos líquidos iônicos (Aparício et al., 2007).

Modelos preditivos podem ser desenvolvidos, por exemplo, a partir do método de contribuição de grupos, que consiste na ligação empírica dos parâmetros do modelo termodinâmico com diferentes grupos químicos que constituem as moléculas. Métodos de contribuição de grupos têm sido desenvolvidos tanto para equações de estado (Skjøld-Jorgensen, 1988; Holderbaum e Gmehling, 1991; Gros et al., 1996; Le Thi et al., 2006), como para modelos de coeficiente de atividade (Fredenslund et al., 1975; Larsen et al., 1987; Gmehling et al., 1993; Tsavas et al., 2004). As principais vantagens dos métodos de contribuição de grupos são a sua simplicidade e eficiência. No entanto, as abordagens de contribuição de grupos estão limitadas aos tipos de moléculas que estiveram envolvidas no ajuste dos parâmetros, e podem ser imprecisos para as condições de pressão e temperatura que não foram consideradas no processo do ajuste dos parâmetros.

Uma segunda maneira de desenvolver modelos preditivos envolve cálculos de química quântica (Prausnitz e Tavares, 2004; Arlt et al., 2004). Uma abordagem possível é utilizar uma equação de estado baseada em um potencial intermolecular ajustado a cálculos *ab initio*. Tal abordagem é muito semelhante à metodologia utilizada na simulação clássica para desenvolver novos campos de força, e pode fornecer previsões muito precisas para moléculas esféricas (Paricaud, 2006). No entanto, esta abordagem está ainda limitada a casos simples; o desenvolvimento de teorias gerais, que levariam em conta todos os tipos de interações (eletrostática, intramolecular, e polarizabilidade) é muito difícil.

Outra estratégia consiste em relacionar os parâmetros de um modelo termodinâmico macroscópico para cálculos de *ab initio* realizados nas moléculas estudadas. Estes parâmetros serão os mesmos para todas as moléculas e são determinados pelo ajuste de um conjunto grande de dados de equilíbrio líquido-vapor e/ou líquido-líquido. Assim, os únicos dados que caracterizam uma dada mistura são os obtidos dos cálculos *ab initio* na molécula. O modelo de coeficiente de atividade COSMO (COnductor-like Screening MOdel) e suas versões, como COSMO-RS (Klamt 1995; Klamt e Eckert, 2000) e COSMO-SAC (Lin e Sandler, 2002, 2004), foram desenvolvidos com base nessa idéia. Os modelos COSMO-RS e COSMO-SAC são capazes de descrever corretamente, pelo menos qualitativamente, variações estruturais das moléculas. No entanto, é necessário reparametrizar os modelos para uma maior precisão ao estudar novas estruturas moleculares (Banerjee et al., 2008). Um extenso banco de dados de

cálculos *ab initio* correspondente ao modelo COSMO-SAC foi desenvolvido por Mullins et al. (2006).

Há poucos trabalhos que tratam da aplicação do COSMO para a descrição do equilíbrio líquido-líquido em sistemas contendo líquidos iônicos e compostos alifáticos sulfurosos, hidrocarbonetos ou água, e nenhum com compostos aromáticos sulfurosos (Freire et al. 2008; Kumar e Banerjee, 2009).

2.2.1 Equilíbrio líquido-vapor a baixas pressões

Como explicado anteriormente, dependendo da sua estrutura, os líquidos iônicos tendem a ser solúveis, parcialmente solúveis ou insolúveis em diferentes solventes clássicos. Nesse contexto, antes de se realizar experimentos de equilíbrio líquido-vapor, são necessários testes de solubilidade para identificar quais misturas são totalmente miscíveis (Shimizu et al., 2009).

Atualmente, a separação de compostos em misturas líquidas com líquidos iônicos tem recebido muita atenção, por se tratar de um processo novo e com um grande potencial para ser reutilizado sem perdas ao ambiente, caracterizando processos ecologicamente limpos. Os líquidos iônicos em processos de separação líquido-vapor está sendo estudado e no momento o número de publicações cresce a cada dia. Nos processos com ELV utiliza-se tanto baixa como alta pressão. O termo baixa pressão para a pesquisa é considerado quando a pressão total é suficientemente baixa para que todas as correções dos coeficientes de fugacidade sejam a unidade (Sandler, 1999). O termo alta pressão é uma pressão suficientemente grande para que se tenha um efeito numérico maior do que a unidade sobre os coeficientes de fugacidade no equilíbrio de fases em consideração.

Dados confiáveis do equilíbrio líquido-vapor são importantes no projeto e simulação dos processos químicos, para o contínuo desenvolvimento de métodos preditivos de modelagem e também para verificar a validade dos modelos termodinâmicos atuais. Nos modelos termodinâmicos de correlação, UNIQUAC e NRTL, Alvarez e Aznar (2008b) mostraram que ambos os modelos conseguem ajustar os dados experimentais do ELV em misturas contendo líquidos iônicos, e o modelo NRTL é superior, quando os dados experimentais contêm grandes desvios. No caso de métodos preditivos, é desejável métodos de simples aplicação e confiáveis. Assim, o método de contribuição de grupos UNIFAC modificado (Dortmund) pode ser aplicado

para líquidos iônicos com a introdução dos principais grupos de cátions (imidazólio, pirrolidinio) e ânions (bis(trifluorometilsulfônico)imida, trifluorometanossulfonato) (Nebig et al. 2007, 2009; Nebig e Gmehling, 2010). Mas o modelo UNIFAC só pode modelar líquidos iônicos com os grupos estruturais que tem parametrizado. Este é um inconveniente que limita a aplicabilidade do modelo UNIFAC para a seleção de líquidos iônicos. A química quântica baseada no modelo COSMO (COSMO-RS, COSMO-RS(O1) ou COSMO-SAC) tem um conjunto pequeno de parâmetros que não precisa ser ajustado para modelar novos compostos, portanto, pode ser aplicado a novos líquidos iônicos. A primeira aplicação do modelo COSMO no ELV foi publicado em 2005 (Kato e Gmehling, 2005), e muito trabalho foi feito e publicado desde então.

Na maioria de processos indústrias temos misturas com água, metanol ou etanol. Assim, o estudo desses compostos em misturas com líquidos iônicos é de interesse teórico e no projeto técnico de processos. Também, na atualidade, os ésteres orgânicos são importantes intermediários em indústrias química e farmacêuticas, e são principalmente produzidos por reações de esterificação catalisada por algum ácido (Larock, 1999). Vários ácidos minerais têm sido utilizados como catalisadores para esterificação, mas eles são extremamente corrosivos e precisam ser neutralizados no final da reação. Muitas reações orgânicas ácido-catalisadas com base em líquidos iônicos têm sido relatadas, entre os quais a esterificação é um tema atual (Leng et al., 2009). Adicionalmente, outro processo, a oxidação de álcoois para os correspondentes aldeídos ou cetonas, é uma das mais importantes transformações de grupos funcionais em síntese orgânica. Ansari e Gree (2002) têm demonstrado que os líquidos iônicos podem ser utilizados na oxidação de álcoois em aldeídos. A pesquisa nessa área teve dois momentos importantes. Em 2002, o aumento da pesquisa deveu-se à aplicação de líquidos iônicos junto com um catalisador para a produção de aldeídos a partir de álcoois (Ansari e Gree, 2002) e, em 2008, a pesquisa cresceu pela produção de aldeídos apenas usando líquidos iônicos (Luo et al., 2007).

Além disso, no final da reação, uma separação líquido-líquido ou destilação dos produtos da mistura de reação parece muito atraente, no caso de derivados que são suficientemente voláteis. E, após a realização de métodos de purificação no líquido iônico, este poderia ser reciclado. Nesse contexto, um estudo sobre as propriedades físicas e ELV entre misturas de aldeídos/ésteres e líquidos iônicos é necessário para desenvolver processo de síntese ou separação.

2.2.2 Equilíbrio líquido-vapor a altas pressões

Entre as várias aplicações previsíveis para líquidos iônicos como solventes ou em processos de separação, a sua utilização em processos com gases supercríticos é uma das mais interessantes. Blanchard et al. (1999) descreveram várias aplicações potenciais de fluidos supercríticos com líquidos iônicos. Eles demonstraram a possibilidade de utilizar CO₂ supercrítico para remover um soluto de um líquido iônico sem contaminação do soluto extraído, resolvendo uma das deficiências no uso dos líquidos iônicos nos processos de extração: a recuperação dos compostos misturados com líquido iônico. Scurto et al. (2002) propuseram um processo inovador para a separação do líquido iônico de solventes orgânicos usando CO₂ supercrítico, que induz uma separação de fases, devido à expansão da fase líquida orgânica e, com a diminuição da constante dielétrica, força o líquido iônico a separar-se em uma segunda fase líquida. Mais tarde, Scurto et al. (2003) também demonstraram que a separação de soluções aquosas de líquidos iônicos hidrofóbicos ou hidrofílicos pode ser realizada utilizando CO₂ supercrítico.

Uma grande quantidade de trabalhos relativos ao desenvolvimento dos líquidos iônicos com afinidade especial para absorver CO₂ foi realizada. Bates et al. (2002) relataram líquidos iônicos com grupos aminas, enquanto Yuan et al. (2007) usaram líquidos iônicos com grupos hidroxila e amônia, e Sun et al. (2008) usaram líquidos iônicos com grupos hidroxila como um novo catalisador químico para a fixação de CO₂. Adicionalmente, Yu et al. (2006) propuseram líquidos iônicos baseados no ânion glicina ou alanina, e Huang et al. (2008) propuseram líquidos iônicos baseados no cátion guanidínio para absorver SO₂. Essas propostas têm em comum utilizar líquidos iônicos com grupos doadores de elétrons que aumentam a força das interações do grupo - NH₂ o qual é receptor-doador de elétrons; consequentemente, melhora as interações entre NH₂ e CO₂.

O êxito no desenvolvimento de processos baseados em líquidos iônicos usando fluidos supercríticos depende do conhecimento adequado do comportamento de fases dos sistemas. Nesse contexto, dados de equilíbrio líquido-vapor a altas pressões foram determinados pelo grupo do professor João Coutinho (Universidade de Aveiro-Portugal) e nosso grupo aplicou o teste de consistência termodinâmica e a modelagem aos dados experimentais.

Durante o estudo das aplicações dos líquidos iônicos, observou-se que existe uma grande pesquisa no equilíbrio líquido-vapor a altas pressões em sistemas binários do tipo líquido iônico + CO₂ supercrítico. Ao comparar os dados de diferentes grupos de pesquisa, podem-se observar importantes discrepâncias entre os valores experimentais obtidos. Como exemplo, dados do sistema CO₂ supercrítico + [bmim]⁺[PF₆]⁻ a 313,15 K são mostrados na Figura 2.3; é fácil observar as significantes discrepâncias entre os diferentes conjuntos de dados. Similares resultados são obtidos a outras temperaturas.

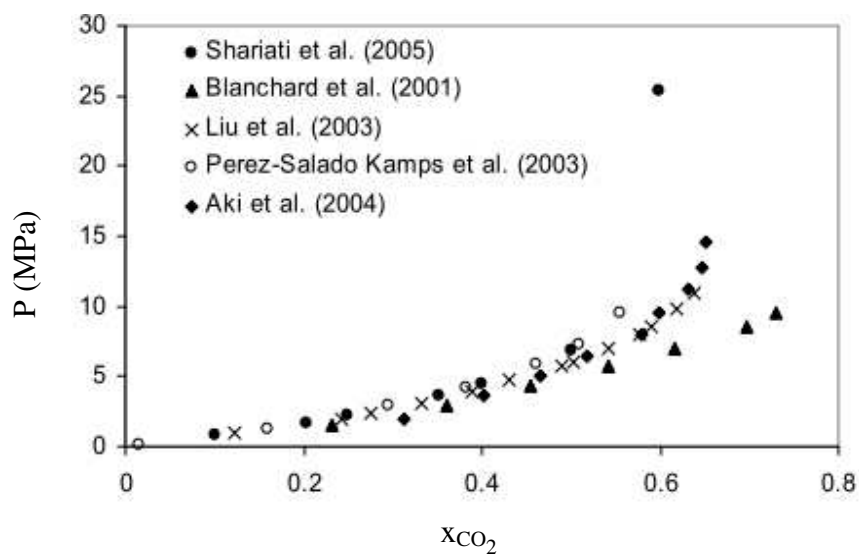


Figura 2.3. Diagrama de fases para o sistema CO₂ supercrítico [bmim]⁺[PF₆]⁻ a 313 K.

Essas diferenças são, evidentemente, devido às imprecisões na medição de propriedades experimentais, o que torna necessário testar as imprecisões inerentes a tais dados. Embora seja difícil ter certeza absoluta sobre a exatidão dos dados experimentais, é possível verificar se esses dados satisfazem a equação de Gibbs-Duhem, estabelecendo se os dados são consistentes ou inconsistentes termodinamicamente.

Um teste de consistência termodinâmica, desenvolvido para sistemas com dados incompletos PTxy e baseado na equação de Gibbs-Duhem, e a equação de estado de Peng-Robinson (Peng e Robinson, 1976) com a regra de mistura de Wong-Sandler (Wong e Sandler, 1992), utilizando o modelo UNIQUAC (Abrams e Prausnitz, 1975) para os coeficientes de atividade, foi desenvolvido por Alvarez e Aznar (2008a). Além disso, é mostrado que o modelo proporciona uma excelente representação dos dados experimentais.

2.2.3 Equilíbrio líquido-líquido

Comunidades científicas e industriais estão cada vez mais preocupadas com processos ecológicos, o que levou a busca de solventes mais benignos. Como os líquidos iônicos não apresentam pressão de vapor mensurável em condições ambientais, eles são uma alternativa atraente a partir do ponto de vista das emissões, originando, o estudo de novos processos líquido-líquido, por exemplo, dessulfurização (Gao et al., 2009), síntese com alto rendimento (Welton, 1999), extração (Swatloski et al., 2002) e descontaminação (Visser et al., 2002; Yang et al., 2004). Em contrapartida, alguns líquidos iônicos são tóxicos e têm considerável solubilidade em água, sendo preocupante as liberações aquosas, e originando o interesse em coeficientes de partição do sistema octanol-água para líquidos iônicos (Domańska et al., 2003). Isto representa uma pesquisa particular do equilíbrio ternário líquido-líquido.

2.3. PRINCIPAIS APLICAÇÕES DOS LÍQUIDOS IÔNICOS

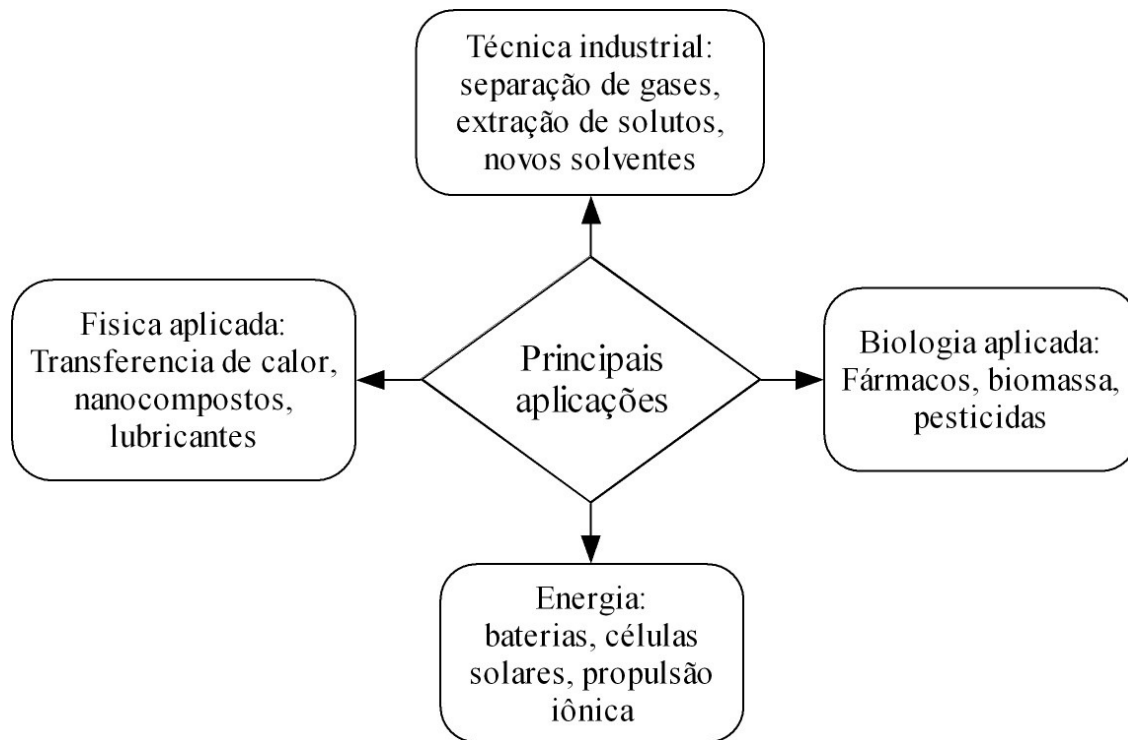


Figura 2.4. Algumas aplicações dos líquidos iônicos até o momento.

O estudo inicial em torno dos líquidos iônicos no que diz respeito à química verde tem sido o interesse pelo fato de ter baixas pressões de vapor; portanto, não emitem compostos orgânicos voláteis. Mas a substituição de solventes orgânicos voláteis é apenas uma parte da pesquisa, pois como já relatado, são materiais que estão tendo uma infinidade de aplicações em vários domínios

das ciências físicas. Algumas aplicações podem ser observadas na Figura 2.4 (Renner, 2001; Atkins et al., 2004).

2.3.1 Catalisadores homogêneos e heterogêneos

Para algumas aplicações, os líquidos iônicos oferecem a vantagem de catalisadores homogêneos ou heterogêneos. Isso ocorre porque um líquido iônico pode ser selecionado para ser imiscível com os reagentes ou produtos, mas dissolver os catalisadores. Esta vantagem foi utilizada em uma patente de produção de biodiesel, onde os reagentes são miscíveis nos líquidos iônicos de pirazólio ou amônio, mas não no produto biodiesel (Seddon et al., 2009).

2.3.2 Processos biocatalíticos

Nestes tipos de processos, o líquido iônico pode ser utilizado como solvente ou co-solvente em sistemas aquosos ou em sistemas bifásicos. Os primeiros resultados descrevendo os líquidos iônicos como meios de reação enzimática foram apresentados por Erbeldinger et al. (2000) e Lau et al. (2000). Essas pesquisas mostraram que as enzimas são estáveis em líquidos iônicos, abrindo a possibilidade aos líquidos iônicos de serem usados em reações biológicas.

2.3.3 Remoção de íons metálicos

Líquidos iônicos projetados para remover cádmio e mercúrio da água em uma extração líquido-líquido foram apresentados por Visser et al. (2002). Assim, quando este líquido iônico, insolúvel em água, entra em contato com água contaminada, arrebata os íons metálicos seqüestrando-os para um posterior processo de purificação.

2.3.4 Purificação de gases

Os líquidos iônicos podem seletivamente dissolver e remover os gases de uma corrente gasosa. Assim, um gás com valores altos de momento dipolar ou com afinidade química tem maior valor de solubilidade nos líquidos iônicos (Anthony et al., 2005).

2.3.5 Degradação fotolítica de compostos orgânicos em líquidos iônicos

Estudos sugerem que a transformação fotolítica é um dos principais mecanismos que contribuem para a degradação de aromáticos clorados. Assim, a radiação UV direta de compostos hidrofílicos (clorofenóis) ou hidrofóbicos (bifenilos policlorados (PCBs), hidrocarbonetos policíclicos

aromáticos (PAHs)) envolve tanto homólise e heterólise da ligação C-Cl, seguido por uma série de reações subsequentes. Embora a degradação proteolítica de clorofenóis em água tem sido provada ser viável, esta técnica pode não ser rentável, quando a concentração de contaminantes na água é baixa e o volume de água poluída é grande.

Yang e Dionysiou (2004) relatam uma nova aplicação dos líquidos iônicos como meio de solvente para fotodegradação de compostos orgânicos e clorofenóis em dois líquidos iônicos, a um determinado cumprimento de onda UV. Essa tecnologia pode ser usada para eliminar uma variedade de impurezas orgânicas e subprodutos contidos no líquido iônico, desde que esse não seja sensível à radiação.

2.3.6 Projeto de líquidos iônicos para aplicações específicas

A síntese de líquidos iônicos estáveis à umidade ambiente e suas propriedades químicas e físicas únicas permitiram a aplicação generalizada destes materiais, com contribuições significativas da sua utilização como alternativa aos solventes orgânicos tradicionais e como exclusivos meios de reação e de síntese. Na maioria das pesquisas, a característica do líquido iônico que tem sido amplamente explorada é a capacidade de dissolver uma grande variedade de solutos. Adicionalmente, o líquido iônico não é simplesmente uma molécula grande com interações de van der Waals; pelo contrário, eles podem interagir fortemente com as moléculas dissolvidas. Isto foi confirmado por Rogers e colaboradores (Swatloski et al., 2002) ao produzir soluções de celulose a concentrações de uso industrial utilizando líquidos iônicos. Eles observaram que ânions como o cloreto pode ser fundamental para facilitar a dissolução de biomoléculas no líquido iônico, como celulose e outros oligossacarídeos.

Aumentar a capacidade dos líquidos iônicos para interagir com moléculas dissolvidas em formas específicas é o foco de novos projetos de investigação. Líquidos iônicos novos estão sendo sintetizados nos grupos de pesquisa, nos quais um grupo funcional específico é incorporado como parte da estrutura do cátion ou ânion. Estes grupos funcionais podem dar um padrão de reatividade particular ao líquido iônico, reforçando a sua capacidade de interação com tipos específicos de soluto. Por exemplo:

- líquidos iônicos do tipo Brønsted anexando grupos ácidos sulfônicos mostram boas atividades catalíticas para a produção de ésteres (Xing et al., 2005).

- líquidos iônicos contendo grupos amino são eficientes para absorver CO₂ desde fluxos de gases (Bates et al., 2002).
- líquidos iônicos com grupos aromáticos mostraram maior eficiência na extração de aromáticos em sistemas bifásicos aquosos (Yang e Dionysiou, 2004).
- líquidos iônicos contendo grupos de tioeter aprimoram a remoção dos metais Hg²⁺ e Cd²⁺(Visser et al., 2002).

3. MATERIAIS E MÉTODOS

PREFÁCIO

Neste capítulo são apresentados os materiais, aparelhos e os métodos experimentais aplicados para obter os dados experimentais na síntese e caracterização de líquidos iônicos puros e suas misturas. A importância de utilizar líquidos iônicos contendo mínimas quantidades de água encaminha o desenvolvimento de métodos de secagem e manuseio que são explicados no capítulo.

3.1. OBJETIVOS

O estudo é definido pelos seguintes compostos: sais de imidazólio ou de hidroxiamina, solventes hidroxílicos (etanol, metanol, água), ésteres (acetato de metila, acetato de etila, acetato de propila), e aldeídos (propanal, pentanal, e hexanal). Assim, o principal objetivo é a síntese de líquidos iônicos contendo o cátion amônio e os estudos termodinâmicos envolvidos neste trabalho são o equilíbrio líquido-vapor (ELV), o equilíbrio líquido-líquido (ELL) e as propriedades físicas densidade, velocidade do som, viscosidade aparente e índice de refração. Com os resultados, espera-se melhorar a base de dados termodinâmica de compostos puros e misturas binárias contendo líquidos iônicos biodegradáveis e de baixa toxicidade. Este capítulo tem o objetivo de explicar a metodologia experimental para:

- Determinar a densidade, velocidade do som, viscosidade aparente e índice de refração dos líquidos iônicos puros em função da temperatura.
- Determinar o equilíbrio líquido-vapor de misturas binárias contendo líquidos iônicos e aldeídos ou ésteres.
- Determinar o equilíbrio líquido-líquido de misturas ternárias contendo líquido iônico + composto sulfuroso + n-dodecano.

3.2. MATERIAIS

3.2.1. REAGENTES

Todos os produtos químicos utilizados nesta parte do trabalho foram de qualidade Merck ou Sigma-Aldrich, com pureza superior de 99% em massa, exceto a água e alguns líquidos iônicos,

que foram obtidos no nosso laboratório. A água reagente foi obtida pela destilação da água procedente do serviço público e logo purificada usando troca iônica (Figura 3.1). Alguns líquidos iônicos foram sintetizados seguindo os procedimentos descritos mais adiante. Os compostos puros foram armazenados em recipientes de vidro cor âmbar, protegidos da luz solar e umidade a temperatura constante. Os reagentes foram desgaseificados usando ultra-som antes do uso. As densidades das substâncias puras são apresentadas na Tabela 3.1 e comparadas com valores de literatura.

Tabela 3.1. Densidades a 298,15 K.

Componente	MM	ρ (g/cm ³)	
	g/mol	Exp	lit
Propanal	58,08	0,79485	0,7911 ^a
Pentanal	86,134	0,80473	0,8089 ^b
Hexanal	100,161		
Acetato de metila	74,079	0,92682	0,9282 ^c
Acetato de etila	88,106	0,89490	0,8928 ^c
Acetato de propila	102,133	0,88261	0,8823 ^c
Água	18,015	0,997040	0,99705 ^f
Metanol	32,042	0,786710	0,78637 ^f
Etanol	46,069	0,785261	0,78493 ^f
Dibenzotiofeno	184,26	-	-
n-dodecano	170,33	0,74515	0,74532 ^g
m-2-HEAA	135,16	1,10087	1,10083 ^d
m-2-HEAB	163,21	1,03945	1,03924 ^d
m-2-HEAH	191,27	0,99417	-
2-HE ₂ AB	193,24	1,10658	-
N-(2-HE)edAB	280,36	1,07344	-
[emim] ⁺ [EtSO ₄] ⁻	236,29	1,23693	1,23763 ^e
[bmim] ⁺ [MeSO ₄] ⁻	250,32	1,21203	1,21222 ^h

^aRenuncio et al. (1996); ^bTarakad e Scheller (1979); ^cSarkara e Roy. (2009); ^dÁlvarez et al. (2010a); ^eCalvar et al. (2008), ^fRiddick et al., 1998, ^gAlonso et al. (2008), ^hPereiro et al., 2007.



Figura 3.1. Destilador e coluna de troca iônica para purificação da água.

3.2.2. APARELHOS UTILIZADOS

Na determinação do erro na medição nos aparelhos foi utilizada a precisão sendo diferente da resolução do aparelho, medição dada pelo aparelho. A precisão da medição foi calculada pelo método de propagação de erros. Densidades e velocidades de som foram medidas para substâncias puras no intervalo 278,15-323,15 K e, para misturas binárias, no intervalo 288,15-323,15 K, usando densímetros Anton Paar DSA 5000 (Figura 3.2) ou DMA 5000. As misturas binárias foram analisadas em toda a faixa de composição. Os aparelhos utilizam a vibração de um tubo para a medida da densidade, com uma precisão de $\pm 5 \times 10^{-5} \text{ g cm}^{-3}$ e a propagação de uma onda de som através do líquido para a velocidade do som, com uma precisão de $\pm 1 \times 10^{-2} \text{ ms}^{-1}$. Os aparelhos foram calibrados à pressão atmosférica com água bidestilada e ar seco. A temperatura dos densímetros foi mantida com uma precisão de $\pm 1 \times 10^{-2} \text{ K}$. As misturas binárias foram preparadas pela pesagem direta dos elementos constitutivos em uma balança eletrônica, cuja precisão é $\pm 2 \times 10^{-4} \text{ g}$. Foram tomadas precauções para minimizar perdas pela evaporação ou absorção de umidade durante o armazenamento e preparo das soluções.



Figura 3.2. Foto do analizador de densidade e velocidade do som, modelo DSA 5000.

Para as análises do índice de refração foi utilizado um refratômetro Mettler-Toledo modelo RE 40D, mostrado na Figura 3.3. Este aparelho consegue medir valores desde 1,32 até 1,70 no índice de refração, com uma precisão de $\pm 1 \times 10^{-4}$. A medição é baseada na linha D do sódio ($\lambda=589,3$ nm), sendo simbolizada a medição por n_D . O índice de refração foi medido com o refratômetro dentro da caixa de acrílico com atmosfera de nitrogênio seco. O refratômetro foi calibrado com ar e água a 298,15 K sempre no início de cada medição. O aparelho utiliza aproximadamente 0,3 ml de amostra.



Figura 3.3. Foto do Refratômetro Mettler-Toledo, modelo RE 40D.

A viscosidade aparente das amostras de líquido iônico foi analisada por um reômetro Visco Elite L (Fungilab) em diferentes temperaturas, mostrado na Figura 3.4. Os cones utilizados foram o

TL5, TL6 e TL7, e o intervalo da velocidade foi selecionado de acordo com a faixa de torque (mínimo de 10% e máximo de 90%), como sugerido pelas instruções do fabricante. A temperatura foi controlada com o auxílio do banho termostático e medida com um termômetro calibrado.



Figura 3.4. Foto do reômetro Visco Elite, modelo L.

A umidade no líquido iônico foi medida pelo aparelho titulador tipo Karl-Fisher (Mettler-Toledo modelo DL-31), o qual é mostrado na Figura 3.5. Este utiliza CombiTitran 5 e metanol seco fornecido pela Merck.



Figura 3.5. Foto do Titulador de Karl-Fisher, modelo DL31.

Os dados experimentais do equilíbrio líquido-vapor neste estudo foram obtidos a partir do eboliômetro Fischer Labodest com recirculação dinâmica. O instrumento é capaz de manipular pressões de 0,25 kPa até 400 kPa e temperaturas até 523,15K. Uma vista geral da unidade experimental é mostrada na Figura 3.6.

O aparelho é construído em vidro e inclui uma bomba Cottrell para atingir o equilíbrio, manta de aquecimento a vácuo, condensador, evaporador de circulação e tampas com septos para retirar amostras por meio de seringas. O aparelho é montado em uma armação de alumínio provida de portas de policarbonato na frente e no topo, e fechado com painéis de alumínio na parte posterior. Inclui um aquecedor de imersão, agitador magnético, sensores de temperatura PT-100 (para fase líquida e vapor) e controle da temperatura pelo módulo *Phase Equilibrium Controller Fischer Minitron*. As medições de pressão com precisão de $\pm 1,0$ Pa foram feitas com um manômetro em U contendo glicerina como fluido manométrico e a temperatura pode ser determinada com precisão de até $\pm 0,1$ K.



Figura 3.6. Foto do eboliômetro Fisher Labodest, modelo VLE-602.

O equilíbrio líquido-líquido foi realizado em uma célula de equilíbrio, a qual é provida de uma câmara encamisada feita de vidro e coletores laterais para retirada das amostras de ambas as fases. Os coletores são selados com septos que permitem a introdução da seringa sem perdas de massa por vazamento. A Figura 3.7 apresenta um modelo da célula de equilíbrio e a partir da Figura 3.8 observa-se a célula em repouso para separar as fases de uma mistura contendo líquido iônico (fase inferior).

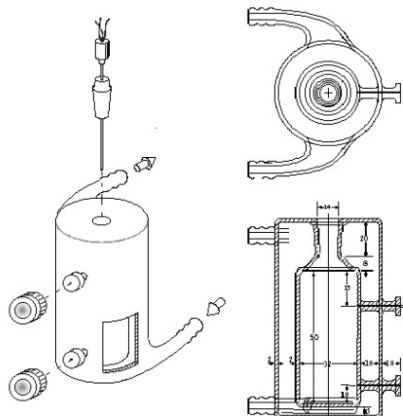


Figura 3.7. Célula de equilíbrio, vista lateral e superior. Unidades em mm. Fonte: Stragevitch, 1997.



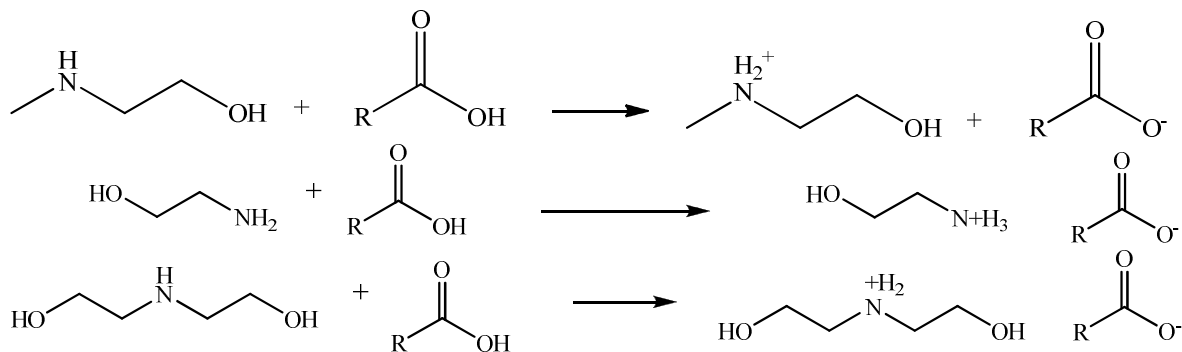
Figura 3.8. Célula em repouso para obter duas fases límpidas.

3.3. SÍNTESE DE LÍQUIDOS IÔNICOS E CARATERIZAÇÃO

3.3.1 SÍNTESE DE LÍQUIDOS IÔNICOS

Os líquidos iônicos contendo o cátion amônio foram sintetizados pelo método de neutralização ácido-base utilizando como reagentes hidroxiamina e ácido orgânico. A amina foi colocada em um balão de três bocas feito inteiramente de vidro, equipado com um condensador de refluxo, um funil e um sensor PT-100 para controlar a temperatura. O balão foi montado em um banho termostático à temperatura de 288,15 K, como observado na Figura 3.9. Essa é a menor temperatura possível, que não permite condensar água no balão. O ácido orgânico foi adicionado gota a gota ao balão sob agitação com uma barra de agitação magnética. A reação é uma

neutralização ácido-base simples (Bicak, 2005), que produz um sal de éster da base utilizada; este processo, de uma forma geral para etanolamina e 2-(metilamino)etanol, pode ser expresso como:



onde R é o grupo alquil presente no ácido orgânico, sendo ácido fórmico (R=H), ácido acético (R=metil), ácido propiônico (R=etil), ácido butanóico (R=n-propil), ácido isobutanoico (R=i-propil), ácido pentanóico (R=n-butil), ácido hexanóico (R=n-pentil) e ácido oléico (R=8-heptadecene).

Estas reações químicas são altamente exotérmicas, de modo que um controle adequado da temperatura é essencial ao longo de toda a reação química. Caso contrário, a evolução da reação a alta temperatura pode produzir a desidratação do sal até a amida correspondente, como no caso de sais de nylon (saís de diaminas com ácidos dicarboxílicos).



Figura 3.9. Foto da montagem utilizada para a síntese dos líquidos iônicos.

A espectroscopia de ressonância magnética nuclear (RMN) foi utilizada para verificar a estrutura dos líquidos iônicos sintetizados.

3.3.2 DESIDRATAÇÃO DE LÍQUIDOS IÔNICOS

Conforme mencionado no Capítulo 2 desta tese, as propriedades físicas dos líquidos iônicos são influenciadas efetivamente pelo teor de água. Assim, para reduzir ao máximo o teor de água e de compostos voláteis, uma metodologia de desidratação dos líquidos iônicos, desenvolvida durante esta tese foi utilizada antes da determinação de dados do equilíbrio de fases.

Metodologia

A umidade contida em um composto exerce uma pressão de vapor que depende da natureza da interação entre as moléculas e da temperatura. Em contato com uma fase gasosa contendo vapor com pressão parcial p , o composto irá perder ou ganhar umidade do ar até que a pressão parcial da umidade no composto seja igual a p .

A água pode estar adsorvida nas paredes das células ou estruturas sólidas, em solução dentro das células ou em pequenos poros dentro do composto. Esta umidade exerce uma pressão de vapor menor que a pressão de vapor da água líquida pura porque tem uma maior interação com o composto. A água também pode estar presente sobre a superfície do composto, ou em grandes cavidades dentro do composto, de modo que sua pressão de vapor seja igual à pressão da água líquida, porque neste caso a água não tem interações moleculares com o composto.

Segundo a literatura, a desidratação de líquidos iônicos é feita em alto vácuo a temperatura ambiente ou levemente superior a esta durante várias horas (Welton, 1999; Carvalho et al. 2009). Nessa metodologia, precisa-se de uma bomba de alto vácuo num sistema turbomolecular capaz de atingir a pressão de 1×10^{-4} Pa. Também precisa-se determinar o armazenamento adequado dos líquidos iônicos.

A cor dos líquidos iônicos sintetizados variou de transparente a amarelo-escuro quando os processos de reação e de purificação (forte agitação e aquecimento a 323,15 K durante 48 h, para vaporizar o ácido orgânico residual) foram concluídos. A temperatura de 323,15 K foi obtida empiricamente. A fim de diminuir ao máximo o teor de água, foram testadas três metodologias de desidratação de 100 g de etilsulfato de 1-etil-3-metilimidazólio $[\text{emim}]^+[\text{EtSO}_4]^-$ utilizando vácuo. Os testes de desidratação utilizaram um recipiente projetado para a evaporação de voláteis sob vácuo (Figura 3.10) com agitação. Os métodos testados foram os seguintes:

1-Desidratação do líquido iônico durante 48 h a 343,15 K à pressão absoluta de 70 Pa.

2-Desidratação do líquido iônico durante 36 horas a 343,15 K à pressão absoluta de 70 Pa, usando um processo em batelada a cada 2 horas. O vácuo é mantido durante 2 horas, logo é fechado e permitido o ingresso de ar durante 15 minutos à pressão ambiente.

3- Desidratação do líquido iônico durante 36 horas a 343,15 K à pressão absoluta de 70 Pa, usando um processo em batelada a cada 2 horas. A pressão é mantida durante 2 horas, logo é fechado e permitido o ingresso de nitrogênio tipo N50 durante 15 minutos à pressão ambiente.

A umidade do líquido iônico foi medida no início da desidratação e em cada início da desidratação do tipo batelada por um titulador potenciométrico de Karl-Fisher modelo DL31 (Mettler-Toledo).

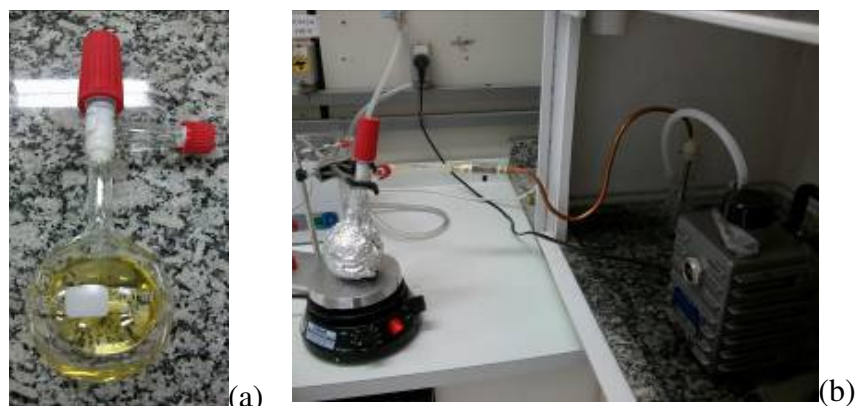


Figura 3.10. Balão (a) e sistema de vácuo (b) projetado para a desidratação e armazenamento do líquido iônico.

3.3.3 MANUSEIO DOS LÍQUIDOS IÔNICOS PUROS E SUAS MISTURAS

Como comentado no item anterior, a desidratação dos líquidos iônicos é necessária pela sua natureza higroscópica. Além disso, a manipulação de tais compostos químicos precisa ser adequada para que se evite capturar água durante a exposição à umidade do ambiente. Assim, os líquidos iônicos devem ser manipulados em uma atmosfera seca.

Metodologia

Uma caixa de acrílico com entrada e saída de linhas de gás foi projetada e construída para o manuseio dos líquidos iônicos em atmosfera seca de nitrogênio (Figura 3.11). Num primeiro momento, uma corrente de nitrogênio foi passada dentro da caixa durante 4 horas, tempo

necessário para atingir uma umidade relativa menor que 10%. O método foi validado com a exposição de sílica-gel dentro e fora da caixa. Dentro da caixa foram expostos 25 cm³ de sílica-gel e 25 cm³ de sílica-gel fora da caixa. A umidade das duas amostras foi comparada visualmente, já que a sílica-gel é um indicador de umidade quando se apresenta na cor rosa.

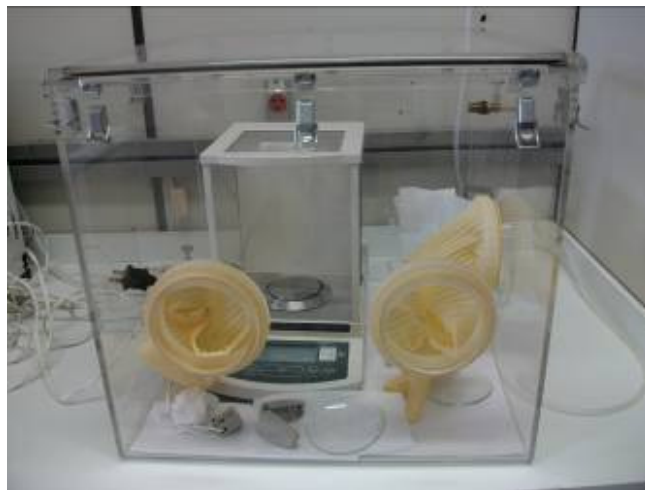


Figura 3.11. Caixa de acrílico para obter uma atmosfera seca.

3.3.4 CARATERIZAÇÃO

3.3.4.1 Ressonância Magnética Nuclear

A espectroscopia de Ressonância Magnética Nuclear representa uma importante técnica para a investigação a nível molecular, sendo capaz de fornecer informações estrutural e dinâmica para qualquer estado da matéria. As propriedades estruturais e físico-químicas dos líquidos iônicos podem ser estudadas com métodos convencionais de RMN líquido (Giernoth et al., 2005). Essas técnicas podem ser úteis na avaliação da composição química e para a análise quantitativa das espécies. Além disso, experimentos de espectroscopia de RMN ordenada por difusão (DOSY, *NMR Diffusion-Ordered SpectroscopY*) podem ser usados para determinar os coeficientes de autodifusão, que estão relacionados ao tamanho molecular e à viscosidade das amostras.

Nesta tese, a espectroscopia de ressonância magnética nuclear (RMN) foi utilizada para verificar a estrutura dos líquidos iônicos sintetizados. Os espectros de ¹H e ¹²C foram os principais a serem analisados. Os experimentos de RMN nos líquidos iônicos foram feitos a 298,15 K para aqueles de baixa viscosidade e a 333,15 K para os de alta viscosidade, com aparência de creme. Os equipamentos utilizados foram o 11.7 T Varian Inova-750 Spectrometer (750 MHz) na Universidade de Santiago de Compostela e o Bruker Avance II (300 MHz) na Universidade

Estadual de Campinas. Os espectros de RMN foram processados com o software Mestre-C (Cobas e Sardina, 2003).

3.3.4.2 Propriedades físicas

Como parte da caracterização dos líquidos iônicos sintetizados, foram estudadas as propriedades físico-químicas em estado puro ou em misturas com aldeídos, ésteres, metanol, etanol e água. Entre as propriedades físico-químicas foram medidas a temperatura de degradação, densidade, velocidade do som, viscosidade aparente e índice de refração.

3.3.4.3 Calorimetria diferencial exploratória

A calorimetria diferencial exploratória (Differential Scanning Calorimetry, DSC) monitora os efeitos do calor associados com as transições de fase e reações químicas em função da temperatura. Nos experimentos no DSC, a diferença no fluxo de calor para a amostra e a referência é baseada numa mesma temperatura, sendo que o fluxo de calor é registrada como função da temperatura. A temperatura da amostra e da referência é aumentada a uma taxa constante. Uma vez que o DSC opera à pressão constante, o fluxo de calor é equivalente às mudanças de entalpia.

$$\left(\frac{dq}{dt} \right)_P = \left(\frac{dH}{dt} \right)_P \quad 3.1$$

Aqui, dH/dt é o fluxo de calor medido em mcal sec⁻¹. A diferença de fluxo de calor entre a amostra e a referência é:

$$\Delta \left(\frac{dH}{dt} \right)_P = \left(\frac{dH}{dt} \right)_{P,amostra} - \left(\frac{dH}{dt} \right)_{P,Blanco} \quad 3.2$$

A variação (Δ) pode ser positiva ou negativa. Em um processo endotérmico, como a maioria das transições de fase, o calor é absorvido, portanto, o fluxo de calor para a amostra é maior do que o de referência. Portanto, $\Delta dH/dt$ é positivo. Exemplos de processos endotérmicos são a desnaturação de proteínas, desidratação, reações de redução, e algumas reações de decomposição. Em um processo exotérmico, como cristalização, reações de oxidação, e algumas reações de decomposição, o $\Delta dH/dt$ é negativo.

O calorímetro é composto por dois suportes, um para a amostra e outro para a referência, como mostrado na Figura 3.12. Ambos são construídos com platina para permitir a operação em alta temperatura. A amostra é selada em um pequeno compartimento de alumínio. A referência é, geralmente, um compartimento vazio e vedado. O compartimento da amostra armazena até aproximadamente 15 mg de material e logo é colocada no suporte. No âmbito de cada suporte tem-se um aquecedor de resistência e um sensor de temperatura. As correntes são aplicadas aos dois aquecedores para aumentar a temperatura na taxa selecionada. A diferença na voltagem dos dois suportes, necessária para manter os suportes na mesma temperatura, é usada para calcular $\Delta dH / dt$. Um diagrama esquemático de um DSC é mostrado na Figura 3.12. Um fluxo de gás nitrogênio ultra puro é mantido sobre as amostras para gerar uma atmosfera reproduzível e seca. A atmosfera de nitrogênio também elimina a oxidação em ar das amostras para altas temperaturas.

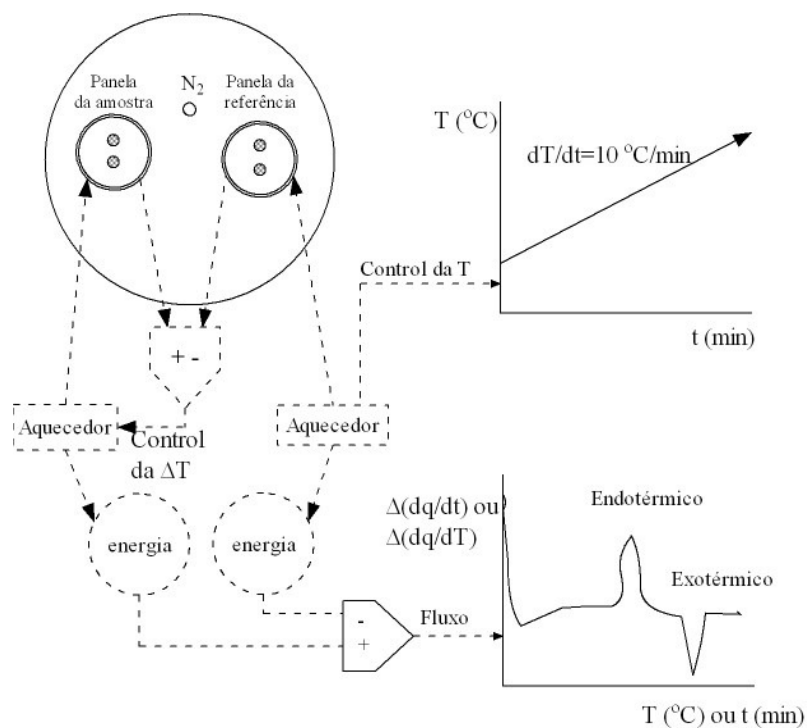


Figura 3.12. Esquema de um DSC.

A amostra foi pesada em um compartimento de alumínio para ter uma massa entre 9 e 15 mg. Foi usada uma balança analítica com uma precisão de $\pm 0,02$ mg, Mettler-Toledo, modelo XP26. Um recipiente vazio e sua tampa foram mantidos como referência durante a experiência. Assim, pode-se obter o termograma na faixa de temperatura 20-550 °C, com uma taxa de $10 \text{ } ^\circ\text{C min}^{-1}$.

3.3.4.4 Propriedades volumétricas

A fim de explorar a força e a natureza das interações entre as espécies do líquido iônico foi calculado o raio molecular, r (Iloukhani e Rostami, 2007), a partir de dados de velocidade do som e densidade.

$$b = \frac{M}{\rho} - \left(\frac{RT}{\rho \cdot u^2} \right) \cdot \left(\left[1 + \frac{M \cdot u^2}{3RT} \right]^{1/2} - 1 \right) \quad 3.3$$

$$r = \left(\frac{3b}{16\pi N_A} \right)^{1/3} \quad 3.4$$

Onde M é a massa molecular, N_A é o numero de Avogadro, R e π são constantes universais.

Os íons do líquido iônico foram considerados como sendo de formato esférico. Portanto, o raio efetivo dessas moléculas pode ser calculado utilizando a equação de Stokes-Einstein. Nessa fórmula, para o cálculo da difusividade browniana a difusividade varia diretamente com a temperatura absoluta e inversamente com a viscosidade e o raio molecular.

$$D = \frac{kT}{r6\pi\eta} \quad 3.5$$

onde D é a difusividade browniana ($\text{m}^2 \text{ s}^{-1}$), k é a constante de Boltzmann (J K^{-1}), T é a temperatura absoluta (K), π é 3,14159, η é a viscosidade do meio (Pa s) e r é o raio da molécula.

A difusividade foi obtida por experiências tipo DOSY nas técnicas de ressonância magnética nuclear. A comparação dos raios moleculares obtidos pelas equações de Stokes-Einstein e termoacústica permite inferir a estrutura mais adequada do líquido iônico.

A fim de explorar a força e a natureza das interações entre os compostos, foi determinado o comprimento livre entre as superfícies das moléculas (Jacobson, 1952), L_f , que pode ser obtido por

$$L_f = 2V_a / Y \quad 3.6$$

onde Y é a área superficial molar e V_a é o volume molar disponível, calculado por

$$Y = (36\pi N V_o^2)^{1/3} \quad 3.7$$

$$V_a = V - V_0 \quad 3.8$$

$$V_0 = V(1 - T/T_c)^{0.3} \quad 3.9$$

Onde V_o é o volume molar à temperatura absoluta zero, V é o volume molar a temperatura T , e T_c é a temperatura crítica. Para os compostos com valores desconhecidos das propriedades críticas experimentais, como no caso dos líquidos iônicos, o método de Pandey et al. 2002 pode ser aplicado para calcular o volume molar disponível.

3.4. SOLUÇÕES CONTENDO LÍQUIDOS IÔNICOS

3.4.1. PROPRIEDADES FÍSICO-QUÍMICAS

A densidade e a velocidade do som para as misturas foram correlacionadas por meio da seguinte equação:

$$Z = \sum_{i=0}^p \left(\left(\sum_{j=0}^q B_{ij} T^j \right) x_1^{i-1} \right) \quad 3.10$$

onde Z é a densidade ou a velocidade do som da mistura, x_1 é a fração molar do solvente, p e q são os graus do polinômio usado, B_{ij} são os parâmetros ajustáveis do modelo, e T é a temperatura absoluta.

O volume molar em excesso (V^E) e as variações na compressibilidade isentrópica ($\delta\kappa_S$) foram calculados pelas seguintes equações:

$$V^E = \sum_{i=1}^N x_i M_i \left(\frac{1}{\rho} - \frac{1}{\rho_i} \right) \quad 3.11$$

$$\delta\kappa_S = \kappa_S - \sum_{i=1}^N x_i \kappa_{Si} \quad 3.12$$

onde N é o número de compostos na solução, x_i é a fração molar; M_i é a massa molar; ρ_i é a densidade do composto puro i , ρ é a densidade da solução, κ_S é a compressibilidade isentrópica

da solução, κ_{Si} é a compressibilidade isentrópica do componente puro i calculada com a equação de Newton-Laplace:

$$\kappa_s = \frac{1}{\rho u^2} \quad 3.13$$

Onde ρ é a densidade da solução e u é a velocidade do som na solução.

As propriedades derivadas foram ajustadas pela equação de Redlich-Kister:

$$Q_{12} = x_1 x_2 - \sum_{i=0}^p \left(\left(\sum_{j=0}^q B_{ij} T^j \right) (x_1 - x_2)^i \right) \quad 3.14$$

onde Q_{12} é o V^E ou $\delta\kappa_s$ e as outras variáveis são as anteriormente citadas. O volume molar aparente (ϕ_V) e a compressibilidade isentrópica molar aparente (ϕ_{κ_s} , $\text{cm}^3 \text{ mol}^{-1} (\text{TPa})^{-1}$) para o líquido iônico foram calculados segundo:

$$\phi_V = 1000 \left(\frac{\rho_1 - \rho}{m \rho_1 \rho} \right) + \frac{M_2}{\rho_1} \quad 3.15$$

$$\phi_{\kappa_s} = 1000 \left(\frac{\kappa_s - \kappa_{S1}}{m \rho} \right) + \kappa_s \phi_V \quad 3.16$$

onde ρ é a densidade da solução, ρ_1 é a densidade do solvente, M_2 é a massa molar do líquido iônico, m é a molalidade da solução, κ_s é a compressibilidade isentrópica da solução e κ_{S1} é compressibilidade isentrópica do solvente. Essas propriedades derivadas foram correlacionadas pela equação modificada de Redlich-Mayer, onde os parâmetros ajustáveis são dependentes da temperatura:

$$\phi_F = \left(\sum_{j=0}^q \phi_{Fi}^o T^j \right) + \sum_{i=0}^p \left(\left(\sum_{j=0}^q \phi_i^F T^j \right) m^{A_i} \right) \quad 3.17$$

onde F representa qualquer propriedade molar aparente e ϕ_{Fi}^o e ϕ_i^F são parâmetros ajustáveis.

O coeficiente de expansão térmica (α_p) mostra a dependência do volume com a temperatura, e está definida como:

$$\alpha_P = \frac{1}{V} \left(\frac{\partial V}{\partial T} \right)_P = - \left(\frac{\partial \ln \rho}{\partial T} \right)_P \quad 3.18$$

3.4.2. EQUILÍBRIO DE FASES

Antes de iniciar os experimentos para determinar o equilíbrio líquido-vapor é necessário desenvolver e validar a metodologia para obter os dados experimentais no ebuliômetro. Primeiramente, a metodologia foi baseada no livro de Hala et al. (1967) e a experiência adquirida no ebuliômetro tipo Othmer na estadia na Universidade Federal de Bahia (Álvarez et al., 2010b). Neste item do trabalho foram feitas pesquisas em ebuliômetros baseados no método de recirculação dinâmica, um tipo Othmer e principalmente no tipo Fisher. Estes tipos de ebuliômetros, como é o caso do Fisher Labodest, não são úteis para sistemas de limitada miscibilidade na fase líquida (Gomis et al., 2000). Além disso, a presença de sistemas de miscibilidade parcial levaria ao fenômeno do equilíbrio trifásico líquido-líquido-vapor.

Neste trabalho, relatamos os dados de ELV a 101,3 kPa, para oito soluções binárias com aldeídos (propanal, pentanal), éster (acetato de metila, acetato de etila, acetato de propila) e etanol. Os aldeídos e ésteres são de alta polaridade e solventes com ponto de ebulação moderado usados em uma variedade de aplicações de engenharia. Os líquidos iônicos utilizados foram baseados no cátion imidazólio e amônio. Dados para estes sistemas contendo um líquido iônico não estão disponíveis na literatura.

Os dados foram modelados termodinamicamente por duas maneiras diferentes, correlação e predição, utilizando a equação de estado de Peng-Robinson (Peng e Robinson, 1976) e a regra de mistura de Wong-Sandler (Wong e Sandler, 1992). Na correlação (Álvarez e Aznar, 2008b), foram usados os modelos de energia livre de Gibbs em excesso de NRTL (Renon e Prausnitz, 1968) e UNIQUAC (Abrams e Prausnitz, 1975) e, na predição, foi usado o modelo COSMO-SAC (Lin e Sandler, 2002).

3.4.2.1. Equilíbrio líquido-vapor a baixas pressões

a) Validação do Procedimento Experimental

Os líquidos iônicos são solventes higroscópicos e apresentam viscosidade e tensão superficial maiores que os solventes comuns (Welton, 1999). Por estes motivos, uma nova metodologia

experimental foi desenvolvida e validada para a determinação da curva de calibração e dos dados do equilíbrio líquido-vapor. O sistema binário etanol + etilsulfato de 1-etil-3-metilimidazólio foi selecionado para ser reproduzido (Calvar et al., 2008).

b) Metodologia

Como primeira etapa, foram preparadas soluções binárias de 12 ml, cobrindo todo o intervalo de composições, do sistema etanol + etilsulfato de 1-etil-3-metilimidazólio. As soluções foram preparadas dentro da caixa de acrílico descrita na seção 2.4.4, sob atmosfera seca de nitrogênio. Foram feitas medições do índice de refração (refratômetro Mettler-Toledo D41) destas soluções, podendo-se construir curvas de calibração relacionando a composição molar e o índice de refração da solução.

Logo, foram determinados os dados do equilíbrio líquido-vapor no ebuliômetro Fischer Labodest. Começa-se o procedimento com solvente puro, seguido da adição sucessiva de quantidades conhecidas de líquido iônico para cada ponto experimental, a fim de cobrir o maior intervalo de composições. Em cada experimento, ao atingir o equilíbrio, foram retiradas amostras das fases de vapor e líquido e logo determinada a composição pelas curvas de calibração.

c) Procedimento experimental no ebuliômetro

- 1 O banho termostático é ligado para manter 283,15 K nos condensadores do ebuliômetro por 30 minutos antes de colocar a amostra.
- 2 No ebuliômetro são colocados aproximadamente 110 ml de solvente puro. Esse volume pode variar de 90 ml até 110 ml, para permitir recirculação da fase líquida, ao ser aquecida a amostra.
- 3 Fecha-se todas as válvulas e adiciona-se nitrogênio até atingir o deslocamento adequado no manômetro para obter 101,3 kPa de pressão.
- 4 Inicia-se a agitação do líquido, aos $\frac{3}{4}$ da máxima velocidade que agita a solução. Logo, o aquecimento é aumentado lentamente a cada 10 min até observar ebullição do solvente puro. O líquido e vapor deve fluir através da bomba Cottrell, para garantir uma troca intensa de

material das fases. A fase vapor é condensada e ambas as fases são recirculadas ao recipiente original.

- 5 Manter constante a taxa de gotejamento do vapor condensado, em duas gotas por segundo durante todo o experimento, através do aumento ou diminuição do calor fornecido.
- 6 A recirculação da fase líquida pode ser observada como gotejamento mais intenso que a fase vapor com finos fios líquidos. No caso de não ser observada a recirculação da fase líquida, aumentar o volume da amostra até obter recirculação. No caso de observar a recirculação de quantidades grandes de líquido, retirar líquido até observar gotejamento na recirculação.
- 7 As condições do equilíbrio podem ser supostas quando a vazão de recirculação das duas fases, a temperatura e a pressão permanecem constantes durante 30 minutos. Essas condições podem ser atingidas ao manter a pressão do sistema e a taxa de gotejamento do vapor condensado constantes durante 30 minutos. Logo, são retiradas amostras da fase vapor e líquida.
- 8 As amostras foram retiradas utilizando seringas diretamente do líquido de ambas as fases, uma para a fase vapor condensado e uma para a fase líquida.
- 9 Logo é retirado 1 ml do líquido contido no eboliômetro e adiciona-se 1,5 ml de líquido iônico purificado utilizando seringas. Repetir os passos 3 a 9, até obter uma solução, na qual não é possível estabilizar a temperatura. Recomenda-se fazer os experimentos de maneira ininterrupta, em toda a faixa de composições, parar evitar reiniciar o eboliômetro com a amostra estagnada, que origina superaquecimento na mistura.

Durante a obtenção dos dados, no intervalo de baixa concentração do solvente volátil, a temperatura é alta e torna-se instável, e o líquido iônico poderia se decompor. Assim, as experiências do ELV foram realizadas enquanto a temperatura de equilíbrio manteve-se estável (Calvar et al., 2008).

A determinação das composições das duas fases em equilíbrio foi feita por refratometria, utilizando um refratômetro digital e a curva de calibração adequada para cada sistema binário. Não foi utilizado densimetria por duas razões: pouca quantidade de amostra (<0,5 ml) é retirada do eboliômetro e amostras viscosas contém muitas bolhas que atrapalham a correta medição.

d) Síntese e purificação dos líquidos iônicos

Dos líquidos iônicos inicialmente propostos no projeto de doutorado, só um deles foi solúvel nos aldeídos e nenhum deles foi solúvel nos ésteres. A motivação principal para esta etapa foi a necessidade de se obter misturas binárias totalmente solúveis nos ésteres e aldeídos propostos no projeto. De acordo com a experiência adquirida no estágio na Universidad de Santiago de Compostela, decidiu-se pela síntese, purificação e caracterização de líquidos iônicos próticos. Essa família de líquidos iônicos foi escolhida por ser pouco estudada na literatura. Inicialmente, foram sintetizados quatro líquidos iônicos para testes de solubilidade com os aldeídos e ésteres, acetato de 2-hidroxietilamônio (2-HEAA), acetato de N-metil-2-hidroxietilamônio (m-2-HEAA), propionato de N-metil-2-hidroxietilamônio (m-2-HEAPr) e butirato de N-metil-2-hidroxietilamônio (m-2-HEAB). Destes líquidos iônicos, apenas o último, m-2-HEAB, apresentou solubilidade com o acetato de metila e acetato de etila. Por isso, após uma análise da estrutura molecular dos líquidos iônicos obtidos, optou-se por sintetizar, purificar e caracterizar um quinto líquido iônico que fosse solúvel nos ésteres, o hexanoato de N-metil-2-hidroxietilamônio (m-2-HEAH), o qual foi solúvel a temperatura ambiente nos três ésteres estudados, mas não nos aldeídos. A metodologia da síntese, purificação e caracterização dos cinco líquidos iônicos é apresentada na seção 2.4.2.

e) Testes de solubilidade

O objetivo desta etapa foi determinar os sistemas completamente miscíveis (soluções) para a posterior determinação dos dados do equilíbrio líquido-vapor.

Foram preparadas misturas binárias de líquidos iônicos e solventes, sendo as massas iguais a 3 g de cada composto. As misturas foram preparadas em frascos de 12 cm³, agitadas com um agitador magnético durante 2 horas e mantidas em repouso durante 6 horas a 298,15 K e 323,15 K. Logo a solubilidade das misturas é constatada por inspeção visual. As misturas completamente miscíveis apresentam uma única fase límpida.

f) ELV dos sistemas binários aldeído ou éster + líquido iônico

O objetivo desta etapa foi determinar o equilíbrio líquido-vapor das soluções binárias totalmente solúveis. A saber, sistemas binários aldeído (propanal ou pentanal) + etilsulfato de 1-etil-3-metilimidazólio, éster (acetato de metila, acetato de etila ou acetato de propila) + butirato de N-

metil-2-hidroxietilamônio, e éster (acetato de metila, acetato de etila ou acetato de propila) + hexanoato de N-metil-2-hidroxietilamônio, à pressão de 101,3 kPa.

Propanal, pentanal, acetato de metila, acetato de etila, acetato de propila e etilsulfato de 1-etil-3-metilimidazólio foram adquiridos da Sigma-Aldrich. Os líquidos iônicos m-2-HEAB e m-2-HEAH foram sintetizados dentro deste trabalho, como descrito anteriormente. A pureza dos aldeídos e ésteres foi informada pelo fabricante como 99,5% (em massa) e foi verificada com a medição da densidade. Estes compostos foram utilizados sem maior purificação. A pureza do líquido iônico $[emim]^+[EtSO_4]^-$ foi de 95% (em massa); a pureza do m-2-HEAB e m-2-HEAH foram maior que 97% (em massa) segundo dados de RMN. A única purificação feita nos líquidos iônicos foi a desidratação. Os líquidos iônicos foram desidratados a pressão absoluta de 70 Pa durante 40 horas com armazenagem de nitrogênio, antes de cada uso, como descrito nas seções anteriores. Os dados experimentais foram modelados com a EdE de Peng-Robinson e a regra de mistura de Wong-Sandler.

3.4.2.2. Equilíbrio líquido-vapor a altas pressões

A parte experimental do ELV a altas pressões foi feita pelo grupo do professor Dr. João Coutinho. As experiências foram feitas numa célula de equilíbrio de alta pressão desenvolvida com base na concepção de Daridon e colaboradores (Vitu et al., 2008), que consiste de um cilindro horizontal oco de aço inox, fechado em uma extremidade por um pistão móvel e na outra extremidade por uma janela de safira. O procedimento experimental utiliza o método sintético.

3.4.2.3. Equilíbrio líquido-líquido

A determinação do equilíbrio líquido-líquido utiliza a metodologia experimental baseada na determinação dos pontos de névoa e linhas de amarração, como apresentado por Oliveira et al. (2010). Esta metodologia de obtenção dos pontos de névoa é uma aplicação clássica na determinação do equilíbrio líquido-líquido (Maduro, 2009). No sistema ternário, é feito um mapeamento da região bifásica, limitada pela curva binodal. A curva é obtida pela titulação de uma solução binária com o terceiro componente do sistema, até o surgimento da segunda fase, observado na turbidez permanente da mistura. Inicia-se com uma composição conhecida da solução binária, inserida na célula de equilíbrio, onde a temperatura é mantida constante. As massas são pesadas dentro da própria célula e a solução binária é colocada sob agitação. O

terceiro componente é adicionado gota a gota por meio de uma seringa à solução binária, até que o sistema ternário se torne levemente turvo e permaneça assim durante mais de 30 min., isto é o ponto de névoa. Então, mede-se a massa do terceiro componente que foi adicionada e calcula-se a composição da mistura ternária obtida. Coleta-se uma amostra desta mistura no ponto de névoa e mede-se a(s) propriedade(s) de interesse. Com a determinação de vários destes pontos pode-se determinar uma curva de calibração, que relaciona a variação da propriedade física medida com a composição do sistema na curva binodal.

Em seguida, para determinar as linhas de amarração, são escolhidos pontos aleatórios dentro da região bifásica delimitada pela curva binodal, determinada com o método anteriormente descrito. A vantagem de conhecer a região bifásica é que se pode estimar, pela regra da alavanca, um ponto da mistura que, após a separação, se dividirá em duas fases de quantidades similares. A massa de cada componente é medida diretamente no interior da célula de equilíbrio. À continuação, cada sistema líquido é agitado com um agitador magnético por 12 horas. Após a agitação, o sistema é deixado em repouso por 24 horas, tempo suficiente para uma separação em duas fases límpidas, ocorrendo o equilíbrio líquido-líquido.

A amostragem de cada fase é feita com seringas e agulhas a temperatura ambiente. Foram retiradas três alíquotas de cada fase para obter um valor médio das propriedades físicas necessárias na curva de calibração. Os experimentos foram conduzidos a pressão atmosférica de Campinas, o qual tem o valor médio de 95 kPa (CEPAGRI, 2010).

A composição das fases obtidas é determinada pela curva de calibração, que relaciona uma ou duas propriedades físicas com a composição. Nos sistemas ternários utilizam-se duas curvas de calibração (duas propriedades) para resolver um sistema de duas incógnitas e determinar a composição. Entretanto, as composições dos componentes do sistema ternário podem ser função de uma única propriedade física (Letcher e Siswana, 1992; Briggs e Cummings, 1943; Oliveira et al., 2010). Esta metodologia permite utilizar a composição dos pontos de névoa como a curva de calibração, já que os pontos de névoa coincidem com os extremos das linhas de amarração. Este método, já validado, foi utilizado no projeto. A propriedade a utilizar foi o índice de refração.

3.5. ALGUMAS APLICAÇÕES DOS LÍQUIDOS IÔNICOS

3.5.1 SEPARAÇÃO DO AZEÓTROPO ETANOL + ÁGUA.

Normalmente, para produzir etanol anidro por destilação extrativa, o agente líquido para a separação (o entrainer) é o benzeno. Esta operação é energeticamente favorável, mas tem condições de saúde perigosas e controle operacional instável. Outros agentes líquidos utilizados na destilação extrativa, tais como furfural, pentano, éter etílico, etileno glicol e tolueno, foram limitados pela legislação ambiental (Ligero e Ravagnani, 2003).

Outra variante da destilação extrativa é a utilização de um entrainer salino (sal não volátil), como o cloreto de cálcio e acetato de potássio, que é introduzido no platô superior da coluna de destilação, desce através das placas e é removida nos produtos de fundo.

Recentemente, a investigação crescente se dirige para avaliar e aplicar líquidos iônicos como agentes de separação. Assim, o líquido iônico pode ser utilizado como um entrainer adequado no processo de destilação extrativa, e pode ser superior ao entrainer comumente usado devido à sua baixa volatilidade e baixa corrosividade.

Metodologia

No primeiro trabalho, o processo de destilação extrativa foi simulado e otimizado com o software HYSYS ®. O equilíbrio líquido-vapor para o sistema foi calculado pelo modelo termodinâmico NRTL, cujos parâmetros de interação foram obtidos da literatura. O planejamento experimental foi utilizado em combinação com a modelagem e a simulação para determinar as condições operacionais que minimizem o gasto energético no revedor. Os resultados das simulações mostraram que ambos, os agentes de separação apresentam similar gasto energético para produzir etanol de alta pureza, mas o líquido iônico permite produzir etanol sem contaminantes.

No segundo trabalho, os dados de ELV foram medidos usando um ebuliômetro de equilíbrio líquido-vapor tipo Othmer, com recirculação em ambas as fases (Ocón e Espantoso, 1958, Resa et al., 2004). A Figura 3.13 mostra o ebuliômetro modificado de Othmer. Um termômetro modelo Yokogawa 7563 e um sensor de platina Pt100 foram usados para medir a temperatura da célula, com uma incerteza de $\pm 0,07$ K. Os dados obtidos pelo termômetro e o sensor foram padronizados pelo Laboratório de Metrologia da Universidade Federal da Bahia, certificada pelo Instituto

Nacional de Metrologia, Normalização e Qualidade Industrial (INMETRO). Para a medição de pressão foi utilizado um manômetro diferencial de tubo em U contendo glicerol, com uma precisão de $\pm 0,01$ kPa. O nitrogênio foi injetado no eboliômetro para manter uma pressão constante de 101,32 kPa, de acordo com a pressão local do laboratório. A pressão local foi calculada pela diferença de altitude com a estação meteorológica localizada no Aeroporto Internacional de Salvador. O volume total do eboliômetro é aproximadamente de 720 cm³, dos quais aproximadamente 360 cm³ foram ocupados pela solução líquida. O eboliômetro foi aquecido através de uma bobina de resistência controlada por um transformador de tensão Variac. Durante a operação, uma solução líquida foi colocada na câmara de ebulação e logo foi aquecida. A mistura de vapor e líquido contida na câmara de ebulação é levada até a câmara de equilíbrio, onde o vapor e as fases líquidas são separados após fluir diretamente ao longo da haste do termômetro. O vapor é condensado no condensador e retorna até a câmara de mistura. O equilíbrio foi atingido normalmente em aproximadamente 30-60 minutos, conforme indicado pela temperatura constante do ponto de ebulação. O sistema foi mantido em equilíbrio por aproximadamente 1 h, e em seguida, amostras de vapor e líquido foram retiradas.



Figura 3.13. Foto do Eboliômetro tipo Othmer.

3.5.2 ABSORÇÃO DE CO₂ EM UM FLUXO DE GÁS.

O potencial dos líquidos iônicos para aplicação industrial na captura de CO₂ e processos de separação de gás é amplamente reconhecida. Esta seção estuda a solubilidade a altas pressões e a

absorção a baixas pressões de CO₂ em líquidos iônicos. Dentro do grupo enorme de líquidos iônicos existentes, aqueles baseados em bases conjugadas de ácidos carboxílicos parecem ser particularmente promissores.

As operações industriais onde um ou mais componentes de uma fase gasosa são absorvidos em uma fase líquida são comuns nas indústrias de processo químico. Em muitos casos, esse contato é útil para alcançar as reações desejadas entre os componentes de ambas as fases. Reatores de borbulhamento têm um amplo leque de aplicações em química, bioquímica e farmacêutica (Lee e Tsui, 1999), devido ao contato efetivo que tem o gás com a fase líquida, para realizar as reações químicas. A transferência de massa do gás em um líquido é geralmente a velocidade limitante. Nesses processos, a maioria dos compostos utilizados na fase líquida são fluidos não-newtonianos. Sabe-se que o coeficiente volumétrico de transferência de massa k_{La} , é um dos parâmetros mais importantes que regem o desempenho dos reatores gás-líquido.

Metodologia

No primeiro trabalho, o ELV a altas pressões foi determinado para uma mistura binária de CO₂ supercrítico + LI prótico, e logo para a mistura ternária CO₂ supercrítico + CH₄ supercrítico + m-2-HEAA. A metodologia experimental foi implementada pelo grupo do Prof. Coutinho.

No segundo trabalho, uma investigação experimental é realizada para avaliar a capacidade de dois líquidos iônicos, formato de 2-hidroxietilamônio (2-HEAF) e formato de N-metil-2-hidroxietilamônio (m-2-HEAF), para a absorção de CO₂. Os estudos de absorção foram realizados em uma coluna semi-contínua de gás-líquido. Os valores dos k_{La} são obtidos para várias velocidades do fluxo gás e diferentes temperaturas.

O conjunto de aparelhos utilizado para a absorção de CO₂ em líquidos iônicos é mostrado na Figura 3.14, e consiste principalmente de um tubo de vidro rodeada de mangueiras de silicones para manter a temperatura desejada utilizando um fluxo de água. A temperatura da água foi controlada por meio de um banho termostático com uma exatidão na temperatura de $\pm 0,1$ K. Um sensor PT100 (Senso term II, J.P. Selecta) com uma exatidão de $\pm 0,1$ K foi utilizado para medir a temperatura do sistema. O gás CO₂ foi introduzido através de 95 ml de líquido iônico carregado no tubo de vidro. Existem chaves para a alimentação e saída de CO₂. A velocidade do fluxo de gás que ingressa foi medida com um aparelho Control Electronics 0154 (Brooks Instruments), o

qual tem uma precisão de $\pm 0,01$ ml CO₂/min. A velocidade do fluxo do gás de saída foi medida com um aparelho ADM 2000 (Agilent), o qual tem uma precisão de $\pm 0,1$ ml CO₂/min. A concentração de CO₂ absorvido nos líquidos iônicos foi determinada para 288,2 K, 298,2 e 308,2 K à pressão ambiente (≈ 100 kPa), e duas velocidades de fluxo (149 e 199 ml/min).



Figura 3.14. Foto dos aparelhos utilizados para medir a absorção de CO₂ nos líquidos iônicos.

Cada experimento foi feito em triplicata com um desvio padrão de $\pm 1,5$ ml/min na velocidade de fluxo do CO₂. A absorção atingiu um quase equilíbrio (valores quase constantes do fluxo de saída de CO₂) e depois de varias horas nesse equilíbrio, o experimento foi finalizado. O efeito da água nos líquidos iônicos também foi estudado e foram feitos três ciclos de absorção e desorção para estudar a perda da habilidade de absorção de CO₂ nos líquidos iônicos.

A quantidade de gás absorvido pode ser determinada com a medida da taxa de gás que ingressa e sai no sistema para um fluxo de gás puro. Se for conhecida a vazão do gás, em sistemas de baixa pressão, pode-se aproximar o fluxo mássico por:

$$F = \frac{P_{gas} V_{gas}}{RT} \quad 3.19$$

onde F é o fluxo mássico em mol/min, P é a pressão do gás, V_{gas} é a vazão do gás em ml/min, T é a temperatura absoluta e R a constante geral dos gases. Assim, a diferença entre o fluxo mássico

que ingressa e o fluxo mássico que sai do reator origina o fluxo mássico absorvido no sistema (ΔF). Assim, em um intervalo de tempo t , a quantidade de gás absorvido é:

$$gás \text{ absorvido} = \int_0^t \Delta F(t) dt \quad 3.20$$

O procedimento para determinar o coeficiente volumétrico de transferência de massa é baseado na medição da quantidade de gás absorvida por unidade de tempo e unidade de volume de acordo com a seguinte equação (Vázquez et al., 1997):

$$\frac{dC}{dt} = k_L a(C^* - C) \quad 3.21$$

onde C^* é a concentração interfacial do composto gás na fase líquida no equilíbrio (ou seja, a solubilidade do gás na fase líquida) e C é a concentração de dióxido de carbono no líquido, que é calculado a partir dos dados experimentais de taxa de absorção,

$$\ln\left(\frac{C^*}{C^* - C}\right) = k_L at \quad 3.22$$

Integrando a Equação 3.21, a Equação 3.22 foi obtida. Então, plotando $\ln [C^* / (C^* - C)]$ contra o tempo e ajustando aos dados uma linha reta que passa pela origem, e o coeficiente angular é k_{La} sendo independente do tempo nas condições deste trabalho. A concentração de dióxido de carbono na maior parte do líquido aumenta com o tempo até a fase líquida ficar quase saturada.

3.5.3 DESSULFURIZAÇÃO DO PETRÓLEO

Na indústria do petróleo, combustíveis com baixo teor de enxofre costumam ser obtidos através do processo de hidrodesulfurização (HDS), que consiste em uma hidrogenação catalítica a altas temperaturas e pressões. Embora o processo HDS tenha-se mostrado efetivo na remoção do enxofre na forma de sulfurosos alifáticos, a sua eficiência encontra-se limitada pelas cada vez mais severas condições operacionais e o alto custo energético envolvido (Alonso et al., 2008).

Os estudos que tratam da remoção do enxofre no óleo diesel envolvem a contaminação de alcanos (óleo diesel modelo) com um composto sulfuroso e a remoção deste com alguma técnica. Em alguns casos é utilizado óleo diesel real, contaminado com enxofre, onde as técnicas

utilizadas apresentam resultados menos eficientes na remoção do composto sulfuroso (Gao et al., 2009). Os estudos mais interessantes na literatura mostram a dessulfurização de um óleo modelo contaminado com compostos aromáticos sulfurosos refratários ao processo HDS (Egorova e Prins, 2004), como o dibenzotifeno (DBT), 4-metildibenzotifeno (4-MDBT) e o 4,6-dimetildibenzotifeno (4,6-DMDBT) (Oliveira, 2009).

Assim, a extração líquida do enxofre de um combustível é um processo onde o soluto (composto sulfuroso) tem preferência pelo solvente em relação ao diluente (combustível). Na literatura existem alguns trabalhos sobre a extração de compostos sulfurosos do óleo diesel (geralmente um óleo modelo) com líquidos iônicos, geralmente a condições de operação mais brandas do que HDS (Francisco et al., 2010). Assim, estes estudos mostram que esta alternativa pode ser viável como complemento à HDS num processo de dessulfurização profunda.

Este trabalho sintetizou líquidos iônicos próticos biodegradáveis e visando à máxima dessulfurização do óleo diesel modelo, foram testados três líquidos iônicos. Os dados de remoção de DBT foram confirmados por experimentos de equilíbrio líquido-líquido no sistema ternário líquido iônico + aromático sulfuroso (DBT) + óleo diesel modelo (n-dodecano).

Metodologia

O n-dodecano foi utilizado como óleo diesel modelo, o dibenzotifeno foi empregado como aromático sulfuroso e líquidos iônicos próticos foram usados como solventes.

Os experimentos foram feitos em células de equilíbrio líquido-líquido (Figura 3.15), como é sugerido por Sandler (2006). A temperatura das células foi mantida por um banho termostático Tecnal TE-184 com uma precisão de $\pm 0,1^{\circ}\text{C}$.

O método do ponto de névoa de Letcher e Siswana (1992) foi utilizado para determinar a curva binodal na fase rica em líquido iônico, e por gotejamento de n-dodecano a uma solução binária de concentração conhecida de DBT + m-2-HEAB até obter turbidez perene no tempo. Logo, o índice de refração (n_D) da fase iônica foi medido em triplicata com um refratômetro digital Mettler-Toledo RE 40D, para determinar as curvas de calibração concentração-índice de refração. O índice de refração da solução binária n-dodecano + DBT foi obtida de Oliveira (2009).

Nas experiências de equilíbrio de fases, misturas ternárias de composição conhecida dentro do intervalo de imiscibilidade foram preparadas pesando os componentes dentro da célula de equilíbrio. A massa adicionada foi medida com uma balança analítica Shimadzu AX200, que tem uma precisão de $\pm 1 \times 10^{-4}$ g. As misturas foram agitadas com um agitador magnético Fisatom 752 durante 12 horas, para permitir o contato entre as fases. Depois de 24 horas em repouso são formadas duas fases límpidas em equilíbrio. Cada fase formada foi analisada por meio do índice de refração; a média das triplicatas foi usada para calcular a composição de cada fase.

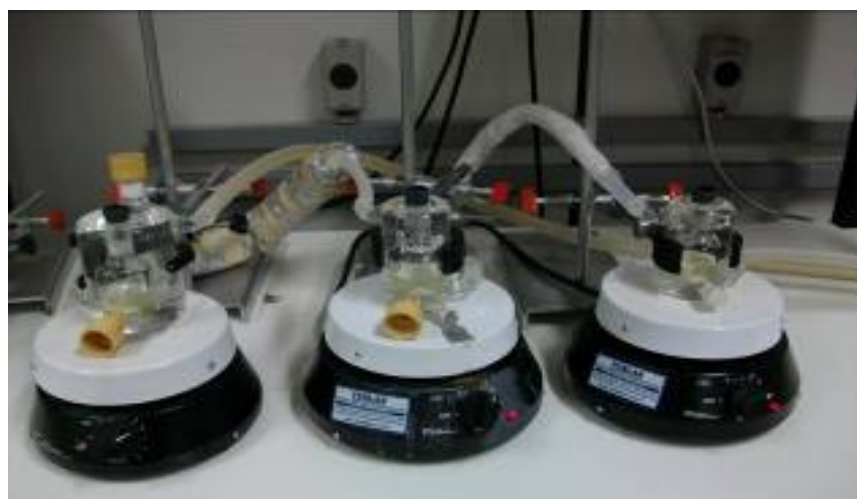


Figura 3.15. Foto de três células em série para determinar o ELL, com mistura sob agitação.

3.6. EQUAÇÕES UTILIZADAS

Para a simulação de processos químicos como, por exemplo, destilação ou extração líquido-líquido, no qual o equilíbrio de fases tem que ser conhecido, esse conhecimento do comportamento real de misturas é de grande importância. Além disso, a predição do comportamento é importante, já que nem sempre é possível obter todos os dados experimentais da mistura de interesse nas condições de temperatura, de pressão e de composição relacionadas ao estudo. Sendo assim, é necessário utilizar modelos fenomenológicos específicos com os dados experimentais disponíveis e de confiança para obter a melhor interpolação e extrapolação dos dados.

De uma forma geral, o equilíbrio de fases é representado pela condição de isofugacidade, quer dizer, as fugacidades de cada um dos componentes na mistura devem ser iguais ao longo de todas as fases (π). Esta condição pode ser representada por:

$$\bar{f}_i^I(T, P, x^I) = \bar{f}_i^{II}(T, P, x^{II}) = \dots = \bar{f}_i^\pi(T, P, x^\pi) \quad 3.23$$

As fugacidades são geralmente representadas pelo coeficiente de fugacidade (ϕ), quando há uma fase vapor envolvida, ou pelo coeficiente de atividade (γ), quando há uma fase líquida envolvida.

3.6.1. MODELAGEM DAS CARACTERÍSTICAS DE SOLVATAÇÃO

A relação entre a constante de Henry e as características de solvatação pode ser dada pela energia de Gibbs. A energia de Gibbs de solvatação corresponde à mudança na energia de Gibbs quando o soluto é transferido, a uma temperatura constante, desde o estado do gás ideal puro à pressão normal para o estado padrão de diluição infinita do soluto no solvente, sendo dada por (Letcher, 2007).

$$\Delta_{sol}G = RT \ln(H / p^o) \quad 3.24$$

onde p^o é a pressão do estado padrão. As diferenças parciais molares de entalpia e entropia entre os dois estados podem ser obtidas através do cálculo das derivadas parciais correspondentes da energia de Gibbs com respeito à temperatura.

$$\Delta_{sol}H = -T^2 \frac{\partial}{\partial T}(\Delta_{sol}G/T)_P \quad 3.25$$

$$\Delta_{sol}S = -\left(\frac{\partial \Delta_{sol}G}{\partial T}\right)_P \quad 3.26$$

Assim, com os resultados para a constante de Henry de CO₂ em diferentes líquidos iônicos foram correlacionados em função da temperatura por uma equação empírica do tipo:

$$\ln(H_{12} / p^o) = A\left(\frac{1}{T}\right) + B \quad 3.27$$

onde os coeficientes A e B são obtidos por regressão dos dados. Assim o efeito da temperatura sobre a solubilidade do CO₂ pode ser relacionada com a entropia parcial molar e a entalpia parcial molar de solvatação (Hildebrand e Scott, 1970) e pode ser calculado a partir de uma adequada correlação (Equação 3.27) das constantes de Henry:

$$\Delta_{sol}H = -T^2 \frac{\partial}{\partial T}(\Delta_{sol}G/T)_P = RA \quad 3.28$$

$$\Delta_{sol}S = -\left(\frac{\partial \Delta_{sol}G}{\partial T}\right)_P = -RB \quad 3.29$$

A entalpia parcial molar de solvatação dá uma indicação da força de interação entre o gás e o líquido iônico, enquanto que a entropia molar parcial indica a quantidade de ordem presente na mistura gás-líquido iônico.

3.6.2. MODELAGEM USANDO O COEFICIENTE DE FUGACIDADE

As mais comuns e industrialmente importantes EdEs são as equações cúbicas derivadas da EdE de van der Waals. Entre elas, a EdE de Peng-Robinson provou combinar a simplicidade e a precisão necessária para a predição e correlação de propriedades volumétricas e termodinâmicas de fluidos, embora possam ser apresentados problemas na aplicação da EdE de PR aos sistemas perto do ponto crítico. A EdE de PR é:

$$P = \frac{RT}{V - b} - \frac{a}{V(V + b) + b(V - b)} \quad 3.30$$

$$a = a_c \alpha(T) \quad a_c = 0.457235(RT_c/P_c)^2 \quad b = 0.077796(RT_c/P_c) \quad 3.31$$

$$\alpha(T) = [1 + F(1 - T_r^{0.5})]^2 \quad F = 0.37464 + 1.54226\omega - 0.26992\omega^2 \quad 3.32$$

onde T_r é a temperatura reduzida e ω é o fator acêntrico de Pitzer. Para misturas tem-se:

$$P = \frac{RT}{V - b_m} - \frac{a_m}{V(V + b_m) + b_m(V - b_m)} \quad 3.33$$

As constantes a_m e b_m são expressos em função da concentração dos diferentes componentes da mistura, através de regras, chamadas regras de mistura. Neste trabalho, a regra de mistura usada foi a de Wong-Sandler

$$b_m = \frac{\sum_i \sum_j x_i x_j \left(b - \frac{a}{RT} \right)_{ij}}{1 - \sum_i \frac{x_i a_{ii}}{b_{ii} RT} - \frac{A_\infty^E}{\Omega RT}} \quad 3.34$$

$$a_m = b_m \left[\sum_i \frac{x_i a_{ii}}{b_{ii}} + \frac{A_\infty^E}{\Omega} \right] \quad 3.35$$

$$\left(b - \frac{a}{RT} \right)_{ij} = \frac{(b_{ii} + b_{jj})}{2} - \frac{(1 - k_{ij})\sqrt{a_{ii}a_{jj}}}{RT} \quad 3.36$$

nessas equações, a_m e b_m são as constantes da EdE, $\Omega = \ln(\sqrt{2}-1)/\sqrt{2}$ para a EdE de PR, e A_∞^E , a energia livre de Helmholtz em excesso ao limite da pressão infinita. Assumindo que $A_\infty^E \approx A_0^E$ $\approx G_0^E$, onde G_0^E é a energia livre de Gibbs em excesso ao limite da pressão zero, essa pode ser calculada usando um modelo do coeficiente de atividade, tal como NRTL ou UNIQUAC. As variáveis a_{ii} e b_{ii} são as constantes da EdE, definidas como:

$$a_{ii} = 0.457235(RT_c/P_c)^2 [1 + F(1 - T_r^{0.5})], \quad F = 0.37464 + 1.54226\omega - 0.26992\omega^2 \quad 3.37$$

$$b_{ii} = 0.077796(RT_c/P_c) \quad 3.38$$

onde T_r é a temperatura reduzida, T_c é a temperatura crítica, P_c é a pressão crítica e ω é o fator acêntrico de Pitzer.

3.6.3. MODELAGEM UTILIZANDO O COEFICIENTE DE ATIVIDADE

O coeficiente de atividade está relacionado com o arranjo molecular na solução, incluindo também a formação ou quebra das ligações no processo de mistura das espécies puras, determinando assim as interações moleculares. Do mesmo modo, ele define as formas das curvas de equilíbrio e há diversos modelos que podem representá-lo; alguns deles serão mostrados mais adiante. A introdução do coeficiente de atividade na Equação 3.23, resulta em:

$$\gamma_i^I(T, P, x^I)x_i^I f_i^I(T, P) = \gamma_i^{II}(T, P, x^{II})x_i^{II} f_i^{II}(T, P) = \dots = \gamma_i^\pi(T, P, x^\pi)x_i^\pi f_i^\pi(T, P) \quad 3.39$$

Tendo cada espécie na fase líquida à temperatura do sistema, tem-se:

$$\gamma_i^I(T, P, x^I)x_i^I = \gamma_i^{II}(T, P, x^{II})x_i^{II} = \dots = \gamma_i^\pi(T, P, x^\pi)x_i^\pi \quad 3.40$$

Junto com as restrições, $\sum x_i^\pi = 1$, constituem o sistema básico de equações para o cálculo do ELL.

Para o cálculo ou correlação do equilíbrio líquido-líquido, que inclui o coeficiente de atividade, é necessário usar uma expressão para a energia livre de Gibbs em excesso como uma função da temperatura e composição, a qual relaciona o coeficiente de atividade à fração molar.

Dados de equilíbrio para sistemas que envolvem compostos sulfurosos e líquidos iônicos são escassos. Assim, modelos de predição que não requerem ajuste de parâmetros baseados em dados experimentais são de crucial importância. Nesse contexto, a simulação molecular pode ser muito útil para predizer as propriedades PVT de compostos aromáticos (Aparício et al., 2007).

3.6.4. MODELOS PARA A ENERGIA LIVRE DE GIBBS EM EXCESSO

a) Correlação dos dados

O modelo NRTL (*non random, two liquid*) utiliza o conceito da composição local para expressar a dependência do coeficiente de atividade com a composição. Esta idéia considera que as moléculas presentes em um sistema líquido não se encontram aleatoriamente distribuídas, mas que existe certa ordem (não aleatoriedade). Esta não aleatoriedade, que é fruto das interações existentes entre as moléculas, provoca o surgimento de regiões com composição diferente da composição global do sistema; daqui a expressão “composição local”. As equações do modelo NRTL para o cálculo do coeficiente de atividade em sistemas multicomponentes são:

$$\ln \gamma_i = \frac{\sum_j \tau_{ji} G_{ji} x_j}{\sum_k G_{ki} x_k} + \sum_j \frac{x_j G_{ij}}{\sum_k G_{kj} x_k} \left[\tau_{ij} - \frac{\sum_k x_k \tau_{kj} G_{ki}}{\sum_k G_{kj} x_k} \right] \quad 3.41$$

$$\tau_{ij} = \frac{\Delta g_{ij}}{RT} \quad (\tau_{ij} \neq \tau_{ji}) \quad 3.42$$

$$G_{ij} = \exp(-\alpha_{ij} \tau_{ij}) \quad (\alpha_{ij} = \alpha_{ji}) \quad 3.43$$

Este modelo apresenta três parâmetros ajustáveis para cada par binário (Δg_{ij} , Δg_{ji} e α_{ij}). Os parâmetros Δg_{ij} e Δg_{ji} estão relacionados à energia característica da interação entre as moléculas do tipo i e j , enquanto o parâmetro α_{ij} está relacionado com o grau de ordem (ou não aleatoriedade) da mistura.

Outro modelo para o coeficiente de atividade baseado no conceito da composição local, mas que tem base na Mecânica Estatística é o modelo UNIQUAC (UNIversal QUAsi-Chemical). Abrams e Prausnitz (1975) desenvolveram uma equação que, de alguma maneira, é uma extensão da teoria quase-química de Guggenheim para moléculas não-randômicas a misturas contendo componentes de diferente tamanho. A equação UNIQUAC para G^E consiste em duas partes: uma

parte combinatorial, que descreve as contribuições entrópicas dos componentes, e uma parte residual, que expressa as forças intermoleculares que são responsáveis pela entalpia de mistura. Para um sistema multicomponente, a equação UNIQUAC é a soma das duas parcelas:

$$g^E = g^E_{comb} + g^E_{res} \quad 3.44$$

$$\frac{g^E_{comb}}{RT} = \sum_i x_i \ln \frac{\Phi_i^*}{x_i} + \frac{z}{2} \sum_i q_i x_i \ln \frac{\theta_i}{\Phi_i^*} \quad 3.45$$

$$\frac{g^E_{res}}{RT} = - \sum_i q'_i x_i \ln \left(\sum_j \theta'_j \tau_{ji} \right) \quad 3.46$$

onde as frações de segmento e as frações de área estão dadas por:

$$\Phi_i^* = \frac{r_i x_i}{\sum_j r_j x_j} \quad \theta_i = \frac{q_i x_i}{\sum_j q_j x_j} \quad \theta'_i = \frac{q'_i x_i}{\sum_j q'_j x_j} \quad 3.47$$

O número de coordenação z é fixado como 10, e, para qualquer componente i , o coeficiente de atividade é dado por:

$$\ln \gamma_i = \ln \frac{\Phi_i^*}{x_i} + \frac{z}{2} q_i \ln \frac{\theta_i}{\Phi_i^*} + l_i - \frac{\Phi_i^*}{x_i} \sum_j x_j l_j - q'_i \ln \left(\sum_j \theta'_j \tau_{ji} \right) + q'_i - q'_i \sum_j \frac{\theta'_j}{\sum_k \theta'_k \tau_{kj}} \quad 3.48$$

$$l_j = \frac{z}{2} (r_j - q_j) - (r_j - 1) \quad 3.49$$

Para cada mistura binária existem dois parâmetros ajustáveis, τ_{ij} e τ_{ji} , que, pela sua vez, são dados por:

$$\tau_{ij} = \exp \left(- \frac{\Delta u_{ij}}{RT} \right) \equiv \exp \left(- \frac{a_{ij}}{T} \right) \quad 3.50$$

$$\tau_{ji} = \exp \left(- \frac{\Delta u_{ji}}{RT} \right) \equiv \exp \left(- \frac{a_{ji}}{T} \right) \quad 3.51$$

Da mesma maneira que no modelo NRTL, os parâmetros Δu_{ij} e Δu_{ji} estão relacionados à energia característica da interação entre as moléculas do tipo i e j .

O modelo UNIQUAC precisa dos parâmetros estruturais da área e volume de van der Waals relativos a um segmento padrão, r_i e q_i . A área superficial e o volume de van der Waals são propriedades características de uma molécula e, a princípio, podem ser derivados diretamente da estrutura molecular. Tradicionalmente, o método desenvolvido por Bondi (1968) é muito popular para calcular estas quantidades, mas segundo o próprio autor, o método é válido apenas para grupos ligados ao carbono. Por outro lado, um método mais geral, proposto inicialmente por Lee e Richards (1971), usa o conceito de superfície acessível por solvente (*solvent accessible surface – AS*). Considerando esta metodologia, Álvarez e Aznar (2008b) calcularam os parâmetros estruturais r e q para diversos solventes e líquidos iônicos, através de cálculos de química computacional.

b) Predição dos dados

Uma descrição detalhada do modelo COSMO e uma revisão de todas as aplicações possíveis podem ser encontradas no livro de Klamt (2005). Essencialmente, na abordagem do modelo COSMO, as interações moleculares são representadas pelas interações entre segmentos de superfície das moléculas. Estes segmentos de superfície são determinados pelas cargas superficiais formadas, que são distribuídas sobre a superfície da cavidade que está ao redor da molécula na mistura. Cada composto é caracterizado por cálculos *ab initio* realizados na molécula solvatada em um condutor. Estes cálculos fornecem o volume molecular, a superfície molecular e os chamados perfis sigma, que correspondem à distribuição das cargas de superfície sobre a superfície da cavidade da molécula.

Neste trabalho foi utilizado o modelo COSMO-SAC, já que existe disponível um amplo banco de dados de compostos (VT-2005) com dados *ab initio* (Mullins et al., 2006). Também serão calculados os dados *ab initio* para alguns compostos do presente projeto, seguindo as recomendações dadas em Mullins et al. (2006).

Aqui são apresentadas as equações principais do modelo COSMO-SAC. Mais detalhes sobre a teoria podem ser encontrados em Lin e Sandler (2002). O coeficiente de atividade γ_i , necessário no equilíbrio líquido-líquido, pode ser determinado a partir do modelo COSMO-SAC, em que o coeficiente de atividade da espécie i é calculado pela soma das contribuições residuais e combinatoriais.

$$\ln \gamma_i = \ln \gamma_i^{res} + \ln \gamma_i^{com} \quad 3.52$$

A parte residual é calculada a partir de uma consideração de solvatação molecular em um condutor perfeito. A distribuição das cargas selecionadas na superfície molecular, o chamado perfil sigma $p(\sigma)$, é determinada a partir de cálculos de mecânica quântica. As interações moleculares na fase líquida são assumidas como sendo a soma das contribuições das interações de segmento de superfície através das cargas selecionadas. Com estes pressupostos, a contribuição residual toma a seguinte forma:

$$\ln \gamma_i^{res} = n_i \sum_{\sigma_m} p_i(\sigma_m) \ln [\Gamma_s(\sigma_m) - \Gamma_i(\sigma_m)] \quad 3.53$$

onde n_i é o numero de segmentos de superfície contidos na espécie i , $\Gamma_s(\sigma)$ é o coeficiente de atividade do segmento i (cuja densidade de carga selecionada é σ) na solução S (para o qual a probabilidade de encontrar um segmento de densidade de carga σ é representada pelo símbolo $p_s(\sigma)$):

$$\ln \Gamma_s(\sigma_m) = -\ln \left\{ \sum_{\sigma_n} p_s(\sigma_n) \Gamma_s(\sigma_n) \exp \left[\frac{-\Delta W(\sigma_m, \sigma_n)}{RT} \right] \right\} \quad 3.54$$

onde $W(\sigma_m, \sigma_n)$ é a interação eletrostática entre dois segmentos da densidade de carga σ_m e σ_n . O modelo de Staverman–Guggenheim (SG) é usado para o termo combinatório:

$$\ln \gamma_i^{com} = \ln \frac{\Phi_i}{x_i} + \frac{z}{2} q_i \ln \frac{\theta_i}{\Phi_i} + l_i - \frac{\Phi_i}{x_i} \sum_j x_j l_j \quad 3.55$$

$$\Phi_i = \frac{r_i x_i}{\sum_j r_j x_j} \quad \theta_i = \frac{q_i x_i}{\sum_j q_j x_j} \quad l_i = (z/2)(r_i - q_i) - (r_i - 1) \quad 3.56$$

onde θ_i é a fração de área de superfície, Φ_i é a fração de volume, z é o numero de coordenação ($z = 10$), e os parâmetros $r_i = V_i^{mol}/V_{ref}$ e $q_i = A_i^{mol}/A_{ref}$ são os parâmetros de volume e área superficial normalizados para a molécula i . V_i^{mol} e A_i^{mol} são o volume e área da molécula i determinada pelo método COSMO *ab initio*, e $V_{ref}=66,69 \text{ \AA}^3$ e $A_{ref}=79,53 \text{ \AA}^2$.

3.6.5. PREDIÇÃO DA DENSIDADE

A equação de estado de Peng-Robinson pode ser escrita em termos do fator de compressibilidade (Z) usando:

$$Z^3 - (1-B)Z^2 + (A-3B^2-2B)Z - (AB-B^2-B^3) = 0 \quad 3.57$$

onde A e B são dadas por:

$$A = \frac{a_m P}{(RT)^2} \quad 3.58$$

$$B = \frac{b_m P}{RT} \quad 3.59$$

onde as constantes a_m e b_m são expressos em função da concentração dos diferentes componentes na mistura, através das chamadas regras de mistura.

A Equação 3.57 produz uma ou três raízes reais, dependendo do número de fases do sistema. Foi mostrado que o modelo proporciona uma excelente representação dos dados experimentais líquido-vapor (Álvarez e Aznar, 2008b). Para a predição da densidade do líquido, a raiz conveniente é a menor positiva. A translação no volume pode ser adotada na equação de estado, para melhorar as estimativas do volume feitas pela equação de estado de Peng-Robinson. Então, o valor de correção para cada componente puro (Δv_i) é dado pela diferença entre o volume calculado pelo modelo termodinâmico e o volume experimental:

$$\Delta v_i = V_{i,exp} - V_{i,cal} \quad 3.60$$

onde $V_{i,cal}$ é o volume molar do composto i calculado pelo modelo termodinâmico e $V_{i,exp}$ é o volume molar experimental do composto i . Em seguida, o volume da mistura é obtido pela correção do volume aplicado por:

$$V = V_{cal} + \sum_i \Delta v_i x_i \quad 3.61$$

onde x_i é a fração molar do líquido do composto puro i , V_{cal} é o volume molar do líquido da mistura calculadas com o modelo termodinâmico, e V é o volume molar predito e corrigido da mistura.

3.6.6. ESTIMAÇÃO DOS PARÂMETROS

Os valores iniciais dos parâmetros nas equações polinomiais foram aproximados por meio de um algoritmo genético, mMyGA (Álvarez et al., 2008). Depois disso, os parâmetros foram reajustados utilizando um algoritmo de otimização não-linear baseado no algoritmo de Marquardt. A otimização utiliza a minimização no desvio padrão entre o valor experimental e calculado, definido como:

$$\sigma = \left[\sum_{i=1}^N \frac{(F_{\text{exp}} - F_{\text{cal}})_i^2}{N - m} \right]^{1/2} \quad 3.62$$

onde N é o número de pontos experimentais, m é o número de parâmetros na curva e F_{cal} e F_{exp} são os valores calculados pelo modelo e obtidos experimentalmente, respectivamente.

4. RESULTADOS E DISCUSSÃO

PREFÁCIO

Neste capítulo, são apresentados os resultados experimentais para os objetivos expostos. Também são apresentadas três aplicações dos líquidos iônicos como alternativa à indústria nacional nas áreas de secagem de etanol, purificação de gases e dessulfurização do petróleo.

4.1. SÍNTESE DE LÍQUIDOS IÔNICOS E CARATERIZAÇÃO

Esta seção apresenta a síntese e caraterização de líquidos iônicos que incorporam o cátion de N-metil-2-hidróxi etil amônio e ânion de ácidos orgânicos.

4.1.1 DESIDRATAÇÃO DOS LÍQUIDOS IÔNICOS

Segundo a metodologia proposta no capítulo anterior, o objetivo é determinar o tempo necessário de vácuo aplicado a uma amostra de 100 g de líquido iônico. A umidade inicial do líquido iônico etilsulfato de 1-etil-3-metilimidazólio foi de 4% (massa) e o primeiro método obteve uma umidade final de 1,5%. Os métodos 2 e 3 permitiram uma maior desidratação, como pode ser observado na Figura 4.1. O método 2 obteve a estabilização da umidade em 1% (massa) com 16 horas de vácuo. O método 3 obteve uma umidade final de 0,01% (massa) com 35 horas de vácuo.

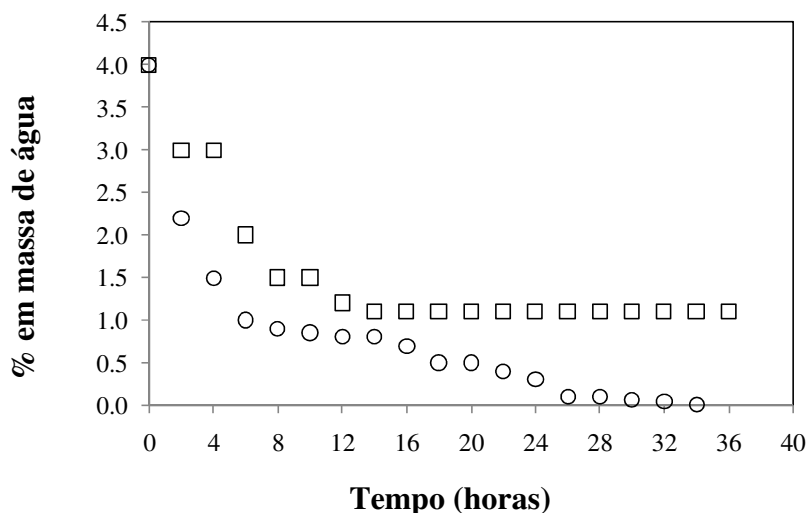


Figura 4.1. Perfil da desidratação em batelada do líquido iônico etilsulfato de 1-etil-3-metilimidazólio vs. tempo. No tempo zero é medida a umidade inicial. (□) armazenagem em ar, (○) armazenagem em nitrogênio.

Segundo os resultados com o líquido iônico etilsulfato de 1-etil-3-metilimidazólio, a metodologia ótima é uma desidratação em batelada com armazenagem em nitrogênio. A metodologia foi validada com o líquido iônico hexanoato de N-metil-2-hidroxietilamônio, atingindo uma umidade final de 0,0862% em massa. O perfil de desidratação pode ser observado na Figura 4.2.

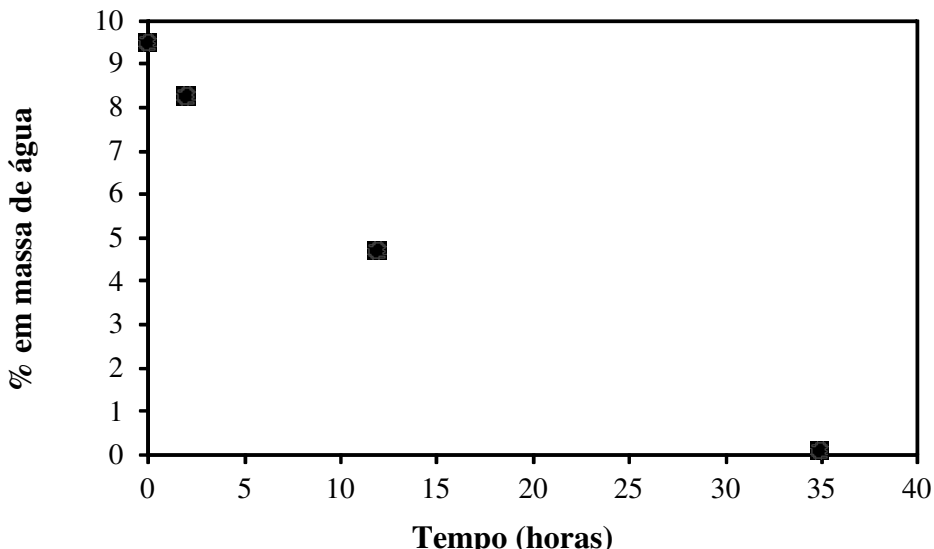


Figura 4.2. Perfil da desidratação em batelada do líquido iônico hexanoato de N-metil-2-hidroxietilamônio vs. Tempo, com armazenagem em nitrogênio.

Após a purificação, a composição química foi estudada por RMN e as propriedades físicas foram medidas.

4.1.2 CALORIMETRIA DIFERENCIAL EXPLORATÓRIA

Os experimentos no DSC foram principalmente feitos para determinar a temperatura de decomposição térmica dos líquidos iônicos sintetizados no laboratório de Equilíbrio de Fases e no laboratório de Termodinâmica Aplicada (Universidade Federal da Bahia). A estrutura química de todos os líquidos iônicos foram verificadas com espectros de RMN para hidrogênio e carbono. A temperatura de decomposição térmica de dezessete líquidos iônicos são apresentados na Tabela 4.1 e de três líquidos iônicos são mostrados na Figura 4.3.

A Figura 4.3 mostra que os três líquidos iônicos tem perfis parecidos variando na intensidade deles. A inclinação observada a partir da temperatura de 293,15 K até o início do pico descendente é devido à perda de umidade durante o aquecimento. Logo é observado um maior

decaimento que dá início ao pico de degradação da amostra, à temperatura de 423,15 K. Assim, os experimentos que utilizaram esses líquidos iônicos não sobrepassaram os 423,15 K.

Tabela 4.1. Temperatura de degradação (T_d) de líquidos iônicos sintetizados

Sigla	Nome	T_d °C
2-HDEABE	Benzoato de 2 hidroxi dietanol amônio	227,6
2-HEAFT	Ftalato de 2 hidroxi monoetanol amônio	213,7
2-HDEAFT	Ftalato de hidroxi dietanol amônio	236,9
2-HEAES	Estearato de 2 hidroxi monoetanol amônio	104,7
2-HDEAES	Estearato de 2 hidroxi dietanol amônio	104,9
2-HEAL	Lactato de 2 hidroxi monoetanol amônio	291,3
2-HDEAL	Lactato de 2 hidroxi dietanol amônio	210,6
2-HEASU	Succinato de 2 hidroxi monoetanol amônio	196,7
2-HDEASU	Succinato de 2 hidroxi dietanol amônio	206,1
2-HEACI	Citrato de 2 hidroxi monoetanol amônio	200,5
2-HDEACI	Citrato de 2 hidroxi dietanol amônio	213,3
2-HDEAFU	Fumarato de 2 hidroxi dietanol amônio	183,6
2-HEAMA	Maleato de 2 hidroxi monoetanol amônio	195,1
2-HDEAMA	Maleato de 2 hidroxi monoetanol amônio	183,5
m-2-HEAA	Acetato de n-metil-2-hidroxietilamônio	200,1
m-2-HEAB	Butirato de n-metil-2-hidroxietilamônio	206,4
e m-2-HEAH	Hexanoato de n-metil-2-hidroxietilamônio	211,3

A Tabela 4.1 mostra que os líquidos iônicos próticos são sensíveis a temperaturas próximas aos 473 K, excepto para os baseados no ânion do ácido esteárico, que decompõe termicamente aos 378 K.

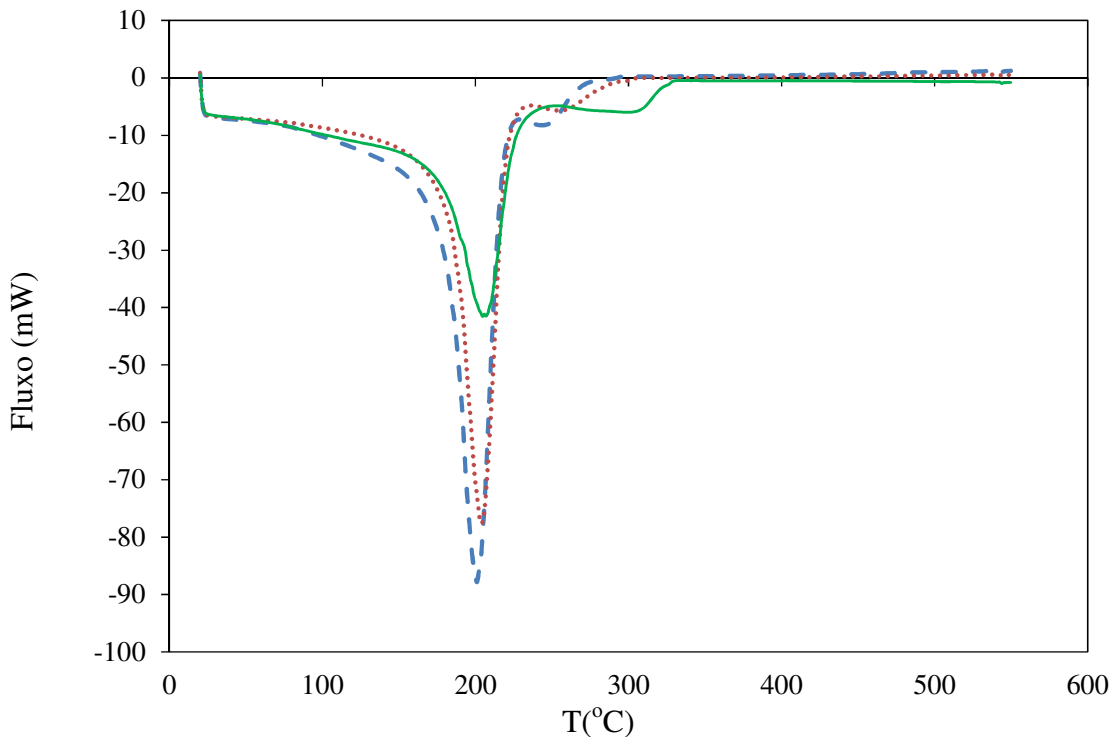
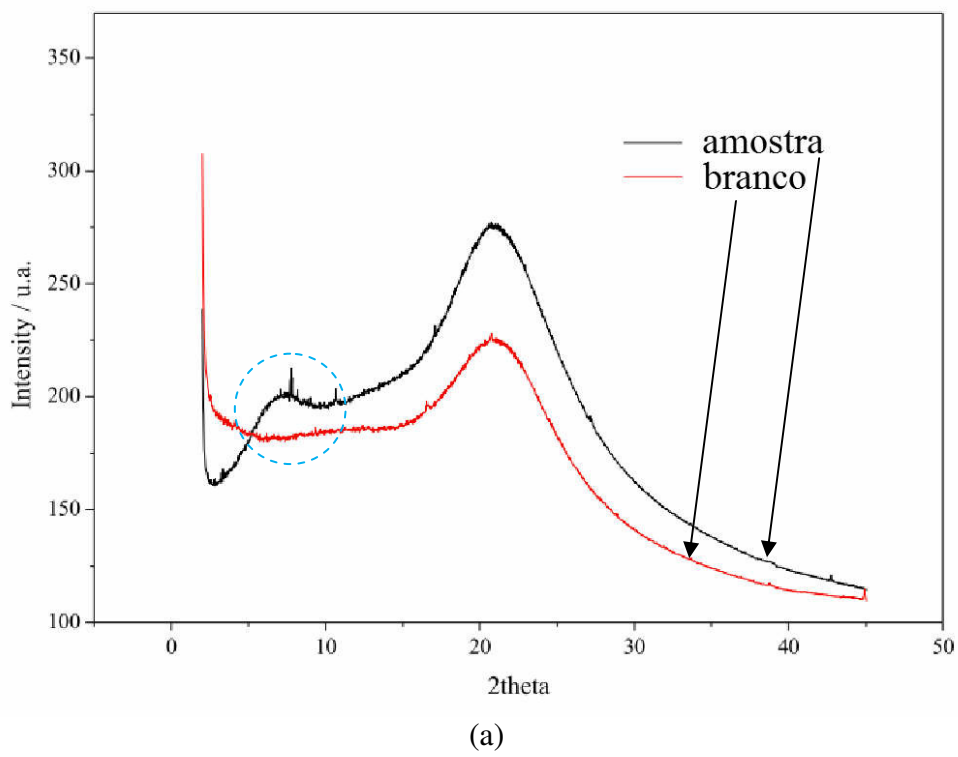


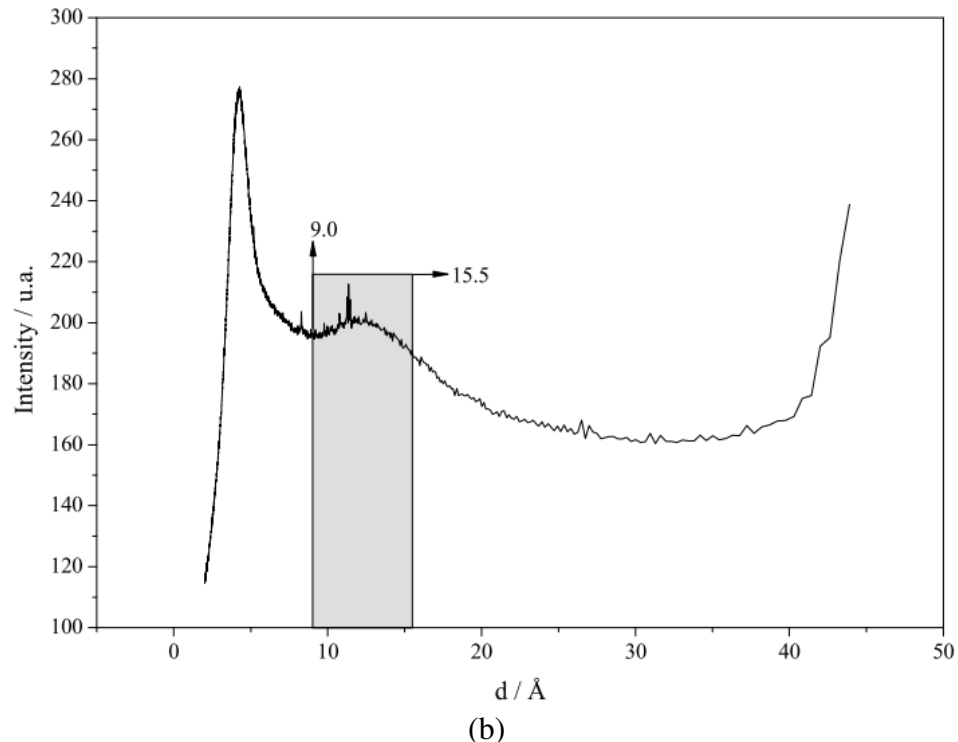
Figura 4.3. Fluxo de calor contra a temperatura, para m-2-HEAA (—), m-2-HEAB(···) e m-2-HEAH (—).

4.1.3 DIFRAÇÃO DE RAIOS X

A Figura 4.4 mostra os gráficos clássicos de difração de raios X para amostras de acetato de 2-hidroxietilamônio (2-HEAA) puro. A Figura 4.4.a mostra o estudo da otimização do ângulo de medição das distâncias intermoleculares. Nesta figura, observa-se que, a diferentes ângulos, tem-se medições na amostra só para valores baixos do ângulo de medida (pico da intensidade da amostra maior ao branco utilizado). Em vermelho, a medida do branco (capilar+ar) e em preto, a medida da amostra (capilar+amostra). Logo, a amostra precisa de medições em baixo ângulo, resultado que confirma a formação de agregados de grandes tamanhos. A Figura 4.4.b mostra graficamente intensidade contra distância intermolecular. Esta figura mostra um ordenamento molecular com (9 a 15) Å. Esse ordenamento semelha estar associado ao tamanho da cadeia anfifílica. Se houve algum ordem ou agregação tipo bicapas, por exemplo, deveria aparecer um pico entre (18 e 30) Å, resultado que não é observado.



(a)



(b)

Figura 4.4. Gráficos clássicos de difração de raios X. (a) Intensidade contra o ângulo de medição, 2θ , (b) Intensidade contra distâncias intramoleculares.

4.1.4 DEGRADAÇÃO DE ALGUNS LÍQUIDOS IÔNICOS

Graves et al., (2007) reporta a obtenção de amidas pela degradação dos líquidos iônicos com cadeia alquílica curta no ânion. Considerando este fenômeno, depois de dois meses dos líquidos iônicos terem sido sintetizados, foi analisada novamente a estrutura química por experiências de ^1H RMN. Os resultados mostraram que o líquido iônico Formiato de N-metil-2-hidroxietilamônio apresenta novos compostos, aparentemente pela degradação no tempo. Segundo a Figura 4.5, a degradação desse líquido iônico tem dois possíveis produtos: o N-metil-N-propilformamide ou o formiato de 2-(metilamino)etil.

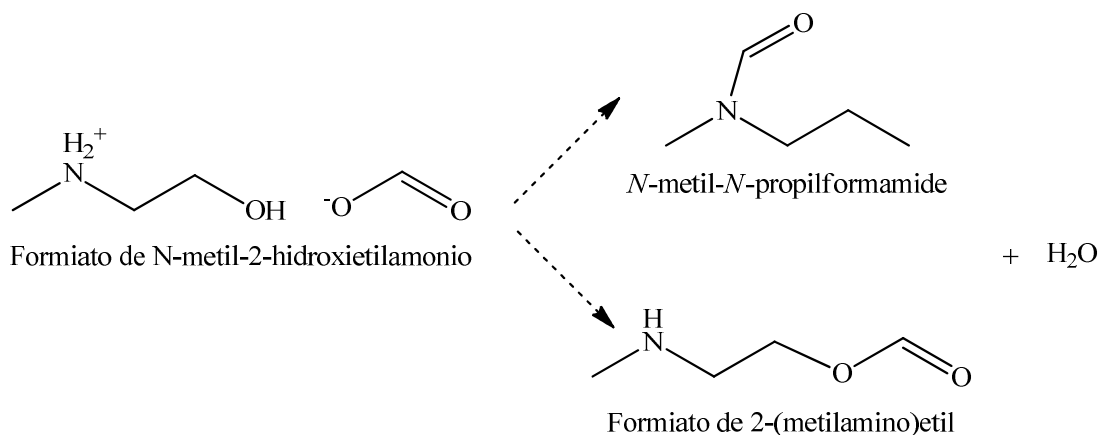


Figura 4.5. Produtos possíveis pela degradação de formiato de N-metil-2-hidroxietilamônio.

A Figura 4.6 mostra os espectros de ^1H RMN para o líquido iônico formiato de N-metil-2-hidroxietilamônio recentemente sintetizado (a) e depois de 2 meses (b). Entretanto, os espectros da Figura 4.6.b mostram novos picos pertencentes à estrutura química de um éster, o formiato de 2-(metilamino)etil. Este resultado confirma a formação de éster na degradação deste tipo de líquido iônico.

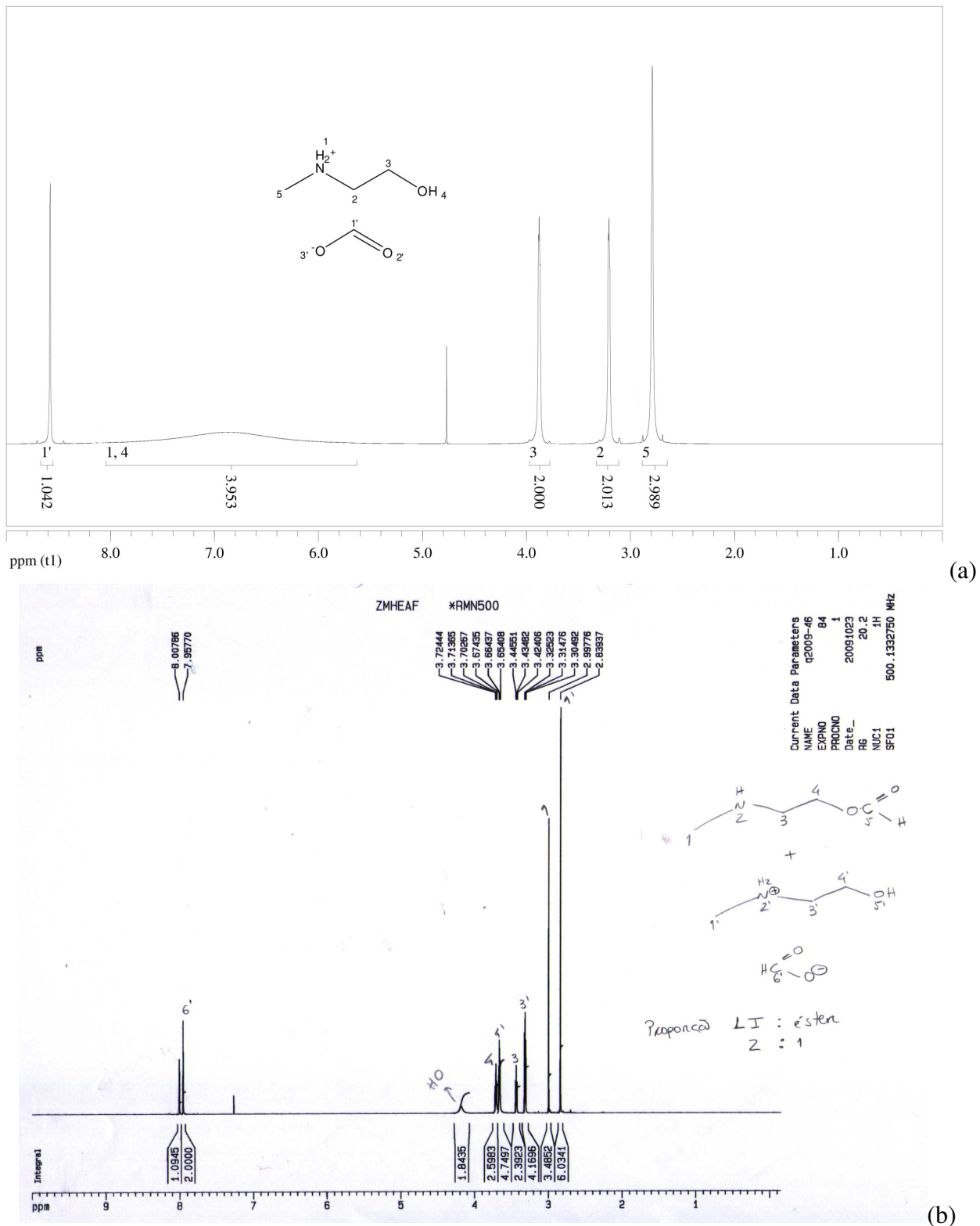


Figura 4.6. Espectros de hidrogenio para o m-2-HEAF. (a) Após uma semana de ter sido sintetizado. Fonte: CACTUS-USC, (b) após dois meses de ter sido sintetizado. Fonte: Prof. Coutinho

Nos resultados gerais, pode-se observar que a adição de carbonos no ânion diminui a densidade do líquido iônico, e a adição de grupos hidroxila ou amônio no cátion para um tipo de anion aumenta a densidade do líquido iônico, como observado na Figura 4.7.

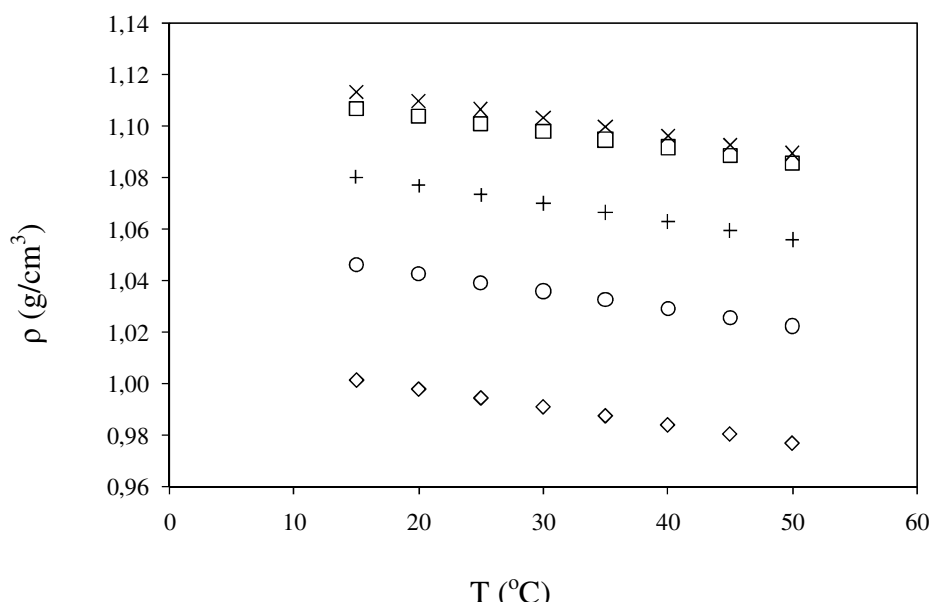


Figura 4.7: Densidade em função da temperatura a pressão ambiente para líquidos iônicos puros: m-2-HEAA (\square), m-2-HEAB (\circ), m-2-HEAH (\diamond), 2-HE2AB (x) e N-(2-HE)edAB (+).

A Figura 4.7. mostra que para o líquido iônico m-2-HEAB, contendo o ânion butirato, a adição de grupos hidroxila ou amônio no cátion aumenta a densidade do novo líquido iônico. Os dados experimentais são apresentados na Tabela 4.2.

Tabela 4.2: Densidade experimental para líquidos iônicos puros com umidade inferior a 1000 ppm.

2HE ₂ AB		N-(2-HE)edAB		m-2-HEAH		m-2-HEAB		m-2-HEAA	
T (°C)	ρ/g/cm ³	T (°C)	ρ/g/cm ³	T (°C)	ρ/g/cm ³	T (°C)	ρ/g/cm ³	T (°C)	ρ/g/cm ³
15,01	1,113343	15,01	1,080216	15,01	1,001459	15,00	1,046008	15,00	1,106802
20,00	1,109969	20,00	1,076849	20,00	0,997979	20,00	1,042640	20,00	1,103755
25,00	1,106580	25,00	1,073441	25,00	0,994536	25,00	1,039245	25,00	1,100827
30,00	1,103181	30,00	1,070012	30,00	0,991089	30,00	1,035872	30,00	1,097843
35,01	1,099772	35,00	1,066542	35,00	0,987623	35,00	1,032530	35,00	1,094833
40,00	1,096280	40,00	1,063037	40,00	0,984126	40,01	1,029145	40,01	1,091784
45,00	1,092850	45,00	1,059482	45,00	0,980605	45,01	1,025722	45,01	1,088717
50,00	1,089433	50,01	1,055839	50,01	0,977064	50,01	1,022262	50,01	1,085620

Artigos publicados:

O primeiro artigo analisa as propriedades físicas de seis novos líquidos iônicos como função do comprimento da cadeia alquílica do ânion.

ÁLVAREZ, V.H.; DOSIL, N.; GONZALEZ-CABALEIRO, R.; MATTEDI, S., MARTIN-PASTOR, M.; IGLESIAS, M.; NAVAZA, J. M. Brønsted Ionic Liquids for Sustainable Processes: Synthesis and Physical Properties, *J. Chem. Eng. Data*, v.55, p. 625–632, 2010.

O segundo artigo estuda as propriedades físicas de dois novos líquidos iônicos contendo o ânion tipo oleato.

ÁLVAREZ, V.H.; R.; MATTEDI, S., MARTIN-PASTOR, M.; AZNAR, M.; IGLESIAS, M. Synthesis and thermophysical properties of new protic long-chain ionic liquids with oleate anion, *Fluid Phase Equilibr.*, aceito (doi:10.1016/j.fluid.2010.08.022), 2010.

Artigo 4.1: Brønsted ionic liquids for sustainable processes: Synthesis and physical properties

J. Chem. Eng. Data 2010, 55, 625–632

625

Brønsted Ionic Liquids for Sustainable Processes: Synthesis and Physical Properties[†]

Víctor H. Álvarez,^{‡,§} Noelia Dosal,[‡] Rebeca Gonzalez-Cabaleiro,[‡] Silvana Mattedi,^{||} Manuel Martin-Pastor,[⊥] Miguel Iglesias,^{*,‡} and José M. Navaza[‡]

Chemical Engineering Department - ETSE, University of Santiago de Compostela, P.O. Box 15782, Santiago de Compostela, Spain, School of Chemical Engineering, State University of Campinas, P.O. Box 6066, 13083-970 Campinas-SP, Brazil, Chemical Engineering Department, Polytechnic School, Federal University of Bahia, 40210-630 Salvador-BA, Brazil, and Unidade de Resonancia Magnética, RIAIDT, edif. CACTUS, University of Santiago de Compostela, P.O. Box 15706, Santiago de Compostela, Spain

This report describes the synthesis of ionic liquids that incorporate the *N*-methyl-2-hydroxyethylammonium cation with various carboxylic acid anions and the study of some of their physical properties, including self-diffusion coefficients, density, speed of sound, viscosity, and refractive index. ¹H and ¹³C NMR spectra were used to characterize the chemical structure of the species in concordance with FT-IR spectra. DOSY NMR spectra was used to determine the self-diffusion coefficients of the components, which were consistent with the formation of a lamellar or micellar liquid-crystal phase in samples containing an alkyl chain in the anion species. Thermoacoustic parameters showed that anion alkyl chain has an influence on the molecular packing of these ionic liquids. In addition, the effect of temperature on the properties seems to be related to the size and the type of aliphatic chain of the ionic liquid.

Introduction

Ionic liquids (ILs) are versatile new media for many chemical synthesis, enzymatic catalysis, and green engineering processes. ILs consist solely of a collection of positive and negative ions of hydrophobic or hydrophilic nature. However, unlike conventional molten salts, these materials often melt below 373 K. This is achieved because the ion-pair packing prevents an ordered electrostatic net structure as a result of steric hindrance, and therefore, a solid phase cannot form under ambient conditions.

ILs can be used as solvents because of their low melting points and their ionic structure. In some cases where ILs are used as solvents, better selectivity for organic reactions or molecular absorption is obtained than with conventional organic solvents because of specific interactions among the ions. In the past few years, room-temperature ILs have found a number of applications as clean solvents and catalysts for green chemistry, as electrolytes for batteries, in photochemistry, for electrosynthesis,^{1–5} and others.

One of the properties of ILs of interest for chemistry is their negligible vapor pressure, which means that no volatile organic pollution is created during their manipulation in industrial operations. Their liquid range can be as large as 300 °C, allowing for large reaction kinetic control and easy separation of organic molecules by distillation without loss of the IL. Until now, many ILs have been based on the imidazolium cation and, in a lesser proportion, on alkylpyridinium cations and trialkylamines.⁶ By variation of the anion or the alkyl chain of the cation, a wide range of properties such as hydrophobicity,

viscosity, density, and solvation power can be modulated, opening the possibility of tailored ILs designed for specific industrial applications.⁷ In this way, Bicak⁸ synthesized an IL formed from the neutralization of monoethanolamine with formic acid. Greaves et al.⁹ proposed different protic ILs obtained from primary amines and organic and inorganic acids. Iglesias and co-workers^{10–12} synthesized a family of these ILs by modifying the aliphatic chain of the organic acid and/or using secondary and tertiary hydroxylamines. These authors explained the low cost, simplicity of synthesis, and different applications of this new IL family. Moreover, the very low toxicity and the degradability of this kind of IL was verified.¹³ Thus, sustainable processes can be originated with their use. Therefore, available physicochemical properties or a thermodynamic database for this class of IL, either pure or in mixtures, can be of technological and/or theoretical interest.

Structural and physicochemical properties of ILs can be studied with conventional liquid NMR methods.¹⁴ These techniques can be useful in assessing the chemical composition of the ILs and for quantitative analysis of the species. In addition, NMR diffusion-ordered spectroscopy (DOSY) experiments can be used to determine self-diffusion coefficients, which are related to the molecular size and viscosity of these samples.

Continuing with our previous studies, this paper presents the synthesis and study of a series of physicochemical properties of ammonium-based ILs. We present the synthesis of six ILs, *N*-methyl-2-hydroxyethylammonium formate (m-2-HEAF), *N*-methyl-2-hydroxyethylammonium acetate (m-2-HEAA), *N*-methyl-2-hydroxyethylammonium propionate (m-2-HEAPr), *N*-methyl-2-hydroxyethylammonium butyrate (m-2-HEAB), *N*-methyl-2-hydroxyethylammonium isobutyrate (m-2-HEAiB), and *N*-methyl-2-hydroxyethylammonium pentanoate (m-2-HEAP). For these ILs, the following physicochemical properties were studied: density (ρ), speed of sound (u), refractive index (n_D), apparent viscosity (η), and self-diffusion coefficient (D).

[†] Part of the “2009 Iberian Conference on Ionic Liquids”.

^{*} Corresponding author. E-mail: miguel.iglesias@usc.es.

[‡] Chemical Engineering Department, University of Santiago de Compostela.

[§] State University of Campinas.

^{||} Federal University of Bahia.

[⊥] Unidade de Resonancia Magnética, University of Santiago de Compostela.

Experimental Section

Materials and Methods. 2-(Methylamino)ethanol (mass fraction purity 0.99) was obtained from Aldrich, and the organic acid (mass fraction purity 0.995) was obtained from Sigma. These components were used as received, as the water content (< 0.5 %) could be removed after the synthesis. During the course of the experiments, the purity of the solvents was monitored by the density and the speed of sound measurements.

The densities and the speeds of sound of the pure liquids were measured using a DSA-5000 digital vibrating tube densimeter (Anton Paar, Austria). This apparatus performs an automatic viscosity correction when used with high-viscosity liquids. The accuracy is ± 0.01 K for temperature, and the uncertainty is $\pm 1 \cdot 10^{-4}$ g·cm⁻³ for the density measurement and ± 0.1 m·s⁻¹ for the speed of sound, as calculated by propagation of errors. Dry air and distilled water were used as reference fluids to calibrate the densimeter at each temperature. The mass of each component was determined on a Kern 770 mass balance having an accuracy of 0.0001 g. The apparent viscosities of IL samples were analyzed using a Visco Elite L rheometer (Fungilab, Spain) at different temperatures. The spindles used were the TL5, TL6, and TL7, and the speed ranges were selected in accordance with the torque range (minimum 10 % and maximum 90 %), as suggested by the manufacturer's instructions. The temperature was controlled with a thermostatic bath and measured with a calibrated thermometer close to the jacket of the viscosimeter. The refractive indexes of the ILs were analyzed by an automatic digital RX-5000 refractometer (Atago, Japan). The temperature was controlled with a thermostatic bath and measured with a PT 100 sensor provided in the refractometer that had a precision of ± 0.1 K for the temperature measurement. The thermostatic bath used was the Frigiterm equipment (J.P. Selecta S.A., Spain) with a temperature stability of ± 0.1 K.

Each refractive index was obtained as the mean of three measurements with a standard deviation of $2 \cdot 10^{-5}$, and the apparent viscosity was obtained as the mean of five different spindle rate measurements with a standard deviation of 0.5 mPa·s at temperatures from (308 to 323) K and 4.0 mPa·s at temperatures from (288 to 303) K.

FT-IR Spectroscopy. The FT-IR spectra were obtained with a Varian FT-IR 670 spectrometer set to acquire the medium- and high-IR-range spectrum [(7900 to 20) cm⁻¹]. The device has a resolution of 0.10 cm⁻¹ and a signal-to-noise ratio of 12 000:1 with 75 % light attenuation. The ATR method was used for the synthesized ILs, and the sample film for these measurements was formed using a drop of IL.

NMR Spectroscopy. All of the NMR experiments were performed at 298 K in an 11.7 T Varian Inova-750 spectrometer operating at 750 MHz proton frequency. The spectra were processed with Mestre-C software.¹⁵

Samples of m-2-HEAF, m-2-HEAA, m-2-HEAPR, m-2-HEAB, m-2-HEAiB, and m-2-HEAP were studied by NMR spectroscopy. Sample preparation required only the transfer to a 5 mm NMR tube. An external reference standard capillary containing deuterated 3-(trimethylsilyl)propionic acid-*d*₄ (TSP) [0.1 M in dimethyl sulfoxide (DMSO)] was introduced coaxially in the tube. The TSP signal at approximately 0 ppm was used to determine absolute concentrations in the one-dimensional (1D) proton spectrum, and the DMSO was used for deuterium lock. The integral of the ¹H NMR signal of TSP in the capillary was calibrated with respect to a sample of 0.2 M sucrose

dissolved in D₂O prepared in a 5 mm NMR tube. The anomeric glucose proton appearing at 5.2 ppm was chosen for the calibration.

The following NMR experiments were acquired for each sample:

A quantitative 1D ¹H NMR experiment was acquired with a 33° pulse and a conveniently long interscan relaxation time (*d*₁ = 10 s). These conditions were used to ensure the exactness of the signal integration.

1D ¹³C, 1D ¹⁵N, 2D total correlation spectroscopy (TOCSY), 2D heteronuclear multiple-quantum coherence (HMQC), and 2D heteronuclear multiple-bond quantum coherence (HMBC) NMR spectra were acquired using standard methodologies.

NMR DOSY experiments were measured with the convection-compensated double-stimulated echo sequence.¹⁶ Diffusion encoding and decoding periods were done with pulsed-field bipolar gradients, and the duration of a pair of bipolar gradients was 4 ms. The gradient power level (*G* in eqs 1 and 2) used for diffusion encoding/decoding was varied linearly between (2 and 62) G·cm⁻¹ in 50 steps, with acquisition of the free-induction decay at each step. The DOSY experiment was repeated with diffusion delay periods of (200, 300, and 400) ms.

The diffusion of the TSP signal in m-2-HEAA was determined by DOSY experiments at two diffusion delays of (50 and 10) ms. The DOSY experiment was done with an internal diffusion reference consisting of 300 mg of TSP.

The self-diffusion coefficients were calculated in each DOSY experiment by fitting the intensity of each NMR signal to the following equation:¹⁶

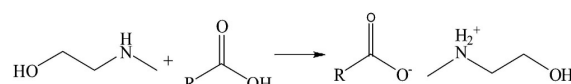
$$\frac{I(G)}{I(0)} = e^{-DG} \quad (1)$$

where *I*(*G*) is the signal integral in the presence of the gradient, *I*(0) is the intensity of the signal with the lowest gradient, *D* is the self-diffusion coefficient, and *Q* is the gradient strength, which was calculated according to the following equation:

$$Q = q^2 \left(t + \frac{4\delta}{3} + \frac{5\tau_1}{4} + \frac{\tau_2}{4} \right) \quad (2)$$

where *t* is the diffusion delay used in the experiment and *q* and the delay variables (*δ*, *τ*₁, and *τ*₂) are explained in the original reference.¹⁶

Preparation of the ILs. 2-(Methylamino)ethanol was placed in a three-necked flask made entirely of glass and equipped with a reflux condenser, a PT-100 temperature sensor for controlling the temperature, and a dropping funnel. The flask was mounted in a thermostatic bath. The organic acids were added dropwise to the flask under stirring with a magnetic stir bar. The reaction is a simple acid–base neutralization⁸ that creates an ester salt of *N*-methyl-2-ethanolamine, which, in a general form, can be expressed as follows:



where *R* is the alkyl group present in the organic acid: formic acid (*R* = H), acetic acid (*R* = Me), propionic acid (*R* = Et), butanoic acid (*R* = *n*-Pr), isobutanoic acid (*R* = *i*-Pr), and pentanoic acid (*R* = *n*-Bu). These chemical reactions are highly exothermic, an adequate control of temperature is essential throughout the chemical reaction; otherwise, heat evolution may produce the dehydration of the salt to the corresponding amide,

as in the case for nylon salts (salts of diamines with dicarboxylic acids). The color varied in each case from transparent to dark-yellow when the reaction process and purification (strong agitation and slight heating for the vaporization of residual nonreacted acid for at least for 48 h) were completed. In order to decrease the water content as much as possible, the IL was dried for 48 h at ambient temperature under a vacuum of 20 kPa with stirring before each use. This time permitted a constant value of the refractive index with respect to drying time to be obtained.

The water content in the ILs was not measured because the room humidity was not completely controlled. In addition, comparisons with standard samples of m-2-HEAA containing H₂O showed a low influence of the humidity on the density. Viscosity was the property most affected by humidity.

Thermodynamic Data Treatment. The measured densities, speeds of sound, and refractive indexes of the ILs were correlated as functions of temperature according to eq 3:

$$Z = A_0 + A_1 T + A_2 T^2 \quad (3)$$

where Z is the property (density, speed of sound, or refractive index), the A_i are adjustable parameters, and T is the absolute temperature. The apparent viscosity was fitted with an Arrhenius-type equation (normally used for Newtonian fluids), as shown in eq 4:

$$\eta = A_0 e^{A_1/T} \quad (4)$$

where η is the apparent viscosity, T is the absolute temperature, and the A_i are adjustable parameters.

The ions of the IL were considered as a large spherical shapes. Therefore, the effective radius of these molecules can be calculated using the Stokes–Einstein equation for the calculation of the Brownian diffusivity (eq 5), in which the diffusivity D varies directly with absolute temperature and inversely with both viscosity and molecular radius:

$$D = \frac{kT}{r^2 \eta} \quad (5)$$

where k is the Boltzmann's constant, T is the absolute temperature, η is the viscosity of the medium, and r is the radius of the species.

In order to explore the strength and nature of the interactions between the species of the IL, the molecular radius r was calculated from the sound velocity and density data as follows:¹⁷

$$r = \left(\frac{3b}{16\pi N_A} \right)^{1/3} \quad (6)$$

in which N_A is Avogadro's constant and b is given by:

$$b = \frac{M}{\rho} - \left(\frac{RT}{\rho u^2} \right) \cdot \left(\left[1 + \frac{Mu^2}{3RT} \right]^{1/2} - 1 \right) \quad (7)$$

where M is the molecular weight, ρ is the density, u is the speed of sound, and R is the gas constant.

Parameter Estimation. The first-approximation parameter estimation for each model was performed using a genetic algorithm code, mMyGA, with a whole-interval search.¹⁸ Next, the resulting fitting parameters were refined using a nonlinear optimization algorithm based on the Marquardt algorithm. Finally, regression was performed with the minimization of the standard deviation between the experimental and calculated values, where the standard deviation (σ) is defined as:

$$\sigma = \left[\sum_{i=1}^N \frac{(F_{\text{exptl}} - F_{\text{calcd}})_i^2}{N} \right]^{1/2} \quad (8)$$

where N is the number of experimental data points and F_{calcd} and F_{exptl} are the property values calculated by the model and obtained from experimental, respectively.

Results and Discussion

The FT-IR and NMR spectra obtained for the ILs studied herein are given in the Supporting Information.

The results of the FT-IR analyses were very similar for all of the ILs. These spectra showed a broad band in the (3500 to 2400) cm⁻¹ range that is characteristic of the ammonium structure. The OH stretching vibration is embedded in this band. The broad band centered at 1600 cm⁻¹ is a combined band of the carbonyl stretching and N–H plane bending vibrations. Figure 1 displays the FT-IR spectrum of m-2-HEAPr, which shows these bands. The Supporting Information shows the FT-IR spectrum for m-2-HEAF.

NMR spectroscopy provided further insight into the chemical composition of the ILs. The chemical composition was determined by the combination of 1D ¹H, 1D ¹³C, 1D ¹⁵N, 2D TOCSY, 2D HMQC, and 2D HMBC spectra. The 2D experiments provided H–H and H–C through-bond correlations that assisted the NMR signal assignment and confirmed the synthesized structure. For instance, Figure 2 shows the 2D TOCSY spectrum of m-2-HEAPr. The off-diagonal H–H correlation peaks observed in this spectrum correspond to pairs of protons that are connected by covalent bonds to the same molecule and form part of the same coupled spin system. For each IL studied herein, the cation/anion ratio obtained from quantitative analysis of the nonexchangeable signals in the 1D proton spectra (see Figures S1–S6) is ca. 1 ± 0.06, which is in agreement with the expected value for an IL.

Study of the DOSY NMR Spectra. For each ¹H NMR signal, DOSY NMR experiments provided the self-diffusion coefficient of the molecular species to which the signal belonged. Figure 3 shows an example of the analysis of the DOSY diffusion decay curves of m-2-HEAPr at diffusion delays of (200, 300, and 400) ms. This figure shows similar decay curves for the nonexchangeable protons of the same charged component. Nevertheless, there is an unexpected difference between the cation and anion components that is beyond the experimental curve fitting error. Results of the analysis of the DOSY experiments of the other ILs studied herein are given in Table 1 and show that the same situation occurs for the other ILs studied herein, except for m-2-HEAF.

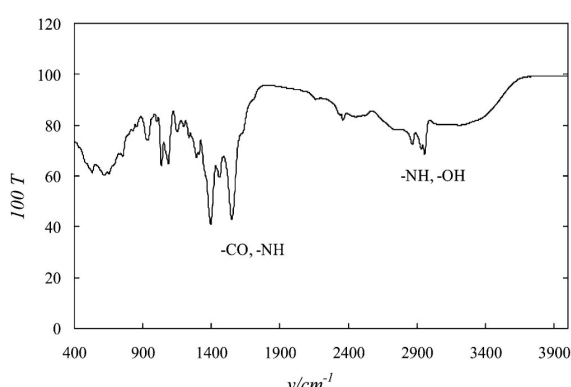


Figure 1. FT-IR spectrum for m-2-HEAPr.

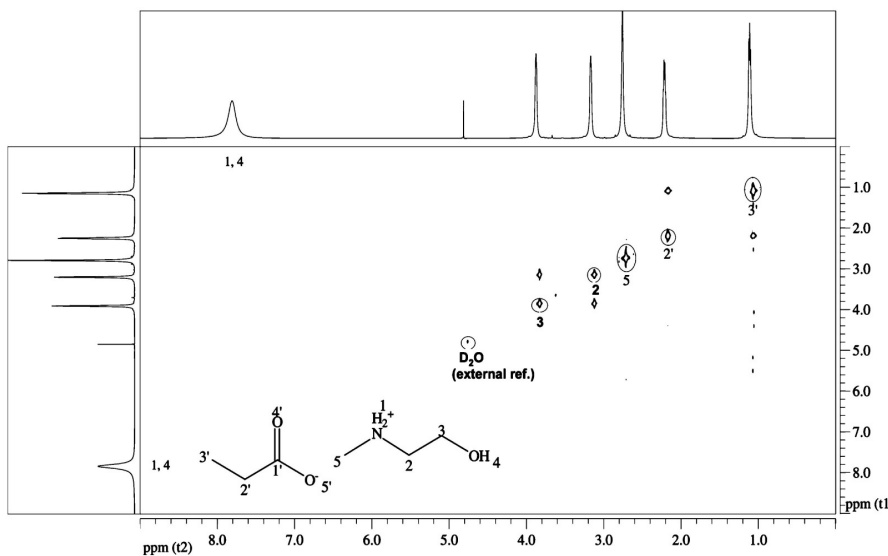


Figure 2. TOCSY spectrum for m-2-HEAPr. The vertical and horizontal traces shown correspond to the 1D proton spectrum. The broad NH_2^+ signal centered at ~ 7.5 ppm does not appear in the TOCSY spectrum because of its fast transverse relaxation.

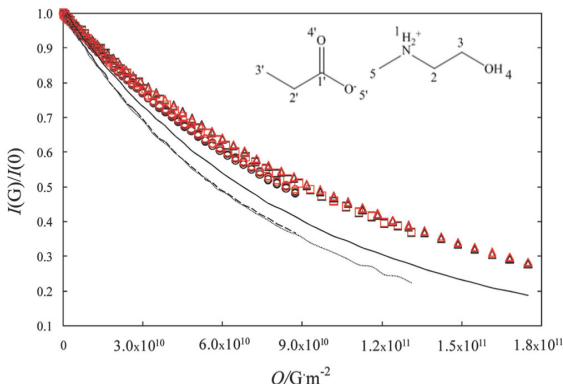


Figure 3. DOSY diffusion decay curves of m-2-HEAPr at three diffusion delays: ○ and dashed line, 200 ms; □ and dotted line, 300 ms; △ and solid line, 400 ms. The symbols are the values for the noninterchangeable species, in black and red for cations and anions, respectively. The lines are the values for the interchangeable species NH_2^+ .

Another observation from the diffusion results of Table 1 is that for all of the samples except m-2-HEAF, the diffusion coefficients of the nonexchangeable protons of the ILs in both the cationic and anionic species were affected by the specific diffusion time parameter that was used for the acquisition of the DOSY experiment. In the range of diffusion times studied, from (100 to 400) ms, the trend observed is that the self-diffusion coefficient systematically decreases with increasing diffusion time parameter. We verified that this trend is also present in a sample of m-2-HEAA mixed with 300 μ g of TSP as an internal diffusion reference compound. In this case, the diffusion measured for the TSP compound was similarly affected by the diffusion time of the experiment. These observations cannot be explained by the eventual presence of thermal convection in the IL samples,¹⁹ since this effect would increase the diffusion coefficient either with turbulent or constant laminar flux currents, while the observed effect was exactly the opposite. In this regard, the constant laminar flux was already eliminated with the compensated double-stimulated-echo¹⁶ version of the DOSY experiment that was used here.

Table 1. Analysis of the DOSY NMR Spectra Measured for the ILs Studied^a

<i>t</i> ms	<i>D</i> $10^{-12} m^2 \cdot s^{-1}$		
	<i>D</i> ⁺	<i>D</i> ⁻	<i>D</i> ^{NH_2^+}
<i>N</i> -Methyl-2-hydroxyethylammonium Formate			
0	35.7 ^b	57.0 ^b	
200	34.90 \pm 0.01	55.80 \pm 0.03	^c
300	34.10 \pm 0.01	54.60 \pm 0.03	^c
400	34.00 \pm 0.01	54.40 \pm 0.03	^c
<i>N</i> -Methyl-2-hydroxyethylammonium Acetate			
0	7.69 ^b	7.94 ^b	
200	6.72 \pm 0.03	7.02 \pm 0.04	9.23 \pm 0.08
300	6.01 \pm 0.02	6.30 \pm 0.02	7.88 \pm 0.03
400	5.69 \pm 0.02	6.03 \pm 0.02	7.86 \pm 0.04
<i>N</i> -Methyl-2-hydroxyethylammonium Propionate			
0	9.39 ^b	9.23 ^b	
200	8.41 \pm 0.02	8.29 \pm 0.02	11.8 \pm 0.05
300	7.68 \pm 0.02	7.65 \pm 0.02	11.7 \pm 0.06
400	7.36 \pm 0.01	7.30 \pm 0.02	10.0 \pm 0.05
<i>N</i> -Methyl-2-hydroxyethylammonium Butyrate			
0	10.5 ^b	9.64 ^b	
200	9.46 \pm 0.05	8.66 \pm 0.04	20.2 \pm 0.01
300	8.66 \pm 0.03	7.88 \pm 0.03	17.9 \pm 0.01
400	8.36 \pm 0.03	7.60 \pm 0.02	16.5 \pm 0.01
<i>N</i> -Methyl-2-hydroxyethylammonium Isobutyrate			
0	10.8 ^b	10.0 ^b	
200	9.70 \pm 0.03	9.02 \pm 0.02	16.8 \pm 0.01
300	9.13 \pm 0.03	8.43 \pm 0.02	14.3 \pm 0.01
400	8.59 \pm 0.03	7.98 \pm 0.02	8.09 \pm 0.02
<i>N</i> -Methyl-2-hydroxyethylammonium Pentanoate			
0	11.2 ^b	10.4 ^b	
100	10.5 \pm 0.02	9.80 \pm 0.01	22.7 \pm 0.02
200	10.1 \pm 0.02	9.37 \pm 0.02	19.3 \pm 0.01
300	9.28 \pm 0.02	8.68 \pm 0.02	17.4 \pm 0.02

^a Symbol definitions: *t*, diffusion time used to encode/decode diffusion in the DOSY experiment; *D*⁺ and *D*⁻, average self-diffusion coefficients of the noninterchangeable signals of the cation and anion, respectively; *D* ^{NH_2^+} , apparent diffusion coefficient of the exchangeable proton signal of NH_2^+ . The \pm values are the uncertainties of the curve fitting.

^b Extrapolated value for 0 ms diffusion time. ^c Signal not detected because of fast relaxation.

The conclusion is that the NMR diffusion results possibly reflect the existence of an aggregation exchange equilibrium in

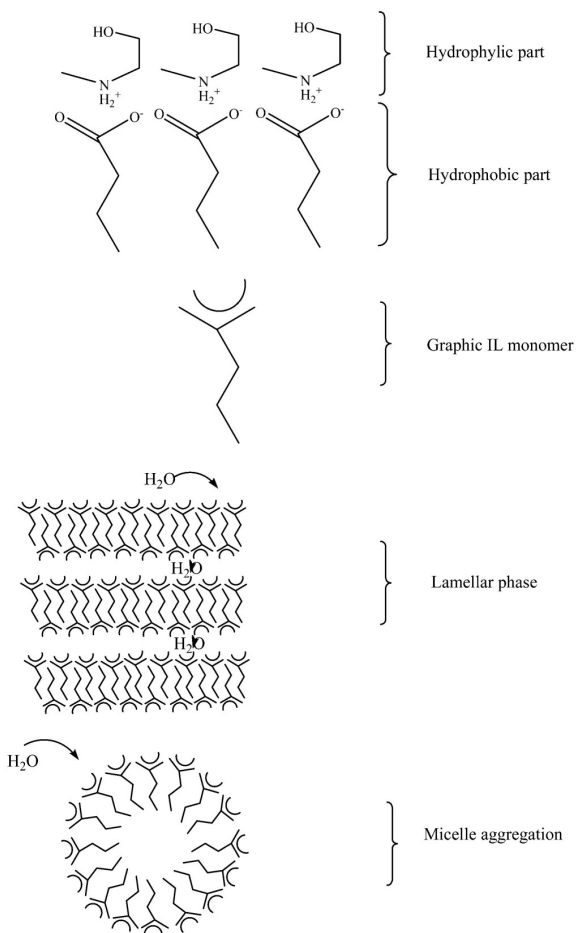


Figure 4. Scheme illustrating the postulated lamellar or micellar liquid-crystal phase of m-2-HEAB.

all of the IL samples except m-2-HEAF. The presence of aggregation is also supported by low-angle X-ray scattering measurements of m-2-HEAB. There is a peak corresponding to aggregates of a size between 9 and 15.5 Å, which is much larger than the optimized molecular modeling of m-2-HEAB in the monomeric state [radius of (3.2 to 3.5) Å]. Moreover, dilution studies recently conducted in our lab have shown the existence of a critical micelle concentration phenomenon in this type of IL (work in preparation).

We speculate that given the amphiphilic nature of these ILs, the alkyl chains of the anion may aggregate to form a lamellar or micellar liquid-crystal phase, as represented in Figure 4. Compartmental diffusion^{20,21} occurring in a lamellar/micellar phase would explain the dependence of the diffusion coefficient on the diffusion time in Table 1, including the anomalous case of m-2-HEAF, which lacks the alkyl chain and therefore would not form a lamellar/micellar phase nor exhibit a compartmental diffusion effect.

In the lamellar structure shown Figure 4, the highly hydrophobic alkyl chains of the anion molecules would be packed together in the lamellar/micellar phase, leaving the polar carboxylate anion head groups exposed to the hydrophilic interlamellar/micellar space, in close contact with the cation species and eventually with the water traces. In fact, the formation of lamellar/micellar phases is not uncommon in amphiphilic molecules.²²

In compartmental systems, the self-diffusion coefficients can be determined by setting a very low diffusion time parameter in the DOSY experiment. However, such an experiment would require special diffusion probes in the spectrometer hardware. A more feasible possibility is to extrapolate the determined self-diffusion coefficients in Table 1 to zero diffusion time, assuming a linear dependence with the diffusion time. Therefore, the self-diffusion coefficients corrected by this method correspond to the authentic diffusion of the species in the compartment.

The corrected values of the diffusion coefficients in Table 1 and the apparent viscosity data in Table 2 can be used to determine the corresponding effective molecular radius of the species by means of the Stokes–Einstein equation (eq 5), which assumes a spherical shape for the molecular entity. However, it was found that the effective radii thus obtained (data not shown) tend to be too small and do not have physical meaning for any of the samples studied except m-2-HEAF, which does not form the lamellar/micellar phase. Clearly, the assumption of spherical shape is not valid for the ILs studied, except in the case of m-2-HEAF.

One important observation from the data in Table 1 is the consistent difference between the diffusion coefficients determined for the cation (D^+) and anion (D^-) for the same sample and same diffusion time. These differences are very remarkable for m-2-HEAF, while for the other ILs the values are relatively more similar. In any case, these differences observed are beyond the experimental fitting error. This behavior is not totally explained by the different compartmental diffusion expected for the cation and anion species in the lamellar/micellar phase, since the m-2-HEAF sample also shows this behavior.

There exists the potential presence of neutral species in the IL mediated by proton exchange reactions (e.g., with the H_2O traces). Thus, the NMR signals of the nonexchangeable protons of one of the components may reflect the combined diffusion of both charged and neutral species that may eventually be different, as the neutral species is in principle the faster one. Therefore, the diffusion coefficients determined with the DOSY experiment and shown in Table 1 could reflect an average of both diffusion coefficients. On this basis, the faster diffusion obtained for the anion than the cation ($D^- > D^+$) in m-2-HEAF in Table 1 probably reflects the presence of relevant mole fraction of neutral formic acid in the sample.

It is also interesting to note from the diffusion coefficients of Table 1 the effect of the length of the alkyl chain. Clearly, the trend observed in these data is that the larger the alkyl chain, the faster is the self-diffusion coefficient of the IL species. This result possibly suggests that the larger the alkyl chain, the larger is the fluidity of the lamellar phase.

A final observation from the data in Table 1 is the diffusion coefficient of the broad signal of NH_2^+ centered at ~7.5 ppm, which is much larger than D^+ and D^- for all of the ILs studied. The diffusion coefficients determined for the NH_2^+ labile protons ($D^{NH_2^+}$) are apparent values, since the signal is affected by fast exchange with other labile protons, in particular with H_2O traces due to inherent sample hygroscopicity and possibly with the OH-4 proton. The detected fast chemical exchange of the NH_2^+ protons is consistent with the exposure of this group to the hydrophilic region in the lamellar/micellar phase model proposed in Figure 4.

Physicochemical Properties. The macroscopic physical properties of the ILs (density, speed of sound, apparent viscosity, and refractive index) were measured, and the results are given in the Supporting Information with the significant figures reported by the device.

Table 2. Molar Mass (M), Experimental Density (ρ), Sound Velocity (u), Refractive Index (n_D), Apparent Viscosity (η), and Molecular Radius (r) Values for the ILs at 298.15 K

	m-2-HEAF	m-2-HEAA	m-2-HEAPr	m-2-HEAB	m-2-HEAiB	m-2-HEAP
$M/\text{g}\cdot\text{mol}^{-1}$	121.135	135.162	149.188	163.215	163.215	177.241
$\rho/\text{g}\cdot\text{cm}^{-3}$	1.12825	1.10083	1.07127	1.03924	1.04337	1.01621
$u/\text{m}\cdot\text{s}^{-1}$	1815.3	1794.8	1690.0	1614.6	1611.3	1548.8
n_D	1.4458 ^a	1.4494	1.4534 ^b	1.4549	1.4511 ^c	1.4538 ^d
$\eta/\text{mPa}\cdot\text{s}$	20.27	106.06	215.06	298.15	163.08	234.44
$r/\text{\AA}$	2.17	2.27	2.37	2.46	2.46	2.55

^a $T = 298.35 \text{ K}$. ^b $T = 298.20 \text{ K}$. ^c $T = 298.05 \text{ K}$. ^d $T = 298.19 \text{ K}$.**Table 3.** Fitting Parameters for Physical Properties and Root-Mean-Square Deviations (σ) in Accordance with Equations 3 and 4 for the Six ILs

	$\rho/\text{g}\cdot\text{cm}^{-3}$	$u/\text{m}\cdot\text{s}^{-1}$	n_D	$\eta/\text{mPa}\cdot\text{s}$
<i>N</i> -Methyl-2-hydroxyethylammonium Formate				
A_2	$(2.3341 \pm 0.11) \pm 10^{-7}$	$(6.8704 \pm 0.22) \pm 10^{-4}$	$(8.4066 \pm 4.6) \pm 10^{-7}$	—
A_1	$(-6.9777 \pm 0.066) \pm 10^{-4}$	-2.3677 ± 0.013	$(-7.7232 \pm 2.8) \pm 10^{-4}$	3949.4 ± 80.0
A_0	1.3155 ± 0.001	2460.1 ± 2.1	1.60127 ± 0.043	$(3.7268 \pm 1.0) \pm 10^{-5}$
σ	4.4 ± 10^{-5}	0.1	1.4 ± 10^{-4}	0.6
<i>N</i> -Methyl-2-hydroxyethylammonium Acetate				
A_2	$(-3.6574 \pm 0.099) \pm 10^{-7}$	$(-1.7489 \pm 0.89) \pm 10^{-4}$	$(-1.5213 \pm 1.7) \pm 10^{-7}$	—
A_1	$(-3.8318 \pm 0.061) \pm 10^{-4}$	-2.4895 ± 0.055	$(-1.5188 \pm 1.0) \pm 10^{-4}$	5541.8 ± 130.0
A_0	1.2476 ± 0.00094	2552.9 ± 8.5	1.5082 ± 0.016	$(9.2245 \pm 4.1) \pm 10^{-7}$
σ	4.2 ± 10^{-5}	0.4	5.4 ± 10^{-5}	3.2
<i>N</i> -Methyl-2-hydroxyethylammonium Propionate				
A_2	$(-3.9113 \pm 0.096) \pm 10^{-7}$	$(7.8612 \pm 1.0) \pm 10^{-4}$	$(-3.2619 \pm 0.29) \pm 10^{-7}$	—
A_1	$(-4.1827 \pm 0.059) \pm 10^{-4}$	-3.4777 ± 0.062	$(-7.9162 \pm 1.8) \pm 10^{-5}$	5676.0 ± 61.0
A_0	1.2308 ± 0.00091	2657.4 ± 9.6	1.5060 ± 0.0027	$(1.1871 \pm 0.25) \pm 10^{-6}$
σ	4.0 ± 10^{-5}	0.4	9.4 ± 10^{-6}	3.9
<i>N</i> -Methyl-2-hydroxyethylammonium Butyrate				
A_2	$(-3.5249 \pm 0.090) \pm 10^{-7}$	$(3.2216 \pm 0.14) \pm 10^{-3}$	$(-6.8333 \pm 0.74) \pm 10^{-7}$	—
A_1	$(-4.6411 \pm 0.056) \pm 10^{-4}$	-5.1731 ± 0.086	$(1.1181 \pm 0.45) \pm 10^{-4}$	5848.1 ± 59.0
A_0	1.2090 ± 0.00085	2871.1 ± 13.0	1.4824 ± 0.0069	$(9.2333 \pm 1.8) \pm 10^{-7}$
σ	3.8 ± 10^{-5}	0.6	2.4 ± 10^{-5}	5.2
<i>N</i> -Methyl-2-hydroxyethylammonium Isobutyrate				
A_2	$(-5.1390 \pm 0.084) \pm 10^{-7}$	$(6.1754 \pm 0.69) \pm 10^{-4}$	$(-4.8174 \pm 2.9) \pm 10^{-7}$	—
A_1	$(-3.3539 \pm 0.052) \pm 10^{-4}$	-3.2309 ± 0.042	$(-1.1006 \pm 18.0) \pm 10^{-5}$	5004.3 ± 65.0
A_0	1.1891 ± 0.00079	2520.0 ± 6.5	1.4971 ± 0.027	$(8.5719 \pm 1.9) \pm 10^{-6}$
σ	3.5 ± 10^{-5}	0.3	9.7 ± 10^{-5}	2.6
<i>N</i> -Methyl-2-hydroxyethylammonium Pentanoate				
A_2	$(-3.3810 \pm 0.084) \pm 10^{-7}$	$(3.5359 \pm 0.12) \pm 10^{-3}$	$(-3.1521 \pm 3.7) \pm 10^{-7}$	—
A_1	$(-4.7268 \pm 0.052) \pm 10^{-4}$	-5.3202 ± 0.072	$(-1.1653 \pm 2.2) \pm 10^{-4}$	5340.6 ± 64.1
A_0	1.1873 ± 0.00079	2821.1 ± 11.0	1.5166 ± 0.034	$(3.9396 \pm 0.86) \pm 10^{-6}$
σ	3.5 ± 10^{-5}	0.5	1.2 ± 10^{-4}	4.6

The densities and speeds of sound for all of the ILs were studied from (278.15 to 338.15) K with a temperature step of 0.25 K. The viscosity was studied from (288.15 to 323.15) K with a temperature step of 2.5 K for m-2-HEAF, m-2-HEAPr, m-2-HEAB, and m-2-HEAP and 5.0 K for m-2-HEAA and m-2-HEAiB. The range studied for the refractive index was (280 to 323) K with a step of 5.0 K for all of the ILs. These data are provided in the Supporting Information. Table 2 shows the properties at 298.15 K, and Table 3 gives the values of the fitting parameters and the deviations for density, speed of sound, and refractive index (eq 3) and apparent viscosity (eq 4) for all temperatures studied. All but four of the fitting parameter values for the quadratic functions have uncertainties less than the respective parameter values.

For each IL sample, the effective radius r determined from the thermoacoustic data (eq 6) is given in Table 2. As discussed above, all of the studied ILs except m-2-HEAF form a lamellar/micellar phase. Systems forming lamellar/micellar phases do not fulfill the conditions for the applicability of the Stokes–Einstein equation (eq 5), and therefore, the effective radii determined with the thermoacoustic equation and given in Table 2 are likely to be more reliable for these systems. The data in Table 2 show that the effective radius increases with the length

of the alkyl chain, with the value being consistent with the sum of the sizes of the cation and anion in the ionic pair.

In Figures 5 to 8, the temperature trends of these physical properties are gathered. The isentropic compressibilities, κ_s , were calculated from the Newton–Laplace equation, and

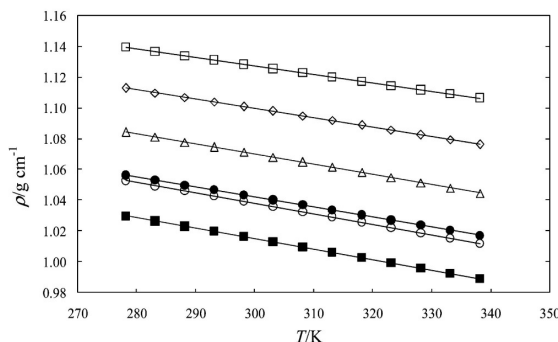


Figure 5. Selected data for the densities of the ILs as functions of temperature: □, m-2-HEAF; ◇, m-2-HEAA; △, m-2-HEAPr; ○, m-2-HEAB; ●, m-2-HEAiB; ■, m-2-HEAP. The solid lines show the corresponding fits to eq 3.

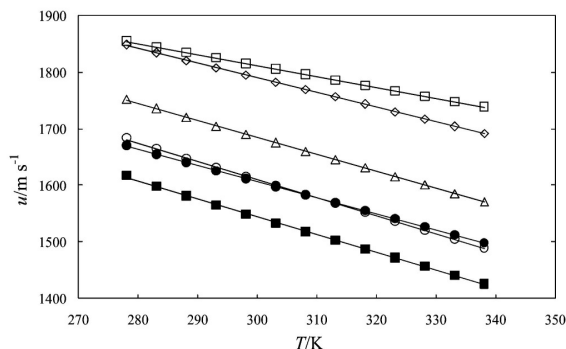


Figure 6. Selected data for the speeds of sound of the ILs as functions of temperature: □, m-2-HEAF; ◇, m-2-HEAA; △, m-2-HEAPr; ○, m-2-HEAB; ●, m-2-HEAiB; ■, m-2-HEAP. The solid lines show the corresponding fits to eq 3.

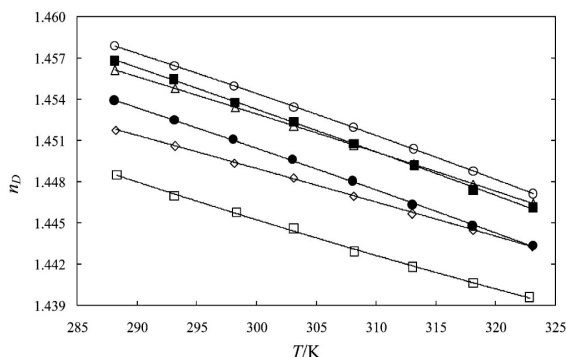


Figure 7. Refractive indexes of the ILs as functions of temperature: □, m-2-HEAF; ◇, m-2-HEAA; △, m-2-HEAPr; ○, m-2-HEAB; ●, m-2-HEAiB; ■, m-2-HEAP. The solid lines show the corresponding fits to eq 3.

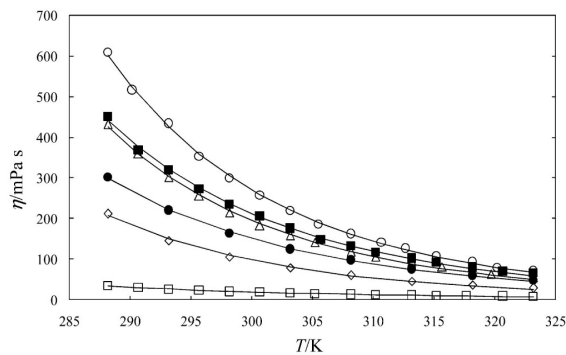


Figure 8. Viscosities of the ILs as functions of temperature: □, m-2-HEAF; ◇, m-2-HEAA; △, m-2-HEAPr; ○, m-2-HEAB; ●, m-2-HEAiB; ■, m-2-HEAP. The solid lines show the corresponding fits to eq 4.

these values for the six ILs are shown in Figure 9. These figures show a decreasing trend in the packing efficiency of the ILs as the molecular weight rises.

The measured apparent viscosities are shown in Figure 8. They exhibit Newtonian behavior, and their values vary exponentially with temperature. In Figure 8, the lowest viscosity corresponds to m-2-HEAF; this IL also shows the largest diffusion coefficient as determined by NMR (Table 1). However, for the other ILs, the NMR diffusion coefficients in Table 1 are relatively similar while the viscosity increases with the length of the alkyl chain (Figure 8). The observation that the enhancement in macroscopic viscosity is unrelated to the NMR diffusion coefficients suggests that the latter do

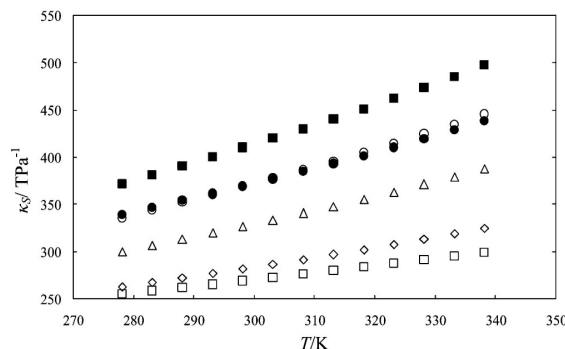


Figure 9. Isentropic compressibilities of the ILs as functions of temperature: □, m-2-HEAF; ◇, m-2-HEAA; △, m-2-HEAPr; ○, m-2-HEAB; ●, m-2-HEAiB; ■, m-2-HEAP.

not reflect the macroscopic diffusion of the IL but just the relatively much faster local or compartmental diffusion in the lamellar/micellar phase, which is in agreement with the nonapplicability of the Stokes–Einstein equation mentioned above.

The apparent viscosities and refractive indexes in Figures 7 and 8 increase with the length of the alkyl chain in the IL. The results for m-2-HEAP were unreliable because of its high hygroscopicity, which affected the measurements (data are shown).

The effect of temperature on the density, speed of sound, refractive index, and apparent viscosity can be seen in Figures 5 to 8. For all of the samples studied, there is an inverse relationship between these properties and the temperature, in agreement with the expectation for fluids.

Conclusions

Six ammonium-based Brønsted acid ILs have been synthesized, and their NMR spectra confirmed the molecular structures.

The diffusion NMR results suggest the existence of an ordered lamellar/micellar liquid-crystal phase for those ILs that contain an alkyl chain in the anion species. For systems forming lamellar/micellar phases, the inherent anisotropy suggests that local structure models should be applied to best explain the macroscopic behavior in terms of the molecular arrangement.

Acknowledgment

The advice from Dr. Bruno Dacuña Mariño (X-ray unit, USC) for suggestions, acquisition, and interpretation of X-ray data is greatly acknowledged.

Supporting Information Available:

Figures S1–S13 and Tables S1–S3. This material is available free of charge via the Internet at <http://pubs.acs.org>.

Literature Cited

- (1) Sheldon, R. Catalytic reactions in ionic liquids. *Chem. Commun.* **2001**, 2399–2407.
- (2) Bates, E. D.; Mayton, R. D.; Ntai, I.; Davis, J. H., Jr. CO₂ capture by a task-specific ionic liquid. *J. Am. Chem. Soc.* **2002**, *124*, 926–927.
- (3) Huddleston, J. G.; Willauer, H. D.; Swatloski, R. P.; Visser, A. E.; Rogers, R. D. Room temperature ionic liquids as novel media for “clean” liquid–liquid extraction. *Chem. Commun.* **1998**, 1765–1766.
- (4) Zhang, S.; Zhang, Q.; Zhang, Z. C. Extractive desulfurization and denitrogenation of fuels using ionic liquids. *Ind. Eng. Chem. Res.* **2004**, *43*, 614–622.

- (5) Fuller, J.; Carlin, R. T.; Osteryoung, R. A. The room temperature ionic liquid 1-ethyl-3-methylimidazolium tetrafluoroborate: Electrochemical couples and physical properties. *J. Electrochem. Soc.* **1997**, *144*, 3881–3886.
- (6) Marsh, K. N.; Boxall, J. A.; Lichtenthaler, R. Room temperature ionic liquids and their mixtures - A review. *Fluid Phase Equilib.* **2004**, *219*, 93–98.
- (7) Kato, R.; Gmehling, J. Activity coefficients at infinite dilution of various solutes in the ionic liquids $[\text{MMIM}]^+[\text{CH}_3\text{SO}_4]^-$, $[\text{MMIM}]^+[\text{CH}_3\text{OC}_2\text{H}_5\text{SO}_4]^-$, $[\text{MMIM}]^+[(\text{CH}_3)_2\text{PO}_4]^-$, $[\text{C}_2\text{H}_5\text{NC}_2\text{H}_5]^+[(\text{CF}_3\text{SO}_2)_2\text{N}]^-$ and $[\text{C}_5\text{H}_5\text{NH}]^+[\text{C}_2\text{H}_5\text{OC}_2\text{H}_4\text{OSO}_3]^-$. *Fluid Phase Equilib.* **2004**, *226*, 37–44.
- (8) Bicak, N. A new ionic liquid: 2-hydroxyethylammonium formate. *J. Mol. Liq.* **2005**, *116*, 15–18.
- (9) Greaves, T. L.; Weerawardena, A.; Fong, C.; Krodkiewska, I.; Drummond, C. Protic ionic liquids: solvents with tunable phase behavior and physicochemical properties. *J. Phys. Chem. B* **2006**, *110*, 22479–22487.
- (10) Iglesias, M.; Torres, A.; Gonzalez-Olmos, R.; Salvatierra, D. Effect of temperature on mixing thermodynamics of a new ionic liquid: {2-Hydroxyethylammonium formate (2-HEAF) + short hydroxylic solvents}. *J. Chem. Thermodyn.* **2008**, *40*, 119–133.
- (11) Cota, I.; Gonzalez-Olmos, R.; Iglesias, M.; Medina, F. New short aliphatic chain ionic liquids: synthesis, physical properties, and catalytic activity in aldol condensations. *J. Phys. Chem. B* **2007**, *111*, 12468–12477.
- (12) Iglesias M.; Garcia R.; Gonzalez-Olmos, R.; Salvatierra, D.; Mattedi S. Synthesis and influence of temperature on thermodynamic properties of new ionic liquids. Presented at the 1st International Congress on Green Process Engineering (GPE 2007), Toulouse, France, April 24–26, 2007.
- (13) Sierra, J.; Martí, E.; Mengibar, A.; González-Olmos, R.; Iglesias, M.; Cruañas, R.; Garau, M. A. Effect of new ammonium based ionic liquids on soil microbial activity. Presented at the 5th Society of Environmental Toxicology and Chemistry World Congress, Aug 3–7, 2008, Sydney, Australia.
- (14) Giernoth, R.; Bankmann, D.; Schlörer, N. High performance NMR in ionic liquids. *Green Chem.* **2005**, *7*, 279–282.
- (15) Cobas, J. C.; Sardina, F. J. Nuclear magnetic resonance data processing. MestRe-C: A software package for desktop computers. *Concepts Magn. Reson.* **2003**, *19A*, 80–96.
- (16) Jerschow, A.; Muller, N. Suppression of convection artifacts in Stimulated-Echo Diffusion experiments. Double-Stimulated-Echo experiments. *J. Magn. Reson.* **1997**, *125*, 372–375.
- (17) Iloukhani, H.; Rostami, Z. Measurement of some thermodynamic and acoustic properties of binary solutions of *N,N*-dimethylformamide with 1-alkanols at 30 °C and comparison with theories. *J. Solution Chem.* **2003**, *32*, 451–462.
- (18) Álvarez, V. H.; Larico, R.; Ianos, Y.; Aznar, M. Parameter estimation for VLE calculation by global minimization: Genetic algorithm. *Braz. J. Chem. Eng.* **2008**, *25*, 409–418.
- (19) Jerschow, A. Thermal convection currents in NMR flow profiles and implications for coherence pathway selection. *J. Magn. Reson.* **2000**, *145*, 125–131.
- (20) Shemesh, N.; Özarslan, E.; Bassar, P. J.; Cohen, Y. Measuring small compartmental dimensions with low-*q* angular double-PGSE NMR: The effect of experimental parameters on signal decay. *J. Magn. Reson.* **2009**, *198*, 15–23.
- (21) Sen, P. N. Time-dependent diffusion coefficient as a probe of geometry. *Concepts Magn. Reson.* **2004**, *23A*, 1–21.
- (22) Burdacea, G. Lyotropic liquid crystals I. Specific structures. *Rom. Rep. Phys.* **2004**, *56*, 66–86.

Received for review June 30, 2009. Accepted December 1, 2009. V.H.A. acknowledges the Movilidad Internacional Santander Scholarship. S.M. is thankful for the financial support for her postdoctoral leave from CNPQ-Brazil. They are also grateful for the support of the PF&PT research team at the University of Santiago de Compostela (USC) during their stay there. M.I. is thankful for the support of the Dirección Xeral de Investigación, Desenvolvimiento e Innovación, Consellería de Innovación e Industria (Xunta de Galicia, Spain).

JE900550V

Artigo 4.2: Synthesis and thermophysical properties of two new protic long-chain ionic liquids with the oleate anion

G Model
FLUID-8621; No. of Pages 9

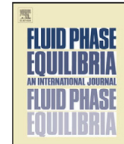
ARTICLE IN PRESS

Fluid Phase Equilibria xxx (2010) xxx–xxx



Contents lists available at ScienceDirect

Fluid Phase Equilibria
journal homepage: www.elsevier.com/locate/fluid



Synthesis and thermophysical properties of two new protic long-chain ionic liquids with the oleate anion

Víctor H. Álvarez^{a,b}, Silvana Mattedi^c, Manuel Martín-Pastor^d, Martín Aznar^b, Miguel Iglesias^{a,c,*}

^a Chemical Engineering Department – ETSE, University of Santiago de Compostela, P.O. Box 15782, Santiago de Compostela, Spain

^b School of Chemical Engineering, State University of Campinas, P.O. Box 6066, 13083-970 Campinas-SP, Brazil

^c Chemical Engineering Department, Polytechnic School, Federal University of Bahia, Rua Aristides Novis 2, Federação, 40210-630 Salvador-BA, Brazil

^d Unidade de Resonancia Magnética, RIADT, CACTUS, University of Santiago de Compostela, P.O. Box 15706, Santiago de Compostela, Spain

ARTICLE INFO

Article history:

Received 25 March 2010

Received in revised form 14 August 2010

Accepted 29 August 2010

Available online xxx

Keywords:

Ionic liquid

Synthesis

Thermodynamics

Aggregation equilibrium

ABSTRACT

This work reports the synthesis of 2-hydroxy ethylammonium oleate and bis(2-hydroxy ethyl)ammonium oleate ionic liquids, which have a long aliphatic chain as well as the study of some of their physical properties, in particular the effect of temperature on their density, speed of sound, viscosity, and refractive index. ¹H and ¹³C NMR spectra were used to characterize the chemical structure of the species in concordance with FT-IR spectra. DOSY NMR spectra were used to determine the self-diffusion coefficients of 2-hydroxy ethylammonium oleate ionic liquid, which were consistent with the formation of a lamellar or micellar liquid crystal phase; due the similar structure, a similar aggregation in the bis(2-hydroxy ethyl)ammonium oleate ionic liquid it is expected.

© 2010 Elsevier B.V. All rights reserved.

1. Introduction

In the last years, the environmental impact of substances has become an important aspect for the correct development of the industrial process. Currently, there are several new environmentally benign chemicals that can replace those that are harmful to the environment. Ionic liquids, which are composed of anion and cations of hydrophobic or hydrophilic nature, and often melt at low temperatures, are a good example of these chemicals. Ionic liquids have unique properties, such as low volatility, non-flammability, high thermal stability, and high solvation capacity, which allow them to be tailored as clean solvents in catalytic process, electrolytes for batteries, photochemistry, electro synthesis, among others [1–5]. Also, their liquid range can be as large as 300 °C, allowing for large reaction kinetic control and easy separation of organic molecules by distillation without loss of the ionic liquid.

Up to date, many ionic liquids have been based on the imidazolium cation and, in a lesser proportion, on alkyl pyridinium and trialkylamines [6]. Besides, ionic liquids can be classified in two types, aprotic ionic liquids (AILs) and protic ionic liquids (PILs). Protic ionic liquids are interesting because they have a high mobile proton, in addition to the classic tailored properties obtained by

changing the anion or cation with different alkyl chains [7]. PILs are produced through proton transfer from a Brønsted acid to a Brønsted base. In this way, Bicak [8] synthesized an ionic liquid formed from the neutralization of monoethanolamine with formic acid. Greaves et al. [9] proposed different PILs from primary amines and organic and inorganic acids. Iglesias and co-workers [10–12] synthesized a family of these PILs by modifying the aliphatic chain of the organic acid and/or using secondary and tertiary hydroxylamines. These authors emphasized the low cost, simplicity of synthesis and different applications of this new ionic liquid family. Moreover, the very low toxicity of this kind of ionic liquids was verified [13]. Therefore, available physico-chemical properties or thermodynamic databases of this class of ionic liquid, either pure or in mixtures, can be of technological and/or theoretical interest.

Structural and physico-chemical properties of ionic liquids can be studied with conventional liquid NMR methods [14]. They can be useful to assess the chemical composition of the ionic liquids and for the quantitative analysis of the species. Besides, NMR DOSY (Diffusion Ordered SpectroscopY) experiments can be used to determine self-diffusion coefficients, which are related to the molecular size and viscosity. This paper presents the synthesis and study of two ammonium based protic ionic liquids with long-chain anion, 2-hydroxy ethylammonium oleate (2-HEAO) and bis(2-hydroxy ethyl)ammonium (2-HE₂AO). Density, speed of sound, refractive index, and apparent viscosity were studied for both ionic liquids, and the self-diffusion coefficient for the 2-HEAO.

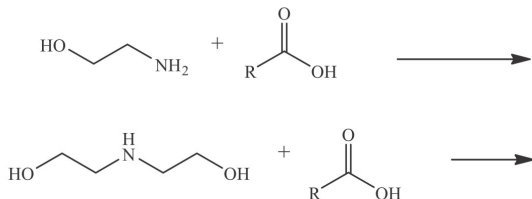
* Corresponding author. Tel.: +34 981 563 100x14216; fax: +34 981 595 012.
E-mail address: miguel.iglesias@usc.es (M. Iglesias).

2. Experimental**2.1. Materials**

Monoethanolamine and diethanolamine were obtained from Aldrich, with 99% purity by mass, while oleic acid was obtained from Sigma, with purity greater than 99.5% by mass. These components were used as received. During the course of the experiments, the purity of solvents was monitored by density and speeds of sound measurements.

2.2. Preparation of the ionic liquids

The amine was placed in a three-necked flask made entirely of glass, equipped with a reflux condenser, a PT-100 temperature sensor for temperature control, and a dropping funnel. The flask was mounted in a thermostatic bath. The oleic acid was added drop-wise to the flask under stirring with a magnetic bar. The reaction is a simple acid-base neutralization, producing an ester and a salt of 2-ethanolamine, which, in a general form, should be expressed as follows:



where R is the alkyl radical present in the oleic acid. These chemical reactions are exothermic, so an adequate temperature control is essential throughout the chemical reaction. The ionic liquid, a yellow liquid with graze appearance, was obtained when the reaction process and purification (strong agitation and slight heating for the vaporization of residual nonreacted acid for at least for 48 h) were completed. In order to decrease the water content as much as possible, the ionic liquid was dried for 48 h at 323 K under vacuum of 20 kPa with stirring, before each use.

Humidity in the ionic liquid was measured using a Karl–Fisher coulometric (Mettler–Toledo DL-32, Spain) titrator with Hydranal Coulomat E supplied by Riedel de Haen as anodic/cathodic solution. Due to the high viscosity of the fluids direct measurement are very difficult so the samples were diluted in absolute ethanol. The solution was gravimetric prepared with a precision balance (Mettler–Toledo ABS4-S/FACT), the humidity of the solvent and solution was measured and the ionic liquid humidity was calculated through a material balance.

2.3. Density, speed of sound, viscosity and refractive index measurements

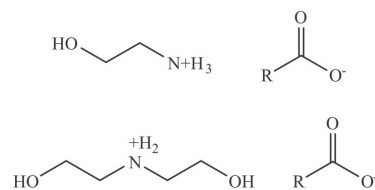
The densities and the speeds of sound of the pure liquids were measured using a DSA 5000 digital vibrating tube densimeter (Anton Paar, Austria). The uncertainty is ± 0.01 K for temperature, $\pm 2 \times 10^{-6}$ g cm $^{-3}$ for density, and ± 0.01 m s $^{-1}$ for speed of sound. Dry air and distilled water were used as reference fluids to calibrate the densimeter at each temperature. The mass of each component was determined on a Kern 770 mass balance with an accuracy of $\pm 1 \times 10^{-4}$ g. The apparent viscosities of ionic liquids were analyzed using a Visco Elite L rheometer (Fungilab, Spain) at different temperatures. The spindles used were the TL5 and L4, and the speed ranges were selected in accordance with torque range (minimum 10% and maximum 90%), as suggested by the manufacturer. The temperature was controlled with a thermostatic

bath (J.P. Selecta S.A., Spain) and measured with a calibrated thermometer. The refractive indexes were analyzed by an automatic digital RX-5000 refractometer (Atago, Japan) with an uncertainty of $\pm 1 \times 10^{-5}$ for the measurement. The temperature was controlled with a Frigiterm thermostatic bath (J.P. Selecta, Spain). The thermostatic bath has a temperature stability of ± 0.1 K, and it is measured with a PT sensor built-in the refractometer, with an uncertainty of ± 0.1 K.

2.4. FT-IR and NMR spectroscopy

The FT-IR spectra were obtained with a Varian FT-IR 670 spectrometer set to medium and high frequency spectra (7900–20 cm $^{-1}$), using the ATR method. The device has a resolution of 0.10 cm $^{-1}$ and a relation signal-noise of 5 s of 12,000:1 with 75% of light attenuation.

All the NMR experiments were performed at 298 K in an 11.7 T Varian Inova-750 spectrometer (operating at 750 MHz proton frequency). The NMR spectra were processed with the Mestre-C software [15].



Samples of 2-HEAO and 2-HE₂AO were studied by NMR. Sample preparation required only the transfer to a 5 mm NMR tube. An external reference standard capillary containing deuterated 3-(trimethylsilyl)-propionic-D4 acid (TSP) 0.1 M in dimethyl sulfoxide (DMSO) was introduced coaxially in the NMR tube. The TSP signal at ~0 ppm was used to determine the absolute concentrations in the 1D proton spectrum and the DMSO was used for deuterium lock. The integral of the ¹H NMR signal of TSP in the capillary was calibrated with a sample of sucrose 0.2 M dissolved in D₂O prepared in a 5 mm NMR tube. The anomeric glucose proton appearing at ~5.2 ppm was chosen for the calibration.

For each sample there were performed the following NMR experiments:

- (i) 1D-¹H NMR quantitative experiments were performed with a 33° pulse and a conveniently long interscan relaxation time (d_1 10 s). These conditions were used to assure the exactness of the signal integration.
- (ii) NMR spectra 1D ¹³C, 2D TOCSY, 2D HMQC and 2D HMBC were obtained using standard methodology.
- (iii) NMR DOSY experiments were performed with the convection compensated double stimulated echo sequence [16]. Diffusion encoding and decoding periods were made with pulse-field bipolar gradients, whose duration was 4 ms. The gradient power level (g in Eqs. (1) and (2) below) used for diffusion encoding-decoding was varied linearly between 2 and 62 G cm $^{-1}$ in 50 steps, with acquisition of the FID at each step. The DOSY experiments were repeated with 50, 100, 200 and 300 ms diffusion delay period.

The self-diffusion coefficients were calculated in each DOSY experiment by fitting the intensity of each NMR signals to the fol-

lowing equation [16]:

$$\frac{I(G)}{I(0)} = e^{-DQ} \quad (1)$$

where $I(G)$ is the signal integral in the presence of the gradient and $I(0)$ is the intensity of the signal with the lowest gradient, D is the self-diffusion coefficient and the gradient strength Q is calculated according to:

$$Q = q^2 \left(t + \frac{4\delta}{3} + \frac{5\tau_1}{4} + \frac{\tau_2}{4} \right) \quad (2)$$

where t is the diffusion delay used in the experiment and q and the delay variables (δ , τ_1 , and τ_2) are explained in the original Ref. [16].

The DOSY experiment is sensitive to reactions that may occur within any of molecules present in the sample. Two type of exchange reactions that were found to be relevant for the interpretation of the results in the study of 2-HEAO were:

i. *Exchange type I: DOSY and chemical exchange among labile protons.*

Labile protons of the IL may undergo fast chemical exchange with other labile protons and with the residual H_2O solvent. In such situation the observed diffusion coefficient for the NMR signal, D_{obs} , is an apparent diffusion coefficient that can be calculated from all the species that intervene according to Eq. (3) [17]

$$D_{obs} = \chi_A D_A + \chi_B D_B + \chi_C D_C + \dots \quad (3)$$

where A, B, C refers to the molecular species with exchangeable protons, D_A , D_B and D_C are their respective diffusion coefficients, and χ_A , χ_B , χ_C are their respective molar fractions, with $\chi_A + \chi_B + \chi_C + \dots = 1$.

ii. *Exchange type II: DOSY and bimolecular association.* Consider the case of bimolecular association equilibrium between the cation and anion of the IL that takes to the transient formation of an ion-pair with slow or intermediate exchange with the single species respect to the diffusion time scale. The DOSY experiment permit to detect this type of exchange when there is modulation in the determined diffusion coefficient of the non-labile protons respect to the diffusion delay time (Δ) used in the experiment [18].

3. Thermodynamic data treatment

The measured density, speed of sound and refractive index of the ionic liquids were correlated as a function of temperature in accordance to:

$$Z = A_0 + A_1 T + A_2 T^2 \quad (4)$$

where Z is density ($g\text{ cm}^{-3}$) or speed of sound (m s^{-1}) or refractive index, A_i represents the fitting parameters, and T is the absolute temperature (K). The apparent viscosity (η) was fitted with an Arrhenius type equation, normally used for Newtonian fluids:

$$\eta = A_0 e^{(A_1/T)} \quad (5)$$

where η is viscosity (mPa s), T is the absolute temperature (K), and A_i are adjustable parameters.

The ions were considered as large spherical shapes. Therefore, the effective radius of these molecules can be calculated using the Stokes-Einstein equation. In this formula, for the calculation of Brownian diffusivity, the diffusivity varies directly with absolute temperature and varies inversely with both viscosity and molecular radius:

$$D = \frac{kT}{r6\pi\eta} \quad (6)$$

where D is the Brownian diffusivity ($\text{m}^2\text{ s}^{-1}$), k is the Boltzmann's constant (J K^{-1}), T is the absolute temperature (K), η is the viscosity of the medium (Pa s) and r is the radius of the species.

In order to explore the strength and nature of the interactions between the ionic liquid species, the molecular radius, r , were calculated from the sound velocity and density data [19].

$$b = \frac{M}{\rho} - \left(\frac{RT}{\rho \cdot u^2} \right) \cdot \left(\left[1 + \frac{M \cdot u^2}{3RT} \right]^{1/2} - 1 \right) \quad (7)$$

$$r = \left(\frac{3b}{16\pi N_A} \right)^{1/3} \quad (8)$$

where b is the van der Waal's constant, M is the molecular weight, N_A is the Avogadro's number, and R is the universal gas constant.

4. Parameter estimation

For all models, the first approximation parameter estimation was performed using a genetic algorithm code, mMyGA, using a whole interval search [20]. After that, the fitting parameters were computed using a non-linear optimization procedure based on Marquardt algorithm. The regression was performed with the minimization of the standard deviation between experimental and calculated values, σ , defined as:

$$\sigma = \left[\sum_{i=1}^N \frac{(F_{exp} - F_{cal})_i^2}{N} \right]^{1/2} \quad (9)$$

where N is the number of experimental points and F_{cal} and F_{exp} are the calculated and experimental values of the property, respectively.

5. Results and discussion

The results of the FT-IR analyses were very similar for the two ionic liquids. The spectra showed a broad band in the $3500\text{--}2400\text{ cm}^{-1}$ range that is characteristic of the ammonium structure. The OH stretching vibration is embedded in this band. The broad band centered at 1600 cm^{-1} is a combined band of the carbonyl stretching and N–H plane bending vibrations. The FT-IR spectra with these bands are shown in Figs. S1 and S2 in the supplementary material.

NMR provided further insight in the chemical composition of the ionic liquids. The chemical composition was determined by combination of 1D ^1H , 1D ^{13}C , 1D ^{15}N , 2D-TOCSY, 2D-HMQC and 2D-HMBC. The 2D experiments provided H–H or H–C through-bond correlations that assisted the NMR signal assignment and confirmed the structure synthesized. For instance, the 2D TOCSY spectrum of 2-HE₂AO is shown in Fig. 1. The off-diagonal H–H correlations peaks observed in this spectrum correspond to a pair of protons that are connected by covalent bonds to the same molecule and are part of the same coupled spin system. For each ionic liquid studied here, the ratio cation:anion obtained from the quantitative analysis of the non-exchangeable signals in the ^1H proton spectra (see Fig. 2 and Fig. S3 in the supplementary material) is ca. 1 ± 0.07 , which is in agreement with the expected for ionic liquids.

In equilibrium with air, the ILs 2-HEAO and 2-HE₂AO contains 0.0159 ± 0.0008 and 0.0126 ± 0.0008 of water in weight fraction. After the drying procedure, the humidity determined (expressed as water weight fraction) of 2-HEAO and 2-HE₂AO was 0.0058 ± 0.0009 and 0.0057 ± 0.0005 , respectively.

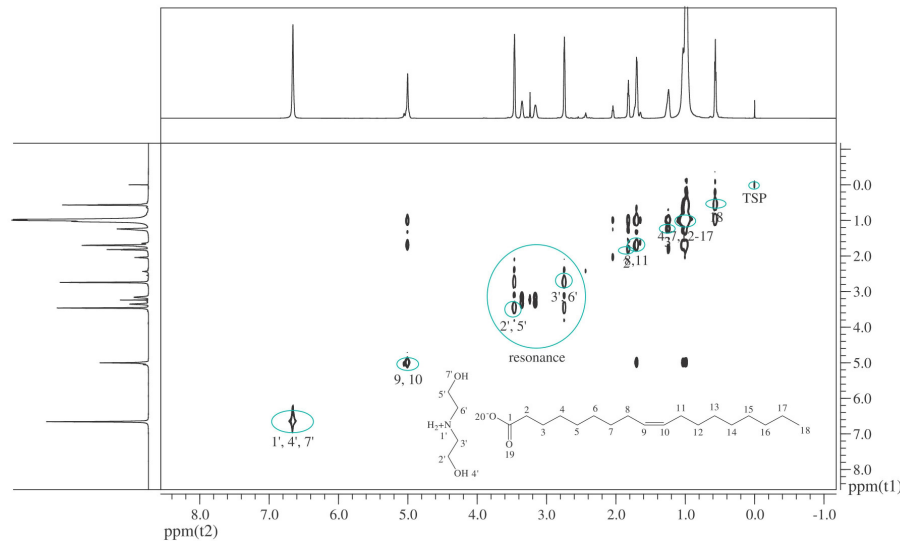


Fig. 1. TOCSY spectrum for the 2-HE₂AO. The vertical and horizontal traces shown correspond to the 1D proton spectrum.

5.1. Study of the exchange reactions by diffusion NMR experiments

DOSY NMR experiments based in the stimulated echo permit to determine the self-diffusion coefficient of the molecular species that generates a given NMR signal [12,16]. In the DOSY experiment, the intensity of a given NMR signal is attenuated by the diffusion of the species it belongs to as a function of the total gradient strength used in the experiment according to Eqs. (1) and (2). Fitting the signal intensities of the DOSY experiments for the 2-HEAO to the previous equations provided the results of Table 1; a similar behavior

is expected for the 2-HE₂AO. Then, the DOSY experiment was not done for the 2-HE₂AO ionic liquid.

For the discussion of the DOSY results, it is illustrative to consider the DOSY decay curves of Fig. 3 that correspond to the three different protons of 2-HEAO at 50 and 300 ms. The faster decay of the intensity of the labile NH₂⁺ protons at ~7.7 ppm respect to the other two signals gives an apparent diffusion coefficient for this signal faster than the non-exchangeable protons of the ethanol amine of 2-HEAO. This is reflected in the diffusion coefficients of Table 1, in which the diffusion of the NH₂⁺ group is much faster than D⁺ and D⁻ in the 2-HEAO. This result can be clearly attributed to the chemi-

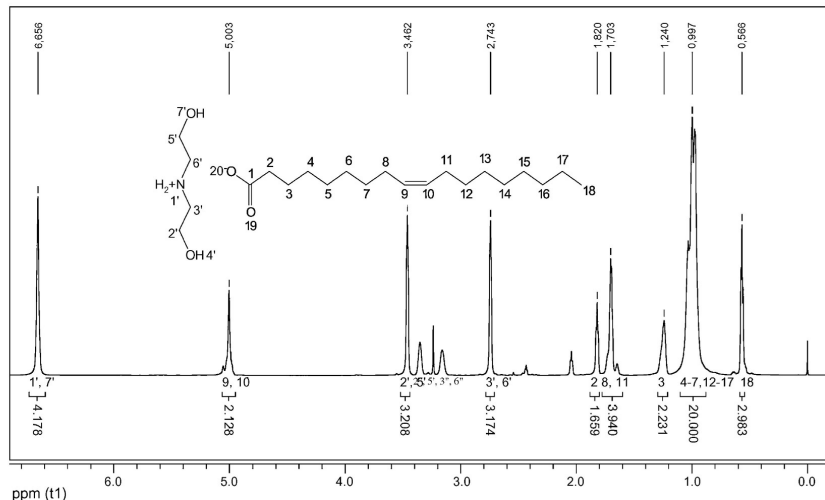


Fig. 2. 1D proton spectrum for the 2-HE₂AO at 353.15 K.

Please cite this article in press as: V.H. Álvarez, et al., Synthesis and thermophysical properties of two new protic long-chain ionic liquids with the oleate anion, *Fluid Phase Equilibr.* (2010), doi:10.1016/j.fluid.2010.08.022

Table 1

Analysis of the DOSY NMR experiments measured for the 2-HEAO at 353.15 K.

Δ (ms)	D^* ($\times 10^{-12} \text{ m}^2 \text{ s}^{-1}$)	D^- ($\times 10^{-12} \text{ m}^2 \text{ s}^{-1}$)	$D^{\text{NH}_2^+}$ ($\times 10^{-12} \text{ m}^2 \text{ s}^{-1}$)	r^* (Å)	r^- (Å)	
0	25,552 ^a	32,023 ^a			0.001	0.0001
50	31.6 ± 0.02	32.6 ± 0.01	39.3 ± 0.02		0.84	0.81
100	22.5 ± 0.02	21.6 ± 0.01	28.3 ± 0.02		1.18	1.23
200	17.1 ± 0.02	16.4 ± 0.02	22.8 ± 0.01		1.55	1.61
300	15.4 ± 0.02	14.7 ± 0.02	21.0 ± 0.02		1.72	1.81

^a Extrapolated value for 0.0001 ms diffusion time with the model: $D = a + bt^{0.5} + ct^{-0.5}$.

cal exchange of the labile protons of NH_2^+ with other labile protons (e.g. OH proton) in the sample and with H_2O traces due to its inherent hygroscopicity (exchange type I). On the other hand, in Fig. 3 the comparison of the DOSY decay curves of the non-exchangeable protons of cation and anion components of 2-HEAO show that their decays are very similar as expected if the two species were forming an ion-pair (see below).

Restricting our analysis to the non-exchangeable protons of 2-HEAO, the results of Table 1 show that, for both cation and anion, the determined diffusion coefficient is modulated by the specific diffusion time period Δ that is used in the DOSY experiment. In the range of Δ from 50 to 300 ms, the trend observed is that the self-diffusion coefficient systematically decreases the larger is the diffusion time parameter. This observation cannot be explained by the eventual presence of thermal convection in the IL samples [21], since this effect would increase the diffusion coefficient either with turbulent or constant laminar flux currents, while the effect observed is exactly the opposite. On this regard, the constant laminar flux is already eliminated with the compensated double-stimulated-echo [16] version of the DOSY experiment that was used here. The conclusion is that the NMR diffusion of Table 1 is possible reflecting an undergoing bimolecular association exchange equilibrium between the cation and anion species of 2-HEAO to form an ion-pair (exchange type II). Further evidence of the formation of the ion-pair in 2-HEAO was obtained from NOESY NMR experiments that proved the spatial proximity between the non-exchangeable protons of the cation and the anion (data not shown).

One important observation in the data of Table 1 is that there are consistent differences between the diffusion coefficients determined for the cation (D^*) and anion (D^-) species within the same sample and same diffusion delay period Δ . In any case, these differences observed are beyond the experimental fitting error. On this basis, the faster diffusion observed for one ion respect to the other in 2-HEAO in Table 1 is probably reflecting the presence of a certain

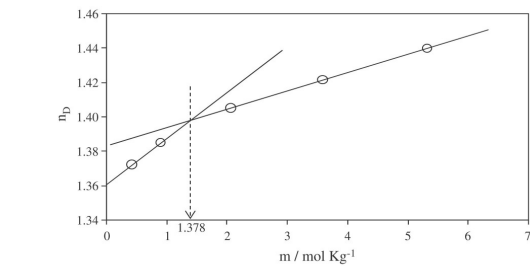


Fig. 4. Refractive index at 298.15 K vs. molality of 2-HEAO diluted in ethanol.

amount of the free anion and free cation species in the equilibrium that takes to the formation of the ion-pair both, with these free species having a slightly different diffusion.

The exchange of type II described in the analysis of the DOSY results of Table 1, also permits the possibility that a number of ion-pairs of 2-HEAO self-associate to form a high-molecular weight aggregate such as a lamellar phase or a micelle. On this regard, compartmental diffusion [22,23] occurring in a lamellar/micellar phase would explain the dependence of the diffusion coefficient with the diffusion delay period Δ in Table 1. Independent evidence of such aggregation process was obtained by measurement of the refractive index in dilution studies of 2-HEAO or 2- HE_2AO with ethanol as solvent. In Figs. 4 and 5 are represented the refractive index against the molality of 2-HEAO and 2- HE_2AO , respectively, with discontinuities at molality ~ 1.378 and ~ 0.914 , respectively. These discontinuities could indicate the presence of a critical micelle concentration (cmc). The analysis by low angle X-ray scattering of diluted samples of ILs below and above the cmc, (2-HEAO molalities of 0.4 and 2.2, and 2- HE_2AO molalities of 0.7 and 1.0), showed that the sample below the cmc does not lead to the formation of high-molecular weight aggregates, on the contrary, the sample with molality over the cmc shows a broad peak correspondingly to a high-molecular weight aggregate of a size between 25 and 30 Å, as can be seen in Figs. 6 and 7. In these figures, also can be appreciate a broad peak correspondingly to aggregates of a size between 3.5 and 4.5 Å. In

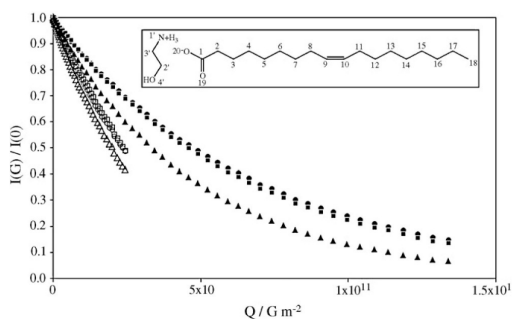
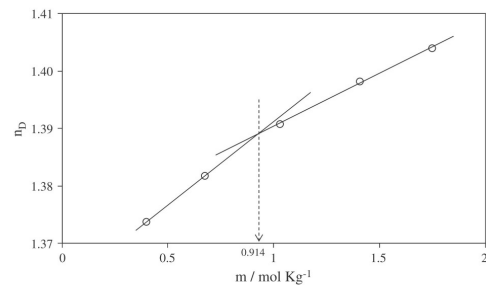


Fig. 3. DOSY signal intensity decay $I(G)/I(0)$ of different ^1H NMR signals of 2-HEAO as a function of the gradient strength Q applied. The open symbols are data at 50 ms and the closed symbols are data at 300 ms. The symbols (○) and (●) correspond to non-exchangeable ^1H NMR signals of the anion (9C) and cation (2C), respectively. The symbols (△) corresponds to the chemically exchangeable protons of the NH_2^+ group (1N).

Fig. 5. Refractive index at 298.15 K vs. molality of 2- HE_2AO diluted in ethanol.

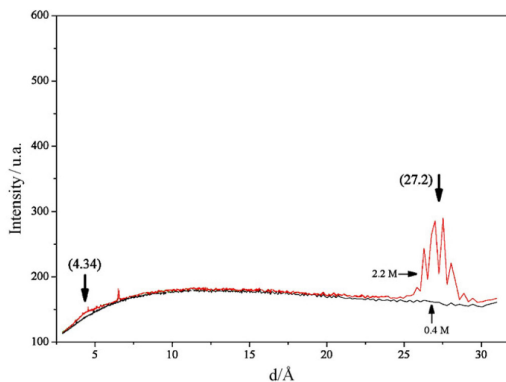


Fig. 6. Low angle X-ray scattering measurements for a mixture of ethanol + 2-HEAO with molalities of 0.4 M and 2.2 M

addition, this size is similar to the aggregates in aqueous mixtures of the 2-hydroxy ethylammonium acetate, as can be seen in Fig. 8. This size is similar for the three ILs indicating a similar aggregation for structure for the pair cation–anion and probably interchanging protons.

We speculate that given the amphiphilic nature of these ILs, the alkyl chains of the anion may aggregate to form a liquid crystal lamellar or micellar phase that is represented in Fig. 9. In the lamellar structure shown Fig. 9, the highly hydrophobic alkyl chains of anion molecules would be packed together in the lamellar/micellar phase leaving the polar carboxylate anion head exposed to the hydrophilic inter-lamellar/micellar space, in close contact with the cation species and eventually with the water traces. In fact, the formation of lamellar/micellar phases is not uncommon in amphiphilic molecules [24].

In compartmental systems, the DOSY self-diffusion coefficients can be determined by setting a very low diffusion period parameter in the DOSY experiment [22,23]. However, such experiment would require special diffusion probes in the spectrometer hardware. A more feasible possibility is to extrapolate the determined self-diffusion coefficients in Table 1 to diffusion time assuming a nonlinear dependence with the diffusion time. Therefore, the self-diffusion coefficients corrected by this method correspond to the authentic diffusion of the species in the compartment. Thus, the

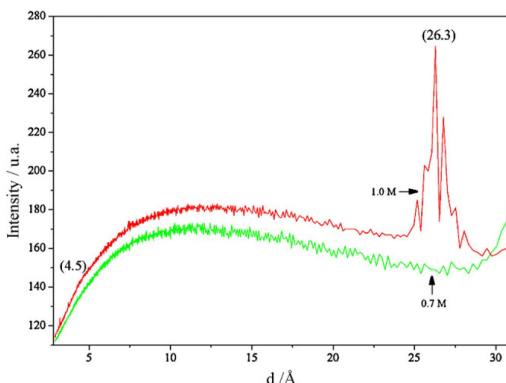


Fig. 7. Low angle X-ray scattering measurements for a mixture of ethanol + 2-HE₂AO with molalities of 0.7 M and 1.0 M

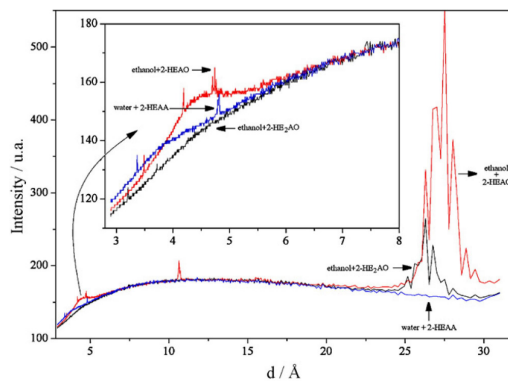


Fig. 8. Comparisons for low angle X-ray scattering measurements for a mixture of ethanol + 2-HEAO and ethanol + 2-HE₂AO at cmc concentrations and water + 2-HEAA at 2.2 M.

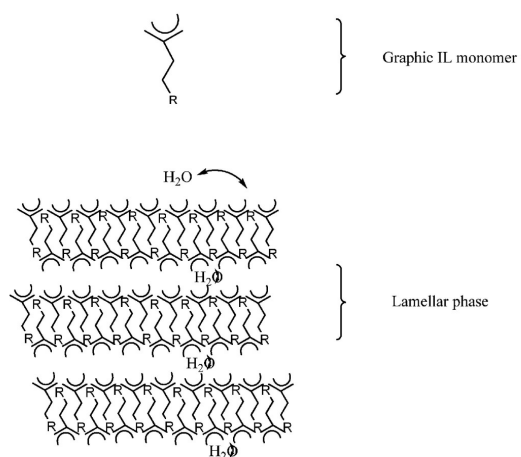
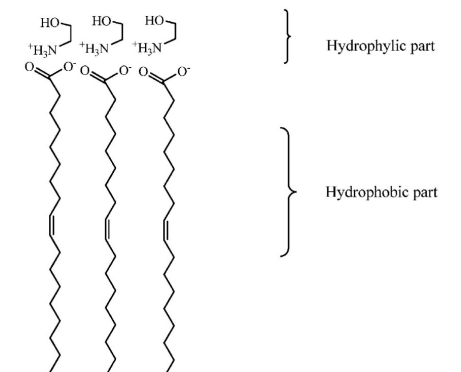


Fig. 9. Scheme of a lamellar liquid crystal phase of 2-HEAO.

Table 2

Molecular mass (M), experimental density (ρ), speed of sound (u), refractive index (n_D), molecular radius (r) at 298.15 K, and viscosity (η) at 353.15 K.

	2-HEAO	2-HE ₂ AO
$M/\text{g mol}^{-1}$	343.54	387.60
$\rho/\text{g cm}^{-3}$	0.936505	0.965108
$u/\text{m s}^{-1}$	1509.91	1521.33
n_D	1.48994	1.48855
$\eta/\text{mPa s}^a$	97.5	79.7
$r/\text{\AA}$	3.31	3.41

^a At 353.15 K.

corrected values of diffusion in Table 1 together with the viscosity data of Table 2 can be used to determine the correspondingly effective molecular radius of the species by means of the Stokes–Einstein equation in Eq. (6). The effective radii calculated with this method are given in Table 1. Clearly, the effective radii calculated from DOSY data suggest that this experiment is essentially reflecting the size of the cation and anion when they form the ion-pair and not that of the aggregate of a size between 25 and 30 Å.

For each IL sample, the effective radius determined with the thermo-acoustic equation in Eq. (8) in Table 2 is very different from the determined with the NMR diffusion coefficient of Table 1 and the Stokes–Einstein equation. Systems forming lamellar/micellar phases do not fulfill the conditions for the applicability of the Stokes–Einstein equation, and long aliphatic chain molecules do not fulfill the conditions for the applicability of the thermo-acoustic equation therefore the effective radius determined in Tables 1 and 2 are not reliable for these ILs.

5.2. Physicochemical properties

The macroscopic physical properties of the ionic liquids, densities, speed of sound, viscosity and refractive index were measured and they are given in supplementary material. Besides, the two ionic liquids are partially soluble in water and soluble in methanol or ethanol.

The density and speed of sound for all ionic liquids were studied from 278.15 to 338.15 K, with an interval of 0.25 K between each temperature. The viscosity was studied from 338.15 to 368.15 K, with an interval of 10 K between each temperature. The refractive index was studied between 278.15 and 333.15 K, with an interval of 10 K. Table 2 shows the properties at 298.15 K or 353.15 K, and Table 3 contains the fitting parameters and deviations for density, speed of sound and refractive index, by Eq. (4), and viscosity, by Eq. (5), for all temperatures studied.

The effect of temperature in the density, speed of sound, refractive index and apparent viscosity can be seen in Figs. 10–15. In all the samples studied there is an inverse relationship between these properties and the temperature, which is in agreement with the

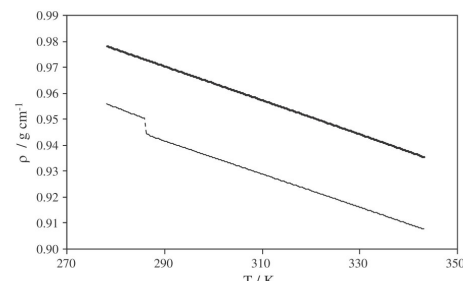


Fig. 10. Density. (—) 2-HEAO, (—) 2-HE₂AO.

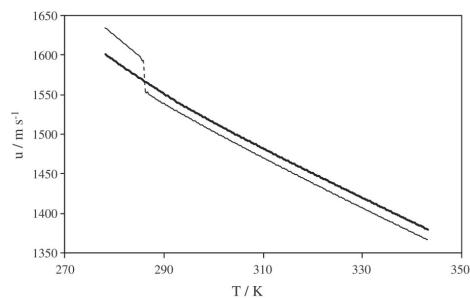


Fig. 11. Speed of sound. (—) 2-HEAO, (—) 2-HE₂AO.

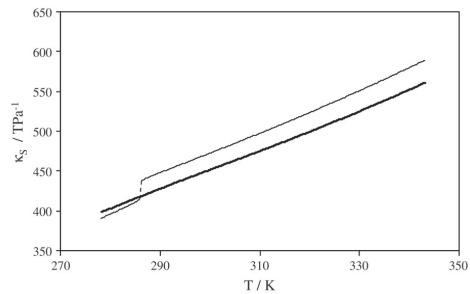


Fig. 12. Isentropic compressibility vs. temperature. (—) 2-HEAO, (—) 2-HE₂AO.

Table 3

Fitting parameters for physical properties and root-mean-square deviations σ in accordance with Eqs. (4) and (5) for the ionic liquids.

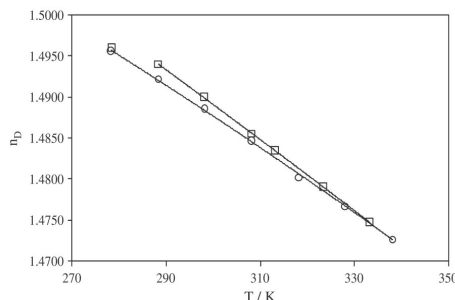
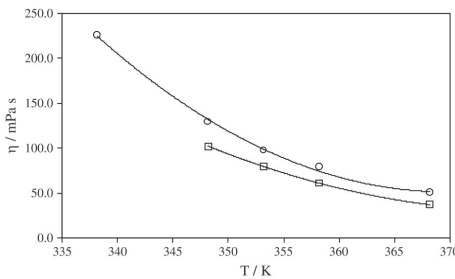
	$\rho/\text{g cm}^{-3}$	$u/\text{m s}^{-1}$	n_D	$\eta/\text{m Pa s}^{-1}$
2-hydroxy ethylammonium oleate				
A_0	-3.7744×10^{-8} ^a	5.6622×10^{-3} ^a	-1.7561×10^{-6}	1.2438×10^{-6} ^b
A_1	-6.1533×10^{-4} ^a	-6.8079 ^a	6.7200×10^{-4}	6429.4 ^b
A_2	1.1233 ^a	3036.7 ^a	1.4455	–
σ	5.1	0.4	$5.2e-4$	2.6
bis(2-hydroxyethyl)ammonium oleate				
A_0	-1.2656×10^{-7}	9.8505×10^{-3}	-2.6515×10^{-6}	9.5620×10^{-7} ^c
A_1	-5.7614×10^{-4}	-9.4434	1.2212×10^{-3}	6437.7 ^c
A_2	1.1482	3462.7	1.3606	–
σ	$2.0e-5$	1.2	$2.0e-3$	0.6

^a From 286.15 to 343.15 K.

^b From 338.15 to 369.15 K.

^c From 348.15 to 369.15 K.

Please cite this article in press as: V.H. Álvarez, et al., Synthesis and thermophysical properties of two new protic long-chain ionic liquids with the oleate anion, *Fluid Phase Equilibr.* (2010), doi:10.1016/j.fluid.2010.08.022

**Fig. 13.** Refractive index vs. temperature. (○) 2-HEAO, (□) 2-HE₂AO, (solid line) fit.**Fig. 14.** Apparent viscosity vs. temperature over the melting point. (○) 2-HEAO, (□) 2-HE₂AO, (solid lines) fit.

expected for fluids. The isentropic compressibility (Fig. 12) were calculated from the Newton–Laplace equation and refractive index (Fig. 13) show a decreasing trend in the packing efficiency for the 2-HE₂AO, the compound with a larger alkyl chain in the cation. Also, these figures show an inflection at ~287 K for the 2-HEAO, that can be explained for the formation of a new molecular structure, as a new physical phase.

The viscosities are shown in Figs. 14 and 15. Both ionic liquids have a Newtonian behavior from 338.15 up to 368.15 K and their value varies exponentially with temperature. Besides, the both ionic liquids show a non-Newtonian behavior below 338.15 K. The observation that the enhancement in macroscopic viscosity is unrelated with the NMR diffusion coefficients suggests that the later are not reflecting the macroscopic diffusion of the ionic liquid but just the relatively much faster local or compartmental diffu-

sion in the lamellar/micellar phase, which is in agreement with the non-applicability of the Stokes–Einstein equation commented above.

6. Conclusions

Two ammonium-based Brønsted acid ionic liquids with long aliphatic chain were synthesized: 2-hydroxy ethylammonium oleate and bis(2-hydroxy ethyl)ammonium oleate, and the NMR spectra confirmed the molecular structure. The diffusion NMR results, measurements of low angle X-ray scattering and index of refraction of dilute mixtures in ethanol suggest the existence of an ordered lamellar/micellar phase liquid crystal for those ionic liquids. On the other hand, the diffusion NMR data is rather insensitive to the diffusion of such large aggregate, and essentially reflect the diffusion of the single ion-pair. However, the observed dependence of the diffusion coefficient with the diffusion delay Δ of the experiment strongly suggests the effects of compartmental diffusion which is consistent with the formation of a lamellar/micelle phase. For systems forming lamellar/micellar phases, the inherent anisotropy suggests that local structure models should be applied in order to best explain the macroscopic behavior from the molecular arrangement.

List of symbols

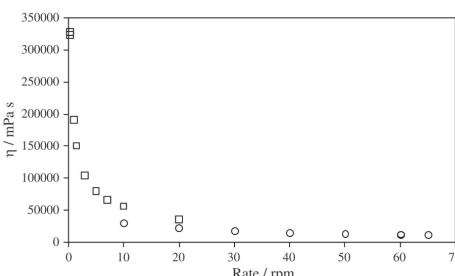
Δ	diffusion delay period used to encode–decode diffusion in the DOSY experiment
D^+	average self-diffusion coefficients of the non-interchangeable signals of cation
D^-	average self-diffusion coefficients of the non-interchangeable signals of anion
$D_{\text{NH}_2^+}$	apparent diffusion coefficient of the exchangeable proton signal of NH_2^+
r^+	effective radius of the cation calculated with the Stokes–Einstein equation
r^-	effective radius of the anion calculated with the Stokes–Einstein equation
k	Boltzmann's constant
AILs	aprotic ionic liquids
NMR	nuclear magnetic resonance
n_D	refractive index
PILs	protic ionic liquids
u	speed of sound

Greek letters

η	viscosity
σ	standard deviation between experimental and calculated values
κ_S	the isentropic compressibilities
ρ	density

Acknowledgments

V.H. Álvarez acknowledges the Mobilidade Internacional Santander scholarship and the FAPESP (Fundação de Amparo à Pesquisa do Estado de São Paulo), Process No. 2006/03711-1. S. Mattedi thanks the financial support for her postdoctoral leave from CNPq-Brazil. They also would like to thank the support of the PF&PT research team (USC) during their stay in Santiago de Compostela. Miguel Iglesias would like to acknowledge to the Fundación Ibercaja (Programa de Excelencia en Investigación 2009) for its support in developing this research. M. Aznar is the recipient of a CNPq-Brazil fellowship.

**Fig. 15.** Apparent viscosity vs. the rate of the spindle at 328 K. (○) 2-HEAO, (□) 2-HE₂AO.

Appendix A. Supplementary data

Supplementary data associated with this article can be found, in the online version, at doi:[10.1016/j.fluid.2010.08.022](https://doi.org/10.1016/j.fluid.2010.08.022).

References

- [1] R. Sheldon, Chem. Commun. 23 (2001) 2399–2407.
- [2] E.B. Bates, R.D. Mayton, I. Ntai, J.H. Davis Jr., J. Am. Chem. Soc. 124 (2002) 926–927.
- [3] J.G. Huddleston, H.D. Willauer, R.P. Swatloski, A.E. Visser, R.D. Rogers, Chem. Commun. 16 (1998) 1765–1766.
- [4] S. Zhang, Q. Zhang, Z.C. Zhang, Ind. Eng. Chem. Res. 43 (2004) 614–622.
- [5] J. Fuller, R.T. Carlin, R.A. Osteryoung, J. Electrochem. Soc. 144 (1997) 3881–3886.
- [6] K.N. Marsh, J.A. Boxall, R. Lichtenhaler, Fluid Phase Equilib. 219 (2004) 93–98.
- [7] R. Kato, J. Gmehling, Fluid Phase Equilib. 226 (2004) 37–44.
- [8] N. Bicak, J. Mol. Liq. 116 (2005) 15–18.
- [9] T.L. Greaves, A. Weerawardena, C. Fong, I. Krodkiewska, C. Drummond, J. Phys. Chem. B 110 (2006) 22479–22487.
- [10] M. Iglesias, A. Torres, R. Gonzalez-Olmos, D. Salvatierra, J. Chem. Thermodyn. 40 (2008) 119–133.
- [11] I. Cota, R. González-Olmos, M. Iglesias, F. Medina, J. Phys. Chem. B 111 (2007) 12468–12477.
- [12] V.H. Álvarez, N. Dosil, R. Gonzalez-Cabaleiro, S. Mattedi, M. Martin-Pastor, M. Iglesias, J.M. Navaza, J. Chem. Eng. Data 55 (2010) 625–632.
- [13] J. Sierra, E. Martí, A. Mengíbar, R. González-Olmos, M. Iglesias, R. Cruañas, M.A. Garau, 5th Society of Environmental Toxicology and Chemistry Congress, Sydney, Australia, 2008.
- [14] R. Giernoth, D. Bankmann, N. Schlörer, Green Chem. 7 (2005) 279–282.
- [15] J.C. Cobas, F.J. Sardina, Concepts Magn. Reson. 19 (2003) 80–96.
- [16] A. Jerschow, N. Muller, J. Magn. Reson. 125 (1997) 372–375.
- [17] K.S. Cameron, L. Fielding, Magn. Reson. Chem. 40 (2002) S106–S109.
- [18] A. Chen, C.S. Johnson Jr., M. Lin, M.J. Shapiro, J. Am. Chem. Soc. 120 (1998) 9094–9095.
- [19] H. Iloukhani, Z. Rostami, J. Sol. Chem. 32 (2003) 451–462.
- [20] V.H. Álvarez, R. Larico, Y. Iano, M. Aznar, Braz. J. Chem. Eng. 25 (2008) 409–418.
- [21] A. Jerschow, J. Magn. Reson. 145 (2000) 125–131.
- [22] N. Shemesh, E. Özarslan, P.J. Basser, Y. Cohen, J. Magn. Reson. 198 (2009) 15–23.
- [23] P.N. Sen, Concepts NMR 23A (2004) 1–21.
- [24] G. Burducea, Roman. Rep. Phys. 56 (2004) 66–86.

Please cite this article in press as: V.H. Álvarez, et al., Synthesis and thermophysical properties of two new protic long-chain ionic liquids with the oleate anion, Fluid Phase Equilibr. (2010), doi:[10.1016/j.fluid.2010.08.022](https://doi.org/10.1016/j.fluid.2010.08.022)

4.2. MISTURAS CONTENDO LÍQUIDOS IÔNICOS

A validação da metodologia utilizando a sílica-gel permitiu observar que a caixa de acrílico pode manter uma atmosfera seca menor que 10% durante 5 horas, tempo que a sílica-gel permanece de cor azul. Além deste tempo, mesmo na atmosfera de nitrogênio, a sílica-gel começa a mostrar uma coloração rosa, indicando a presença de umidade. Tempo suficiente para preparar as soluções binárias dos líquidos iônicos com os solventes.

4.2.1. PROPRIEDADES FÍSICO-QUÍMICAS

Nesta seção foram estudadas as interações entre solventes típicos orgânicos com líquidos iônicos, que geralmente são usadas na indústria em termos de densidade e velocidade do som em função da temperatura e concentração molar. Os volumes de excesso e desvio de compressibilidade isentrópica obtidas da densidade e velocidade do som foram calculados de modo a ampliar o conhecimento de como estes interagem com os líquidos iônicos e solventes. Os solventes estudados neste capítulo são ésteres (o mais usado no mundo inteiro), aldeídos (o mais usado no Brasil), etanol (devido ao seu uso importante no Brasil), metanol e água, dados experimentais apresentados na seguinte seção como artigos.

Artigo publicado:

O presente artigo estuda as propriedades volumétricas de soluções de solventes hidroxílicos e o líquido iônico 2-HEAA. Outros estudos de soluções binárias são apresentados juntos com dados do ELV, nos artigos do seguinte item.

Álvarez, V.H.; Mattedi, S.; Martin-Pastor, M.; Aznar, M.; Iglesias, M. Thermophysical properties of binary mixtures of ionic liquid 2-hydroxy ethylammonium acetate + (water, methanol or ethanol), *J. Chem. Thermodyn.*, submetido, 2010.

Artigo 4.3: Thermophysical properties of binary mixtures of ionic liquid 2-hydroxy ethylammonium acetate + (water, methanol or ethanol)

Víctor H. Álvarez^{a,d}, Silvana Mattedi^b, Manuel Martín-Pastor^c, Martín Aznar^a, Miguel Iglesias^{d¹}

^a*School of Chemical Engineering, State University of Campinas (UNICAMP), P.O. Box 6066,
13083-970, Campinas-SP, Brazil*

^b*Chemical Engineering Department, Polytechnic School, Federal University of Bahia (UFBA),
40210-630, Salvador-BA, Brazil*

^c*Unidade de Resonancia Magnética, RIAIDT, edif. CACTUS. University of Santiago de
Compostela (USC), P.O. Box 15706, Santiago de Compostela, Spain*

^d*Chemical Engineering Department – ETSE, University of Santiago de Compostela (USC), P.O.
Box 15782, Santiago de Compostela, Spain*

Abstract

In this work, density and speed of sound data of binary mixtures of an ionic liquid consisting of 2-hydroxy ethylammonium acetate (2-HEAA) + (water, methanol or ethanol) have been measured throughout the entire concentration range, from 288.15 K to 323.15 K at atmospheric pressure. The excess molar volumes, variations of the isentropic compressibility, the apparent molar volume, isentropic apparent molar compressibility and thermal expansion coefficient were calculated from the experimental data. The excess molar volumes were negative throughout the whole composition range. Compressibility data in combination with low angle X-ray scattering and NMR measurements proved that the presence of micelles formed due to ion pair interaction above a critical concentration of the ionic liquid in the mixtures. The Peng-Robinson equation of state coupled with the Wong-Sandler mixing rule and COSMO-SAC model was used to predict densities and the calculated deviations were lower than 3%, for binary mixtures in all composition range.

Keywords: protic ionic liquid; aggregation; intermolecular free length; COSMO-SAC

1. Introduction

Ionic liquids are organic salts which are liquid at room temperature. They have emerged as possible "green" solvents because they have very low vapor pressure and are stable within a wide temperature range and therefore have no polluting gas emissions. Through the adequate combination of cations and anions, the design of ionic liquids can enable the development of more efficient processes and products. Ionic liquids can be used as solvents in catalytic reactions [1], separation processes [2,3], electrolytic cells [4], heat transfer fluids [5] and other applications. However, there are two main problems with these new solvents: i) their resistance to photodegradation [6] and low biodegradability [7], turning them into persistent pollutants that break through classical treatment systems into natural waters; ii) their expensive production costs; for example, through using the task-specific ionic liquids designed by tethering amine

¹ Corresponding author: Tel.: + 34 981 563 100 ext.14216; fax: + 34 981 595 012. Email address:
miguel.iglesias@usc.es (M. Iglesias).

functional groups to improve the absorption of CO₂ the process costs are increased [8]. These facts have led to the search for a new class of ionic liquids.

Bicak [9] synthesized 2-hydroxy ethylammonium formate (2-HEAF) through the reaction of monoethanolamine with formic acid. Yuan et al. [10] and Iglesias and co-workers [11,12] synthesized several ionic liquids from this hydroxyl ethylammonium family, by modifying the aliphatic chain of the organic acid, emphasizing the low cost, simplicity of synthesis and different applications of this new family. Moreover, it was verified that some ionic liquids in this family present a negligible toxicity [13]. As a part of the characterization of these new compounds, physicochemical properties for pure ionic liquids and its mixtures with organic substances and water are of technological and theoretical interest.

Among several thermodynamic properties, volumetric and isentropic compressibilities are some of the most important for design and theoretical study. Previous studies [14] have shown that the addition of even small amounts of a low molecular weight solvent can dramatically increase or decrease the density and viscosity of ionic liquids. In a previous work, the densities and speed of sound for pure 2-HEAF and its binary mixtures with water, methanol or ethanol were studied [15].

Therefore, this work is a continuation of our research on the thermophysical properties of ammonium based ionic liquids. The ionic liquid 2-hydroxy ethylammonium acetate (2-HEAA) is synthesized and purified. The density and speed of sound data for the binary systems 2-HEAA + (water or methanol or ethanol) at temperatures from 298.15 up to 313.15 K over the whole composition range are reported at atmospheric pressure. The measured data is used to obtain the excess molar volumes, variations in the isentropic compressibility, the apparent molar volume, the apparent molar isentropic compressibility, and the thermal expansion coefficient of the mixtures. Compressibility data, in combination with low angle X-ray scattering and NMR measurements proved the formation of a complex mediated by ion pair interaction over a critical concentration of the ionic liquid in the mixtures.

2. Experimental

2.1. Materials and methods

Ethanolamine was obtained from Aldrich at 99 % purity by mass, while acetic acid was obtained from Sigma at 99.6 % purity by mass. The alcohols used in the preparation of the samples were supplied by Merck with purity levels greater than 99.6 % by mass. These compounds were used as received, without further purification. Double distilled deionized water was used for preparation of the solutions. During the experiments, the purity of solvents was monitored by density and speed of sound measurements. In Table 1, experimental density and speed of sound of pure compounds are compared with literature data. The pure compounds were protected from sunlight and maintained at constant humidity and temperature.

Table 1. Physical properties of pure compounds at 298.15 K and properties of the substances used in the modeling.

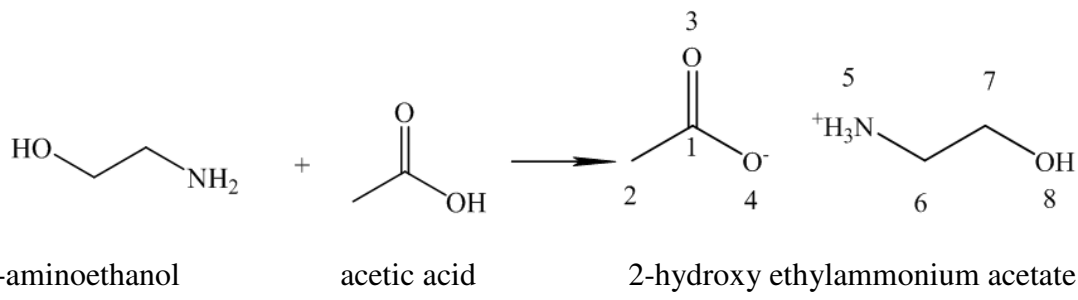
Compound	MM/ (g mol ⁻¹)	r/(Å)		ρ /(g cm ⁻³)		u/(m s ⁻¹)		T_c (K)	P_c (MPa)	ω	COSMO Segments ^g	V_{COSMO} (Å ³) ^g
		Exp.	Lit.	Exp.	Lit.	Exp.	Lit.					
2-HEAA	121.14	2.2	1.149039	-	1790.73	-	699.22 ^e	4.139 ^e	0.93590 ^e	717	160.550	
water	18.02	1.2	0.997040	0.99705 ^a	1496.89	1496.69 ^b	647.13 ^f	22.055 ^f	0.34486 ^f	136	25.750	
methanol	32.04	1.6	0.786710	0.78637 ^a	1102.98	1102.00 ^c	512.50 ^f	8.084 ^f	0.56583 ^f	258	48.548	
ethanol	46.07	1.8	0.785261	0.78493 ^a	1143.50	1143.00 ^d	514.00 ^f	6.137 ^f	0.64356 ^f	384	69.856	

^a[35], ^b[36], ^c[37], ^d[38], ^e[39], ^f[40], ^g[this work], MM : molecular mass, r : molecular radii, ρ : density, u : speed of sound, T_c : critical temperature, P_c : critical pressure, ω : Pitzer acentric factor, V_{COSMO} : molecular volume calculated by the COSMO salvation model.

Density and speed of sound of the pure liquids and mixtures were measured using a DSA 5000 density and speed of sound meter (Anton Paar) with accuracy of ± 0.01 K for temperature, $\pm 5 \times 10^{-6}$ g·cm⁻³ for density and ± 0.01 m·s⁻¹ for speed of sound. Dry air and double distilled deionized water was used as a reference fluid to calibrate the densimeter. The mass of each compound was determined on a Kern 770 mass balance with an accuracy of $\pm 1 \times 10^{-4}$ g.

2.2. Ionic liquid synthesis

Ethanolamine was placed in a triple necked glass flask equipped with a reflux condenser, a PT-100 temperature sensor for controlling temperature and a dropping funnel. The flask was mounted in an ice bath. The acetic acid was added dropwise to the flask while stirring with a magnetic bar. Stirring was continued for 24 h at room temperature in order to obtain a final viscous liquid. The reaction is a simple acid–base neutralization forming a Brønsted ionic liquid, as shown in Figure 1. Ionic liquid 2-HEAA is hygroscopic, and in order to decrease the water content as much as possible, it was dried for 48 h at room temperature under a vacuum of 20 kPa while stirring, before each use.



2.3. Experimental procedure

Each mixture was prepared with a known mass of ionic liquid and solvent, both injected into a glass vial using a syringe. The mixtures were sealed in the vials with an aluminum cap and a rubber plug. Also, the empty space in the vials was minimized, in order to avoid evaporation losses. The mixtures were injected into the DSA 5000 densimeter, and simultaneous measurements of density and speed of sound at each temperature and atmospheric pressure (≈ 100

kPa) were obtained. The density and speed of sound experimental uncertainties were less than $\pm 3 \cdot 10^{-5}$ g·cm⁻³ and ± 0.5 m.s⁻¹, respectively.

2.4. NMR spectroscopy

All the NMR experiments were performed at 298 K in a 17.6 T Varian Inova-750 spectrometer (operating at 750 MHz proton frequency). The spectra was processed with Mestre-C software [16].

Four NMR samples were prepared, pure 2-HEAA and three binary mixtures of 2-HEAA + water (molar ratio 30:70), 2-HEAA + methanol (molar ratio 30:70) and 2-HEAA + ethanol (molar ratio 40:60). Sample preparation required only the transfer of the mixture to a 5 mm NMR tube. An external reference standard capillary containing a deuterated 3-(trimethylsilyl)-propionic-D₄ acid (TSP) 0.1 M in DMSO that was introduced coaxially in the tube. The external DMSO was used for deuterium lock. The external TSP was used for chemical shift referencing of the ¹H and ¹³C NMR spectra (TSP resonates at 0 ppm in these two types of spectra). The external TSP proton signal was also used for the determination of absolute concentrations with the ¹H NMR spectra. For this task, the integral of the ¹H-NMR signal of TSP in the capillary was calibrated with respect to a sample of 0.2 M of sucrose dissolved in D₂O prepared in a 5 mm NMR. The anomeric glucose proton appearing at \approx 5.2 ppm was chosen for the calibration.

For each sample, a 1D-¹H NMR quantitative experiment was performed with a 33° pulse and a conveniently long interscan relaxation time (d_1 10 s). These conditions were used to assure the exactness of the signal integration. NMR spectra 1D ¹³C, 1D ¹⁵N, 2D TOCSY, 2D HMQC and 2D HMBC were acquired using standard methodology.

3. Data treatment

3.1. Volumetric and compressibility properties

The density and speed of sound for the mixtures were correlated by:

$$Z = \sum_{i=0}^p \left(\left(\sum_{j=0}^q B_{ij} T^j \right) x_1^{i-1} \right) \quad (1)$$

where Z is the density or speed of sound of the mixture, x_1 is the mole fraction of the solvent, p and q are the polynomial degrees, B_{ij} are the fitting parameters, and T is the absolute temperature. The excess molar volumes (V^E) and changes of isentropic compressibility ($\delta\kappa_S$) were calculated by:

$$V^E = \sum_{i=1}^N x_i M_i \left(\frac{1}{\rho} - \frac{1}{\rho_i} \right) \quad (2)$$

$$\delta\kappa_S = \kappa_S - \sum_{i=1}^N x_i \kappa_{Si} \quad (3)$$

where N is the number of compounds in the mixture, x_i is the mole fraction; M_i denotes molar mass; ρ_i is the density of the pure compound i , ρ is the density of the mixture, κ_S is the isentropic

compressibility of the mixture, κ_{Si} is the isentropic compressibility of the pure compound i calculated from the Newton-Laplace equation. These derived properties were fitted to a Redlich-Kister-type equation:

$$Q_{12} = x_1 x_2 - \sum_{i=0}^p \left(\left(\sum_{j=0}^q C_{ij} T^j \right) (x_1 - x_2)^i \right) \quad (4)$$

where Q_{12} is V^E or $\delta\kappa_S$ and the other variables are the same as above.

The apparent molar volume (ϕ_V) and the isentropic apparent molar compressibility, (ϕ_{κ_S} , $\text{cm}^3 \text{ mol}^{-1} \text{TPa}^{-1}$) were calculated by:

$$\phi_V = 1000 \left(\frac{\rho_1 - \rho}{m \rho_1 \rho} \right) + \frac{M_2}{\rho_1} \quad (5)$$

$$\phi_{\kappa_S} = 1000 \left(\frac{\kappa_S - \kappa_{S1}}{m \rho} \right) + \kappa_S \phi_V \quad (6)$$

where ρ is the density of the mixture, ρ_1 is the density of the solvent, M_2 is the molar mass of ionic liquid, m is the molality of the solution, κ_S is the isentropic compressibility of the solution and κ_{S1} is the isentropic compressibility of the solvent. These derived values were correlated by a modified Redlich–Mayer equation, where the fitting parameters show a temperature dependence:

$$\phi_F = \left(\sum_{j=0}^q \phi_{Fi}^o T^j \right) + \sum_{i=0}^p \left(\left(\sum_{j=0}^q \phi_{ij}^F T^j \right) m^{A_i} \right) \quad (7)$$

where F represents any apparent molar property and ϕ_{Fi}^o and ϕ_{ij}^F are fitting parameters.

The thermal expansion coefficient (α_P) shows the temperature dependence of volume, and is defined as:

$$\alpha_P = \frac{1}{V} \left(\frac{\partial V}{\partial T} \right)_P = - \left(\frac{\partial \ln \rho}{\partial T} \right)_P \quad (8)$$

3.2. Molecular radii and intermolecular free length

In order to explore the strength and nature of the interactions between the compounds, other thermodynamic properties were calculated from the speed of sound and density data. For pure components these properties are; the molar volume, V , the van der Waals constant, b , and the molecular radius, r [17]:

$$M = \sum_i^N x_i M_i \quad (9)$$

$$V = M / \rho \quad (10)$$

$$b = V - \left(\frac{RT}{\rho \cdot u^2} \right) \cdot \left(\left[1 + \frac{M \cdot u^2}{3RT} \right]^{1/2} - 1 \right) \quad (11)$$

$$r = \left(\frac{3b}{16\pi N_A} \right)^{1/3} \quad (12)$$

where N_A is the Avogadro number and R is the universal gas constant. The free length between the surfaces of the molecules [18], L_f , can be obtained by:

$$L_f = 2V_a / Y \quad (13)$$

where Y is the molar surface area and V_a is the available volume, calculated by

$$Y = (36\pi N V_o^2)^{1/3} \quad (14)$$

$$V_a = V - V_0 \quad (15)$$

$$V_0 = V(1 - T/T_c)^{0.3} \quad (16)$$

where V_o is volume at zero absolute temperature, and T_c is the critical temperature. For compounds without experimental critical properties data, such as ionic liquids, the method of Pandey et al. [19] can be applied to calculate the available volume.

3.3. Density predictions

The calculation of the molar volume of the mixture at a specific temperature and pressure can be predicted by an equation of state. The Peng-Robinson equation of state [20], coupled with the Wong-Sandler mixing rule [21] using the predictive liquid activity coefficient model COSMO-SAC [22] was used as a thermodynamic model to predict the density. In the COSMO model, for each compound, the equilibrium molecular geometry is first determined by minimization of the molecular energy at 0 K. The next step for COSMO-SAC calculation was to estimate the cavity volume (V_{COSMO}), the total number of segments (COSMO Segments), and the sigma profile of each compound. The calculations were done using the quantum chemistry package DMol3 built in the Accelrys Materials Studio v4.3. The sigma profile, $p(\sigma)$, is a file containing the probability of finding a surface segment with screening charge density, σ . The detailed settings for DMol3 can be found elsewhere [23] and, for the molecular description of the ionic liquid, the ion-pair approach [24] was used. The sigma profile of ionic liquid has been obtained for the molecule as a whole. The activity coefficient was then calculated [23]. The Peng-Robinson equation can be written in terms of the compressibility factor (Z) by:

$$Z^3 - (1-B)Z^2 + (A-3B^2-2B)Z - (AB-B^2-B^3) = 0 \quad (17)$$

where A and B are given by:

$$A = \frac{a_m P}{(RT)^2} \quad (18)$$

$$B = \frac{b_m P}{RT} \quad (19)$$

where the constants a_m and b_m are expressed as functions of the concentration of the different components in the mixture, through the so-called mixing rules. In this work, the Wong-Sandler mixing rules are used:

$$b_m = \frac{\sum_i \sum_j x_i x_j \left(b - \frac{a}{RT} \right)_{ij}}{1 - \sum_i \frac{x_i a_{ii}}{b_{ii} RT} - \frac{A_\infty^E}{\Omega RT}} \quad (20)$$

$$a_m = b_m \left[\sum_i \frac{x_i a_{ii}}{b_{ii}} + \frac{A_\infty^E}{\Omega} \right] \quad (21)$$

$$\left(b - \frac{a}{RT} \right)_{ij} = \frac{(b_{ii} + b_{jj})}{2} - \frac{(1 - k_{ij}) \sqrt{a_{ii} a_{jj}}}{RT} \quad (22)$$

In these equations, k_{ij} is the adjustable interaction parameter, $\Omega = \ln(\sqrt{2}-1)/\sqrt{2}$ for the PR EoS, and A_∞^E , the excess Helmholtz free energy at the limit of infinite pressure, can be calculated using the COSMO-SAC₅ activity coefficient model, and a_{ii} and b_{ii} are the EoS constants, defined as

$$a_{ii} = 0.457235(RT_c/P_c)^2 [1 + F(1 - T_r^{0.5})], \quad F = 0.37464 + 1.54226\omega - 0.26992\omega^2 \quad (23)$$

$$b_{ii} = 0.077796(RT_c/P_c) \quad (24)$$

where T_r is the reduced temperature, T_c is the critical temperature, P_c is the critical pressure, and ω is the Pitzer's acentric factor.

Equation 17 yields one or three real roots, depending on the number of phases in the system. It was shown that this model provides an excellent representation of the vapor-liquid experimental data [25]. For the prediction of the liquid density, the root of interest is the smallest positive one. An equation of state does not necessarily yield the accurate volumetric behavior of fluids and their mixtures. Therefore, a volume translation can be adopted in the equation of state, to improve the volumetric behavior [26]. Translation along the volume axis affects only the saturated density calculations, and leaves vapor pressure conditions unchanged [26]. This property may be exploited to improve the volume estimations made by the Peng-Robinson equation of state. Then, the correction value for each pure component (Δv_i) is given by the difference between the volume calculated by the thermodynamic model and the experimental volume:

$$\Delta v_i = V_{i,\text{exp}} - V_{i,\text{cal}} \quad (25)$$

where $V_{i,cal}$ is the molar volume of the compound i calculated by the thermodynamic model, and $V_{i,exp}$ is the experimental molar volume of the compound i . Then, the volume of the mixture was obtained using the correction of the volume applied by

$$V = V_{cal} + \sum_i \Delta v_i x_i \quad (26)$$

where x_i is the liquid molar fraction of the pure compound i , V_{cal} is the liquid molar volume of the mixture calculated with the thermodynamic model, and V is the predicted corrected molar volume of the mixture.

4. Parameter estimation

In this work, the first approximation parameter estimation was performed using a genetic algorithm code, mMyGA [27] using a whole interval search. After that, the fitting parameters were best tuned using a non-linear optimization algorithm based on the Marquardt algorithm. The optimization used the minimization of the standard deviation between experimental and calculated values, defined as:

$$\sigma = \left[\sum_{i=1}^N \frac{(F_{exp} - F_{cal})_i^2}{N-m} \right]^{1/2} \quad (27)$$

where N is the number of experimental points, m is the number of parameters in the curve fit, and F_{cal} and F_{exp} are the property values calculated by the model and obtained experimentally, respectively.

5. Results and discussion

The 2-HEAA ionic liquid is completely soluble in water, methanol and ethanol, and is not soluble in some alkanes such as n-octane and n-dodecane. The moisture in the LI's was not measured during the experiments of the properties, but comparisons were made of the measured density with standard mixtures of 2-HEAA with H₂O. The density shows low influence on the humidity. Thus, it was observed that values of the measured density for pure 2-HEAA are comparable with mixtures containing less than 1200 ± 130 ppm of H₂O. The humidity was determined using the DL31 Karl Fischer titrator (Mettler Toledo).

5.1. Volumetric and compressibility properties

Density and speed of sound data for some temperatures are presented in Tables 2 to 4. The complete data is presented in the supporting information. Table 5 contains the fitting parameters for equation (1). Figures 2 and 3 show these properties as a function of composition and temperature. These figures show a stronger inflection at dilute 2-HEAA-water mixtures, which is a very different shape than for other hydroxylic mixtures. In all figures, the black points represent the experimental data and the lines are the results for the fitted model.

Table 2. Density (ρ), speed of sound (u), isentropic compressibility (κ_s), isobaric expansibility (α), excess molar volume (V^E), change of isentropic compressibility ($\delta\kappa_s$), apparent molar volume (ϕ_V) and isentropic apparent molar compressibility (ϕ_{κ_s}) for binary mixtures water (1) + 2-HEAA (2) over the range of temperature (288.15-323.15) K.

water (1) + 2-HEAA (2)								
x_1	x_2	$\rho / (\text{g}\cdot\text{cm}^{-3})$	$u / (\text{m}\cdot\text{s}^{-1})$	$\kappa_s / (\text{TPa}^{-1})$	$V^E / (\text{cm}^3\text{mol}^{-1})$	$\delta\kappa_s / (\text{TPa}^{-1})$	$\alpha \times 10^3 / (\text{K}^{-1})$	$\phi_V / (\text{g cm}^{-3})$
$T = 323.15 \text{ K}$								
1.0000	0.0000	0.988040	1542.13	425.58	0.0000	0.00	0.4706	-
0.9490	0.0510	1.040148	1691.79	335.90	-0.3697	-82.88	0.4803	105.6
0.8981	0.1019	1.068467	1751.19	305.19	-0.5548	-106.81	0.4899	110.5
0.8037	0.1963	1.097974	1792.35	283.51	-0.7592	-115.92	0.5012	115.1
0.7106	0.2894	1.112140	1793.89	279.41	-0.8089	-107.61	0.5016	117.6
0.6041	0.3959	1.121292	1778.92	281.82	-0.7894	-91.01	0.5022	119.3
0.4984	0.5016	1.126361	1765.89	284.71	-0.7018	-74.04	0.5013	120.4
0.4179	0.5821	1.128951	1762.79	285.05	-0.6141	-62.97	0.4950	121.0
0.3163	0.6837	1.130791	1753.26	287.69	-0.4516	-46.79	0.4881	121.5
0.2237	0.7763	1.132672	1751.03	287.94	-0.3451	-34.20	0.4808	121.9
0.1239	0.8761	1.133996	1740.16	291.21	-0.2018	-17.63	0.4799	122.3
0.0863	0.9137	1.134359	1741.50	290.67	-0.1415	-13.17	0.4843	122.4
0.0000	1.0000	1.135075	1735.99	292.34	0.0000	0.00	0.4955	-
$T = 313.15 \text{ K}$								
1.0000	0.0000	0.992210	1529.34	430.91	0.0000	0.00	0.3846	-
0.9490	0.0510	1.044653	1692.01	334.37	-0.3674	-89.05	0.4465	105.1
0.8981	0.1019	1.073540	1759.23	300.98	-0.5600	-114.96	0.4632	110.0
0.8037	0.1963	1.103422	1807.09	277.52	-0.7692	-124.54	0.4882	114.6
0.7106	0.2894	1.117687	1811.06	272.78	-0.8199	-115.61	0.4935	117.1
0.6041	0.3959	1.126901	1797.72	274.58	-0.8017	-98.15	0.4962	118.8
0.4984	0.5016	1.131979	1785.34	277.15	-0.7142	-80.05	0.4948	119.9
0.4179	0.5821	1.134527	1782.34	277.46	-0.6239	-67.91	0.4897	120.5
0.3163	0.6837	1.136367	1773.15	279.89	-0.4616	-50.55	0.4875	121.0
0.2237	0.7763	1.138213	1771.26	280.03	-0.3522	-36.80	0.4849	121.4
0.1239	0.8761	1.139504	1760.85	283.03	-0.2058	-19.13	0.4854	121.8
0.0863	0.9137	1.139839	1762.29	282.49	-0.1429	-14.16	0.4888	121.9
0.0000	1.0000	1.140545	1757.17	283.96	0.0000	0.00	0.4973	-
$T = 303.15 \text{ K}$								
1.0000	0.0000	0.995650	1509.48	440.80	0.0000	0.00	0.2986	-
0.9490	0.0510	1.049299	1688.61	334.23	-0.3797	-98.14	0.4126	104.5
0.8981	0.1019	1.078395	1764.80	297.74	-0.5697	-126.24	0.4365	109.4
0.8037	0.1963	1.108745	1820.63	272.10	-0.7821	-136.28	0.4751	114.1
0.7106	0.2894	1.123167	1827.54	266.58	-0.8322	-126.43	0.4854	116.6
0.6041	0.3959	1.132471	1816.05	267.74	-0.8126	-107.67	0.4903	118.3
0.4984	0.5016	1.137555	1804.60	269.94	-0.7213	-88.02	0.4882	119.4
0.4179	0.5821	1.140067	1801.86	270.16	-0.6261	-74.50	0.4843	120.0
0.3163	0.6837	1.141902	1793.18	272.35	-0.4600	-55.54	0.4869	120.6
0.2237	0.7763	1.143669	1791.71	272.37	-0.3412	-40.23	0.4890	121.0
0.1239	0.8761	1.145068	1781.98	275.02	-0.1997	-21.10	0.4908	121.3
0.0863	0.9137	1.145431	1783.58	274.44	-0.1381	-15.47	0.4932	121.4
0.0000	1.0000	1.146216	1779.04	275.65	0.0000	0.00	0.4992	-
$T = 293.15 \text{ K}$								

1.0000	0.0000	0.998200	1482.53	455.80	0.0000	0.00	0.2126	-	-
0.9490	0.0510	1.053411	1681.43	335.77	-0.3960	-110.39	0.3788	103.8	-3326.1
0.8981	0.1019	1.082965	1768.09	295.38	-0.5870	-141.19	0.4098	108.9	8642.8
0.8037	0.1963	1.113953	1833.14	267.14	-0.8045	-151.59	0.4620	113.7	17878.3
0.7106	0.2894	1.128588	1843.39	260.75	-0.8540	-140.41	0.4774	116.2	22662.5
0.6041	0.3959	1.138005	1834.17	261.20	-0.8321	-119.84	0.4843	118.0	26114.5
0.4984	0.5016	1.143092	1823.86	262.99	-0.7352	-98.11	0.4817	119.1	28297.6
0.4179	0.5821	1.145540	1821.56	263.09	-0.6321	-82.81	0.4789	119.7	29312.4
0.3163	0.6837	1.147451	1813.61	264.96	-0.4659	-61.76	0.4863	120.3	30479.7
0.2237	0.7763	1.149335	1812.94	264.72	-0.3512	-44.52	0.4931	120.7	31080.3
0.1239	0.8761	1.150746	1804.56	266.86	-0.2068	-23.53	0.4963	121.0	31875.3
0.0863	0.9137	1.151087	1806.51	266.20	-0.1419	-17.09	0.4977	121.1	31963.9
0.0000	1.0000	1.151866	1803.21	267.00	0.0000	0.00	0.5010	-	-
<i>T = 288.15 K</i>									
1.0000	0.0000	0.999100	1466.40	465.46	0.0000	0.00	0.1696	-	-
0.9490	0.0510	1.055262	1676.33	337.23	-0.4061	-117.87	0.3618	103.4	-5837.2
0.8981	0.1019	1.085138	1768.92	294.51	-0.5988	-150.25	0.3965	108.6	6977.8
0.8037	0.1963	1.116518	1838.97	264.84	-0.8196	-160.73	0.4555	113.5	16803.6
0.7106	0.2894	1.131278	1851.11	257.97	-0.8685	-148.69	0.4733	116.1	21828.3
0.6041	0.3959	1.140754	1843.14	258.04	-0.8446	-126.96	0.4814	117.8	25407.4
0.4984	0.5016	1.145825	1833.58	259.59	-0.7431	-103.94	0.4784	118.9	27661.7
0.4179	0.5821	1.148341	1831.56	259.59	-0.6411	-87.59	0.4762	119.6	28718.1
0.3163	0.6837	1.150311	1824.35	261.20	-0.4759	-65.33	0.4860	120.1	29902.2
0.2237	0.7763	1.152168	1824.40	260.76	-0.3568	-46.95	0.4952	120.6	30513.3
0.1239	0.8761	1.153585	1817.14	262.53	-0.2102	-24.90	0.4990	120.9	31291.9
0.0863	0.9137	1.153920	1819.47	261.78	-0.1439	-18.01	0.4999	121.0	31378.9
0.0000	1.0000	1.154702	1817.23	262.25	0.0000	0.00	0.5020	-	-

Table 3. Density (ρ), speed of sound (u), isentropic compressibility (κ_S), isobaric expansibility (α), excess molar volume (V^E), change of isentropic compressibility ($\delta\kappa_S$), apparent molar volume (ϕ_V) and isentropic apparent molar compressibility (ϕ_{κ_S}) for binary mixtures methanol (1) + 2-HEAA (2) over the range of temperature (288.15-323.15) K.

methanol (1) + 2-HEAA (2)									
x_1	x_2	$\rho /$ (g·cm ⁻³)	$u /$ (m·s ⁻¹)	$\kappa_S /$ (TPa ⁻¹)	$V^E /$ (cm ³ mol ⁻¹)	$\delta\kappa_S /$ (TPa ⁻¹)	$\alpha \times 10^3 /$ (K ⁻¹)	$\phi_V /$ (g cm ⁻³)	$\phi_{\kappa_S} /$ (cm ³ mol ⁻¹ TPa ⁻¹)
<i>T = 323.15 K</i>									
1.0000	0.0000	0.762809	1021.99	1255.14	0.0000	0.00	1.2467	-	-
0.9508	0.0492	0.819344	1107.05	995.86	-0.7322	-211.90	1.1022	102.8	-93553.6
0.9049	0.0951	0.862394	1172.35	843.68	-1.1792	-319.86	0.9858	112.7	-50366.0
0.8013	0.1987	0.932105	1292.08	642.62	-1.4950	-421.18	0.8221	128.0	-2616.5
0.7100	0.2900	0.977831	1382.74	534.88	-1.5808	-441.03	0.7303	136.2	15066.7
0.6214	0.3786	1.011420	1455.93	466.43	-1.4769	-424.21	0.6688	141.9	25149.4
0.5175	0.4825	1.043940	1533.18	407.51	-1.3597	-383.12	0.6204	146.7	31858.8
0.3993	0.6007	1.072543	1603.68	362.53	-1.1052	-314.20	0.5633	150.7	36926.1
0.3289	0.6711	1.087182	1641.12	341.52	-0.9666	-267.46	0.5345	152.7	38941.3
0.2203	0.7797	1.106186	1661.68	327.40	-0.6989	-177.01	0.5224	155.1	43193.8
0.1703	0.8297	1.114370	1714.67	305.22	-0.6116	-151.08	0.4993	156.1	42032.5
0.0672	0.9328	1.128103	1712.30	302.34	-0.2982	-54.66	0.4945	157.8	45767.1
0.0000	1.0000	1.135075	1735.99	292.34	0.0000	0.00	0.4704	-	-
<i>T = 313.15 K</i>									

1.0000	0.0000	0.772458	1053.97	1165.38	0.0000	0.00	1.2358	-	-
0.9508	0.0492	0.828348	1137.85	932.43	-0.6914	-189.58	1.0779	102.7	-78323.9
0.9049	0.0951	0.870876	1202.11	794.61	-1.1133	-286.92	0.9662	112.2	-40585.8
0.8013	0.1987	0.939757	1320.02	610.69	-1.4075	-379.53	0.8090	127.0	1327.4
0.7100	0.2900	0.984961	1409.34	511.15	-1.4883	-398.60	0.7200	134.9	16857.5
0.6214	0.3786	1.018167	1481.29	447.61	-1.3880	-384.09	0.6597	140.4	25759.2
0.5175	0.4825	1.050423	1557.49	392.45	-1.2848	-347.69	0.6087	145.0	31629.3
0.3993	0.6007	1.078571	1627.38	350.08	-1.0341	-285.79	0.5560	149.0	36063.5
0.3289	0.6711	1.093067	1664.30	330.29	-0.9053	-243.55	0.5328	150.9	37829.3
0.2203	0.7797	1.112052	1683.43	317.31	-0.6683	-160.80	0.5223	153.2	41721.4
0.1703	0.8297	1.119912	1736.74	296.04	-0.5681	-138.03	0.5004	154.2	40536.5
0.0672	0.9328	1.133642	1733.82	293.44	-0.2843	-49.72	0.4975	155.9	43962.7
0.0000	1.0000	1.140545	1757.17	283.96	0.0000	0.00	0.4891	-	-
<i>T = 303.15 K</i>									
1.0000	0.0000	0.781983	1086.46	1083.37	0.0000	0.00	1.2248	-	-
0.9508	0.0492	0.837209	1168.82	874.32	-0.6506	-169.30	1.0535	102.7	-64822.6
0.9049	0.0951	0.879233	1232.00	749.33	-1.0483	-257.20	0.9466	111.8	-32021.5
0.8013	0.1987	0.947318	1348.07	580.87	-1.3207	-341.98	0.7959	126.1	4701.8
0.7100	0.2900	0.992018	1435.98	488.86	-1.3952	-360.25	0.7097	133.7	18337.2
0.6214	0.3786	1.024855	1506.71	429.81	-1.2966	-347.78	0.6506	139.0	26188.7
0.5175	0.4825	1.056745	1581.73	378.24	-1.1971	-315.45	0.5971	143.5	31333.1
0.3993	0.6007	1.084544	1651.03	338.25	-0.9536	-259.88	0.5487	147.3	35198.2
0.3289	0.6711	1.098865	1687.70	319.50	-0.8298	-221.79	0.5312	149.1	36727.2
0.2203	0.7797	1.117835	1705.67	307.49	-0.6196	-146.08	0.5223	151.4	40280.6
0.1703	0.8297	1.125586	1759.39	287.01	-0.5231	-126.20	0.5016	152.3	39070.0
0.0672	0.9328	1.139378	1756.27	284.54	-0.2715	-45.35	0.5006	154.0	42197.4
0.0000	1.0000	1.146216	1779.04	275.65	0.0000	0.00	0.5078	-	-
<i>T = 293.15 K</i>									
1.0000	0.0000	0.791418	1119.49	1008.22	0.0000	0.00	1.2139	-	-
0.9508	0.0492	0.845970	1199.77	821.20	-0.6112	-150.54	1.0291	102.6	-52607.7
0.9049	0.0951	0.887505	1262.08	707.38	-0.9865	-230.32	0.9270	111.4	-24534.7
0.8013	0.1987	0.954823	1376.31	552.90	-1.2390	-308.02	0.7829	125.1	7572.5
0.7100	0.2900	0.999035	1462.77	467.81	-1.3079	-325.44	0.6994	132.5	19536.7
0.6214	0.3786	1.031502	1532.41	412.84	-1.2103	-314.77	0.6415	137.6	26444.7
0.5175	0.4825	1.063019	1606.20	364.64	-1.1132	-285.98	0.5854	142.0	30954.7
0.3993	0.6007	1.090449	1675.24	326.77	-0.8744	-236.16	0.5414	145.7	34296.7
0.3289	0.6711	1.104702	1712.12	308.81	-0.7628	-201.96	0.5295	147.4	35587.5
0.2203	0.7797	1.123695	1728.63	297.82	-0.5813	-132.45	0.5222	149.7	38854.1
0.1703	0.8297	1.131238	1784.03	277.74	-0.4801	-115.48	0.5028	150.6	37571.2
0.0672	0.9328	1.145100	1781.08	275.29	-0.2602	-41.49	0.5036	152.2	40411.7
0.0000	1.0000	1.151866	1803.21	267.00	0.0000	0.00	0.5265	-	-
<i>T = 288.15 K</i>									
1.0000	0.0000	0.796694	1136.34	972.06	0.0000	0.00	1.2084	-	-
0.9508	0.0492	0.850323	1214.76	796.96	-0.5640	-140.17	1.0170	103.0	-45383.0
0.9049	0.0951	0.891619	1276.77	688.01	-0.9300	-216.52	0.9172	111.3	-20510.5
0.8013	0.1987	0.958564	1390.34	539.68	-1.1762	-291.32	0.7763	124.7	9002.7
0.7100	0.2900	1.002523	1476.08	457.81	-1.2442	-308.39	0.6943	131.8	20118.4
0.6214	0.3786	1.034793	1545.44	404.62	-1.1487	-298.73	0.6370	136.9	26532.0
0.5175	0.4825	1.066135	1618.37	358.12	-1.0561	-271.49	0.5796	141.1	30752.9
0.3993	0.6007	1.093447	1688.04	320.95	-0.8274	-224.69	0.5378	144.8	33790.9
0.3289	0.6711	1.107676	1725.14	303.35	-0.7245	-192.34	0.5287	146.5	34965.1

0.2203	0.7797	1.126677	1740.76	292.90	-0.5600	-125.69	0.5222	148.7	38103.9
0.1703	0.8297	1.134061	1797.77	272.83	-0.4533	-110.30	0.5033	149.6	36758.2
0.0672	0.9328	1.147970	1795.27	270.28	-0.2526	-39.64	0.5051	151.2	39445.2
0.0000	1.0000	1.154702	1817.23	262.25	0.0000	0.00	0.5359	-	-

Table 4. Density (ρ), speed of sound (u), isentropic compressibility (κ_s), isobaric expansibility (α), excess molar volume (V^E), change of isentropic compressibility ($\delta\kappa_s$), apparent molar volume (ϕ_V) and isentropic apparent molar compressibility (ϕ_{κ_s}) for binary mixtures ethanol (1) + 2-HEAA (2) over the range of temperature (288.15-323.15) K.

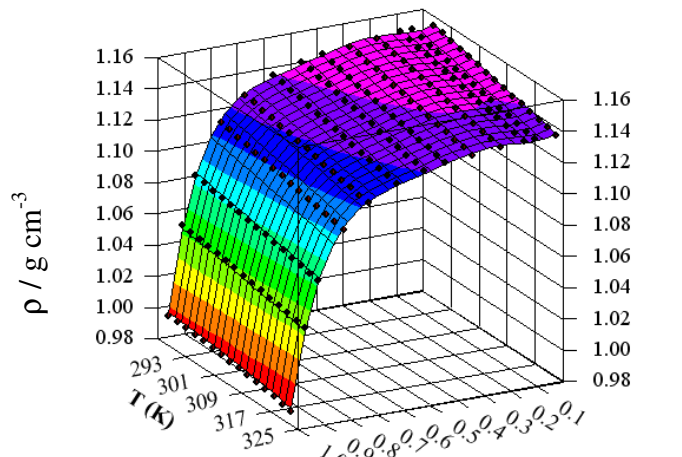
ethanol (1) + 2-HEAA (2)									
x_1	x_2	$\rho / (\text{g} \cdot \text{cm}^{-3})$	$u / (\text{m} \cdot \text{s}^{-1})$	$\kappa_s / (\text{TPa}^{-1})$	$V^E / (\text{cm}^3 \cdot \text{mol}^{-1})$	$\delta\kappa_s / (\text{TPa}^{-1})$	$\alpha \times 10^3 / (\text{K}^{-1})$	$\phi_V / (\text{g cm}^{-3})$	$\phi_{\kappa_s} / (\text{cm}^3 \cdot \text{mol}^{-1} \cdot \text{TPa}^{-1})$
$T = 323.15 \text{ K}$									
1.0000	0.0000	0.763296	1059.58	1166.92	0.0000	0.00	1.1736	-	-
0.9503	0.0497	0.800468	1104.68	1023.72	-0.4468	-99.73	1.0890	105.1	-50018.0
0.8990	0.1010	0.834368	1146.05	912.50	-0.7379	-166.09	1.0031	112.9	-22006.7
0.7990	0.2010	0.890443	1220.99	753.30	-0.9921	-237.81	0.8772	124.4	8689.9
0.6991	0.3009	0.938735	1310.52	620.25	-1.1682	-283.47	0.7446	132.5	19860.9
0.5943	0.4057	0.981801	1373.74	539.72	-1.2227	-272.35	0.7062	139.0	31929.1
0.5054	0.4946	1.013188	1436.95	478.00	-1.1724	-256.32	0.6563	143.5	36585.0
0.3970	0.6030	1.046544	1512.70	417.58	-1.0423	-222.00	0.6208	147.9	40057.2
0.3235	0.6765	1.066976	1559.36	385.44	-0.9493	-189.83	0.5777	150.5	41867.1
0.2082	0.7918	1.095472	1618.89	348.31	-0.7563	-126.15	0.5305	153.9	44545.9
0.1175	0.8825	1.115061	1667.21	322.64	-0.5472	-72.47	0.5152	156.2	45740.0
0.0461	0.9539	1.128270	1706.71	304.28	-0.2863	-28.39	0.4816	157.8	46298.7
0.0000	1.0000	1.135075	1735.99	292.34	0.0000	0.00	0.4706	-	-
$T = 313.15 \text{ K}$									
1.0000	0.0000	0.772204	1092.85	1084.29	0.0000	0.00	1.1428	-	-
0.9503	0.0497	0.809131	1137.22	955.64	-0.4258	-88.89	1.0595	104.8	-39947.6
0.8990	0.1010	0.842694	1177.60	855.73	-0.6956	-147.75	0.9787	112.4	-15023.9
0.7990	0.2010	0.898225	1250.96	711.42	-0.9280	-211.99	0.8602	123.6	11919.6
0.6991	0.3009	0.946069	1338.66	589.84	-1.0945	-253.60	0.7746	131.4	21573.7
0.5943	0.4057	0.988723	1400.95	515.32	-1.1470	-244.25	0.6976	137.7	32147.2
0.5054	0.4946	1.019833	1463.15	458.03	-1.1024	-230.39	0.6491	142.1	36168.3
0.3970	0.6030	1.052873	1537.67	401.70	-0.9818	-200.03	0.6109	146.4	39139.9
0.3235	0.6765	1.073170	1583.47	371.63	-0.9017	-171.24	0.5720	148.9	40694.5
0.2082	0.7918	1.101310	1642.51	336.57	-0.7166	-114.05	0.5347	152.2	42993.0
0.1175	0.8825	1.120845	1690.20	312.30	-0.5335	-65.71	0.5183	154.4	43993.6
0.0461	0.9539	1.133958	1729.87	294.70	-0.2891	-26.17	0.4985	155.9	44407.1
0.0000	1.0000	1.140545	1757.17	283.96	0.0000	0.00	0.4892	-	-
$T = 303.15 \text{ K}$									
1.0000	0.0000	0.780944	1126.50	1009.06	0.0000	0.00	1.1120	-	-
0.9503	0.0497	0.817614	1169.98	893.50	-0.4038	-79.12	1.0299	104.5	-31146.1
0.8990	0.1010	0.850864	1209.48	803.42	-0.6536	-131.58	0.9543	112.0	-9175.8
0.7990	0.2010	0.905897	1281.19	672.50	-0.8655	-189.13	0.8433	122.8	14535.4
0.6991	0.3009	0.953327	1367.04	561.30	-1.0221	-227.05	0.8046	130.3	22892.0
0.5943	0.4057	0.995593	1428.42	492.27	-1.0711	-219.22	0.6890	136.5	32162.4
0.5054	0.4946	1.026430	1489.56	439.09	-1.0294	-207.20	0.6419	140.7	35643.3
0.3970	0.6030	1.059371	1562.83	386.48	-0.9320	-180.36	0.6009	144.9	38174.9

0.3235	0.6765	1.079281	1607.96	358.36	-0.8412	-154.55	0.5663	147.3	39509.5
0.2082	0.7918	1.107257	1666.99	325.00	-0.6760	-103.37	0.5389	150.5	41440.7
0.1175	0.8825	1.126691	1714.49	301.94	-0.5112	-59.90	0.5215	152.7	42257.2
0.0461	0.9539	1.139621	1755.41	284.76	-0.2727	-24.71	0.5155	154.2	42499.5
0.0000	1.0000	1.146216	1779.04	275.65	0.0000	0.00	0.5078	-	-
<i>T = 293.15 K</i>									
1.0000	0.0000	0.789553	1160.63	940.22	0.0000	0.00	1.0812	-	-
0.9503	0.0497	0.825955	1203.03	836.55	-0.3818	-70.22	1.0004	104.2	-23390.2
0.8990	0.1010	0.858918	1241.51	755.35	-0.6142	-116.89	0.9300	111.5	-4077.7
0.7990	0.2010	0.913490	1311.66	636.29	-0.8086	-168.61	0.8263	122.0	16675.6
0.6991	0.3009	0.960535	1395.69	534.45	-0.9569	-203.18	0.8347	129.3	23892.6
0.5943	0.4057	1.002435	1456.17	470.46	-1.0032	-196.62	0.6804	135.3	32018.8
0.5054	0.4946	1.033003	1516.31	421.04	-0.9637	-186.18	0.6347	139.4	35025.5
0.3970	0.6030	1.065672	1588.44	371.91	-0.8738	-162.39	0.5910	143.5	37178.7
0.3235	0.6765	1.085334	1633.15	345.45	-0.7829	-139.34	0.5606	145.8	38300.1
0.2082	0.7918	1.113260	1693.35	313.26	-0.6455	-93.92	0.5430	149.0	39840.2
0.1175	0.8825	1.132524	1741.70	291.08	-0.4916	-55.04	0.5246	151.1	40456.0
0.0461	0.9539	1.145666	1786.64	273.44	-0.2934	-24.60	0.5324	152.5	40416.5
0.0000	1.0000	1.151866	1803.21	267.00	0.0000	0.00	0.5264	-	-
<i>T = 288.15 K</i>									
1.0000	0.0000	0.793828	1177.84	908.03	0.0000	0.00	1.0658	-	-
0.9503	0.0497	0.830092	1219.72	809.75	-0.3709	-66.19	0.9856	104.1	-20009.2
0.8990	0.1010	0.862917	1257.67	732.65	-0.5951	-110.17	0.9178	111.2	-1863.3
0.7990	0.2010	0.917271	1327.03	619.07	-0.7816	-159.15	0.8178	121.6	17566.8
0.6991	0.3009	0.964134	1410.01	521.70	-0.9263	-192.00	0.8497	128.8	24302.4
0.5943	0.4057	1.005849	1470.21	459.95	-0.9707	-186.07	0.6761	134.7	31885.7
0.5054	0.4946	1.036288	1529.90	412.28	-0.9325	-176.32	0.6311	138.7	34676.3
0.3970	0.6030	1.068792	1601.60	364.75	-0.8435	-153.90	0.5860	142.8	36653.9
0.3235	0.6765	1.088470	1646.28	338.98	-0.7636	-132.18	0.5578	145.1	37663.4
0.2082	0.7918	1.116268	1707.89	307.12	-0.6309	-89.60	0.5451	148.2	38989.2
0.1175	0.8825	1.135661	1756.70	285.34	-0.5007	-52.80	0.5261	150.3	39513.4
0.0461	0.9539	1.148757	1806.70	266.69	-0.3089	-25.34	0.5409	151.7	39220.7
0.0000	1.0000	1.154702	1817.23	262.25	0.0000	0.00	0.5357	-	-

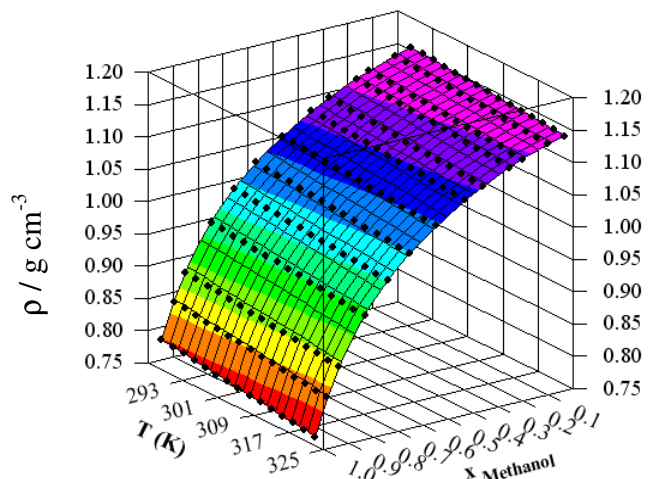
Table 5. Fitting parameters and root mean square deviations for density and speed of sound of binary systems by equation (1).

	water + 2-HEAA		methanol + 2-HEAA		ethanol + 2-HEAA	
	$\rho/\text{g cm}^{-3}$	$u/(\text{m s}^{-1})$	$\rho/\text{g cm}^{-3}$	$u/(\text{m s}^{-1})$	$\rho/\text{g cm}^{-3}$	$u/(\text{m s}^{-1})$
B ₀₀	1.3464	4184.9	1.3374	4202.8	1.3469	4401.7
B ₀₁	-7.4641x10 ⁻⁴	-13.272	-6.9222 x 10 ⁻⁴	-13.386	-7.5335x10 ⁻⁴	-14.628
B ₀₂	2.8436x10 ⁻⁷	0.0176	2.0078x10 ⁻⁷	0.0178	2.9807x10 ⁻⁷	0.0197
B ₁₀	-0.16937	-14842.2	0.44286	-15717.0	1.6770	9467.1
B ₁₁	3.3045x10 ⁻⁴	94.608	-3.6008x10 ⁻³	97.2439	-1.1627x10 ⁻²	-61.744
B ₁₂	-3.5697x10 ⁻⁸	-0.1489	5.8162x10 ⁻⁶	-0.1516	1.8616x10 ⁻⁵	0.0945
B ₂₀	3.1374	50367.1	-5.0092	92325.3	-16.658	-170181.2
B ₂₁	-1.3470x10 ⁻²	-342.90	3.2596x10 ⁻²	-574.7251	0.10595	1068.8
B ₂₂	1.8222x10 ⁻⁵	0.5594	-5.2185x10 ⁻⁵	0.8881	-1.7109x10 ⁻⁴	-1.6712
B ₃₀	-15.091	-45612.2	13.446	-307867.8	46.929	663468.4
B ₃₁	7.3916x10 ⁻²	441.16	-9.0051x10 ⁻²	1917.4627	-0.30127	-4163.4
B ₃₂	-1.0880x10 ⁻⁴	-0.8207	1.4177x10 ⁻⁴	-2.9713	4.8542x10 ⁻⁴	6.5155
B ₄₀	24.178	-109368.9	-15.119	530651.3	-52.692	-1138623.4
B ₄₁	-0.12308	307.3537	0.10280	-3325.9	0.33875	7131.8
B ₄₂	1.8480x10 ⁻⁴	-0.1673	-1.6075x10 ⁻⁴	5.1689	-5.4580x10 ⁻⁴	-11.1661
B ₅₀	-12.676	241274.9	5.9765	-445788.7	20.384	910959.9
B ₅₁	6.5159x10 ⁻²	-1093.8	-4.2031x10 ⁻²	2810.9	-0.13154	-5694.6
B ₅₂	-9.8456x10 ⁻⁵	1.3701	6.5179x10 ⁻⁵	-4.3805	2.1192x10 ⁻⁴	8.9181
B ₆₀		-128408.6		144487.7		-277167.1
B ₆₁		630.41		-916.24		1729.3
B ₆₂		-0.8453		1.4309		-2.7087
σ	1.8×10^{-3}	3.9	7.0×10^{-4}	8.5	4.4×10^{-4}	1.45

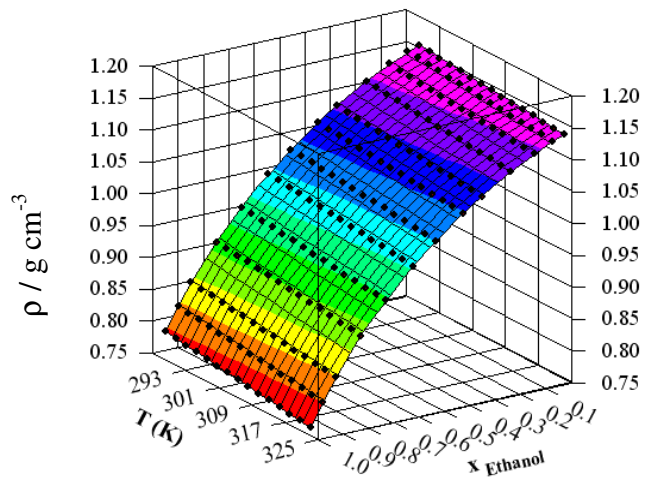
ρ : density, u : velocity of sound, B_{ij} : the fitting parameters of equation (1), σ : standard deviation between experimental and calculated values



(a)



(b)



(c)

Figure 2. Density versus mole fraction and temperature, (a) water + 2-HEAA, (b) methanol + 2-HEAA, (c) ethanol + 2-HEAA.

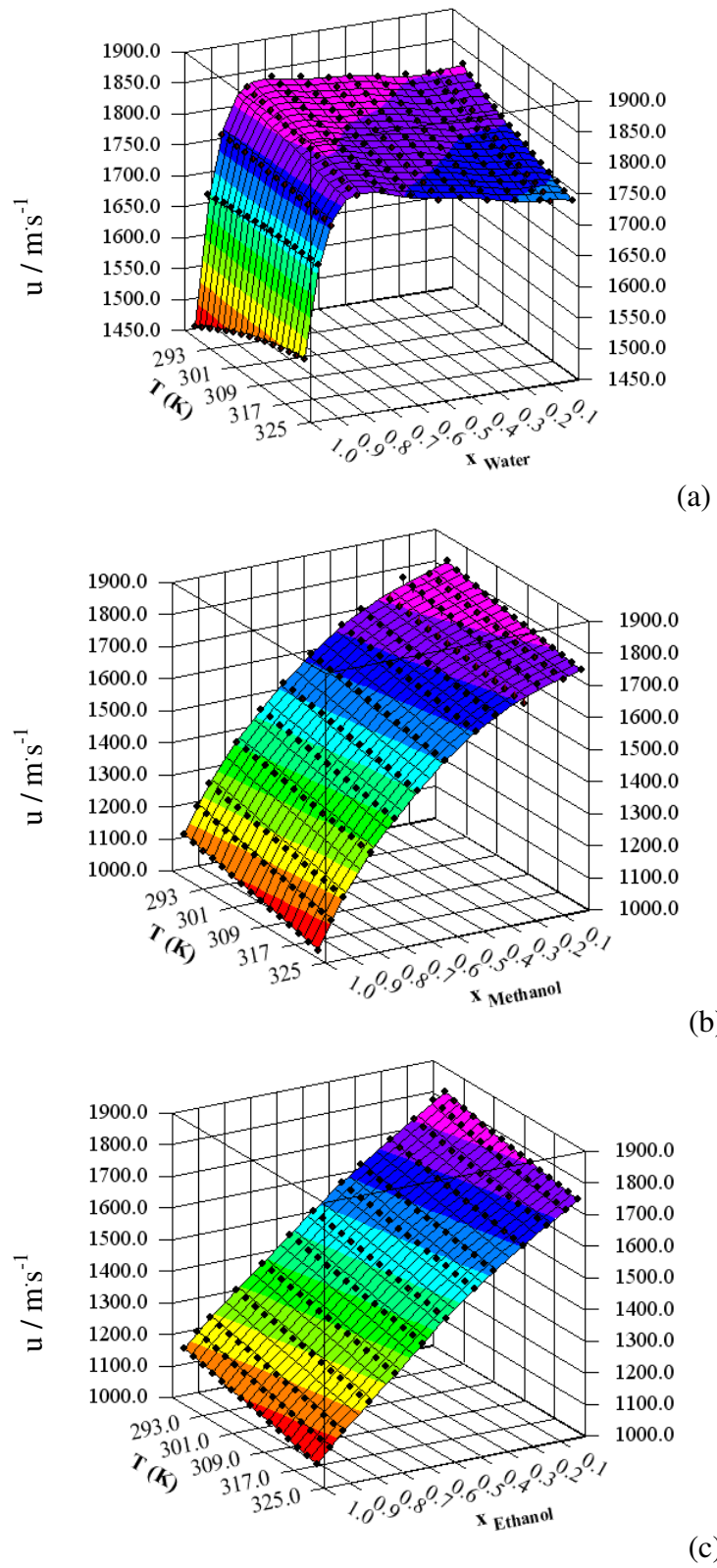
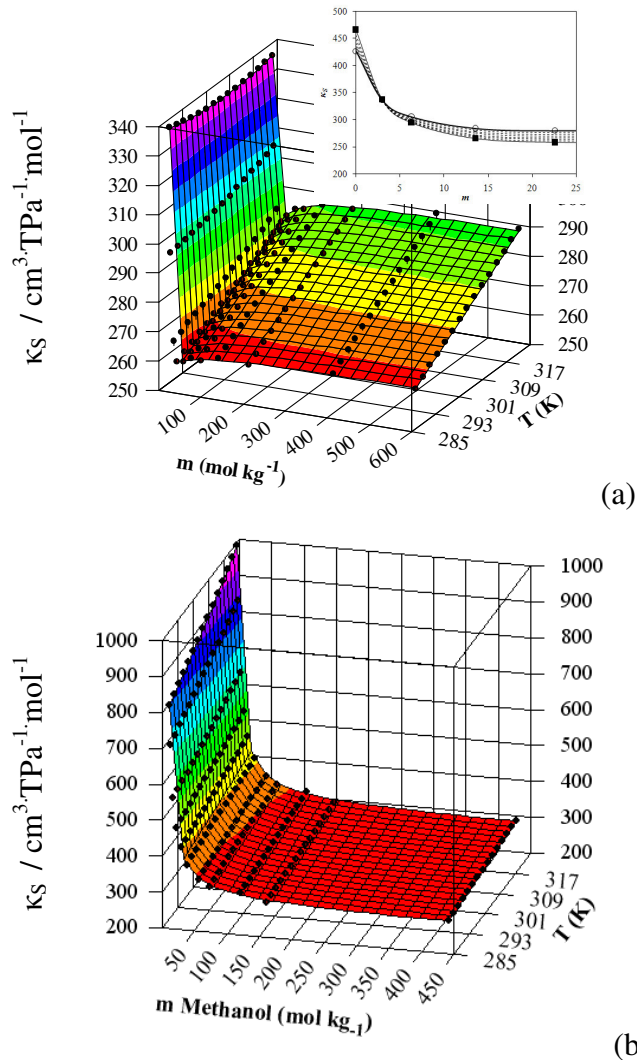


Figure 3. Speed of sound versus mole fraction and temperature, (a) water + 2-HEAA, (b) methanol + 2-HEAA, (c) ethanol + 2-HEAA.

In Figure 4, the isentropic compressibilities are plotted versus the molality and temperature for the three binary mixtures. These figures show the solutions in ethanol as more compressible than the others at a particular concentration and temperature. This shows that there exists a different solvation process in ethanol, due to ethanol exhibiting a weak ion (+) solvent interaction from its poor hydrogen bonding capability (hydrophilic –OH groups) and steric structure (hydrophobic –CH₂-CH₃ groups). On the other hand, water exhibits stronger ion (+) solvent interactions because it has stronger hydrogen bonds and a higher dipole interaction value than both alcohols. In addition, the different interaction between water + 2-HEAA can be explained for a different packing shape, as was shown in Figures 4 and 5(a). In these figures, dilute mixtures of ionic liquid show different packing. This type of behavior, as suggested by different authors [28], holds over this very narrow interval of concentration where the compressibility isotherms cross one another in the formation of a clathrate-like structure. This behavior has a defined stoichiometry corresponding to the concentration at which the crossing occurs. The structure is independent of temperature and is created at a 0.95 water molar fraction.



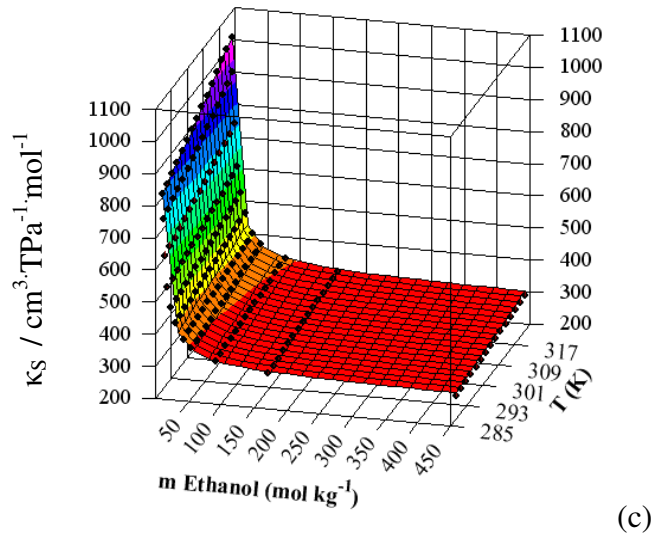
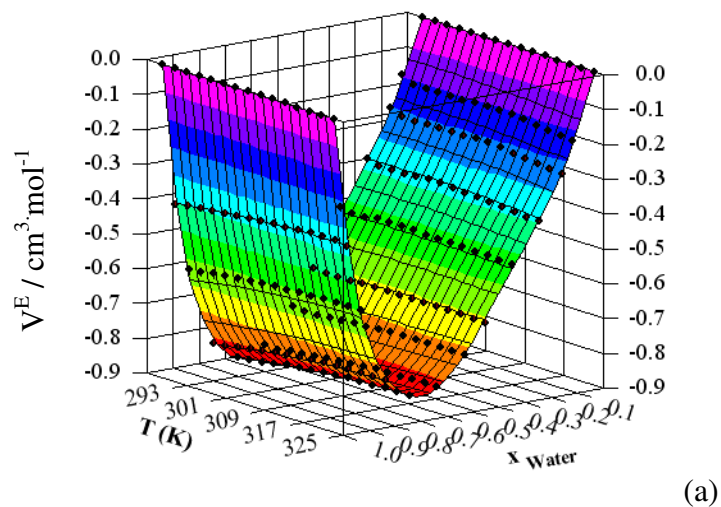


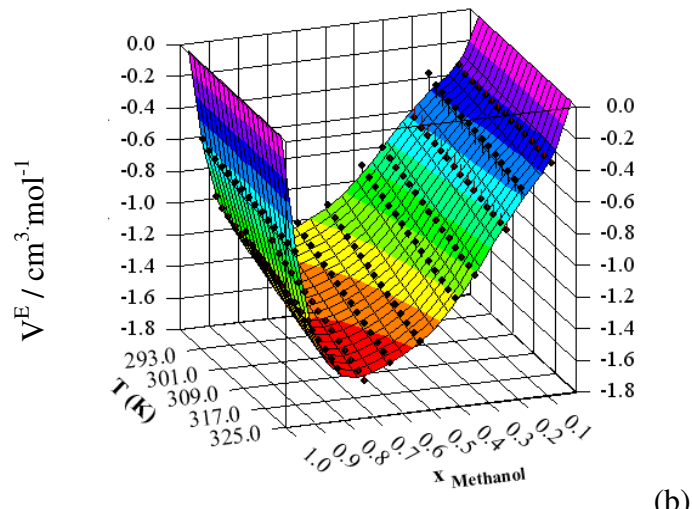
Figure 4. Isentropic compressibility versus molality of 2-HEAA and temperature in mixtures solvent + 2-HEAA. a) water + 2-HEAA, b) methanol + 2-HEAA, c) ethanol + 2-HEAA. For the inside figure in (a): (■) 288.15 K, (○) 323.15 K.

Figure 4 shows a different behavior for the aqueous mixture and this can be explained by the presence of aggregation species of the ionic liquid. In this figure, the increase of the concentration of 2-HEAA at each isotherm induces the decrease of κ_S due to the solvation of ions and breaking the net structure of the solvent. Also, the decrease of κ_S up to a critical concentration (< 5 m) shows the structure of the solvent as the dominant contributor for the behavior mixture. After this point, the stabilized value of the compressibility reflects a new structure formed, the attraction between the ionic pair of 2-HEAA.

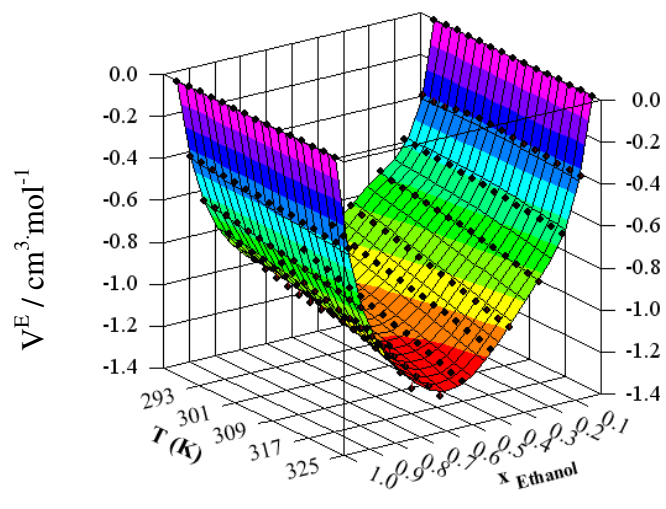
The excess molar volumes and changes of isentropic compressibility are shown in Figures 5 and 6, respectively, and the complete data is presented in the supporting information. Table 6 contains the fitting parameters for these properties. One can note that the values of V^E are negative for all measured temperatures over the whole composition range. The negative values of the excess molar volumes V^E , contributing to a contraction in volume, are dominant. Therefore, these binary mixtures with 2-HEAA could be classified as “contractive” mixtures. Also, these figures show that the introduction of alcohols in the ionic liquid structure results in a considerable decrease in the excess molar properties to more negative values, showing the polar effect of the molecules. In other cases, the introduction of water results in a weak decrease of the excess molar properties.



(a)



(b)



(c)

Figure 5. Excess molar volume versus mole fraction and temperature, (a) water + 2-HEAA, (b) methanol + 2-HEAA, (c) ethanol + 2-HEAA.

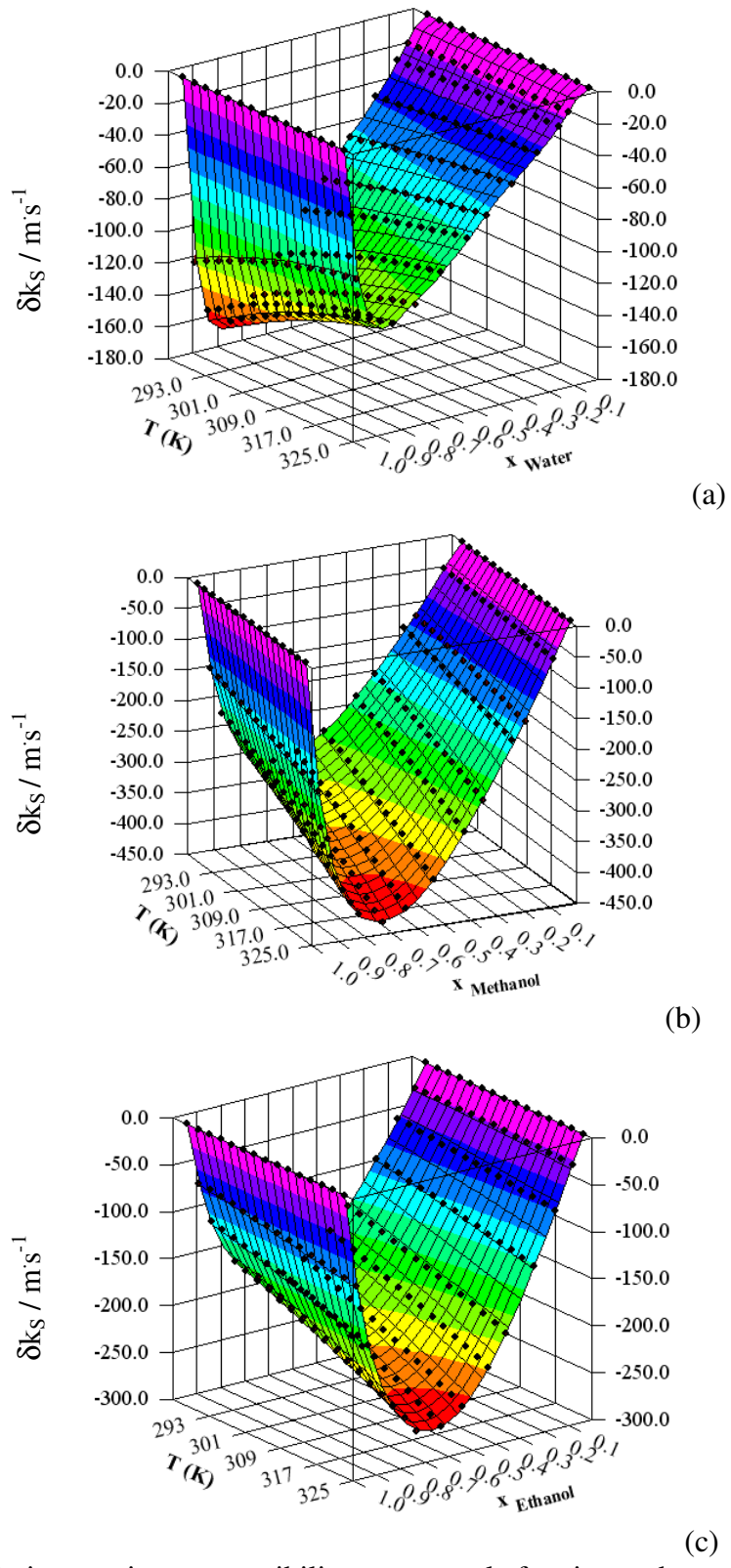


Figure 6. Changes in isentropic compressibility versus mole fraction and temperature, (a) water + 2-HEAA, (b) methanol + 2-HEAA, (c) ethanol + 2-HEAA.

Table 6. Fitting parameters and root mean square deviations for excess molar volume and changes of isentropic compressibility of binary systems by equation (4).

	water + 2-HEAA		methanol + 2-HEAA		ethanol + 2-HEAA	
	$V^E/(\text{cm}^3 \text{ mol}^{-1})$	$\delta\kappa_S/(\text{m s}^{-1})$	$V^E/(\text{cm}^3 \text{ mol}^{-1})$	$\delta\kappa_S/(\text{m s}^{-1})$	$V^E/(\text{cm}^3 \text{ mol}^{-1})$	$\delta\kappa_S/(\text{m s}^{-1})$
C ₀₀	-9.4625	-4963.8	14.205	-2098.6	-4.7857	-2035.9
C ₀₁	3.9516x10 ⁻²	26.864	-8.8707x10 ⁻²	17.997	3.0934x10 ⁻²	16.966
C ₀₂	-6.0256x10 ⁻⁵	-3.8535x10 ⁻²	8.5749x10 ⁻⁵	-5.0004x10 ⁻²	-9.6540x10 ⁻⁵	-4.2847x10 ⁻²
C ₁₀	-27.589	-7330.6	3.9113	-2445.2	-78.328	-2600.9
C ₁₁	0.15444	41.399	-3.4848x10 ⁻²	20.028	0.50680	19.501
C ₁₂	-2.3356x10 ⁻⁴	-6.1138x10 ⁻²	4.2250x10 ⁻⁵	-4.8874x10 ⁻²	-8.3084x10 ⁻⁴	-4.0261x10 ⁻²
C ₂₀	-34.115	-1250.4	-46.793	-4009.2	-86.419	-503.32
C ₂₁	0.21804	5.8319	0.30739	28.096	0.56556	5.2340
C ₂₂	-3.5782x10 ⁻⁴	-8.0912x10 ⁻³	-5.1838x10 ⁻⁴	-5.4185x10 ⁻²	-9.2255x10 ⁻⁴	-1.2964x10 ⁻²
C ₃₀	100.06	5647.2	-19.114	-6449.9	131.66	-4501.5
C ₃₁	-0.63409	-35.009	0.12965	41.992	-0.84825	29.580
C ₃₂	1.0118x10 ⁻³	5.4289x10 ⁻²	-2.7718x10 ⁻⁴	-7.1066x10 ⁻²	1.3725x10 ⁻³	-5.0329x10 ⁻²
C ₄₀	-16.248	-16931.0	76.608	4237.5	69.891	-4078.5
C ₄₁	8.8638x10 ⁻²	97.086	-0.51030	-20.527	-0.48202	26.334
C ₄₂	-1.3697x10 ⁻⁴	-0.14418	7.8617x10 ⁻⁴	1.2827x10 ⁻²	7.6434x10 ⁻⁴	-4.5624x10 ⁻²
C ₅₀	-127.53	-28002.0	78.161	6595.0	84.238	10681.0
C ₅₁	0.79312	164.29	-0.50560	-35.982	-0.53472	-66.728
C ₅₂	-1.2521x10 ⁻³	-0.24786	8.5285x10 ⁻⁴	3.8388x10 ⁻²	8.4280x10 ⁻⁴	0.10238
σ	8.2×10^{-3}	2.0	3.9×10^{-2}	3.0	1.5×10^{-2}	0.8

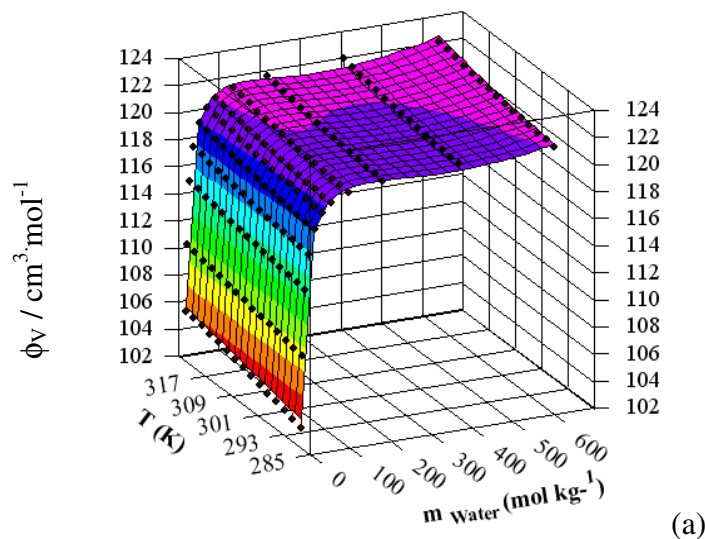
V^E : excess molar volumes, $\delta\kappa_S$: changes of isentropic compressibility, C_{ij}: the fitting parameters of equation (4), σ : standard deviation between experimental and calculated values

The apparent molar volume and isentropic apparent molar compressibility data is given in Tables 2 to 4. Table 7 contains the fitting parameters for these properties. Figure 7 shows that the apparent molar volume, ϕ_V , increases rapidly at low concentration range (below 20 mol/kg), while at higher concentrations it is almost constant (all three mixtures showed the same trend). Figure 8 shows that the apparent molar isentropic compressibility, ϕ_{κ_S} , have the same trend for the three studied mixtures . The values increase rapidly at low concentrations (below 100 mol/kg), while in the high concentration range it is almost constant. Also, in both figures, the properties increase with temperature at all concentrations.

Table 7. Fitting parameters and root mean square deviations for apparent molar volume and apparent molar isentropic compressibility of binary systems by equation (7).

	water + 2-HEAA		methanol + 2-HEAA		ethanol + 2-HEAA	
	ϕ_V (g cm ⁻³)	ϕ_{k_s} (cm ³ mol ⁻¹ Pa ⁻¹)	ϕ_V (g cm ⁻³)	ϕ_{k_s} (cm ³ mol ⁻¹ TPa ⁻¹)	ϕ_V (g cm ⁻³)	ϕ_{k_s} (cm ³ mol ⁻¹ TPa ⁻¹)
A ₀	0.5000	-0.3646	0.5000	0.4317	0.5000	-0.4112
A ₁	0.5156	-0.4451	0.5447	0.3022	0.4876	-46.3230
A ₂	0.5204	-0.3072	0.5167	0.5431	0.4990	-0.4835
A ₃		-0.0669		-0.5099		-0.4444
ϕ_{00}^F	1518.8823	854848.0537	367.6583	-89102.7339	-5420.501	-21933599.278
ϕ_{01}^F	1.3230	-4776.2086	4.8507	120.6279	417.8004	77891.6765
ϕ_{02}^F	0.0053	-3.6090	0.0124	1.0882	-0.0584	149.9512
ϕ_{10}^F	-5352.721	2019028.2191	209.8587	114779.5780	-243.2035	-3106906.2111
ϕ_{11}^F	-7.1726	3008.0711	1.7437	-221.6724	40.2388	4444.3224
ϕ_{12}^F	-0.0174	-9.9991	0.0060	-1.1218	-0.0029	52.1173
ϕ_{20}^F	3862.0575	-183089.8343	-581.346	19713.4049	5684.8633	-79177468.965
ϕ_{21}^F	5.7782	-2782.2268	-6.4314	-11.9528	-458.0162	64054.8273
ϕ_{22}^F	0.0123	13.0427	-0.0184	-0.3036	0.0614	1754.9602
ϕ_{30}^F		-66520.5599		7992880.2045		60457283.1874
ϕ_{31}^F		601.4567		5961.2746		-161089.4619
ϕ_{32}^F		-1.2153		-184.0703		-713.6817
ϕ_F^{00}	51.6883	-3232966.510	131.7442	-8127728.480	63.7519	40340860.2458
ϕ_F^{01}	0.1442	7293.9306	-0.3523	-4155.3416	0.0697	21910.4892
ϕ_F^{02}	-0.0002	-2.8359	0.0002	178.7909	-0.0003	-1197.4583
σ	0.3	116.5	0.5	1068.8	0.6	407.2

ϕ_V : apparent molar volume, ϕ_{k_s} : isentropic apparent molar compressibility, A₀, A₁, A₂, A₃, ϕ_{ij}^F , ϕ_F^{00} , ϕ_F^{01} , ϕ_F^{02} : the fitting parameters of equation (7), σ : standard deviation between experimental and calculated values



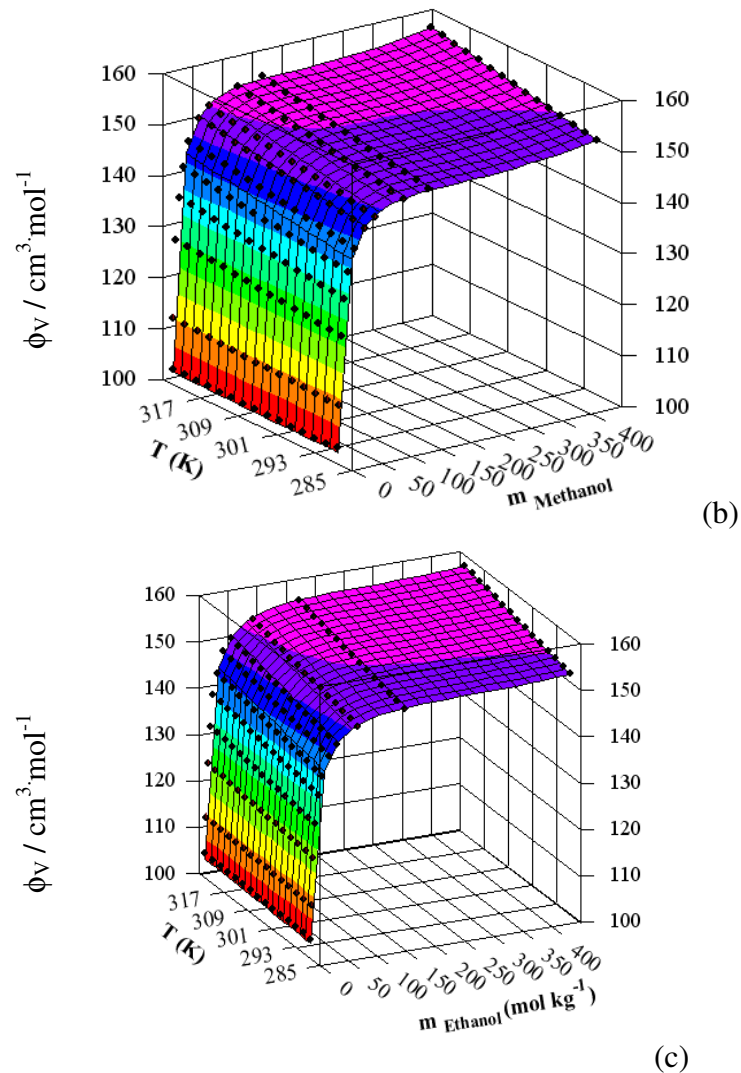


Figure 7. Apparent molar volume versus molality and temperature, (a) water + 2-HEAA, (b) methanol + 2-HEAA, (c) ethanol + 2-HEAA.

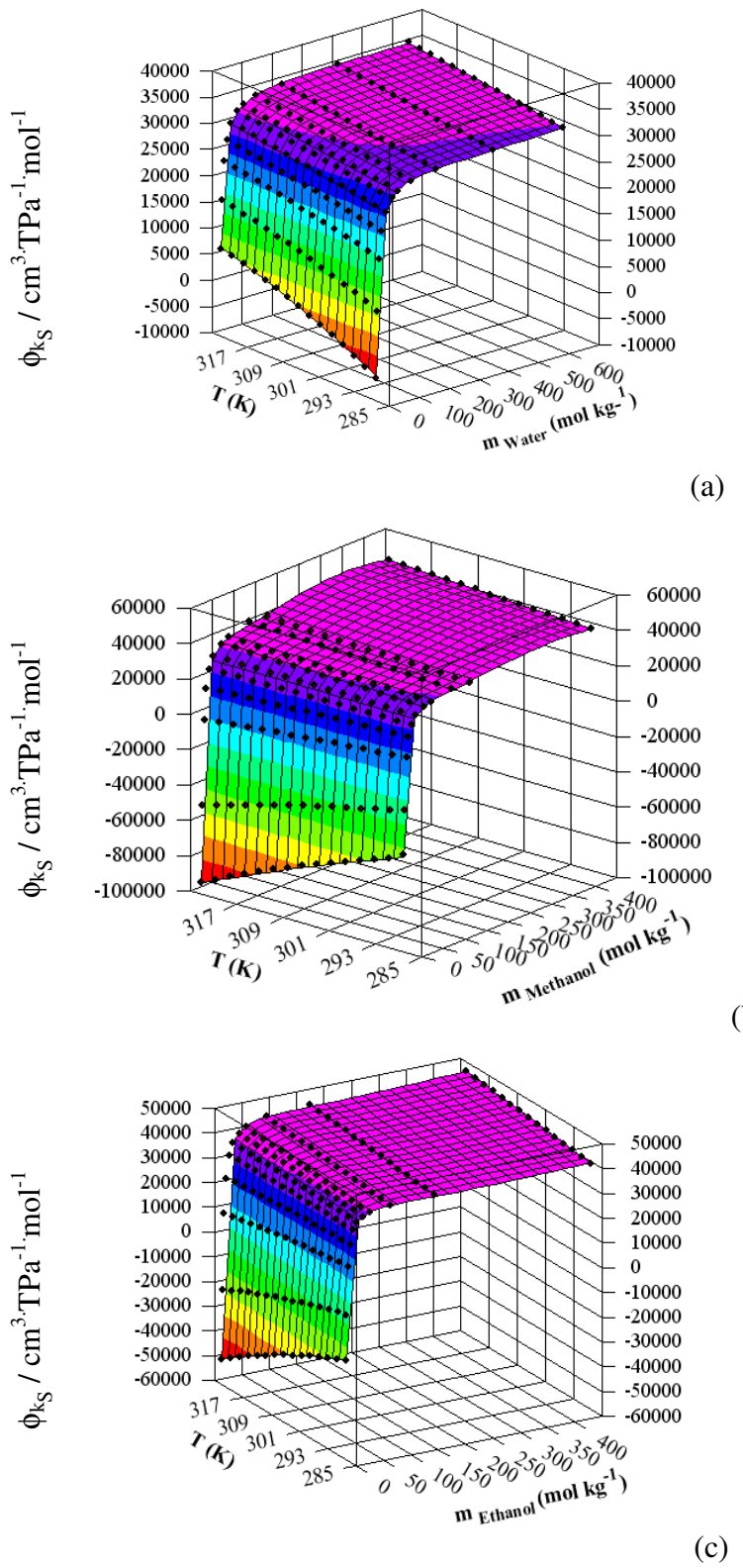


Figure 8. Isentropic compressibility versus molality and temperature, (a) water + 2-HEAA, (b) methanol + 2-HEAA, (c) ethanol + 2-HEAA.

The values for apparent molar volumes at infinite dilution ϕ_V^0 were obtained by extrapolation at infinite dilution ($m \rightarrow 0$), based on the extended Redlich-Mayer relation, Equation (7). The values of ϕ_V^0 for several temperatures are shown in Figure 9. This figure shows that the apparent molar volume at infinite dilution for aqueous mixture is greater than in other alcoholic mixtures. This is a different behavior from classic ionic liquids [29,30].

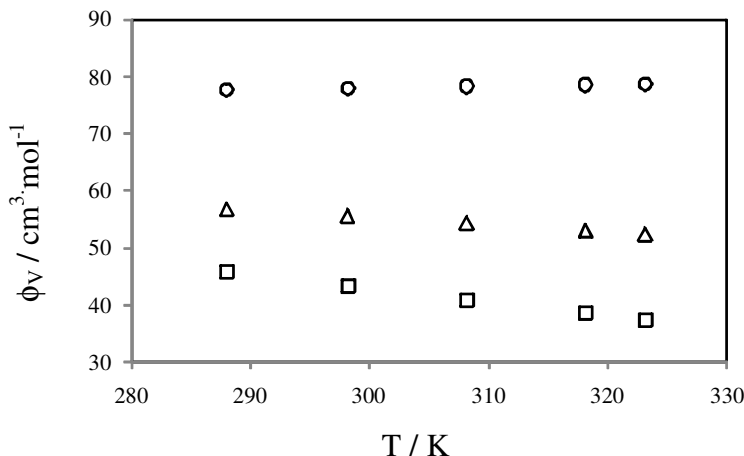
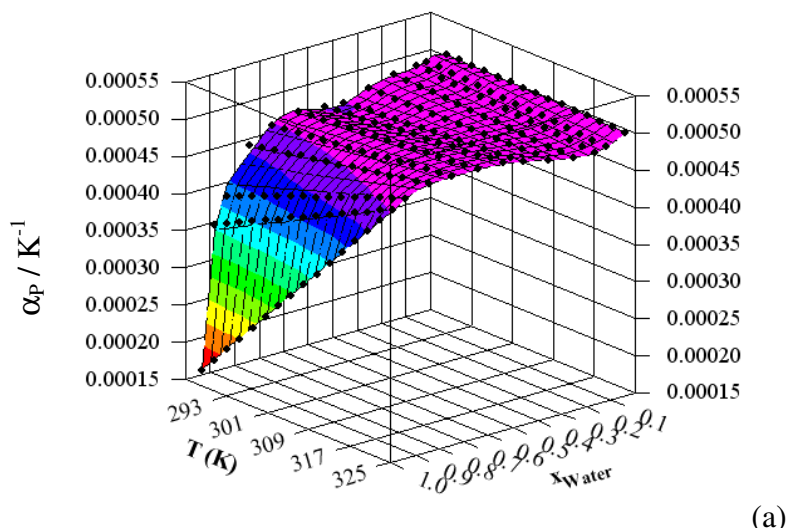


Figure 9. Apparent molar volume at infinite dilution versus temperature. Binary system with water (o), methanol (□) and ethanol (Δ).

The values for the thermal expansion coefficient are shown in Tables 2 to 4 and the behavior is shown in Figure 10. The value deduced for α_P is particularly sensitive to the type of mathematical function used to fit the density data. The fit can be done with a linear function; however, subtle effects stem from the non-linear behavior of most fluids, and therefore a piece of information may be lost. In these figures, the ionic liquid shows a decrease of thermal expansion coefficient with the rise of temperature, a different behavior for hydroxylic solvents. This interesting behavior has been reported previously for lubricants [31]. This behavior shows a very polar attraction among the high ordering molecules of the ionic liquid.



(a)

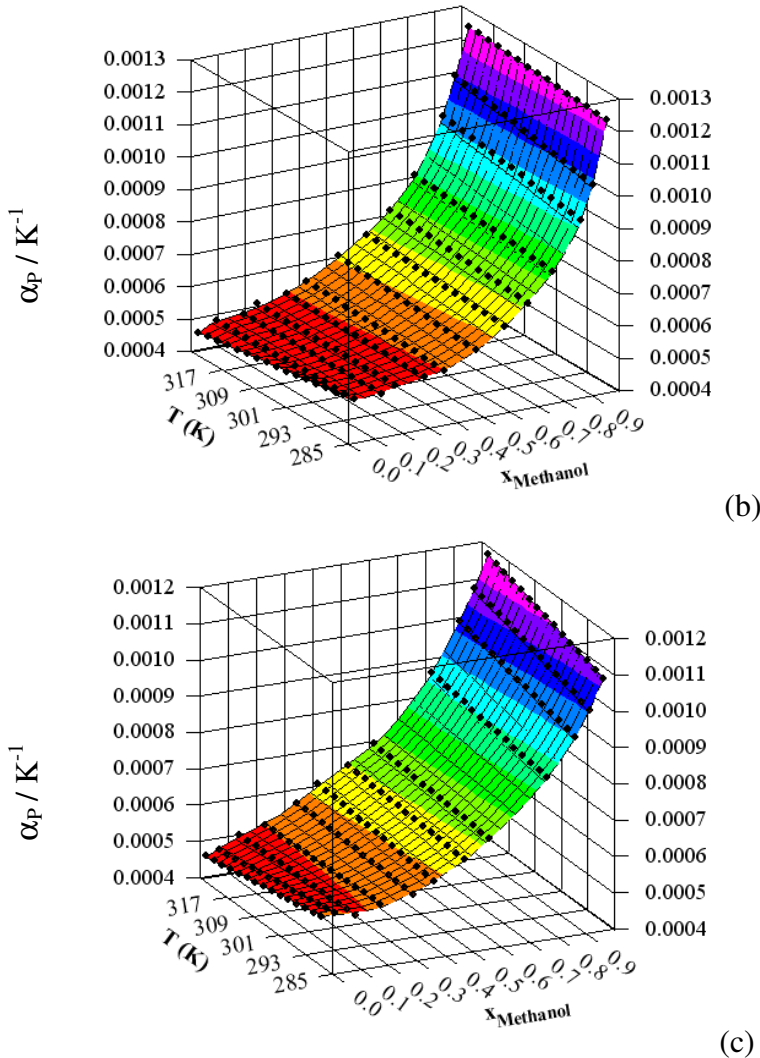


Figure 10. Thermal expansion coefficient versus mole fraction of the solvent and temperature, (a) water + 2-HEAA, (b) methanol + 2-HEAA, (c) ethanol + 2-HEAA.

5.2. The molecular radii and the intermolecular free length

In order to gain a greater understanding of the 2-HEAA structure, a comparative study of the packing for several compounds was made. The adiabatic compressibility against the free length for normal fluids shows a linear trend and different kinds of liquids are out of this trend [18]. Values for these properties are presented in Table S4 in the supporting information. Figure 11 shows the linear tendency for normal fluids, associate fluids (carboxylic acid) with a slope fall to the left of the line corresponding to normal liquids, and aggregates fluids (such as ionic liquids), with a slope fall to the right of the line. This figure shows that n-methyl-2-hydroxyethylammonium formate (m-2-HEAF, ■) is an ionic liquid without aggregation [10] while 1-hexyl-3-methylimidazolium bromide ([C₆mim][Br], Δ), 1-methyl-3-octylimidazolium tetrafluoroborate ([moim][BF₄], ◇), 1-butyl-3-methylimidazolium tetrafluoroborate [bmim][BF₄], ×, and n-methyl-2-hydroxyethylammonium pentanoate (m-2-HEAP, □), [32, 33, 34] are self aggregate ionic liquids. The 2-HEAA (◆) seems to be in the set of aggregate fluids.

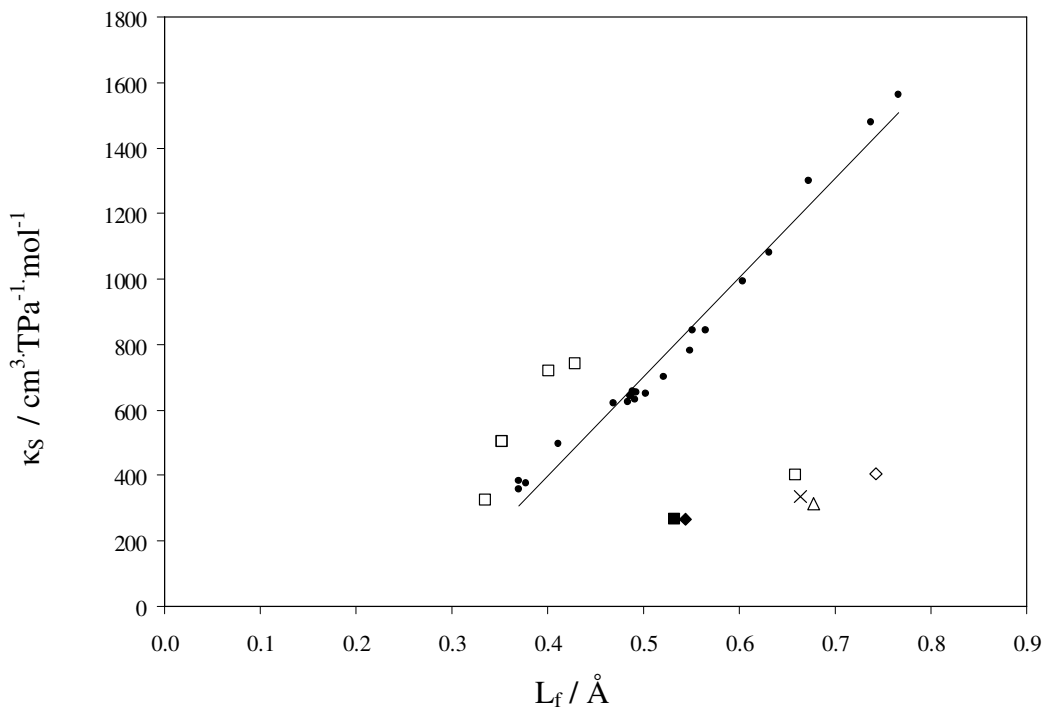


Figure 11. Isentropic compressibility as function of intermolecular free length in normal fluids (●), carboxylic acids (□) and ILs. 2-HEAA, ♦; m-2-HEAF, ■; m-2-HEAP, □; [c₆mim][Br], Δ; [c₁oim][BF₄], ◇; [c₄mim][BF₄], ×. The line shows the tendency of normal compounds.

The linear extrapolation of the curves in Figure 4 allows for the break point for the isentropic compressibility at each temperature to be obtained. For instance, in Figure 12 these are represented by the curves of the aqueous dilution of 2-HEAA corresponding to 288.15 and 323.15 K. The break point for the isentropic compressibilities occurs at the critical molalities of ≈ 4.5 and ≈ 4.9 at 288.15 K and 323.15 K respectively. The break point represents the critical point where the ionic liquid forms an ionic pair in this mixture. The presence of the ionic pair coupling is also supported by the low angle X-ray scattering measurements (Figure 13). Mixtures with concentrations lower than the critical concentration in Figure 12 do not show peaks in Figure 13; otherwise, mixtures with concentrations higher than this limit show a peak in Figure 13 corresponding to aggregates with sizes between 3.4 and 4.0 Å. This size is similar to the molecular diameter of 2-HEAA, showing that the cation and the anion (the ionic pair) is near each other. The ionic pair decoupling at dilute concentrations can be explained by the easy biodegradation [13] of these kind of ionic liquids.

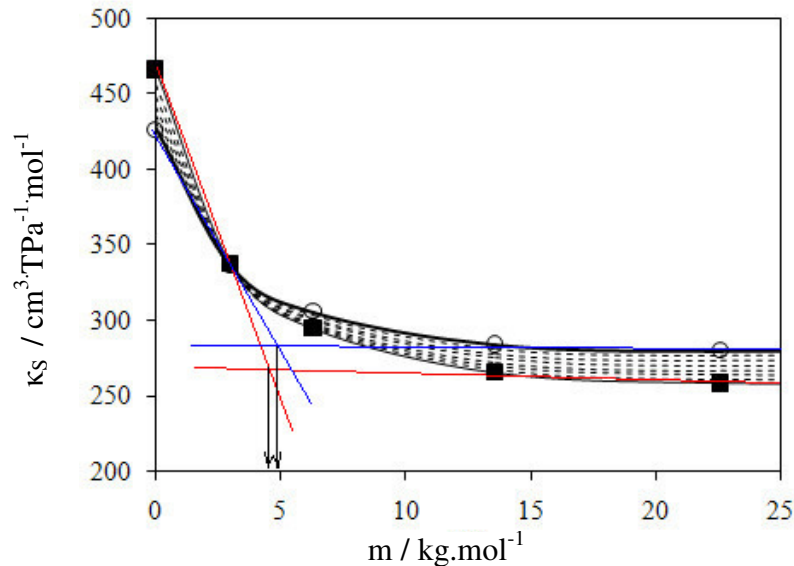


Figure 12. Isentropic compressibility as function of molality of 2-HEAA in water at 288.15 K (squares) and 323.15 K (circles). The linear extrapolation of these curves to determine the break point is indicated.

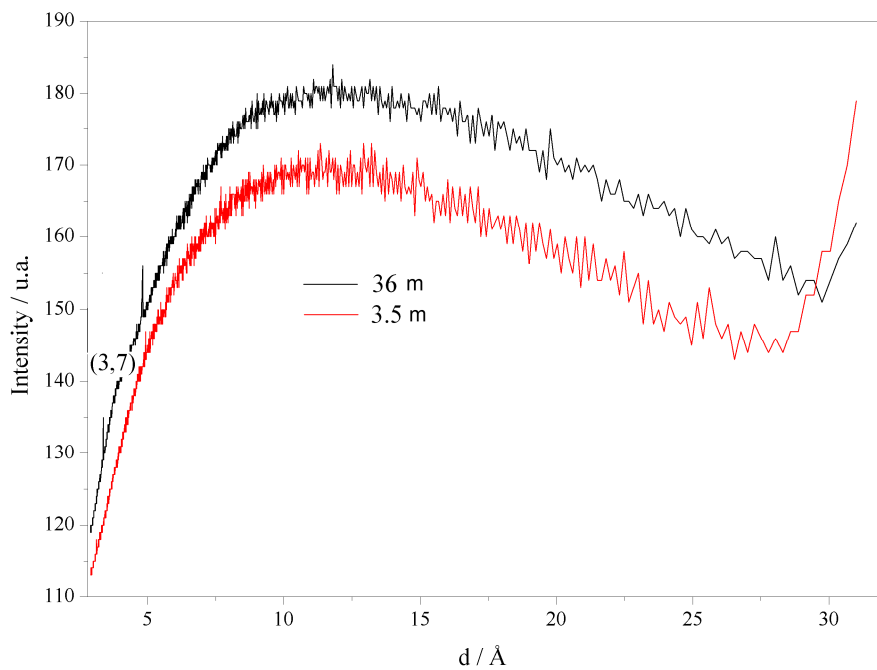


Figure 13. Low angle x-ray scattering measurements for a mixture of water + 2-HEAA with a molalities of 36 m and 3.5 m.

5.3. NMR studies

In mixtures with molar fractions of water greater than 60%, the increase of temperature presents low values for both excess volume and changes of isentropic compressibilities. This behavior could be explained by an initial chemical absorption of water taking place in 2-HEAA at low temperatures, but, as the sites become saturated, a physical solvation becomes dominant. For a deeper understanding of these interactions, NMR spectroscopy measurements of 2-HEAA in the

pure state and in mixtures with a solvent that contains a hydroxylic group were made. In particular, the following mixtures were prepared at the minimum excess volume; 2-HEAA:H₂O molar ratio 30:70, 2-HEAA:MeOH molar ratio 30:70 and 2-HEAA:EtOH molar ratio 40:60. The ¹H-NMR and ¹³C-NMR spectra of the four NMR samples can be seen in Figures S1 and S2 in the supporting information, and the chemical shifts are given in Table 8.

Table 8

¹H-NMR and ¹³C-NMR chemical shifts (ppm) of pure 2-HEAA and binary mixtures. The atom labeling scheme of Figure 1 was used for 2-HEAA.

atom label	pure 2-HEAA	2-HEAA:water 30:70	2-HEAA:methanol 30:70	2-HEAA:ethanol 40:60
¹ H-NMR chemical shifts / (ppm)				
2	1.5	1.5	1.8	1.7
5	7.4	5.8	6.8	7.1
6	2.7	2.6	2.9	2.8
7	3.4	3.3	3.6	3.6
8	3.5	3.5	3.5	3.5
¹³ C-NMR chemical shifts / (ppm)				
1	180.9	180.5	181.1	180.7
2	25.9	24.4	25.6	25.8
6	43.8	42.4	44.1	44.0
7	60.3	58.8	60.5	60.4

In Table 8, the comparison between the ¹H-NMR and ¹³C-NMR chemical shifts of the pure 2-HEAA and its mixtures with H₂O, MeOH and EtOH reveals that most of the ¹H and ¹³C-NMR signals had chemical shifts very comparable with these four samples, with the only exception being the proton signals of the NH₃⁺ group (labeled as 5 in Fig. 1). The proton chemical shift attributed to the NH₃⁺ group in pure 2-HEAA and in the mixture 2-HEAA + H₂O are 7.4 and 5.8 ppm, respectively. Such a remarkable difference reveals the fast proton chemical exchange equilibrium occurring in the mixture 2-HEAA + H₂O among the labile protons of the NH₃⁺ group and H₂O, which causes the single signal finally observed in the ¹H spectrum at the average chemical shift of the two type of protons, though weighted by their respective molar fraction. An additional mechanism that could contribute to this aforementioned exchange is the possible Brønsted acid/base proton exchange of the carboxylate group and/or hydroxilic groups of 2-HEAA with the H₂O protons. Similarly, chemical exchange of the labile protons explains the difference of chemical shift of the signal attributed by the NH₃⁺ group in the 2-HEAA + MeOH and 2-HEAA + EtOH mixtures with respect to the pure 2-HEAA.

The integration of the ¹H-NMR signals is also consistent with the existence of fast exchange equilibrium in the mixtures of 2-HEAA with any of the protic solvents studied. If one considers the ¹H-NMR spectrum of pure 2-HEAA, when the integral area of the non-exchangeable protons of the methylene group 7 (see Fig. 1) is normalized to 2, the relative integral area of the NH₃⁺ group (labeled as 5 in Fig. 1) is 3.3. The value of 3.3 is slightly over the expected number of three protons of the NH₃⁺ group; the excess of 0.3 in the integral imply that there are contributions of other hydrogen atoms in this signal. The most likely explanation is that the sample has captured a small amount of water from the ambient due to its inherent hygroscopicity. Based on this

assumption, it was not unexpected that, in the hydroxylic mixtures, the same analysis results in a much higher relative integral of the NH_3^+ group of 6.9, 5.8 and 5.0 for the 2-HEAA + H_2O , 2-HEAA + MeOH and 2-HEAA + EtOH mixtures, respectively. Clearly, the value of the integral reveals the chemical exchange contribution of a larger amount of protic solvent to the NH_3^+ integral signal.

These NMR results prove the existence of a relatively fast chemical exchange equilibrium of the labile protons in the 2-HEAA/hydroxylic solvent mixtures. The existence of such equilibrium requires that the two components of the mixture are in very close proximity. The spatial arrangement of the two components is likely stabilized by the formation of hydrogen bonds. The aqueous 2-HEAA shows a greater interaction in the NH_3^+ , CH_3^- and $-\text{CH}_2-$ groups than the alcohols, which could probably reflect the transient formation of a complex with a relative long half life between 2-HEAA and one or more molecules of H_2O . In such a complex, the properties of the water molecules structured around the 2-HEAA are different from the remaining bulk aqueous solvent molecules. In order to obtain more detailed information of the solution structure and dynamics of the complexes, specific NMR experiments are being conducted; however, such study is beyond the scope of the present work.

The previous results show that the solubility of hydroxylic solvents in 2-HEAA depends primarily on the strength of the interaction of the hydroxylic solvent with the cation. Furthermore, the ionic liquid hydrogen bond donor behavior was dominated by the hydrogen bond basicity of the hydroxylic solvent, with a low contribution from the hydrogen bond basicity of the cation. Due this behavior, 2-HEAA is completely miscible in hydroxylic solvents at low pressures, and can be used as a potential solvent or additive for green processes.

5.4. Density predictions

Figure 14 compares the σ -profile for 2-HEAA, water, methanol, and ethanol compounds. The σ -profile of these compounds can be qualitatively divided in three main regions, which are separated in Figure 14 by two vertical lines located at the cutoff values for the hydrogen bond donor ($\sigma_{\text{HB}} < -0.0084 \text{ e}/\text{\AA}^2$) and acceptor ($\sigma_{\text{HB}} > 0.0084 \text{ e}/\text{\AA}^2$) group[22]. For 2-HEAA, the σ -profile reveals to be as broad as the σ -profiles of the hydroxylic solvents. Also, the σ -profile of this ionic liquid is dominated by a huge peak of slightly negative screening charge density at $\sigma = -0.003$, which is due to polarization of $-\text{CH}_2-$ groups by the ammonium-hydrogen, hydroxyl-hydrogen and oxygen atoms. The two peaks located at about 0.009 and 0.012 correspond to the negatively charged $-\text{COO}^-$ and lone pairs of the oxygen in the $-\text{OH}$ groups, respectively. Considering the high-polarity region $\sigma_{\text{HB}} > 0.0084 \text{ e}/\text{\AA}^2$, these groups can be considered as hydrogen-bond acceptor groups [22,24]. On the left hand side of the histogram, two low peaks at values lower than the cutoff $-0.0084 \text{ e}/\text{\AA}^2$ can be observed, which are affected by the alkyl chain. These peaks are related to the ammonium-hydrogen and hydroxyl-hydrogen; they may contribute to hydrogen bonds as donors. Finally, the distribution of the charge densities around zero ($-0.0084 \text{ e}/\text{\AA}^2 < \sigma < 0.0084 \text{ e}/\text{\AA}^2$) corresponds to the non-polar alkyl groups of the cation, being those for positive and negative signs assigned to carbon and hydrogen atoms, respectively. Figure 14 shows that the higher number of carbon atoms in the alkyl chain which implies the increasing of the area below each histogram of charge densities around the non-polar area (water < methanol < ethanol < 2-HEAA). In this way, the σ -profile with high values at $\sigma = 0$ show more repulsive interactions between polar and non-polar segments, affecting the cohesive properties of the molecule. The same idea can be applied to mixtures of compounds with very different σ -profiles,

i.e. the binary mixture water + 2-HEAA is another non ideal system studied here. Interestingly, high deviations of the predicted density for the aqueous systems at high concentrations of 2-HEAA can be observed, as shown in Figure 15. The thermodynamic model was used with interaction parameter values of zero. The physical properties used in the model for all substances are reported in Table 1. The predictive results show percentage relative deviations for the mixtures of 2-HEAA with water, methanol and ethanol as 3.0%, 0.8%, and 0.5%, respectively. This suggests that σ -profile is an adequate a priori parameter to quantitatively characterize the non-ideality of volumetric behavior.

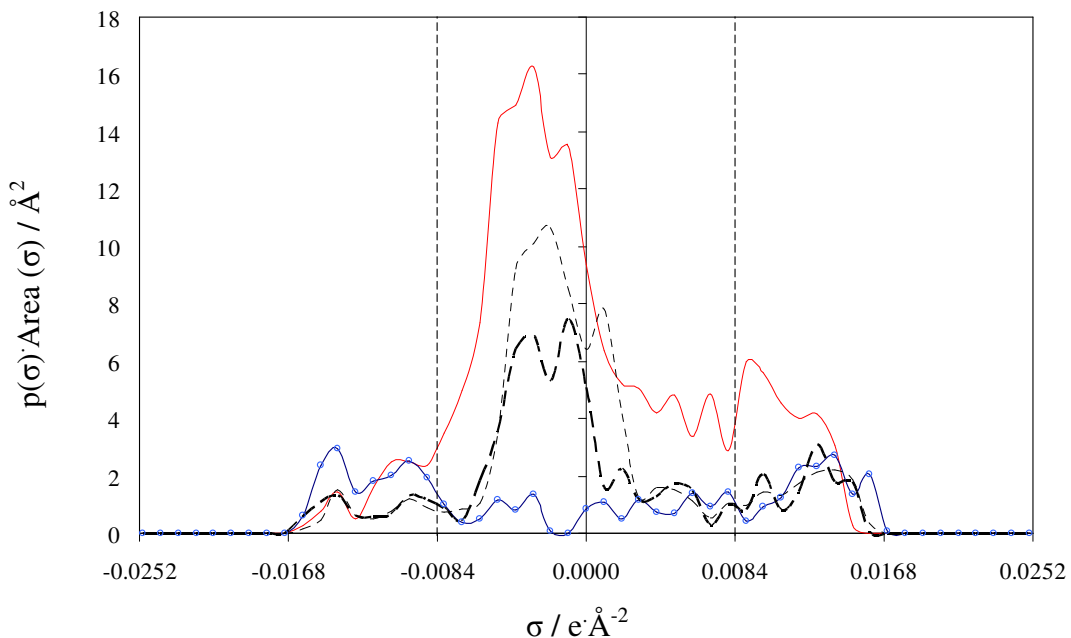


Figure 14. Sigma profiles employed for 2-HEAA (—), water (\ominus), methanol (--) and ethanol (---). Note that, due to the definition as conductor screening charges, electrostatically positive parts of the molecules have negative σ and vice versa.

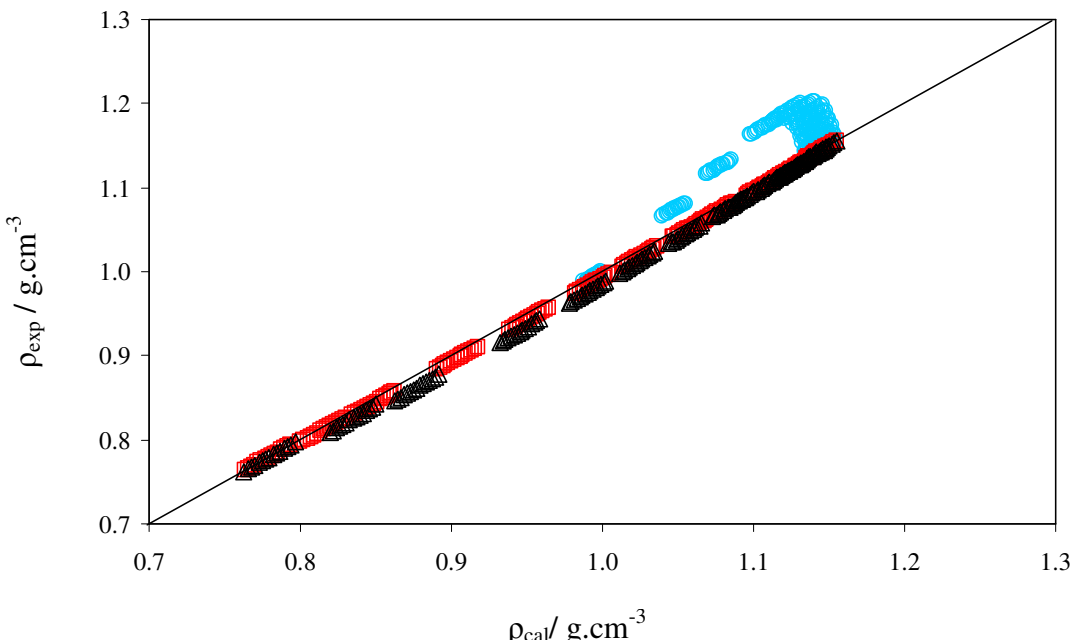


Figure 15. Comparison of experimental and PR-WS/COSMO-SAC model predicted values of density ($\text{g}\cdot\text{cm}^{-3}$) for binary mixtures, water + 2-HEAA (\circ), methanol + 2-HEAA (Δ) and ethanol + 2-HEAA (\square) in the whole composition interval.

Conclusions

Density and speed of sound data of binary mixtures 2-hydroxy ethylammonium acetate + (water or methanol or ethanol) have been measured between 298.15 to 313.15 K and atmospheric pressure. Other properties, such as excess molar volume and variations in the isothermal compressibility were also calculated. The values of V^E are negative within the temperature and concentration ranges studied.

The aggregation, dynamic behavior and hydrogen-bond network in 2-HEAA + (water or methanol or ethanol) mixtures were studied using thermo-acoustic, X-ray and NMR techniques. The results show a slight perturbation of ionic liquid structure in nonpolar regions by the presence of hydroxyl solvents. The formation of a water structure around the NH_3^+ was observed at different water compositions.

The densities for water+2-HEAA, methanol+2-HEAA and ethanol+2-HEAA binary systems have been predicted using the Peng-Robinson equation of state coupled with the Wong-Sandler mixing rule using the COSMO-SAC model. COSMO-SAC is also revealed as a valuable computational tool to describe the intermolecular interaction of systems containing 2-HEAA. In addition, the σ -profile is suggested as a simple molecular parameter to characterize the non ideality of the mixtures respect to volumetric properties.

Acknowledgments

V.H. Álvarez acknowledges the Movilidade Internacional Santander Scholarship and FAPESP (Fundação de Amparo à Pesquisa do Estado de São Paulo), grant 06/03711-1. S. Mattedi thanks

the financial support from CNPq (National Counsel of Scientific and Technological Development, Brazil) for her postdoctoral leave. They also would like to thank the PF&PT research team (USC) for the experimentation facilities and hospitality during their stay in Santiago de Compostela.

M. Aznar is the recipient of a CNPq (National Counsel of Scientific and Technological Development, Brazil) fellowship.

M. Iglesias would like to acknowledge the Fundacion Ibercaja (Programa de Excelencia en Investigacion 2009) for its support in developing this research.

The help and suggestions from Dr. Bruno Dacuña Mariño (X-ray unity, USC) for acquisition and interpretation of X-ray data are also gratefully acknowledged.

References

- [1] R. Sheldon, Chem. Commun. 23 (2001) 2399-2407.
- [2] J.G. Huddleston, H.D. Willauer, R.P. Swatloski, A.E. Visser, R.D. Rogers, Chem. Commun. 16 (1998) 1765-1766.
- [3] S. Zhang, Q. Zhang, Z.C. Zhang, Ind. Eng. Chem. Res. 43 (2004) 614-622.
- [4] J. Fuller, R.T. Carlin, R.A. Osteryoung, J. Electrochem Soc. 144 (1997) 3881-3886.
- [5] M.E. Van Valkenburg, R.L. Vaughn, M. Williams, J.S. Wilkes, Thermochim. Acta 425 (2005) 181-188.
- [6] P. Stepnowski, A. Zaleska, J. Photochem Photobiol A: Chem. 170 (2005) 45-50.
- [7] N. Gathergood, P.J. Scammells, Aust J Chem. 55 (2002) 557-560.
- [8] E.D. Bates, R.D. Mayton, I. Ntai, J.H.Jr. Davis, J. Am. Chem. Soc. 124 (2002) 926-927.
- [9] N. Bicak, J. Mol. Liq. 116 (2005) 15-18.
- [10] X. Yuan, S. Zhang, J. Liu, X. Lu, Fluid Phase Equilib., 257 (2007) 195–200.
- [11] I. Cota, R. Gonzalez-Olmos, M. Iglesias, F. Medina, J. Phys. Chem. B 111 (2007) 12468-12477.
- [12] V.H. Álvarez, N. Dosil, R. Gonzalez-Cabaleiro, S. Mattedi, M. Martin-Pastor, M. Iglesias, J. M. Navaza, J. Chem. Eng. Data 55 (2010) 625-632.
- [13] J. Sierra, E. Martí, A. Mengíbar, R. González-Olmos, M. Iglesias, R. Cruañas, M.A. Garau, 5º Society of Environmental Toxicology and Chemistry Congress, Sydney, 2008.
- [14] G. Annat, D.R. MacFarlane, M. Forsyth, J. Phys. Chem. B 111 (2007) 9018-9024.
- [15] M. Iglesias, A. Torres, R. Gonzalez-Olmos, D. Salvatierra, J. Chem. Thermodyn. 40 (2008) 119-133.
- [16] J.C. Cobas, F.J. Sardina, Concepts Magn. Reson. 19 (2003) 80-96.
- [17] H. Iloukhani, Z. Rostami, J. Sol. Chem. 32 (2003) 451-462.
- [18] B. Jacobson, Acta Chem. Scand. 6 (1952) 1485-1498.
- [19] J. D. Pandey, R. Dey, B.D. Bhatt, PhysChemComm. 5 (2002) 37-39.
- [20] D. Peng, D.B. Robinson, Ind. Eng. Chem. Fundam. 15 (1976) 59–64.
- [21] D.S.H. Wong, S.I. Sandler, AIChE J. 38 (1992) 671–680.
- [22] S.T. Lin, S.I. Sandler, Ind. Eng. Chem. Res. 41 (2002) 899-913.
- [23] <http://www.design.che.vt.edu/VT-Databases.html>, access on January (2010).
- [24] M. Diedenhofen, A. Klamt, Fluid Phase Equilib. In press (2010).
- [25] V.H. Álvarez, M. Aznar, J. Chin. Inst. Chem. Eng. 39 (2008) 353–360.
- [26] A. Peneloux, E. Rauzy, R. Freze, Fluid Phase Equilib. 8 (1982) 7-23.
- [27] V.H. Álvarez, R. Larico, Y. Ianos, M. Aznar, Braz. J. Chem. Eng. 25 (2008) 409-418.
- [28] J.D. Holbrey, W.M. Reichert, M. Nieuwenhuyzen, O. Sheppard, C. Hardacre, R.D. Rogers, Chem. Commun. 4 (2003) 476-477.

- [29] J.F. Brennecke, E.J. Maginn, AIChE J. 47 (2001) 2384-2389.
- [30] M.T. Zafarani-Moattar, H. Shekaari, J. Chem. Thermodyn. 37 (2005) 1029-1035.
- [31] O. Fandiño, A. S. Pensado, L. Lugo, E. R. López, J. Fernández, Green Chem. 7 (2005) 775-783.
- [32] A.J. Kumar, Solution Chem. 37 (2008) 203-214.
- [33] T. Singh, A. Kumar, Colloids and Surfaces A: Physicochem. Eng. Aspects 318 (2008) 263-268.
- [34] Q.Q. Baltazar, J. Chandawalla, K. Sawyer, J.L. Anderson, Colloids and Surfaces A: Physicochem. Eng. Aspects 302 (2007) 150-156
- [35] J.A. Riddick, W.B. Bunger, T.K. Sakano, Organic Solvents, Physical Properties and Methods of Purification, 4th ed., Wiley Interscience, New York, 1986.
- [36] V.A. Del Grossso, C.W. Mader, J. Acous. Soc. Am. 52 (1972) 1442-1446.
- [37] J.M. Resa, C. González, J.M. Goenaga, J. Chem. Eng. Data 50 (2005) 1570-1575.
- [38] H. Lloukhani, B. Samiey, M.A. Moghaddasi, J. Chem. Thermodyn. 38 (2006) 190-200.
- [39] V.H. Álvarez, J.O. valderrama, Alimentaria 254 (2004) 55-66.
- [40] Diadem Public v.1.2, The DPPR Information and Data Evaluation Manager (2000).

4.2.2. EQUILÍBRIO DE FASES

Neste capítulo serão analisadas as interações entre os aldeídos ou ésteres com líquidos iônicos em termos do equilíbrio líquido-vapor a 101,325 kPa. Os coeficientes de atividade e parâmetros de interação binária de vários modelos foram obtidos. Além disso, foram realizadas previsões precisas do ELV. Os líquidos iônicos estudados nesta parte foram o sulfato de 1-etil-3-metilimidazólio, butirato de N-metil-2-hidroxietilamônio e hexanoato de N-metil-2-hidroxietilamônio. Os solventes utilizados foram propanal, pentanal, acetato de metila, acetato de etila e acetato de propila.

4.2.2.1 Testes de solubilidade para os sistemas binários e equilíbrio líquido-vapor a baixas pressões

Os resultados indicaram que os sistemas completamente miscíveis acima da temperatura de ebulição do solvente mais volátil são: etilsulfato de 1-etil-3-metilimidazólio + propanal ou pentanal, butirato de N-metil-2-hidroxietilamônio + acetato de metila, acetato de etila ou acetato de propila, e hexanoato de N-metil-2-hidroxietilamônio + acetato de metila, acetato de etila ou acetato de propila. Este último líquido iônico foi projetado especialmente para ser solúvel nos três ésteres estudados, como comentado no capítulo anterior. Os resultados dos testes de solubilidade das misturas binárias são apresentados nas Tabelas 4.3 e 4.4.

Os resultados mostram que as misturas entre os líquidos iônicos próticos e aldeídos são exotérmicas, produzindo um sistema de duas fases. A temperatura das misturas atingida com o propanal, pentanal e hexanal foram 95 °C, 60 °C e 56 °C, respectivamente. As misturas dos aldeídos com os líquidos iônicos tipo imidazólio atingiram o máximo de 35 °C.

Os resultados também mostraram que a solubilidade do líquido iônico prático em ésteres é influenciada pela cadeia alquílica do ânion. Assim, os líquidos iônicos com cadeias alquílicas curtas (acetato e propionato de N-metil-2-hidroxietilamônio) não apresentam solubilidade nos ésteres, o butirato de N-metil-2-hidroxietilamônio apresenta solubilidade no acetato de metila. Considerando este fato, foi sintetizado o hexanoato de N-metil-2-hidroxietilamônio, que mostrou solubilidade completa em todos os ésteres, nas duas temperaturas estudadas. Essa observação mostra como é possível projetar um líquido iônico para ser solúvel em um determinado solvente. Ainda sendo um exemplo simples, pode-se observar a característica mais importante nos líquidos iônicos, sua projeção para uma função específica.

Os resultados mostraram que o cátion influie na solubilidade dos nos ésteres, como observado para os líquidos iônicos 2-HE₂AB e N-(2-HE)edAB, mantendo o anion butirato.

Por outro lado, o líquido iônico baseado no cátion imidazólio com cadeia alquílica curta no cátion é solúvel no propanal e no pentanal, mas não no hexanal nem ésteres.

Tabela 4.3. Solubilidade de misturas binárias de líquido iônico + solvente a 298,15 K.

	propanal	pentanal	hexanal	acetato de metila	acetato de etila	acetato de propila
[emim] ⁺ [EtSO ₄] ⁻	Sim	Sim	Não	Não	Não	Não
[bmim] ⁺ [MeSO ₄] ⁻	Não	Não	Não	Não	Não	Não
2-HEAA	Não	Não	Não	Não	Não	Não
m-2-HEAA	Não	Não	Não	Não	Não	Não
m-2-HEAPr	Não	Não	Não	Não	Não	Não
m-2-HEAB	Não	Não	Não	Sim	Sim	Não
m-2-HEAH	Não	Não	Não	Sim	Sim	Sim
2-HE ₂ AB	Não	Não	Não	Não	Não	Não
N-(2-HE)edAB	Não	Não	Não	Sim	Não	Não

Tabela 4.4. Solubilidade de misturas binárias de líquido iônico + solvente a 323,15 K.

	propanal	pentanal	hexanal	acetato de metila	acetato de etila	acetato de propila
[emim] ⁺ [EtSO ₄] ⁻	Sim	Sim	Não	Não	Não	Não
[bmim] ⁺ [MeSO ₄] ⁻	Não	Não	Não	Não	Não	Não
2-HEAA	Não	Não	Não	Não	Não	Não
m-2-HEAA	Não	Não	Não	Não	Não	Não
m-2-HEAPr	Não	Não	Não	Não	Não	Não
m-2-HEAB	Não	Não	Não	Sim	Sim	Sim
m-2-HEAH	Não	Não	Não	Sim	Sim	Sim
2-HE ₂ AB	Não	Não	Não	Não	Não	Não
N-(2-HE)edAB	Não	Não	Não	Sim	Não	Não

4.2.2.2 Equilíbrio líquido-vapor a baixa pressão

O líquido iônico utilizado foi desidratado com o método anteriormente descrito e logo utilizado na preparação das soluções e no ELV dos sistemas binários aldeído/ester + líquido iônico a 101,3 kPa. A equação de estado de Peng-Robinson com a regra de mistura de Wong-Sandler utilizando o modelo COSMO-SAC foi utilizado na predição do ELV e da densidade das soluções.

Pode-se observar a influencia do crescimento da cadeia alquilica no anion do líquido iônico (m-2-HEAB e m-2-HEAH) e a pouca influencia de um líquido iônico dicatiónico (N-(2-HE)edAB), como mostra a Figura 4.8.

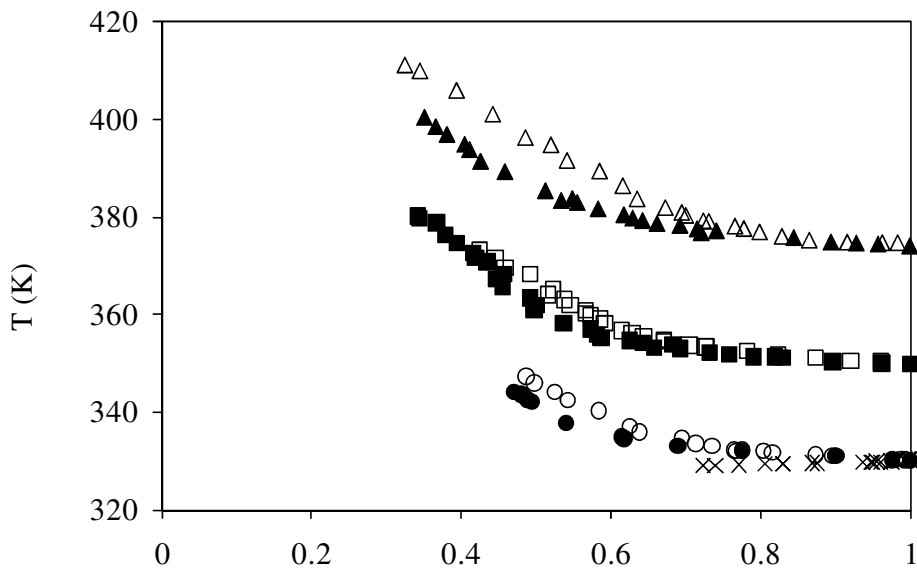


Figura 4.8: Temperatura contra. composição do sistema binário ester + líquido iônico: Acetato de metila, (\circ); acetato de etila, (\square); e acetato de propila, (Δ). Os símbolos fechados é o ELV com m-2-HEAB, os simbolos avertos é o ELV co m-2-HEAH e o simbolo X é o ELV com N-(2-HE)edAB.

A influencia do líquido iônico prótico e aprótico sobre a pressão de um sistema binário, pode ser observada em um solvente comum, o etanol, como mostra a Figura 4.9.

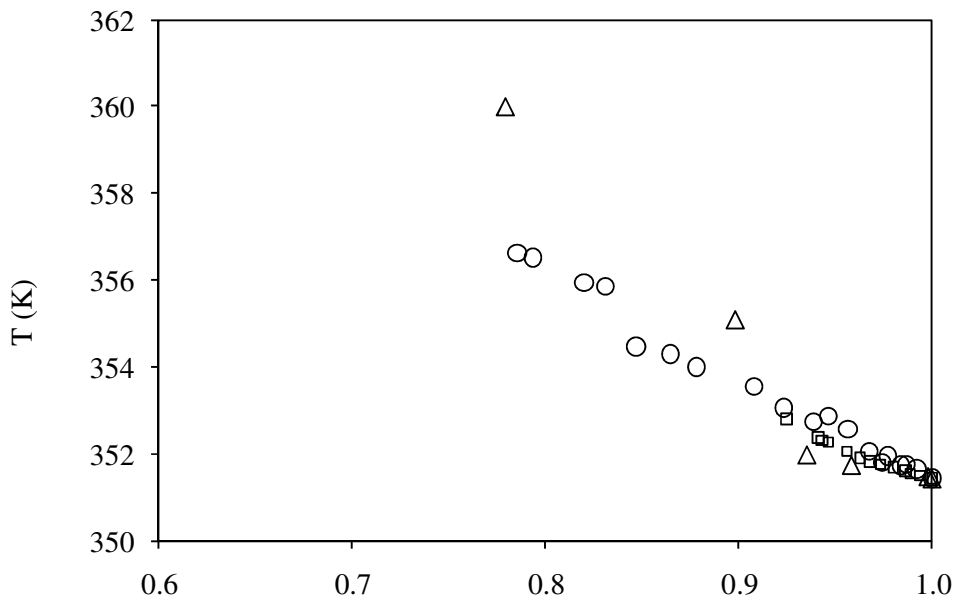


Figura 4.9: Temperatura contra. composição de sistemas binário etanol + líquido iônico: [emim][EtSO₄], (Δ); 2-HE2AB, (\circ); N-(2-HE)edAB, (\square).

A Figura 4.9 mostra o ELV para o sistema binário etanol + líquido iônico: etanol + [emim][EtSO₄], etanol + 2-HE₂AB e etanol + N-(2-HE)edAB. Esta figura mostra que os sistemas contendo líquidos iônicos proticos tem maior temperatura de ebulação que os aproticos a baixa concentração de líquido iônico. Dos líquidos iônicos próticos, o líquido iônico dication apresenta o sistema binário com menor temperatura de ebulação.

Os dados experimentais para o ELV e índice de refração para os sistemas são apresentados nas tabelas 4.5 e 4.6, respectivamente.

Tabela 4.5. Dados experimentais do ELV para os sistemas binários contendo etanol.

Etanol+[emim][EtSO ₄]		etanol + N-(2-HE)edAB		etanol + 2-HE ₂ AB		methyl acetate + N-(2-HE)edAB	
x ₁	T (K)	x ₁	T (K)	x ₁	T (K)	x ₁	T (K)
1.0000	351.44	1.0000	351.44	1.0000	351.44	0.9981	330.20
0.9979	351.49	0.9936	351.50	0.9917	351.65	0.9966	330.35
0.9582	351.75	0.9883	351.55	0.9837	351.73	0.9917	330.25
0.9351	351.99	0.9861	351.60	0.9743	351.80	0.9813	330.15
0.8980	355.10	0.9798	351.69	0.9864	351.75	0.9785	329.96
0.7790	360.00	0.9730	351.75	0.9767	351.94	0.9743	329.91
0.6538	365.20	0.9678	351.82	0.9675	352.05	0.9604	329.78
0.5459	376.00	0.9626	351.91	0.9562	352.57	0.9549	329.95
0.4418	384.80	0.9555	352.06	0.9465	352.86	0.9465	329.77
0.3454	404.00	0.9461	352.27	0.9384	352.75	0.9499	329.75
		0.9428	352.31	0.9234	353.05	0.9367	329.67
		0.9410	352.38	0.9080	353.54	0.8752	329.58
		0.9246	352.80	0.8781	354.00	0.8686	329.55
				0.8645	354.30	0.8294	329.40
				0.8469	354.47	0.8299	329.35
				0.8308	355.85	0.8059	329.30
				0.8199	355.95	0.7708	329.21
				0.7935	356.51	0.7387	329.17
				0.7852	356.62	0.7232	329.15

Tabela 4.6. Indice de refração a 20 °C para os sistemas binários contendo etanol ou acetato de metila.

etanol + N-(2-HE)edAB		etanol + 2-HE ₂ AB		methyl acetate + N-(2-HE)edAB	
X ₁	n _D	X ₁	n _D	X ₁	n _D
0.0000	1.4803	0.0000	1.476	0.0000	1.4803
0.0691	1.4774	0.0813	1.4742	0.0667	1.4763
0.1401	1.4767	0.1504	1.472	0.1041	1.4715
0.1925	1.4745	0.2607	1.4693	0.1952	1.4663
0.3276	1.4649	0.4294	1.4577	0.3576	1.4537
0.5176	1.4561	0.5662	1.4456	0.4850	1.4434
0.6519	1.4429	0.6708	1.4352	0.5933	1.437
0.7467	1.4345	0.7498	1.4231	0.6875	1.4238
0.8170	1.4234	0.8183	1.4114	0.7675	1.4115
0.8676	1.4134	0.8760	1.3991	0.8362	1.3994
0.9104	1.4011	0.9230	1.387	0.8972	1.3874
0.9453	1.3883	0.9642	1.3743	0.9510	1.3753
0.9750	1.3751	0.9829	1.3679	0.9757	1.368
0.9881	1.3681	1.0000	1.3614	1.0000	1.3615
1.0000	1.3614				

Artigos publicados:

Os seguintes artigos apresentam os dados experimentais das soluções binárias e o ELV dos sistemas estudados.

ÁLVAREZ V.H.; MATTEDI S.; AZNAR M. Isobaric Vapor-Liquid Equilibria of 1-Ethyl-3-Methylimidazolium Ethylsulfate Plus (Propionaldehyde or Valeraldehyde): Experimental Data and Prediction, *Journal of Chemical Thermodynamics*, submetido.

ÁLVAREZ V.H.; MATTEDI S.; AZNAR M. Density, Refractive Index and Vapor-Liquid Equilibria of N-Methyl-2-Hydroxyethylammonium Hexanoate plus (Methyl Acetate or Ethyl Acetate or Propyl Acetate) at Several Temperatures, em preparação.

ÁLVAREZ V. H.; MATTEDI S.; AZNAR M. Density, Refractive Index and Vapor-Liquid Equilibria of 1-ethyl-3-methylimidazolium ethylsulfate plus (Propanal or pentanal) at Several Temperatures, em preparação.

Artigo 4.4: Isobaric vaporliquid equilibria of 1-ethyl-3-methylimidazolium ethylsulfate plus (propionaldehyde or valeraldehyde): experimental data and prediction

V. H. Álvarez¹, S. Mattedi² and M. Aznar¹

¹School of Chemical Engineering, University of Campinas (UNICAMP), Av. Albert Einstein 500,
13083-852, Campinas-SP, Brazil

²Chemical Engineering Department, Polytechnic School, Federal University of Bahia (UFBA), R.
Aristides Novis 2, 40210-630, Salvador-BA, Brazil

This paper reports the density, refraction index, and vapor liquid equilibria (VLE) for binary systems aldehyde + 1-ethyl-3-methylimidazolium ethylsulfate ([emim][EtSO₄]): propionaldehyde + [emim][EtSO₄] and valeraldehyde + [emim][EtSO₄]. Excess molar volumes, deviations in the refraction index, apparent molar volume, and thermal expansion coefficient were calculated from experimental data and fitted to typical correlations. A qualitative analysis of the variation of the properties with changes in solvent and temperature was performed. The Peng–Robinson equation of state, coupled with the Wong–Sandler mixing rule, is used to describe the experimental data. To calculate activity coefficients we used three different models: NRTL, UNIQUAC and COSMO-SAC. Since the predictive liquid activity coefficient model COSMO-SAC is used in the Wong–Sandler mixing rule, the resulting thermodynamic model is a completely predictive one. The prediction results for the density and for the vapor-liquid equilibria have a deviation lower than 2.3% and 1.6%, respectively. The vapor-liquid equilibria predictions show a good description for the propionaldehyde system and only a qualitative description for the valeraldehyde system.

KEYWORDS: vapor–liquid equilibria; protic ionic liquid; COSMO-SAC; molecular interactions

1. Introduction

Room-temperature ionic liquids constitute a new class of substances that are considered as potential substitutes to many traditional organic solvents in reaction and separation processes (Huddleston et al., 1998; Zhang et al., 2004). In spite of their importance and interest, accurate values for many of the fundamental physical-chemical properties of these compounds are either scarce or absent. In order to design any process involving ionic liquids in industrial scale, it is necessary to know several physical properties, including density and vapor liquid equilibria. Since it is impossible to measure all the possible combinations of systems, it is necessary to make measurements on selective systems to provide results that can be used to develop correlations and predictive methods.

Due to the vast number and nature of the possible ionic liquids, the interest in asymmetric mixtures is strong. These mixtures, containing lighter and heavier components, can easily be found in several industries, such as paints and polymers production. Among the main measured properties of these mixtures are the density and the refraction index. The liquid density is a key property in solvent extraction, design and processing. The measurement of the refraction index is easy, accurate and simple, and uses a small quantity of sample (≈ 0.3 mL).

The selection of the most suitable ionic liquid for each separation process is not simple, since there is not enough information about the influence of the structure of the ionic liquid on its physical and solvent properties. Besides, experimental phase equilibrium data are required for developing thermodynamic models and for understanding their thermodynamic behavior. Vapor–liquid equilibria (VLE) data allow checking the potential of excess Gibbs energy (G^E) models, which are used for the description of the nonideal behavior of systems containing ionic liquids.

The oxidation of alcohols to the corresponding aldehydes and ketones is one of the most important functional group transformations in organic synthesis. Ansari and Gree (2002) demonstrated that ionic liquids can be employed in the oxidation of alcohols to aldehydes. Figure 1 shows the trend of the open literature publications about ionic liquids and aldehydes, from 1998 to 2009 (ISI web of knowledge, 2010). In this figure, two important years can be easily identified, 2002 and 2008. In 2002, ionic liquids were used together with a catalyst to obtain aldehydes from alcohols (Ansari and Gree, 2002), and in 2008, aldehydes were obtained from ionic liquids only (Luo et al., 2007). After the oxidation reaction, a direct distillation of the aldehydes from the reaction mixture is very attractive, mainly in the case of aldehydes that are volatile enough; besides, after purification, the ionic liquid could be recycled. Therefore, a study about physical properties and VLE between mixtures of aldehydes and ionic liquids is required to develop such separation process.

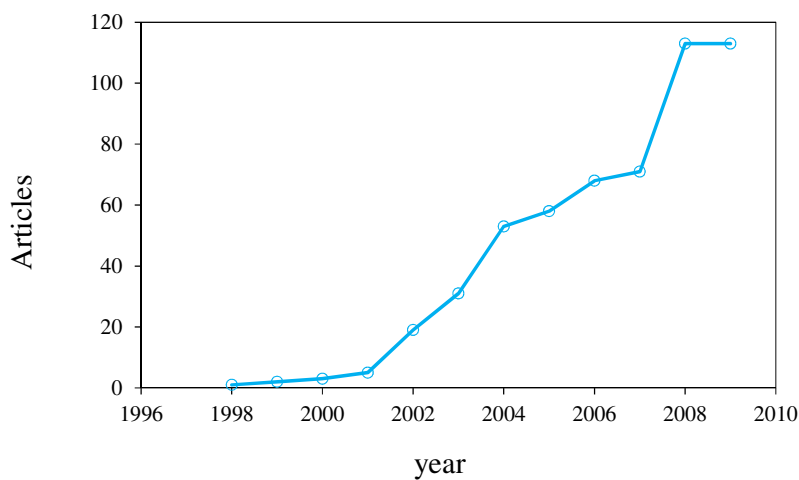


Figure 1. Open literature produced for each year about ionic liquids and aldehydes.

In this work, experimental density and refraction index data of pure 1-ethyl-3-methylimidazolium ethylsulfate, [emim][EtSO₄], have been measured at several temperatures. Experimental density, refraction index and vapor–liquid equilibria (VLE) data over the whole composition range for propionaldehyde (also known as propanal) + [emim][EtSO₄] and valeraldehyde (also known as pentanal) + [emim][EtSO₄] have been determined at 101.3 kPa. Excess molar volumes, deviations in the refraction index, apparent molar volume, and thermal expansion coefficient were calculated from experimental data. Density and VLE data were predicted using the Peng–Robinson equation of state (Peng and Robinson, 1976) coupled with the Wong–Sandler mixing rule (Wong and Sandler, 1992) using the COSMO–SAC model (Li and Sandler, 2002) for the calculation of the liquid-phase activity coefficients.

2. Experimental Section

2.1. Chemicals

Both aldehydes and [emim][EtSO₄] were supplied by Sigma–Aldrich, with mass fraction higher than 0.99 and 0.95, respectively. These compounds were ultrasonically degassed before each use.

2.2. Drying

In order to reduce the water content (lower than 0.1 % mass fraction, determined using a Mettler–Toledo 756 Karl Fisher titrator), [emim][EtSO₄] was dried by heating to 343.15 K and stirring under high vacuum (7 Pa) for two days, always immediately prior to its use. The ionic liquid was kept in bottles with nitrogen gas. Table 1 shows a good agreement between experimental and literature density data of the pure components at 298.15 K.

Table 1. Densities of pure compounds at 298.15 K.

Compound	ρ (g cm ⁻³)	
	exp	lit
propionaldehyde	0.79485	0.7911 ^a
valeraldehyde	0.80473	0.8089 ^b
[emim][EtSO ₄]	1.23686	1.23763 ^c

^aRenuncio et al. (1996); ^bTarakad and Scheller (1979); ^cCalvar et al. (2008).

2.3. Apparatus and procedure

Samples were prepared by introducing, with a syringe, known masses of the pure liquids into stoppered bottles, in an inert-atmosphere glove box, using a Mettler AX-205 Delta Range analytical balance, with a precision of $\pm 1 \times 10^{-4}$ g. A glove box was used because the ionic liquid is moisture sensitive. Densities were measured using an Anton Paar DMA 4000 digital vibrating–tube densimeter. The repeatability and the uncertainty in experimental measurement have been found to be lower than $\pm 5 \times 10^{-6}$ g·cm⁻³ for the density. The DMA 4000 automatically corrects the influence of viscosity on the measured density.

Refraction indices were determined using an automatic refractometer Mettler Toledo D4 with a resolution of $\pm 10^{-4}$ and an uncertainty in the experimental measurements of $\pm 2 \times 10^{-4}$.

The VLE data were measured using a glass Fischer Labodest vapor-liquid equilibrium still, model 602D. The temperature was measured by a Pt100 platinum sensor. For the pressure measurement, a differential U–tube glycerol manometer was used, with an uncertainty of ± 0.01 kPa. Nitrogen was injected into the still to maintain a constant pressure of 101.32 kPa, in agreement with the local atmospheric pressure. During the operation, a liquid binary mixture of aldehyde + [emim][EtSO₄] was placed inside the boiling chamber and heated. The mixture of vapor and liquid in the boiling chamber was carried upward to the equilibrium chamber, where the vapor and liquid phases were separated after flowing directly along the thermometer stem. The vapor was condensed in the condenser and went to the mixing chamber. The equilibrium was usually reached in about 30-

60 minutes, as indicated by the constant boiling temperature. The system was maintained in equilibrium for about 30 min, and then samples of the vapor and liquid were taken out by syringes. The compositions of the vapor and liquid phases were determined by refractometric analysis. The refraction index of both phases was measured at 288.15 K and the results were compared with samples of known composition, through an inverse interpolation.

3. Modeling

3.1. Physical properties

The density and refraction index for the mixtures were correlated by:

$$Z = \sum_{i=0}^p \left(\left(\sum_{j=0}^q B_{ij} T^j \right) x_1^{i-1} \right) \quad (1)$$

where Z is the density or refraction index of the mixture, x_1 is the mole fraction of the solvent, p and q are the polynomial degrees, B_{ij} are the fitting parameters, and T is the absolute temperature.

The excess molar volumes (V^E) and deviations in the refraction index (δn_D) were calculated from experimental values as follows:

$$V^E = \sum_{i=1}^N x_i M_i \left(\frac{1}{\rho} - \frac{1}{\rho_i} \right) \quad (2)$$

$$\delta n_D = n_D - \sum_{i=1}^N x_i n_{Di} \quad (3)$$

where N is the number of compounds in the mixture, x_i is mole fraction, M_i denotes molar mass, ρ_i is the density of the pure compound i , ρ is the density of the mixture, and n_D and n_{Di} are the refraction index of the mixture and of the pure component i , respectively. These derived properties were fitted to a Redlich–Kister-type equation:

$$Q = x_1 x_2 \sum_{i=0}^p \left(\left(\sum_{j=0}^q C_{ij} T^j \right) (x_1 - x_2)^i \right) \quad (4)$$

where Q is V^E or δn_D , C_{ij} are the fitting parameters and the other variables are the same as above.

The apparent molar volume (ϕ_V) for the binary mixtures was calculated by:

$$\phi_V = 1000 \left(\frac{\rho_1 - \rho}{m \rho_1 \rho} \right) + \frac{M_2}{\rho_1} \quad (5)$$

where ρ is the density of the mixture, ρ_1 is the density of the solvent, M_2 is the molar mass of the ionic liquid, and m is the molality of the solution. These derived values were correlated by a modified Redlich–Mayer equation, where the fitting parameters show temperature dependence:

$$\phi_V = \left(\sum_{j=0}^q \phi_{Fj}^o T^j \right) + \sum_{i=0}^p \left(\left(\sum_{j=0}^q \phi_{ij}^F T^j \right) m^{A_i} \right) \quad (6)$$

where A_i , ϕ_{Fj}^o and ϕ_{ij}^F are fitting parameters.

The thermal expansion coefficient (α_P) shows the temperature dependence of volume, and it is defined as:

$$\alpha_P = \frac{1}{V} \left(\frac{\partial V}{\partial T} \right)_P = - \left(\frac{\partial \ln \rho}{\partial T} \right)_P \quad (7)$$

3.2. Vapor-liquid equilibrium

The most common method used for the correlation of phase equilibria in mixtures at high and low pressure is the use of equations of state (EoS). The most common and industrially important EoS are the cubic equations derived from the van der Waals EoS; among these, the Peng–Robinson EoS (Peng and Robinson, 1976) has proven to combine the simplicity and accuracy required for the prediction and correlation of volumetric and thermodynamic properties of fluids, although there can be problems when applying the PR EoS to systems near the critical point.

Recently, Álvarez and Aznar (2008a, 2008b) applied an extension of this approach to several supercritical fluid + ionic liquid systems, using the Peng–Robinson equation of state coupled with the Wong–Sandler mixing rule (Wong and Sandler, 1992) using the UNIQUAC or NRTL model (Abrams and Prausnitz, 1975) for the excess Gibbs free energy, GE, using three or four adjustable parameters, respectively. In addition, by using the Wong–Sandler mixing rule, any cubic EoS can be made predictive for mixtures, i.e., without the need of any adjustable binary interaction parameter, when a predictive model for G^E is used. For example, G^E can be determined from the COSMO–SAC model (Lin and Sandler, 2002), in which the activity coefficient γ_i of species i is calculated from the sum of the residual and combinatorial contributions:

$$\ln \gamma_i = \ln \gamma_i^{res} + \ln \gamma_i^{com} \quad (8)$$

The residual part is calculated considering molecular solvation in a perfect conductor. The distribution of screening charges on the molecular surface, called the sigma profile, $p(\sigma)$, is first determined from quantum mechanical calculations. The molecular interactions in the liquid phase are assumed to be the sum of contributions of surface segment interactions through the screening charges. With these assumptions, the residual term takes the following form:

$$\ln \gamma_i^{res} = n_i \sum_{\sigma_m} p_i(\sigma_m) \ln [\Gamma_s(\sigma_m) - \Gamma_i(\sigma_m)] \quad (9)$$

where n_i is the number of surface segments contained in species i , $\Gamma_S(\sigma)$ is the activity coefficient of segment i (whose screening charge density is σ) in solution S (for which the probability of finding a segment of charge density σ is denoted $p_S(\sigma)$):

$$\ln \Gamma_S(\sigma_m) = -\ln \left\{ \sum_{\sigma_n} p_S(\sigma_n) \Gamma_S(\sigma_n) \exp \left[\frac{-\Delta W(\sigma_m, \sigma_n)}{RT} \right] \right\} \quad (10)$$

where $W(\sigma_m, \sigma_n)$ is the electrostatic interaction between two segments of charge density σ_m and σ_n . The Staverman–Guggenheim model is used for the combinatorial term:

$$\ln \gamma_i^{com} = \ln \frac{\Phi_i}{x_i} + \frac{z}{2} q_i \ln \frac{\theta_i}{\Phi_i} + l_i - \frac{\Phi_i}{x_i} \sum_j x_j l_j \quad (11)$$

$$\Phi_i = \frac{r_i x_i}{\sum_j r_j x_j} \quad \theta_i = \frac{q_i x_i}{\sum_j q_j x_j} \quad (12)$$

$$l_i = (z/2)(r_i - q_i) - (r_i - 1) \quad (13)$$

where θ_i is the surface area fraction, Φ_i is the volume fraction, z is the coordination number ($z=10$), and r_i and q_i are the normalized volume and surface area parameters for species i .

3.3. Density predictions

The calculation of the molar volume of the mixture at a specific temperature and pressure can be predicted by an equation of state. The Peng–Robinson equation of state, coupled with the Wong–Sandler mixing rule and using the predictive liquid activity coefficient model COSMO–SAC, was used as thermodynamic model to predict the density and VLE. The Peng–Robinson equation can be written in terms of the compressibility factor, Z , by:

$$Z^3 - (1-B)Z^2 + (A - 3B^2 - 2B)Z - (AB - B^2 - B^3) = 0 \quad (14)$$

where A and B are given by:

$$A = \frac{a_m P}{(RT)^2} \quad (15)$$

$$B = \frac{b_m P}{RT} \quad (16)$$

where the constants a_m and b_m are expressed as functions of the concentration of the different components in the mixture, through the so-called mixing rules. In this work, the Wong–Sandler mixing rules are used:

$$b_m = \frac{\sum_i \sum_j x_i x_j \left(b - \frac{a}{RT} \right)_{ij}}{1 - \sum_i \frac{x_i a_{ii}}{b_{ii} RT} - \frac{A_\infty^E}{\Omega RT}} \quad (17)$$

$$a_m = b_m \left[\sum_i \frac{x_i a_{ii}}{b_{ii}} + \frac{A_\infty^E}{\Omega} \right] \quad (18)$$

$$\left(b - \frac{a}{RT} \right)_{ij} = \frac{(b_{ii} + b_{jj})}{2} - \frac{(1 - k_{ij}) \sqrt{a_{ii} a_{jj}}}{RT} \quad (19)$$

In these equations, k_{ij} is the adjustable interaction parameter, $\Omega = \ln(\sqrt{2}-1)/\sqrt{2}$ for the PR EoS; A_∞^E , the excess Helmholtz free energy at the limit of infinite pressure, is calculated using the COSMO-SAC activity coefficient model, and a_{ii} and b_{ii} are the EoS constants, defined as

$$a_{ii} = 0.457235(RT_c/P_c)^2 [1 + F(1 - T_r^{0.5})], \quad F = 0.37464 + 1.54226\omega - 0.26992\omega^2 \quad (20)$$

$$b_{ii} = 0.077796(RT_c/P_c) \quad (21)$$

where T_r is the reduced temperature, T_c is the critical temperature, P_c is the critical pressure, and ω is the Pitzer acentric factor.

Equation 14 yields one or three real roots, depending on the number of phases in the system. For the prediction of the liquid density, the root of interest is the smallest positive one. It was shown that this model provides an excellent representation of the vapor-liquid experimental data (Álvarez and Aznar, 2008). However, an equation of state does not necessarily yield the accurate volumetric behavior of fluids and their mixtures. In order to improve the description of liquid densities, a volume translation is used (Peneloux et al., 1982, Loria et al., 2009). Then, the difference between the volume calculated by the thermodynamic model and the experimental volume for pure compounds, can be defined:

$$\Delta V_i = V_{i,\text{exp}} - V_{i,\text{cal}} \quad (22)$$

where $V_{i,\text{cal}}$ is the molar volume of the compound i calculated by the thermodynamic model, and $V_{i,\text{exp}}$ is the experimental molar volume of the compound i . Then, the volume of the mixture is obtained using the correction of the volume applied by

$$V = V_{\text{cal}} + \sum_i \Delta V_i x_i \quad (23)$$

where x_i is the liquid molar fraction of the pure compound i , V_{cal} is the liquid molar volume of the mixture calculated with the thermodynamic model, and V is the predicted corrected molar volume of the mixture.

3.4. Computational details

For each system, the VLE phase diagram is predicted by using the Peng–Robinson EoS with the Wong–Sandler/COSMO–SAC mixing rule. For a given liquid phase composition, the bubble point pressure calculation, as detailed by Michelsen and Mollerup (2007), is performed to obtain the system pressure and the vapor phase compositions. In order to make the models predictive, the binary interaction parameters k_{ij} in the combining rules are set to zero.

In the COSMO model, for each compound, the equilibrium molecular geometry is first determined by minimization of the molecular energy at 0 K. The next step for COSMO–SAC calculation is to estimate the volume of the cavity (V_{COSMO}), the total number of segments (COSMO segments), and the sigma profile of each compound. In this step, a solvation calculation in a perfect conductor was performed using the equilibrium geometry to obtain the surface screening charges on the compound. These calculations were done using the quantum chemistry package DMol3 built in Accelrys Materials Studio v4.3. The sigma profile, $p(\sigma)$, is a file containing the probability of finding a surface segment with screening charge density, σ . The complete detailed settings for DMol3 were the same used by Mullins et al. (2006). The molecular description of the ionic liquid was obtained using the ion-pair approach (Diedenhofen and Klamt, 2010). Therefore, the sigma profile has been obtained for the molecule as a whole. Note that, for each species, the quantum mechanical part of this calculation only has to be done once. The activity coefficient is then calculated (Mullins et al., 2006).

The absolute average error in pressure or density (F) from the calculation is determined as:

$$|\Delta F| \% = \frac{100}{N} \sum_{i=1}^N \left| \frac{F_i^{\text{cal}} - F_i^{\text{exp}}}{F_i^{\text{exp}}} \right| \quad (24)$$

where N is the number of data point, superscripts *exp* and *cal* denote the values from experiment and calculation, respectively.

4. Parameter Estimation

The parameters for the polynomial Redlich–Kister and Redlich–Mayer equations were firstly approximated using a genetic algorithm code, mMyGA (Álvarez et al., 2008), using a whole interval search. After that, the fitting parameters were best tuned using a non-linear optimization algorithm based on the Marquardt algorithm. The optimization used the minimization of the standard deviation (s) between experimental and calculated values, defined as:

$$s = \left[\sum_{i=1}^N \frac{(F_{\text{exp}} - F_{\text{cal}})_i^2}{N-m} \right]^{1/2} \quad (25)$$

where N is the number of experimental points, m is the number of parameters in the curve fit, and F_{cal} and F_{exp} are the values of the property calculated by the model and obtained experimentally, respectively.

5. Results and Discussion

The [emim][EtSO₄] structure was checked by 1D hydrogen NMR spectrum as shown in the supporting information. [emim][EtSO₄] shows completely solubility in water, methanol, ethanol, propionaldehyde and valeraldehyde, from 288.15 to 323.15 K, and it is not soluble in some alkanes as n-octane and n-dodecane. The water content of pure ionic liquid and the mixtures was less than 320 ± 50 ppm.

5.1. Physical properties

Densities and excess molar volumes of the binary mixtures aldehyde (1) + [emim][EtSO₄] (2) at 298.15 K, and refraction indices and deviations in the refraction indices at atmospheric pressure (\approx 96 kPa) are listed in Tables 2 and 3, respectively. The complete data are presented in the supporting information and the Tables 4 and 5 contain the fitting parameters by Equation (1) for these properties.

Table 2. Density and excess volume for the aldehyde (1) + [emim][EtSO₄] (2) at 298.15 K.

propionaldehyde + [emim][EtSO ₄]			valeraldehyde + [emim][EtSO ₄]		
x_1	ρ (g/cm ³)	V^E	x_1	ρ (g/cm ³)	V^E
0.0000	1.23686	0.0000	0.0000	1.23686	0.0000
0.0770	1.22094	0.3357	0.0792	1.21193	0.7703
0.1702	1.20892	-0.5959	0.1010	1.20759	0.5564
0.2146	1.20181	-0.9340	0.2039	1.18549	-0.4193
0.3671	1.17521	-2.3390	0.3008	1.16215	-1.3149
0.4184	1.16288	-2.6072	0.4074	1.13350	-2.3246
0.5246	1.13230	-3.0373	0.5048	1.10270	-3.0903
0.6160	1.10102	-3.4659	0.6047	1.06669	-3.8475
0.7074	1.06218	-3.8166	0.7012	1.02935	-4.8701
0.8104	1.00373	-3.9102	0.8024	0.98252	-5.7690
0.9022	0.92591	-3.0568	0.8970	0.92662	-6.0413
0.9521	0.86519	-1.7250	0.9513	0.88782	-5.8717
1.0000	0.79485	0.0000	1.0000	0.80473	0.0000

Table 3. Refraction index and deviations for aldehyde (1) + [emim][EtSO₄] (2) at 298.15 K.

propionaldehyde + [emim][EtSO ₄]			valeraldehyde + [emim][EtSO ₄]		
x_1	n_D	δn_D	x_1	n_D	δn_D
1.0000	1.3648	0.0000	1.0000	1.3960	0.0000
0.9521	1.3854	0.0150	0.9513	1.4231	0.0229
0.9022	1.4100	0.0338	0.8970	1.4310	0.0262
0.8104	1.4260	0.0390	0.8024	1.4403	0.0273
0.7074	1.4369	0.0379	0.7012	1.4486	0.0270
0.6160	1.4467	0.0370	0.6047	1.4554	0.0255
0.5246	1.4532	0.0328	0.5048	1.4621	0.0237
0.4184	1.4627	0.0299	0.4074	1.4672	0.0204
0.3671	1.4641	0.0253	0.3008	1.4718	0.0159
0.2146	1.4730	0.0163	0.2039	1.4759	0.0116
0.1702	1.4768	0.0150	0.1010	1.4788	0.0057
0.0770	1.4789	0.0062	0.0792	1.4793	0.0044
0.0000	1.4817	0.0000	0.0000	1.4817	0.0000

Table 4. Fitting parameters and root mean square deviations for density and refraction index of binary systems by equation (1).

	propionaldehyde + [emim][EtSO ₄]		valeraldehyde + [emim][EtSO ₄]	
	ρ (g cm ⁻³)	n_D	ρ (g cm ⁻³)	n_D
B ₀₀	1.468	1.485	1.450	1.484
B ₀₁	-8.970×10^{-4}		-8.029×10^{-4}	
B ₀₂	3.705×10^{-7}		2.279×10^{-7}	
B ₁₀	4.384×10^{-1}	-1.002×10^{-1}	-1.377×10^0	-7.173×10^{-2}
B ₁₁	-3.306×10^{-3}		8.037×10^{-3}	
B ₁₂	5.268×10^{-6}		-1.294×10^{-5}	
B ₂₀	-1.587	2.057×10^{-1}	1.658	1.351×10^{-1}
B ₂₁	7.789×10^{-3}		-1.514×10^{-2}	
B ₂₂	-1.386×10^{-5}		2.437×10^{-5}	
B ₃₀	8.465×10^{-1}	-2.195×10^{-1}	-5.482×10^{-1}	-1.421×10^{-1}
B ₃₁	-1.124×10^{-3}		1.336×10^{-2}	
B ₃₂	5.241×10^{-6}		-2.369×10^{-5}	
B ₄₀	3.566×10^{-2}		-1.919×10^{-1}	
B ₄₁	-3.934×10^{-3}		-5.665×10^{-3}	
B ₄₂	3.375×10^{-6}		1.079×10^{-5}	
<i>s</i>	3.3×10^{-3}	4.8×10^{-4}	7.6×10^{-3}	2.0×10^{-4}

s: standard deviation between experimental and calculated values

Table 5. Fitting parameters and root mean square deviations for excess molar volume and deviations of refraction index of binary systems by equation (4).

	propionaldehyde + [emim][EtSO ₄]		valeraldehyde + [emim][EtSO ₄]	
	V^E (cm ³ mol ⁻¹)	δn_D	V^E (cm ³ mol ⁻¹)	δn_D
C ₀₀	1.682×10^1	1.280×10^{-1}	9.126	9.566×10^{-2}
C ₀₁	-9.653×10^{-2}		-7.037×10^{-2}	
C ₁₀	2.017×10^1	6.733×10^{-2}	-9.665	7.259×10^{-2}
C ₁₁	-9.412×10^{-2}		-3.082×10^{-3}	
C ₂₀	1.337×10^1	1.101×10^{-1}	1.362	-1.803×10^{-2}
C ₂₁	-6.959×10^{-2}		-8.129×10^{-2}	
C ₃₀	1.453×10^2	1.960×10^{-1}	-3.670×10^1	-1.261×10^{-1}
C ₃₁	-5.722×10^{-1}		-2.568×10^{-1}	
C ₄₀	1.480×10^1	5.052×10^{-2}	-2.905×10^1	2.500×10^{-1}
C ₄₁	-8.652×10^{-2}		2.375×10^{-1}	
C ₅₀	-6.020×10^2	-9.338×10^{-2}	-4.509×10^1	3.950×10^{-1}
C ₅₁	2.044		1.209	
C ₆₀	-1.917×10^1		1.335×10^1	
C ₆₁	1.286×10^{-1}		-3.274×10^{-1}	
C ₇₀	5.450×10^2		1.987×10^1	
C ₇₁	-1.844		-1.248	
<i>s</i>	4.4×10^{-2}	2.1×10^{-3}	9.3×10^{-2}	1.1×10^{-3}

s: standard deviation between experimental and calculated values

Figure 2 shows the density as a function of composition and temperature. This figure shows a similar behavior for the two binary mixtures. Density increased with the decrease of temperature and the increase of ionic liquid composition. In all figures, the open points are the experimental data and the lines are model fittings. Figures 3 and 4 show the experimental excess molar volume and the deviations in the refraction index, respectively, as well as the fitted curves for the binary mixtures aldehyde + [emim][EtSO₄]. In Figure 3a we can observe that the excess molar volumes show a minimum at $x_1 = 0.65$ for the propionaldehyde + [emim][EtSO₄] system and at $x_1 = 0.9$ for the valeraldehyde + [emim][EtSO₄] system; besides, both systems present a positive V^E with a maximum at $x_1 = 0.1$.

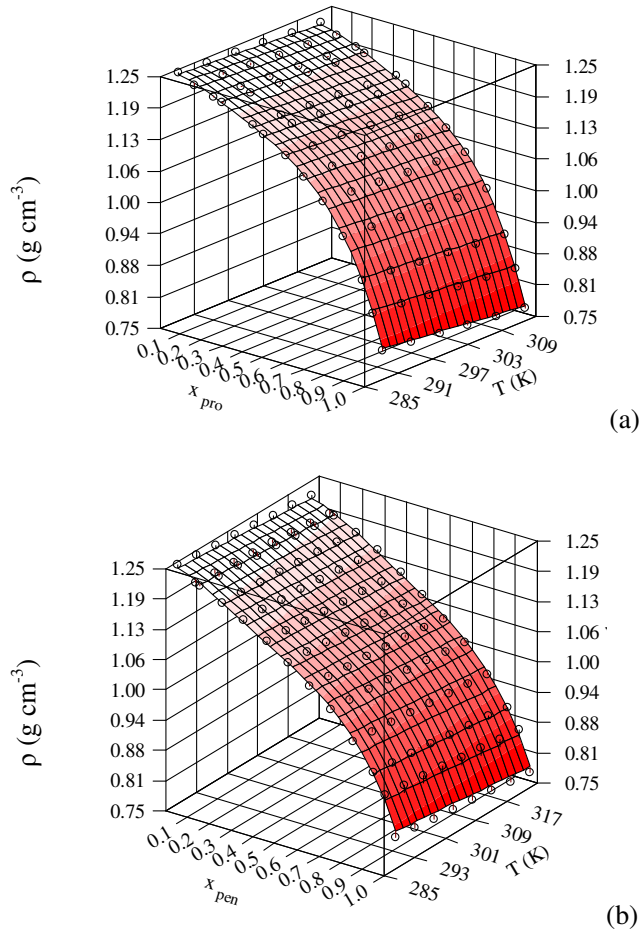


Figure 2. Density versus mole fraction and temperature, (a) propionaldehyde + [emim][EtSO₄], (b) valeraldehyde + [emim][EtSO₄].

Excess molar volumes are the results of the intermolecular interactions due to the difference between the real and the ideal molar volumes. Sigmoidal-shaped curves have been observed for these systems; it has been suggested that this shape results from two opposing effects. The positive excess molar volumes obtained in the ionic liquid-rich region may be attributed to the breakdown of the hydrogen bonded structure of the ionic liquid. In the aldehyde-rich region, the negative excess molar volumes observed may be attributed to the accommodation of the ionic liquid interstitially in the hydrogen bonded structure of the aldehyde (solvation of the ionic liquid). From

the results, it could be seen that V^E values increase with the increase of the alkyl chain length in the aldehyde.

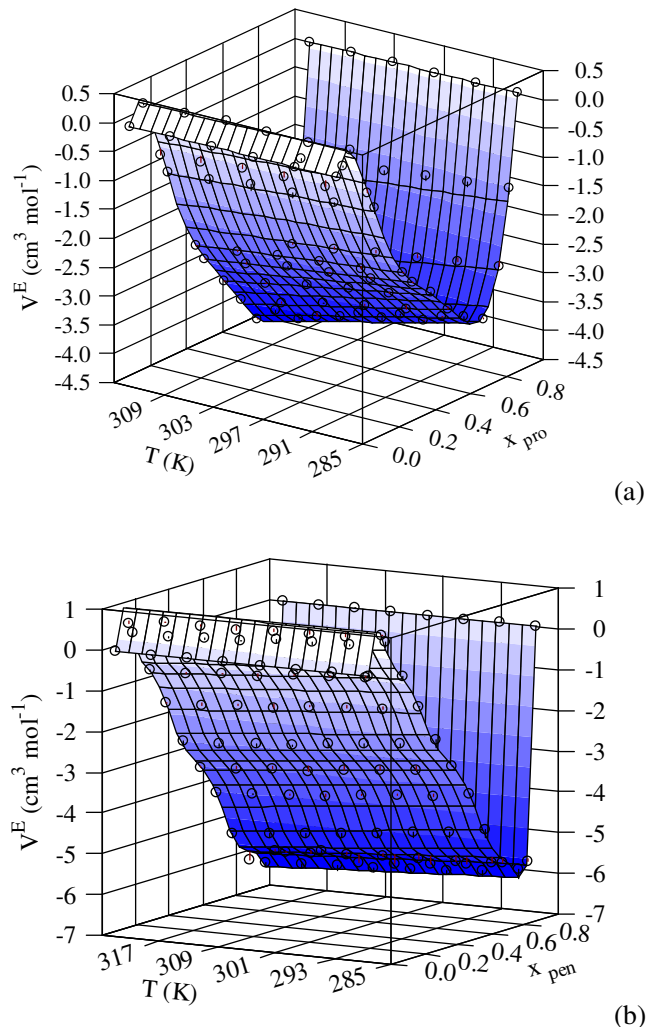


Figure 3. Excess molar volume versus mole fraction and temperature, (a) propionaldehyde + [emim][EtSO₄], (b) valeraldehyde + [emim][EtSO₄].

In these systems, a large negative V^E with a curve skewed to the aldehyde-rich region can be explained by occupation of the free volume or cavities in the open ionic liquid structure by the aldehyde. The observed V^E values may be explained qualitatively as follows: the ionic liquid is partially self-associated in the pure state and the degree of self-association may decrease when small quantities of aldehydes are mixed. This may be due to dissociation of hydrogen-bonding interactions into the ionic liquid and into the aldehyde; with an additional quantity of aldehyde, the aldehyde molecules begin to fill up the cavities in the ionic liquid structure, and the process concludes with the creation of new hydrogen-bonding interactions between the ionic liquid and the aldehyde. A decreasing of V^E reflects the new compact structure or the more efficient packing achieved in the mixture than in the pure compounds. The magnitude of the contributions made by these different types of interactions will vary with the aldehyde and the composition of the mixture. From figure 3 can be seen that the curves are skewed to the aldehyde-rich region. The skewing of

the curves is due to the size of the alkyl chain in the aldehyde; since propionaldehyde has a smaller alkyl chain, changes in V^E are less pronounced. This trend in V^E values can be attributed to an increased interaction between the ionic liquid and the aldehyde with a strong packing effect observed with the increase of the alkyl chain.

The excess molar volumes become more negative as the temperature increases because the kinetic energy of molecules also increases with temperature, which leads to a decrease in interaction of the molecules (Zhong et al., 2007).

In Figure 4, the refraction index deviations are positive for the two systems, and the maximum lies at a mole fraction of approximately 0.85 for both binary systems. According to Nakata and Sakurai (1987) the sign of δn_D is opposite to that of V^E if the behavior of the refraction index is not too nonlinear between n_{D1} and n_{D2} . In our mixtures this rule is truly fulfilled in all the cases.

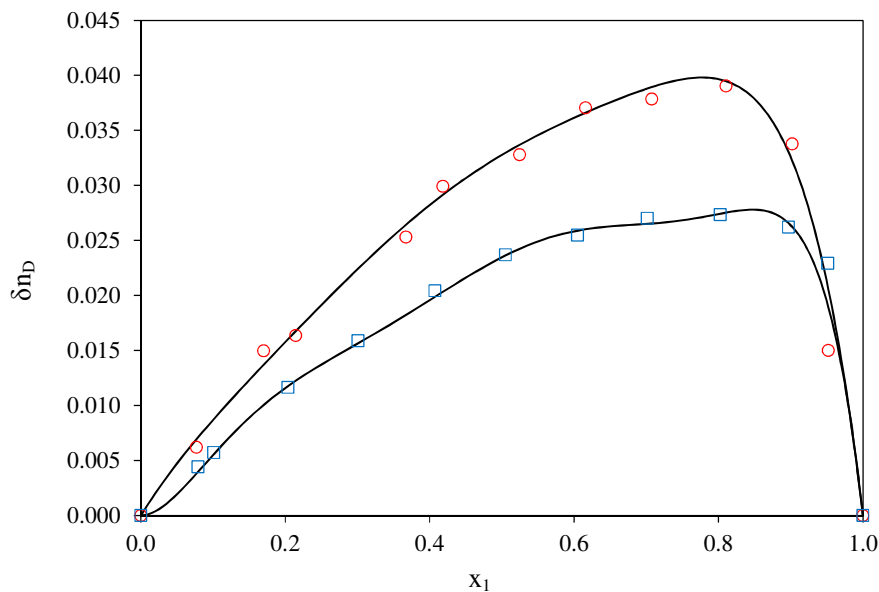


Figure 4. Deviations in the refraction index, propionaldehyde (○), valeraldehyde (□), Redlich-Kister fitted values (-).

At low solute concentrations, the measured volume reflects the contribution of both solvent and solute intrinsic properties. Thus, results have to be carefully interpreted to discriminate between those due to the intrinsic packing of a solute and those due to interactions occurring at the interface in contact with the solvent. This characteristic can be obtained from experimental densities. Thus, the apparent molar volume is used to study the aggregation behavior of the solutes in a wide variety of mixtures (Ruso et al., 2004).

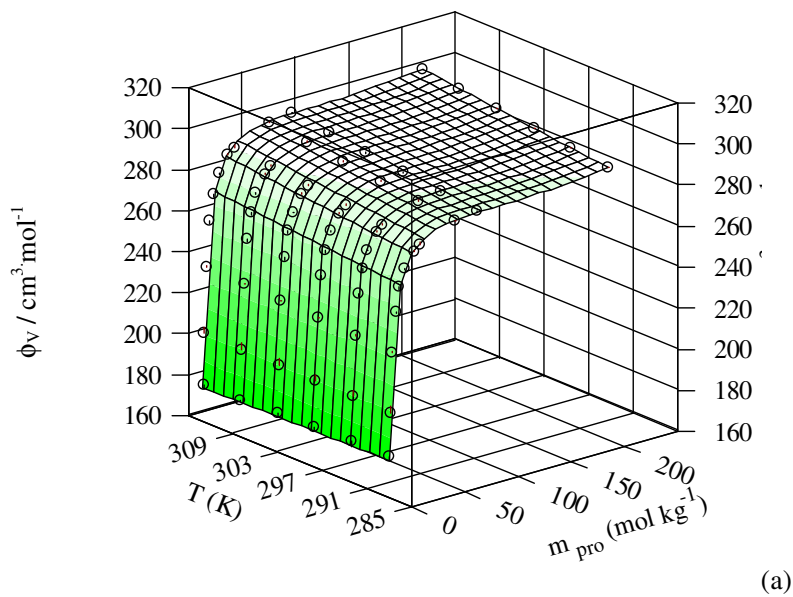
The apparent molar volume data are given in the supplementary information. Table 6 contains the fitting parameters for this property. Figure 5 shows that the apparent molar volume, ϕ_V , rises rapidly at low concentrations (below 15 m), while at higher concentrations is almost constant (all two mixtures shown the same trend). Also, in these figures this property increases with temperature. This behavior can be explained by the presence of aggregation species. Figure 5 shows the increase

of the [emim][EtSO₄] concentration at each isotherm, inducing the increase of ϕ_V due to the solvation of ions and the breaking of the net structure of the solvent. Also, the curves of Figure 5 show that, as the molality of [emim][EtSO₄] increases, the high packing of the solvent is the dominant contributor until a critical concentration; in this point, the quasi constant values of ϕ_V reflect the attraction between the ionic pair of [emim][EtSO₄] as the principal contributor.

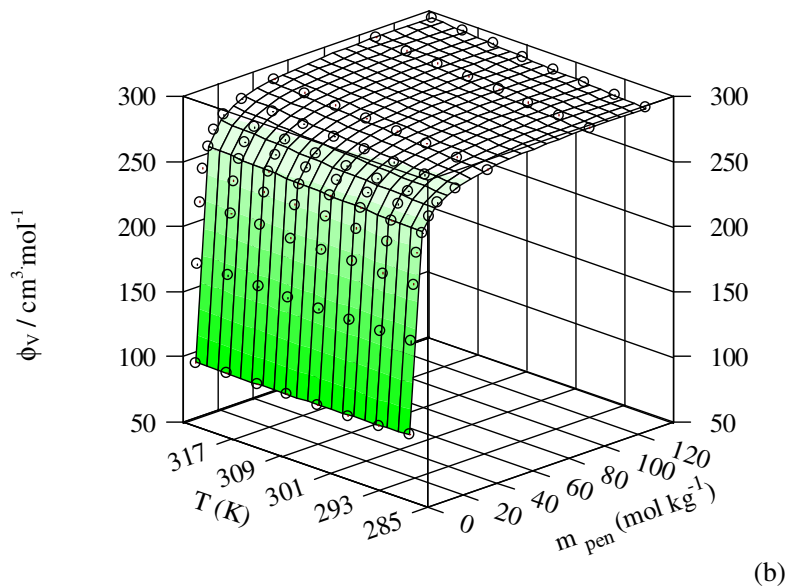
Table 6. Fitting parameters and standard deviations for apparent molar volume of binary systems by equation (6).

	propionaldehyde + [emim][EtSO ₄] ϕ_V (g cm ⁻³)	valeraldehyde + [emim][EtSO ₄] ϕ_V (g cm ⁻³)
A ₀	5.000×10^{-1}	4.728×10^{-2}
A ₁	4.815×10^{-1}	3.197×10^{-2}
A ₂	4.927×10^{-1}	3.110×10^{-2}
ϕ_{00}^F	9.90×10^3	4.792×10^5
ϕ_{01}^F	5.353×10^1	4.435×10^2
ϕ_{02}^F	2.493×10^{-1}	3.405×10^{-1}
ϕ_{10}^F	6.562×10^3	-1.304×10^7
ϕ_{11}^F	4.396×10^1	-1.955×10^4
ϕ_{12}^F	1.769×10^{-1}	-8.521×10^{-2}
ϕ_{20}^F	-1.648×10^4	1.267×10^7
ϕ_{21}^F	-9.700×10^1	1.944×10^4
ϕ_{22}^F	-4.258×10^{-1}	-4.575×10^{-1}
ϕ_F^{00}	2.474×10^2	-1.138×10^5
ϕ_F^{01}	-7.792×10^{-1}	-3.386×10^2
ϕ_F^{02}	1.522×10^{-5}	2.041×10^{-1}
s	1.5	1.2

s: standard deviation between experimental and calculated values



(a)



(b)

Figure 5. Apparent molar volume vs molality and temperature, (a) propionaldehyde + [emim][EtSO₄], (b) valeraldehyde + [emim][EtSO₄].

The values for apparent molar volumes at infinite dilution, ϕ_V^θ , were obtained by extrapolation at infinite dilution ($m \rightarrow 0$), based on the extended Redlich–Mayer relation, Equation (6). The values of ϕ_V^θ for several temperatures are shown in Figure 6 for the propionaldehyde system, but not for the valeraldehyde system, which shows negative values by the extrapolation. This figure shows that the apparent molar volume at infinite dilution for propionaldehyde mixture decreases with the temperature. This behavior and the fact that the values are lower than the pure ionic liquid molar volume confirm the compact structure of the mixture.

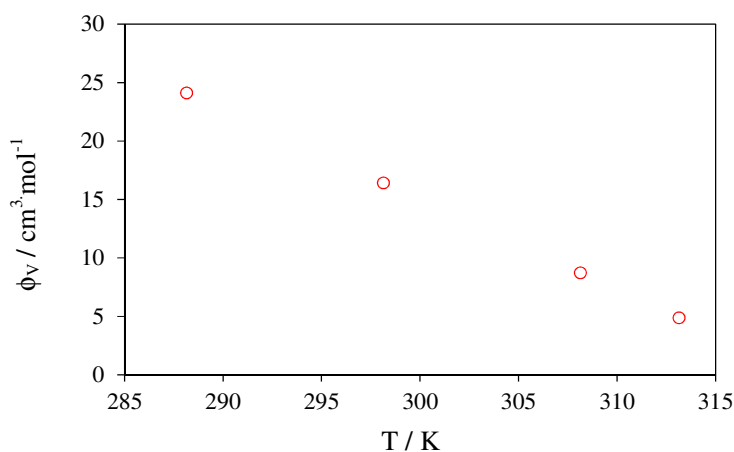


Figure 6. Apparent molar volume at infinite dilution vs. temperature. Binary system with propionaldehyde (o)

The values for the thermal expansion coefficient are shown in the supplementary information and the behavior is shown in Figure 7. The value deduced for α_P is particularly sensitive to the type of mathematical function used to fit the density data. The fit can be done with a linear function; however, subtle effects stem from the nonlinear behavior of most fluids, and therefore a piece of

information may be lost. In these figures, the pure ionic liquid shows a stable value of thermal expansion coefficient with the increase of temperature, while an increase in the value of this coefficient was observed for the binary mixtures and pure aldehydes.

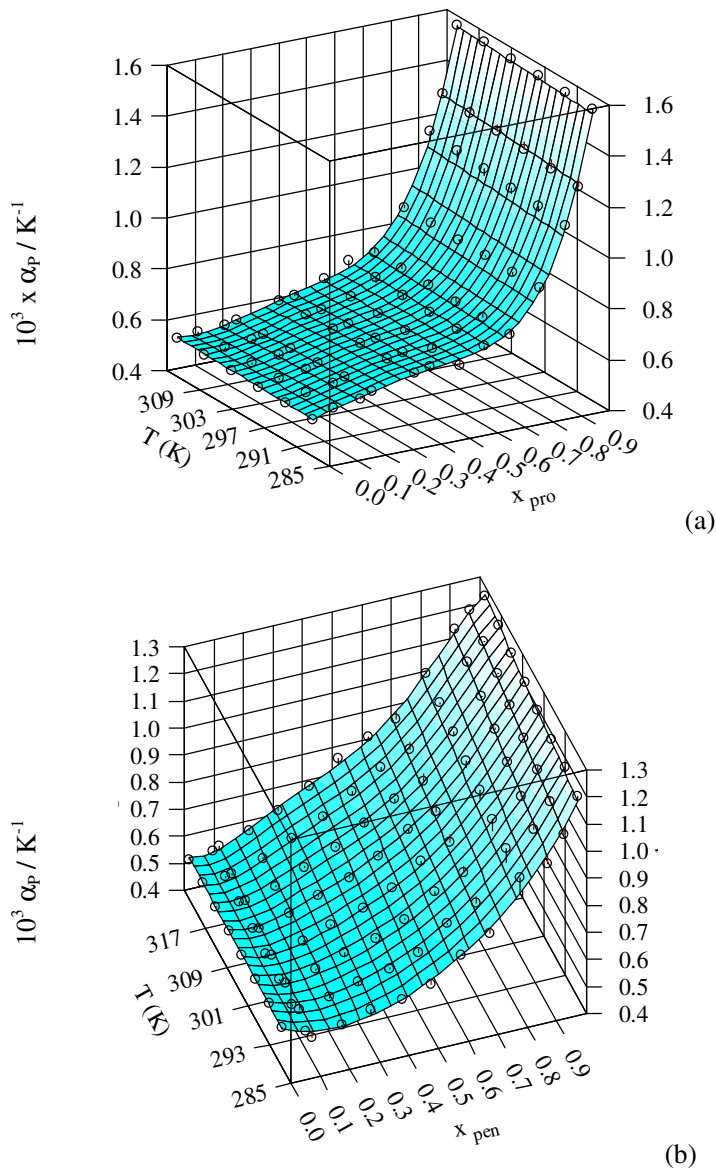


Figure 7. Thermal expansion coefficient vs. solvent mole fraction and temperature, (a) propionaldehyde + [emim][EtSO₄], (b) valeraldehyde + [emim][EtSO₄].

The propionaldehyde mixture exhibits a higher thermal expansion than the valeraldehyde mixture. The results suggest that the increasing of the alkyl chain length in the aldehyde strongly decreases the thermal expansion coefficient. The increasing of the alkyl chain seems to yield a smaller thermal expansion coefficient even at higher concentrations of ionic liquid, the difference between α_p for the binary mixtures being about 20%.

The results of this study suggest that aldehydes are accommodated in the ionic liquid structure in the aldehyde-rich region ($x_1 > 0.5$), possibly by forming hydrogen bonds with both the anion and the cation. The increase on cohesive energy is probably the cause of volumetric compression of the system from the pure aldehyde to $x_1 \approx 0.6$. If the ionic liquid is present in over equimolar amounts ($x_2 > 0.5$), this order become unstable, and the aldehydes rearranges into a different internal order, in which more ionic liquid can be accommodated. Further addition of ionic liquid may be the starting point of ionic liquid aggregates, and some aldehyde molecules not hydrogen-bonded to the ionic liquid appears.

5.2. Density predictions

Figure 8 compares the σ -profile for [emim][EtSO₄], propionaldehyde, and valeraldehyde compounds. The σ -profile of these compounds can be qualitatively divided in three main regions, which are separated in Figure 8 by two vertical lines located at the cutoff values for the hydrogen bond donor ($\sigma_{HB} < -0.0084 \text{ e}/\text{\AA}^2$) and acceptor ($\sigma_{HB} > 0.0084 \text{ e}/\text{\AA}^2$) group (Lin and Sandler, 2002). For [emim][EtSO₄], the σ -profile reveals to be broader than the σ -profiles of the aldehydes. Also, the σ -profile of this ionic liquid is dominated by a huge peak of slightly negative screening charge density at $\sigma = -0.004$, which is due to the polarization of $-\text{CH}_2-$ groups by the amine-hydrogen and oxygen atoms. The two peaks about 0.011 and 0.013 correspond to the negatively charged and lone pairs of the oxygen in the sulfate group. Considering the high-polarity region $\sigma_{HB} > 0.0084 \text{ e}/\text{\AA}^2$, these groups can be considered as hydrogen-bond acceptor groups (Lin and Sandler, 2002; Diedenhofen and Klamt, 2010). On the left-hand side of the histogram, it can be observed one small peak at values lower than the cutoff, $-0.0084 \text{ e}/\text{\AA}^2$, which is affected by the alkyl chain. This peak is related to the amine-hydrogen; it may contribute to hydrogen bonds as donors. Finally, the distribution of the charge densities around zero ($-0.0084 \text{ e}/\text{\AA}^2 < \sigma < 0.0084 \text{ e}/\text{\AA}^2$) corresponds to the non-polar alkyl groups of the cation, being those for positive and negative signs assigned to carbon and hydrogen atoms, respectively. Also, Figure 8 shows that the higher number of carbon atoms in the alkyl chain implies the increasing of the area below each histogram of charge densities around the nonpolar area (propionaldehyde < valeraldehyde < [emim][EtSO₄]). In this way, the σ -profile with high values at $\sigma = 0$ show more repulsive interactions between polar and nonpolar segments, affecting the cohesive properties of the molecule. The same idea can be applied to mixtures, where compounds with very different σ profiles would create a less compact mixture than a mixture of compounds with similar σ profiles. The binary mixture [emim][EtSO₄] + propionaldehyde is the system with the most different σ profiles, so they are more difficult to fit between them, getting a less orderly and compact structure than the system [emim][EtSO₄] + valeraldehyde. Therefore, the mixture [emim][EtSO₄] + valeraldehyde have greater V^E , as can be seen in Figure 3.

The physical properties used in the model for all substances are reported in Table 7. The average relative deviations between calculated and experimental density values for the mixtures of [emim][EtSO₄] with propionaldehyde and valeraldehyde are 1.1%, and 2.3%, respectively (Figure 9). This confirms that σ -profile is an adequate a priori parameter to characterize quantitatively the nonideality of volumetric behavior.

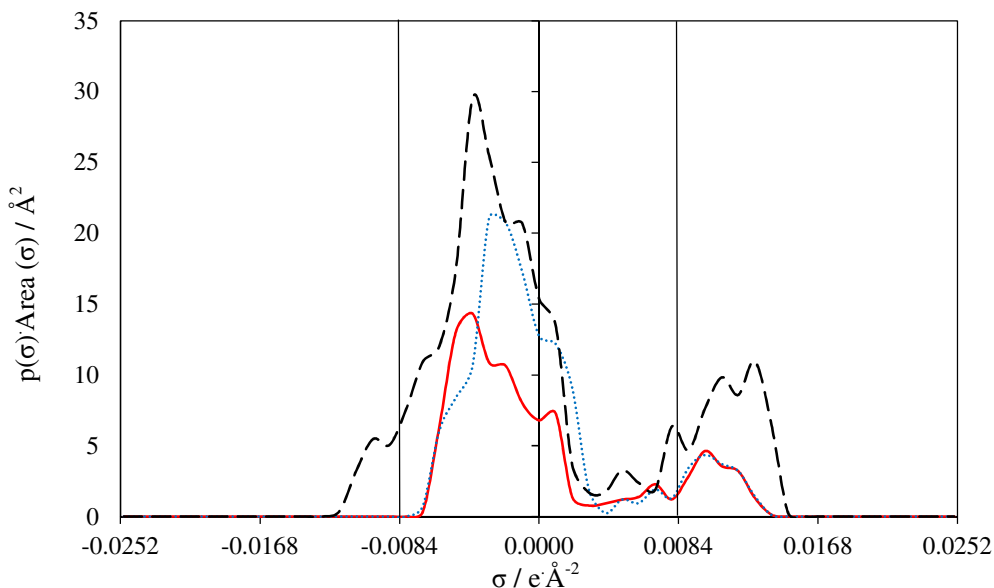


Figure 8. Sigma profiles for [emim][EtSO₄] (— —), propionaldehyde (—), and valeraldehyde (···). Note that, due to the definition as conductor screening charges, electrostatically positive parts of the molecules have negative σ and vice versa.

Table 7. Physical properties used in the modeling.

Compound	<i>MM</i>	<i>T_c</i> (K)	<i>P_c</i> (MPa)	ω	<i>r</i>	<i>q</i>	COSMO segments ^c	<i>V</i> ^{COSMO} (Å ³) ^c
propionaldehyde	58.08	504.4 ^a	4.92 ^a	0.25591 ^a	7.77	4.57	421	85.8253
valeraldehyde	86.13	566.1 ^a	3.97 ^a	0.34716 ^a	12.40	6.59	645	129.8010
[emim][EtSO ₄]	236.29	1067.49 ^b	4.00 ^b	0.37441 ^b	27.53	12.85	1097	282.0909

^aDiadem Public (2000); ^bValderrama and Robles (2007); ^cthis work

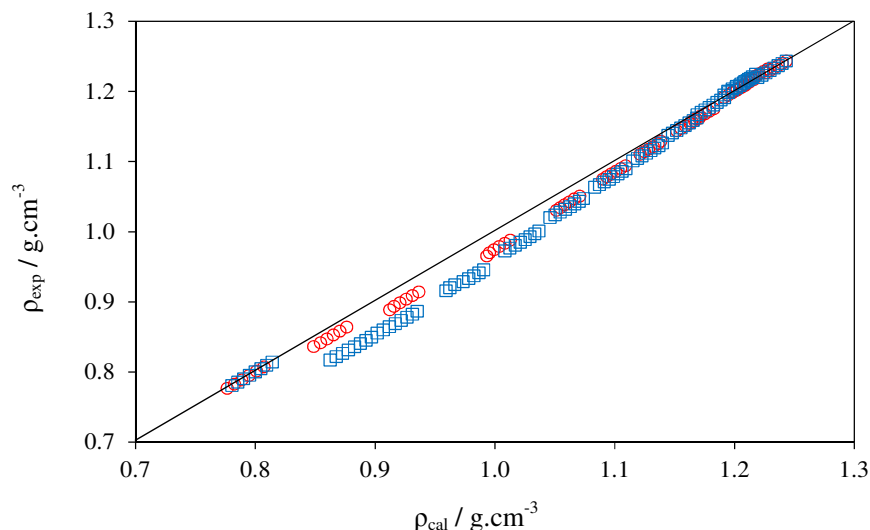


Figure 9. Comparison of experimental and PR-WS/COSMO-SAC model predicted values of density (g.cm⁻³) for binary mixtures propionaldehyde + [emim][EtSO₄] (○) and valeraldehyde + [emim][EtSO₄] (□).

5.3. VLE data

The vapor–liquid equilibrium (VLE) phase diagrams of the two binary mixtures covering a wide range of temperature (313.15–403.15) K at 101.3 kPa are examined. The systems have strong interactions between the species (aldehyde and ionic liquid).

In order to validate the technique, experimental vapor-liquid equilibrium data for the system ethanol (1) + [emim][EtSO₄] (2) were first determined and compared with published data from Calvar et al. (2008). As it could be observed in Figure 10, a good agreement between this work and the data from Calvar et al. (2008) was achieved, and the experimental technique was considered validated.

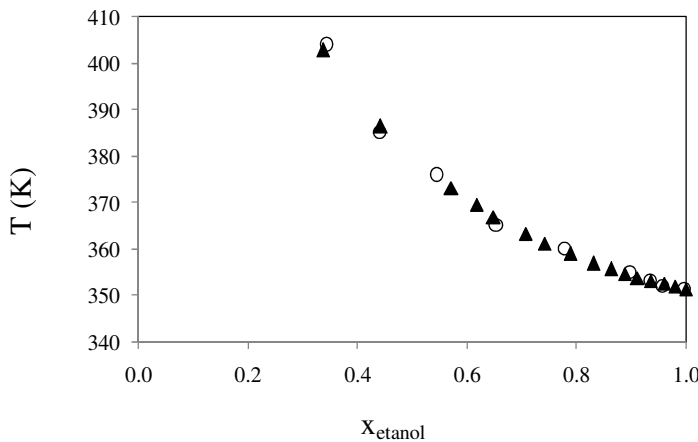


Figure 10. Vapor–liquid equilibrium: (T_x diagram) for the system ethanol + [emim][EtSO₄]. This work (○), Calvar et al. (2008) (▲).

VLE for the binary systems aldehyde (1) + [emim][EtSO₄] (2) have been determined at 101.3 kPa and the results are summarized in Table 8. The parameters used in the thermodynamic model Peng–Robinson EoS with the Wong–Sandler/COSMO–SAC mixing rule are reported in Table 7. The experimental data and predicted results for the systems are shown in Figure 11 and the average relative deviations between these values for the mixtures of [emim][EtSO₄] with propionaldehyde and valeraldehyde are 0.3%, and 1.6%, respectively. The representation of the phase behavior has a good trend for the propionaldehyde mixture only, and the pure vapor phase is correctly predicted for both mixtures. The Peng–Robinson EoS with the Wong–Sandler using NRTL or UNIQUAC model are shown in Figure 12 and the average relative deviations are below than 0.15% for the binary systems. For these systems the interaction parameters are shown in the Table 9.

Table 8. Vapor liquid equilibria at 101.3 kPa for the binary systems with [emim][EtSO₄].

propionaldehyde (1) + [emim][EtSO ₄] (2)		valeraldehyde (1) + [emim][EtSO ₄] (2)	
x_1	T (K)	x_1	T (K)
1.0000	321.2	1.0000	376.2
0.9164	322.8	0.9595	378.3
0.8633	323.6	0.9403	381.2
0.8449	324.0	0.8916	384.2
0.8159	324.7	0.8859	385.4
0.7601	326.1	0.8638	386.7
0.7526	326.1	0.8522	388.2
0.7208	327.3	0.8175	392.0
0.6694	331.2	0.8016	396.0
0.6352	333.7		
0.6171	335.2		

Table 9. Details of the fitted results for the systems studied using the PR+WS/UNIQUAC or PR+WS/NRTL models.

Model	k_{ij}	α	A_{ij}	A_{ji}	% ΔT
propanal (1) + [emim][EtSO ₄] (2)					
NRTL	0,1049	0,3470	-9446,8691	22616,1934	0,06
UNIQUAC	0,3691	-	-3173,4609	7032,0225	0,12
pentanal (1) + [emim][EtSO ₄] (2)					
NRTL	0,1836	0,4171	-0,0214	-9287,5674	0,14
UNIQUAC	-0,6838	-	-3875,4272	22743,0293	0,14

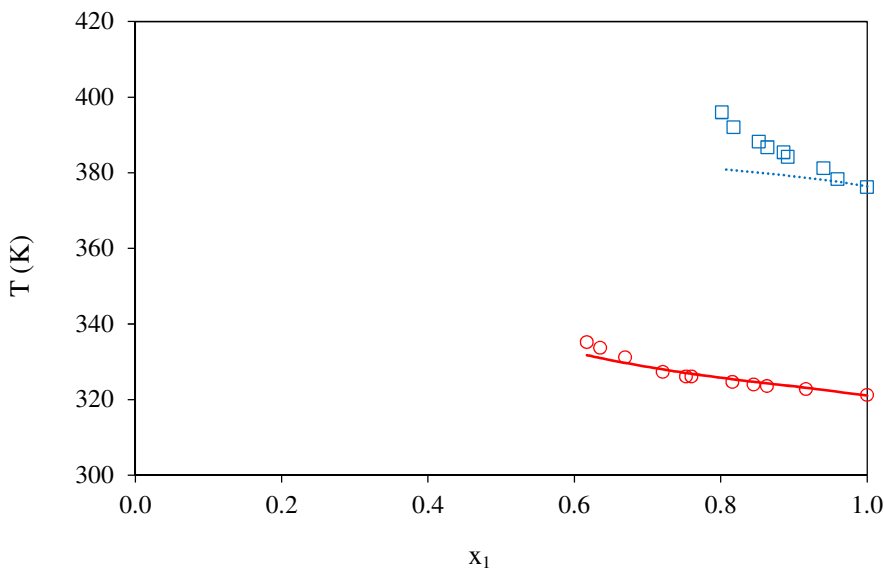


Figure 11. Vapor–liquid equilibrium (T_x diagram): propionaldehyde + [emim][EtSO₄] (○) and valeraldehyde + [emim][EtSO₄] (□); lines are predicted values.

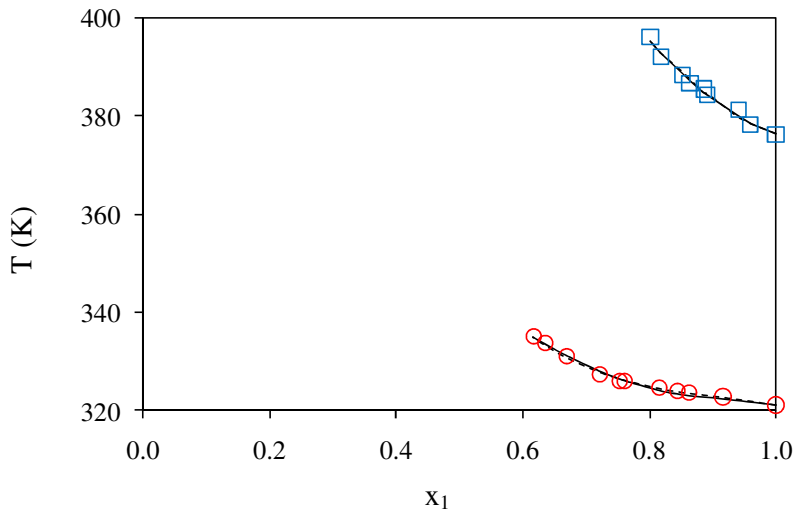


Figure 12. Vapor–liquid equilibrium (T_x diagram): propionaldehyde + [emim][EtSO₄] (○) and valeraldehyde + [emim][EtSO₄] (□); lines are NRTL or UNIQUAC models.

6. Conclusions

Density and refraction index of binary mixtures aldehyde + 1–ethyl–3–methylimidazolium ethylsulfate have been measured at atmospheric pressure. Other properties, such as excess molar volume and deviations in the refraction index were also calculated. The values of V^E are negative at high concentrations of aldehyde and positive in the opposite case. The obtained results indicate that ionic liquid interactions with aldehydes generate a new packing order depending of the mixture composition and the alkyl chain length in the aldehyde.

The vapor–liquid equilibrium of binary systems propionaldehyde + [emim][EtSO₄] and valeraldehyde + [emim][EtSO₄] at 101.3 kPa was measured by a dynamic method.

The Peng–Robinson equation of state coupled with the Wong–Sandler mixing rule using the COSMO–SAC model was used to predict the density and vapor liquid equilibrium.

The predicted densities show deviations below than 2.3 %. COSMO–SAC is also revealed as a valuable computational tool to describe the intermolecular interaction of systems containing [emim][EtSO₄]. In addition, the σ -profile is suggested as a simple molecular parameter to characterize the nonideality of the mixtures respect to volumetric properties.

The experimental VLE data were predicted and fitted by the thermodynamic model with deviations below than 1.6 % and 0.15% respectively.

Acknowledgments

V.H. Álvarez acknowledges the financial support from FAPESP (Fundação de Amparo à Pesquisa do Estado de São Paulo), grant 06/03711-1. M. Aznar and S. Mattedi are recipients of CNPq (Brazil) fellowships

References

- Abrams, D.S.; Prausnitz, J.M. Statistical thermodynamics of liquid mixtures: a new expression for the excess Gibbs energy of partly or completely miscible systems, *AIChE J.*, 21, 116–128, 1975.
- Accelrys Materials Studio, <http://accelrys.com/products/materials-studio/>, accessed January 2010.
- Ansari, I.A.; Gree, R. TEMPO-catalyzed aerobic oxidation of alcohols to aldehydes and ketones in ionic liquid [bmim][PF₆], *Org. Lett.*, 4, 1507–1509, 2002.
- Álvarez, V.H.; Aznar, M. Thermodynamic modeling of vapor–liquid equilibrium of binary systems ionic liquid + supercritical {CO₂ or CHF₃} and ionic liquid + hydrocarbons using Peng–Robinson equation of state, *J. Chin. Inst. Chem. Eng.*, 39, 353–360, 2008a.
- Álvarez, V.H.; Aznar, M. Application of a thermodynamic consistency test to binary mixtures containing an ionic liquid, *The Open Thermodynamics Journal*, v. 2, p. 25-38, 2008b.
- Álvarez, V.H.; Larico, R., Ianos, Y.; Aznar, M. Parameter estimation for VLE calculation by global minimization: genetic algorithm, *Braz. J. Chem. Eng.*, 25, 409–418, 2008.
- Álvarez, V.H.; Dosil, N.; Gonzalez-Cabaleiro, R.; Mattedi, S., Martin-Pastor, M.; Iglesias, M.; Navaza, J.M. Brønsted ionic liquids for sustainable processes: synthesis and physical properties, *J. Chem. Eng. Data*, 55, 625–632, 2010.
- Álvarez, V.H.; Aznar, M. An efficient approach to optimal interpolation of experimental data, *J. Taiwan Inst. Chem. Eng.*, 41, 184–189, 2010.
- Calvar, N.; González, B.; Gómez E.; Dominguez, Á. Vapor–liquid equilibria for the ternary system ethanol + water +1-ethyl-3-methylimidazolium ethylsulfate and the corresponding binary systems containing the ionic liquid at 101.3 kPa, *J. Chem. Eng. Data*, 53, 820–825, 2008.
- Diadem Public 1.2, The DIPPR Information and Data Evaluation Manager, 2000.
- Diedenhofen, M.; Klamt, A. COSMO–RS as a tool for property prediction of IL mixtures – A review, *Fluid Phase Equilib.* 294, 31–38, 2010.
- Huddleston, J.G.; Willauer, H.D.; Swatloski, R.P.; Visser, A.E.; Rogers, R.D. Room temperature ionic liquids as novel media for clean liquid–liquid extraction, *Chem. Commun.*, 1765–1766, 1998.
- ISI web of knowledge, <http://apps.isiknowledge.com/>, accessed in july, 2010.
- Loria, H.; Pereira-Almao, P.; Satyro M. Prediction of density and viscosity of bitumen using the Peng–Robinson equation of state, *Ind. Eng. Chem. Res.* 48, 10129–10135, 2009.
- Lin, S.T.; Sandler, S.I. A priori phase equilibrium prediction from a segment contribution solvation model, *Ind. Eng. Chem. Res.*, 41, 899–913, 2002.
- Luo, S.; Mi, X.; Zhang, L.; Liu, S.; Xu, H.; Cheng J-P. Functionalized ionic liquids catalyzed direct aldol reactions, *Tetrahedron*, 63, 1923–1930, 2007.
- Michelsen, M.L.; Mollerup, J. *Thermodynamic Models: Fundamentals and Computational Aspects*, 2nd ed., Tie-Line Publications, Lyngby, 2007.

Mullins, E.; Oldland, R.; Liu, Y.A.; Wang, S.; Sandler, S.I.; Chen, C.C.; Zwolak, M.; Seavey, K.C. Sigma-profile database for using COSMO-based thermodynamic methods, *Ind. Eng. Chem. Res.*, 45, 4389–4415, 2006.

Nakata, M.; Sakurai, M. Refraction index and excess volume for binary liquid mixtures. Part 1. Analyses of new and old data for binary mixtures, *J. Chem. Soc., Faraday Trans.*, 83, 2449–2457, 1987.

Peneloux, A.; Rauzy, E.; Freze, R. A consistent correction for Redlich–Kwong–Soave volumes, *Fluid Phase Equilib.*, 8, 7–23, 1982.

Peng, D.; Robinson, D.B. A new two-constant equation of state, *Ind. Eng. Chem. Fundam.*, 15, 59–64, 1976.

Renuncio, J.A.R.; Coto, B.; Cabafias, A.; Menduifia, C.; Rubio, R.G.; Pando, C. Excess enthalpies and vapor–liquid equilibrium and surface properties of the highly non-ideal associated mixtures formed by an alcohol and propionaldehyde, *Fluid Phase Equilib.*, 126, 177–194, 1996

Ruso, J.M.; González-Pérez, A.; Prieto, G.; Sarmiento, F.A. Volumetric study of two related amphiphilic beta-blockers as a function of temperature and electrolyte concentration, *Colloids and Surfaces B: Biointerfaces*, 33, 165–175, 2004.

Sarkar, L.; Roy M.N. Studies on liquid–liquid interactions of some ternary mixtures by density, viscosity, ultrasonic speed and refraction index measurements, *Thermoch. Acta*, 496, 124–128, 2009.

Tarakad, R.R.; Scheller, W.A. Isothermal vapor-liquid equilibrium data for the system n-heptane–n-valeraldehyde at 75 and 90°C, *J. Chem. Eng. Data*, 24, 119–120, 1979.

Valderrama, J.O.; Robles, P.A. Critical properties, normal boiling temperatures, and acentric factors of fifty ionic liquids. *Ind. Eng. Chem. Res.*, 46, 1338–1344, 2007.

Wong, D.S.H.; Sandler, S.I. A theoretically correct mixing rule for cubic equations of state. *AIChE J.*, 38, 671–680, 1992.

Zhang, S.; Zhang, Q.; Zhang, Z.C. Extractive desulfurization and denitrogenation of fuels using ionic liquids. *Ind. Eng. Chem. Res.*, 43, 614–622, 2004.

Zhong, Y.; Wang, H.; Diao, K. Densities and excess volumes of binary mixtures of the ionic liquid 1-butyl-3-methylimidazolium hexafluorophosphate with aromatic compound at T=(298.15 to 313.15)K, *J. Chem. Thermodyn.*, 39, 291–296, 2007.

Artigo 4.5: Density, Refractive Index and Vapor-Liquid Equilibria of N-Methyl-2-Hydroxyethylammonium Butyrate plus (Methyl Acetate or Ethyl Acetate or Propyl Acetate) at Several Temperatures

V. H. Álvarez¹, S. Mattedi² and M. Aznar¹

¹*School of Chemical Engineering, State University of Campinas (UNICAMP), P.O. Box 6066, 13083-970, Campinas-SP, Brazil*

²*Chemical Engineering Department, Polytechnic School, Federal University of Bahia (UFBA), 40210-630, Salvador-BA, Brazil*

ABSTRACT – This paper reports the densities, refractive indices, and vapor liquid equilibria for binary systems ester + n-methyl-2-hydroxyethylammonium butyrate (m-2-HEAB): methyl acetate (1) + m-2-HEAB (2), ethyl acetate (1) + m-2-HEAB and propyl acetate (1) + m-2-HEAB (2). The excess molar volumes, deviations in the refractive index, the apparent molar volume, and the coefficient of thermal expansion for the binary systems were fitted to typical equations. The Peng-Robinson equation of state, coupled with the Wong-Sandler mixing rule, is used to describe the experimental data. To calculate activity coefficients we used three different models: NRTL, UNIQUAC and COSMO-SAC. Since the predictive liquid activity coefficient model COSMO-SAC is used in the Wong-Sandler mixing rule, the resulting thermodynamic model is a completely predictive one. The prediction results for the density and for the vapor-liquid equilibria have a deviation lower than 1.0% and 1.1%, respectively. The vapor-liquid equilibria predictions show a good trend for the esters mixture.

KEYWORDS: ionic liquid; COSMO-SAC; excess volume

1. Introduction

Actually, organic esters are important intermediates in chemical and pharmaceutical industries, and they are mostly produced by acid-catalyzed esterification reactions (Larock, 1999). Various mineral acids have been used as catalysts for esterification, but they are extremely corrosive and need to be neutralized at the end of the reaction. Many acid-catalyzed organic reactions based on ILs have been reported, among which esterifications are a hot topic (Zhu et al., 2003) Furthermore, at the end of the reaction, a direct liquid-liquid separation or distillation of the esters compounds from the reaction mixture appears very attractive in the case of derivatives that are volatile enough. And, after performing purification methods on the ionic solvent, it could be recycled.

Room-temperature ionic liquids are neoteric substances, salts that are liquids below approximately 373 K and they are considered as potential substitutes to many traditional organic solvents in reaction and separation processes (Huddleston et al., 1998; Zhang et al., 2004). In spite of their importance and interest, accurate values for many of the fundamental physical-chemical properties of these compounds are either scarce or absent. In order to design any process involving ionic liquids in industrial scale, it is necessary to know several physical properties, including

density and vapor-liquid equilibria between mixtures of esters and ionic liquids. Since it is impossible to measure all the possible combinations of systems, it is necessary to make measurements on selective systems to provide results that can be used to develop correlations and predictive methods.

The majority studies concerning ionic liquids have been based on the imidazolium cation and, to a lesser extent, on the alkyl pyridiniums and trialkylamines (Marsh et al., 2004). In opposition Protic ionic liquids (PIL's) have received limited attention from the academia. The first PIL synthetized was the ethanolammonium nitrate, reported by Gabriel and Weiner in 1882. These PILs were produced by a stoichiometric acid-base Brønsted reaction and their main difference, compared to aprotic ILs (AIL's), is the presence of at least a labile proton, which is/are able to promote extensive hydrogen bonding (Kennedy and Drummond, 2009; Álvarez et al., 2010). Newly, some work has been reported on the synthesis, physicochemical and structural characterization of PILs. Bicak (2005) synthesized the 2-hydroxyethylammonium formate (2-HEAF), an ionic liquid formed by the neutralization of monoethanolamine with formic acid. Greaves et al. (2006) proposed different PILs from primary amines and organic and inorganic acids. Cota et al. (2007), Kurnia et al. (2009) and Alvarez et al. (2010) synthesized a family of these ILs by modifying the aliphatic chain of the organic acid and/or using secondary and tertiary hydroxyamines. There were also studies that use PIL's in catalytic reactions and on the interaction with hydroxilic solvents, showing that 2-HEAF is soluble in water, ethanol and methanol in all the concentration range (Iglesias et al., 2008). Moreover, a relevant aspect, few times considered in the relation application of ILs and the environment, is their potential toxicity. This issue has not been sufficiently studied until now, especially taking into account the need of this information to fulfill the REACH (Registration, Evaluation, Authorization and Restriction of Chemical Substances) requirements (UE) and so, allowing the assessment of hygiene and safety issues derived from their manufacture, use, and transport in the industrial sectors in which these substances will be applied. In what is referred to PIL's from hydroxyamines and organic acids, the first results highlight that total biodegradation and low toxicity are intrinsic characteristics of these family of ionic liquids (Sierra et al., 2008; Peric et al., 2010).

In this work, experimental density and refractive index data of pure m-2-HEAB PIL have been measured at several temperatures. Also, experimental density, refractive index and vapor-liquid equilibria (VLE) data over whole composition range for methyl acetate (1) + m-2-HEAB (2), ethyl acetate (1) + m-2-HEAB (2) and propyl acetate (1) + m-2-HEAB (2) have been determined at 101.3 kPa. The coefficient of thermal expansion, excess molar volumes, and deviations in the refractive index were calculated from experimental data. Density and VLE data were predicted using the Peng-Robinson equation of state (Peng and Robinson, 1976) coupled with the Wong-Sandler mixing rule (Wong and Sandler, 1992) using the COSMO-SAC model (Li and Sandler, 2002) for the calculation of the liquid-phase activity coefficients.

2. Experimental Section

2.1. Chemicals

The esters were supplied by Sigma-Aldrich, with mass fraction higher than 0.99, and were degassed ultrasonically.

2.2. Synthesis

N-methyl-2-hydroxyethylammonium butyrate was prepared according to a slightly modified literature procedure (Álvarez et al., 2010); a quantity of butanoic acid was added dropwise to a quantity of 2-(methylamino)ethanol and cooled in an ice bath under nitrogen at a rate to maintain the reaction temperature below 283.15 K, since the reaction is exothermic. The reaction mixture was stirred at room temperature for 5 h and the progress of the reaction was monitored by refractive index measurements. The ionic liquid n-methyl-2-hydroxyethylammonium butyrate obtained was dried by heating to 343.15 K and stirring under high vacuum (7 Pa) for 48 h. Its purity was ascertained as 98 % mass fraction by NMR method. Then, the ionic liquid was kept in bottles with nitrogen gas.

To reduce the water content (lower than 0.1 % mass fraction, determined using a 756 Karl Fisher titrator), the dried method was applied, always immediately prior to their use.

Table 1 shows a good agreement between experimental and literature density data of the pure components at 298.15 K. The differences between experimental and literature data for pure m-2-HEAB can be explained because physical properties of ionic liquids depend on the water content and other impurities.

Table 1. Density of pure compounds at 298.15 K.

Compound	ρ (g cm ⁻³)	
	exp	lit
methyl acetate	0.92682	0.9282 ^a
ethyl acetate	0.89490	0.8928 ^a
propyl acetate	0.88261	0.8823 ^a
m-2-HEAB	1.03394	1.0392 ^b

^aSarkar and Roy (2009); ^bÁlvarez et al. (2010)

2.3. Apparatus and procedure

Samples were prepared by introducing with a syringe known masses of the pure liquids into stoppered bottles, in an inert-atmosphere glove box, using a Mettler AX-205 Delta Range analytical balance, with a precision of $\pm 10^{-4}$ g. A glove box was used because the ionic liquid is moisture sensitive. Densities were measured using an Anton Paar DMA 4000 digital vibrating-tube densimeter. The repeatability and the uncertainty in experimental measurement have been found to be lower than $\pm 5 \times 10^{-6}$ g cm⁻³ for the density. The DMA 4000 automatically corrects the influence of viscosity on the measured density.

Refractive indices were determined using an automatic refractometer Mettler Toledo D4 with a resolution of $\pm 10^{-4}$ and an uncertainty in the experimental measurements of $\pm 2 \times 10^{-4}$.

3. Modeling

3.1. Properties

The density and refractive index for the mixtures were correlated by:

$$Z = \sum_{i=0}^p \left(\left(\sum_{j=0}^q B_{ij} T^j \right) x_1^{i-1} \right) \quad (1)$$

where Z is the density or speed of sound of the mixture, x_1 is the mole fraction of the solvent, p and q are the polynomial degrees, B_{ij} are the fitting parameters, and T is the absolute temperature.

The excess molar volumes (V^E) and deviations in the refractive index ($\delta\kappa_S$) were calculated from experimental values as follows:

$$V^E = \sum_{i=1}^N x_i M_i \left(\frac{1}{\rho} - \frac{1}{\rho_i} \right) \quad (2)$$

$$\delta n_D = n_D - \sum_{i=1}^N x_i n_{Di} \quad (3)$$

where N is the number of compounds in the mixture, x_i is mole fraction; M_i denotes molar mass; ρ_i is the density of the pure compound i , ρ is the density of the mixture, n_D and n_{Di} are the refractive index of the mixture and the refractive index of the pure components, respectively. These derived properties were fitted to a Redlich-Kister-type equation:

$$Q_{12} = x_1 x_2 \sum_{i=0}^p \left(\left(\sum_{j=0}^q C_{ij} T^j \right) (x_1 - x_2)^i \right) \quad (4)$$

where Q_{12} is V^E or $\delta\kappa_S$ and the other variables are the same as above.

The apparent molar volume (ϕ_V) for the mixtures contend m-2-HEAB were calculated by:

$$\phi_V = 1000 \left(\frac{\rho_1 - \rho}{m \rho_1 \rho} \right) + \frac{M_2}{\rho_1} \quad (5)$$

where ρ is the density of the mixture, ρ_1 is the density of the solvent, M_2 is the molar mass of ionic liquid, m is the molality of the solution. These derived values were correlated by a modified Redlich–Mayer equation, where the fitting parameters show temperature dependence:

$$\phi_F = \left(\sum_{j=0}^q \phi_{Fi}^o T^j \right) + \sum_{i=0}^p \left(\left(\sum_{j=0}^q \phi_{ij}^F T^j \right) m^{A_i} \right) \quad (6)$$

where F represents any apparent molar property and ϕ_{Fi}^o and ϕ_{ij}^F are fitting parameters.

The thermal expansion coefficient (α_P) shows the temperature dependence of volume, and it is defined as:

$$\alpha_P = \frac{1}{V} \left(\frac{\partial V}{\partial T} \right)_P = - \left(\frac{\partial \ln \rho}{\partial T} \right)_P \quad (7)$$

3.2. VLE

The most common method used for the correlation of phase equilibria in mixtures at high and low pressure is the use of equations of state (EoS). The most common and industrially important EoS are the cubic equations derived from van der Waals EoS; among these, the Peng–Robinson EoS (Peng and Robinson, 1976) has proven to combine the simplicity and accuracy required for the prediction and correlation of volumetric and thermodynamic properties of fluids, although there can be problems when applying the PR EoS to systems near the critical point.

Recently, Álvarez and Aznar (2008a, 2008b) applied an extension of this approach to several supercritical fluid + ionic liquid systems, using the Peng–Robinson equation of state coupled with the Wong–Sandler mixing rule (Wong and Sandler, 1992) using the UNIQUAC or NRTL model (Abrams and Prausnitz, 1975) for the excess Gibbs free energy, G^E , using three or four adjustable parameters, respectively.

By using the Wong–Sandler mixing rule, any cubic EoS can be made predictive for mixtures, i.e., without the need of any adjustable binary interaction parameter, when a predictive model for G^E is used. For example, G^E can be determined from the COSMO-SAC model (Lin and Sandler, 2002), in which the activity coefficient γ_i of species i is calculated from the sum of the residual and combinatorial contributions:

$$\ln \gamma_i = \ln \gamma_i^{res} + \ln \gamma_i^{com} \quad (8)$$

The residual part is calculated considering molecular solvation in a perfect conductor. The distribution of screening charges on the molecular surface, called the sigma profile $p(\sigma)$, is first determined from quantum mechanical calculations. The molecular interactions in the liquid phase are assumed to be the sum of contributions of surface segment interactions through the screening charges. With these assumptions, the residual term takes the following form:

$$\ln \gamma_i^{res} = n_i \sum_{\sigma_m} p_i(\sigma_m) \ln [\Gamma_S(\sigma_m) - \Gamma_i(\sigma_m)] \quad (9)$$

where n_i is the number of surface segments contained in species i , $\Gamma_S(\sigma)$ is the activity coefficient of segment i (whose screening charge density is σ) in solution S (for which the probability of finding a segment of charge density σ be denoted $p_S(\sigma)$):

$$\ln \Gamma_s(\sigma_m) = -\ln \left\{ \sum_{\sigma_n} p_s(\sigma_n) \Gamma_s(\sigma_n) \exp \left[\frac{-\Delta W(\sigma_m, \sigma_n)}{RT} \right] \right\} \quad (10)$$

where $W(\sigma_m, \sigma_n)$ is the electrostatic interaction between two segments of charge density σ_m and σ_n . The Staverman–Guggenheim model is used for the combinatorial term:

$$\ln \gamma_i^{com} = \ln \frac{\Phi_i}{x_i} + \frac{z}{2} q_i \ln \frac{\theta_i}{\Phi_i} + l_i - \frac{\Phi_i}{x_i} \sum_j x_j l_j \quad (11)$$

$$\Phi_i = \frac{r_i x_i}{\sum_j r_j x_j} \quad \theta_i = \frac{q_i x_i}{\sum_j q_j x_j} \quad (12)$$

$$l_i = (z/2)(r_i - q_i) - (r_i - 1) \quad (13)$$

where θ_i is the surface area fraction, Φ_i is the volume fraction, z is the coordination number ($z=10$), and r_i and q_i are the normalized volume and surface area parameters for species i .

3.3. Density predictions

The calculation of the molar volume of the mixture at a specific temperature and pressure can be predicted by an equation of state. The Peng-Robinson equation of state, coupled with the Wong-Sandler mixing rule using the predictive liquid activity coefficient model COSMO-SAC was used as thermodynamic model to predict the density. In the COSMO model, for each compound, the equilibrium molecular geometry is first determined by minimization of the molecular energy at 0 K. The next step for COSMO-SAC calculation is to estimate the volume of cavity (V_{COSMO}), the total number of segments (COSMO Segments), and the sigma profile of each compound. The calculations were done using the quantum chemistry package DMol3 built in Accelrys Materials Studio v4.3. The sigma profile, $p(\sigma)$, is a file containing the probability of finding a surface segment with screening charge density, σ . The detailed settings for DMol3 can be found elsewhere (Mullins et al., 2006) and, for the molecular description of the ionic liquid, there is used the ion-pair approach (Diedenhofen and Klamt, 2010). The sigma profile of ionic liquid has been obtained for the molecule as a whole. The activity coefficient is then calculated (Mullins et al., 2006). The Peng-Robinson equation can be written in terms of the compressibility factor (Z) by:

$$Z^3 - (1-B)Z^2 + (A-3B^2-2B)Z - (AB-B^2-B^3) = 0 \quad (14)$$

where A and B are given by:

$$A = \frac{a_m P}{(RT)^2} \quad (15)$$

$$B = \frac{b_m P}{RT} \quad (16)$$

where the constants a_m and b_m are expressed as functions of the concentration of the different components in the mixture, through the so-called mixing rules. In this work, the Wong-Sandler mixing rules are used:

$$b_m = \frac{\sum_i \sum_j x_i x_j \left(b - \frac{a}{RT} \right)_{ij}}{1 - \sum_i \frac{x_i a_{ii}}{b_{ii} RT} - \frac{A_\infty^E}{\Omega RT}} \quad (17)$$

$$a_m = b_m \left[\sum_i \frac{x_i a_{ii}}{b_{ii}} + \frac{A_\infty^E}{\Omega} \right] \quad (18)$$

$$\left(b - \frac{a}{RT} \right)_{ij} = \frac{(b_{ii} + b_{jj})}{2} - \frac{(1 - k_{ij}) \sqrt{a_{ii} a_{jj}}}{RT} \quad (19)$$

In these equations, k_{ij} is the adjustable interaction parameter, $\Omega = \ln(\sqrt{2}-1)/\sqrt{2}$ for the PR EoS, and A_∞^E , the excess Helmholtz free energy at the limit of infinite pressure, is calculated using the COSMO-SAC, activity coefficient model, and a_{ii} and b_{ii} are the EoS constants, defined as

$$a_{ii} = 0.457235(RT_c/P_c)^2 [1 + F(1 - T_r^{0.5})], \quad F = 0.37464 + 1.54226\omega - 0.26992\omega^2 \quad (20)$$

$$b_{ii} = 0.077796(RT_c/P_c) \quad (21)$$

where T_r is the reduced temperature, T_c is the critical temperature, P_c is the critical pressure, and ω is the Pitzer acentric factor.

Equation 14 yields one or three real roots, depending on the number of phases in the system. It was shown that this model provides an excellent representation of the vapor-liquid experimental data (Álvarez and Aznar, 2008a). For the prediction of the liquid density, the root of interest is the smallest positive one. An equation of state does not necessarily yield the accurate volumetric behavior of fluids and their mixtures. In order to improve the description of liquid densities, a volume translation is used (Peneloux et al., 1982, Loria et al., 2009). Then, for the prediction of the liquid density, the root of interest in Equation (14) is the smallest positive one. Then, the difference between the volume calculated by the thermodynamic model and the experimental volume for pure compounds, can be defined:

$$\Delta v_i = V_{i,\text{exp}} - V_{i,\text{cal}} \quad (22)$$

where $V_{i,\text{cal}}$ is the molar volume of the compound i calculated by the thermodynamic model, and $V_{i,\text{exp}}$ is the experimental molar volume of the compound i . Then, the volume of the mixture is obtained using the correction of the volume applied by

$$V = V_{\text{cal}} + \sum_i \Delta v_i x_i \quad (23)$$

where x_i is the liquid molar fraction of the pure compound i , V_{cal} is the liquid molar volume of the mixture calculated with the thermodynamic model, and V is the predicted corrected molar volume of the mixture.

3.4. Computation details

The vapor–liquid equilibrium (VLE) phase diagrams of three binary mixtures covering a wide range of temperature (313.15–403.15) K at 101 kPa are examined. The chosen systems have strong interactions between the species (esters and ionic liquid).

For each system, the VLE phase diagram is predicted by using the Peng-Robinson EoS with the Wong-Sandler/COSMO-SAC mixing rule. For a given liquid phase composition, the bubble point pressure calculation, as detailed by Michelsen and Mollerup (2007), is performed to obtain the system pressure and the vapor phase compositions. In order to make the models predictive, the binary interaction parameters k_{ij} in the combining rules are set to zero.

For each compound, the equilibrium molecular geometry is first determined by minimization of the molecular energy at 0 K using the quantum chemistry package DMol3 implemented in Accelrys Materials Studio v4.3. A solvation calculation in a perfect conductor is then performed using the equilibrium geometry to obtain the surface screening charges on the compound. . The detailed settings for DMol3 was the same that Mullins et al. (2006) applied. The activity coefficient is then calculated from the procedure above using an in-house program. Note that, for each species, the quantum mechanical part of this calculation, which may be time consuming, only has to be done once, regardless of the temperature and the composition of mixture needed. The absolute average error in pressure, vapor phase composition or density from the calculation is determined as:

$$|\Delta F| \% = \frac{100}{N} \sum_{i=1}^N \frac{|F_i^{cal} - F_i^{exp}|}{F_i^{exp}} \quad (24)$$

where N is the number of data point, superscripts *exp* and *cal* denote the values from experiment and our calculation, respectively.

4. Parameter Estimation

In this work, the first approximation parameter estimation was performed using a genetic algorithm code, mMyGA (Álvarez et al., 2008) using a whole interval search. After that, the fitting parameters were best tuned using a non-linear optimization algorithm based on the Marquardt algorithm. The optimization used the minimization of the standard deviation (s) between experimental and calculated values, defined as:

$$s = \left[\sum_{i=1}^N \frac{(F_{exp} - F_{cal})_i^2}{N-m} \right]^{1/2} \quad (25)$$

where N is the number of experimental points, m is the number of parameters in the curve fit, and F_{cal} and F_{exp} are the values of the property calculated by the model and obtained experimentally, respectively.

5. Results and Discussion

The m-2-HEAB was synthetized and the 1D hydrogen spectrum was similar than Álvarez et al., (2010) as can be seen in Figure 1. The m-2-HEAB ionic liquid shows completely solubility in water, methanol and ethanol, and it is not soluble in some alkanes as n-octane and n-dodecane. The humidity of the ionic liquid was determined by using DL31 Karl Fischer titrator (Mettler Toledo) and shows moisture less than 900 ± 50 ppm of H_2O .

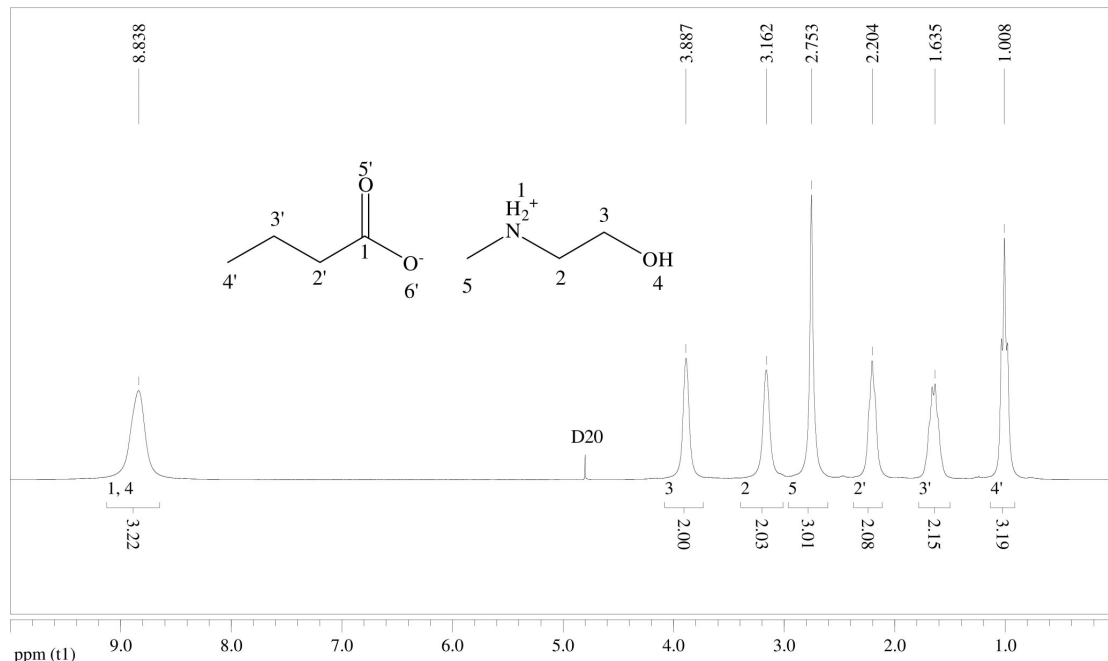


Figure 1. 1D hydrogen spectrum for the m-2-HEAB ionic liquid.

The m-2-HEAB ionic liquid shows completely solubility in methyl acetate, in ethyl acetate, and in propyl acetate from 288.15, 303.15, and 308.15 K, respectively. These data established the lower temperature where the liquids were miscible and thus where the excess properties could be determined.

5.1. Properties

Densities and excess molar volumes of the binary mixtures methyl acetate (1) + m-2-HEAB (2), ethyl acetate (1) + m-2-HEAB (2) and propyl acetate (1) + m-2-HEAB (2) at 298.15 K and refractive indices and deviations in the refractive indices at atmospheric pressure are listed in Tables 2 and 3. The complete data are presented in the supporting information. Table 4 contains the fitting parameters for density and refractive index by equation (1). Figures 2 shows this property as a function of composition and temperature. This figure shows a similar behavior for the three binary mixtures. The increase of the density is obtained by a decrease of the temperature and an increase of

the ionic liquid composition. In all figures, the open points are the experimental data and the lines are the results for the model fitted.

Table 2. Density and excess volume for the esters (1) + m-2-HEAB (2).

methyl acetate + m-2-HEAB (288.15 K)			ethyl acetate + m-2-HEAB (303.15 K)			propyl acetate + m-2-HEAB (313.15 K)		
x_1	ρ (g/cm ³)	V^E	x_1	ρ (g/cm ³)	V^E	x_1	ρ (g/cm ³)	V^E
0.0000	1.04600	0.0000	0.0000	1.03587	0.0000	0.0000	1.02914	0.0000
0.0454	1.04000	0.3520	0.0454	1.02624	0.8080	0.0785	1.01332	0.9322
0.0956	1.03610	0.5246	0.0956	1.02232	0.6510	0.1247	1.00937	0.6252
0.1990	1.02730	0.8605	0.1990	1.01358	0.3460	0.2070	0.99976	0.4202
0.2901	1.02107	0.7075	0.2901	1.00461	0.1635	0.3035	0.98989	-0.1133
0.4120	1.01560	0.4704	0.4120	0.99258	-0.2320	0.4177	0.97759	-0.7700
0.5070	1.01150	-0.0991	0.5070	0.98119	-0.4054	0.5088	0.96473	-0.9609
0.6018	1.00300	-0.2154	0.6018	0.96706	-0.3654	0.6042	0.94838	-0.8692
0.7039	0.99140	-0.1586	0.7039	0.95035	-0.3235	0.6960	0.93130	-0.7187
0.8031	0.97720	-0.0865	0.8031	0.93153	-0.1807	0.7939	0.91241	-0.6133
0.8998	0.95970	-0.0291	0.8998	0.91157	-0.0795	0.8936	0.89100	-0.3774
0.9497	0.95010	0.0118	0.9497	0.90062	-0.0494	0.9454	0.87887	-0.1920
1.0000	0.93990	0.0000	1.0000	0.88876	0.0000	1.0000	0.86570	0.0000

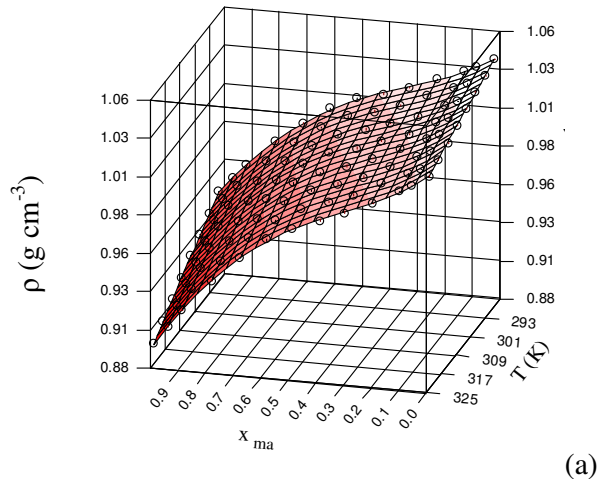
Table 3. Refractive index and deviations for the systems esters (1) + m-2-HEAB(2).

methyl acetate + m-2-HEAB (288.15 K)			ethyl acetate + m-2-HEAB (303.15 K)			propyl acetate + m-2-HEAB (313.15 K)		
x_1	n_D	δn_D	x_1	n_D	δn_D	x_1	n_D	δn_D
1.0000	1.3650	0.0000	1.0000	1.3672	0.0000	1.0000	1.3741	0.0000
0.9483	1.3746	0.0048	0.9497	1.3746	0.0031	0.9454	1.3809	0.0027
0.8979	1.3833	0.0088	0.8998	1.3812	0.0054	0.8936	1.3870	0.0048
0.7912	1.3996	0.0152	0.8031	1.3949	0.0107	0.7939	1.3991	0.0093
0.6898	1.4130	0.0191	0.7039	1.4055	0.0128	0.6960	1.4068	0.0095
0.5928	1.4232	0.0203	0.6018	1.4161	0.0146	0.6042	1.4146	0.0103
0.4973	1.4327	0.0210	0.5070	1.4246	0.0149	0.5088	1.4222	0.0106
0.3983	1.4399	0.0190	0.4120	1.4324	0.0145	0.4177	1.4288	0.0103
0.3079	1.4349	0.0056	0.2901	1.4411	0.0127	0.3035	1.4365	0.0092
0.2074	1.4509	0.0123	0.1990	1.4472	0.0109	0.2070	1.4417	0.0071
0.1097	1.4556	0.0079	0.0956	1.4511	0.0059	0.1247	1.4457	0.0048
0.0646	1.4558	0.0039	0.0454	1.4533	0.0038	0.0785	1.4483	0.0039
0.0000	1.4579	0.0000	0.0000	1.4534	0.0000	0.0000	1.4504	0.0000

Table 4. Fitting parameters and root mean square deviations for density and refractive index of binary systems by equation (1).

	Methyl acetate + m-2-HEAB			Ethyl acetate + m-2-HEAB		
	$\rho/\text{g cm}^{-3}$	n_D		$\rho/\text{g cm}^{-3}$	n_D	
B ₀₀	1.232x10 ⁰	-2.777x10 ⁴		1.199x10 ⁰	-3.073x10 ⁴	
B ₀₁	-6.045x10 ⁻⁴	-9.538x10 ¹		-4.133x10 ⁻⁴	-1.004x10 ²	
B ₀₂	-1.288x10 ⁻⁷	6.655x10 ⁻¹		-4.314x10 ⁻⁷	6.656x10 ⁻¹	
B ₁₀	-4.042x10 ⁻²	-2.777x10 ⁴		6.744x10 ⁻¹	-3.073x10 ⁴	
B ₁₁	-3.270x10 ⁻⁴	-9.538x10 ¹		-5.009x10 ⁻³	-1.004x10 ²	
B ₁₂	2.275x10 ⁻⁹	6.655x10 ⁻¹		7.651x10 ⁻⁶	6.656x10 ⁻¹	
B ₂₀	-4.289x10 ⁻¹	-2.777x10 ⁴		2.726x10 ⁰	-3.073x10 ⁴	
B ₂₁	5.014x10 ⁻³	-9.538x10 ¹		-1.493x10 ⁻²	-1.004x10 ²	
B ₂₂	-8.910x10 ⁻⁶	6.655x10 ⁻¹		2.216x10 ⁻⁵	6.656x10 ⁻¹	
B ₃₀	1.038x10 ⁰	-2.777x10 ⁴		-1.029x10 ¹	-3.073x10 ⁴	
B ₃₁	-9.772x10 ⁻³	-9.539x10 ¹		6.185x10 ⁻²	-1.004x10 ²	
B ₃₂	1.697x10 ⁻⁵	6.655x10 ⁻¹		-9.657x10 ⁻⁵	6.656x10 ⁻¹	
B ₄₀	-5.938x10 ⁻¹			6.943x10 ⁰		2.368x10 ⁻¹
B ₄₁	5.138x10 ⁻³			-4.266x10 ⁻²		-9.480x10 ⁻⁴
B ₄₂	-9.241x10 ⁻⁶			6.703x10 ⁻⁵		3.117x10 ⁻⁶
<i>s</i>	8.9x10 ⁻⁴	3.9		9.2x10 ⁻⁴	8.5	
						1.0x10 ⁻³
						1.45

ρ : density, u : velocity of sound, B_{ij} : the fitting parameters of equation (1), s : standard deviation between experimental and calculated values.



(a)

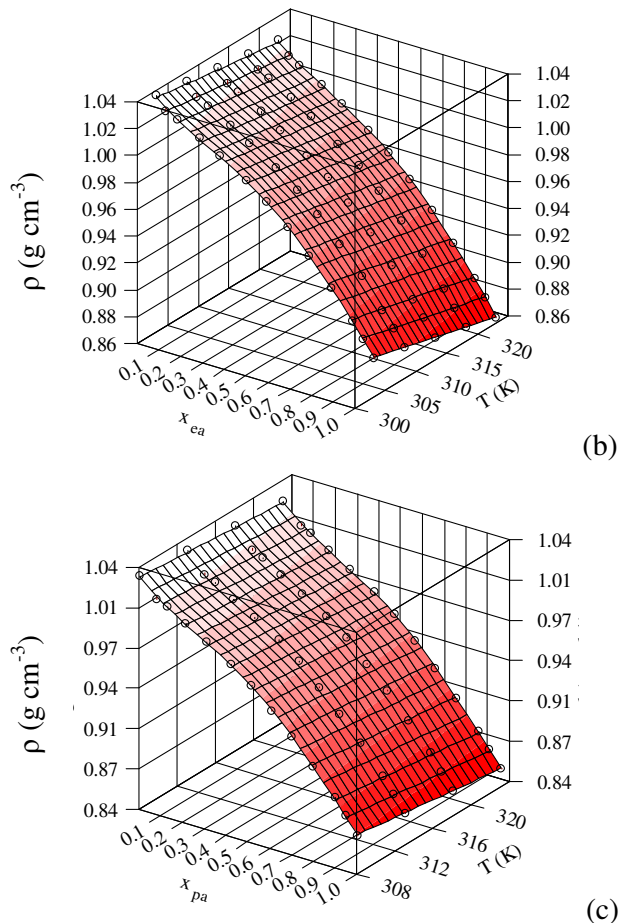
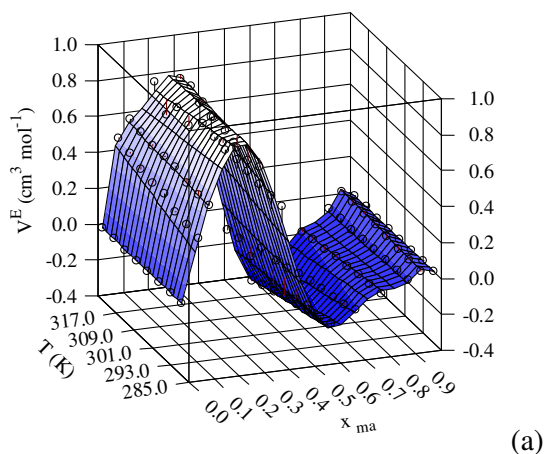


Figure 2. Density versus mole fraction and temperature, (a) methyl acetate + m-2-HEAB, (b) ethyl acetate + m-2-HEAB, (c) propyl acetate + m-2-HEAB.



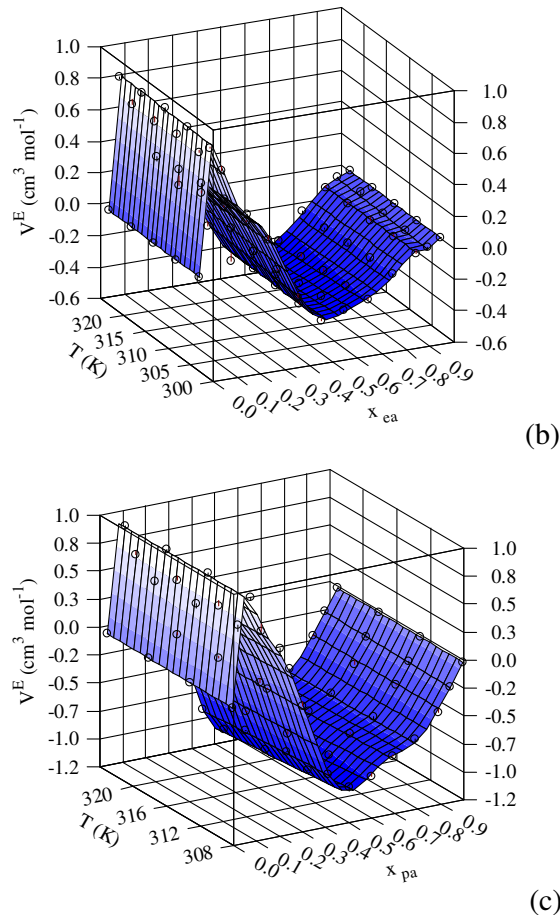


Figure 3. Excess molar volume versus mole fraction and temperature, (a) methyl acetate + m-2-HEAB, (b) ethyl acetate + m-2-HEAB, (c) propyl acetate + m-2-HEAB.

Figure 3 and Figure 4 show the experimental excess molar volume and deviations in the refractive index, respectively, as well as the fitted curves for binary mixtures ester + m-2-HEAB. Table 5 contains the fitting parameters for these properties. In Figure 3a we can observe that the excess molar volumes show a minimum at $x_1 = 0.6$ for the methyl acetate + m-2-HEAB system and $x_1 = 0.5$ for the other two systems; besides, the methyl acetate + m-2-HEAB system presents a maximum at $x_1 = 0.25$ and $x_1 = 0.1$ for the other two systems. The minimum V^E could be due to hydrogen bonds between ester and ionic liquid. At higher concentrations of ester, in the methyl acetate + m-2-HEAB system we can observe a maximum that can be due to the dissociation of the ions in the ionic liquid. In the same way, low concentration of the ester broke the self-associate IL to build a positive V^E . And, a continues introduction of esters in the ionic liquid structure results in considerable decrease in the excess molar properties to more negative values to build association IL-ester, showing the polar effect of the molecules. In other cases, the increase of the alky chain in the ester results in an increase of the excess molar properties, showing the ability of the alkyl chain to fill the holes of the new structure IL-ester.

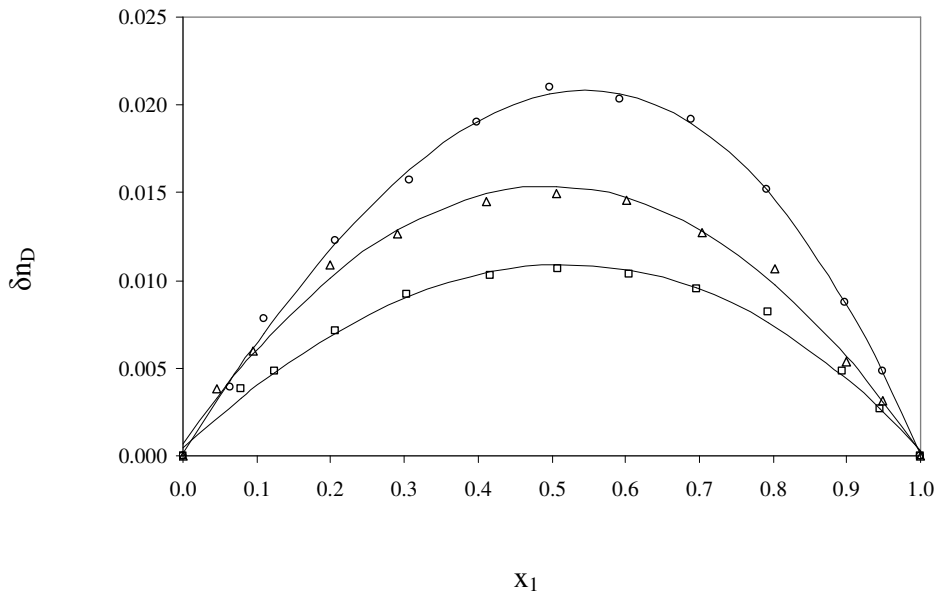


Figure 4. Deviations in the refractive index. Methyl acetate(\circ), ethyl acetate (Δ), propyl acetate (\square), fitted values by the Redlich-Kister model (-).

Table 5. Fitting parameters and root mean square deviations for excess molar volume and deviations of refractive index of binary systems by equation (4).

	Methyl acetate + m-2-HEAB		Ethyl acetate + m-2-HEAB		Propyl acetate + m-2-HEAB	
	$V^E/(cm^3 mol^{-1})$	δn_D	$V^E/(cm^3 mol^{-1})$	δn_D	$V^E/(cm^3 mol^{-1})$	δn_D
C ₀₀	3.522×10^{-1}	8.358×10^{-2}	-1.410×10^0	5.932×10^{-2}	5.642×10^0	4.207×10^{-2}
C ₀₁	-2.220×10^{-3}		-4.827×10^{-4}		-3.047×10^{-2}	
C ₁₀	2.263×10^1	2.046×10^{-2}	1.990×10^1	3.731×10^{-4}	8.886×10^0	-2.466×10^{-3}
C ₁₁	-1.023×10^{-1}		-7.116×10^{-2}		-3.082×10^{-2}	
C ₂₀	1.655×10^1	-3.952×10^{-2}	3.372×10^1	2.424×10^{-2}	-2.587×10^1	2.265×10^{-2}
C ₂₁	-5.146×10^{-3}		-7.384×10^{-2}		1.431×10^{-1}	
C ₃₀	-1.615×10^2	-2.684×10^{-2}	-2.016×10^2	5.451×10^{-3}	-1.027×10^2	4.328×10^{-2}
C ₃₁	5.991×10^{-1}		6.189×10^{-1}		2.362×10^{-1}	
C ₄₀	4.460×10^1	1.754×10^{-1}	-4.874×10^1	-2.229×10^{-2}	5.698×10^1	-5.188×10^{-2}
C ₄₁	-2.512×10^{-1}		6.217×10^{-2}		-3.290×10^{-1}	
C ₅₀	2.592×10^2	2.583×10^{-2}	4.773×10^2	-2.330×10^{-2}	2.363×10^2	-5.718×10^{-2}
C ₅₁	-9.653×10^{-1}		-1.406×10^0		-5.372×10^{-1}	
C ₆₀	-1.085×10^2	-1.643×10^{-1}	1.173×10^1	1.010×10^{-2}	-3.227×10^1	5.576×10^{-2}
C ₆₁	4.374×10^{-1}		8.512×10^{-2}		2.633×10^{-1}	
C ₇₀	-9.517×10^1		-3.437×10^2		-1.879×10^2	
C ₇₁	3.788×10^{-1}		9.433×10^{-1}		3.963×10^{-1}	
s	3.6×10^{-2}	3.7×10^{-4}	2.6×10^{-2}	4.0×10^{-4}	2.9×10^{-2}	1.4×10^{-4}

V^E : excess molar volumes, δn_D : changes of isentropic compressibility, C_{ij}: the fitting parameters of equation (4), s: standard deviation between experimental and calculated values,

In Figure 4, the refractive index deviations are positive values for the three systems, and the maximum lies at a mole fraction of approximately 0.6 for the methyl acetate + m-2-HEAB system and at 0.5 for the other two systems. According to Nakata and Sakurai (1987) the sign of δn_D is opposite to that of V^{EX} if the behavior of the refractive index is not too non-linear between n_{D1} and n_{D2} . In our mixtures this rule is truly fulfilled in all the cases.

The apparent molar volume data are given in the supplementary information. Table 6 contains the fitting parameters for these properties. Figure 5 shows that the apparent molar volume, ϕ_V , rises rapidly at low concentrations (below 30 mol/kg), while at higher concentrations is almost constant (all three mixtures shown the same trend). Also, in the figures the properties increase with temperature at all concentrations.

Table 6. Fitting parameters and standard deviations for apparent molar volume of binary systems by equation (6).

	Methyl acetate + m-2-HEAB	Ethyl acetate + m-2-HEAB	Propyl acetate + m-2-HEAB
	ϕ_V (g cm ⁻³)	ϕ_V (g cm ⁻³)	ϕ_V (g cm ⁻³)
A ₀	8.761x10 ⁻¹	7.977x10 ⁻¹	9.074x10 ⁻¹
A ₁	8.459x10 ⁻¹	7.637x10 ⁻¹	8.356x10 ⁻¹
A ₂	8.825x10 ⁻¹	7.806x10 ⁻¹	8.743x10 ⁻¹
ϕ_{00}^F	-2.809x10 ³	6.180x10 ²	-1.090x10 ³
ϕ_{01}^F	1.872x10 ¹	-2.113x10 ⁰	7.820x10 ⁰
ϕ_{02}^F	-4.604x10 ⁻²	7.789x10 ⁻³	-1.166x10 ⁻²
ϕ_{10}^F	5.847x10 ²	7.526x10 ²	-1.321x10 ³
ϕ_{11}^F	-3.903x10 ⁰	-2.565x10 ⁰	9.481x10 ⁰
ϕ_{12}^F	9.626x10 ⁻³	9.660x10 ⁻³	-1.404x10 ⁻²
ϕ_{20}^F	2.234x10 ³	-1.365x10 ³	2.373x10 ³
ϕ_{21}^F	-1.488x10 ¹	4.657x10 ⁰	-1.702x10 ¹
ϕ_{22}^F	3.657x10 ⁻²	-1.736x10 ⁻²	2.530x10 ⁻²
ϕ_F^{00}	1.229x10 ²	1.373x10 ²	2.457x10 ²
ϕ_F^{01}	1.215x10 ⁻¹	9.423x10 ⁻⁴	-7.048x10 ⁻¹
ϕ_F^{02}	-4.455x10 ⁻⁵	1.573x10 ⁻⁴	1.279x10 ⁻³
s	0.3	0.3	0.3

ϕ_V : apparent molar volume, ϕ_{ks} : isentropic apparent molar compressibility, A₀, A₁, A₂, A₃, ϕ_{ij}^F , ϕ_F^{00} , ϕ_F^{01} , ϕ_F^{02} : the fitting parameters of equation (6), s: standard deviation between experimental and calculated values.

The values for apparent molar volumes at infinite dilution ϕ_V were obtained by extrapolation at infinite dilution ($m \rightarrow 0$), based on the extended Redlich-Mayer relation, Equation (6). The values of ϕ_V for several temperatures are shown in Figure 6. This figure shows that the apparent molar volume at infinite dilution for methyl acetate mixture is greater than other esters mixtures and increase with the raising of the temperature.

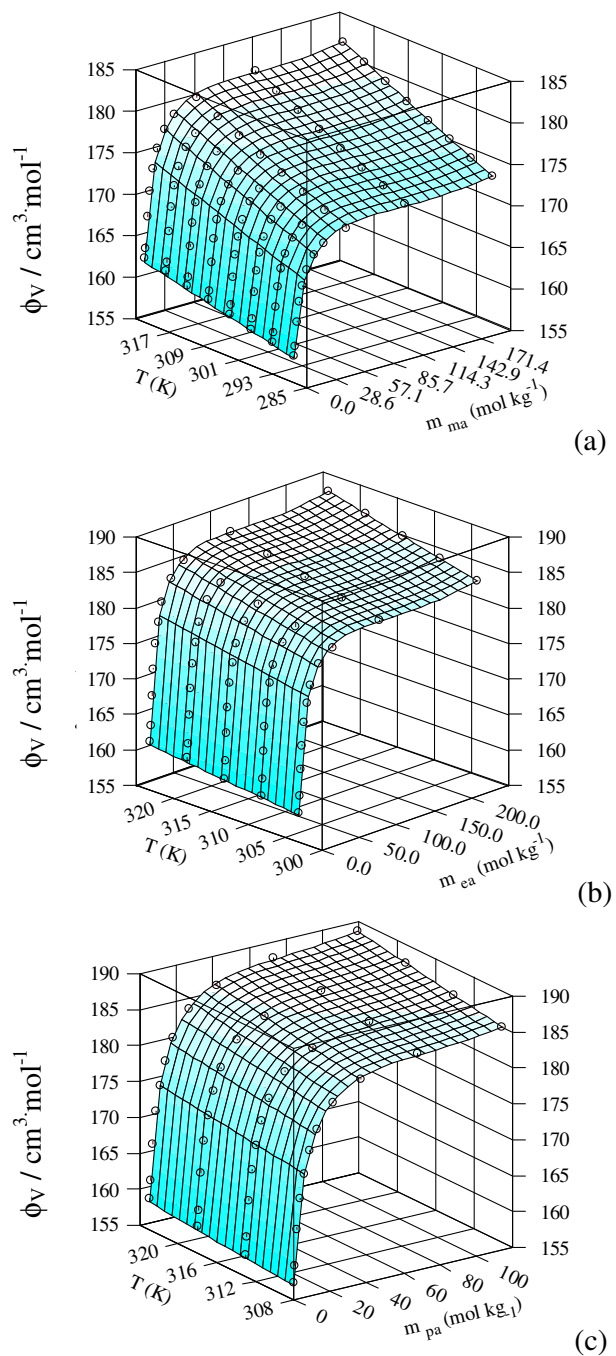


Figure 5. Apparent molar volume versus molality and temperature, (a) methyl acetate + m-2-HEAH, (b) ethyl acetate + m-2-HEAH, (c) propyl acetate + m-2-HEAH.

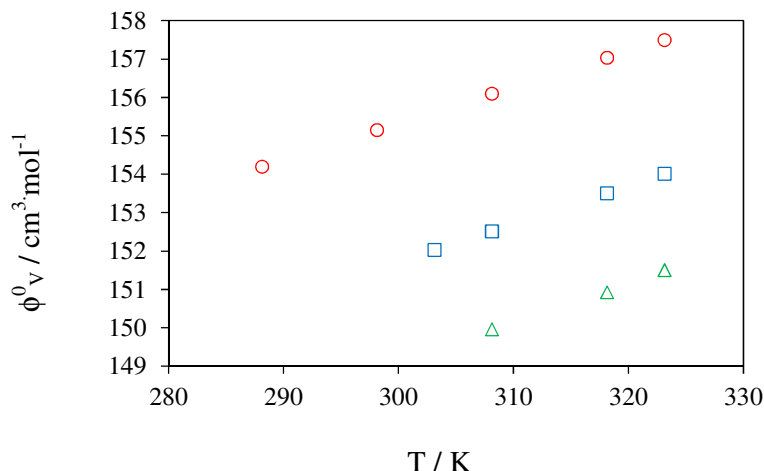
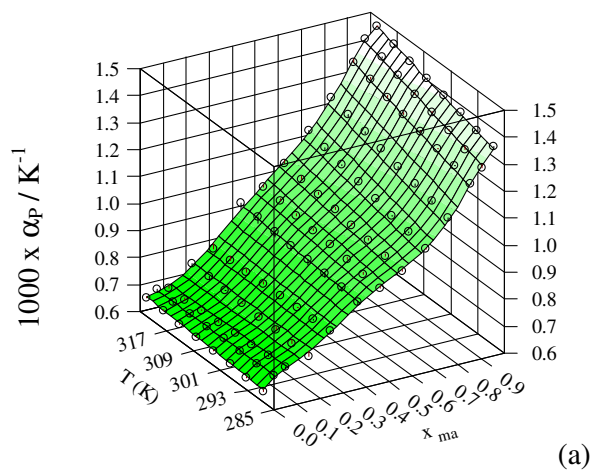


Figure 6. Apparent molar volume at infinite dilution versus temperature. Binary system with methyl acetate (o), ethyl acetate (□) and propyl acetate (Δ).

The values for the thermal expansion coefficient are shown in the supplementary information and the behavior is shown in Figure 7. The value deduced for α_P is particularly sensitive to the type of mathematical function used to fit the density data. The fit can be done with a linear function; however, subtle effects stem from the non-linear behavior of most fluids, and therefore a piece of information may be lost. In these figures, the ionic liquid shows a stable value of thermal expansion coefficient with the rise of temperature, a different behavior for the binary mixtures and esters solvents. For the binary mixtures and esters the thermal expansion coefficient increases with the raise of the temperature and concentration of the ester. This behavior shows a very polar attraction among the high ordering molecules of the ionic liquid.



(a)

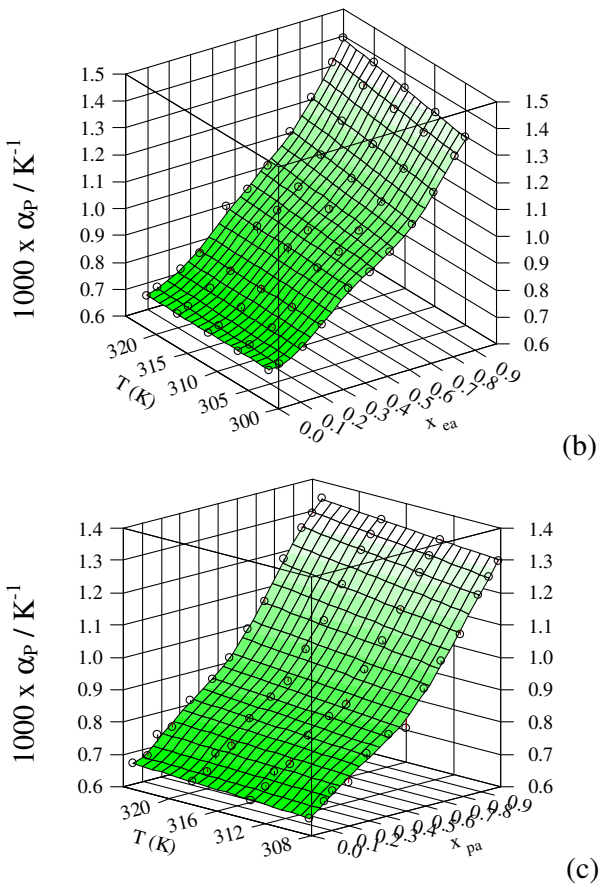


Figure 7. Thermal expansion coefficient versus mole fraction of the solvent and temperature, (a) methyl acetate + m-2-HEAH, (b) ethyl acetate + m-2-HEAH, (c) propyl acetate + m-2-HEAH.

5.2. Density predictions

Figure 8 compares the σ -profile for m-2-HEAB, methyl acetate, ethyl acetate, and propyl acetate compounds. The σ -profile of these compounds can be qualitatively divided in three main regions, which are separated in Figure 8 by two vertical lines located at the cutoff values for the hydrogen bond donor ($\sigma_{\text{HB}} < -0.0084 \text{ e}/\text{\AA}^2$) and acceptor ($\sigma_{\text{HB}} > 0.0084 \text{ e}/\text{\AA}^2$) group (Lin and Sandler, 2002). For m-2-HEAB, the σ -profile reveals to be broad as the σ -profiles of the hydroxylic solvents. Also, the σ -profile of this ionic liquid is dominated by a huge peak of slightly negative screening charge density at $\sigma = -0.003$, which is due to polarization of $-\text{CH}_2-$ groups by the ammonium-hydrogen, hydroxyl-hydrogen and oxygen atoms. The two peaks about 0.009 and 0.012 corresponds to the negatively charged $-\text{COO}^-$ and lone pairs of the oxygen in the $-\text{OH}$ groups, respectively. Considering the high-polarity region $\sigma_{\text{HB}} > 0.0084 \text{ e}/\text{\AA}^2$, these groups can be considered as hydrogen-bond acceptor groups (Lin and Sandler, 2002; Diedenhofen and Klamt, 2010). On the left hand side of the histogram, it can be observed two low peaks at values lower than the cutoff $-0.0084 \text{ e}/\text{\AA}^2$, which are affected by the alkyl chain. These peaks are related to the ammonium-hydrogen and hydroxyl-hydrogen; they may contribute to hydrogen bonds as donors. Finally, the distribution of the charge densities around zero ($-0.0084 \text{ e}/\text{\AA}^2 < \sigma < 0.0084 \text{ e}/\text{\AA}^2$) corresponds to the non-polar alkyl groups of the cation, being those for positive and negative signs assigned to carbon and hydrogen atoms, respectively. Figure 8 shows that the higher number of

carbon atoms in alkyl chain implies the increasing of the area below each histogram of charge densities around the non-polar area (water < methanol < ethanol < m-2-HEAB). In this way, the σ -profile with high values at $\sigma = 0$ show more repulsive interactions between polar and non-polar segments, affecting the cohesive properties of the molecule. The same idea can be applied to mixtures of compounds with very different σ -profiles, i.e. the binary mixture water + m-2-HEAB is the more non ideal system studied here. Interestingly, it can be observed high deviations of the predicted density for the aqueous systems at high concentrations of m-2-HEAB, showed in Figure 9. The thermodynamic model was used with the value of the interaction parameters as zero. The physical properties used in the model for all substances are reported in Table 7. The predictive results show percentage relative deviations for the mixtures of m-2-HEAB with water, methanol and ethanol as 0.8%, 1.0%, and 1.0%, respectively. This suggests that σ -profile is an adequate a priori parameter to characterize quantitatively the non-ideality of volumetric behavior.

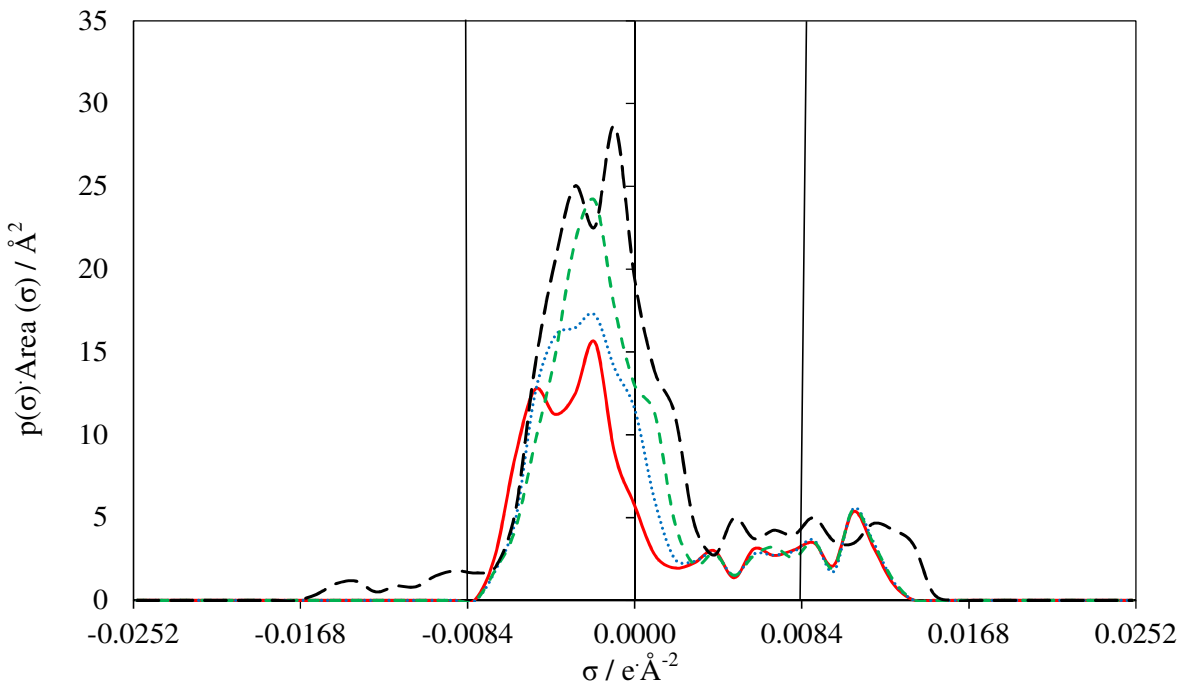


Figure 8. Sigma profiles employed for m-2-HEAB (— —), methyl acetate (—), ethyl acetate (···), and propyl acetate (---). Note that, due to the definition as conductor screening charges, electrostatically positive parts of the molecules have negative σ and vice versa.

Table 7. Properties of the substances used in the modeling

Compound	MM	Tc (K)	Pc (MPa)	ω	r	q	COSMO ^c Segments	V ^{COSMO} (Å³) ^c
methyl acetate ^a	74.08	506.55	4.75	0.33126	8.61	5.08	459	97.0419
ethyl acetate ^a	88.11	523.30	3.88	0.36641	10.91	6.18	571	117.9393
propyl acetate ^a	102.13	549.73	3.36	0.38890	13.21	7.19	676	139.8076
m-2-HEAB ^b	163.21	760.26	2.69	1.04756	14.67	8.33	969	225.8936

^aDiadem public (2000); ^bValderrama and Robles (2007); ^cThis work.

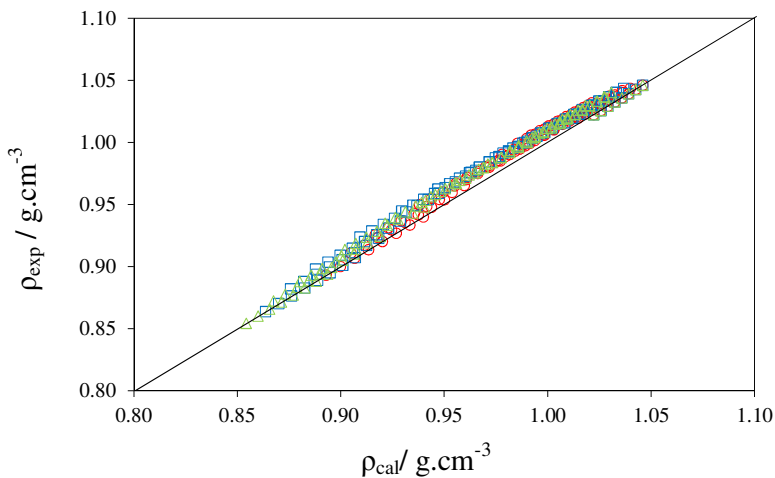


Figure 9. Comparison of experimental and PR-WS/COSMO-SAC model predicted values of density ($\text{g}\cdot\text{cm}^{-3}$) for binary mixtures, methyl acetate + m-2-HEAB (\circ), ethyl acetate + m-2-HEAB (\square) and propyl acetate + m-2-HEAB (Δ) in the whole composition interval.

5.3. VLE data

In order to validate the technique, experimental VLE data for the system ethanol (1) + 1-ethyl-3-methylimidazolium ethylsulfate, [emim] $[\text{EtSO}_4]$ (2) were determined and compared with published data from Calvar et al. (2008). This comparison is shown in Figure 10. From the results in this figure, the experimental technique can be considered as validated and can be used to determine the new experimental data involving m-2-HEAB.

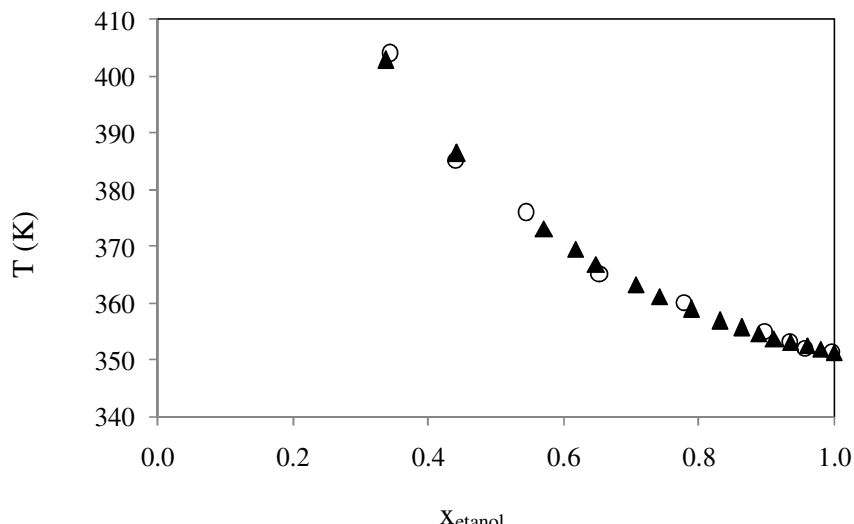


Figure 10. Vapor temperature vs. ethanol mole fraction for the system ethanol + [emim][EtSO_4]. This work (\circ), Calvar et al. (2008) (\blacktriangle).

Vapor-liquid equilibrium for the binary systems ester (1) + m-2-HEAB (2) have been determined at 101.3 kPa and the VLE data are summarized in Table 8. Figure 11 show the predicted

values of the models. Table 9 shows the interaction parameters and the deviation results of the model. The predicted and fitted relative percentage average deviations for the mixtures are below than 2.50% and 0.34%, respectively. The predicted representation of the phase behavior has a good trend and the pure vapor phase is correctly predicted for the mixtures.

Table 8. Vapor liquid equilibria at 101.3 kPa for the binary systems aldehyde (1) + m-2-HEAB (2).

x_1	T (K)	x_1	T (K)	x_1	T (K)
Methyl acetate + m-2-HEAB		Ethyl acetate + m-2-HEAB		Propyl acetate + m-2-HEAB	
1.0000	330.1	1.0000	349.8	1.0000	374.0
0.9746	330.2	0.9612	350.0	0.9575	374.4
0.9004	331.1	0.8956	350.3	0.9283	374.6
0.7753	332.0	0.8294	351.2	0.8944	374.8
0.6889	333.1	0.8188	351.4	0.8446	375.7
0.6174	334.6	0.7904	351.4	0.7410	377.1
0.6137	334.9	0.7576	351.9	0.7207	376.7
0.5399	337.8	0.7312	352.2	0.7153	377.5
0.4938	342.2	0.6925	353.0	0.6922	378.2
0.4872	342.6	0.6824	353.9	0.6616	378.6
0.4798	343.6	0.6581	353.3	0.6423	379.2
0.4696	344.2	0.6419	354.2	0.6289	379.7
		0.6248	354.7	0.6171	380.4
		0.5867	355.3	0.5827	381.6
		0.5807	355.9	0.5548	382.9
		0.5718	357.0	0.5482	383.7
		0.5363	358.3	0.5333	383.3
		0.4995	361.9	0.5121	385.3
		0.4974	361.0	0.4579	389.2
		0.4915	363.4	0.4253	391.3
		0.4558	368.2	0.4040	394.8
		0.4554	365.5	0.4106	393.7
		0.4471	367.3	0.3803	396.8
		0.4339	370.8	0.3653	398.4
		0.4190	371.6	0.3502	400.3
		0.4162	372.7		
		0.3938	374.7		
		0.3780	376.3		
		0.3663	378.8		
		0.3439	379.6		
		0.3423	380.2		

Table 9. Details of the fitted results for the systems studied using the PR+WS/UNIQUAC or PR+WS/NRTL models.

Model	k_{ij}	α	A_{ij}	A_{ji}	% ΔT
acetato de metila (1) + m-2-HEAB (2).					
NRTL	0,1944	0,3133	40019,0625	61398,9180	0,34
UNIQUAC	0,8970	-	6086,4258	-3537,9409	0,16
acetato de etila (1) + m-2-HEAB (2)					
NRTL	-0,0039	0,3920	-33397,7070	-747,0703	0,32
UNIQUAC	0,6648	-	-3484,8975	7225,5708	0,22
acetato de propila (1) + m-2-HEAB (2).					
NRTL	-0,7653	0,3230	-78984,4844	-2586,5935	0,10
UNIQUAC	0,5977	-	-3334,3506	6417,3892	0,14

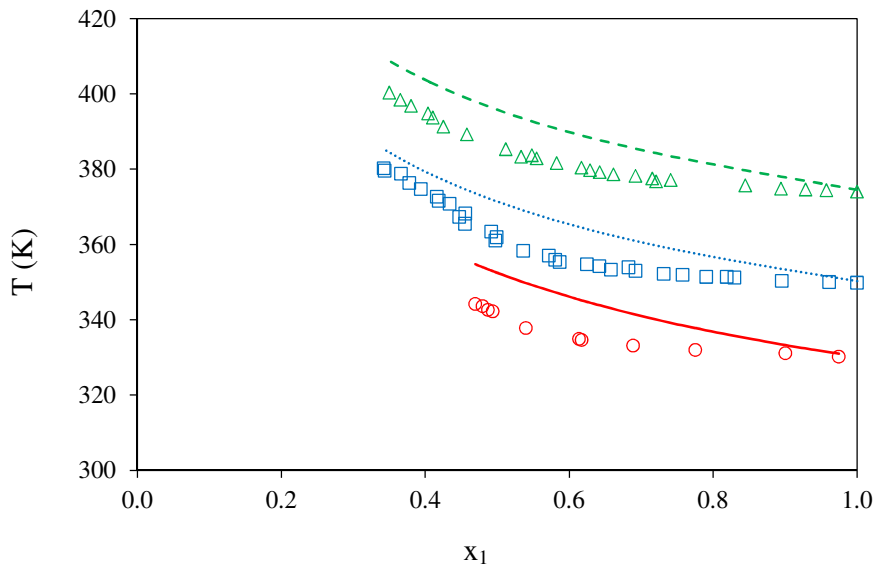


Figure 11. Temperature vs. composition of the ester. (○) methyl acetate (1) + m-2HEAB (2), (□) ethyl acetate (1) + m-2HEAB (2), (Δ) propyl acetate (1) + m-2HEAB (2), and predicted values as lines (—).

6. Conclusions

Density and refractive index of binary mixtures ester + N-methyl-2-hydroxyethylammonium butyrate have been measured at atmospheric pressure. Other properties, such as excess molar volume and deviations in the refractive index were also calculated. The values of V^E are negative at high concentrations of ester and positive in the opposite case.

The densities for methyl acetate + m-2-HEAB, ethyl acetate + m-2-HEAB and propyl acetate + m-2-HEAB binary systems have been predicted using the Peng-Robinson equation of state coupled with the Wong-Sandler mixing rule using the COSMO-SAC model. COSMO-SAC is also revealed as a valuable computational tool to describe the intermolecular interaction of systems containing m-2-HEAB. In addition, the σ -profile is suggested as a simple molecular parameter to characterize the non ideality of the mixtures respect to volumetric properties.

The vapor-liquid equilibrium of binary systems ester (methyl acetate, ethyl acetate or propyl acetate) + N-methyl-2-hydroxyethylammonium butyrate at 101.3 kPa was measured by a dynamic

method. The experimental density and VLE data were predicted by using the Peng-Robinson equation of state with the Wong-Sandler mixing rule and COSMO-SAC model. The prediction results for density are reliable with low deviations than 1%, and for the VLE are only reliable for a qualitative description.

Acknowledgments

V.H. Álvarez acknowledges the financial support from FAPESP (Fundação de Amparo à Pesquisa do Estado de São Paulo), process 2006/03711-1. M. Aznar and S. Mattedi are recipients of CNPq (Brazil) fellowships

References

- ABRAMS, D.S.; PRAUSNITZ, J.M. Statistical thermodynamics of liquid mixtures: a new expression for the excess Gibbs energy of partly or completely miscible systems. *AIChE J.*, v.21, p.116–128, 1975
- Accelrys Materials Studio, <http://accelrys.com/products/materials-studio/>, accessed January 2010.
- ÁLVAREZ, V.H.; AZNAR, M. Thermodynamic modeling of vapor–liquid equilibrium of binary systems ionic liquid + supercritical {CO₂ or CHF₃} and ionic liquid + hydrocarbons using Peng–Robinson equation of state. *J. Chin. Inst. Chem. Eng.*, v. 39, p.353–360, 2008.
- Álvarez, V.H.; Aznar, M. Application of a thermodynamic consistency test to binary mixtures containing an ionic liquid, *The Open Thermodynamics Journal*, v. 2, p. 25-38, 2008b.
- ÁLVAREZ, V.H.; LARICO, R., IANOS, Y.; AZNAR, M. Parameter estimation for VLE calculation by global minimization: Genetic algorithm, *Braz. J. Chem. Eng.* 2008, 25, 409-418
- ÁLVAREZ, V.H.; DOSIL, N.; GONZALEZ-CABALEIRO, R.; MATTEDI, S., MARTIN-PASTOR, M.; IGLESIAS, M.; NAVAZA, J. M. Brønsted Ionic Liquids for Sustainable Processes: Synthesis and Physical Properties, *J. Chem. Eng. Data*, v.55, p. 625–632, 2010.
- ÁLVAREZ V.H.; AZNAR, M. An efficient approach to optimal interpolation of experimental data. *J. Taiwan Inst. Chem. Eng.*, v.41, p.184–189, 2010.
- CALVAR, N.; GONZÁLEZ, B.; GÓMEZ E.; DOMINGUEZ, Á. Vapor–liquid equilibria for the ternary system ethanol + water +1-ethyl-3-methylimidazolium ethylsulfate and the corresponding binary systems containing the ionic liquid at 101.3 kPa, *J. Chem. Eng. Data*, v.53, p.820-825, 2008
- Diadem Public 1.2, The DPPR Information and Data Evaluation Manager, 2000.
- DIEDENHOFEN, M.; KLAMT, A. COSMO-RS as a tool for property prediction of IL mixtures—A review, *Fluid Phase Equilib.* In press (2010).
- HUDDLESTON, J.G.; WILLAUER, H.D.; SWATLOSKI, R.P.; VISSER, A.E.; ROGERS, R.D. Room temperature ionic liquids as novel media for clean liquid–liquid extraction. *Chem. Commun.*, p.1765-1766, 1998.
- LAROCK, R. C. *Comprehensive Organic Transformations*, VCH, New York, 1999.

LORIA, H.; PEREIRA-ALMAO, P.; SATYRO M. Prediction of Density and Viscosity of Bitumen Using the Peng-Robinson Equation of State, *Ind. Eng. Chem. Res.* v48, p. 10129–10135, 2009.

LIN, S.T.; SANDLER, S.I. A priori phase equilibrium prediction from a segment contribution solvation model. *Ind. Eng. Chem. Res.*, v.41, p.899-913, 2002

MICHELSSEN, M.L.; MOLLERUP, J. *Thermodynamic Models: Fundamentals and Computational Aspects*, 2nd edition, Tie-Line Publications, Lyngby, 2007.

MULLINS, E.; OLDDLAND, R.; LIU, Y.A.; WANG, S.; SANDLER, S.I.; CHEN, C.C.; ZWOLAK, M.; SEAVEY, K.C. Sigma-profile database for using COSMO-based thermodynamic methods. *Ind. Eng. Chem. Res.*, v.45, p.4389–4415, 2006.

NAKATA, M.; SAKURAI, M. Refractive index and excess volume for binary liquid mixtures. Part 1. Analyses of new and old data for binary mixtures. *J. Chem. Soc., Faraday Trans. 1*, v. 83, p.2449 - 2457, 1987.

PENELOUX, A.; RAUZY, E.; FREZE, R. A consistent correction for Redlich-Kwong-Soave volumes, *Fluid Phase Equilib.* 8 (1982) 7-23.

PENG, D.; ROBINSON, D.B. A new two-constant equation of state. *Ind. Eng. Chem. Fundam.*, v.15, p.59–64, 1976.

SARKAR, L.; ROY M. N. Studies on liquid–liquid interactions of some ternary mixtures by density, viscosity, ultrasonic speed and refractive index measurements, *Thermoch. Acta*, v. 496, p.124–128, 2009.

VALDERRAMA, J.O.; ROBLES, P.A. Critical properties, normal boiling temperatures, and acentric factors of fifty ionic liquids. *Ind. Eng. Chem. Res.*, v.46 p.1338-1344, 2007

WONG, D.S.H.; SANDLER, S.I. A theoretically correct mixing rule for cubic equations of state. *AIChE J.*, v.38, p.671–680. 1992.

ZHANG, S.; ZHANG, Q.; ZHANG, Z. C. Extractive desulfurization and denitrogenation of fuels using ionic liquids. *Ind. Eng. Chem. Res.*, v.43, p. 614-622, 2004.

ZHU, H-P.; YANG, F.; TANG, J.; HE, M-Y. Brønsted acidic ionic liquid 1-methylimidazolium tetrafluoroborate: a green catalyst and recyclable medium for esterification, *Green Chemistry*, v. 5, p. 38–39, 2003

K.N. Marsh, J.A. Boxall, R. Lichtenthaler, Room temperature ionic liquids and their mixtures-a review, *Fluid Phase Equilib.* 219 (2004) 93-98.

S. Gabriel, J. Weiner, Ueber einige Abkömmlinge des Propylamins, *Ber.* 21 (1888) 2669-2679.

KENNEDY, D.F.; DRUMMOND, C.J. Large Aggregated Ions Found in Some Protic Ionic Liquids, *J. Phys. Chem. B* 113 (2009) 5690-5693.

BICAK, N. A new ionic liquid: 2-hydroxyethylammonium formate. *J. Mol. Liq.* 2005, 116, 15–18.

GREAVES T. L.; WEERAWARDENA A.; FONG C.; KRODKIEWSKA I.; DRUMMOND C. J.
Protic Ionic Liquids: Solvents with Tunable Phase Behavior and Physicochemical Properties, *J. Phys. Chem. B* 2006, 110, 22479-22487.

COTA, I.; GONZÁLEZ-OLMOS, R.; IGLESIAS, M.; MEDINA F. New short chain aliphatic chain ionic liquids: synthesis, physical properties and catalytic activity in aldol condensations. *J. Phys. Chem. B* 111(2007) 12468-12477.

KURNIA, K.; WILFRED, C.; MURUGESAN, T. Thermophysical properties of hydroxyl ammonium ionic liquids, *J. Chem. Thermodyn.* 41 (2009) 517-521.

IGLESIAS M.; TORRES A.; GONZALEZ-OLMOS R., SALVATIERRA D. Effect of temperature on mixing thermodynamics of a new ionic liquid: {2-hydroxyethylammonium formate (2-HEAF) + short hydroxylic solvents}, *J. Chem. Thermodyn.*, 40 (2008), 119-133.

PERIC, B.; SIERRA, J.; MARTI, E.; GONZALEZ-OLMOS, R.; IGLESIAS, M.; CRUAÑAS, R.; GARAU, M.A. 20th Society of Environmental Toxicology and Chemistry Congress, SETAC Europe Annual Meeting, Science and Technology for Environmental Protection, Sevilla (Spain), May, 2010.

SIERRA, J.; MARTÍ, E.; MENGÍBAR, A.; GONZÁLEZ-OLMOS, R.; IGLESIAS, M.; CRUAÑAS, R.; GARAU, M.A. 5º society of environmental toxicology and chemistry congress, SETAC 2008. Sydney (Australia), August, 2008.

Artigo 4.6: Density, Refractive Index and Vapor-Liquid Equilibria of N-Methyl-2-Hydroxyethylammonium Hexanoate plus (Methyl Acetate or Ethyl Acetate or Propyl Acetate) at Several Temperatures

V. H. Álvarez¹, S. Mattedi² and M. Aznar¹

¹*School of Chemical Engineering, State University of Campinas (UNICAMP), P.O. Box 6066, 13083-970, Campinas-SP, Brazil*

²*Chemical Engineering Department, Polytechnic School, Federal University of Bahia (UFBA), 40210-630, Salvador-BA, Brazil*

ABSTRACT – This paper reports the densities, refractive indices, and vapor liquid equilibria for binary systems ester + n-methyl-2-hydroxyethylammonium hexanoate (m-2-HEAH): methyl acetate (1) + m-2-HEAH (2), ethyl acetate (1) + m-2-HEAH and propyl acetate (1) + m-2-HEAH (2). The excess molar volumes, deviations in the refractive index, the apparent molar volume, and the coefficient of thermal expansion for the binary systems were fitted to typical equations. The Peng-Robinson equation of state, coupled with the Wong-Sandler mixing rule, is used to describe the experimental data. To calculate activity coefficients we used three different models: NRTL, UNIQUAC and COSMO-SAC. Since the predictive liquid activity coefficient model COSMO-SAC is used in the Wong-Sandler mixing rule, the resulting thermodynamic model is a completely predictive one. The prediction results for the density and for the vapor-liquid equilibria have a deviation lower than 1.6% and 1.1%, respectively. The vapor-liquid equilibria predictions show a good trend for the esters mixture.

KEYWORDS: ionic liquid; COSMO-SAC; excess volume

1. Introduction

Room-temperature ionic liquids constitute a new class of substances that are considered as potential substitutes to many traditional organic solvents in reaction and separation processes (Huddleston et al., 1998; Zhang et al., 2004). In spite of their importance and interest, accurate values for many of the fundamental physical-chemical properties of these compounds are either scarce or absent. In order to design any process involving ionic liquids in industrial scale, it is necessary to know several physical properties, including density and vapor liquid equilibria. Since it is impossible to measure all the possible combinations of systems, it is necessary to make measurements on selective systems to provide results that can be used to develop correlations and predictive methods.

Due to the vast number and nature of the possible ionic liquids, the interest in asymmetric mixtures is strong. These mixtures, containing lighter and heavier components, can easily be found among several industries such as those producing paints and polymers. One of the among principal properties of the mixtures is the density and the property of easy measurement is the refractive index. The liquid density is a key property in solvent extraction, design and processing. The measurement of refractive index is easy and simple, it use a little quantity of sample (≈ 0.3 ml) and the sample can be easily save of bubbles, and the results are accurate.

The prediction of the most suitable IL for each separation process is limited since there is not enough information about the influence of the structure of the IL on its physical and solvent properties. Besides, experimental phase equilibrium data are required for developing thermodynamic models and for understanding their thermodynamic behavior. Vapor–liquid equilibria (VLE) data permit checking the potential of excess Gibbs energy (G^E) models which are used for the description of the nonideal behavior of systems containing IL.

In recent times room temperature ionic liquids have attracted increasing interest in the area of green chemistry. Although ionic liquid was initially introduced as an alternative green reaction medium, today it has marched far beyond showing its significant role in controlling the reaction as catalyst (Ranu et al., 2006). Then, a number of ionic liquids with unique properties have been developed and applied to catalyze many types of reactions. Some acidic ionic liquids, which exhibit a stable acidic anion, have been utilized to catalyze esterification reaction (Zhu et al., 2003).

The Figure 1 shows the trend of the open literature production about ionic liquids and esters, from 1999 to 2009. Also, this figure shows two important years for the increase of this research. In 2003, the increased of the research was due to the application of ionic liquids as catalyst to produce esters from alcohols and organic acid (Zhu et al., 2003), and in 2007, the research was increased due the production of biodiesel (fatty acid methyl esters) in ionic liquids (Ha et al., 2007). Furthermore, a direct distillation of the esters compounds from the reaction mixture appears very attractive in the case of derivatives that are volatile enough. And, after performing purification methods on the ionic solvent, it could be recycled. Then, a study about physical properties and VLE between mixtures of aldehydes and ionic liquids are required for to develop a separation process.

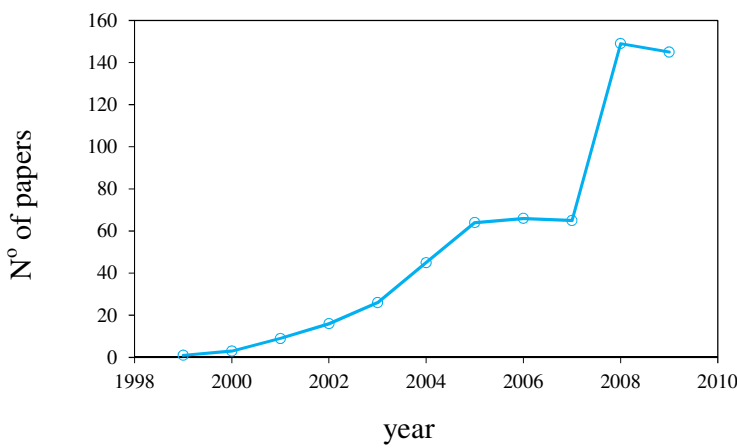


Figure 1. Open literature production about ionic liquids and esters.

The majority studies concerning ionic liquids have been based on the imidazolium cation and, to a lesser extent, on the alkyl pyridiniums and trialkylamines (Marsh et al., 2004). In opposition Protic ionic liquids (PIL's) have received limited attention from the academia. The first PIL synthetized was the ethanolammonium nitrate, reported by Gabriel and Weiner in 1882. These PILs were produced by a stoichiometric acid-base Brønsted reaction and their main difference, compared to aprotic ILs (AIL's), is the presence of at least a labile proton, which is/are able to

promote extensive hydrogen bonding (Kennedy and Drummond, 2009; Álvarez et al., 2010). Newly, some work has been reported on the synthesis, physicochemical and structural characterization of PILs. Bicak (2005) synthesized the 2-hydroxyethylammonium formate (2-HEAF), an ionic liquid formed by the neutralization of monoethanolamine with formic acid. Greaves et al. (2006) proposed different PILs from primary amines and organic and inorganic acids. Cota et al. (2007), Kurnia et al. (2009) and Alvarez et al. (2010) synthesized a family of these ILs by modifying the aliphatic chain of the organic acid and/or using secondary and tertiary hydroxyamines. There were also studies that use PIL's in catalytic reactions and on the interaction with hydroxilic solvents, showing that 2-HEAF is soluble in water, ethanol and methanol in all the concentration range (Iglesias et al., 2008). Moreover, a relevant aspect, few times considered in the relation application of ILs and the environment, is their potential toxicity. This issue has not been sufficiently studied until now, especially taking into account the need of this information to fulfill the REACH (Registration, Evaluation, Authorization and Restriction of Chemical Substances) requirements (UE) and so, allowing the assessment of hygiene and safety issues derived from their manufacture, use, and transport in the industrial sectors in which these substances will be applied. In what is referred to PIL's from hydroxyamine and organic acid, the first results highlight that total biodegradation and low toxicity are intrinsic characteristics of these family of ionic liquids (Sierra et al., 2008; Peric et al., 2010).

In this work, experimental density and refractive index data of pure m-2-HEAH PIL's have been measured at several temperatures. Experimental density, refractive index and vapor-liquid equilibria (VLE) data over whole composition range for methyl acetate (1) + m-2-HEAH (2), ethyl acetate (1) + m-2-HEAH (2) and propyl acetate (1) + m-2-HEAH (2) have been determined at 101.3 kPa. The coefficient of thermal expansion, excess molar volumes, and deviations in the refractive index were calculated from experimental data.

2. Experimental Section

2.1. Chemicals

The esters were supplied by Sigma-Aldrich, with mass fraction higher than 0.99, and were degassed ultrasonically before each use.

2.2. Synthesis

N-methyl-2-hydroxyethylammonium butyrate was prepared according to a slightly modified literature procedure (Álvarez et al., 2010); a quantity of hexanoic acid was added dropwise to a quantity of 2-(methylamino)ethanol and cooled in an ice bath under nitrogen at a rate to maintain the reaction temperature below 283.15 K, since the reaction is exothermic. After, the reaction mixture was obtained, it was stirred at room temperature for additional 5 h and the progress of the reaction was monitored by refractive index measurements. To reduce the water content (lower than 0.1 % mass fraction, determined using a 756 Karl Fisher titrator) the m-2-HEAH ionic liquid was dried by heating to 343.15 K and stirring under high vacuum (7 Pa) for two days, always immediately prior to their use. The ionic liquid was kept in bottles with nitrogen gas.

Table 1 shows a comparison between experimental and literature density data of the pure components at 298.15 K, but not for the m-2-HEAH why is a new ionic liquid.

Table 1. Density of pure compounds at 298.15 K.

Compound	ρ (g cm ⁻³)	
	exp	lit
methyl acetate	0.92682	0.9282 ^a
ethyl acetate	0.89490	0.8928 ^a
propyl acetate	0.88261	0.8823 ^a
m-2-HEAH	0.99417	-

^aSarkar and Roy (2009)

2.3. Apparatus and procedure

Samples were prepared by introducing with a syringe known masses of the pure liquids into stoppered bottles, in an inert-atmosphere glove box, using a Mettler AX-205 Delta Range analytical balance, with a precision of $\pm 10^{-4}$ g. A glove box was used because the ionic liquid is moisture sensitive. Densities were measured using an Anton Paar DMA 4000 digital vibrating-tube densimeter. The repeatability and the uncertainty in experimental measurement have been found to be lower than $\pm 5 \times 10^{-6}$ g cm⁻³ for the density. The DMA 4000 automatically corrects the influence of viscosity on the measured density.

Refractive indices were determined using an automatic refractometer Mettler Toledo D4 with a resolution of $\pm 10^{-4}$ and an uncertainty in the experimental measurements of $\pm 2 \times 10^{-4}$.

3. Modeling

3.1. Properties

The density and refractive index for the mixtures were correlated by:

$$Z = \sum_{i=0}^p \left(\left(\sum_{j=0}^q B_{ij} T^j \right) x_1^{i-1} \right) \quad (1)$$

where Z is the density or refractive index of the mixture, x_1 is the mole fraction of the solvent, p and q are the polynomial degrees, B_{ij} are the fitting parameters, and T is the absolute temperature.

The excess molar volumes (V^E) and deviations in the refractive index (δn_D) were calculated from experimental values as follows:

$$V^E = \sum_{i=1}^N x_i M_i \left(\frac{1}{\rho} - \frac{1}{\rho_i} \right) \quad (2)$$

$$\delta n_D = n_D - \sum_{i=1}^N x_i n_{Di} \quad (3)$$

where N is the number of compounds in the mixture, x_i is mole fraction; M_i denotes molar mass; ρ_i is the density of the pure compound i , ρ is the density of the mixture, n_D and n_{Di} are the refractive index of the mixture and the refractive index of the pure components, respectively. These derived properties were fitted to a Redlich-Kister-type equation:

$$Q = x_1 x_2 \sum_{i=0}^p \left(\left(\sum_{j=0}^q C_{ij} T^j \right) (x_1 - x_2)^i \right) \quad (4)$$

where Q is V^E or δn_D , C_{ij} are the fitting parameters and the other variables are the same as above.

The apparent molar volume (ϕ_V) for the mixtures contend m-2-HEAH were calculated by:

$$\phi_V = 1000 \left(\frac{\rho_1 - \rho}{m \rho_1 \rho} \right) + \frac{M_2}{\rho_1} \quad (5)$$

where ρ is the density of the mixture, ρ_1 is the density of the solvent, M_2 is the molar mass of ionic liquid, m is the molality of the solution. These derived values were correlated by a modified Redlich–Mayer equation, where the fitting parameters show temperature dependence:

$$\phi_V = \left(\sum_{j=0}^q \phi_{Fj}^o T^j \right) + \sum_{i=0}^p \left(\left(\sum_{j=0}^q \phi_{ij}^F T^j \right) m^{A_i} \right) \quad (6)$$

where ϕ_{Fj}^o and ϕ_{ij}^F are fitting parameters.

The thermal expansion coefficient (α_P) shows the temperature dependence of volume, and it is defined as:

$$\alpha_P = \frac{1}{V} \left(\frac{\partial V}{\partial T} \right)_P = - \left(\frac{\partial \ln \rho}{\partial T} \right)_P \quad (7)$$

3.2. VLE

The most common method used for the correlation of phase equilibria in mixtures at high and low pressure is the use of equations of state (EoS). The most common and industrially important EoS are the cubic equations derived from van der Waals EoS; among these, the Peng–Robinson EoS (Peng and Robinson, 1976) has proven to combine the simplicity and accuracy required for the prediction and correlation of volumetric and thermodynamic properties of fluids, although there can be problems when applying the PR EoS to systems near the critical point.

Recently, Álvarez and Aznar (2008a, 2008b) applied an extension of this approach to several supercritical fluid + ionic liquid systems, using the Peng–Robinson equation of state coupled with the Wong–Sandler mixing rule (Wong and Sandler, 1992) using the UNIQUAC or NRTL model (Abrams and Prausnitz, 1975) for the excess Gibbs free energy, G^E , using three or four adjustable parameters, respectively. In addition, by using the Wong–Sandler mixing rule, any cubic EoS can be

made predictive for mixtures, i.e., without the need of any adjustable binary interaction parameter, when a predictive model for G^E is used. For example, G^E can be determined from the COSMO-SAC model (Lin and Sandler, 2002), in which the activity coefficient γ_i of species i is calculated from the sum of the residual and combinatorial contributions:

$$\ln \gamma_i = \ln \gamma_i^{res} + \ln \gamma_i^{com} \quad (8)$$

The residual part is calculated from a consideration of molecular solvation in a perfect conductor. The distribution of screening charges on the molecular surface, called the sigma profile $p(\sigma)$, is first determined from quantum mechanical calculations. The molecular interactions in the liquid phase are assumed to be the sum of contributions of surface segment interactions through the screening charges. With these assumptions, the residual term takes the following form:

$$\ln \gamma_i^{res} = n_i \sum_{\sigma_m} p_i(\sigma_m) \ln [\Gamma_S(\sigma_m) - \Gamma_i(\sigma_m)] \quad (9)$$

where n_i is the number of surface segments contained in species i , $\Gamma_S(\sigma)$ is the activity coefficient of segment i (whose screening charge density is σ) in solution S (for which the probability of finding a segment of charge density σ be denoted $p_S(\sigma)$):

$$\ln \Gamma_S(\sigma_m) = -\ln \left\{ \sum_{\sigma_n} p_S(\sigma_n) \Gamma_S(\sigma_n) \exp \left[\frac{-\Delta W(\sigma_m, \sigma_n)}{RT} \right] \right\} \quad (10)$$

where $W(\sigma_m, \sigma_n)$ is the electrostatic interaction between two segments of charge density σ_m and σ_n . The Staverman–Guggenheim model is used for the combinatorial term:

$$\ln \gamma_i^{com} = \ln \frac{\Phi_i}{x_i} + \frac{z}{2} q_i \ln \frac{\theta_i}{\Phi_i} + l_i - \frac{\Phi_i}{x_i} \sum_j x_j l_j \quad (11)$$

$$\Phi_i = \frac{r_i x_i}{\sum_j r_j x_j} \quad \theta_i = \frac{q_i x_i}{\sum_j q_j x_j} \quad (12)$$

$$l_i = (z/2)(r_i - q_i) - (r_i - 1) \quad (13)$$

where θ_i is the surface area fraction, Φ_i is the volume fraction, z is the coordination number ($z=10$), and r_i and q_i are the normalized volume and surface area parameters for species i .

3.3. Density predictions

The calculation of the molar volume of the mixture at a specific temperature and pressure can be predicted by an equation of state. The Peng-Robinson equation of state, coupled with the Wong-Sandler mixing rule using the predictive liquid activity coefficient model COSMO-SAC was used as thermodynamic model to predict the density and VLE. The Peng-Robinson equation can be written in terms of the compressibility factor (Z) by:

$$Z^3 - (1-B)Z^2 + (A-3B^2-2B)Z - (AB-B^2-B^3) = 0 \quad (14)$$

where A and B are given by:

$$A = \frac{a_m P}{(RT)^2} \quad (15)$$

$$B = \frac{b_m P}{RT} \quad (16)$$

where the constants a_m and b_m are expressed as functions of the concentration of the different components in the mixture, through the so-called mixing rules. In this work, the Wong-Sandler mixing rules are used:

$$b_m = \frac{\sum_i \sum_j x_i x_j \left(b - \frac{a}{RT} \right)_{ij}}{1 - \sum_i \frac{x_i a_{ii}}{b_{ii} RT} - \frac{A_\infty^E}{\Omega RT}} \quad (17)$$

$$a_m = b_m \left[\sum_i \frac{x_i a_{ii}}{b_{ii}} + \frac{A_\infty^E}{\Omega} \right] \quad (18)$$

$$\left(b - \frac{a}{RT} \right)_{ij} = \frac{(b_{ii} + b_{jj})}{2} - \frac{(1 - k_{ij}) \sqrt{a_{ii} a_{jj}}}{RT} \quad (19)$$

In these equations, k_{ij} is the adjustable interaction parameter, $\Omega = \ln(\sqrt{2}-1)/\sqrt{2}$ for the PR EoS, and A_∞^E , the excess Helmholtz free energy at the limit of infinite pressure, is calculated using the COSMO-SAC, activity coefficient model, and a_{ii} and b_{ii} are the EoS constants, defined as

$$a_{ii} = 0.457235(RT_c/P_c)^2 [1 + F(1 - T_r^{0.5})], \quad F = 0.37464 + 1.54226\omega - 0.26992\omega^2 \quad (20)$$

$$b_{ii} = 0.077796(RT_c/P_c) \quad (21)$$

where T_r is the reduced temperature, T_c is the critical temperature, P_c is the critical pressure, and ω is the Pitzer acentric factor.

Equation 14 yields one or three real roots, depending on the number of phases in the system. It was shown that this model provides an excellent representation of the vapor-liquid experimental data (Álvarez and Aznar, 2008). However, an equation of state does not necessarily yield the accurate volumetric behavior of fluids and their mixtures. In order to improve the description of liquid densities, a volume translation is used (Peneloux et al., 1982, Loria et al., 2009). Then, for the prediction of the liquid density, the root of interest in Equation (14) is the smallest positive one. Then, the difference between the volume calculated by the thermodynamic model and the experimental volume for pure compounds, can be defined:

$$\Delta V_i = V_{i,\text{exp}} - V_{i,\text{cal}} \quad (22)$$

where $V_{i,cal}$ is the molar volume of the compound i calculated by the thermodynamic model, and $V_{i,exp}$ is the experimental molar volume of the compound i . Then, the volume of the mixture is obtained using the correction of the volume applied by

$$V = V_{cal} + \sum_i \Delta v_i x_i \quad (23)$$

where x_i is the liquid molar fraction of the pure compound i , V_{cal} is the liquid molar volume of the mixture calculated with the thermodynamic model, and V is the predicted corrected molar volume of the mixture.

3.4. Computation details

For each system, the VLE phase diagram is predicted by using the Peng-Robinson EoS with the Wong-Sandler/COSMO-SAC mixing rule. For a given liquid phase composition, the bubble point pressure calculation, as detailed by Michelsen and Mollerup (2007), is performed to obtain the system pressure and the vapor phase compositions. In order to make the models predictive, the binary interaction parameters k_{ij} in the combining rules are set to zero.

In the COSMO model, for each compound, the equilibrium molecular geometry is first determined by minimization of the molecular energy at 0 K. The next step for COSMO-SAC calculation is to estimate the volume of cavity (V_{COSMO}), the total number of segments (COSMO Segments), and the sigma profile of each compound. In this step, a solvation calculation in a perfect conductor was performed using the equilibrium geometry to obtain the surface screening charges on the compound. These calculations were done using the quantum chemistry package DMol3 built in Accelrys Materials Studio v4.3. The sigma profile, $p(\sigma)$, is a file containing the probability of finding a surface segment with screening charge density, σ . The detailed settings for DMol3 can be found elsewhere (Mullins et al., 2006). The molecular description of the ionic liquid was obtained using the ion-pair approach (Diedenhofen and Klamt, 2010). Therefore, the sigma profile of ionic liquid has been obtained for the molecule as a whole. Note that, for each species, the quantum mechanical part of this calculation, only has to be done once, irrespective of the temperature and the composition of mixture required. The activity coefficient is then calculated (Mullins et al., 2006).

The absolute average error in pressure, vapor phase composition or density (F) from the calculation is determined as:

$$|\Delta F| \% = \frac{100}{N} \sum_{i=1}^N \frac{|F_i^{cal} - F_i^{exp}|}{F_i^{exp}} \quad (24)$$

where N is the number of data point, superscripts exp and cal denote the values from experiment and our calculation, respectively.

4. Parameter Estimation

In this work, the first approximation parameter estimation was performed using a genetic algorithm code, mMyGA (Álvarez et al., 2008) using a whole interval search. After that, the fitting

parameters were best tuned using a non-linear optimization algorithm based on the Marquardt algorithm. The optimization used the minimization of the standard deviation (s) between experimental and calculated values, defined as:

$$s = \left[\sum_{i=1}^N \frac{(F_{\text{exp}} - F_{\text{cal}})_i^2}{N - m} \right]^{1/2} \quad (25)$$

where N is the number of experimental points, m is the number of parameters in the curve fit, and F_{cal} and F_{exp} are the values of the property calculated by the model and obtained experimentally, respectively.

5. Results and Discussion

The m-2-HEAH was synthetized and the 1D hydrogen spectrum is shown in Figure 2. The m-2-HEAH ionic liquid shows completely solubility in water, methanol and ethanol, and it is not soluble in some alkanes as n-octane and n-dodecane. The humidity of the ionic liquid was determined by DL31 Karl Fischer titrator (Mettler Toledo) and shows moisture less than 600 ± 50 ppm of H₂O.

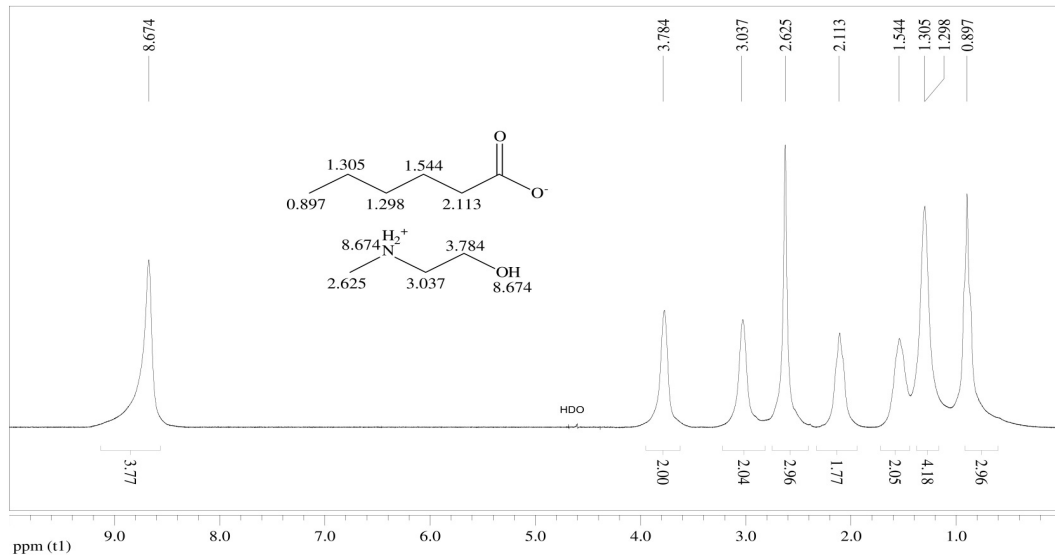


Figure 2. 1D hydrogen spectrum for the m-2-HEAH ionic liquid.

5.1. Properties

Densities and excess molar volumes of the binary mixtures ester (1) + m-2-HEAH (2) at 298.15 K, and refractive indices and deviations in the refractive indices at atmospheric pressure (≈ 96 kPa) are listed in Tables 2 and 3, respectively. The complete data are presented in the supporting information. Tables 4 and 5 contain the fitting parameters for these properties by Equation (1), and Figures 3 and 4 show these properties as a function of composition and temperature. These figures show a similar behavior for the three binary mixtures. The increase of the density is obtained by a decrease of the temperature and an increase of the ionic liquid composition. In all figures, the open points are the experimental data and the lines are the results for the model fitted. Figure 4 and

Figure 5 show the experimental excess molar volume and deviations in the refractive index, respectively, as well as the fitted curves for binary mixtures ester + m-2-HEAH. Table 5 contains the fitting parameters for these properties. In Figure 4a we can observe that the excess molar volumes show a minimum at $x_1= 0.6$ for the methyl acetate +m-2-HEAH system and $x_1=0.5$ for the other two systems; besides, the systems present a maximum at $x_1=0.1$. This minimum could be due to hydrogen bonds between ester and ionic liquid. Also, Figure 4 shows that the increase of the alkyl chain in the esters introduced in the ionic liquid structure results in considerable decrease in the excess molar properties to more negative values, showing the polar effect of the molecules. In other cases, the introduction of methyl acetate results in weak decrease of the excess molar properties.

Table 2. Density and excess volume for the esters (1) + m-2-HEAH (2) at 298.15 K.

methyl acetate + m-2-HEAH			ethyl acetate + m-2-HEAH			propyl acetate + m-2-HEAH		
x_1	ρ (g/cm ³)	V^E	x_1	ρ (g/cm ³)	V^E	x_1	ρ (g/cm ³)	V^E
1.0000	0.92682	0.0000	1.0000	0.89490	0.0000	1.000	0.88261	0.0000
0.9512	0.93435	-0.0116	0.9499	0.90468	-0.0575	0.949	0.89302	-0.1664
0.9011	0.94120	-0.0295	0.9017	0.91311	-0.0915	0.898	0.90320	-0.3880
0.7999	0.95332	-0.1276	0.8031	0.92828	-0.1543	0.804	0.92108	-0.8855
0.6976	0.96381	-0.3073	0.7005	0.94277	-0.3603	0.702	0.93554	-1.0104
0.5982	0.97163	-0.4118	0.5971	0.95448	-0.4463	0.601	0.94877	-1.1677
0.5063	0.97700	-0.4092	0.4946	0.96456	-0.5318	0.500	0.95995	-1.2307
0.4030	0.98215	-0.4090	0.3986	0.97194	-0.4642	0.402	0.96850	-1.0791
0.3045	0.98615	-0.3761	0.3111	0.97730	-0.2946	0.304	0.97404	-0.5347
0.2149	0.98890	-0.2733	0.1973	0.98515	-0.3655	0.202	0.98082	-0.2537
0.1336	0.99073	-0.1101	0.1039	0.98814	0.0868	0.109	0.98743	-0.1675
0.0512	0.99231	0.0721	0.0719	0.99014	0.0459	0.045	0.99153	-0.0881
0.0000	0.99417	0.0000	0.0000	0.99417	0.0000	0.000	0.99417	0.0000

Table 3. Refractive index and deviations for the systems esters (1) + m-2-HEAH(2) at 288.15 K.

methyl acetate + m-2-HEAH			ethyl acetate + m-2-HEAH			propyl acetate + m-2-HEAH		
x_1	n_D	δn_D	x_1	n_D	δn_D	x_1	n_D	δn_D
1.0000	1.3650	0.0000	1.0000	1.3746	0.0000	1.0000	1.3867	0.0000
0.9512	1.3750	0.0054	0.9499	1.3836	0.0048	0.9489	1.3938	0.0034
0.9011	1.3847	0.0104	0.9017	1.3911	0.0081	0.8978	1.4003	0.0061
0.7999	1.4017	0.0177	0.8031	1.4041	0.0127	0.8036	1.4110	0.0099
0.6976	1.4147	0.0210	0.7005	1.4158	0.0156	0.7024	1.4208	0.0123
0.5982	1.4252	0.0221	0.5971	1.4255	0.0165	0.6005	1.4290	0.0130
0.5063	1.4332	0.0213	0.4946	1.4336	0.0159	0.4999	1.4369	0.0136
0.4030	1.4402	0.0185	0.3986	1.4405	0.0146	0.4022	1.4428	0.0123
0.3045	1.4459	0.0149	0.3111	1.4452	0.0118	0.3040	1.4473	0.0097
0.2149	1.4516	0.0121	0.1973	1.4519	0.0088	0.2022	1.4533	0.0082
0.1336	1.4546	0.0073	0.1039	1.4560	0.0050	0.1089	1.4556	0.0036
0.0512	1.4582	0.0032	0.0719	1.4566	0.0028	0.0454	1.4578	0.0012
0.0000	1.4599	0.0000	0.0000	1.4599	0.0000	0.0000	1.4599	0.0000

Table 4. Fitting parameters and root mean square deviations for density and refractive index of binary systems by equation (1).

	Methyl acetate + m-2-HEAB			Ethyl acetate + m-2-HEAB		
	$\rho/\text{g cm}^{-3}$	n_D		$\rho/\text{g cm}^{-3}$	n_D	$\rho/\text{g cm}^{-3}$
B ₀₀	1.202E+00	1.460E+00		1.185E+00	1.460E+00	1.141E+00
B ₀₁	-6.963E-04			-6.042E-04		-2.793E-04
B ₀₂	-3.671E-09			-1.286E-07		-7.138E-07
B ₁₀	-3.019E-01	-4.592E-02		3.224E-01	-4.311E-02	1.484E-01
B ₁₁	2.073E-03			-1.635E-03		-3.783E-04
B ₁₂	-3.832E-06			1.285E-06		-1.294E-06
B ₂₀	1.263E+00	2.116E-02		-1.020E+00	1.876E-03	-6.373E-01
B ₂₁	-8.415E-03			4.521E-03		6.447E-04
B ₂₂	1.417E-05			-3.396E-06		6.135E-06
B ₃₀	-1.704E+00	-7.043E-02		9.139E-01	-4.373E-02	1.060E+00
B ₃₁	1.152E-02			-3.159E-03		-1.963E-03
B ₃₂	-2.018E-05			-8.589E-07		-7.515E-06
B ₄₀	7.530E-01			-2.161E-01		-5.561E-01
B ₄₁	-5.070E-03			1.567E-04		1.250E-03
B ₄₂	8.621E-06			2.241E-06		2.736E-06
<i>s</i>	2.2x10 ⁻⁴	4.5x10 ⁻⁴		3.4x10 ⁻⁴	4.1x10 ⁻⁴	6.0x10 ⁻⁴
						4.5x10 ⁻⁴

ρ : density, B_{ij} : the fitting parameters of equation (1), s : standard deviation.

Table 5. Fitting parameters and root mean square deviations for excess molar volume and deviations of refractive index of binary systems by equation (4).

	Methyl acetate + m-2-HEAH			Ethyl acetate + m-2-HEAH		
	$V^E/(\text{cm}^3 \text{ mol}^{-1})$	δn_D		$V^E/(\text{cm}^3 \text{ mol}^{-1})$	δn_D	$V^E/(\text{cm}^3 \text{ mol}^{-1})$
C ₀₀	-1.265E+01	8.419E-02		-2.568E+00	6.384E-02	2.304E+01
C ₀₁	9.437E-02			3.713E-02		-1.527E-01
C ₀₂	-1.931E-04			-1.179E-04		1.983E-04
C ₁₀	2.409E+00	3.790E-02		1.125E+02	2.010E-02	-2.531E+02
C ₁₁	-1.520E-02			-7.063E-01		1.698E+00
C ₁₂	2.106E-05			1.096E-03		-2.860E-03
C ₂₀	8.068E+01	1.140E-02		-1.138E+02	1.043E-02	-1.666E+02
C ₂₁	-5.291E-01			5.490E-01		1.048E+00
C ₂₂	8.670E-04			-5.528E-04		-1.568E-03
C ₃₀	-1.287E+02	-9.461E-03		-4.581E+02	8.477E-03	1.546E+03
C ₃₁	8.537E-01			3.142E+00		-1.018E+01
C ₃₂	-1.355E-03			-5.296E-03		1.663E-02
C ₄₀	-9.571E+01			1.798E+02		3.940E+02
C ₄₁	6.171E-01			-9.179E-01		-2.721E+00
C ₄₂	-9.544E-04			1.087E-03		4.633E-03
C ₅₀	1.533E+02			4.165E+02		-2.018E+03
C ₅₁	-1.039E+00			-3.043E+00		1.343E+01
C ₅₂	1.674E-03			5.383E-03		-2.218E-02
<i>s</i>	1.1x10 ⁻²	2.9x10 ⁻⁴		4.0x10 ⁻²	3.0x10 ⁻⁴	8.8x10 ⁻²
						4.3x10 ⁻⁴

V^E : excess molar volumes, C_{ij} : the fitting parameters of equation (4), s : standard deviation.

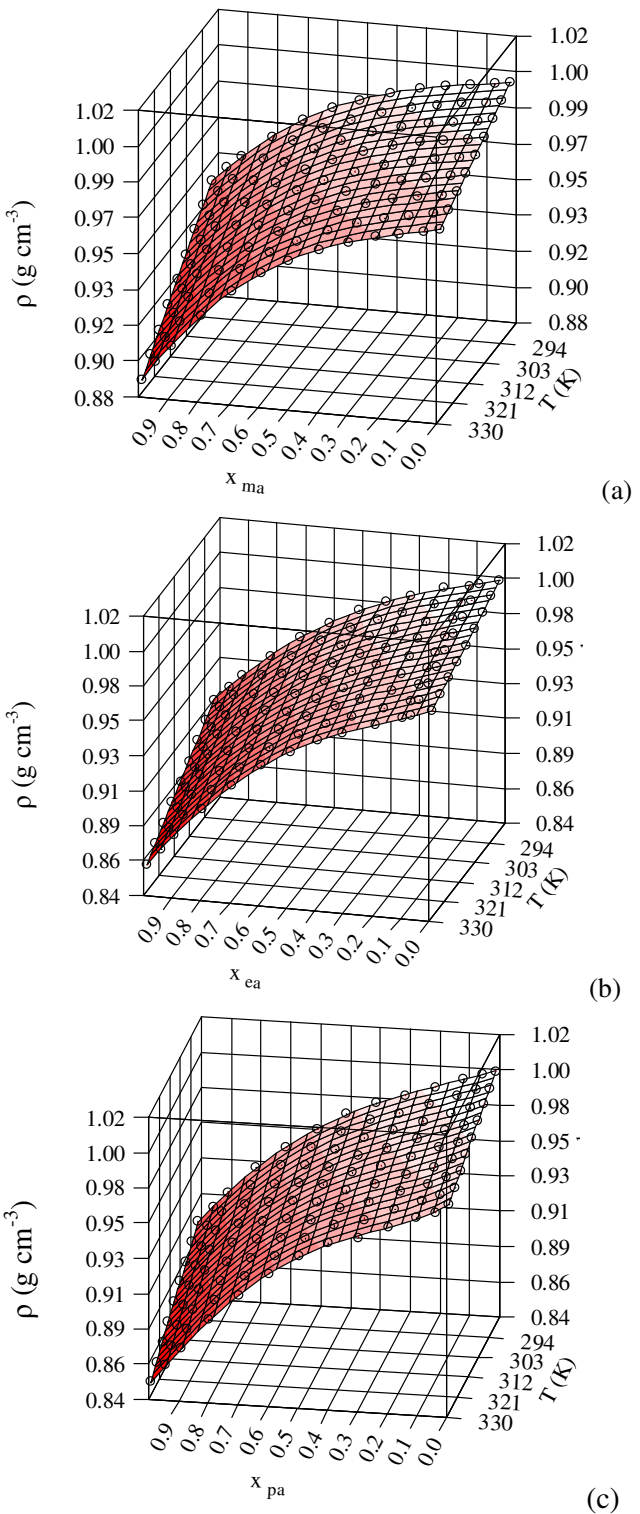
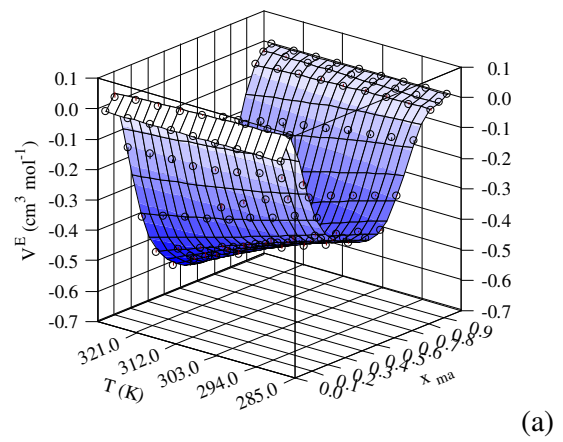
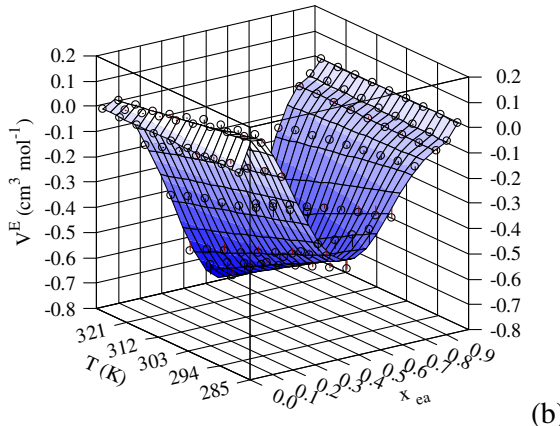


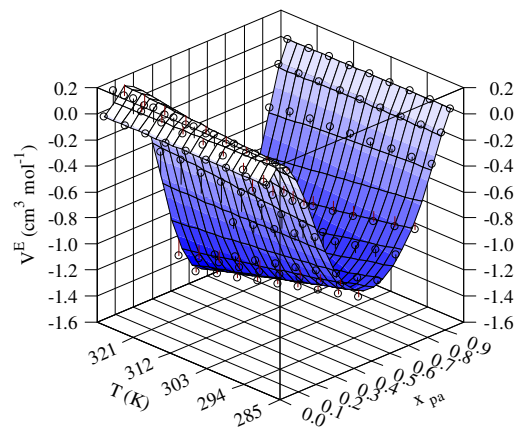
Figure 3. Density versus mole fraction and temperature, (a) methyl acetate + m-2-HEAH, (b) ethyl acetate + m-2-HEAH, (c) propyl acetate + m-2-HEAH.



(a)



(b)



(c)

Figure 4. Excess molar volume versus mole fraction and temperature, (a) methyl acetate + m-2-HEAH, (b) ethyl acetate + m-2-HEAH, (c) propyl acetate + m-2-HEAH.

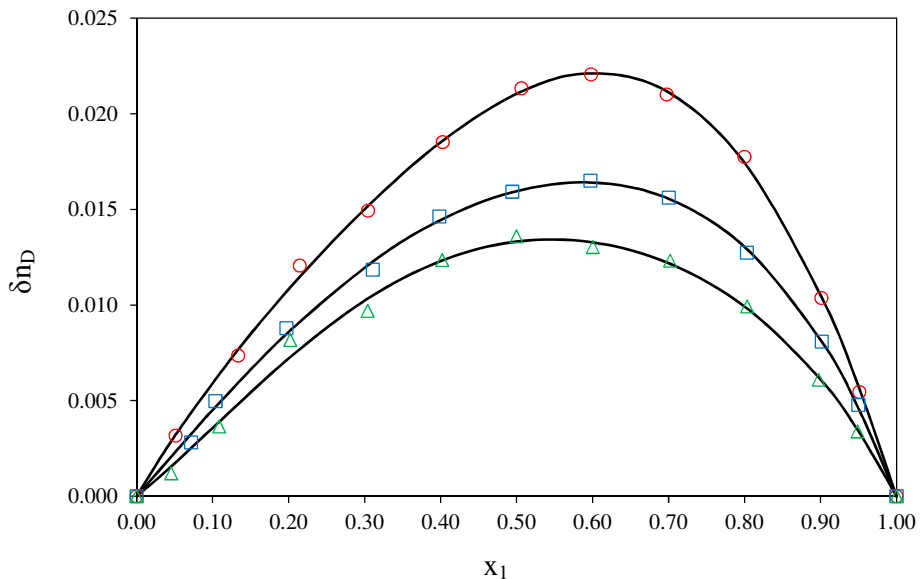


Figure 5. Deviations in the refractive index. Methyl acetate(\circ), ethyl acetate (\square), propyl acetate (Δ), fitted values by the Redlich-Kister model (-).

Excess molar volumes are the results of the intermolecular interactions that are due to the difference between the real and the ideal molar volumes. Sigmoidal-shaped curves have been observed for these systems, it has been suggested that this shape results from two opposing effects. The behavior in the IL rich region, the positive excess molar volumes may be attributed to the breakdown of the hydrogen bonded structure of ester or IL. The behavior in the ester rich region, the negative excess molar volumes may be attributed to the accommodation of the IL interstitially in the hydrogen bonded structure of the ester (solvation of the IL). From the results the, V^E , values increase with the increase of the alkyl chain length in the ester.

From figure 4 can be seen that the curves are skewed to the ester-rich region. The skewing of the curves is due to the size of the alkyl chain in the aldehyde, since methyl acetate has a smaller alkyl chain, changes in V^E is less pronounced. This trend in V^E values can be attributed to an increased interaction between IL and ester and to a stronger packing effect for the increase of the alkyl chain.

The excess molar volumes become more negative as the temperature increases because the kinetic energy of molecules also increases with temperature, which leads to a decrease in interaction of the molecules (Zhong and Wang 2007).

In the systems, a large negative V^E with a curve skewed to the ester-rich region can be explained by occupation of the free volume or cavities in the open IL structure by the ester. The observed V^E values may be explained qualitatively as follows: the IL is partially self-associated in the pure state and the degree of self-association may decrease when bit quantities of ester are mixed. This may be due to dissociation of hydrogen-bonding interactions into the IL and into the aldehyde. Additional quantity of ester, begin the ability of the ester molecules to fill up the cavities in the loose IL structure, and conclude with the creation of new hydrogen-bonding interactions IL-aldehyde. A decrease magnitude of V^E reflects the new compact structure or the

more efficient packing found in the mixture than in the pure compounds. The magnitude of the contributions made by these different types of interactions will vary with the ester and the composition of the mixture.

In Figure 5, the refractive index deviations are positive values for the three systems, and the maximum lies at a mole fraction of approximately 0.65 for the methyl acetate + m-2-HEAH system and at 0.6 for the other two systems. According to Nakata and Sakurai (1987) the sign of δn_D is opposite to that of V^{EX} if the behavior of the refractive index is not too non-linear between n_{D1} and n_{D2} . In our mixtures this rule is truly fulfilled in all the cases.

Table 6. Fitting parameters and standard deviations for apparent molar volume of binary systems by equation (6).

	Methyl acetate + m-2-HEAH	Ethyl acetate + m-2-HEAH	Propyl acetate + m-2-HEAH
	ϕ_V (g cm ⁻³)	ϕ_V (g cm ⁻³)	ϕ_V (g cm ⁻³)
A ₀	0.5000	0.5000	0.5000
A ₁	-2.991E-02	-4.992E-01	1.217E-01
A ₂	-2.978E-02	-4.996E-01	1.216E-01
ϕ_{00}^F	9.696E+00	-4.287E+04	5.961E+00
ϕ_{01}^F	-9.336E-02	2.817E+02	-3.641E-02
ϕ_{02}^F	2.795E-04	-4.447E-01	1.780E-04
ϕ_{10}^F	-6.171E+02	2.040E+04	3.442E+02
ϕ_{11}^F	1.028E+01	-1.401E+02	-3.236E+00
ϕ_{12}^F	-4.410E-02	2.160E-01	2.725E-02
ϕ_{20}^F	6.161E+02	2.235E+04	-3.446E+02
ϕ_{21}^F	-1.027E+01	-1.407E+02	3.239E+00
ϕ_{22}^F	4.405E-02	2.274E-01	-2.727E-02
ϕ_F^{00}	1.482E+02	3.701E+02	1.584E+02
ϕ_F^{01}	1.713E-01	-1.329E+00	8.809E-02
ϕ_F^{02}	-1.141E-04	2.376E-03	-8.552E-06
s	0.1	0.6	0.6

ϕ_V : apparent molar volume, A₀, A₁, A₂, A₃, ϕ_{ij}^F , ϕ_F^{00} , ϕ_F^{01} , ϕ_F^{02} : the fitting parameters of equation (7), s: standard deviation between experimental and calculated values

The apparent molar volume data are given in the supplementary information. Table 6 contains the fitting parameters for these properties. Figure 5 shows that the apparent molar volume, ϕ_V , rises rapidly at low concentrations (below 20 mol/kg), while at higher concentrations is almost constant (all three mixtures shown the same trend). Also, in the figures the properties increase with temperature at all concentrations. The apparent molar volume is used to know an aggregation behavior of the solutes in a wide variety of mixtures (Ruso et al., 2004). The behavior for ester mixtures can be explained by the presence of aggregation species. Figure 6 shows the increase of the concentration of m-2-HEAH at each isotherm, inducing the increase of ϕ_V due to solvation of ions and breaking off the net structure of the solvent. Also, the curves of Figure 6 show that, as the molality of m-2-HEAH is increased from pure solvent, the high packing of the solvent is the dominant contributor, up to a critical concentration, in this point the quasi constant values of ϕ_V reflects the attraction between the ionic pair of m-2-HEAH as the principal contributor.

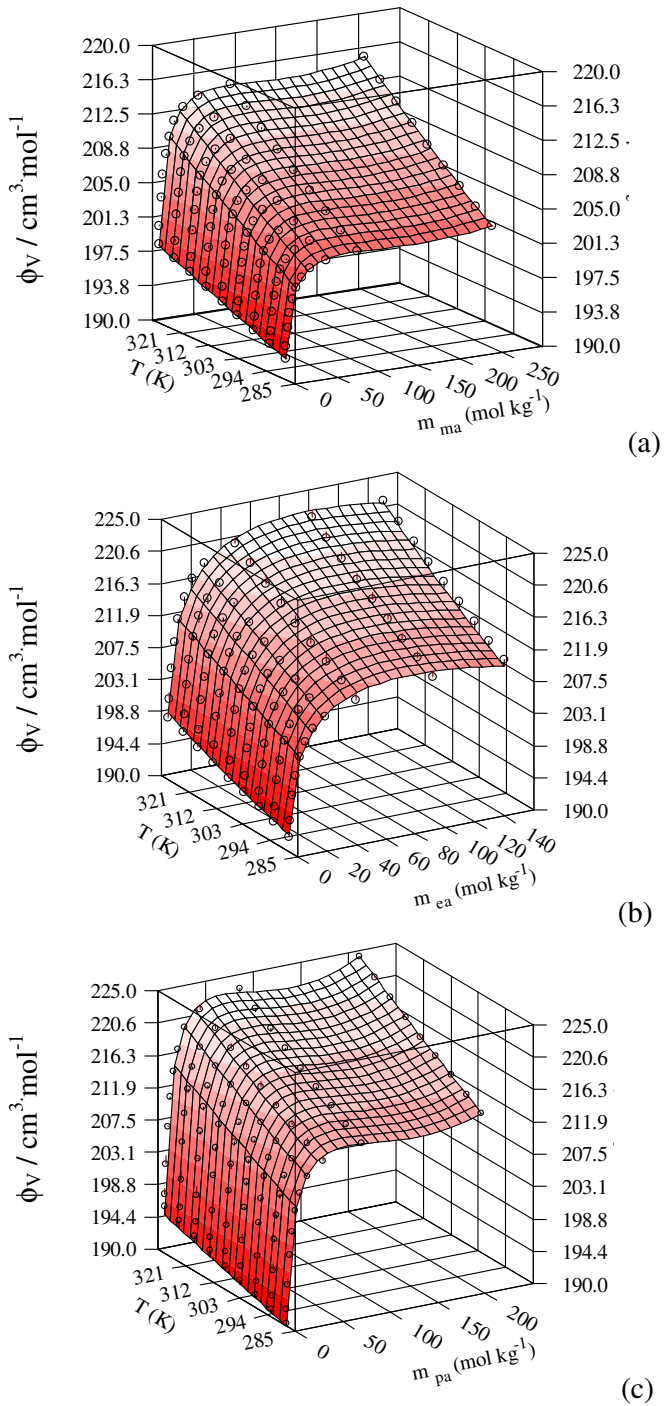


Figure 6. Apparent molar volume versus molality and temperature, (a) methyl acetate + m-2-HEAH, (b) ethyl acetate + m-2-HEAH, (c) propyl acetate + m-2-HEAH.

The values for apparent molar volumes at infinite dilution ϕ_V were obtained by extrapolation at infinite dilution ($m \rightarrow 0$), based on the extended Redlich-Mayer relation, Equation (6). The values of ϕ_V for several temperatures are shown in Figure 7. This figure shows that the apparent molar volume at infinite dilution for methyl acetate mixture is greater than other esters mixtures.

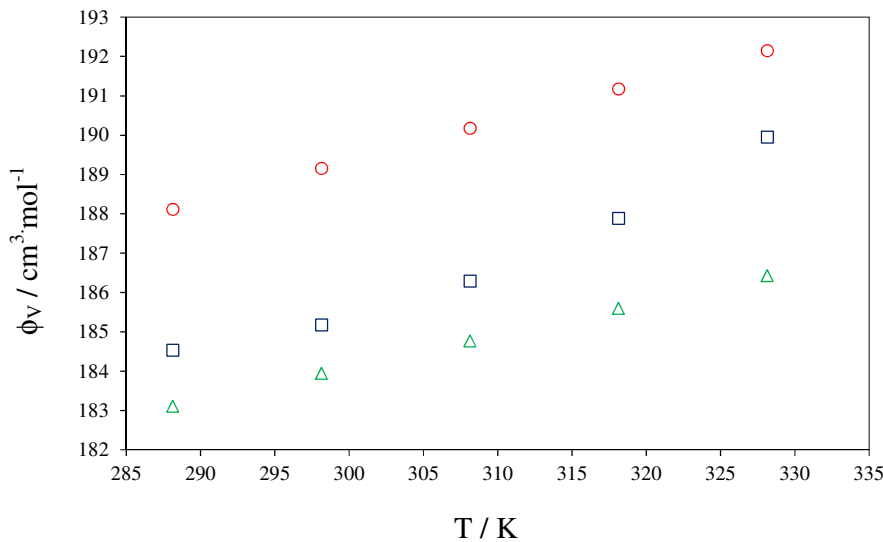
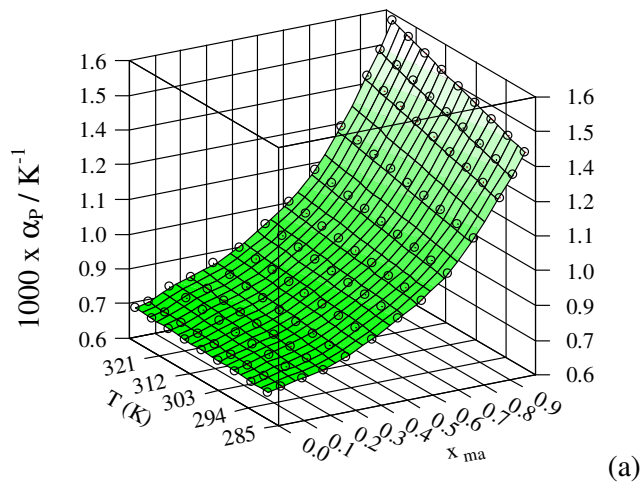


Figure 7. Apparent molar volume at infinite dilution versus temperature. Binary system with methyl acetate (○), ethyl acetate (□) and propyl acetate (Δ).

The values for the thermal expansion coefficient are shown in the supplementary information and the behavior is shown in Figure 8. The value deduced for α_P is particularly sensitive to the type of mathematical function used to fit the density data. The fit can be done with a linear function; however, subtle effects stem from the non-linear behavior of most fluids, and therefore a piece of information may be lost. In these figures, the ionic liquid shows a stable value of thermal expansion coefficient with the rise of temperature, a different behavior for binary mixtures and esters solvents. This behavior shows a very polar attraction among the high ordering molecules of the ionic liquid.



(a)

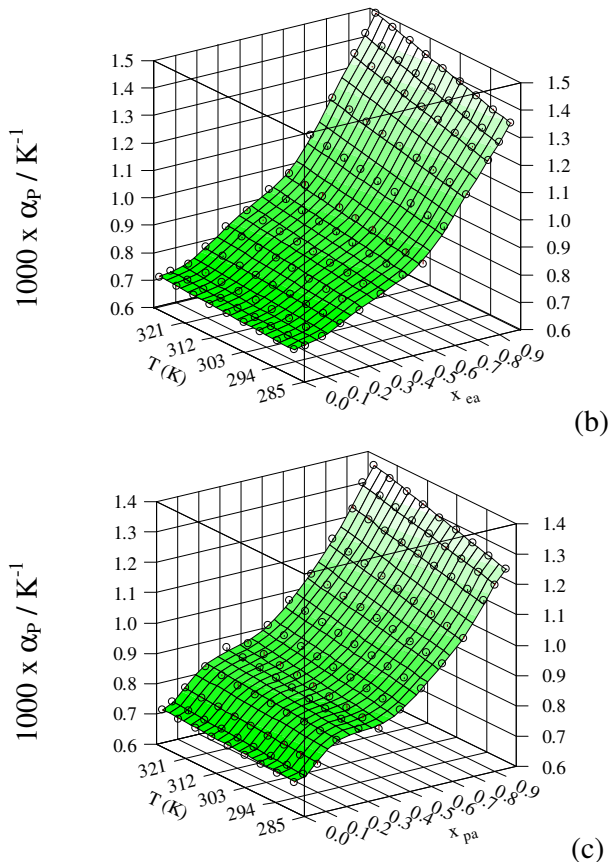


Figure 8. Thermal expansion coefficient versus mole fraction of the solvent and temperature, (a) methyl acetate + m-2-HEAH, (b) ethyl acetate + m-2-HEAH, (c) propyl acetate + m-2-HEAH.

The methyl acetate mixture exhibit a higher thermal expansion than the others mixture. The results also suggest that the presence of the alkyl chain length in the ester decreases the thermal expansion coefficient. The presence of the alkyl chain seems to yield a smaller thermal expansion coefficient even at high concentration of IL, the difference between α_p for the binary mixtures being about 10%.

5.2. Density predictions

Figure 9 compares the σ -profile for m-2-HEAH, methyl acetate, ethyl acetate, and propyl acetate compounds. The σ -profile of these compounds can be qualitatively divided in three main regions, which are separated in Figure 9 by two vertical lines located at the cutoff values for the hydrogen bond donor ($\sigma_{HB} < -0.0084 \text{ e}/\text{\AA}^2$) and acceptor ($\sigma_{HB} > 0.0084 \text{ e}/\text{\AA}^2$) group (Lin and Sandler, 2002). For m-2-HEAH, the σ -profile reveals to be broader than the σ -profiles of the esters solvents. Also, the σ -profile of this ionic liquid is dominated by a huge peak of slightly negative screening charge density at $\sigma = -0.001$, which is due to polarization of $-\text{CH}_2-$ groups by the ammonium-hydrogen, hydroxyl-hydrogen and oxygen atoms. The two peaks about 0.009 and 0.012 corresponds to the negatively charged $-\text{COO}^-$ and lone pairs of the oxygen in the $-\text{OH}$ groups, respectively. Considering the high-polarity region $\sigma_{HB} > 0.0084 \text{ e}/\text{\AA}^2$, these groups can be considered as hydrogen-bond acceptor groups (Lin and Sandler, 2002; Diedenhofen and Klamt, 2010). On the left hand side of the histogram, it can be observed two low peaks at values lower than

the cutoff $-0.0084 \text{ e}/\text{\AA}^2$, which are affected by the alkyl chain. These peaks are related to the ammonium-hydrogen and hydroxyl-hydrogen; they may contribute to hydrogen bonds as donors. Finally, the distribution of the charge densities around zero ($-0.0084 \text{ e}/\text{\AA}^2 < \sigma < 0.0084 \text{ e}/\text{\AA}^2$) corresponds to the non-polar alkyl groups of the cation, being those for positive and negative signs assigned to carbon and hydrogen atoms, respectively. Figure 9 shows that the higher number of carbon atoms in alkyl chain implies the increasing of the area below each histogram of charge densities around the non-polar area (methyl acetate < ethyl acetate < propyl acetate < m-2-HEAH). In this way, the σ -profile with high values at $\sigma = 0$ show more repulsive interactions between polar and non-polar segments, affecting the cohesive properties of the molecule. The same idea can be applied to mixtures of compounds with very different σ -profiles, i.e. the binary mixture propyl acetate + m-2-HEAH is the more non ideal system studied here. Interestingly, it can be observed high deviations of the predicted density for this binary system, showed in Figure 10. The physical properties used in the model for all substances are reported in Table 7. The predictive results show percentage average relative deviations for the mixtures of m-2-HEAH with methyl acetate, ethyl acetate and propyl acetate are 1.3%, 1.3%, and 1.6%, respectively. This suggests that σ -profile is an adequate a priori parameter to characterize quantitatively the non-ideality of volumetric behavior.

Table 7. Properties of the substances used in the modeling

Compound	<i>MM</i>	<i>T_c</i> (K)	<i>P_c</i> (MPa)	ω	<i>r</i>	<i>q</i>	COSMO ^c Segments	<i>V</i> ^{COSMO} (Å ³) ^c
methyl acetate ^a	74.08	506.55	4.75	0.33126	8.61	5.08	459	97.0419
ethyl acetate ^a	88.11	523.30	3.88	0.36641	10.91	6.18	571	117.9393
propyl acetate ^a	102.13	549.73	3.36	0.38890	13.21	7.19	676	139.8076
m-2-HEAH ^b	191.27	804.82	2.29	1.11210	26.68	12.76	1212	271.5216

^aDiadem public (2000); ^bValderrama and Robles (2007); ^cThis work

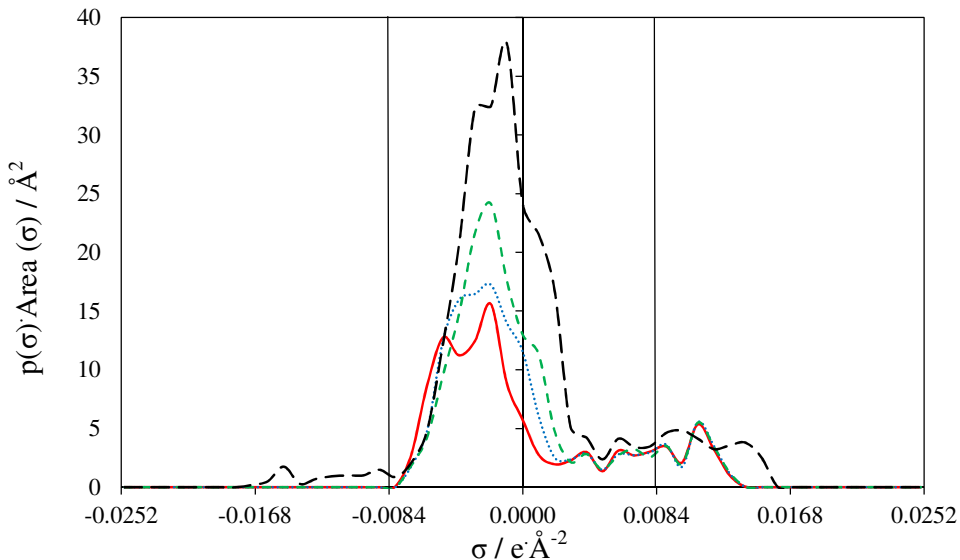


Figure 9. Sigma profiles employed for m-2-HEAH (— —), methyl acetate (—), ethyl acetate (···), and propyl acetate (— · · —). Note that, due to the definition as conductor screening charges, electrostatically positive parts of the molecules have negative σ and vice versa.

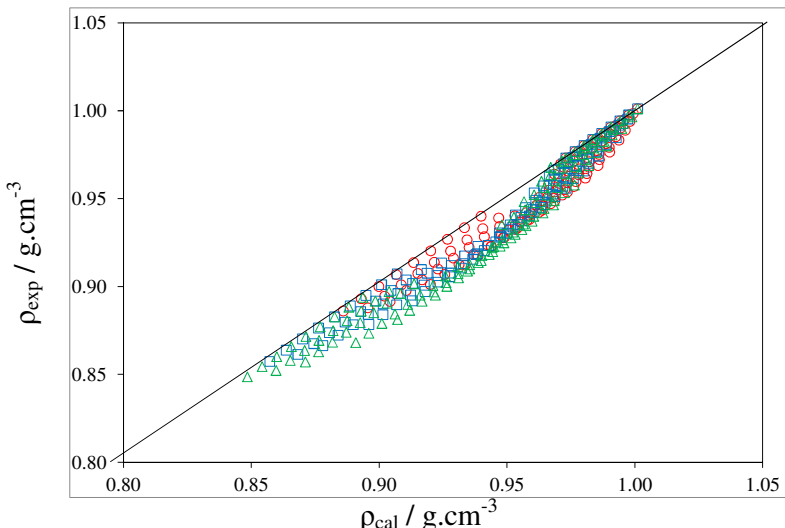


Figure 10. Comparison of experimental and PR-WS/COSMO-SAC model predicted values of density ($\text{g}\cdot\text{cm}^{-3}$) for binary mixtures, methyl acetate + m-2-HEAH (○), ethyl acetate + m-2-HEAH (□) and propyl acetate + m-2-HEAH (Δ) in the whole composition interval.

5.3. VLE data

The vapor–liquid equilibrium (VLE) phase diagrams of three binary mixtures covering a wide range of temperature (313.15–403.15) K at 101.3 kPa are examined. The chosen systems have strong interactions between the species (esters and ionic liquid).

In order to validate the technique, experimental vapor-liquid equilibrium data for the system ethanol (1) + 1-ethyl-3-methylimidazolium ethylsulfate, [emim] $[\text{EtSO}_4]$ (2) were determined and compared with published data from Calvar et al. (2008). This comparison is shown in Figure 11. From the results in this figure, the experimental technique can be considered as validated and can be used to determine the new experimental data involving m-2-HEAH.

VLE for the binary systems ester (1) + m-2-HEAH (2) have been determined at 101.3 kPa and the results are summarized in Table 8. The parameters used in the thermodynamic model Peng–Robinson EoS with the Wong–Sandler/COSMO-SAC mixing rule are reported in Table 7, and applied for the prediction of VLE experimental data. The predicted results for the systems are shown in Figure 12 and the percentage average relative deviations for the mixtures of m-2-HEAH with methyl acetate, ethyl acetate and propyl acetate are 1.1%, 1.0%, and 0.6%, respectively. The representation of the phase behavior has a good trend and the vapor phase, free of ionic liquid, is correctly predicted.

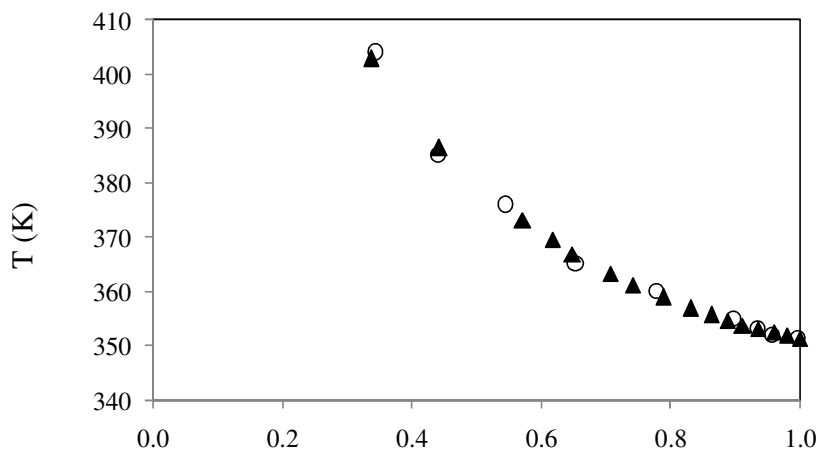


Figure 11. Vapor temperature vs. ethanol mole fraction for the system ethanol + [emim][EtSO₄]. This work (○), Calvar et al. (2008) (▲).

Table 8. Vapor liquid equilibria at 101.3 kPa for the binary systems m-2-HEAH.

x_1	T (K)	x_1	T (K)	x_1	T (K)
Methyl acetate (1) + m-2-HEAH (2)		Ethyl acetate (1) + m-2-HEAH (2)		Propyl acetate (1) + m-2-HEAH (2)	
1.0000	330.1	1.0000	349.8	1.0000	374.0
0.9927	330.2	0.9604	350.3	0.9837	374.7
0.9876	330.4	0.9195	350.5	0.9630	374.7
0.8987	331.1	0.8734	351.3	0.9162	374.8
0.8953	331.0	0.8223	351.8	0.8654	375.2
0.8729	331.3	0.7817	352.5	0.8289	376.0
0.8149	331.8	0.7275	353.4	0.7989	376.9
0.8032	332.0	0.7263	353.4	0.7780	377.6
0.7751	332.2	0.7041	353.7	0.7660	378.1
0.7670	332.1	0.6705	354.6	0.7310	379.1
0.7634	332.2	0.6702	354.8	0.7237	379.2
0.7344	333.1	0.6431	355.6	0.7002	380.3
0.7130	333.6	0.6278	356.3	0.6948	380.9
0.6943	334.7	0.6143	356.7	0.6728	381.9
0.6379	335.9	0.5909	358.2	0.6350	383.7
0.6240	337.1	0.5862	359.1	0.6159	386.4
0.5834	340.3	0.5728	360.0	0.5849	389.4
0.5416	342.5	0.5660	360.3	0.5413	391.6
0.5241	344.1	0.5654	360.9	0.5198	394.8
0.4971	346.0	0.5451	361.9	0.4856	396.3
0.4867	347.3	0.5373	363.1	0.4419	401.1
		0.5228	365.1	0.3935	406.0
		0.5160	364.1	0.3444	410.0
		0.4912	368.2	0.3243	411.2
		0.4581	369.6		
		0.4447	371.5		
		0.4249	373.1		

Table 9. Details of the fitted results for the systems studied using the PR+WS/UNIQUAC or PR+WS/NRTL models.

Model	k_{ij}	α	A_{ij}	A_{ji}	% ΔT
Methyl acetate (1) + m-2-HEAH (2).					
NRTL	0,4180	0,5148	38413,7188	-2460,9375	0,06
UNIQUAC	0,5513	-	-3078,2317	13298,9502	0,10
Ethyl acetate (1) + m-2-HEAH (2)					
NRTL	0,4664	0,5341	-1186,5233	-2478,7903	0,12
UNIQUAC	0,6412	-	-3361,8164	7130,1270	0,16
Propyl acetate (1) + m-2-HEAH (2).					
NRTL	-0,7133	0,2218	32111,6641	-2812,3711	0,16
UNIQUAC	0,5293	-	-3427,6592	6317,1387	0,19

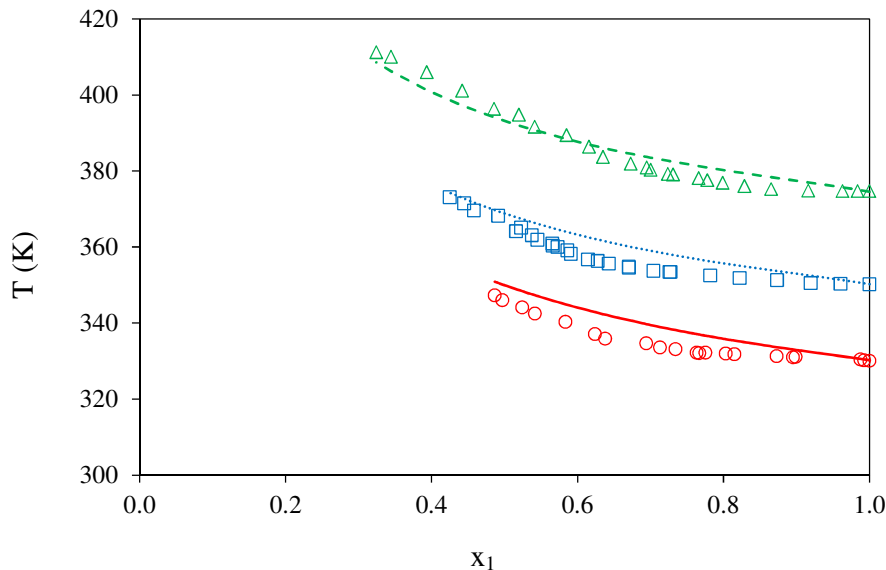


Figure 12. Temperature vs. composition of the ester. (○) methyl acetate (1) + m-2HEAH (2), (□) ethyl acetate (1) + m-2HEAH(2), (Δ) propyl acetate (1) + m-2HEAH (2), and predicted values(-).

6. Conclusions

Density and refractive index of binary mixtures ester + N-methyl-2-hydroxyethylammonium hexanoate have been measured at atmospheric pressure. Other properties, such as excess molar volume and deviations in the refractive index were also calculated. The values of V^E are negative at high concentrations of ester and positive in the opposite case.

The Peng-Robinson equation of state coupled with the Wong-Sandler mixing rule using the COSMO-SAC model was used to predict the density and vapor liquid equilibrium.

For the binary systems ester (methyl acetate, ethyl acetate or propyl acetate) + m-2-HEAH, the predicted densities show deviations below than 1.6 %. COSMO-SAC is also revealed as a valuable computational tool to describe the intermolecular interaction of systems containing m-2-HEAH. In addition, the σ -profile is suggested as a simple molecular parameter to characterize the non ideality of the mixtures respect to volumetric properties.

The vapor-liquid equilibrium of binary systems ester + m-2-HEAH at 101.3 kPa was measured by a dynamic method. The experimental VLE data were predicted by the thermodynamic model with deviations below than 1.1 %.

Acknowledgments

V.H. Álvarez acknowledges the financial support from FAPESP (Fundação de Amparo à Pesquisa do Estado de São Paulo), process 2006/03711-1. M. Aznar and S. Mattedi are recipients of CNPq (Brazil) fellowships

References

ABRAMS, D.S.; PRAUSNITZ, J.M. Statistical thermodynamics of liquid mixtures: a new expression for the excess Gibbs energy of partly or completely miscible systems. *AIChE J.*, v.21, p.116–128, 1975

Accelrys Materials Studio, <http://accelrys.com/products/materials-studio/>, accessed January 2010.

ÁLVAREZ, V.H.; AZNAR, M. Thermodynamic modeling of vapor–liquid equilibrium of binary systems ionic liquid + supercritical {CO₂ or CHF₃} and ionic liquid + hydrocarbons using Peng–Robinson equation of state. *J. Chin. Inst. Chem. Eng.*, v. 39, p.353–360, 2008.

Álvarez, V.H.; Aznar, M. Application of a thermodynamic consistency test to binary mixtures containing an ionic liquid, *The Open Thermodynamics Journal*, v. 2, p. 25-38, 2008b.

ÁLVAREZ, V.H.; LARICO, R., IANOS, Y.; AZNAR, M. Parameter estimation for VLE calculation by global minimization: Genetic algorithm, *Braz. J. Chem. Eng.* 2008, 25, 409-418

ÁLVAREZ, V.H.; DOSIL, N.; GONZALEZ-CABALEIRO, R.; MATTEDI, S., MARTIN-PASTOR, M.; IGLESIAS, M.; NAVAZA, J. M. Brønsted Ionic Liquids for Sustainable Processes: Synthesis and Physical Properties, *J. Chem. Eng. Data*, v.55, p. 625–632, 2010.

ÁLVAREZ V.H.; AZNAR, M. An efficient approach to optimal interpolation of experimental data. *J. Taiwan Inst. Chem. Eng.*, v.41, p.184–189, 2010.

CALVAR, N.; GONZÁLEZ, B.; GÓMEZ E.; DOMINGUEZ, Á. Vapor–liquid equilibria for the ternary system ethanol + water +1-ethyl-3-methylimidazolium ethylsulfate and the corresponding binary systems containing the ionic liquid at 101.3 kPa, *J. Chem. Eng. Data*, v.53, p.820-825, 2008

Diadem Public 1.2, The DPPR Information and Data Evaluation Manager, 2000.

DIEDENHOFEN, M.; KLAMT, A. COSMO-RS as a tool for property prediction of IL mixtures—A review, *Fluid Phase Equilib.* In press (2010).

HA, S. H.; LAN, M. N.; LEE, S. H.; HWANG, S. M.; KOO Y-M. Lipase-catalyzed biodiesel production from soybean oil in ionic liquids, *Enzyme and Microbial Technology* 41, 480–483, 2007.

HUDDLESTON, J.G.; WILLAUER, H.D.; SWATLOSKI, R.P.; VISSER, A.E.; ROGERS, R.D. Room temperature ionic liquids as novel media for clean liquid–liquid extraction. *Chem. Commun.*, p.1765-1766, 1998.

LORIA, H.; PEREIRA-ALMAO, P.; SATYRO M. Prediction of Density and Viscosity of Bitumen Using the Peng-Robinson Equation of State, *Ind. Eng. Chem. Res.* v48, p. 10129–10135, 2009.

LIN, S.T.; SANDLER, S.I. A priori phase equilibrium prediction from a segment contribution solvation model. *Ind. Eng. Chem. Res.*, v.41, p.899-913, 2002

MICHELSEN, M.L.; MOLLERUP, J. *Thermodynamic Models: Fundamentals and Computational Aspects*, 2nd edition, Tie-Line Publications, Lyngby, 2007.

MULLINS, E.; OLDDLAND, R.; LIU, Y.A.; WANG, S.; SANDLER, S.I.; CHEN, C.C.; ZWOLAK, M.; SEAVEY, K.C. Sigma-profile database for using COSMO-based thermodynamic methods. *Ind. Eng. Chem. Res.*, v.45, p.4389–4415, 2006.

NAKATA, M.; SAKURAI, M. Refractive index and excess volume for binary liquid mixtures. Part 1. Analyses of new and old data for binary mixtures. *J. Chem. Soc., Faraday Trans. 1*, v. 83, p.2449 - 2457, 1987.

PENELOUX, A.; RAUZY, E.; FREZE, R. A consistent correction for Redlich-Kwong-Soave volumes, *Fluid Phase Equilib.* 8 (1982) 7-23.

PENG, D.; ROBINSON, D.B. A new two-constant equation of state. *Ind. Eng. Chem. Fundam.*, v.15, p.59–64, 1976.

RANU,B. C.; BANERJEE S.; JANA R. Ionic liquid as catalyst and solvent: the remarkable effect of a basic ionic liquid, [bmIm]OH on Michael addition and alkylation of active methylene compounds, *Tetrahedron* 63, 776–782, 2007.

RUSO, J. M.; GONZÁLEZ-PÉREZ, A.; PRIETO,G.; SARMIENTO F.A Volumetric study of two related amphiphilic beta-blockers as a function of temperature and electrolyte concentration, *Colloids and Surfaces B: Biointerfaces* 33, 165–175, 2004.

SARKAR, L.; ROY M. N. Studies on liquid–liquid interactions of some ternary mixtures by density, viscosity, ultrasonic speed and refractive index measurements, *Thermoch. Acta*, v. 496, p.124–128, 2009.

VALDERRAMA, J.O.; ROBLES, P.A. Critical properties, normal boiling temperatures, and acentric factors of fifty ionic liquids. *Ind. Eng. Chem. Res.*, v.46 p.1338-1344, 2007

WONG, D.S.H.; SANDLER, S.I. A theoretically correct mixing rule for cubic equations of state. *AICHE J.*, v.38, p.671–680. 1992.

ZHANG, S.; ZHANG, Q.; ZHANG, Z. C. Extractive desulfurization and denitrogenation of fuels using ionic liquids. *Ind. Eng. Chem. Res.*, v.43, p. 614-622, 2004.

ZHU, H-P.; YANG, F.; TANG, J.; HE, M-Y. Brønsted acidic ionic liquid 1-methylimidazolium tetrafluoroborate: a green catalyst and recyclable medium for esterification, *Green Chemistry*, v. 5, p. 38–39, 2003

K.N. Marsh, J.A. Boxall, R. Lichtenthaler, Room temperature ionic liquids and their mixtures-a review, *Fluid Phase Equilib.* 219 (2004) 93-98.

S. Gabriel, J. Weiner, Ueber einige Abkömmlinge des Propylamins, *Ber.* 21 (1888) 2669-2679.

KENNEDY, D.F.; DRUMMOND, C.J. Large Aggregated Ions Found in Some Protic Ionic Liquids, *J. Phys. Chem. B* 113 (2009) 5690-5693.

BICAK, N. A new ionic liquid: 2-hydroxyethylammonium formate. *J. Mol. Liq.* 2005, 116, 15–18.

GREAVES T. L.; WEERAWARDENA A.; FONG C.; KRODKIEWSKA I.; DRUMMOND C. J. Protic Ionic Liquids: Solvents with Tunable Phase Behavior and Physicochemical Properties, *J. Phys. Chem. B* 2006, 110, 22479-22487.

COTA, I.; GONZÁLEZ-OLMOS, R.; IGLESIAS, M.; MEDINA F. New short chain aliphatic chain ionic liquids: synthesis, physical properties and catalytic activity in aldol condensations. *J. Phys. Chem. B* 111(2007) 12468-12477.

KURNIA, K.; WILFRED, C.; MURUGESAN, T. Thermophysical properties of hydroxyl ammonium ionic liquids, *J. Chem. Thermodyn.* 41 (2009) 517-521.

IGLESIAS M.; TORRES A.; GONZALEZ-OLMOS R., SALVATIERRA D. Effect of temperature on mixing thermodynamics of a new ionic liquid: {2-hydroxyethylammonium formate (2-HEAF) + short hydroxylic solvents}, *J. Chem. Thermodyn.*, 40 (2008), 119-133.

PERIC, B.; SIERRA, J.; MARTI, E.; GONZALEZ-OLMOS, R.; IGLESIAS, M.; CRUAÑAS, R.; GARAU, M.A. 20th Society of Environmental Toxicology and Chemistry Congress, SETAC Europe Annual Meeting, Science and Technology for Environmental Protection, Sevilla (Spain), May, 2010.

SIERRA, J.; MARTÍ, E.; MENGÍBAR, A.; GONZÁLEZ-OLMOS, R.; IGLESIAS, M.; CRUAÑAS, R.; GARAU, M.A. 5º society of environmental toxicology and chemistry congress, SETAC 2008. Sydney (Australia), August, 2008.

4.2.2.3 Equilíbrio líquido-vapor a altas pressões

Um teste de consistência termodinâmica (Álvarez e Aznar, 2008a; Álvarez e Aznar, 2009) foi desenvolvido para sistemas com dados isotérmicos incompletos tipo PTxy. O teste é baseado na equação de Gibbs-Duhem, e na equação de Estado de Peng-Robinson com a regra de mistura de Wong-Sandler usando o modelo UNIQUAC ou NRTL para os coeficientes de atividade. Foi mostrado que o modelo proporciona uma excelente representação dos dados experimentais e o teste de consistência consegue mostrar que os dados aqui relatados são termodinamicamente consistentes ou inconsistentes.

A constante de Henry para os sistemas binários CO₂ + líquidos iônicos foi estimada pelo modelo termodinâmico utilizado no teste de consistência, usando uma aproximação numérica da inclinação limite quando a solubilidade se aproxima de zero. Logo foi obtida uma função empírica que relaciona a constante de Henry em função da temperatura. Com essa correlação, pode ser calculada a entropia parcial molar e a entalpia parcial molar da solução (Letcher, 2007), para relacionar o efeito da temperatura sobre a solubilidade do CO₂. A entalpia molar parcial de dissolução do gás indica a força de interação entre o gás e líquido iônico, enquanto que a entropia molar parcial indica a quantidade de ordem presente na mistura gás-líquido iônico.

A variação com a temperatura da solubilidade para os oito gases estudados, expressa na lei de Henry, está diretamente relacionada com as propriedades termodinâmicas de solvatação que, no caso dos solutos gasosos em baixas pressões, é praticamente idêntica para as propriedades termodinâmicas da solução (Hildebrand et al., 1970).

Como os dados de solubilidade obtidos são suficientemente precisos, as propriedades termodinâmicas de solvatação podem ser usadas para inferir sobre os mecanismos moleculares relacionados com a solvatação do CO₂ em diferentes líquidos iônicos. Essas propriedades fornecem informações valiosas tanto sobre as interações soluto-solvente e sobre a estrutura molecular das soluções: a entalpia da solução está intimamente relacionada com a ligação das interações moleculares gás-líquido iônico e a entropia de solvatação dá indicações sobre a estrutura do solvente molecular em torno do soluto. Os valores da energia de Gibbs, entalpia e entropia de solvatação são apresentados na Tabela 4.7 para os CO₂ nos líquidos iônicos a 298,15 K.

Tabela 4.7. Funções termodinâmicas da solvatação do CO₂ nos líquidos iônicos estudados.

Líquido iônico	MM g/mol	$\Delta_{\text{solv}}H$ kJ/mol	$T \cdot \Delta_{\text{solv}}S _{T=298\text{ K}}$ kJ/mol	$\Delta_{\text{solv}}G$ kJ/mol
[c ₄ mim] ⁺ [Ac] ⁻	198,26	-32,52	-23,82	-8,70
[c ₄ mim] ⁺ [TFA] ⁻	252,23	-19,34	-22,70	3,36
[THTDP] ⁺ [Tf ₂ N] ⁻	764,00	-10,53	-12,42	1,89
[THTDP] ⁺ [Cl] ⁻	519,31	-17,80	-19,11	1,31
[c ₂ mim] ⁺ [Tf ₂ N] ⁻	391,31	-13,33	-16,52	3,19
[c ₅ mim] ⁺ [Tf ₂ N] ⁻	433,39	-13,96	-16,60	2,64
[c ₄ mim] ⁺ [DCA] ⁻	205,26	-14,46	-13,07	-1,39
[c ₄ mim] ⁺ [Tf ₂ N] ⁻	419,36	-16,60	-18,63	2,03
m-2-HEAF	121,14	-18,28	-24,37	6,10
m-2-HEAA	135,16	-27,48	-30,28	2,81

Na Tabela 4.7 todas as entalpias de solvatação são negativas, isto corresponde a uma hidratação exotérmica, com os máximos valores para [c₄mim]⁺[Ac]⁻ e m-2-HEAA. Para a parte entrópica da solvatação, todos os valores são negativos e com os máximos valores para m-2-HEAF e m-2-HEAA.

O comportamento observado para a entalpia de solvatação, provavelmente, significa que as interações solvente-soluto são de natureza diferente no líquido iônico com ânion acetato. O mesmo é observado no caso da entropia de solvatação para o qual o comportamento é diferente no caso de líquidos iônicos contendo cátion amônio.

Artigos publicados:

Na seguinte listagem de artigos, os dois primeiros apresentam o desenvolvimento do método de consistência termodinâmica e os seguintes artigos apresentam os dados experimentais de sistemas contendo CO₂ supercrítico e sua modelagem.

ÁLVAREZ V.H.; AZNAR M. Application of a thermodynamic consistency test to binary mixtures containing an ionic liquid, *The Open Thermodynamics Journal*, v. 2, p. 25-38, 2008.

ÁLVAREZ V.H.; AZNAR M. An efficient approach to optimal interpolation of experimental data, *Journal of the Taiwan Institute of Chemical Engineers*, v. 41, p. 184-189, 2010.

CARVALHO P.J.; ÁLVAREZ V.H.; MACHADO J.J.B.; PAULY J.; DARIDON J-L.; MARRUCHO I.M.; AZNAR M.; COUTINHO J.A.P. High pressure phase behavior of carbon dioxide in 1-alkyl-3-methylimidazolium bis(trifluoromethylsulfonyl)imide ionic liquids, *J. Supercrit. Fluids*, v. 48, p. 99–107, 2009.

CARVALHO P.J.; ÁLVAREZ V.H.; MARRUCHO I.M.; AZNAR M.; COUTINHO J.A.P. High pressure phase behavior of carbon dioxide in 1-butyl-3-methylimidazolium bis(trifluoromethylsulfonyl)imide and 1-butyl-3-methylimidazolium dicyanamide ionic liquids, *J. of Supercritical Fluids*, v. 50, p. 105–111, 2009.

CARVALHO, P.J.; ÁLVAREZ V.H.; SCHRÖDER B.; GIL A.M., MARRUCHO I.M.; AZNAR M., SANTOS L.M.N.B.F.; COUTINHO J.A. P. Specific solvation interactions of CO₂ on acetate and trifluoroacetate imidazolium based ionic liquids at high pressures, *J. Phys. Chem. B*, v. 113, p. 6803-6812, 2009.

CARVALHO P.J.; ÁLVAREZ V.H.; MARRUCHO I.M.; AZNAR M.; COUTINHO J.A.P. High carbon dioxide solubilities in trihexyltetradecylphosphonium-based ionic liquids, the journal of supercritical fluids, *J. of Supercritical Fluids*, v.52, p. 258–265, 2010.

Artigo 4.7: Application of a thermodynamic consistency test to binary mixtures containing an ionic liquid

The Open Thermodynamics Journal, 2008, 2, 25-38

25

Application of a Thermodynamic Consistency Test to Binary Mixtures Containing an Ionic Liquid

Víctor H. Álvarez and Martín Aznar*

School of Chemical Engineering, State University of Campinas, UNICAMP, P.O. Box 6066, 13083-970, Campinas-SP, Brazil

Abstract: A thermodynamic consistency test developed for high pressure binary vapor-liquid mixtures is applied to mixtures containing a supercritical solvent and an ionic liquid. Several authors have reported vapor-liquid equilibrium data on the binary systems supercritical $\text{CO}_2 + 1\text{-butyl-3-methyl imidazolium hexafluorophosphate } \{[\text{bmim}]\text{[PF}_6\}\}$, supercritical $\text{CO}_2 + 1\text{-butyl-3-methyl imidazolium nitrate } \{[\text{bmim}]\text{[NO}_3\}\}$, supercritical $\text{CO}_2 + 1\text{-butyl-3-methyl imidazolium tetrafluoroborate } \{[\text{bmim}]\text{[BF}_4\}\}$ and supercritical $\text{CHF}_3 + 1\text{-butyl-3-methyl imidazolium hexafluorophosphate } \{[\text{bmim}]\text{[PF}_6\}\}$, but some of these data differ dramatically. The Peng-Robinson equation of state, coupled with the Wong-Sandler mixing rules, has been used for modeling the vapor-liquid equilibrium of these binary mixtures. Then, the proposed thermodynamic consistency test has been applied. The results show that the consistency test can be applied with confidence, determining consistency or inconsistency of the experimental data.

INTRODUCTION

Recently, Blanchard *et al.* [1], Pérez-Salado Kamps *et al.* [2], Liu *et al.* [3] Aki *et al.* [4], Shiflett and Yokozeki [5] and Shariati *et al.* [6] measured the vapor-liquid equilibrium of the binary system supercritical $\text{CO}_2 + [\text{bmim}]\text{[PF}_6]$ at different temperatures. In the same way, Blanchard *et al.* [1] and Aki *et al.* [4] reported vapor-liquid equilibrium data for the system supercritical $\text{CO}_2 + [\text{bmim}]\text{[NO}_3\}$; Aki *et al.* [4], Kroon *et al.* [7] and Shiflett and Yokozeki [5] studied the system supercritical $\text{CO}_2 + [\text{bmim}]\text{[BF}_4\}$, while Shiflett and Yokozeki [8] and Shariati *et al.* [6] presented data about the system supercritical $\text{CHF}_3 + [\text{bmim}]\text{[PF}_6\}$. All these data show important discrepancies among the different sets. As an example, all the data for the system $\text{CO}_2 + [\text{bmim}]\text{[PF}_6]$ at 313.15 K are plotted in Fig. (1); it is easy to see the significant discrepancies among the different data sets. Similar results are obtained at the other temperatures.

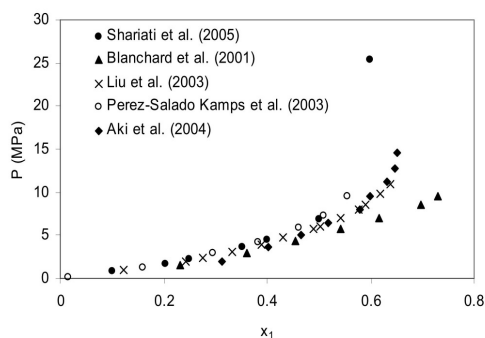


Fig. (1). Phase behavior for system supercritical $\text{CO}_2 + [\text{bmim}]\text{[PF}_6\}$ at 313.15 K.

*Address correspondence to this author at the School of Chemical Engineering, State University of Campinas, UNICAMP, P.O. Box 6066, 13083-970, Campinas - SP, Brazil; Tel: +55-19-3788-3962; Fax: +55-19-3788-3965; E-mail: maznar@feq.unicamp.br

These discrepancies are of course due to inaccuracies in measuring experimental properties; this makes necessary to test the inaccuracies inherent of such data. Although it is difficult to be absolutely certain about the exactness of experimental data, it is possible to verify if such data satisfy the Gibbs-Duhem equation, establishing if they are thermodynamic consistent or inconsistent. Good reviews about consistency tests are found in Raal and Mühlbauer [9] and Prausnitz *et al.* [10]. Jackson and Wilsak [11] analyzed several consistency tests, mainly for complete high pressure VLE data, that is, experimental PTxy data covering the entire concentration range in both phases; the authors conclude that each test provides different information that, sometimes, can bias the operator. Bertucco *et al.* [12] proposed a consistency test applicable to isothermal, binary VLE data at moderate and high pressures, also for the entire concentration range in both phases. Valderrama and Álvarez [13] presented a new method to test the thermodynamic consistency of incomplete binary VLE data; that is, where PTxy data are not fully available for the entire concentration range, and for low liquid solute concentrations in the vapor phase (mole fractions $< 10^{-3}$). For these cases, the classic derivative or integral methods are not applicable.

In these tests, the criteria on consistency are always statistical. But any of these tests still cannot decide whether the underlying data are of high or bad quality. This depends on inaccuracies in measuring experimental properties. The consistency tests only can say if the data satisfy or not the thermodynamic constraints imposed by the Gibbs-Duhem equation.

In this work, an extension of the consistency test of Valderrama and Álvarez [13] is applied to four systems supercritical fluid + ionic liquid; this test is useful when the data do not cover the entire concentration range in liquid or gas phase, that is, where PTxy data are not fully available for the entire concentration range, and for low solute liquids concentrations in the vapor phase. So far, few attempts have been done to treat binary mixtures as presented in this work.

The consistency test for binary gas-ionic liquid mixtures proposed in this work can be considered as a modeling procedure and can be easily extended to other multicomponent mixtures. In the method, a thermodynamic model that can accurately fit the experimental data must be also used to apply the consistency test. The fitting of the experimental data requires the calculation of some model parameters using a defined objective function that must be optimized. The test was first validated with the binary system $\text{CO}_2 + \text{n-butane}$, and next applied to the binary systems $\text{CO}_2 + [\text{bmim}][\text{PF}_6]$, $\text{CO}_2 + [\text{bmim}][\text{NO}_3]$, $\text{CO}_2 + [\text{bmim}][\text{BF}_4]$, and $\text{CHF}_3 + [\text{bmim}][\text{PF}_6]$.

The binary mixtures selected for this study present some interesting peculiarities that make them appropriate for the thermodynamic test for binary mixtures that is presented here. The ionic liquid themselves, $[\text{bmim}][\text{PF}_6]$, $[\text{bmim}][\text{NO}_3]$ and $[\text{bmim}][\text{BF}_4]$, present very different physicochemical characteristics and properties, that determine different phase behavior. The $[\text{PF}_6]$ anion was found to hydrolyze completely after addition of excess water at 100°C [14]. On the other hand, $[\text{bmim}][\text{NO}_3]$, as most nitrate salts, is water-miscible, while $[\text{bmim}][\text{PF}_6]$ is not; ionic liquids with the $[\text{BF}_4]$ anion may be miscible in water or not, depending on the nature of the cation; specifically, $[\text{bmim}][\text{BF}_4]$ is miscible in water. Table 1 presents some properties of the components of the binary mixtures included in this work. In this table, the critical properties for ionic liquids are from [15], while the structural parameters r and q are from [16].

The mixtures studied also have some special characteristics. For the binary mixtures $\text{CO}_2 + \text{ionic liquid}$, the concentration of the ionic liquid in supercritical CO_2 is so small that it could not be detected with experimental equipment [1-7]. On the other hand, for the binary mixtures $\text{CHF}_3 + \text{ionic liquid}$, the concentration of the ionic liquid in supercritical CHF_3 is appreciable [6, 8].

For the systems $\text{CO}_2 + [\text{bmim}][\text{PF}_6]$, $\text{CO}_2 + [\text{bmim}][\text{BF}_4]$ and $\text{CHF}_3 + [\text{bmim}][\text{PF}_6]$, Shariati *et al.* [6] measured isopleths, i.e. lines at constant overall composition; therefore, their VLE data are obtained by interpolation of the original data. Several authors used different interpolated functions to build a Px diagram [17, 18]. The interpolation method used in this work is discussed in appendix A.

THERMODYNAMIC MODELING

The thermodynamic relationship used to analyze the thermodynamic consistency of experimental VLE data is the Gibbs-Duhem equation. Once a thermodynamic model (such an equation of state with appropriate mixing and combining rules) accurately fit the data fulfilling the equality of fugacities required by the fundamental phase equilibrium equation, that model is used to check that the Gibbs-Duhem equation is also fulfilled. Once should notice that these two steps, modeling of the data and the application of the Gibbs-Duhem equation are independent, so that good modeling does not guarantee consistency and that consistent data cannot necessarily be well represented by a defined model. Recently, Álvarez and Aznar [16] and Álvarez *et al.* [19] presented some results for mixtures $\text{CO}_2 + \text{ionic liquid}$ using the Peng-Robinson [20] equation of state (EoS), and the results showed good agreement with the experimental data. Redlich-Kong type equations were also used by Shiflett and Yokozeki [5].

The thermodynamic model used to fit the experimental data must be also used to apply the consistency test. Then the proposed test is a modeling procedure, similar to the Van Ness-Byer-Gibbs test [21]. Once the model parameters are determined and the calculated solubilities are within acceptable limits of deviations, the Gibbs-Duhem equation is applied. The equations defining the consistency criteria for binary mixtures have been presented by Valderrama and Álvarez [13]. The development for binary mixtures containing ionic liquids has not been yet presented in the literature, and is summarized as follows.

The test use the Peng-Robinson (PR) EoS with the Wong-Sandler [22] mixing rule, coupled with the UNIQUAC model [23] for the excess Gibbs free energy, as the standard thermodynamic model in a bubble-point calculation; of course, other models could be used. The complete model is described below:

$$P = \frac{RT}{V - b} - \frac{a}{V(V + b) + b(V - b)} \quad (1)$$

$$a = a_c \alpha(T) \quad (2)$$

$$a_c = 0.457235(RT_c/P_c)^2 \quad (3)$$

Table 1. Properties of Compounds Used in This Work

Components	M (g/mol)	T _c (K) ^{a,c}	P _c (MPa) ^{a,c}	ω ^{a,c}	r	q
carbon dioxide	44.01 ^a	304.21 ^a	7.383 ^a	0.2236 ^a	3.26 ^b	2.39 ^b
fluoroform	70.01 ^a	299.01 ^a	4.816 ^a	0.2642 ^a	4.36 ^b	3.19 ^b
n-butane	284.18 ^d	708.9 ^c	1.73 ^c	0.7553 ^c	24.01 ^b	15.16 ^b
[bmim][PF ₆]	226.02 ^d	632.3 ^c	2.04 ^c	0.8489 ^c	21.75 ^d	14.08 ^d
[bmim][BF ₄]	201.22 ^d	946.3 ^c	2.73 ^c	0.6039 ^c	21.09 ^b	13.70 ^b
[bmim][NO ₃]	44.01 ^a	304.21 ^a	7.383 ^a	0.2236 ^a	3.26 ^b	2.39 ^b

^aDiadem Public[31], ^bÁlvarez and Aznar [16], ^cValderrama and Robles [15], ^dthis work.

$$b = 0.077796(RT_c/P_c) \quad (4)$$

$$\alpha(T) = [1 + F(1 - T_r^{0.5})]^2 \quad (5)$$

$$F = 0.37464 + 1.54226\omega - 0.26992\omega^2 \quad (6)$$

where T_r is the reduced temperature, T_c is the critical temperature, P_c is the critical pressure, R is the gas constant, and ω is the acentric factor. For mixtures:

$$P = \frac{RT}{V - b_m} - \frac{a_m}{V(V + b_m) + b_m(V - b_m)} \quad (7)$$

The mixture constants a_m and b_m are expressed by the Wong-Sandler (WS) mixing rules:

$$b_m = \frac{\sum_i \sum_j x_i x_j \left(b - \frac{a}{RT} \right)_{ij}}{1 - \sum_i \frac{x_i a_i}{b_i RT} - \frac{A_\infty^E}{\Omega RT}} \quad (8)$$

$$a_m = b_m \left[\sum_i \frac{x_i a_i}{b_i} + \frac{A_\infty^E}{\Omega} \right] \quad (9)$$

$$\left(b - \frac{a}{RT} \right)_{ij} = \frac{(b_i + b_j)}{2} - \frac{(1 - k_{ij})\sqrt{a_i a_j}}{RT} \quad (10)$$

where $\Omega = \ln(\sqrt{2} - 1)/\sqrt{2}$ for PR EoS, x is the molar fraction, A_∞^E is the excess Helmholtz energy at infinite pressure and k_{ij} is a binary interaction parameter.

The excess Helmholtz energy at infinite pressure A_∞^E can be approximated by the excess Gibbs energy at zero pressure G_∞^E [24], and the latter can be expressed by the UNIQUAC model [23] as:

$$G^E = G_{\text{comb}}^E + G_{\text{res}}^E \quad (11)$$

$$\frac{G_{\text{comb}}^E}{RT} = \sum_i x_i \ln \frac{\Phi_i^*}{x_i} + \frac{z}{2} \sum_i q_i x_i \ln \frac{\theta_i}{\Phi_i^*} \quad (12)$$

$$\frac{G_{\text{res}}^E}{RT} = - \sum_i q_i x_i \ln \left(\sum_j \theta_j \tau_{ji} \right) \quad (13)$$

$$\Phi_i^* = \frac{r_i x_i}{\sum_j r_j x_j} \quad (14)$$

$$\theta_i = \frac{q_i x_i}{\sum_j q_j x_j} \quad (15)$$

$$\tau_{ij} = \exp \left(- \frac{A_{ij}}{RT} \right) \quad (16)$$

where A_{ij} and A_{ji} represent the interaction energy between molecules i and j . Φ_i^* and θ_i are the volume and surface area fractions, z is the coordination number ($z = 10$), and r and q are the structural parameters for the volume and surface area.

For the modeling, the relative deviations in the pressure and solute concentration in the gas phase for data point "i" are defined as:

$$\% \Delta P_i = 100(P_i^{\text{cal}} - P_i^{\text{exp}}) / P_i^{\text{exp}} \quad (17)$$

$$\% \Delta y_{2i} = 100 \left[(y_2^{\text{cal}} - y_2^{\text{exp}}) / y_2^{\text{exp}} \right]_i \quad (18)$$

The proposed test uses the Gibbs-Duhem equation expressed in the integral form:

$$\int \frac{1}{Py_2} dP = \int \frac{(1 - y_2)}{y_2(Z - 1)} \frac{d\phi_1}{\phi_1} + \int \frac{1}{(Z - 1)} \frac{d\phi_2}{\phi_2} \quad (19)$$

where P is the pressure of the system, y_2 is the mole fraction of the ionic liquid in the gas phase, ϕ_1 and ϕ_2 are the fugacity coefficients of the component 1 and 2 in the gas phase, and Z is the compressibility factor. Both sides of this equation are denoted as follows:

$$A_P = \int \frac{1}{Py_2} dP \quad (20)$$

$$A_\phi = \int \frac{(1 - y_2)}{y_2(Z - 1)} \frac{d\phi_1}{\phi_1} + \int \frac{1}{(Z - 1)} \frac{d\phi_2}{\phi_2} \quad (21)$$

The values for A_P are obtained with experimental Py_2 data, while the values for A_ϕ are obtained with calculated values of Z , ϕ_i and y_2 . Thus, for one data set to be considered as consistent, A_ϕ and A_P should be similar within acceptable deviations. In order to define the acceptable deviations, an individual percent area deviation ($\% \Delta A_i$) between the A_ϕ and A_P values can be defined as:

$$\% \Delta A_i = 100 \left[(A_\phi - A_P) / A_P \right]_i \quad (22)$$

This is the parameter that determines the consistency of the data set.

The method implies the minimization of the deviations, Eqs. (20), (21) and (22), where the experimental values of concentration of ionic liquid in the gas phase (y_2) are needed; however, since these concentrations are almost negligible, its measurement is difficult [6]; this is the basis for the physical criterion for values of y_2 , and this value can be lesser than 10^{-3} with an experimental uncertainties of 10^{-5} . These values are empirically based in different experimental results for solubility of solids in gas. Therefore, the consistency test presented here use values for y_2 calculated through the bubble pressure calculation, restricted only for values not well detected with equipments to be used as physically significant values in Eqs. (18) and (19). As a comparison, Banerjee *et al.* [25] predicted y_{fluid} values in the range 0.99-1.00.

The objective function for the consistency test includes a minimization of deviations in VLE data, and the integral areas ($\% \Delta A_i$). The inclusion of vapor concentrations in the objective function allows low deviations in pressure and predicts true physical concentrations in the vapor phase [13]. Then the consistency of VLE data set is tested by the objective function, OF,

$$\text{OF} = \sum_{i=1}^{N-1} \left[\frac{A_p - A_\phi}{\sigma_A} \right]_i^2 + \sum_{i=1}^N \left[\frac{P_i^{\text{cal}} - P_i^{\text{exp}}}{\sigma_P} \right]_i^2 + \sum_{i=1}^N \left[\frac{y_{\text{fluid}}^{\text{cal}} - 1}{\sigma_y} \right]_i^2 \quad (23)$$

where N is the number of data points, P is the pressure, y_{fluid} is the vapor mole fraction of the supercritical fluid for data point i, the superscripts "exp" and "cal" refers to the experimental and calculated values respectively, and σ_A , σ_P and σ_y are the standard deviations of the measured quantities. For simplification, the experimental uncertainties (or interpolation errors) of the pressure data were used for σ_P , the value 10^{-5} (or 10^{-3} when there are dew point data) for σ_y and the value of A_p for σ_A . Equation (23) was used to put a reasonable weight on the measured quantities according to their experimental accuracy. The accepted deviation defined by $\% \Delta P < 10$ is used as constraint for every data point in the minimization method. The minimization method was performed using a genetic algorithm code, implemented and fully explained in Álvarez *et al.* [19].

There are three possible answers for the consistency test: (i) the data are thermodynamically consistent (TC); (ii) the data are not fully consistent (NFC); and (iii) the data are thermodynamically inconsistent (TI). When individual pressure and area deviations are greater than a defined limit, the worst data point is eliminated and the remaining data set is analyzed. If this data set passes the test, the conclusion is that the original data are not fully consistent and the remaining data set is thermodynamically consistent.

These intervals defined for consistency criteria are based on information presented in the literature related to the accuracy of experimental data for this type of mixtures (ionic liquids, solids and heavy alkanes dissolved in a high pressure gas) and on the criteria used by Valderrama and Álvarez [13]. In order to analyze the limits for consistency criteria, calculations of error propagation on the measured experimental data have been performed by using the general equation of error propagation [26], with the liquid phase mole fraction, the temperature and the interaction parameters as the independent measured variables. The calculated individual area A_ϕ , evaluated using two consecutive points, is the dependent variable. The error (EA) and the percent error ($\% \Delta EA$) in the calculated area are:

$$\begin{aligned} EA &= \left| \frac{\partial A_\phi}{\partial x} \right| \Delta x + \left| \frac{\partial A_\phi}{\partial T} \right| \Delta T + \left| \frac{\partial A_\phi}{\partial k_{ij}} \right| \Delta k_{ij} \\ &+ \left| \frac{\partial A_\phi}{\partial A_{ij}} \right| \Delta A_{ij} + \left| \frac{\partial A_\phi}{\partial A_{ji}} \right| \Delta A_{ji} \end{aligned} \quad (24)$$

$$\% \Delta EA = 100 EA / A_\phi \quad (25)$$

In this work, there were admitted maximum uncertainties of 0.005 for the experimental liquid phase mole fraction, 0.5 K for the temperature, and 1% for each interaction parameter. The error propagation was refined because the interaction parameters were used as independent variables. The partial derivatives in Eq. (19) were numerically calculated

for several mixtures, giving a direct relationship between the estimated percent errors $\% \Delta A$ and the relative percent deviations of the pressure $\% \Delta P$. For a thermodynamically consistent data, a VLE fit yields minimal deviations in the individual areas; a $\% \Delta P_i$ below that 5% yields $\% \Delta A_i$ below that 10% and a $\% \Delta P_i$ between 5% up to 10% yields $\% \Delta A_i$ below that 20%. Over these limits, the experimental data has high chance to be thermodynamically inconsistent. These limits defined for the consistency criterion produce randomly distributed deviations on VLE.

Then, according the study on error propagation studied and the observations by Valderrama and Álvarez [13], the maximum deviation must be within the range -20% to +20% for $\% \Delta A_i$ and -10 to +10 for $\% \Delta P_i$. Of course, these limits are not strict. When only one data point is slightly out of limits, the data set can be consider thermodynamic consistent. However, if several data points are out of limits, there is an evident tendency of inconsistency. The rule of thumb for remove bad data points is: (i) data point with $\% \Delta P_i > 10$ and $\% \Delta A_i > 20$; (ii) data point with $\% \Delta A_i > 20$; (iii) data point with $\% \Delta P_i < 5$ and $\% \Delta A_i > 10$.

This procedure is applied when there are less than 50% of the individual areas with deviations in the limits defined. If it is not the case, the data set is considered thermodynamically inconsistent. The empirical value of 50% is based in robust regression theory, which says that more than 50% of spurious data destroy the tendency of data, showing that the data have systematic experimental error [27]. When the thermodynamic model cannot fit more than 30% of data points in the data set within the limits defined for individual pressure and ionic liquid concentration in the gas phase, another thermodynamic model should be used.

RESULTS

Twenty-eight isotherms for five binary mixtures were chosen to show the application of the proposed thermodynamic consistency test. The mixtures were carefully selected so that several phase behavior and features of the test could be emphasized.

In the discussion below, the difference between experimental and calculated values is calculated as the average percent deviation, expressed in absolute form [28], as follows:

$$\% |\Delta P| = \frac{100}{N} \sum_{i=1}^N \left[\left| \frac{P_i^{\text{cal}} - P_i^{\text{exp}}}{P_i^{\text{exp}}} \right| \right] \quad (26)$$

$$\% |\Delta y_2| = \frac{100}{N} \sum_{i=1}^N \left[\left| \frac{y_{2i}^{\text{cal}} - y_{2i}^{\text{exp}}}{y_{2i}^{\text{exp}}} \right| \right] \quad (27)$$

The physical properties for all substances are shown in Table 1, where the structural parameters r and q were calculated according to [16]. Tables 2-5 show all the experimental data. In Table 2 and Fig. (1), for the $\text{CO}_2 + [\text{bmim}][\text{PF}_6]$ system, the data determined by Blanchard *et al.* [1], Liu *et al.* [3] and Aki *et al.* [4] show greater deviations from the data by Pérez-Salado Kamps *et al.* [2] or Shariati *et al.* [6]; the discrepancies become even more significant with increasing pressure at constant temperature. In Table 3, for the system $\text{CO}_2 + [\text{bmim}][\text{NO}_3]$, the data by Blanchard *et al.* [1] present a lower solubility of CO_2 than those by Aki *et al.* [4]. In

Table 4, for the system $\text{CO}_2 + [\text{bmim}][\text{BF}_4]$, the data by Aki *et al.* [4] show greater deviations from the data by Kroon *et al.* [7] or Shiflett and Yokozeki [5]. In Table 5, for the system $\text{CHF}_3 + [\text{bmim}][\text{PF}_6]$, the data by Shariati *et al.* [6] and Shiflett and Yokozeki [8] show the same values in the same pressure range, but the work by Shariati *et al.* [6] presents data with high pressures. All these discrepancies can be mainly attributed to the different experimental techniques used to measure the solubility, to ionic liquid impurities, and also to ionic liquid degradation [14]. Besides, it is important to note that some of the data from Shariati *et al.* [6] show liquid-liquid-vapor boundaries; consequently, it is to be expected that this phenomenon highly affects the quality of their vapor-liquid representation in this region of the phase diagram. This complex phase behavior could be the cause for the apparent inconsistencies in the data.

Table 2. Different Reports of VLE for the Supercritical CO_2 (1) + $[\text{bmim}][\text{PF}_6]$ (2) System

NP	Range of Data			Ref
	T (K)	P (MPa)	x_1	
8	313.15	0.8-52.7	0.1-0.7	[5]
8	323.15	0.9-58.7	0.1-0.7	
8	333.15	1.1-64.0	0.1-0.7	
7	313.15	0.1-9.5	0.02-0.6	
10	333.15	0.4-9.2	0.04-0.5	
7	313.15	1.5-9.6	0.2-0.7	[1]
7	323.15	1.7-9.2	0.2-0.7	
7	333.15	1.6-9.3	0.2-0.7	
13	313.15	0.9-10.9	0.1-0.6	[3]
10	323.15	0.6-11.6	0.1-0.6	
9	333.15	1.5-12.9	0.2-0.6	
9	323.15	0.01-2.0	0.002-0.2	
9	313.3 (first)	2.0-14.6	0.3-0.6	[4]
6	313.3 (second)	1.6-8.7	0.2-0.6	
6	313.3 (third)	1.4-8.5	0.2-0.6	
8	333.3	1.7-13.2	0.2-0.6	

The test was applied with the objective function (Eq. 23), the uncertainty for pressure, $\sigma_p = 0.05\%$ and the uncertainty for concentration in the gas phase, $\sigma_y = 0.001$. The concentrations y_2 were calculated through the bubble point and used for A_p and A_ϕ . The mixture $\text{CO}_2 + \text{n-butane}$ was already examined by Bertucco *et al.* [12] and Valderrama and Álvarez [13], and has been used here to validate the proposed method. Both papers used the experimental y_2 value. For these authors, the original data set is not fully consistent. In the analysis of Valderrama and Álvarez [13], the last two points give $\% \Delta A_i$ out of the limits; after removing these

points, the remaining data set was considered thermodynamically consistent. The results are shown in Table 6. As expected, the original data set was found to be not fully consistent, since the last two points give an area deviation outside the defined range (bold and italic type in Table 6). After removing these points, the model fitted the remaining data set with $\% |\Delta P| = 0.2$ and $\% |\Delta y_2| = 2.1$, and the data set was regarded thermodynamically consistent. In this way, the model predicts consistently the concentrations y_2 , and yield results that confirm those obtained by other authors. In this calculation, the proposed method shows characteristics of a robust regression [28], since the y_2 predicted is correct and outlying points do not have a great influence on the tendency of the bulk data. The data from Blanchard *et al.* [1], which were discarded in a later work by the same authors, was used as a test for the proposed method, which correctly indicated that this data set was thermodynamically inconsistent.

Table 3. Different Reports of VLE for the Supercritical CO_2 (1) + $[\text{bmim}][\text{NO}_3]$ (2) System

NP	Range of Data			Ref
	T (K)	P (MPa)	x_1	
7	313.15	1.5-9.2	0.2-0.5	[1]
7	333.15	1.8-9.3	0.2-0.5	
6	313.15	1.3-9.3	0.1-0.5	[4]
6	333.1	1.3-8.9	0.07-0.4	

Table 4. Different Reports of VLE for the Supercritical CO_2 (1) + $[\text{bmim}][\text{BF}_4]$ (2) System

NP	Range of Data			Ref
	T (K)	P (MPa)	x_1	
5	298.15	1.2-5.1	0.2-0.5	[4]
5	298.15	0.7-4.8	0.1-0.5	[7]
9	298.15	0.01-2.0	0.002-0.28	[5]

Table 5. Different Reports of VLE for the Supercritical CHF_3 (1) + $[\text{bmim}][\text{PF}_6]$ (2) System

NP	Range of Data				Ref
	T (K)	P (MPa)	x_1	y_1	
9	323	0.05-2.0	0.005-0.2	-	[5]
9	348	0.01-2.0	0.001-0.2	-	
12	323	0.8-26.2	0.1-0.9	0.956-0.99	[6]
12	348	1.1-37.0	0.1-0.9	0.956-0.99	

Table 6. Detailed Results for System Supercritical CO₂ (1) + n-Butane (2) at 344.26 K from [31]

A _P	A _φ	%ΔA _i	P ^{exp}	P ^{cal}	%ΔP	y ₂ ^{exp}	y ₂ ^{cal}	%Δy ₂	x ₁
(18 data points) k _{ij} = 0.1600, A ₁₂ = 593.459, A ₂₁ = 1735.860, ΔP (%) = 0.2, Δy ₂ (%) = 2.1									
0.20	0.22	6.63	0.862	0.856	-0.78	0.970	0.975	0.55	0.002
0.20	0.20	-1.49	1.035	1.039	0.40	0.827	0.825	-0.23	0.017
0.20	0.19	-1.71	1.207	1.209	0.17	0.723	0.724	0.15	0.031
0.38	0.38	1.00	1.379	1.378	-0.06	0.645	0.647	0.34	0.045
0.37	0.37	-0.06	1.724	1.727	0.19	0.538	0.535	-0.59	0.074
0.36	0.35	-1.19	2.068	2.072	0.20	0.464	0.460	-0.87	0.103
0.35	0.35	1.51	2.414	2.414	0.03	0.408	0.407	-0.33	0.132
0.34	0.34	0.36	2.758	2.765	0.24	0.365	0.366	0.21	0.162
0.33	0.33	-0.67	3.103	3.112	0.29	0.332	0.335	0.77	0.192
0.63	0.62	-0.79	3.447	3.455	0.23	0.306	0.310	1.33	0.222
0.59	0.58	-1.11	4.137	4.142	0.11	0.268	0.274	2.28	0.283
0.55	0.55	-0.45	4.826	4.824	-0.05	0.246	0.250	1.57	0.345
0.52	0.51	-1.48	5.516	5.510	-0.11	0.230	0.233	1.39	0.409
0.48	0.48	0.55	6.205	6.188	-0.28	0.220	0.223	1.16	0.474
0.44	0.45	1.92	6.895	6.880	-0.22	0.216	0.217	0.56	0.543
0.20	0.21	3.60	7.584	7.581	-0.04	0.222	0.219	-1.24	0.618
0.13	0.25	101.06^a	7.930	7.937	0.09	0.242	0.226	-6.58	0.661
			8.164	8.240	0.94	0.287	0.238	-17.15^a	0.713
(17 data points) k _{ij} = 0.1701, A ₁₂ = 272.129, A ₂₁ = 1997.902, ΔP (%) = 0.3, Δy ₂ (%) = 1.4									
0.20	0.22	7.08	0.862	0.856	-0.76	0.970	0.975	0.53	0.002
0.20	0.20	-1.27	1.035	1.040	0.49	0.827	0.824	0.31	0.017
0.20	0.19	-1.63	1.207	1.210	0.30	0.723	0.723	0.03	0.031
0.38	0.38	0.91	1.379	1.380	0.08	0.645	0.646	0.20	0.045
0.37	0.37	-0.31	1.724	1.729	0.31	0.538	0.534	0.76	0.074
0.36	0.35	-1.55	2.068	2.074	0.28	0.464	0.459	1.06	0.103
0.35	0.35	1.07	2.414	2.415	0.05	0.408	0.406	0.54	0.132
0.34	0.34	-0.10	2.758	2.764	0.20	0.365	0.365	0.04	0.162
0.33	0.33	-1.11	3.103	3.109	0.20	0.332	0.334	0.47	0.192
0.63	0.62	-1.12	3.447	3.450	0.09	0.306	0.309	0.96	0.222
0.59	0.59	-1.16	4.137	4.133	-0.10	0.268	0.273	1.71	0.283
0.56	0.56	-0.02	4.826	4.814	-0.26	0.246	0.248	0.72	0.345
0.53	0.52	-0.41	5.516	5.502	-0.26	0.230	0.230	0.17	0.409
0.49	0.50	2.51	6.205	6.186	-0.30	0.220	0.219	0.51	0.474
0.45	0.47	5.22	6.895	6.893	-0.04	0.216	0.212	1.68	0.543
0.21	0.22	8.27	7.584	7.619	0.45	0.222	0.213	4.18	0.618
			7.930	7.995	0.82	0.242	0.218	9.85	0.661

^aOut of limits data point. Shaded line: removed data point.

Table 7 presents results for the application of the test to the binary systems containing ionic liquid. In this table, NP is the number of data points, T is the temperature, k_{ij}, A₁₂ and A₂₁ are the interaction parameter of the model, where 1

stands for the supercritical fluid (CO₂ or CHF₃) and 2 stands for the ionic liquid. This table is divided in sections for each system studied.

Table 7. Results of the Consistency Test Using PR+WS/UNIQUAC, with Estimated k_{ij} , A_{12} and A_{21} Parameters

Reference	NP	T (K)	k_{ij}	A_{12} kJ/kmol	A_{21} kJ/kmol	$ \Delta P (\%)$	Result
$\text{CO}_2 + [\text{bmim}][\text{PF}_6]$							
[5]	8	313	0.3061	4562.630	-536.211	1.2	NFC/TC
	8	323	0.3041	4367.418	-461.895	1.2	NFC/TC
	8	333	0.3271	4631.519	-492.994	1.6	NFC/TC
[2]	7	313	0.5724	1532.211	354.253	1.9	TC
	10	333	0.6182	1976.688	245.462	0.4	TC
[1]	7	313	0.2888	130.813	1364.330	6.2	TI
	7	323	0.2476	716.755	526.845	3.7	TI
	7	333	0.2077	1896.333	-185.649	5.6	TI
[3]	13	313	0.4722	272.421	1333.819	3.3	TI
	10	323	0.9987	-1686.089	3848.819	3.7	TI
	9	333	0.9999	-1296.043	2854.631	4.2	TI
[5]	9	323	0.5188	2135.729	144.314	7.4	NFC/TC
[4]	9	313(first)	0.6469	-163.857	1570.101	8.5	TI
	6	313(second)	0.3050	344.647	1430.118	3.6	TI
	6	313(third)	0.3843	1301.887	431.109	8.3	TI
	8	333	0.8466	70.647	1434.796	3.2	TI
$\text{CO}_2 + [\text{bmim}][\text{NO}_3]$							
[1]	7	313	0.7307	737.260	244.341	8.1	TI
	7	333	0.2245	975.738	241.039	6.4	TI
[4]	6	313	0.0825	-441.908	2382.438	6.3	NFC/TC
	6	333	-0.4347	-724.243	3032.147	2.0	TI
$\text{CO}_2 + [\text{bmim}][\text{BF}_4]$							
[4]	5	298	0.9999	-1869.427	3969.204	2.5	TI
[7]	5	298	0.2832	2591.745	-140.975	0.7	TC
[5]	9	298	0.4961	1249.692	298.008	3.1	TC
$\text{CHF}_3 + [\text{bmim}][\text{PF}_6]$							
[8]	8	323	0.9522	-1985.123	3675.940	4.0	NFC/TC
	9	348	0.9999	-1955.672	3669.472	7.8	NFC/TC
[6]	12	323	0.4378	-1822.636	3604.477	7.9	NFC/TC
	12	348	0.5651	-1723.135	3302.432	3.1	NFC/TC

TC: thermodynamically consistent; TI: thermodynamically inconsistent; NFC: not fully consistent.

More detailed results for the system $\text{CO}_2 + [\text{bmim}][\text{PF}_6]$ are shown in Tables 8 up to 12. These tables are divided in two parts. The upper part shows the original data set, while the lower part shows the remaining data after removing some points. Each part shows the interaction parameters for the thermodynamic model. Tables 8-10 show detailed results for the data from Shariati *et al.* [6]. In Table 8, which presents detailed results at 313.15 K, the upper part shows that these data have deviations outside the established limits in the two final values of $\% \Delta A_i$ (bold and italic type); the lower part shows that, when one point from the original data set is

eliminated (the one with the highest area deviation, shaded in the upper part), the deviations for the remaining seven points are within the defined limits of -20% to +20%. Therefore, the original set with eight data points is not fully consistent, but a new set with the remaining seven points is thermodynamically consistent; however, the last point has a high probability to be inconsistent, because two $\% \Delta P_i < 5$ yields $\% \Delta A_i > 10$. The same procedure is applied for the data at 323.15 and 333.15 K, as shown in Tables 9 and 10, respectively; both of data sets are not fully consistent.

Table 8. Detailed Results for CO₂ + [bmim][PF₆] at 313.15 K from [5]

A _P	A _φ	%ΔA _i	P ^{exp}	P ^{cal}	%ΔP	y ₁ ^{cal}	y ₂ ^{cal}	x ₁
(8 data points) k _{ij} = 0.3061, A ₁₂ = 4562.630, A ₂₁ = -536.211, ΔP (%) = 1.2								
243439.9	249882.6	2.6	0.78	0.77	-1.54	0.9999957	0.0000043	0.100
101610.3	99044.5	-2.5	1.74	1.75	0.50	0.9999972	0.0000028	0.203
179993.4	177695.2	-1.3	2.28	2.28	-0.16	0.9999973	0.0000027	0.250
58676.9	62042.6	5.7	3.71	3.69	-0.50	0.9999969	0.0000031	0.351
84064.8	91159.8	8.4	4.52	4.55	0.64	0.9999962	0.0000038	0.399
153996.2	178073.3	15.6^a	6.91	7.20	4.22	0.9999882	0.0000118	0.501
234254.1	724645.2	209.3^a	25.31	24.92	-1.54	0.9999911	0.0000089	0.598
			52.73	53.09	0.69	0.9999985	0.0000015	0.650
(7 data points) k _{ij} = 0.2458, A ₁₂ = 4189.500, A ₂₁ = -429.368, ΔP (%) = 0.6								
229858.0	234248.3	1.9	0.78	0.77	-0.69	0.9999956	0.0000044	0.100
91395.4	88095.0	-3.6	1.74	1.75	0.86	0.9999970	0.0000030	0.203
154891.0	150069.9	-3.1	2.28	2.28	-0.09	0.9999970	0.0000030	0.250
47050.8	48479.4	3.0	3.71	3.67	-1.23	0.9999962	0.0000038	0.351
64467.2	66282.2	2.8	4.52	4.49	-0.61	0.9999951	0.0000049	0.399
92311.9	80323.9	-13.0^a	6.91	6.97	0.82	0.9999833	0.0000167	0.501
			25.31	25.32	0.05	0.9999711	0.0000289	0.598

^aOut of limits data point. Shaded line: removed data point.

Tables 11 and 12 present detailed results for the data from Pérez-Salado Kamps *et al.* [2], at 313.15 and 333.15 K, respectively; these data are thermodynamically consistent, meaning that all the deviations are within the defined ranges, -20% to 20%; however, in both tables the last point has a high probability to be inconsistent, because the two %ΔP_i < 5 yields %ΔA_i greater than 10. Tables 13 shows the detailed results for the system CO₂ + [bmim][NO₃]. The data from Blanchard *et al.* [1] are thermodynamically inconsistent, since more than 50% of %ΔA_i showed deviations outside the established limits. Table 14 shows the detailed results for the system CO₂ + [bmim][BF₄]₂ at 298.15 K from Shiflett and Yokozeki [5] are thermodynamic consistent; in this latter, there is a high probability of inconsistency in the data point x₁ = 0.002, because is the sole data point with %ΔP = 11.94, slightly out of the limits. Tables 15 and 16 show the detailed results for the system CHF₃ + [bmim][PF₆]. The data from Shiflett and Yokozeki [8] and Shariati *et al.* [6] are not fully consistent. Table 16 shows that Shariati *et al.* [6] report dew point data, where ionic liquid exists in the gas phase. In this table, y₂ is an interpolated value for the pressure and the method predicts this concentration of ionic liquid with a deviation less than 3.5%.

CONCLUSIONS

A thermodynamic model, composed by the Peng-Robinson EoS coupled with the Wong-Sandler/UNIQUAC mixing rule, was used to accurately correlate experimental vapor-liquid equilibrium data in binary systems containing ionic liquids. The model was also able to predict the low ionic liquid concentrations in the vapor phase. A thermodynamic consistency test based on this model and on the Gibbs-Duhem equation, that allows the analysis of individual data points in a binary vapor-liquid equilibrium data set, i.e., to eliminate doubtful points, was proposed. The test was applied to several data sets from literature involving three ionic liquids and two supercritical solvents. For the system CO₂ + [bmim][PF₆]₂, only the original data sets from Pérez-Salado Kamps *et al.* [2] are thermodynamically consistent, although the data from Shariati *et al.* [6] must be considered with care, since they show some liquid-liquid-vapor boundaries, a complex phase behavior which could be the cause for the apparent inconsistencies. For the system CO₂ + [bmim][NO₃]₂, only the data from Aki *et al.* [4] at 313.15 are not fully consistent. For the system CO₂ + [bmim][BF₄]₂, the data sets from Kroon *et al.* [7] and Shiflett and Yokozeki [5] are considered thermodynamically consistent. Finally, for the system CHF₃ + [bmim][PF₆]₂, all data sets are not fully consistent.

Table 9. Detailed Results for CO₂ + [bmim][PF₆] at 323.15 K from [5]

A _P	A _φ	%ΔA _i	P ^{exp}	P ^{cal}	%ΔP	y ₁ ^{cal}	y ₂ ^{cal}	x ₁
(8 data points) k _{ij} = 0.3041, A ₁₂ = 4367.418, A ₂₁ = -461.895, ΔP (%) = 1.2								
114652.3	117845.3	2.8	0.93	0.91	-1.45	0.999991	0.000009	0.100
46947.9	44844.3	-4.5	2.07	2.08	0.73	0.999994	0.000006	0.203
78068.5	77354.9	-0.9	2.74	2.72	-0.47	0.999994	0.000006	0.250
24264.8	25311.3	4.3	4.46	4.44	-0.57	0.999992	0.000008	0.351
34438.9	36501.6	6.0	5.47	5.49	0.35	0.999990	0.000010	0.399
48309.7	66691.5	38.1 ^a	8.70	9.01	3.56	0.999961	0.000039	0.501
97440.1	450648.4	362.5 ^a	29.24	28.75	-1.66	0.999981	0.000019	0.598
			58.71	59.07	0.60	0.999997	0.000004	0.650
(7 data points) k _{ij} = 0.2523, A ₁₂ = 3914.281, A ₂₁ = -327.957, ΔP (%) = 0.6								
108661.7	110901.9	2.1	0.93	0.92	-0.49	0.999991	0.000009	0.100
42422.4	40082.0	-5.5	2.07	2.09	1.21	0.999993	0.000007	0.203
67612.6	65771.2	-2.7	2.74	2.73	-0.28	0.999993	0.000007	0.250
19566.3	19897.7	1.7	4.46	4.41	-1.15	0.999991	0.000009	0.351
26508.9	26525.5	0.1	5.47	5.43	-0.76	0.999987	0.000013	0.399
26216.0	27204.9	3.8	8.70	8.70	0.04	0.999943	0.000058	0.501
			29.24	29.24	0.00	0.999938	0.000062	0.598

^aOut of limits data point. Shaded line: removed data point.Table 10. Detailed Results for CO₂ + [bmim][PF₆] at 333.15 K from [5]

A _P	A _φ	%ΔA _i	P ^{exp}	P ^{cal}	%ΔP	y ₁ ^{cal}	y ₂ ^{cal}	x ₁
(8 data points) k _{ij} = 0.3271, A ₁₂ = 4631.519, A ₂₁ = -492.994, ΔP (%) = 1.6								
58678.7	60481.4	3.1	1.09	1.07	-1.99	0.999983	0.000017	0.100
23837.0	22818.6	-4.3	2.43	2.44	0.44	0.999988	0.000012	0.203
39136.6	39221.2	0.2	3.23	3.21	-0.71	0.999988	0.000012	0.250
12199.5	12771.3	4.7	5.29	5.28	-0.22	0.999985	0.000015	0.351
19222.2	19988.9	4.0	6.53	6.59	0.83	0.999979	0.000021	0.399
41320.0	79219.8	91.7 ^a	10.94	11.41	4.33	0.999931	0.000069	0.501
132303.0	1361502.8	929.1 ^a	34.57	33.51	-3.08	0.999987	0.000013	0.598
			64.04	63.29	-1.16	0.999998	0.000002	0.650
(6 data points) k _{ij} = 0.9854, A ₁₂ = -273.858, A ₂₁ = 1824.747, ΔP (%) = 0.5								
130003.7	132586.3	2.0	1.09	1.08	-0.40	0.999985	0.0000105	0.100
87022.6	82412.2	-5.3	2.43	2.46	1.05	0.9999961	0.0000039	0.203
261518.7	262161.8	0.2	3.23	3.21	-0.47	0.9999973	0.0000027	0.250
185890.9	193607.5	4.2	5.29	5.26	-0.49	0.9999987	0.0000013	0.351
662853.3	663250.0	0.1	6.53	6.56	0.37	0.9999990	0.0000010	0.399
			10.94	10.94	0.00	0.9999994	0.0000006	0.501

^aOut of limits data point. Shaded line: removed data point.

Table 11. Detailed Results for CO₂ + [bmim][PF₆] at 313.15 K from [2]

A _P	A _φ	%ΔA _i	P ^{exp}	P ^{cal}	%ΔP	y ₁ ^{cal}	y ₂ ^{cal}	x _i
(7 data points) k _{ij} = 0.5724, A ₁₂ = 1532.211, A ₂₁ = 354.253, ΔP (%) = 1.9								
442117.3	429754.6	-2.8	0.105	0.109	3.7	0.9999771	0.0000229	0.0156
454063.1	438556.3	-3.4	1.292	1.286	-0.5	0.9999976	0.0000024	0.1594
279632.6	283292.0	1.3	2.893	2.814	-2.7	0.9999986	0.0000014	0.2958
228775.9	235887.4	3.1	4.242	4.150	-2.2	0.9999987	0.0000013	0.3833
124000.5	121025.7	-2.4	5.844	5.778	-1.1	0.9999984	0.0000016	0.4617
76344.5	90541.4	18.6^a	7.293	7.177	-1.6	0.9999978	0.0000022	0.5096
			9.480	9.652	1.8	0.9999875	0.0000125	0.5551

^aOut of limits data point.**Table 12.** Detailed Results for CO₂ + [bmim][PF₆] at 333.15 K from [2]

A _P	A _φ	%ΔA _i	P ^{exp}	P ^{cal}	%ΔP	y ₁ ^{cal}	y ₂ ^{cal}	x _i
(10 data points) k _{ij} = 0.6182, A ₁₂ = 1976.688, A ₂₁ = 245.462, ΔP (%) = 0.4								
88824.8	87849.8	-1.1	0.42	0.43	0.9	0.9999678	0.0000322	0.0423
64236.0	63659.3	-0.9	1.75	1.74	-0.2	0.9999906	0.0000094	0.1527
41086.4	41740.7	1.6	2.89	2.87	-0.6	0.9999933	0.0000067	0.2286
32594.8	31931.7	-2.0	3.73	3.73	-0.1	0.9999941	0.0000059	0.2773
47083.6	47903.2	1.7	4.49	4.47	-0.5	0.9999944	0.0000056	0.3144
35797.3	35570.3	-0.6	5.81	5.81	0.0	0.9999945	0.0000055	0.3707
16312.0	16834.6	3.2	7.09	7.08	-0.1	0.9999942	0.0000058	0.4142
13887.2	12788.9	-7.9	7.82	7.84	0.2	0.9999937	0.0000063	0.4359
9750.2	11454.1	17.5^a	8.56	8.52	-0.5	0.9999932	0.0000068	0.4532
			9.18	9.25	0.7	0.9999923	0.0000077	0.4696

^aOut of limits data point.**Table 13.** Detailed Results for the CO₂ + [bmim][NO₃] at 313.15 K from [1]

A _P	A _φ	%ΔA _i	P ^{exp}	P ^{cal}	%ΔP	y ₁ ^{cal}	y ₂ ^{cal}	x _i
(7 data points) k _{ij} = 0.7307, A ₁₂ = 737.260, A ₂₁ = 244.341, ΔP (%) = 8.1								
540231601.8	384832576.6	-28.8^a	1.547	1.768	14.31^a	1.0	0.0	0.196
419272612.9	352823607.3	-15.8	2.905	2.792	-3.90	1.0	0.0	0.276
344310882.7	310156934.0	-9.9	4.263	3.862	-9.40	1.0	0.0	0.342
257814341.1	284461023.8	10.3	5.670	4.998	-11.85^a	1.0	0.0	0.397
110543090.0	197680291.6	78.8^a	7.118	6.424	-9.75	1.0	0.0	0.449
15815696.6	24430743.2	54.5^a	8.372	8.477	1.25	1.0	0.0	0.497
			9.200	9.779	6.29	1.0	0.0	0.513
(6 data points) k _{ij} = 0.5337, A ₁₂ = 73.609, A ₂₁ = 1087.130, ΔP (%) = 4.3								
208409124.6	160663801.3	-22.9^a	2.905	3.106	6.92	1.0	0.0	0.276
127470852.8	103236320.5	-19.0	4.263	4.193	-1.65	1.0	0.0	0.342
68574153.0	66838886.9	-2.5	5.670	5.295	-6.61	1.0	0.0	0.397
20644385.6	31853700.4	54.3^a	7.118	6.615	-7.07	1.0	0.0	0.449
1750040.9	2299166.8	31.4^a	8.372	8.409	0.44	1.0	0.0	0.497
			9.200	9.493	3.18	0.999997	0.000003	0.513

^aOut of limits data point. Shaded line: removed data point.

Table 14. Detailed Results for the CO₂ + [bmim][BF₄] at 298.15 K from [5]

A _P	A _φ	%ΔA _i	P ^{exp}	P ^{cal}	%ΔP	y ₁ ^{cal}	y ₂ ^{cal}	x ₁
(5 data points) k _{ij} = 0.4961, A ₁₂ = 1249.692, A ₂₁ = 298.008, ΔP (%) = 3.1								
5300.9	5219.2	-1.5	0.010	0.011	11.94 ^a	0.999235	0.000765	0.002
6312.1	5890.6	-6.7	0.050	0.055	9.88	0.999845	0.000155	0.010
35180.2	33760.9	-4.0	0.100	0.105	4.98	0.999919	0.000081	0.019
32905.3	33149.1	0.7	0.400	0.400	0.21	0.999978	0.000022	0.069
31530.0	31044.4	-1.5	0.700	0.705	0.62	0.999987	0.000013	0.116
30081.1	30111.1	0.1	1.000	0.998	-0.13	0.999990	0.000010	0.158
19145.8	18793.7	-1.8	1.300	1.302	0.11	0.999992	0.000008	0.197
45205.2	45778.8	1.3	1.500	1.495	-0.36	0.999993	0.000007	0.221
			2.000	2.002	0.11	0.999994	0.000006	0.277

^aOut of limits data point.**Table 15.** Detailed Results for the CHF₃ + [bmim][PF₆] at 323.10 K from [8]

A _P	A _φ	%ΔA _i	P ^{exp}	P ^{cal}	%ΔP	y ₁ ^{cal}	y ₂ ^{cal}	x ₁
(8 data points) k _{ij} = 0.9522, A ₁₂ = -1985.123, A ₂₁ = 3675.940, ΔP (%) = 4.0								
7401.2	8459.8	14.3	0.050	0.041	-18.57 ^a	0.9998576	0.0001424	0.005
51290.7	56615.4	10.4	0.100	0.089	-10.44	0.9999357	0.0000643	0.011
56487.0	55091.9	-2.5	0.400	0.406	1.64	0.9999865	0.0000135	0.050
58146.3	56810.9	-2.3	0.700	0.703	0.36	0.9999925	0.0000075	0.086
60305.3	61356.3	1.7	1.000	0.995	-0.56	0.9999949	0.0000051	0.121
42105.9	42865.8	1.8	1.299	1.299	-0.01	0.9999963	0.0000037	0.156
109615.1	108640.6	-0.9	1.500	1.502	0.14	0.9999969	0.0000031	0.179
			1.999	1.999	-0.02	0.9999978	0.0000022	0.231
(7 data points) k _{ij} = 0.8961, A ₁₂ = -1917.752, A ₂₁ = 3550.764, ΔP (%) = 1.9								
50441.7	55778.4	10.6	0.0996	0.0888	-10.83	0.9999352	0.0000648	0.011
54802.0	53575.3	-2.2	0.3996	0.4051	1.38	0.9999862	0.0000138	0.050
55614.6	54489.0	-2.0	0.7004	0.7021	0.24	0.9999922	0.0000078	0.086
56820.1	57916.9	1.9	1.0004	0.9945	-0.59	0.9999947	0.0000053	0.121
39149.7	39896.6	1.9	1.2993	1.2995	0.02	0.9999960	0.0000040	0.156
99935.3	98824.2	-1.1	1.5001	1.5029	0.19	0.9999966	0.0000034	0.179
			1.9993	1.9987	-0.03	0.9999975	0.0000025	0.231

^aOut of limits data point. Shaded line: removed data point.

Table 16. Detailed Results for the CHF₃ + [bmim][PF₆] at 323.10 K from [6]

A _P	A _φ	%ΔA _i	P ^{exp}	P ^{cal}	%ΔP	y ₂ ^{exp}	y ₂ ^{cal}	x _i
(12 data points) k _{ij} = 0.3821, A ₁₂ = -1446.267, A ₂₁ = 2826.518, ΔP (%) = 4.0								
93020.068	91092.305	-2.1	0.810	0.824	1.7	<10 ⁻³	9.70*10 ⁻⁶	0.102
69309.529	66173.159	-4.5	1.667	1.675	0.5	<10 ⁻³	6.70*10 ⁻⁶	0.203
46882.596	47214.62	0.7	2.604	2.570	-1.3	<10 ⁻³	6.50*10 ⁻⁶	0.302
27470.452	27663.524	0.7	3.598	3.564	-0.9	<10 ⁻³	7.80*10 ⁻⁶	0.400
15714.417	14861.863	-5.4	4.598	4.568	-0.6	<10 ⁻³	1.12*10 ⁻⁵	0.483
6185.105	7915.197	28.0^a	5.728	5.633	-1.6	<10 ⁻³	2.07*10 ⁻⁵	0.552
3889.665	2477.174	-36.3^a	6.951	7.219	3.9	<10 ⁻³	8.63*10 ⁻⁵	0.621
433.438	284.36	-34.4^a	11.337	10.726	-5.4	<10 ⁻³	8.29*10 ⁻⁴	0.700
45.358	52.182	15.0	18.535	16.433	-11.3	<10 ⁻³	3.86*10 ⁻³	0.780
3.729	10.313	176.5^a	23.745	22.757	-4.1	≈ 0.010	0.012	0.850
1.163	1.64	41.0^a	25.278	27.179	7.5	≈ 0.020	0.028	0.900
			26.225	28.623	9.2	≈ 0.044	0.037	0.925
(7 data points) k _{ij} = 0.2901, A ₁₂ = -1158.594, A ₂₁ = 2360.242, ΔP (%) = 0.6								
83947.1	83886.1	-0.1	0.810	0.811	0.13	<10 ⁻⁴	0.000010	0.102
58230.7	56888.2	-2.3	1.667	1.672	0.30	<10 ⁻⁴	0.000008	0.203
35903.0	36604.3	2.0	2.604	2.591	-0.49	<10 ⁻⁴	0.000008	0.302
18888.5	18728.4	-0.8	3.598	3.608	0.28	<10 ⁻⁴	0.000011	0.400
9799.4	8757.6	-10.6	4.598	4.608	0.21	<10 ⁻⁴	0.000018	0.483
3673.4	4166.8	13.4	5.728	5.620	-1.88	<10 ⁻⁴	0.000035	0.552
			6.951	7.011	0.86	<10 ⁻⁴	0.000138	0.621

^aOut of limits data point. Shaded line: removed data point.**ACKNOWLEDGEMENTS**

The financial support of CAPES and FAPESP (Brazil) is gratefully acknowledged.

NOMENCLATURE**Symbols**

<i>A, B, C, D</i>	= Parameters in interpolation functions	<i>k_{ij}</i>	= Binary interaction parameter
<i>A</i>	= Area	<i>P</i>	= Pressure
<i>A^E</i>	= Excess Helmholtz energy	<i>q</i>	= Structural parameter for surface area in UNIQUAC
<i>A_{ij}</i>	= Energy interaction parameter in UNIQUAC	<i>R</i>	= Universal gas constant
<i>a, a_c, b</i>	= Constants in Peng-Robinson EoS	<i>r</i>	= Structural parameter for volume in UNIQUAC
<i>a_m, b_m</i>	= Mixture constants in Peng-Robinson EoS	<i>T</i>	= Temperature
<i>EA</i>	= Error in calculated areas	<i>T_c</i>	= Critical temperature
<i>F</i>	= Dependence on the acentric factor in the <i>α</i> function	<i>T_r</i>	= Reduced temperature (<i>T_r = T/T_c</i>)
<i>G^E</i>	= Excess Gibbs energy	<i>V</i>	= Molar volume
		<i>y</i>	= Mole fraction of supercritical fluid in the vapor phase
		<i>x</i>	= Mole fraction in the liquid phase
		<i>Z</i>	= Compressibility factor
		<i>z</i>	= Coordination number in UNIQUAC (<i>z</i> = 10)

Abbreviations

<i>EoS</i>	=	Equation of State
<i>NFC</i>	=	Not fully consistent
<i>TC</i>	=	Thermodynamically consistent
<i>TI</i>	=	Thermodynamically inconsistent
<i>UNIQUAC</i>	=	UNIversal-QUAsiChemical model
$\% \Delta$	=	Percent deviation

Greek letters

$\alpha(T)$	=	Temperature function in the Peng-Robinson EoS
ω	=	Acentric factor
Ω	=	Characteristic constant in Wong-Sandler mixing rule
Φ	=	Volume fraction in UNIQUAC
θ	=	Surface area fraction in UNIQUAC
Δ	=	Interval (for temperature, pressure and mole fraction)
ϕ	=	Fugacity coefficient
τ	=	Exponential interaction parameter in UNIQUAC
σ	=	Standard deviation in measured properties

Super/subscripts

<i>A</i>	=	Area
<i>cal</i>	=	Calculated
<i>E</i>	=	Excess property
<i>comb</i>	=	Combinatorial
<i>exp</i>	=	Experimental
<i>fluid</i>	=	Supercritical fluid
<i>i, j</i>	=	Components
<i>P</i>	=	Pressure
<i>res</i>	=	Residual
<i>Y</i>	=	Vapor-phase composition
∞	=	Infinite pressure

APPENDIX A: PX DIAGRAM FROM ISOPLETHS

By interpolating between isopleths, it is possible to plot the *Px* diagram at constant temperature. Since both bubble- and dew-points are available in several isopleths, each *Px* diagram illustrates both the solubility of the supercritical fluid in the ionic liquid-rich phase and the solubility of the ionic liquid in the supercritical fluid phase. Then, values of other than the known discrete points may be needed (i.e., interpolation). This process, for discrete data, is performed by fitting an approximating function to the discrete data set. Many types of approximating functions can be used and several authors calculated *Px* diagram from isopleths, but without recommending one specific method for the best interpolation or curve fitted for the isopleths. A *Px* diagram appears in Fig. (A.1).

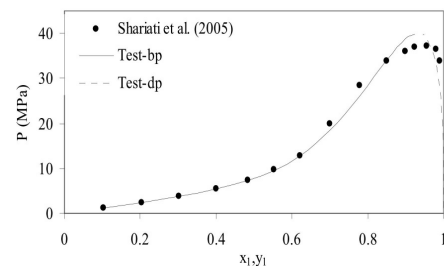


Fig. (A.1). *Px* diagram for the system supercritical $\text{CHF}_3 + [\text{bmim}][\text{PF}_6]$ at 348.10 K.

In this work, there were used interpolation functions for a set of discrete data in two ways: exact fit, such as cubic spline [29] and approximate fit, by using low degree polynomials [17, 18], where the parameters were fitted through the least squares approximation. Five interpolation functions were tested.

The method for select the best interpolation function is based on the hypothesis that experimental error should be randomly distributed. The error defined in order to accept the interpolation function as accurate for the data is based on the work by Hoffman [30], using the general equation of error interpolation of Weierstrass approximation theorem. Then, the error defined ($\%|\Delta E|$) used temperature T as the independent measured variable and pressure P as the dependent measured variable for the isopleths data. In order to confirm this error, several calculations of errors in the interpolated experimental data were performed. The absolute average percent deviations for the interpolation $\%|\Delta E|$ is defined as:

$$\%|\Delta E| = \frac{100}{N} \sum_{i=1}^N |P_i^{\text{exp}} - f(T_1^{\text{exp}}, \dots, T_j^{\text{exp}}, \dots, T_N^{\text{exp}})_{j \neq i}| / P_i^{\text{exp}}$$

where N is the number of data points, T_i^{exp} is the experimental temperature at point “ i ”, P_i^{exp} is the experimental pressure at point “ i ”, and f is the interpolated function fitted with all other experimental data points but “ i ” and evaluated at “ i ”. The interpolation error is used on five interpolation functions over each isopleth; so, the interpolation function with the minimum value of $\%|\Delta E|$ is established as the optimal for the isopleth. After that, the chosen interpolation function is fitted with all experimental data and used to plot the *Px* diagram. In this way, the optimal interpolation function has the natural tendency of data, suffers a minimal influence by the removing of one data point, does not present over fitting and has the best representation for large or rough data sets.

The isopleths from Shariati and co-workers used in the consistency thermodynamic were used; one set of such data is shown in Fig. (A.1). The interpolation functions and the results are shown in Table A1. In this table, N_i is the number of isopleths interpolated, $\%|\Delta E|$ is the average percent deviations for the interpolation, $\%|\Delta P|$ is the absolute average percent deviation for pressure, and A, B, C and D are the fitted parameters for the interpolation functions.

Table A1. Interpolation Functions, Errors (%|ΔE|) and Relative Deviation in Pressure (%|ΔP|)

Function	N _i	% ΔE	% ΔP
cubic spline	8	0.20	0.00
P = AT ² + BT + C	9	0.28	0.22
P = AT ³ + BT ² + CT + D	11	0.19	0.11
P = e ^(A+B/T)	1	0.53	0.45
P = e ^(A+B/T²)	1	0.57	0.50

Table A1 shows that the value of %|ΔE| is always greater than %|ΔP|. Also, it shows that the cubic spline has %|ΔP| = 0, because cubic spline yields the exact experimental pressure P_i for each experimental temperature T_i . In contrast, %|ΔE| by definition uses a function fitted without the data point “ i ”, evaluated in the point “ i ” and then does not allow over fitting.

For systems with P_x diagram from interpolated isopleths data, the mean value of %|ΔE| for all isopleths was used for σ_p . The mean value of %|ΔE| for CO₂ + [bmim][PF₆], CO₂ + [bmim][BF₄] and CHF₃ + [bmim][PF₆] are 0.39%, 0.33% and 0.13%, respectively. These values are within the reported experimental error, which has a range from 0.04% for high pressure to 1.7% for low pressure. Considering these values, when a reported experimental data set does not show experimental uncertainties, the value $\sigma_p = 0.1\%$ was used.

REFERENCES

- [1] L.A. Blanchard, Z. Gu and J.F. Brennecke, “High-pressure phase behavior of ionic liquid/CO₂ systems,” *J. Phys. Chem. B*, vol. 105, pp. 2437-2444, March 2001.
- [2] A. Pérez-Salado Kamps, D. Tuma, J. Xia and G. Maurer, “Solubility of CO₂ in the ionic liquid [bmim][PF₆],” *J. Chem. Eng. Data*, vol. 48, pp. 746-849, June 2003.
- [3] Z. Liu, W. Wu, B. Han, Z. Dong, G. Zhao, J. Wang, T. Jiang and G. Yang, “Study on the phase behaviors, viscosities, and thermodynamic properties of CO₂/[C₄mim][PF₆] / methanol system at elevated pressures,” *Chem. Eur. J.*, vol. 9, pp. 3897-3903, August 2003.
- [4] S.V.N.K. Aki, B.R. Mellein, E.M. Saurer and J.F. Brennecke, “High-pressure phase behavior of carbon dioxide with imidazolium-based ionic liquids,” *J. Phys. Chem. B*, vol. 108, pp. 20355-20365, December 2004.
- [5] M.B. Shiflett and A. Yokozeki, “Solubilities and diffusivities of carbon dioxide in ionic liquids: [bmim][PF₆] and [bmim][BF₄],” *Ind. Eng. Chem. Res.*, vol. 44, pp. 4453-4464, June 2005.
- [6] A. Shariati, K. Gutkowski and C.J. Peters, “Comparison of the phase behavior of some selected binary systems with ionic liquids,” *AICHE J.*, vol. 51, pp. 1532-1540, May 2005.
- [7] M.C. Kroon, A. Shariati, M. Costantini, J. Van Spronsen, G. Wittkamp, R.A. Sheldon and C.J. Peters, “High-pressure phase behavior of systems with ionic liquids: Part V. the binary system carbon dioxide + 1-butyl-3-methylimidazolium tetrafluoroborate,” *J. Chem. Eng. Data*, vol. 50, pp. 173-176, February 2005.
- [8] M.B. Shiflett and A. Yokozeki, “Solubility and diffusivity of hydrofluorocarbons in room-temperature ionic liquids,” *AICHE J.* vol. 52, pp. 1205-1219, March 2006.
- [9] J.D. Raal and A.D. Mühlbauer, *Phase Equilibria: Measurement and Computation*, Taylor & Francis, Washington, DC, 1998.
- [10] J.M. Prausnitz, R.N. Lichenthaler and E.G. Azevedo, *Molecular Thermodynamics of Fluid Phase Equilibria*, 3rd edition, Prentice Hall, Englewood Cliffs, New Jersey, 1999.
- [11] O.L. Jackson and R.A. Wilsak, “Thermodynamic consistency tests based on the Gibbs-Duhem equation applied to isothermal, binary vapor-liquid equilibrium data: data evaluation and model testing,” *Fluid Phase Equilib.*, vol. 103, pp. 155-197, February 1995.
- [12] A. Bertucco, M. Barolo and N. Elvassore, “Thermodynamic consistency of vapor-liquid equilibrium data at high-pressure,” *AICHE J.*, vol. 43, pp. 547-554, February 1997.
- [13] J.O. Valderrama and V.H. Álvarez, “A versatile thermodynamic consistency test for incomplete phase equilibrium data of high-pressure gas-liquid mixtures,” *Fluid Phase Equilib.*, vol. 226, pp. 149-159, December 2004.
- [14] P. Wasserscheid and T. Welton, *Ionic Liquids in Synthesis*, Wiley-VCH, Weinheim, 2002.
- [15] J.O. Valderrama and P.A. Robles, “Critical properties, normal boiling temperatures, and acentric factors of fifty ionic liquids,” *Ind. Eng. Chem. Res.*, vol. 46, pp. 1338-1344, February 2007.
- [16] V.H. Álvarez and M. Aznar, “Vapor-liquid equilibrium of binary systems ionic liquid + supercritical {CO₂ or CHF₃} and ionic liquid + hydrocarbons using Peng-Robinson equation of state,” XXII Interamerican Congress of Chemical Engineering, 672, Buenos Aires, October 2006.
- [17] A.R. Cruz Duarte, M.M. Mooijer-van den Heuvel, C.M.M. Duarte and C.J. Peters, “Measurement and modelling of bubble and dew points in the binary systems carbon dioxide + cyclobutanone and propane + cyclobutanone,” *Fluid Phase Equilib.*, vol. 214, pp. 121-136, December 2003.
- [18] C.J. Peters, J.L. De Roo and R.N. Lichenthaler, “Measurements and calculations of phase equilibria of binary mixtures of ethane + eicosane. Part 1: vapour + liquid equilibria,” *Fluid Phase Equilib.*, vol. 34, pp. 287-308, July 1987.
- [19] V.H. Álvarez, R. Larico, Y. Yanos and M. Aznar, “Parameter estimation for VLE calculation by global minimization: genetic algorithm,” *Braz. J. Chem. Eng.*, 2007, in press.
- [20] D.Y. Peng and D.B. Robinson, “A new two-constant equation of state,” *Ind. Eng. Chem. Fund.*, vol. 15, pp. 59-64, February 1976.
- [21] H.C. Van Ness, S.M. Byer and R.E. Gibbs, “Vapor-liquid equilibrium. Part 1. An appraisal of data reduction methods,” *AICHE J.*, vol. 19, pp. 238-244, March 1973.
- [22] D.H.S. Wong and S.I. Sandler, “A theoretically correct mixing rule for cubic equations of state,” *AICHE J.*, vol. 38, pp. 671-680, May 1992.
- [23] D.S. Abrams and J.M. Prausnitz, “Statistical thermodynamics of liquid-mixtures – a new expression for the excess Gibbs energy of partly or completely miscible systems,” *AICHE J.*, vol. 21, pp. 116-128, January 1975.
- [24] J. Mollerup, “A note on the derivation of mixing rules from excess Gibbs energy models,” *Fluid Phase Equilib.*, vol. 25, pp. 323-327, March 1986.
- [25] T. Banerjee, M.K. Singh and A. Khanna, “Prediction of binary VLE for imidazolium based ionic liquid systems using COSMO-RS,” *Ind. Eng. Chem. Res.*, vol. 45, pp. 3207-3219, April 2006.
- [26] R.H. Perry, D.W. Green and J.O. Maloney, *Perry's Chemical Engineers' Handbook*, 7th ed., McGraw-Hill, New York, 1999.
- [27] V.H. Álvarez, R.M. Maduro and M. Aznar, “Robust and Efficient Implementation of Strategies for Chemical Engineering Regression Problems”, 18th European Symposium on Computer Aided Process Engineering, 2008, accepted.
- [28] J.O. Valderrama and V.H. Álvarez, “Correct way of reporting results when modelling supercritical phase equilibria using equations of state,” *Can. J. Chem. Eng.*, vol. 83, pp. 578-581, June 2005.
- [29] W.H. Press, S.A. Teukolsky, W.T. Vetterling and B.P. Flannery, *Numerical Recipes in Fortran 77. The Art of Scientific Computing*, Vol. 1, 2nd ed., Cambridge University Press, New York, 1992.
- [30] J.D. Hoffman, *Numerical Methods for Engineers and Scientists*, 2nd ed., Marcel Dekker, Inc., New York, 2001.
- [31] Diadem Public 1.2. The DIPPR Information and Data Evaluation Manager, 2000.

Received: March 31, 2008

Revised: April 01, 2008

Accepted: April 18, 2008

Artigo 4.8: An efficient approach to optimal interpolation of experimental data

Journal of the Taiwan Institute of Chemical Engineers 41 (2010) 184–189



An efficient approach to optimal interpolation of experimental data[☆]

Víctor H. Álvarez, Martín Aznar*

School of Chemical Engineering, State University of Campinas, UNICAMP, P.O. Box 6066, 13083-970 Campinas, SP, Brazil

ARTICLE INFO

Article history:

Received 10 February 2009

Received in revised form 2 July 2009

Accepted 8 August 2009

Keywords:

Interpolation method

Thermodynamic data

Consistency test

ABSTRACT

In this work, a computational method is proposed in order to choose the best interpolation function for experimental data. The optimal interpolation function follows the natural tendency of data, suffers a minimal influence by removing one data point, does not present over fitting and yields the best representation for large or rough data sets. High pressure Px data of binary mixtures containing ionic liquid were used as case studies: supercritical $\text{CO}_2 + 1\text{-hexyl-3-methyl imidazolium hexafluorophosphate} ([\text{hmim}][\text{PF}_6])$, supercritical $\text{CO}_2 + 1\text{-butyl-3-methyl imidazolium tetrafluoroborate} ([\text{bmim}][\text{BF}_4])$ and supercritical $\text{CHF}_3 + 1\text{-butyl-3-methyl imidazolium hexafluorophosphate} ([\text{bmim}][\text{PF}_6])$. The common practice of using the correlation coefficient to analyze the accuracy of the interpolation model is critically discussed. As a validation of the method, a thermodynamic consistency test is applied to the interpolated data. The results show that the mean values of the interpolation error for $\text{CO}_2 + [\text{hmim}][\text{PF}_6]$, $\text{CO}_2 + [\text{bmim}][\text{BF}_4]$ and $\text{CHF}_3 + [\text{bmim}][\text{PF}_6]$ are 0.47%, 0.33% and 0.13%, respectively. These values are within the reported experimental error, which has a range from 0.04% to 1.7%.

© 2010 Published by Elsevier B.V. on behalf of Taiwan Institute of Chemical Engineers.

1. Introduction

Interpolated data are needed in several engineering problems; an example of these problems is the construction of a Px diagram from experimental isopleths, a typical vapor–liquid equilibrium (VLE) problem. By interpolating between isopleths, it is possible to plot the Px diagram at constant temperature. Since both bubble- and dew-points are available in several isopleths, each Px diagram illustrates both the solubility of the solute in the solvent-rich phase and the solubility of the solvent in the solute-rich phase. Then, values of other than the known discrete points may be needed. This interpolation process is performed by fitting an approximating function to the discrete data set.

Many types of interpolation functions can be used and several authors calculated Px diagram from isopleths, but without recommending one specific method for the best interpolation function. Then, there are not scientific papers that develop and give solutions about how to choose the best interpolation function;

however, this solution is always demanded by readers and referees when interpolated data are used.

In several applications of interpolation functions to experimental data, it has been a common practice to analyze the results using definitions of errors and deviations that we consider misleading and that do not give a clear indication about how accurate are the models employed in the analyses. Sentences such as "...fairly good representation data for these systems were found" or "...in general, the correlation of the experimental data of this work by the polynomial is acceptable", which are commonly found in the literature, must be taken with care. Three main problems are found in this kind of analysis: (i) the polynomial interpolation may oscillate wildly between the data points; this problem is commonly resolved by the use of spline interpolation, but this function can over fit the data set and the R^2 also shows a high value; (ii) when calculated and experimental data are used to analyze the accuracy of a interpolation, the differences between experimental and correlated values are presented using different definitions of errors and deviations, which mislead the correct correlation; (iii) the interpolation methods do not measure the natural tendency of the individual data points. The typical interpolation is used to predict new data but this characteristic is not measurement.

Another question arises as to whether the assumptions and methods that are taught are still sufficient for the data analysis needs of a chemical engineer. For example, Clancey (1947) examined approximately 250 error distributions involving

* A previous version of this paper was presented as a poster (in Portuguese) at the XVII Brazilian Congress of Chemical Engineering, Recife, 2008.

Abbreviations: NFC, not fully consistent; TC, thermodynamically consistent; UNIQUAC, universal quasichemical; VLE, vapor–liquid equilibrium.

* Corresponding author. Tel.: +55 19 3788 3962; fax: +55 19 3788 3965.

E-mail address: maznar@feq.unicamp.br (M. Aznar).

Nomenclature

A	areas in the Gibbs–Duhem equation
A, B, C, D	coefficients for interpolation functions
f	interpolation function
k_{ij}	binary interaction parameter
N	number of experimental points
OF	objective function
P	pressure
R^2	correlation coefficient
r, q	UNIQUAC volume and surface parameters
T	temperature
x	liquid phase mole fraction
y	vapor phase mole fraction
Z	compressibility factor
<i>Greek symbols</i>	
σ	standard deviation
ΔA	individual area deviation
ΔE	absolute average deviation for error interpolation
ΔP	absolute average deviation for pressure
ω	acentric factor
ϕ	fugacity coefficient
<i>Superscripts/subscripts</i>	
calc	calculated
c	critical
exp	experimental
i, j	indexes

50,000 chemical analyses of metals and found that only 10–15% of the series presents a normal distribution of errors. This may be due for outliers or leverage point in the data (Rousseeuw, 1984). If the data are assumed with normally distributed error but their actual distribution has tails, then estimates based on the maximum likelihood principle not only cease to be “best”, but they may have unacceptably low statistical efficiency. These potential deficiencies have been investigated since the 1960s, and some solutions were proposed (Rousseeuw, 1984). In order to evaluate the robustness of the methods, the term “breakdown point” can be defined as the smallest fraction of contamination which a given sample may contain without spoiling the estimator completely (Rousseeuw, 1984). The breakdown point for least squares is 0%, which means that a single outlier in a data set destroys the estimator. In the last years, several estimators with high breakdown point (50%) were proposed (Rousseeuw, 1984). A simple and robust estimator is the least absolute values; this regression protects against outlying on y_i considering normal errors on x_i (Harter, 1977), as is the case for temperature-dependent data. Thus, the goal of this work is to propose a simple estimator for the error analysis of interpolation methods.

In this work, interpolation functions were applied to a discrete vapor–liquid equilibrium data set in two ways: exact fit, such as cubic spline (Press *et al.*, 1992) and approximate fit, by using low degree polynomials (Cruz-Duarte *et al.*, 2003; Peters *et al.*, 1987), where the parameters were fitted through the least squares approximation. Five different interpolation functions were tested, and in each case one of them yielded the best fit over the experimental data. The method is applied to the experimental isopleths of the systems $\text{CO}_2 + [\text{hmim}][\text{PF}_6]$, $\text{CO}_2 + [\text{bmim}][\text{BF}_4]$ and $\text{CHF}_3 + [\text{bmim}][\text{PF}_6]$. As a validation of the method, an

extended isothermal thermodynamic consistency test is applied to the interpolated data.

2. Model analysis

Some authors give interpolation data by fitting exponential curves to the experimental data points and evaluating the fit through the correlation coefficient (R^2). Peters *et al.* (1987) gave interpolation data by fitting polynomial curves to the experimental data points and evaluated the fit with a good tendency of data curve.

These methods to select the best interpolation function are based on the hypothesis that experimental errors are randomly distributed. Another, error defined in order to accept the interpolation function as accurate for the data can be based on the general equation of error interpolation of Weierstrass approximation theorem (Hoffman, 2001) with the least absolute residues. The method intuitively makes the fit procedure to be significantly quicker with robust properties. There are some occasions where the standard deviation of the errors in the y values (σ_y) is not constant; in this case weighted fitting is required. The purpose of weighted fitting is to obtain the best estimates of the parameters by forcing the curve close to those data that are known with high precision, while giving much less weight to those data that exhibit large scatter. Therefore, the propose method was called the absolute average percent deviations for the error interpolation ($\%|\Delta E|$), and for the P_x data, the temperature is the independent measured variable and pressure is the dependent measured variable for the isopleth data, defined as

$$\%|\Delta E| = \frac{100}{N} \sum_{i=1}^N \frac{|P_i^{\text{exp}} - f(T_1^{\text{exp}}, \dots, T_j^{\text{exp}}, \dots, T_N^{\text{exp}})_{j \neq i}|}{\sigma_{P_i^{\text{exp}}}} \quad (1)$$

where N is the number of data points, T_i^{exp} is the experimental temperature at point “ i ”, P_i^{exp} is the experimental pressure at point “ i ”, and f is the interpolated function fitted with all other experimental data points but “ i ” and evaluated at “ i ”. It is possible that the absolute values of σ_y are unknown, then can be replaced by dependent variable values, as,

$$\%|\Delta E| = \frac{100}{N} \sum_{i=1}^N \frac{|P_i^{\text{exp}} - f(T_1^{\text{exp}}, \dots, T_j^{\text{exp}}, \dots, T_N^{\text{exp}})_{j \neq i}|}{P_i^{\text{exp}}} \quad (2)$$

The last equation is generally preferred. The interpolation error is used on five interpolation functions over each isopleth; so, the interpolation function with the minimum value of $\%|\Delta E|$ is established as the optimal for the isopleth. After that, the chosen interpolation function is fitted with all experimental data and used to plot the P_x diagram. In order to known the applicability of the proposed equation on functions with over fitting, the cubic spline approximation was used. There were also included 2 exponential functions (Cruz-Duarte *et al.*, 2003) and two polynomial functions (Peters *et al.*, 1987).

Other definitions of error are used to analyze the data fit, such as the prediction error sum of squares (PRESS), the correlation coefficient (R^2), and the absolute average percent deviation for pressure ($\%|\Delta P|$):

$$\%|\Delta P| = 100 \left| \frac{P_i^{\text{cal}} - P_i^{\text{exp}}}{P_i^{\text{exp}}} \right| \quad (3)$$

Also, generalized correlation coefficients and standard deviations may be used to assess statistical goodness of fit or compatibility between experimental data and model results. However, from the practical point of view, the error interpolation (Eq. (1)) should be used to draw conclusions about how accurate is a curve fit in order to correlate or predict an experimental data point. This is of special

Table 1
VLE data for supercritical systems studied.

Sys	Ni	Range of data				
		T (K)	P (MPa)	x ₁		
CO ₂ + [hmim][PF ₆]	1	98	298–364	0.6–94.6	0.1–0.7	–
CHF ₃ + [bmim][PF ₆]	2	173	303–363	0.6–41.0	0.1–0.9	0.96–0.99
CO ₂ + [bmim][BF ₄]	3	53	278–368	0.6–67.6	0.1–0.6	–

importance for applications such as thermodynamic consistency tests for high pressure data, cases in which an accurate interpolation is required of data without normal errors.

The interpolation method was applied to three systems show in Table 1. System 1 is CO₂ (1) + [hmim][PF₆] (2) from Shariati and Peters (2004), system 2 is CHF₃ (1) + [bmim][PF₆] (2) from Shariati *et al.* (2005), while system 3, CO₂ (1) + [bmim][BF₄] (2) is taken from Kroon *et al.* (2005). In this table, N_i is the number of isopleths, T is the temperature, P is the pressure and x₁ and y₁ are the molar fraction in liquid and vapor phase, respectively.

The isopleth at x₁ = 0.102 for the CHF₃ + [bmim][PF₆] and x₁ = 0.299 for the CO₂ + [hmim][PF₆] systems were selected as examples for the analysis of results. The interpolation functions used and the results for the selected data are shown in Table 2. In this table, %|ΔE| is the average percent deviations for the method proposed, ΔPRESS is the deviations from PRESS, %|ΔP| is the absolute average percent deviation for pressure, R² is the coefficient of correlation, and A, B, C and D are the fitted variables for the functions.

Table 2 shows that different expressions for deviations used to express the goodness of fit for a given function can lead to different conclusions. In this table, the value of %|ΔE| is always greater than the other error definitions. Also, it shows that the cubic spline yields %|ΔP| = 0, because cubic spline yields the exact experimental pressure for each experimental temperature. The same problem appears with the coefficient of correlation using cubic spline, R² = 1, because the cubic spline passes through every data point. On the other hand, %|ΔE| and ΔPRESS, by definition, uses the function fitted without the data point “i”, evaluated in the point “i” not allowing over fitting. Then, only the proposed method (%|ΔE|) and PRESS make possible to compare the functions with natural over fitting (cubic spline) with other functions in order to analyze the data fit. Table 2 shows also that, according with the proposed method; the cubic spline was the worst function. Therefore, the cubic spline is dropped out and only the functions 2–5 are used as interpolation functions in this discussion. The residual scatter for these functions are shown in Fig. 1 for the CHF₃ + [bmim][PF₆]. This figure shows that all residual errors are low; however, the selected functions are different for each definition of error and the results are shown in Table 3.

The confidence intervals (in particular the 95% confidence interval) on the variable values and data point errors fit can be very useful indicators of the fit between the model and the data (Benson-Karhi *et al.*, 2007). If all confidence intervals are smaller than the respective variable values, all of them are significant in the function fit; the best model is obtained with the lowest data point errors (Perry *et al.*, 1999). The results for the CO₂ + [hmim][PF₆] in Table 3 show that all variables in function 3 are not significant, since the confidence intervals are greater than the variable values; therefore, the function is not the best for the data, although would be selected by the R² criterion. Besides, the function 5 shows all the parameters as significant, but their residual errors have two points over the 1%. These results show that the outlier at 348.15 K influences a bad quality of the fit with the PRESS method. On the other hand, all the variables in function 4, selected with the method proposed, are significant, and the residual errors show a best fit on the data with the same tendency, with low influence of

Table 2
Interpolation functions, error (%|ΔE|) and relative deviation in pressure (%|ΔP|).

Function	Formula	% ΔE	ΔPRESS	% ΔP	R ²
CO ₂ + [hmim][PF ₆]	Cubic spline	0.76	0.0014	0.0	1.00000
1	P = AT ² + BT + C	0.54	0.0011	0.411	0.99933
2	P = AT ³ + BT ² + CT + D	0.62	0.0012	0.406	0.99943
3	P = e ^(A+B/T)	0.66	0.0015	0.545	0.99904
4	P = e ^(A+B/T²)	0.61	0.0010	0.516	0.99933
5	P = e ^(A+B/T²)	0.72	0.00054	0.60	0.99946
CHF ₃ + [bmim][PF ₆]	Cubic spline	1.08	0.000100	0.00	1.00000
1	P = AT ² + BT + C	0.54	0.000030	0.41	0.99971
2	P = AT ³ + BT ² + CT + D	0.57	0.000034	0.40	0.99972
3	P = e ^(A+B/T)	0.53	0.000033	0.46	0.99965
4	P = e ^(A+B/T²)	0.72	0.000054	0.60	0.99946

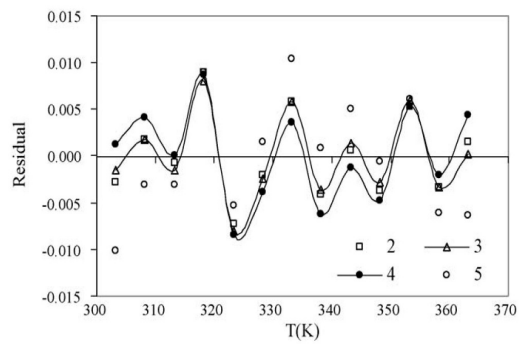


Fig. 1. Residual error for functions 2–5 for the CHF₃ + [bmim][PF₆] system.

the outlier on the fit. This result is observed in all function fits using the proposed method. The results for the CHF₃ + [bmim][PF₆] show similar residual errors for the method proposed and PRESS, but the proposed method select an function with two parameters only. Table 3 shows the relative residual errors close to 1% with bold values.

Three interpolated isotherms from isopleths using the proposed method are shown in Table 4. In this table, the interpolated temperature was 323.15 K, P is the pressure and x₁ and y₁ are the mole fraction of component 1 in liquid and vapor phase, respectively.

The interpolated isotherms for CO₂ + [hmim][PF₆], CO₂ + [bmim][BF₄] and CHF₃ + [bmim][PF₆] have %|ΔE| = 0.68%, 0.28% and 0.13%, respectively. These values are within the reported experimental error, which has a range from 0.04% to 1.7%. Therefore, the optimal interpolation function follows the natural tendency of data, suffers a minimal influence by removing one data point, does not present over fitting and yields the best representation for large or rough data sets.

3. Consistency test

The interpolated data of Table 4 were tested with a thermodynamic consistency test. The equations defining the consistency criteria for binary mixtures have been presented by Valderrama and Álvarez (2004). The test uses the Peng–Robinson (1976) EoS with the Wong–Sandler (1992) mixing rule coupled with the UNIQUAC model (Abrams and Prausnitz, 1975) for the excess Gibbs free energy as the standard thermodynamic model in a bubble point calculation. The development for binary mixtures containing ionic liquids is summarized below.

This thermodynamic model is used to accurately fit the experimental data and thereafter, apply the consistency test.

Table 3

Interpolated values, parameters for the function fit and confidence interval in functions 95% for the selected functions in Table 2.

CO ₂ + [hmim][PF6]											
% ΔE (F2)						ΔPRESS (F5)			% ΔP , R ² (F3)		
A	2.031E-4 ± 6.109E-5						3.861E+0 ± 4.559E-2			-2.143E-6 ± 3.750E-6	
B	-8.015E-2 ± 4.075E-2						-2.867E+5 ± 5.307E+3			2.347E-3 ± 3.750E-3	
C	7.741E+0 ± 6.778E+0						-			-7.935E-1 ± 1.248E+0	
D	-						-			8.671E+1 ± 1.383E+2	
T (K)	P (MPa)	P _{cal} (MPa)	Δ	Δ%	P _{cal} (MPa)	Δ	Δ%	P _{cal} (MPa)	Δ	Δ	Δ%
303.34	2.13	2.118	0.012	0.566	2.108	0.022	1.045	2.136	-0.006	-0.265	
308.35	2.34	2.339	0.001	0.048	2.330	0.010	0.410	2.339	0.001	0.050	
313.36	2.57	2.570	0.000	0.000	2.564	0.006	0.221	2.560	0.010	0.378	
318.39	2.80	2.812	-0.012	-0.439	2.810	-0.010	-0.360	2.799	0.001	0.022	
323.41	3.06	3.064	-0.004	-0.143	3.066	-0.006	-0.192	3.053	0.007	0.225	
328.44	3.31	3.327	-0.017	-0.520	3.332	-0.022	-0.673	3.321	-0.011	-0.328	
333.36	3.60	3.594	0.006	0.160	3.602	-0.002	-0.059	3.594	0.006	0.159	
338.43	3.86	3.880	-0.020	-0.511	3.889	-0.029	-0.761	3.886	-0.026	-0.681	
343.63	4.17	4.183	-0.013	-0.320	4.193	-0.023	-0.553	4.195	-0.025	-0.596	
348.46	4.56	4.475	0.085	1.859	4.483	0.077	1.690	4.488	0.072	1.575	
353.48	4.79	4.789	0.001	0.029	4.792	-0.002	-0.033	4.798	-0.008	-0.173	
358.65	5.09	5.122	-0.032	-0.631	5.117	-0.027	-0.528	5.121	-0.031	-0.619	
363.37	5.43	5.436	-0.006	-0.111	5.420	0.010	0.187	5.419	0.011	0.211	
CHF3 + [bmim][PF6]											
% ΔE (F4)						ΔPRESS (F2)			% ΔP , R ² (F3)		
A	4.837E+0 ± 6.304E-2						5.370E-05 ± 1.005E-5			-1.540E-07 ± 6.603E-7	
B	1.631E+3 ± 2.153E+1						-2.189E-02 ± 6.698E-3			2.076E-04 ± 6.602E-4	
C	-						2.279E+0 ± 1.113E+0			-7.308E-02 ± 2.196E-1	
D	-						-			-	
T (K)	P (MPa)	P _{cal} (MPa)	Δ	Δ%	P _{cal} (MPa)	Δ	Δ%	P _{cal} (MPa)	Δ	Δ	Δ%
303.20	0.58	0.581	-0.001	-0.205	0.577	0.003	0.488	0.578	0.002	0.268	
308.19	0.63	0.634	-0.004	-0.649	0.632	-0.002	-0.277	0.632	-0.002	-0.277	
313.20	0.69	0.690	0.000	-0.016	0.689	0.001	0.112	0.689	0.001	0.213	
318.18	0.74	0.749	-0.009	-1.216	0.749	-0.009	-1.216	0.748	-0.008	-1.095	
323.26	0.82	0.812	0.008	0.976	0.813	0.007	0.854	0.812	0.008	0.976	
328.24	0.88	0.876	0.004	0.441	0.878	0.002	0.230	0.878	0.002	0.282	
333.22	0.94	0.944	-0.004	-0.390	0.946	-0.006	-0.620	0.946	-0.006	-0.620	
338.17	1.02	1.014	0.006	0.611	1.016	0.004	0.401	1.016	0.004	0.356	
343.25	1.09	1.089	0.001	0.111	1.091	-0.001	-0.052	1.091	-0.001	-0.127	
348.22	1.17	1.165	0.005	0.410	1.166	0.004	0.317	1.167	0.003	0.237	
353.23	1.24	1.245	-0.005	-0.423	1.245	-0.005	-0.429	1.246	-0.006	-0.485	
358.22	1.33	1.328	0.002	0.151	1.327	0.003	0.248	1.327	0.003	0.248	
363.25	1.41	1.414	-0.004	-0.314	1.411	-0.001	-0.102	1.410	0.000	-0.012	

The experimental data fit requires the calculation of the model interaction parameters, using an optimized objective function. Although the consistency test is model dependent, good fitting does not guarantee that the data are consistent, since the proposed area test, derived from the Gibbs–Duhem equation, must also be fulfilled. The test uses the Gibbs–Duhem equation expressed in the integral form (Valderrama and Álvarez, 2004):

$$\int \frac{1}{P} dP = \int \frac{1 - y_2}{y_2(Z-1)} \frac{d\phi_1}{\phi_1} + \int \frac{1}{Z-1} \frac{d\phi_2}{\phi_2} \quad (4)$$

where P is the pressure of the system, y₂ is the mole fraction of the ionic liquid in the gas phase, ϕ₁ and ϕ₂ are the fugacity coefficients of the components fluid (1) and ionic liquid (2) in the gas phase, and Z is the compressibility factor. Both sides of this equation are denoted as follows:

$$A_P = \int \frac{1}{P} dP \quad (5)$$

$$A_\phi = \int \frac{1 - y_2}{y_2(Z-1)} \frac{d\phi_1}{\phi_1} + \int \frac{1}{Z-1} \frac{d\phi_2}{\phi_2} \quad (6)$$

The A_P and A_ϕ are evaluated using two consecutive points. The values for A_P are obtained with experimental P_{y2} data, while the values for A_ϕ are obtained with calculated values of Z, ϕ_i and y₂ by

the thermodynamic model. The pressures used as experimental data are calculated as interpolated values by the proposed criteria equation. Thus, for one data set to be considered as consistent, A_ϕ and A_P should be similar within acceptable deviations. In order to define the acceptable deviations, an individual percent area deviation (%ΔA_i) between the A_ϕ and A_P values can be defined as:

$$\% \Delta A_i = 100 \left[\frac{A_\phi - A_P}{A_P} \right]_i \quad (7)$$

The quality of the correlation was analyzed through the relative deviations in the calculated pressure in the gas phase for each point i, defined as:

$$\% \Delta P_i = 100 \frac{P_i^{\text{cal}} - P_i^{\text{exp}}}{P_i^{\text{exp}}} \quad (8)$$

The method implies the minimization of the deviations, Eqs. (7) and (8). Then, the objective function for the consistency test includes a minimization of deviations in VLE data, and the integral areas (%ΔA_i). Besides, the inclusion of vapor concentrations in the objective function allows low deviations in pressure and predicts true physical concentrations in the vapor phase. Then the consistency of VLE data set is determined by the minimization

Table 4
Interpolated VLE data for fluid (1)+IL (2) systems at 323.15 K.

P (MPa)	x ₁	y ₁
CO ₂ +[hmim][PF ₆]		
0.81	0.098	≤0.9999
1.80	0.198	≤0.9999
3.05	0.299	≤0.9999
4.91	0.410	≤0.9999
5.50	0.501	≤0.9999
10.98	0.599	≤0.9999
25.86	0.650	≤0.9999
57.96	0.702	≤0.9999
64.45	0.711	≤0.9999
85.11	0.727	≤0.9999
CHF ₃ +[bmim][PF ₆]		
0.81	0.102	≤0.9999
1.67	0.203	≤0.9999
2.60	0.302	≤0.9999
3.60	0.400	≤0.9999
4.60	0.483	≤0.9999
5.73	0.552	≤0.9999
6.95	0.621	≤0.9999
11.34	0.700	≤0.9999
18.53	0.780	≤0.9999
23.74	0.850	~0.990
25.28	0.900	~0.980
26.22	0.925	~0.956
CO ₂ +[bmim][BF ₄]		
1.056	0.1022	≤0.9999
2.267	0.1998	≤0.9999
4.003	0.3035	≤0.9999
6.084	0.4005	≤0.9999
8.956	0.4825	≤0.9999
20.372	0.5507	≤0.9999
43.393	0.6017	≤0.9999

of the objective function, OF,

$$OF = \sum_{i=1}^{N-1} \left[\frac{A_p - A_{\phi}}{\sigma_A} \right]_i^2 + \sum_{i=1}^N \left[\frac{P^{\text{cal}} - P^{\text{exp}}}{\sigma_P} \right]_i^2 + \sum_{i=1}^N \left[\frac{y_{\text{fluid}}^{\text{cal}} - 1}{\sigma_y} \right]_i^2 \quad (9)$$

where N is the number of data points, P is the pressure, y_{fluid} is the vapor mole fraction of the supercritical fluid for data point "i", the superscripts "exp" and "cal" refer to the experimental and calculated values, respectively, and σ_A , σ_P and σ_y are the standard deviations of the measured quantities. For simplification, the interpolation errors of the pressure data were used for σ_P , the value 10^{-5} (or 10^{-3} when there are dew-point data) for σ_y and the value of A_p for σ_A .

The experimental values of concentration of ionic liquid in the gas phase (y_2) are needed; however, since these concentrations are almost negligible, its measurement is difficult (Shariati *et al.*, 2005); this is the rule of thumb for the physical criterion for y_2 , whose value can be lesser than 10^{-3} with an experimental uncertainty of 10^{-5} . Therefore, the consistency test uses values for y_2 calculated through the bubble point calculation of the thermodynamic model, restricted only for low values to use in Eqs. (5) and (6).

In order to analyze the limits for consistency criteria and the uncertainty caused by the independent variables, calculations of error propagation have been performed (Perry *et al.*, 1999), with the liquid phase mole fraction, the temperature, and the interaction parameters as the independent measured variables. The calculated individual area A_{ϕ} is the dependent variable. Therefore, the error (EA) and the percent error (%ΔEA) in the calculated area are defined:

$$EA = \frac{\partial A_{\phi}}{\partial x} \Delta x + \frac{\partial A_{\phi}}{\partial T} \Delta T + \frac{\partial A_{\phi}}{\partial k_{ij}} \Delta k_{ij} + \frac{\partial A_{\phi}}{\partial A_{ij}} \Delta A_{ij} \quad (10)$$

$$\% \Delta EA = 100 \frac{EA}{A_{\phi}} \quad (11)$$

Table 5
Critical properties.

Component	T _c (K)	P _c (MPa)	ω
CO ₂ ^a	304.21	7.383	0.2236
CHF ₃ ^a	299.01	4.816	0.2642
[hmim][PF ₆] ^b	754.3	1.55	0.8352
[bmim][PF ₆] ^b	708.9	1.73	0.7553
[bmim][BF ₄] ^b	632.3	2.04	0.8489

^a Diadem (2000).

^b Valderrama and Robles (2007).

where uncertainties of 0.005 for the experimental liquid phase mole fraction, 0.5 K for the temperature, and 0.0001 for each interaction parameter were used. The partial derivatives were numerically calculated and applied for several mixtures. The results shows a direct relationship between the estimated percent errors %EA and the fit deviations of the pressure (%ΔP), with a maximum deviations of 17% for %ΔEA and 5% on the %ΔP.

Also, the analysis show a good VLE fit yields minimal deviations in the individual areas; a %ΔP below that 5% gives %ΔA_i below that 10% and a %ΔP_i between 5% up to 10% yields %ΔA_i below that 20%. Therefore, over these limits, the experimental data has high chance to be thermodynamically inconsistent. These limits defined for the consistency criterion produce randomly distributed deviations on VLE. These limits defined are not strict, for example with only one data point slightly out of limits, the data set can be consider thermodynamic consistent. However, if more than 50% of the data points are out of limits, there is an evident tendency of inconsistency. Then, using the analysis of the propagation error a rule of thumb for remove bad data points is: (i) data point with %ΔP_i > 10 and %ΔA_i > 20; (ii) data point with %ΔA_i > 20; (iii) data point with %ΔP_i < 5 and %ΔA_i > 10.

Accepted deviation defined by %ΔP ≤ 10 is used as constraint for every data point for the thermodynamic model. If the thermodynamic model cannot fit more than 30% of data points in the data set within this limit defined for individual pressure and low ionic liquid concentration in the gas phase, another thermodynamic model should be used. In another case, the results are used into Eqs. (5) and (6) to evaluate the consistency of the data.

The deviations accepted for the consistency test are beyond of the uncertainties of the interpolated data, thus is not a cause for data not consistent. Also, the works of Álvarez and Aznar (2006, 2008) show the flexibility of the thermodynamic model for these systems, where the UNIQUAC structural parameters and critical properties have a small influence on the data fit; the interaction parameters are the opposite, since their values have high influence on the data fit. Therefore, to obtain the best interaction parameters, the minimization method was performed using a genetic algorithm code, implemented and fully explained in Álvarez *et al.* (2008).

4. Application of the test

The consistency test using the Peng–Robinson EoS with the Wong–Sandler/UNIQUAC mixing rules was applied to the isotherms of Table 4. The critical properties for all substances are

Table 6
Structural parameters for UNIQUAC.

Component	r	q
CO ₂ ^a	3.26	2.39
CHF ₃ ^a	4.36	3.19
[hmim][PF ₆] ^a	28.08	18.10
[bmim][PF ₆] ^b	24.01	15.16
[bmim][BF ₄] ^b	21.75	14.08

^a Álvarez and Aznar (2008).

^b This work.

Table 7Results of the consistency test, with estimated k_{ij} , A_{12} and A_{21} UNIQUAC parameters.

Sys	k_{ij}	A_{12} (kJ/kmol)	A_{21} (kJ/kmol)	$ \Delta P $ (%)	Result
1	0.3126	9459.9	-1163.3	10.6	NFC
2	0.4378	-1822.6	3604.5	7.9	NFC
3	0.2832	2591.7	-141.0	0.7	TC

shown in Table 5, while the structural parameters r and q for the UNIQUAC model are shown in Table 6. Table 7 shows the results for the consistency test and the interaction parameters for the UNIQUAC model; in this table, TC stands for “thermodynamically consistent” and NFC for “not fully consistent”.

5. Conclusion

A computational method is proposed in order to choose the best interpolation function for Px isopleths. The isothermal data obtained from interpolation are within the reported experimental error. All variables for the function fit are statistically significant. An isothermal consistency test was developed to analyze individual interpolated data points in a binary vapor–liquid equilibrium data set containing ionic liquids, i.e., to eliminate doubtful points, based on the Peng–Robinson EoS with the Wong–Sandler/UNIQUAC mixing rule. The consistency test was applied to the isothermal interpolated data. The systems $\text{CO}_2 + [\text{bmim}][\text{BF}_4]$ was considered thermodynamically consistent, while the systems $\text{CO}_2 + [\text{hmim}][\text{PF}_6]$ and $\text{CHF}_3 + [\text{bmim}][\text{PF}_6]$ were considered not fully consistent.

Acknowledgements

The financial support of the Coordenação de Aperfeiçoamento de Pessoal de Nível Superior (CAPES) and Fundação de Amparo à Pesquisa do Estado de São Paulo (FAPESP) are gratefully acknowledged. M. Aznar is the recipient of a fellowship from Conselho Nacional de Desenvolvimento Científico e Tecnológico (CNPq).

References

- Abrams, D. S. and J. M. Prausnitz, “Statistical Thermodynamics of Liquid-Mixtures—A New Expression for the Excess Gibbs Energy of Partly or Completely Miscible Systems,” *AIChE J.*, **21**, 116 (1975).
- Álvarez, V. H. and M. Aznar, “Vapor–Liquid Equilibrium of Binary Systems Ionic Liquid + Supercritical (CO_2 or CHF_3) and Ionic Liquid + Hydrocarbons Using the Peng–Robinson Equation of State,” In: XXII Interamerican Congress of Chemical Engineering, vol. 1, Buenos Aires (2006).
- Álvarez, V. H. and M. Aznar, “Vapor–Liquid Equilibrium of Binary Systems Ionic Liquid + Supercritical (CO_2 or CHF_3) and Ionic Liquid + Hydrocarbons Using the Peng–Robinson Equation of State,” *J. Chin. Inst. Chem. Eng.*, **39**, 353 (2008).
- Álvarez, V. H., R. Larico, Y. Yanos, and M. Aznar, “Parameter Estimation for VLE Calculation by Global Minimization: Genetic Algorithm,” *Braz. J. Chem. Eng.*, **25**, 409 (2008).
- Benson-Karhi, D., H. Shore, and M. Shacham, “Modeling Temperature-Dependent Properties of Water via Response Modeling Methodology (RMM) and Comparison with Acceptable Models,” *Ind. Eng. Chem. Res.*, **46**, 3446 (2007).
- Clancey, V. J., “Statistical Methods in Chemical Analyses,” *Nature*, **159**, 339 (1947).
- Cruz-Duarte, A. R., M. M. Mooijer-Van Den Heuvel, C. M. M. Duarte, and C. J. Peters, “Measurement and Modelling of Bubble and Dew Points in the Binary Systems Carbon Dioxide + Cyclobutanone and Propane + Cyclobutanone,” *Fluid Phase Equilibr.*, **214**, 121 (2003).
- Diadem Public 1.2. *The DIPPR Information and Data Evaluation Manager*, (2000).
- Harter, H. L., “Nonuniqueness of Least Absolute Values Regression,” *Commun. Statist. Theor. Methods*, **6**, 829 (1977).
- Hoffman, J. D., *Numerical Methods for Engineers and Scientists*, 2nd ed., Marcel Dekker, Inc., New York (2001).
- Kroon, M. C., A. Shariati, M. Costantini, J. Van Spronsen, G. Witkamp, R. A. Sheldon, and C. J. Peters, “High-pressure Phase Behavior of Systems with Ionic Liquids: Part V. The Binary System Carbon Dioxide + 1-Butyl-3-methylimidazolium Tetrafluoroborate,” *J. Chem. Eng. Data*, **50**, 173 (2005).
- Peng, D. Y. and D. B. Robinson, “A New Two Constant Equation of State,” *Ind. Eng. Chem. Fundam.*, **15**, 59–64 (1976).
- Perry, R. H., D. W. Green, and J. O. Maloney, *Perry's Chemical Engineers' Handbook*, 7th ed., McGraw-Hill, New York (1999).
- Peters, C. J., J. L. De Roo, and R. N. Lichtenhaler, “Measurements and Calculations of Phase Equilibria of Binary Mixtures of Ethane + Eicosane. Part 1: Vapour + Liquid Equilibria,” *Fluid Phase Equilibr.*, **34**, 287 (1987).
- Press, W. H., S. A. Teukolsky, W. T. Vetterling, and B. P. Flannery, *Numerical Recipes in Fortran 77. The Art of Scientific Computing*, vol. 1. Cambridge University Press, New York (1992).
- Rousseeuw, P. J., “Least Median of Squares Regression,” *J. Am. Stat. Assoc.*, **79**, 871 (1984).
- Shariati, A., K. Gutkowski, and C. J. Peters, “Comparison of the Phase Behavior of some Selected Binary Systems with Ionic Liquids,” *AIChE J.*, **51**, 1532 (2005).
- Shariati, A. and C. J. Peters, “High-pressure Phase Behavior of Systems with Ionic Liquids. Part III. The Binary System Carbon Dioxide + 1-hexyl-3-methylimidazolium Hexaurophosphate,” *J. Supercrit. Fluids*, **30**, 139 (2004).
- Valderrama, J. O. and V. H. Alvarez, “A Versatile Thermodynamic Consistency Test for Incomplete Phase Equilibrium Data of High-Pressure Gas–Liquid Mixtures,” *Fluid Phase Equilibr.*, **226**, 149 (2004).
- Valderrama, J. O. and P. A. Robles, “Critical Properties, Normal Boiling Temperatures, and Acentric Factors of Fifty Ionic Liquids,” *Ind. Eng. Chem. Res.*, **46**, 1338 (2007).
- Wong, D. H. S. and S. I. Sandler, “A Theoretically Correct Mixing Rule for Cubic Equations of State,” *AIChE J.*, **38**, 671 (1992).

Artigo 4.9: High pressure phase behavior of carbon dioxide in 1-alkyl-3-methylimidazolium bis(trifluoromethylsulfonyl)imide ionic liquids

J. of Supercritical Fluids 48 (2009) 99–107



Contents lists available at ScienceDirect

The Journal of Supercritical Fluids

journal homepage: www.elsevier.com/locate/supflu



High pressure phase behavior of carbon dioxide in 1-alkyl-3-methylimidazolium bis(trifluoromethylsulfonyl)imide ionic liquids

Pedro J. Carvalho^a, Víctor H. Álvarez^c, José J.B. Machado^a, Jérôme Pauly^b, Jean-Luc Daridon^b, Isabel M. Marrucho^a, Martín Aznar^c, João A.P. Coutinho^{a,*}

^a CICECO, Departamento de Química, Universidade de Aveiro, 3810-193 Aveiro, Portugal

^b Laboratoire des Fluides Complexes, UMR 5150, BP 1155, 64013 Pau Cedex, France

^c Faculdade de Engenharia Química, Universidade Estadual de Campinas, 13083-970 Campinas-SP, Brazil

ARTICLE INFO

Article history:

Received 8 August 2008

Received in revised form 9 October 2008

Accepted 10 October 2008

Keywords:

1-Ethyl-3-methyl-imidazolium

bis(trifluoromethylsulfonyl)imide

1-Methyl-3-pentyl-imidazolium

bis(trifluoromethylsulfonyl)imide

Carbon dioxide

Phase behavior

Supercritical

Experimental

High pressure

ABSTRACT

New standards concerning environmental and safety issues are creating an increasing interest on ionic liquids as alternative solvents for a wide range of industrial applications. In this work, a new apparatus developed to measure vapor–liquid phase equilibrium in a wide range of pressures and temperatures was used to measure the phase behavior of the binary systems of carbon dioxide (CO_2) + 1-ethyl-3-methyl-imidazolium bis(trifluoromethylsulfonyl)imide ($[\text{C}_2\text{mim}][\text{Tf}_2\text{N}]$) and CO_2 + 1-methyl-3-pentyl-imidazolium bis(trifluoromethylsulfonyl)imide ($[\text{C}_5\text{mim}][\text{Tf}_2\text{N}]$) at temperatures up to 363 K and pressures up to 50 MPa. A thermodynamic consistency test, developed for systems with incomplete $P/T/x$ data and based on the Gibbs–Duhem equation, was applied to the experimental data measured in this work and the Peng–Robinson EoS using the Wong–Sandler mixing rule was used to describe the experimental data with excellent results.

© 2008 Elsevier B.V. All rights reserved.

1. Introduction

Ionic liquids (ILs), a class of *neoteric* solvents composed of large organic cations and organic or inorganic anions, that cannot form an ordered crystal and thus remain liquid at or near room temperature, are becoming one of the fastest growing “green” media for chemists and engineers, bridging academia and industrial interests. The tunable properties of ILs through an endless combination of cations and anions, allow the design of solvents for the development of more efficient processes and products. Among the several applications foreseeable for ionic liquids such as solvents in organic synthesis [1,2], homogeneous and biphasic transfer catalysts [3–5], separation processes [6–9], their use in processes with supercritical gases is one of the most exciting.

Blanchard et al. [9–11] described several potential applications of supercritical fluids with ILs. They demonstrated the possibility of using supercritical CO_2 to remove a solute from an IL, without contamination of the extracted solute, solving one of the shortcomings of the use of ionic liquids in solvent extraction processes:

the recovery of the compounds from the ionic liquid media. Scurto et al. [12] proposed an innovative process of separating ILs from organic solvents using supercritical CO_2 that induces a phase separation, due to the organic liquid phase expansion and the dielectric constant decrease, forcing the IL to separate into a second liquid phase. Later, Scurto et al. [13] also demonstrated that separation of aqueous solutions of both hydrophobic and hydrophilic ILs can be performed using supercritical CO_2 .

A large amount of work concerning the development of ionic liquids with special affinity towards CO_2 has been carried Bates et al. [6] who reported amine functionalized ILs, while Yuan et al. [14] and Sun et al. [15] used hydroxyl-functionalized ILs as a novel efficient catalyst for chemical fixation of CO_2 . Yu et al. [16] and Huang et al. [17] proposed guanidinium-based ILs, where the electron-donating groups increased the strength of the donor-acceptor interactions on $-\text{NH}_2$ and consequently enhanced the interactions between $-\text{NH}_2$ and CO_2 . Muldoon et al. [18] and Lopez-Castillo [19] reported that CO_2 can be used to enhance the solubility of other gases that typically present low solubilities in ILs. Solinas et al. [20] showed that inducing CO_2 pressure on a system improves the activation, tuning and immobilization of chiral iridium catalysts in IL/ CO_2 for the enantioselective hydrogenation reaction of imines.

* Corresponding author. Tel.: +351 234 401 507; fax: +351 234 370 084.
E-mail address: jcoutinho@ua.pt (J.A.P. Coutinho).

The successful development of IL-based processes using supercritical fluids depends on the adequate knowledge of the phase behavior of the systems. Several authors, such as Brennecke [11,21,22], Peters [23–25] Noble [26], Lim [27], Baltus [28], Outcalt [29], Yokozeki [30] and Majer [31], have been reporting supercritical carbon dioxide solubility in common ILs, but few have focused their studies on the Tf_2N anion-based ionic liquids [23,25–29].

Apart task specific ILs, the Tf_2N anion-based ILs are the ones presenting the highest CO_2 solubility. Although both anion and cation influence the CO_2 solubility, the anion has the strongest influence [21,22,32,33]. The presence of fluoroalkyl groups, known to be "CO₂-philic", make the Tf_2N anion-based ILs compounds with great CO_2 solubilities. However, this behavior is yet poorly understood and while some authors emphasize the role of the interactions between the CO_2 and the Tf_2N anion [21,22,34], others identify the large free volume of the ionic liquid as the main factor responsible for the large solubility [18]. On the other hand, the alkyl chain length of the cations, also influences the CO_2 solubility, indicating an entropic, rather than enthalpic, effect is present [21]. For a given cation, the data available seems to indicate that the longer the alkyl chain, the higher the free volume, and consequently the larger the solubility [11,21,23,24,34–37].

In this work, a new apparatus was developed to investigate the high pressure phase behavior of gas+ionic liquid systems. Two Tf_2N -based ionic liquids were selected in order to further contribute for a more detailed knowledge and thus a better understanding of the solubility of supercritical CO_2 in these fluids. The system of $\text{CO}_2 + 1\text{-ethyl-3-methylimidazolium bis(trifluoromethylsulfonyl)imide} ([\text{C}_2\text{mim}][\text{Tf}_2\text{N}])$ was chosen because it allows the evaluation of the quality of the measurements by direct comparison with literature data [25], and the $\text{CO}_2 + 1\text{-methyl-3-pentyl-imidazolium bis(trifluoromethylsulfonyl)imide} ([\text{C}_5\text{mim}][\text{Tf}_2\text{N}])$ system was studied to investigate the effect of the alkyl chain length on the CO_2 solubility in ionic liquids. Both systems were measured at temperatures up to 363 K and pressures of 50 MPa.

A thermodynamic consistency test [38,39], developed for systems with incomplete PV_{xy} data and based on the Gibbs–Duhem equation, and the Peng–Robinson equation of state [40] with the Wong–Sandler mixing rule [41] using the UNIQUAC model [42] for

the activity coefficients, was applied to describe the experimental data measured in this work. It will be shown that the model provides an excellent representation of the experimental data and the consistency test shows that the data here reported, unlike many other systems available in the literature, is thermodynamically consistent [38,39,43].

2. Experimental

2.1. Materials

Two imidazolium-based ILs, 1-ethyl-3-methyl-imidazolium bis(trifluoromethylsulfonyl)imide, $[\text{C}_2\text{mim}][\text{Tf}_2\text{N}]$ and 3-methyl-1-pentyl-imidazolium bis(trifluoromethylsulfonyl)imide, $[\text{C}_5\text{mim}][\text{Tf}_2\text{N}]$, were used on this study. All compounds were acquired from IoLiTec with mass fraction purities >99% and bromide impurity mass fraction < 10^{-4} . The purities of each ionic liquid stated by the supplier, were checked by ^1H NMR, ^{13}C NMR and ^{19}F NMR.

It is well established that ILs physical properties are influenced by their water content [44–47]. To reduce to negligible values both water and volatile compounds content, vacuum (0.1 Pa), stirring and moderate temperature (353 K), for a period of at least 48 h, were applied prior to the measurements. The final IL water content was determined with a Metrohm 831 Karl Fischer coulometer, indicating a water mass fraction of $(42 \text{ and } 20) \times 10^{-6}$ for $[\text{C}_2\text{mim}][\text{Tf}_2\text{N}]$ and $[\text{C}_5\text{mim}][\text{Tf}_2\text{N}]$, respectively.

The CO_2 used was from Air Liquide with a purity of $\geq 99.998\%$ and H_2O , O_2 , C_nH_m , N_2 and H_2 impurities volume fractions lower than $(3, 2, 2, 8 \text{ and } 0.5) \times 10^{-6}$, respectively.

2.2. Experimental measurements

The high pressure equilibrium cell developed in this work uses the synthetic method and is sketched in Fig. 1. The cell, based on the design of Daridon and co-workers [48–52], consists of a horizontal hollow stainless-steel cylinder, closed at one end by a movable piston and at the other end by a sapphire window. This window, along with a second window on the cell wall through which an optical fiber lights the cell chamber, allows the operator to follow

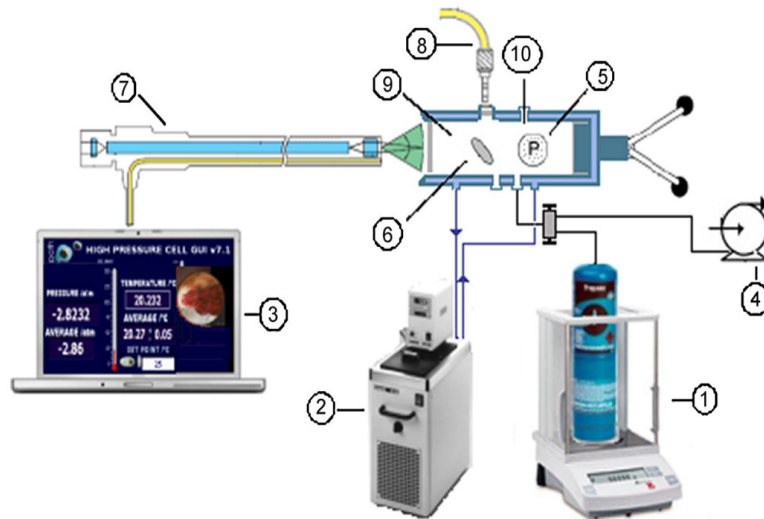


Fig. 1. Schematic apparatus—1: analytical balance; 2: thermostated bath circulator; 3: computer to data and video acquisition; 4: vacuum pump; 5: piezoresistive pressure transducer; 6: magnetic bar; 7: endoscope plus a video camera; 8: light source with optical fiber cable; 9: high-pressure variable-volume cell; 10: temperature probe.

the behavior of the sample with pressure and temperature. The orthogonal positioning of both sapphire windows minimizes the parasitic reflections and improves the observation in comparison to axial lighting.

A small magnetic bar placed inside the cell allows the homogenization of the mixture by means of an external magnetic stirrer. The sapphire window on the cell wall limits the minimum internal volume of the cell to 8 cm^3 , while the maximum value is set to 30 cm^3 . The presence of the magnetic stirrer, as well as the cell reduced volume, help to minimize the inertia and temperature gradients within the sample.

The cell is thermostatted by circulating a heat-carrier fluid through three flow lines directly managed into the cell. The heat-carrier fluid is thermo-regulated with a temperature stability of $\pm 0.01\text{ K}$ by means of a thermostat bath circulator (Julabo MC). The temperature is measured with a high precision thermometer, Model PN 5207 with an accuracy of 0.01 K , connected to a calibrated platinum resistance inserted inside the cell close to the sample. The pressure is measured by a piezoresistive silicon pressure transducer (Kulite) fixed directly inside the cell to reduce dead volumes, that was previously calibrated and certified by an independent laboratory with IPAC accreditation, following the EN 837-1 standard and with accuracy better than 0.2%.

A fixed amount of IL was introduced inside the cell, its exact mass was determined by weighting, using a high weight/high precision balance with an accuracy of 1 mg (Sartorius). In order to avoid any interference of atmospheric gases during the manipulation, after placing the IL inside the cell, it was kept under vacuum overnight, while stirring and heating at 353 K .

The CO_2 was introduced under pressure from an aluminum reservoir tank. Its mass was measured with the precision balance and introduced into the measuring cell by means of a flexible high pressure capillary.

After preparation of a mixture of known composition and the desired temperature at low pressure was reached, the pressure was then slowly increased at constant temperature until the system becomes monophasic. The pressure at which the last bubble disappears represents the equilibrium pressure for the fixed temperature.

The purity of the IL is re-checked by NMR at the end of the study to confirm that no degradation of the IL takes place during the measurements.

3. Thermodynamic modeling and consistency

Valderrama and Álvarez [39] developed a thermodynamic consistency test for systems with incomplete $PTxy$ data, cataloguing them as thermodynamic consistent (TC), thermodynamic inconsistent (TI) or not full consistent (NFC). The authors analyzed the difficulties normally found when modeling this type of mixtures and proposed a methodology to analyze the experimental data, concluding about their thermodynamic consistency or inconsistency. Recently, Álvarez and Aznar [38,43] applied an extension of this approach to several supercritical fluid+IL systems using a method based on the Gibbs–Duhem equation, on the fundamental phase equilibrium equation, and on the Peng–Robinson equation of state [40], with the Wong–Sandler mixing rule [41] using the UNIQUAC model [42] for the activity coefficient.

The test uses the Gibbs–Duhem equation expressed in the integral form, where the left-hand side is denoted as A_p and the right-hand side as A_ϕ , as it follows:

$$A_p = \int \frac{1}{Py_2} dP \quad (1)$$

$$A_\phi = \int \frac{(1-y_2)}{y_2(Z-1)} \frac{d\varphi_1}{\varphi_1} + \int \frac{1}{Z-1} \frac{d\varphi_2}{\varphi_2} \quad (2)$$

The values for A_p are obtained with experimental Py_2 data, and the values for A_ϕ are obtained with calculated values of Z , φ_i and y_2 . The subscripts 1 and 2 denote CO_2 and ionic liquid compounds, respectively. The individual percent area deviation, ΔA_i , is given as:

$$\Delta A_i = 100 \left[\frac{A_\phi - A_p}{A_p} \right]_i \quad (3)$$

where the subscript i refers to the i th data point. The quality of the correlation was analyzed through the relative deviations in the calculated pressure and solute concentration in the gas phase for each point i , defined as:

$$\Delta P_i = 100 \left(\frac{p_i^{\text{cal}} - p_i^{\text{exp}}}{p_i^{\text{exp}}} \right) \quad (4)$$

$$\Delta y_{2i} = 100 \left[\frac{y_2^{\text{cal}} - y_2^{\text{exp}}}{y_2^{\text{exp}}} \right]_i \quad (5)$$

The method implies the minimization of the deviations of Eqs. (3)–(5), setting as the objective function, OF, for the consistency test the minimization of the deviations in VLE data and the individual percent area deviation.

$$OF = \sum_{i=1}^{N-1} \left[\frac{A_p - A_\phi}{\sigma_A} \right]_i^2 + \sum_{i=1}^N \left[\frac{p_i^{\text{cal}} - p_i^{\text{exp}}}{\sigma_p} \right]_i^2 + \sum_{i=1}^N \left[\frac{y_{\text{fluid}}^{\text{cal}} - 1}{\sigma_y} \right]_i^2 \quad (6)$$

where N is the number of data points, P is the pressure, y_{fluid} is the vapor mole fraction of the supercritical fluid for data point i , the superscripts “exp” and “cal” refers to the experimental and calculated values, respectively, and σ_A , σ_p and σ_y are the standard deviations of those quantities. The experimental uncertainties in the pressure data were used for σ_p , the value 10^{-5} for σ_y and the value of A_p for σ_A . The minimization method was performed using a genetic algorithm code, implemented and fully explained in Álvarez et al. [53]. The difference between experimental and calculated values was calculated as the average percent deviation, expressed in absolute form, as follows:

$$|\Delta P| = \frac{100}{N} \sum_{i=1}^N \left[\frac{|p_i^{\text{cal}} - p_i^{\text{exp}}|}{p_i^{\text{exp}}} \right] \quad (7)$$

The isopleths were interpolated with the method proposed by Álvarez and Aznar [43] and the results are shown in Table 1, for the $\text{CO}_2 + [\text{C}_2\text{mim}][\text{TF}_2\text{N}]$ system and for the $\text{CO}_2 + [\text{C}_5\text{mim}][\text{TF}_2\text{N}]$ system, respectively. The physical properties used in the model for all substances are reported in Table 2.

4. Results and discussion

Although measurements were previously carried by us and others in similar apparatuses [48–52], $[\text{C}_2\text{mim}][\text{TF}_2\text{N}]$ was selected to validate the methodology and experimental procedure adopted in this work and the measurements were compared against data by Schilderman et al. [25]. High pressure binary vapor–liquid mixtures data of CO_2 in ILs are scarce and significant discrepancies among data from different authors [25,27,29] are common in literature. The identification of the data with the highest quality available in the literature was carried using the thermodynamic consistency test described above [43]. The most reliable data identified by Álvarez and Aznar [38,43] were those by Schilderman et al. [25] for the system $\text{CO}_2 + [\text{C}_2\text{mim}][\text{TF}_2\text{N}]$, where the isotherms at 313 K , 323 K and

Table 1Interpolated VLE data for the system supercritical CO₂ (1)+[C₂mim][Tf₂N] (2) and CO₂ (1)+[C₅mim][Tf₂N] (2).

T/K	X ₁								
	0.221	0.327	0.418	0.503	0.56	0.606	0.65	0.7	0.75
CO ₂ (1)+[C ₂ mim][Tf ₂ N] (2)									
293.15	–	–	–	–	2.935	3.437	3.942	4.783	
298.15	0.718	1.284	1.915	2.699	3.342	3.922	4.540	5.520	19.065
303.15	0.830	1.453	2.178	3.049	3.784	4.459	5.178	6.497	22.207
313.15	1.073	1.861	2.746	3.835	4.772	5.687	6.681	10.142	28.178
323.15	1.341	2.293	3.372	4.724	5.899	7.121	8.561	14.477	33.729
333.15	1.634	2.757	4.054	5.706	7.164	8.762	10.902	18.933	38.862
343.15	1.953	3.280	4.792	6.770	8.568	10.608	13.585	23.085	43.575
353.15	2.297	3.849	5.587	7.907	10.110	12.660	16.464	27.039	–
363.15	2.666	4.406	6.439	9.105	11.791	14.919	19.429	30.832	–
X ₁									
T/K	0.212	0.351	0.39	0.453	0.619	0.654	0.701	0.751	0.802
CO ₂ (1)+[C ₅ mim][Tf ₂ N] (2)									
298.15	0.702	1.483	1.718	2.143	3.872	4.429	5.205	8.065	29.980
303.15	0.807	1.664	1.905	2.393	4.352	5.005	5.937	10.577	32.753
313.15	1.028	2.050	2.341	2.938	5.445	6.343	7.723	15.399	38.148
323.15	1.266	2.465	2.817	3.540	6.701	7.919	10.281	19.950	43.205
333.15	1.520	2.912	3.345	4.195	8.103	9.717	13.185	24.231	47.993
343.15	1.792	3.388	3.895	4.899	9.635	11.724	16.461	28.241	52.435
353.15	2.080	3.895	4.447	5.647	11.280	13.925	19.720	31.981	56.153

363 K were found to be thermodynamically consistent. A comparison between our data and the data reported by Schilderman et al. [25] showed a good agreement. Moreover, as will be shown below, the data here measured was found to be essentially thermodynamic consistent.

The solubility of carbon dioxide in the studied ILs was measured for mole fractions from (0.2 to 0.8), in the temperature range (293–363) K and pressures from (0.6 to 50) MPa, as reported in Tables 3 and 4 and depicted in Fig. 2a and b. The temperature increase leads to an increase on the equilibrium pressure and by increasing CO₂ concentration, the equilibrium pressures increase gradually, at first, and rapidly for higher CO₂ contents.

Due to the presence of fluoroalkyl groups, Tf₂N anion-based ILs, are “CO₂-philic”, meaning that they present higher CO₂ solubilities than other ILs resulting in lower equilibrium pressures for high CO₂ mole fractions, as can be seen in Fig. 2. This behavior, yet poorly understood, seems to be related to the interaction between the negative fluorine atoms and the positive charge on the carbon of the CO₂ molecule [21,22].

It is known that the substituents on the imidazolium ring can affect the ILs properties [23,24,44,47,54–57]. For CO₂, a slight increase on solubility can be observed with the alkyl chain length at all pressures as shown in Fig. 3 [11,21,23,25]. Nonetheless, in the Tf₂N-based ILs, the alkyl chain length on the imidazolium ring seem to have a lower influence on the solubility than other IL families, even for higher CO₂ concentrations [21,25]. Kazarian et al. [58], using ATR-IR spectroscopy, suggested that the increase in solubility is not related to any specific interactions between the CO₂ and the cation. Shariati et al. [23] and Aki et al. [21]

Table 2
Properties of the substances used in the modeling.

Compound	T _c /K	p _c /MPa	ω	r	q
CO ₂	304.21 ^a	7.38 ^a	0.2236 ^a	3.26 ^c	2.38 ^c
[C ₂ mim][Tf ₂ N]	1214.22 ^b	3.37 ^b	0.2818 ^b	28.77 ^c	18.16 ^c
[C ₅ mim][Tf ₂ N]	1249.43 ^b	2.63 ^b	0.4123 ^b	34.23 ^c	21.84 ^c

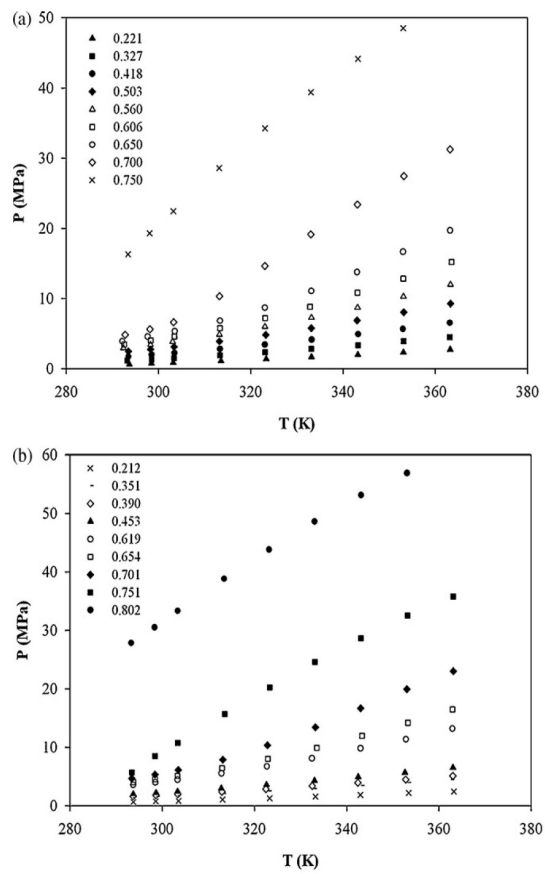
^a [61].^b [62].^c [38].

Fig. 2. Pressure–temperature diagram of the binary systems (a) CO₂+[C₅mim][Tf₂N] and (b) CO₂+[C₂mim][Tf₂N].

Table 3
Bubble point data for the system CO_2 (1)+[C₂mim][Tf₂N] (2).

x_1	T/K	p/MPa												
0.221	293.65	0.620	0.327	293.24	1.130	0.418	293.50	1.688	0.503	293.50	2.398	0.560	292.41	2.879
0.221	298.52	0.725	0.327	298.50	1.295	0.418	298.55	1.945	0.503	298.29	2.706	0.560	298.24	3.351
0.221	303.25	0.837	0.327	303.41	1.462	0.418	303.48	2.185	0.503	303.41	3.076	0.560	303.11	3.778
0.221	313.59	1.083	0.327	313.32	1.868	0.418	313.32	2.745	0.503	313.24	3.845	0.560	313.22	4.780
0.221	323.39	1.345	0.327	323.13	2.292	0.418	323.10	3.365	0.503	323.27	4.725	0.560	323.07	5.883
0.221	333.15	1.645	0.327	333.17	2.758	0.418	333.23	4.054	0.503	333.16	5.708	0.560	333.16	7.173
0.221	343.25	1.957	0.327	343.27	3.287	0.418	343.30	4.836	0.503	343.11	6.769	0.560	343.19	8.569
0.221	353.10	2.276	0.327	353.16	3.850	0.418	353.02	5.565	0.503	353.18	7.912	0.560	353.14	10.115
0.221	363.23	2.680	0.327	363.19	4.408	0.418	363.17	6.436	0.503	363.35	9.128	0.560	363.34	11.821
x_1	T/K	p/MPa												
0.606	292.60	3.387	0.650	292.16	3.825	0.700	292.82	4.736	0.750	293.44	16.076			
0.606	298.29	3.942	0.650	297.70	4.485	0.700	298.15	5.520	0.750	298.09	19.048			
0.606	303.46	4.506	0.650	303.54	5.230	0.700	303.30	6.535	0.750	303.26	22.130			
0.606	313.30	5.686	0.650	313.35	6.715	0.700	313.24	10.180	0.750	313.19	28.187			
0.606	323.11	7.103	0.650	323.10	8.550	0.700	323.09	14.450	0.750	323.14	33.787			
0.606	332.88	8.695	0.650	333.16	10.905	0.700	333.04	18.885	0.750	333.08	38.898			
0.606	343.13	10.649	0.650	343.08	13.565	0.700	343.15	23.085	0.750	343.29	43.565			
0.606	353.07	12.650	0.650	353.05	16.435	0.700	353.22	27.066	0.750	353.08	47.850			
0.606	363.55	14.996	0.650	363.22	19.450	0.700	363.22	30.858						

Table 4
Bubble point data the system CO_2 (1)+[C₅mim][Tf₂N] (2).

x_1	T/K	p/MPa												
0.212	298.65	0.720	0.351	298.77	1.517	0.390	298.65	1.736	0.453	298.70	2.152	0.619	298.55	3.915
0.212	303.61	0.799	0.351	303.34	1.675	0.390	303.39	1.915	0.453	303.38	2.395	0.619	303.33	4.360
0.212	313.15	1.044	0.351	313.21	2.031	0.390	312.99	2.334	0.453	312.85	2.927	0.619	312.90	5.426
0.212	323.35	1.252	0.351	323.05	2.468	0.390	322.52	2.785	0.453	322.62	3.512	0.619	322.72	6.645
0.212	333.25	1.525	0.351	332.85	2.894	0.390	332.54	3.312	0.453	333.07	4.218	0.619	332.50	7.984
0.212	343.00	1.780	0.351	343.19	3.398	0.390	342.47	3.858	0.453	342.53	4.839	0.619	343.04	9.650
0.212	353.49	2.124	0.351	353.26	3.907	0.390	352.85	4.430	0.453	352.65	5.598	0.619	352.86	11.212
0.212	363.29	2.370	0.351	362.68	4.400	0.390	363.05	5.050	0.453	363.05	6.430	0.619	362.95	12.990
0.212	293.75	0.618	0.351	293.65	1.322	0.390	293.73	1.564	0.453	293.75	1.943	0.619	293.75	3.486
x_1	T/K	p/MPa												
0.654	298.47	4.460	0.701	298.45	5.245	0.751	298.42	8.365	0.802	298.37	30.098			
0.654	303.32	5.030	0.701	303.49	5.990	0.751	303.38	10.625	0.802	303.38	32.881			
0.654	313.00	6.344	0.701	313.19	7.732	0.751	313.57	15.435	0.802	313.30	27.460			
0.654	322.96	7.870	0.701	322.85	10.198	0.751	323.34	19.995	0.802	313.44	38.299			
0.654	333.56	9.778	0.701	333.28	13.225	0.751	333.11	24.280	0.802	323.19	43.225			
0.654	343.37	11.776	0.701	343.08	16.438	0.751	343.05	28.266	0.802	333.08	47.960			
0.654	353.30	13.980	0.701	353.06	19.692	0.751	353.20	32.086	0.802	343.14	52.431			
0.654	362.95	16.246	0.701	363.12	22.730	0.751	363.11	35.340	0.802	353.13	56.146			
0.654	293.76	3.974	0.701	293.43	4.617	0.751	293.42	5.609	0.802	363.29	59.805			

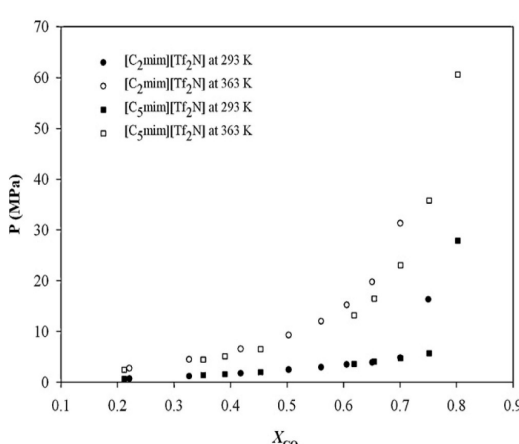


Fig. 3. Pressure–composition diagram of CO_2 in $[\text{C}_n\text{mim}][\text{Tf}_2\text{N}]$.

explained this phenomenon based on entropic rather enthalpic considerations, due to the decrease of the compounds densities with the increase of the alkyl chain length leading to a greater free volume.

The results of the application of the thermodynamic consistency test to the binary systems containing ionic liquid is presented in Table 5. In this table, NP is the number of data points, T is the temperature, k_{12} , A_{12} and A_{21} are the interaction parameters of the model, where 1 stands for the CO_2 and 2 for the ionic liquid. This table is divided in sections for each system studied. The consistency analyses for the $\text{CO}_2 + [\text{C}_2\text{mim}][\text{Tf}_2\text{N}]$ system measured by Schilderman et al. [25] at 363.15 K are also reported here.

Some detailed results are shown in Tables 6–8. These tables are divided in two parts, the upper part shows the original data set, while the lower part shows the remaining data after removing some experimental points that have been found to be thermodynamically inconsistent. Table 6 also includes the detailed results for the system $\text{CO}_2 + [\text{C}_2\text{mim}][\text{Tf}_2\text{N}]$ at 363.15 K by Schilderman et al. [25]. These data have deviations within the established limit values of ΔA_i , being thermodynamically consistent. In Table 7, where

Table 5
Results of the consistency test.

Reference	NP	T/K	k_{12}	$A_{12}/\text{kJ kmol}^{-1}$	$A_{21}/\text{kJ kmol}^{-1}$	$ \Delta p /\%$	Result
$\text{CO}_2 + [\text{C}_2\text{mim}][\text{Tf}_2\text{N}]$							
[17]	8	363.15	-0.1904	3767.474	-1202.621	0.7	TC
	4	293.15	-0.222	49988.291	-1791.751	0.5	TC
	9	298.15	0.0057	20355.366	-2001.440	2.4	NFC/TC
	9	303.15	-0.0090	8795.384	-1923.852	2.0	NFC/TC
	9	313.15	0.0204	5854.406	-1747.716	1.1	NFC/TC
[This work]	9	323.15	0.0108	4879.271	-1604.227	1.0	NFC/TC
	9	333.15	0.0038	4323.089	-1491.756	1.4	NFC/TC
	9	343.15	-0.0077	3830.967	-1359.963	1.6	NFC/TC
	8	353.15	-0.1468	3458.742	-1158.891	0.5	TC
	8	363.15	-0.1317	3048.107	-1016.976	0.8	TC
$\text{CO}_2 + [\text{C}_5\text{mim}][\text{Tf}_2\text{N}]$							
[This work]	9	298.15	0.0639	2642.548	-854.215	1.6	NFC/TC
	9	303.15	0.0606	2477.849	-773.810	1.5	NFC/TC
	9	313.15	0.0489	2232.933	-637.261	1.9	NFC/TC
	9	323.15	0.0364	2057.406	-528.352	2.4	NFC/TC
	9	333.15	0.0247	1907.507	-429.010	2.8	NFC/TC
	9	343.15	0.0195	1805.985	-356.494	2.9	NFC/TC
	9	353.15	0.0172	1728.749	-298.579	3.0	TI

Table 6
Detailed results for CO_2 (1)+[C₂mim][Tf₂N] (2) at 298.15 K.

A_p	A_ϕ	$\% \Delta A_i$	p^{exp}	p^{cal}	$\% \Delta p$	y_1^{cal}	y_2^{cal}	x_1
(8 data points) $k_{12} = -0.1904$, $A_{12} = 3767.474$, $A_{21} = -1202.621$, $ \Delta p (\%) = 0.7$								
10865327.5	10387930.5	-4.4	1.303	1.317	1.1	1.0000	0.0000	0.1230
5441391.3	5567544.7	2.3	2.543	2.514	-1.1	1.0000	0.0000	0.2120
2379790.2	2291077.1	-3.7	4.036	4.044	0.2	1.0000	0.0000	0.3030
701940.6	703925.0	0.3	6.023	5.988	-0.6	1.0000	0.0000	0.3920
78335.4	73487.2	-6.2	8.569	8.602	0.4	1.0000	0.0000	0.4790
31674.7	32701.5	3.2	10.258	10.213	-0.4	1.0000	0.0000	0.5190
4092.1	3503.8	-14.4	12.832	12.973	1.1	1.0000	0.0000	0.5700
-	-	-	14.770	14.676	-0.6	0.9999	0.0001	0.5930

detailed results at 298.15 K for the system $\text{CO}_2 + [\text{C}_2\text{mim}][\text{Tf}_2\text{N}]$ are presented, the upper part shows that these data have deviations in the final values of ΔA_i (bold and italic type) outside the established limits; the lower part shows that when the highest area deviation is eliminated, the deviations for the remaining eight points are within the defined limits of $\pm 20\%$. Therefore, although the original data set with nine data points is not fully thermodynamically consistent, the new set with the remaining eight points is thermodynamically consistent; however, the $x_{\text{CO}_2} = 0.606$ point has a good probability to be inconsistent, because two $\Delta P_i < 5$ yields $\Delta A_i > 10$.

The same procedure is applied for the data of the system $\text{CO}_2 + [\text{C}_5\text{mim}][\text{Tf}_2\text{N}]$, at 298.15, reported in Table 8. Again, although the original data are not fully consistent, the remaining eight points, after removing one data point, are within the defined limits of -20% to $+20\%$, which are thermodynamically consistent. Detailed results for all systems are shown in [Supplementary Information](#). These results show that the $\text{CO}_2 + [\text{C}_2\text{mim}][\text{Tf}_2\text{N}]$ system has greater deviations in the isopleths at $x_1 = 0.75$, while the $\text{CO}_2 + [\text{C}_5\text{mim}][\text{Tf}_2\text{N}]$ system has greater deviations in the isopleths at $x_1 = 0.751$ and $x_1 = 0.802$. Therefore, the isotherms with these compositions are not fully consistent.

Table 7
Detailed results for CO_2 (1)+[C₂mim][Tf₂N] (2) at 298.15 K.

A_p	A_ϕ	$\% \Delta A_i$	p^{exp}	p^{cal}	$\% \Delta p$	y_1^{cal}	y_2^{cal}	x_1
(9 data points) $k_{12} = 0.0057$, $A_{12} = 20355.366$, $A_{21} = -2001.440$, $ \Delta p (\%) = 2.4$								
5.81E+09	5.23E+09	-9.9	0.718	0.763	6.3	1.0000	0.0000	0.221
4.34E+09	4.09E+09	-5.7	1.284	1.294	0.8	1.0000	0.0000	0.327
3.48E+09	3.30E+09	-5.2	1.915	1.889	-1.4	1.0000	0.0000	0.418
1.80E+09	1.82E+09	0.6	2.699	2.619	-3.0	1.0000	0.0000	0.503
1.09E+09	1.21E+09	10.3	3.342	3.248	-2.8	1.0000	0.0000	0.560
7.81E+08	9.40E+08	20.3	3.922	3.874	-1.2	1.0000	0.0000	0.606
7.69E+08	8.71E+08	13.4	4.540	4.618	1.7	1.0000	0.0000	0.650
3.56E+14	2.17E+15	511.2	5.520	5.759	4.3	1.0000	0.0000	0.700
-	-	-	19.065	18.939	-0.7	1.0000	0.0000	0.750
(8 data points) $k_{12} = 0.2655$, $A_{12} = 2013.583$, $A_{21} = -993.493$, $ \Delta p (\%) = 2.4$								
7.39E+09	6.72E+09	-9.2	0.718	0.754	5.0	1.0000	0.0000	0.221
6.19E+09	5.88E+09	-5.0	1.284	1.283	-0.1	1.0000	0.0000	0.327
5.45E+09	5.20E+09	-4.5	1.915	1.877	-1.9	1.0000	0.0000	0.418
2.99E+09	3.01E+09	0.9	2.699	2.609	-3.4	1.0000	0.0000	0.503
1.79E+09	1.97E+09	10.0	3.342	3.237	-3.1	1.0000	0.0000	0.560
1.16E+09	1.38E+09	18.8	3.922	3.859	-1.6	1.0000	0.0000	0.606
8.25E+08	9.02E+08	9.3	4.540	4.589	1.1	1.0000	0.0000	0.650
-	-	-	5.520	5.673	2.8	1.0000	0.0000	0.700

Table 8
Detailed results for CO_2 (1)+[C₅mim][Tf₂N] (2) at 298.15 K.

A_P	A_ϕ	% ΔA_i	p^{exp}	p^{cal}	% Δp	y_1^{cal}	y_2^{cal}	x_1
(9 data points) $k_{12} = 0.0639$, $A_{12} = 2642.548$, $A_{21} = -854.215$, $ \Delta p (\%) = 1.6$								
1.11E+12	9.85E+11	-11.3	0.702	0.728	3.7	1.0000	0.0000	0.212
1.96E+11	2.12E+11	8.0	1.483	1.431	-3.5	1.0000	0.0000	0.351
2.57E+11	2.82E+11	9.7	1.718	1.677	-2.4	1.0000	0.0000	0.390
4.55E+11	4.62E+11	1.5	2.143	2.137	-0.3	1.0000	0.0000	0.453
2.23E+10	2.14E+10	-3.8	3.872	3.911	1.0	1.0000	0.0000	0.619
1.13E+10	1.30E+10	14.2	4.429	4.452	0.5	1.0000	0.0000	0.654
6.92E+09	7.76E+09	12.2	5.205	5.344	2.7	1.0000	0.0000	0.701
5.54E+04	2.71E+04	-51.0	8.065	8.036	-0.4	1.0000	0.0000	0.751
-	-	-	29.980	29.988	0.0	0.9999	0.0001	0.802
(8 data points) $k_{12} = -0.1037$, $A_{12} = 4558.106$, $A_{21} = -1265.823$, $ \Delta p (\%) = 1.5$								
8.94E+11	7.86E+11	-12.1	0.702	0.733	4.3	1.0000	0.0000	0.212
1.37E+11	1.47E+11	7.3	1.483	1.435	-3.2	1.0000	0.0000	0.351
1.67E+11	1.82E+11	8.8	1.718	1.680	-2.2	1.0000	0.0000	0.390
2.67E+11	2.67E+11	0.0	2.143	2.136	-0.3	1.0000	0.0000	0.453
8.66E+09	8.21E+09	-5.1	3.872	3.884	0.3	1.0000	0.0000	0.619
3.92E+09	4.42E+09	12.6	4.429	4.415	-0.3	1.0000	0.0000	0.654
2.03E+09	2.37E+09	16.5	5.205	5.286	1.6	1.0000	0.0000	0.701
-	-	-	8.065	8.061	-0.1	1.0000	0.0000	0.751

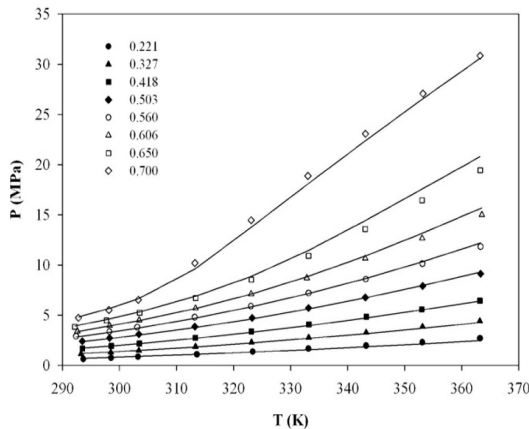


Fig. 4. PT diagram and modeling for the system CO_2 +[C₂mim][Tf₂N].

In Figs. 4 and 5 the description of the experimental data using the model detailed above and the parameters reported in Tables 1 and 9 for the CO_2 +[C₂mim][Tf₂N] and CO_2 +[C₅mim][Tf₂N] systems is presented. As can be seen, using the proposed approach it is possible to obtain a very good description of the experimental data measured in this work.

The Henry's law relates the amount of a given gas dissolved in a given type and the amount of liquid, at a constant temperature, to the fugacity of that gas in equilibrium with that liquid and can be described as

$$H_{12}(T, P) = \lim_{x_1 \rightarrow 0} \frac{f_i^L}{x_1} \quad (8)$$

where $H_{12}(T, P)$ is the Henry's constant, x_1 is the mole fraction of gas dissolved in the liquid phase, and f_i^L is the fugacity of gas in the liquid phase. As shown, Eq. (8) is only rigorously valid in the diluted

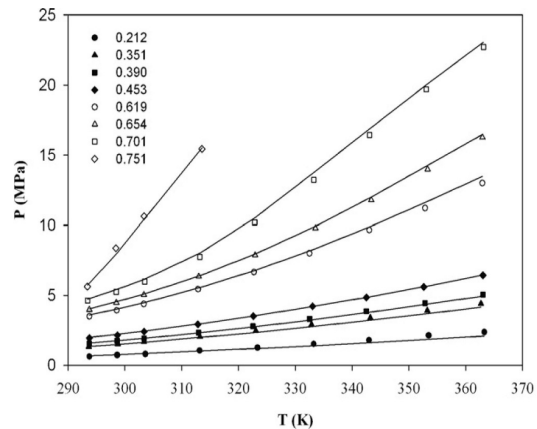


Fig. 5. PT diagram and modeling for the system CO_2 +[C₅mim][Tf₂N].

region limit. The Henry's constant for the CO_2 in the ILs investigated, were estimated by fitting the PR-WS/UNIQUAC model to the data and calculating the limiting slope as the solubility approaches zero.

The results are shown in Table 10, where, $|\Delta P|$ is average absolute deviations for pressure and H_{12} is the Henry's constant calculated. For one additional validation of the calculated Henry's constant for the CO_2 +[C₂mim][Tf₂N] binary system, Henry's constant at 298.15 K and 3.56 MPa, taken from Schilderman et al. [25], was included showing good agreement with linear tendency obtained in this work. The results indicate that Henry's constant decreases slightly (i.e., CO_2 solubility increases) as the length of the carbon chain on the imidazolium ring increases.

The results for the Henry's constant of CO_2 in [C₂mim][Tf₂N] (where the calculated value 3.56 MPa at 298.15 K was included [25]) and CO_2 in [C₅mim][Tf₂N] were correlated as a function of temper-

Table 9
Estimated independent-temperature interaction parameters for the CO_2 (1)+ILs(2) systems.

System	NP	x_1	k_{12}	$A_{12}/\text{kJ kmol}^{-1}$	$A_{21}/\text{kJ kmol}^{-1}$	$ \Delta p (\%)$	Max y_2^a
CO_2 +[C ₂ mim][Tf ₂ N]	72	0.221–0.700	0.1061	4224.889	-1556.505	2.8	5.5
CO_2 +[C ₅ mim][Tf ₂ N]	63	0.212–0.751	0.0113	2613.005	-785.272	3.0	11.8

^a These values are expressed as $y_2 \times 10^5$.

Table 10

Interaction parameter for the model and Henry's constant of CO₂ (1)+ ionic liquids (2).

T/K	$ \Delta p /\%$	H_{12}/MPa
CO ₂ + [C ₂ mim][Tf ₂ N] $k_{ij} = 0.0077$, $A_{12} = 2284.160$, $A_{21} = -723.030$		
313.15	0.7	4.66
323.15	0.7	5.50
333.15	0.7	6.40
343.15	0.8	7.36
353.15	0.8	8.37
363.15	0.8	9.43
CO ₂ + [C ₅ mim][Tf ₂ N] $k_{ij} = 0.0113$, $A_{12} = 2613.005$, $A_{21} = -785.272$		
298.15	2.7	2.88
303.15	2.1	3.18
313.15	1.8	3.81
323.15	2.6	4.49
333.15	3.3	5.24
343.15	3.8	6.03

Table 11

Coefficients A, B and C obtained for CO₂ (1)+ ionic liquids (2).

Ionic liquid (%)	A	B	C	$ \Delta H_{12} $
[C ₂ mim][Tf ₂ N]	-153854.908	-685.377	5.298	0.1
[C ₅ mim][Tf ₂ N]	-189365.718	-488.274	4.827	0.04

ature by an empirical equation of the type:

$$\ln(H_{12}) = A \left(\frac{1}{T} \right)^{(2)} + B \left(\frac{1}{T} \right) + C \quad (9)$$

where, the coefficients A, B and C obtained are listed in Table 11, together with the Henry's constant average absolute deviations, $|\Delta H_{12}|$, obtained for each ionic liquid. The average deviation of 0.1% and a maximum deviation of 0.1% for [C₂mim][Tf₂N] and an average deviation of 0.04% and a maximum deviation of 0.04% for [C₅mim][Tf₂N] were obtained.

The effect of temperature on CO₂ solubility can be related to the partial molar entropy and partial molar enthalpy of solution [59] and can be calculated from an appropriate correlation of Henry's constant:

$$\Delta_{\text{sol}}H = R \left(\frac{\partial \ln(H_{12})}{\partial (1/T)} \right)_P \quad (10)$$

$$\Delta_{\text{sol}}S = -R \left(\frac{\partial \ln(H_{12})}{\partial (1/T)} \right)_P \quad (11)$$

Table 12

Thermodynamic functions of solvation for CO₂ (1)+ ionic liquids (2) at several temperatures.

T/K	$\Delta_{\text{sol}}H/\text{J mol}^{-1}$	$T\Delta_{\text{sol}}S/(\text{J}(\text{mol}^{-1}))$
[C ₂ mim][Tf ₂ N]		
298.15	-14279.3	-14162.1
303.15	-14137.8	-14096.5
313.15	-13868.3	-13872.5
323.15	-13615.5	-13669.2
333.15	-13377.8	-13425.9
343.15	-13154.0	-13177.0
353.15	-12942.9	-12890.0
363.15	-12743.4	-12601.3
[C ₅ mim][Tf ₂ N]		
298.15	-14621.1	-14549.7
303.15	-14446.9	-14429.9
313.15	-14115.2	-14123.1
323.15	-13804.0	-13830.8
333.15	-13511.5	-13492.6
343.15	-13236.1	-13142.6

The partial molar enthalpy of gas dissolution gives an indication of the strength of interactions between the gas and IL, while the partial molar entropy illustrates the amount of ordering present in the gas/IL mixture. The partial molar enthalpy values obtained are similar to those reported by Brennecke's group [21,33] and the magnitude consistent with physical absorption. The results in Table 12 show that although the partial molar enthalpy is slightly higher than the product of the temperature and the partial molar entropy they are of similar magnitude indicating that the solubility of CO₂ in ILs is not entropically driven, as suggested by some authors [22,28,60], neither essentially an enthalpic phenomena, as suggested by others [18,31], but both phenomena control the solubility of CO₂ in ILs.

5. Conclusions

A high pressure cell to measure supercritical fluid+liquid phase behavior was developed and new experimental data for CO₂ solubility in 1-ethyl-1-methyl-imidazolium bis(trifluoromethylsulfonyl)imide and 3-methyl-1-pentyl-imidazolium bis(trifluoromethylsulfonyl)imide in a wide range of temperature, pressure and carbon dioxide mole fractions are reported.

A thermodynamic consistency test based on the Peng–Robinson EoS with the Wong–Sandler/UNIQUAC mixing rule was applied to the measured data showing that they are thermodynamically consistent. The model allows a good description of the experimental data and the estimation of the Henry's constant for these systems. The partial molar enthalpies and the product of the temperature and the partial molar entropies for these systems are of similar magnitude what allows to conclude that this solubility is not driven predominantly by entropic or enthalpic phenomena, as previously admitted by various authors.

Acknowledgments

The authors are thankful for financial support from Fundação para a Ciência e a Tecnologia (Project POCI/EQU/58152/2004) and Ph.D. grant (SFRH/BD/41562/2007) of Pedro J. Carvalho. The authors would like to acknowledge FAPESP (Fundação de Amparo à Pesquisa do Estado de São Paulo), process # 2006/03711-1.

Appendix A. Supplementary data

Supplementary data associated with this article can be found, in the online version, at doi:10.1016/j.supflu.2008.10.012.

References

- J.A. Boon, J.A. Levinsky, J.L. Pfug, J.S. Wilkes, Friedel–Crafts reactions in ambient-temperature molten salts, *J. Org. Chem.* 51 (1986) 480–483.
- S.E. Fry, N.J. Pienta, Effects of molten salts on reactions. Nucleophilic aromatic substitution by halide ions in molten dodecytetrabutylphosphonium salts, *JACS* 107 (1985) 6399–6400.
- H. Zhao, Innovative applications of ionic liquids as green engineering liquids, *Chem. Eng. Commun.* 193 (2006) 1660–1677.
- R. Sheldon, Catalytic reactions in ionic liquids, *Chem. Commun.* (2001) 2399–2407.
- H. Wong, S. Han, A.G. Livingston, The effect of ionic liquids on product yield and catalyst stability, *Chem. Eng. Sci.* 61 (2006) 1338–1341.
- E. Bates, R. Mayton, I. Ntaï, J. Davis, CO₂ capture by a task-specific ionic liquid, *JACS* 124 (2002) 926–927.
- J.L. Anthony, E.J. Maginn, J.F. Brennecke, Solution thermodynamics of imidazolium-based ionic liquids and water, *J. Phys. Chem. B* 105 (2001) 10942–10949.
- J.G. Huddleston, H.D. Willauer, R.P. Swatloski, A.E. Visser, R.D. Rogers, Room temperature ionic liquids as novel media for clean liquid–liquid extraction, *Chem. Commun.* 16 (1998) 1765–1766.

- [9] L. Blanchard, J. Brennecke, Recovery of organic products from ionic liquids using supercritical carbon dioxide, *Ind. Eng. Chem. Res.* 40 (2001) 287–292.
- [10] L.A. Blanchard, D. Hancu, E.J. Beckman, J.F. Brennecke, Green processing using ionic liquids and CO₂, *Nature* 399 (1999) 28–29.
- [11] L. Blanchard, Z. Gu, J. Brennecke, High-pressure phase behavior of ionic liquid/CO₂ systems, *J. Phys. Chem. B* 105 (2001) 2437–2444.
- [12] A. Scurto, S. Aki, J. Brennecke, CO₂ as a separation switch for ionic liquid/organic mixtures, *JACS* 124 (2002) 10276–10277.
- [13] A.M. Scurto, S.N.V.K. Aki, J.F. Brennecke, Carbon dioxide induced separation of ionic liquids and water, *Chem. Commun.* (2003) 572–573.
- [14] X. Yuan, S. Zhang, J. Liu, X. Lu, Solubilities of CO₂ in hydroxyl ammonium ionic liquids at elevated pressures, *Fluid Phase Equilib.* 257 (2007) 195–200.
- [15] J. Sun, S. Zhang, W. Cheng, J. Ren, Hydroxyl-functionalized ionic liquid: a novel efficient catalyst for chemical fixation of CO₂ to cyclic carbonate, *Tetrahedron Lett.* 49 (2008) 3588–3591.
- [16] G. Yu, S. Zhang, X. Yao, J. Zhang, K. Dong, W. Dai, R. Mori, Design of task-specific ionic liquids for capturing CO₂: a molecular orbital study, *Ind. Eng. Chem. Res.* 45 (2006) 2875–2880.
- [17] J. Huang, A. Riisager, R.W. Berg, R. Fehrmann, Tuning ionic liquids for high gas solubility and reversible gas sorption, *J. Mol. Catal. A: Chem.* 279 (2008) 170–176.
- [18] M. Muldoon, S. Aki, J. Anderson, J. Dixon, J. Brennecke, Improving carbon dioxide solubility in ionic liquids, *J. Phys. Chem. B* 111 (2007) 9001–9009.
- [19] Z. Lopez-Castillo, S. Aki, M. Stadther, J. Brennecke, Enhanced solubility of hydrogen in CO₂-expanded liquids, *Ind. Eng. Chem. Res.* 47 (2008) 570–576.
- [20] M. Solinas, A. Pfaltz, P. Cozzi, W. Leitner, Enantioselective hydrogenation of imines in ionic liquid/carbon dioxide media, *JACS* 126 (2004) 16142–16147.
- [21] S.N.V.K. Aki, B.R. Mellein, E.M. Saurer, J.F. Brennecke, High-pressure phase behavior of carbon dioxide with imidazolium-based ionic liquids, *J. Phys. Chem. B* 108 (2004) 20355–20365.
- [22] J.L. Anderson, J.K. Dixon, J.F. Brennecke, Solubility of CO₂, CH₄, C₂H₆, C₂H₄, O₂, and N₂ in 1-hexyl-3-methylpyridinium bis(trifluoromethylsulfonyl)imide: comparison to other ionic liquids, *Acc. Chem. Res.* 40 (11) (2007) 1208–1216.
- [23] A. Shariati, C.J. Peters, High-pressure phase behavior of systems with ionic liquids. II. The binary system carbon dioxide + 1-ethyl-3-methylimidazolium hexafluorophosphate, *J. Supercrit. Fluids* 29 (2004) 43–48.
- [24] A. Shariati, C.J. Peters, High-pressure phase behavior of systems with ionic liquids. Part III. The binary system carbon dioxide + 1-hexyl-3-methylimidazolium hexafluorophosphate, *J. Supercrit. Fluids* 30 (2004) 139–144.
- [25] A.M. Schilderman, S. Raeissi, C.J. Peters, Solubility of carbon dioxide in the ionic liquid 1-ethyl-3-methylimidazolium bis(trifluoromethylsulfonyl)imide, *Fluid Phase Equilibr.* 260 (2007) 19–22.
- [26] A. Finotello, J. Bara, D. Camper, R. Noble, Room-temperature ionic liquids: temperature dependence of gas solubility selectivity, *Ind. Eng. Chem. Res.* 47 (2008) 3453–3459.
- [27] E. Shin, B. Lee, J.S. Lim, High-pressure solubilities of carbon dioxide in ionic liquids: 1-alkyl-3-methylimidazolium bis(trifluoromethylsulfonyl)imide, *J. Supercrit. Fluids* 45 (2008) 282–292.
- [28] Y. Hou, R. Baltus, Experimental measurement of the solubility and diffusivity of CO₂ in room-temperature ionic liquids using a transient thin-liquid-film method, *Ind. Eng. Chem. Res.* 46 (2007) 8166–8175.
- [29] B. Lee, S. Outcal, Solubilities of gases in the ionic liquid 1-n-butyl-3-methylimidazolium bis(trifluoromethylsulfonyl)imide, *J. Chem. Eng. Data* 51 (2006) 892–897.
- [30] M. Shiflett, A. Yokozeki, Solubility of CO₂ in room temperature ionic liquid [hmim][Tf₂N], *J. Phys. Chem. B* 111 (2007) 2070–2074.
- [31] J. Jacquemin, M.F. Costa Gomes, P. Husson, V. Majer, Solubility of carbon dioxide, ethane, methane, oxygen, nitrogen, hydrogen, argon, and carbon monoxide in 1-butyl-3-methylimidazolium tetrafluoroborate between temperatures 283 K and 343 K and at pressures close to atmospheric, *J. Chem. Thermodyn.* 38 (2006) 490–502.
- [32] M. Kanakubo, T. Umecky, Y. Hiejima, T. Aizawa, H. Nanjo, Y. Kameda, Solution structures of 1-butyl-3-methylimidazolium hexafluorophosphate ionic liquid saturated with CO₂: experimental evidence of specific anion–CO₂ interaction, *J. Phys. Chem. B* 109 (2005) 13847–13850.
- [33] J. Anthony, J. Anderson, E. Maginn, J. Brennecke, Anion effects on gas solubility in ionic liquids, *J. Phys. Chem. B* 109 (2005) 6366–6374.
- [34] C. Cadena, J. Anthony, J. Shah, T. Morrow, J. Brennecke, E. Maginn, Why is CO₂ so soluble in imidazolium-based ionic liquids? *JACS* 126 (2004) 5300–5308.
- [35] K. Gutkowski, A. Shariati, C. Peters, High-pressure phase behavior of the binary ionic liquid system 1-octyl-3-methylimidazolium tetrafluoroborate + carbon dioxide, *J. Supercrit. Fluids* 39 (2006) 187–191.
- [36] A. Shariati, C.J. Peters, High-pressure phase equilibria of systems with ionic liquids, *J. Supercrit. Fluids* 34 (2005) 171–176.
- [37] J. Anthony, E. Maginn, J. Brennecke, Solubilities and thermodynamic properties of gases in the ionic liquid 1-n-butyl-3-methylimidazolium hexafluorophosphate, *J. Phys. Chem. B* 106 (2002) 7315–7320.
- [38] V.H. Álvarez, M. Aznar, Thermodynamic modeling of vapor–liquid equilibrium of binary systems ionic liquid + supercritical {CO₂ or CHF₃} and ionic liquid + hydrocarbons using Peng–Robinson equation of state, *J. Chin. Inst. Chem. Eng.* 39 (2008) 353–360.
- [39] José O. Valderrama, V.H. Álvarez, A versatile thermodynamic consistency test for incomplete phase equilibrium data of high-pressure gas–liquid mixtures, *Fluid Phase Equilib.* 226 (2004) 149–159.
- [40] D. Peng, D.B. Robinson, A new two-constant equation of state, *Ind. Eng. Chem. Fundam.* 15 (1976) 59–64.
- [41] D.S.H. Wong, S.I. Sandler, A theoretically correct mixing rule for cubic equations of state, *AIChE J.* 38 (1992) 671–680.
- [42] D.S. Abrams, J.M. Prausnitz, Statistical thermodynamics of liquid mixtures: a new expression for the excess Gibbs energy of partly or completely miscible systems, *AIChE J.* 21 (1975) 116–128.
- [43] V. Álvarez, M. Aznar, Application of a thermodynamic consistency test to binary mixtures containing an ionic liquid, *Open Thermodyn. J.* 2 (2008) 25–38.
- [44] M.G. Freire, P.J. Carvalho, A.M. Fernandes, I.M. Marrucho, A.J. Queimada, J.A. Coutinho, Surface tensions of imidazolium based ionic liquids: anion, cation, temperature and water effect, *J. Colloid Interface Sci.* 314 (2) (2007) 621–630.
- [45] K.R. Seddon, A. Stark, M. Torres, Influence of chloride, water, and organic solvents on the physical properties of ionic liquids, *Pure Appl. Chem.* 72 (12) (2000) 2275–2287.
- [46] J.G. Huddleston, A.E. Visser, W.M. Reichert, H.D. Willauer, G.A. Broker, R.D. Rogers, Characterization and comparison of hydrophilic and hydrophobic room temperature ionic liquids incorporating the imidazolium cation, *Green Chem.* 3 (2001) 156–164.
- [47] R.L. Gardas, M.G. Freire, P.J. Carvalho, I.M. Marrucho, I.M.A. Fonseca, A.G.M. Ferreira, J.A.P. Coutinho, High pressure densities and derived thermodynamic properties of imidazolium based ionic liquids, *J. Chem. Eng. Data* 52 (1) (2007) 80–88.
- [48] S. Vitu, J.N. Jaubert, J. Pauly, J.L. Daridon, D. Barth, Phase equilibria measurements of CO₂ + methyl cyclopentane and CO₂ + isopropyl cyclohexane binary mixtures at elevated pressures, *J. Supercrit. Fluids* 44 (2008) 155–163.
- [49] J. Pauly, J. Coutinho, J.L. Daridon, High pressure phase equilibria in methane + waxy systems. I. methane + heptadecane, *Fluid Phase Equilibr.* 255 (2007) 193–199.
- [50] S.P.M. Ventura, J. Pauly, J.L. Daridon, J.A.L. da Silva, I.M. Marrucho, A.M.A. Dias, J.A.P. Coutinho, High pressure solubility data of carbon dioxide in tri-isobutyl(methyl)phosphonium tosylate–water systems, *J. Chem. Thermodyn.* 40 (2008) 1187–1192.
- [51] A.M.A. Dias, H. Carrier, J.L. Daridon, J.C. Pamies, L.F. Vega, J.A.P. Coutinho, I.M. Marrucho, Vapor–liquid equilibrium of carbon dioxide–perfluoroalkane mixtures: experimental data and SAFT modeling, *Ind. Eng. Chem. Res.* 45 (2006) 2341–2350.
- [52] S.P.M. Ventura, J. Pauly, J.L. Daridon, I.M. Marrucho, A.M.A. Dias, J.A.P. Coutinho, High-pressure solubility data of methane in aniline and aqueous aniline systems, *J. Chem. Eng. Data* 52 (2007) 1100–1102.
- [53] V.H. Álvarez, R. Larico, Y. Ianos, M. Aznar, Parameter Estimation for VLE Calculation by Global Minimization: Genetic Algorithm, *Braz. J. Chem. Eng.* 25 (2008) 409–418.
- [54] M.G. Freire, C.M.S.S. Neves, P.J. Carvalho, R.L. Gardas, A.M. Fernandes, I.M. Marrucho, L.M.N.B.F. Santos, J.A.P. Coutinho, Mutual solubilities of water and hydrophobic ionic liquids, *J. Phys. Chem. B* 111 (45) (2007) 13082–13089.
- [55] M.G. Freire, P.J. Carvalho, R.L. Gardas, I.M. Marrucho, L.M.N.B.F. Santos, J.A.P. Coutinho, Mutual solubilities of water and the [C_nmim][Tf₂N] hydrophobic ionic liquids, *J. Phys. Chem. B* 112 (2008) 1604–1610.
- [56] R.L. Gardas, M.G. Freire, P.J. Carvalho, I.M. Marrucho, I.M.A. Fonseca, A.G.M. Ferreira, J.A.P. Coutinho, P. (rho), T measurements of imidazolium based ionic liquids, *J. Chem. Eng. Data* 52 (2007) 1881–1888.
- [57] P.J. Carvalho, M.G. Freire, I.M. Marrucho, A.J. Queimada, J.A.P. Coutinho, Surface tensions for the 1-alkyl-3-methylimidazolium bis(trifluoromethylsulfonyl)imide ionic liquids, *J. Chem. Eng. Data* 53 (2008) 1346–1350.
- [58] S.G. Kazarian, B.J. Briscoe, T. Welton, Combining ionic liquids and supercritical fluids: in situ ATR–IR study of CO₂ dissolved in two ionic liquids at high pressures, *Chem. Commun.* (2000) 2047–2048.
- [59] J.H. Hildebrand, R.L. Scott, *Regular and Related Solutions*, Van Nostrand Reinhold, New York, 1970.
- [60] J. Anderson, J. Dixon, E. Maginn, J. Brennecke, Measurement of SO₂ solubility in ionic liquids, *J. Phys. Chem. B* 110 (2006) 15059–15062.
- [61] Diadema Public 1.2, The DIPPR Information and Data Evaluation Manager, 2000.
- [62] J. Valderrama, P. Robles, Critical properties, normal boiling temperatures, and acentric factors of fifty ionic liquids, *Ind. Eng. Chem. Res.* 46 (2007) 1338–1344.

Artigo 4.10: High pressure phase behavior of carbon dioxide in 1-butyl-3-methylimidazolium bis(trifluoromethylsulfonyl)imide and 1-butyl-3-methylimidazolium dicyanamide ionic liquids

J. of Supercritical Fluids 50 (2009) 105–111



Contents lists available at ScienceDirect

The Journal of Supercritical Fluids

journal homepage: www.elsevier.com/locate/supflu



High pressure phase behavior of carbon dioxide in 1-butyl-3-methylimidazolium bis(trifluoromethylsulfonyl)imide and 1-butyl-3-methylimidazolium dicyanamide ionic liquids

Pedro J. Carvalho^a, Víctor H. Álvarez^b, Isabel M. Marrucho^a, Martín Aznar^b, João A.P. Coutinho^{a,*}

^a CICECO, Departamento de Química, Universidade de Aveiro, 3810-193 Aveiro, Portugal

^b Faculdade de Engenharia Química, Universidade Estadual de Campinas, 13083-970, Campinas, SP, Brazil

ARTICLE INFO

Article history:

Received 6 April 2009

Received in revised form 22 May 2009

Accepted 28 May 2009

Keywords:

1-Butyl-3-methylimidazolium dicyanamide

1-Butyl-3-methylimidazolium

bis(trifluoromethylsulfonyl)imide

Carbon dioxide

Phase behavior

Supercritical

Experimental

High pressure

Specific solvation interactions

Henry's constant

ABSTRACT

The acidity/basicity of the reaction media has a substantial influence on the efficiency of many reactive processes; therefore, a new class of acidic or basic ionic liquids is gaining special attention due to the possibility of increasing the efficiency of many processes by a wise manipulation of their properties. The absorption of sour gases is one of the processes that can be enhanced by the basic character of the ionic liquid. The fluorination of the cation or anion can also contribute to the gas solubility enhancement. In this work, these two characteristics are evaluated and compared through the study of gas–liquid equilibrium of two ionic liquids, 1-butyl-3-methylimidazolium dicyanamide ([C₄mim][DCA]) and 1-butyl-3-methylimidazolium bis(trifluoromethylsulfonyl)imide ([C₄mim][Tf₂N]), with carbon dioxide (CO₂) at temperatures up to 363 K and pressures up to 74 MPa.

A thermodynamic model based on the Peng–Robinson equation of state with the Wong–Sandler mixing rule, using the UNIQUAC model for the activity coefficients, was used to describe the experimental data and for the estimation of the Henry's constants.

The solubility of CO₂ in 1-butyl-3-methylimidazolium dicyanamide is much lower than anticipated on the basis of the reported pK_a of the anion when compared with the acetate anion. No chemisorption is observed and the solvation enthalpy is quite low, ruling out any Lewis acid/base interaction between the anion and the CO₂. The 1-butyl-3-methylimidazolium bis(trifluoromethylsulfonyl)imide ionic liquid, known to present one of the highest solubilities towards CO₂ due to the presence of fluoroalkyl groups, showed a much larger solubility for CO₂ than 1-butyl-3-methylimidazolium dicyanamide.

© 2009 Elsevier B.V. All rights reserved.

1. Introduction

Acidic or basic ionic liquids (ILs) represent new classes of acids or bases. The study of the acidity/basicity of these task-specific ionic liquids is of great importance since the efficiency of many processes depends on the acidity/basicity of the media or can be controlled by it. These compounds aptness for the fine tuning of their properties through an endless combination of cations and anions, cataloging them as *designer* solvents, allow the design of solvents for the development of more efficient and sustainable processes and products. From the wide range of applications envisioned for ILs, such as catalysts for acid-catalyzed organic reactions [1,2], hydrosilation processes [3], lubricants [4], performance additives [5], media for metal-catalyzed reactions [6], their use as CO₂-selective separation media [7–10] for capture/sequestration

of sour gases like CO₂, H₂S and SO₂ is one of the most exciting and of increasing interest [8,9,11–27]. The development of improved, highly efficient and economically viable separation and storage processes is gaining a special interest both by academia and industry. Nonetheless, and despite of the promising properties of ILs, further research is still required in order to make this *neoteric* solvents feasible candidates for these applications. Being a key parameter in the design of equilibrium stage- and rate-based separations, reliable gas solubility data is of great interest and a fundamental step towards the development of industrial applications, either by the data itself or by developing predictive and simulation tools to aid in such applications development.

Crowhurst et al. [28] reported that the hydrogen bond basicities of ILs are controlled by the anion, while the hydrogen bond donation behavior is dominated by the hydrogen bond basicity of the anions with a smaller contribution from the hydrogen bond acidity of the cation. Therefore, changing to more basic anions leads to a dramatic drop in the acidity. Based on the Pearson's "hard and

* Corresponding author. Tel.: +351 234 401 507; fax: +351 234 370 084.
E-mail address: jcoutinho@ua.pt (J.A.P. Coutinho).

soft acid/base" principles, allowing a strong affinity towards CO₂. Pennline et al. [29] screened quaternary ammonium polyether ILs as potential solvents for CO₂ capture. In a previous work [12], following the works by Shiflett et al. [26] and Yokozeki et al. [30], imidazolium-based IL with the acetate and trifluoroacetate anions were studied by our group. The acetate ion was shown to present a chemical absorption behavior for low CO₂ mole fractions (mole fractions <0.3) and *ab initio* calculations and ¹³C HRMAS NMR spectroscopy provided a deeper understanding of the CO₂-acetate interactions [12].

In the wake of this previous work [12], the purpose of the present study is to further explore the basicity of the anion as a mean to enhance the absorption of carbon dioxide by the ionic liquids. For that purpose, following the suggestion of MacFarlane et al. [31] that dicyanamide would be a basic anion (the pK_a, 5.1, for dicyanoamine reported by MacFarlane is higher than the pK_a for the acetic acid, 4.75), a dicyanamide anion based ionic liquid was chosen here to further investigate the effect of the anion basicity on the solvation of CO₂. The 1-butyl-3-methylimidazolium dicyanamide was thus selected for that purpose and the solubility of the CO₂ in this IL is compared to that in the 1-butyl-3-methylimidazolium bis(trifluoromethylsulfonyl)imide ionic liquid, also studied here and known to present one of the highest solubility towards CO₂ due to the presence of fluoroalkyl groups. Both systems were measured at temperatures up to 363 K and pressures up to 74 MPa.

The Peng–Robinson equation of state [32] with the Wong–Sandler/UNIQUAC mixing rule [33] using the UNIQUAC model [34] for the activity coefficients, was used to model the experimental data measured in this work.

2. Experimental

2.1. Materials

Two ILs based on the 1-butyl-3-methyl-imidazolium cation, 1-butyl-3-methyl-imidazolium bis(trifluoromethylsulfonyl)imide, [C₄mim][Tf₂N] and 1-butyl-3-methyl-imidazolium dicyanamide, [C₄mim][DCA], were used in this study. All compounds were acquired at IoLiTec with mass fraction purities higher than 99% and bromide impurity mass fraction lower than 10⁻⁴. The purities stated by the supplier, of each ionic liquid, were checked by ¹H NMR, ¹³C NMR and ¹⁹F NMR.

It is well known that the phase equilibria and thermophysical properties of ILs are greatly influenced by their water content [35–38]. Blanchard et al. [16] reported that minor amounts of water, dissolved in [C₄mim][PF₆]⁻, lead to a reduction of 77% on the CO₂ solubility. Later, in a systematically study on the influence of water on the solubility of CO₂ for the same compound, Fu et al. [39] reported a less pronounced though significant influence, <15%. Furthermore, being an active proton acceptor, water can dramatically increase the degree of dissociation of an acid in a neutral ionic liquid. Similarly, in a neutral IL the state of a base will be altered by the presence of water and in a basic IL, water will be at least partly dissociated producing OH⁻ [31]. These reports made researchers aware of the importance of implementing purifying procedures prior to the measurements. Thus, in order to reduce to negligible values both water and volatile compounds, vacuum (0.1 Pa), stirring and moderate temperature (353 K), for a period of at least 48 h, were applied prior to the measurements. The final IL water content was determined with a Metrohm 831 Karl Fischer coulometer, indicating a water mass fraction of (44 and 28) × 10⁻⁶ for [C₄mim][Tf₂N] and [C₄mim][DCA], respectively.

The carbon dioxide (CO₂) was acquired from Air Liquide with a purity of ≥99.998% and H₂O, O₂, C_nH_m, N₂ and H₂ impurities volume fractions lower than (3, 2, 2, 8 and 0.5) × 10⁻⁶, respectively.

2.2. Experimental equipment

The high pressure equilibrium cell used in this work is based on a cell designed by Daridon and co-workers [40–44] using the synthetic method. Both the apparatus and the methodology followed here were fully described in previous works [11,12], and shown to be adequate to accurately measure vapor–liquid phase equilibrium in a wide range of pressures and temperatures [11,12,40–44]. The high pressure equilibrium cell consists of a horizontal hollow stainless-steel cylinder, closed at one end by a movable piston and at the other end by a sapphire window. This window, along with a second window on the cell wall through which an optical fiber lights the cell chamber, allows the operator to follow the behavior of the sample with pressure and temperature. The orthogonal positioning of both sapphire windows minimizes the parasitic reflections and improves the observation in comparison to axial lighting. A small magnetic bar placed inside the cell allows the homogenization of the mixture by means of an external magnetic stirrer. The presence of the magnetic stirrer, as well as the cell reduced volume, help to minimize the inertia and temperature gradients within the sample. The cell is thermostabilized by circulating a heat-carrier fluid through three flow lines directly managed into the cell. The heat-carrier fluid is thermo-regulated with a temperature stability of ±0.01 K by means of a thermostat bath circulator (Julabo MC). The temperature is measured with a high precision thermometer, Model PN 5207 with an accuracy of 0.01 K, connected to a calibrated platinum resistance inserted inside the cell close to the sample. The pressure is measured by a piezoresistive silicon pressure transducer (Kulite) fixed directly inside the cell to reduce dead volumes, that was previously calibrated and certified by an independent laboratory with IPAC accreditation, following the EN 837-1 standard and with accuracy better than 0.2%.

A fixed amount of IL was introduced inside the cell, its exact mass was determined by weighting, using a high weight/high precision balance with an accuracy of 1 mg (Sartorius). In order to avoid any interference of atmospheric gases during the manipulation, after placing the IL inside the cell, it was kept under vacuum overnight, while stirring and heating at 353 K.

The CO₂ was introduced under pressure from an aluminum reservoir tank. Its mass was measured with the precision balance and introduced into the measuring cell by means of a flexible high pressure capillary.

After preparation of a mixture of known composition and the desired temperature at low pressure was reached, the pressure was then slowly increased at constant temperature until the system becomes monophasic. The pressure at which the last bubble disappears represents the equilibrium pressure for the fixed temperature.

The purity of the IL is checked again by NMR at the end of the study to confirm that no degradation takes place during the measurements.

2.3. Thermodynamic modeling

As in previous works [11,12] we have applied the Peng–Robinson equation of state [32]:

$$P = \frac{RT}{V - b_m} - \frac{a_m}{V(V + b_m) + b(V - b_m)} \quad (1)$$

where the constants a_m and b_m are expressed as functions of concentration of the different components in the mixture through the Wong–Sandler mixing rule [33]:

$$b_m = \frac{\sum_i \sum_j x_i x_j (b - (a/RT))_{ij}}{1 - \sum_i (x_i a_{ii}/b_{ii} RT) - (A_\infty^E/\Omega RT)} \quad (2)$$

$$a_m = b_m \left[\sum_i \frac{x_i a_{ii}}{b_{ii}} + \frac{A_\infty^E}{\Omega} \right] \quad (3)$$

$$\left(b - \frac{a}{RT} \right)_{ij} = \frac{b_{ii} + b_{jj}}{2} - \frac{(1 - k_{ij}) \sqrt{a_{ii} a_{jj}}}{RT} \quad (4)$$

in these equations, a_m and b_m are the EoS constants, $\Omega = 0.34657$, and the excess Helmholtz free energy at the limit of infinite pressure, that is calculated assuming that $A_\infty^E \approx A_0^E \approx G_0^E$ where G_0^E is the excess Gibbs free energy at the limit of zero pressure calculated here using the UNIQUAC model [34].

The correlation of the experimental data was carried by the minimization of the objective function, OF , for

$$OF = \sum_{i=1}^N \left[\frac{p_{\text{cal}} - p_{\text{exp}}}{\sigma_p} \right]^2_i \quad (5)$$

where N is the number of data points, P is the pressure, the superscripts “exp” and “cal” refers to the experimental and calculated values, respectively, and σ_p is the standard deviation of pressure. The experimental uncertainties in the pressure data were used for σ_p . The minimization method was performed using a genetic algorithm code, implemented and fully explained in Alvarez et al. [45]. The difference between experimental and calculated values was calculated as the average percent deviation, expressed in absolute form, as follows:

$$|\Delta P| = \frac{100}{N} \sum_{i=1}^N \left[\frac{P_i^{\text{cal}} - P_i^{\text{exp}}}{P_i^{\text{exp}}} \right] \quad (6)$$

Furthermore the proposed model was applied, in the diluted region limit, to determine the Henry's constant for the studied systems.

3. Results and discussion

The solubility of carbon dioxide in the studied ILs was measured for mole fractions ranging from 0.2 to 0.8, in the temperature range 293–363 K and pressures from 0.6 to 74 MPa, as reported in Tables 1 and 2 and depicted in Fig. 1. A temperature increase leads to an increase on the equilibrium pressures and by increasing CO_2 concentration, the equilibrium pressures increase gradually, at first, and rapidly for higher CO_2 contents as also observed previously for other ILs [11,12].

The experimental data reported here is generally in agreement with those available in literature, covering however a wider range

of carbon dioxide concentrations, pressures and temperatures, as depicted in Fig. 2. For the system $\text{CO}_2 + [\text{C}_4\text{mim}][\text{Tf}_2\text{N}]$ a good agreement is observed with the data by Shin et al. [46] for CO_2 mole fractions below 0.7. Above these concentrations, their data is scarce and ours provide a more detailed view of the phase diagram. The data by Anthony et al. [15] for this system is available only in the low pressure region and seems to present some deviations from both the data reported here and by Shin et al. [46]. For the system $\text{CO}_2 + [\text{C}_4\text{mim}][\text{DCA}]$ only three isotherms below 10 MPa were reported by Aki et al. [13]. A good agreement is obtained with this data in the lower pressure region while again the data reported here provide a more complete description of the phase diagram for high pressures.

Contrary to what was expected, the higher basicity character of the dicyanamide anion, compared to the bis(trifluoromethylsulfonyl)imide, as expressed in their pK_a values, does not enhance the CO_2 solubility as was previously observed with the acetate anion. The explanation for this fact seems to be that, as shown previously [12], the solubility of CO_2 on an IL is enhanced by a Lewis acid/base interaction between the gas and the anion. The dicyanamide, in spite of its large pK_a value, seems however to be a much weaker Lewis base than the acetate anion.

3.1. Henry's constants

The results of the application of the thermodynamic modeling to the binary systems containing ionic liquids studied in this work are presented in Table 3 for all the experimental data. In this table, T is the temperature, k_{12} , A_{12} and A_{21} are the interaction parameters of the model, where 1 stands for the CO_2 and 2 for the ionic liquid. This table is divided in sections for each system studied. The physical parameters used in the thermodynamic model are reported in Table 4 while the interaction parameters used are presented in Table 3. The proposed model, with temperature independent parameters, was applied to describe the experimental data and estimate the Henry's constant for the studied systems. As depicted in Fig. 3 the model describes well the experimental data for pressures below 30 MPa. Above this pressure higher deviations are observed.

The Henry's law relates the amount of a given gas dissolved in a given type and volume of liquid, at a constant temperature, to the fugacity of that gas in equilibrium with that liquid and can be described as

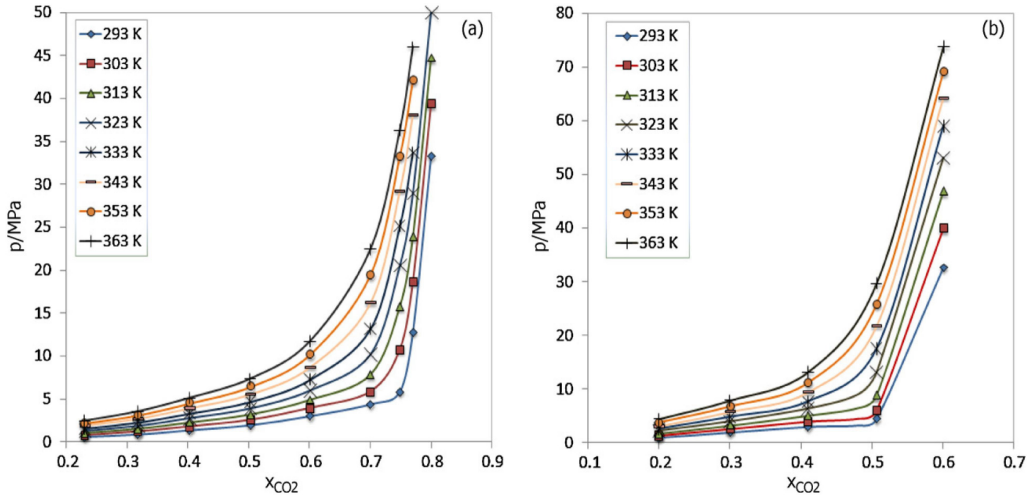
$$H_{12}(T, P) = \lim_{x_1 \rightarrow 0} \frac{f_i^L}{x_1} \quad (7)$$

Table 1
Bubble point data of the system CO_2 (1)+ $[\text{C}_4\text{mim}][\text{Tf}_2\text{N}]$ (2).

x_1	T/K	P/MPa									
0.231	292.65	0.629	0.319	293.21	0.915	0.404	293.53	1.410	0.503	293.22	1.997
0.231	303.18	0.786	0.319	303.05	1.223	0.404	303.10	1.812	0.503	303.12	2.568
0.231	313.32	1.050	0.319	313.19	1.540	0.404	313.17	2.273	0.503	313.10	3.196
0.231	323.22	1.303	0.319	323.27	1.892	0.404	323.26	2.787	0.503	323.20	3.909
0.231	333.19	1.574	0.319	333.17	2.283	0.404	333.23	3.316	0.503	333.12	4.670
0.231	343.00	1.874	0.319	342.87	2.682	0.404	343.11	3.897	0.503	343.24	5.499
0.231	353.20	2.179	0.319	353.09	3.121	0.404	353.12	4.512	0.503	353.17	6.412
0.231	363.26	2.485	0.319	363.19	3.579	0.404	363.17	5.156	0.503	363.18	7.372
x_1	T/K	P/MPa									
0.701	293.37	4.433	0.749	293.32	5.907	0.771	293.42	12.829	0.801	293.26	33.263
0.701	303.19	5.880	0.749	303.19	10.812	0.771	303.31	18.726	0.801	303.19	39.373
0.701	313.11	7.860	0.749	313.12	15.810	0.771	313.23	23.943	0.801	313.25	44.740
0.701	323.09	10.215	0.749	323.11	20.543	0.771	323.13	28.960	0.801	323.30	49.990
0.701	333.10	13.150	0.749	333.17	25.124	0.771	333.28	33.693			
0.701	343.25	16.144	0.749	343.20	29.205	0.771	343.08	38.081			
0.701	353.14	19.437	0.749	353.09	33.219	0.771	353.22	42.030			
0.701	362.99	22.468	0.749	363.18	36.365	0.771	363.25	46.010			

Table 2Bubble point data of the system CO_2 (1)+[C₄mim][DCA] (2).

x_1	T/K	P/MPa												
0.200	293.36	1.018	0.300	293.50	1.980	0.410	293.38	3.015	0.507	293.44	4.496	0.601	293.41	32.606
0.200	303.45	1.360	0.300	303.40	2.590	0.410	303.45	3.950	0.507	302.91	6.056	0.601	303.14	39.866
0.200	313.36	1.771	0.300	313.06	3.230	0.410	313.32	5.088	0.507	313.03	8.856	0.601	313.17	46.749
0.200	322.94	2.260	0.300	323.04	4.005	0.410	323.47	6.395	0.507	322.93	13.184	0.601	323.07	53.174
0.200	332.72	2.644	0.300	333.28	4.860	0.410	333.13	7.743	0.507	333.21	17.566	0.601	333.15	59.007
0.200	343.12	3.108	0.300	343.34	5.776	0.410	343.01	9.452	0.507	343.12	21.750	0.601	343.17	64.217
0.200	353.09	3.745	0.300	353.10	6.722	0.410	353.13	11.166	0.507	353.01	25.759	0.601	353.19	69.002
0.200	363.25	4.328	0.300	363.11	7.776	0.410	363.18	13.106	0.507	363.20	29.583	0.601	363.21	73.640

**Fig. 1.** Pressure–composition diagram of the binary systems (a) CO_2 +[C₄mim][Tf₂N] and (b) CO_2 +[C₄mim][DCA]. The solid curves are guide for easier visual interpretation.

where $H_{12}(T, P)$ is the Henry's constant, x_1 is the mole fraction of gas dissolved in the liquid phase, and f_1^L is the fugacity of the gas in the liquid phase. As shown, Eq. (7) is only rigorously valid in the diluted region limit. The Henry's constants for the CO₂ in the investigated ILs were estimated by fitting the PR-WS/UNIQUAC model to the data and calculating the limiting slope as the solubility approaches zero. This approach introduces some uncertainty on the estimated Henry's constants but the values of these constants for the two studied ILs are different enough to allow a discussion of the interactions between the CO₂ and the

two ionic liquids based on these values. The estimated Henry's constants results, reported in Table 3, indicate that Henry's constant increases slightly (i.e., CO₂ solubility decreases) with the temperature.

The results for the Henry's constant of CO₂ in [C₄mim][DCA] and in [C₄mim][Tf₂N] were correlated as a function of temperature by an empirical equation of the type:

$$\ln(H_{12}) = A \left(\frac{1}{T} \right) + B \quad (8)$$

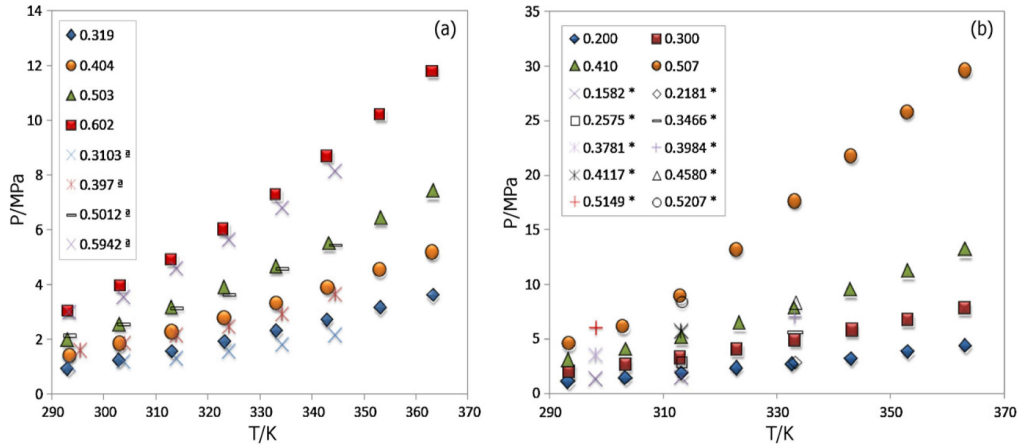
**Fig. 2.** Pressure–temperature–composition diagram of the binary systems (a) CO_2 +[C₄mim][Tf₂N] and (b) CO_2 +[C₄mim][DCA] for this work experimental data and data from ^aRef. [46] and *Ref. [13].

Table 3

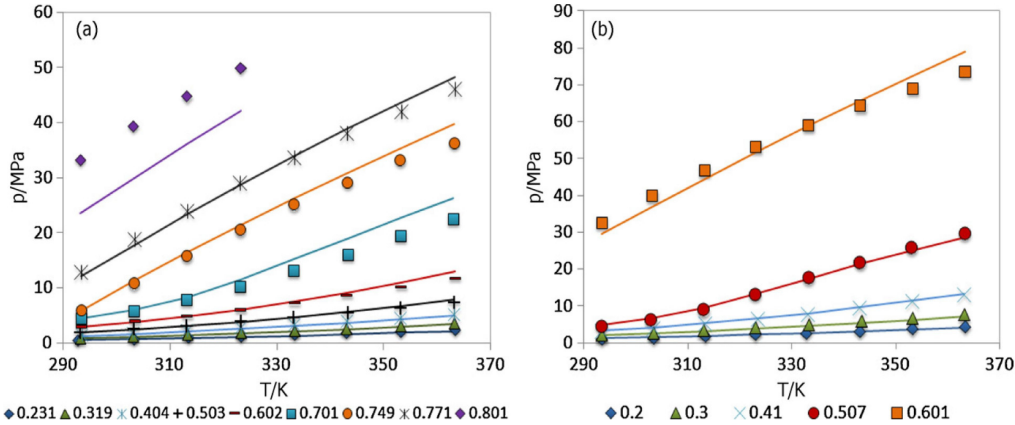
Interaction parameters for the studied systems and predicted Henry's constants.

$\text{CO}_2 + [\text{C}_4\text{mim}][\text{DCA}]$ ($K_{ij} = 0.1255$, $A_{12} = 5075.1963$, $A_{21} = -1168.4022$, $ \Delta P = 5.2\%$)		$\text{CO}_2 + [\text{C}_4\text{mim}][\text{Tf}_2\text{N}]$ ($K_{ij} = 0.2734$, $A_{12} = 5888.6826$, $A_{21} = -1845.7030$, $ \Delta P = 7.9\%$)	
T/K	H_{12}/MPa	T/K	H_{12}/MPa
294	5.13	294	2.05
298	5.59	298	2.25
303	6.19	303	2.53
313	7.49	313	3.14
323	8.92	323	3.84
333	10.48	333	4.62
343	12.14	343	5.47
348	13.01	348	5.93
353	13.90	353	6.41
363	15.74	363	7.42

Table 4

Properties of the substances used in the modeling.

Compound	T_c/K	P_c/MPa	ω	r	q
CO_2	304.21 ^a	7.38 ^a	0.2236 ^a	3.26 ^c	2.38 ^c
$[\text{C}_4\text{mim}][\text{DCA}]$	782.96 ^b	2.44 ^b	0.8419 ^b	22.63 ^c	14.86 ^c
$[\text{C}_4\text{mim}][\text{Tf}_2\text{N}]$	826.30 ^b	2.76 ^b	0.3004 ^b	32.67 ^c	20.68 ^c

^a Ref. [48].^b Calculated with Ref. [49].^c Calculated with Ref. [50].**Fig. 3.** PTx diagram and modeling for the systems $\text{CO}_2 + [\text{C}_4\text{mim}][\text{Tf}_2\text{N}]$ (a) and $\text{CO}_2 + [\text{C}_4\text{mim}][\text{DCA}]$ (b). The solid lines represent the calculations with PR-WS/NRTL EoS.

where the coefficients A and B are listed in Table 5, together with the Henry's constant average absolute deviations, $|\Delta H_{12}|$, obtained for each ionic liquid.

The effect of temperature on CO_2 solubility can be related to the Gibbs energy, the partial molar entropy and partial molar enthalpy of solvation [47] and can be calculated from an appropriate correlation of Henry's constant:

$$\Delta_{\text{solv}}G^\circ = RT(\ln(H_{12}))_p \quad (9)$$

$$\Delta_{\text{solv}}H^\circ = -T^2 \left(\frac{\partial \Delta_{\text{solv}}G^\circ}{\partial T} \right)_T = -RT^2 \left(\frac{\partial \ln H_{12}}{\partial T} \right)_p = RA \quad (10)$$

$$\Delta_{\text{solv}}S^\circ = \frac{\Delta_{\text{solv}}H^\circ - \Delta_{\text{solv}}G^\circ}{T} = -RT \left(\frac{\partial \ln H_{12}}{\partial T} \right)_p - R \ln(H_{12})_p = -RB \quad (11)$$

The partial molar enthalpy of solvation gives an indication of the strength of interactions between the gas and the IL, while the partial molar entropy illustrates the amount of ordering present in the gas/IL mixture. The results presented in Table 5 show that the partial entropies in both fluids are essentially identical, indicating a similar structural solvation interaction. The partial molar enthalpy of solvation of the CO_2 in $[\text{C}_4\text{mim}][\text{Tf}_2\text{N}]$ is lower than in $[\text{C}_4\text{mim}][\text{DCA}]$, indicating a slightly stronger interaction between the CO_2 and

Table 5Coefficients A and B in Eq. (8) and partial molar enthalpy and partial molar entropy of solvation obtained for CO_2 (1)+ILs (2) systems.

Ionic liquid	A	B	$ \Delta H_{12} /\%$	$\Delta_{\text{solv}}H/\text{kJ mol}^{-1}$	$\Delta_{\text{solv}}S/\text{J mol}^{-1}\text{K}^{-1}$	$-T\Delta_{\text{solv}}S _{T=298\text{ K}}/\text{kJ mol}^{-1}$
$[\text{C}_4\text{mim}][\text{DCA}]$	-1739.868	7.564	0.71	-15.03	-64.75	19.29
$[\text{C}_4\text{mim}][\text{Tf}_2\text{N}]$	-1970.775	7.456	0.60	-18.21	-68.09	20.29

the [C₄mim][Tf₂N] when compared with the [C₄mim][DCA]. The enthalpies and entropies of solvation contribution make the solubility of both systems non-spontaneous and moreover, controlled by physical absorption. The partial molar enthalpies of solvation observed for these ILs are also much lower than those previously reported for [C₄mim][acetate] and [C₄mim][TFA] [12] showing that, as discussed previously, in spite of the pK_a of dicyanamide no acid/base interaction is observed for the ILs studied in this work.

4. Conclusions

New gas–liquid equilibrium data of two binary systems, namely, 1-butyl-3-methylimidazolium dicyanamide + CO₂ and 1-butyl-3-methylimidazolium bis(trifluoromethylsulfonyl)imide + CO₂ have been investigated in a wide range of temperatures, pressures and CO₂ mole fractions aiming at understanding the effect of the basicity of the anion in the gas solubility in the ionic liquids.

Contrary to what the dicyanamide anion basicity would suggest the [C₄mim][DCA] ionic liquid do not show a significant enhancement on the CO₂ solubility. In fact, the interaction between the negative fluorine atoms and the positive charge on the carbon of the CO₂ molecule seems to be stronger in the Tf₂N anion based IL.

A thermodynamic model based on the Peng–Robinson EoS with the Wong–Sandler/UNIQUAC mixing rule was used in description of the measured data. The model allows a good description of the experimental data and the estimation of the Henry's constants for these systems.

The partial Gibbs energy, enthalpies and entropies of solvation estimated from Henry's constants show that the solubility of CO₂ in both systems is non spontaneous at standard pressure (0.1 MPa). The entropies of solvation in the two systems are essentially identical and the partial molar enthalpy of solvation of CO₂ in [C₄mim][Tf₂N], when compared to the one of [C₄mim][DCA], indicate similar interactions between the CO₂ and the two ionic liquids.

Acknowledgments

The authors are thankful for financial support from Fundação para a Ciência e a Tecnologia (PTDC/EQU/65252/2006) and Ph.D. grant (SFRH/BD/41562/2007) of Pedro J. Carvalho. The authors would like to acknowledge FAPESP (Fundação de Amparo à Pesquisa do Estado de São Paulo), process # 2006/03711-1. M. Aznar is the recipient of a CNPq fellowship. The authors are also grateful to Catarina M.S.S. Neves for the help with the NMR spectra.

References

- [1] W. Li, Z. Zhang, B. Han, S. Hu, J. Song, Y. Xie, X. Zhou, Switching the basicity of ionic liquids by CO₂, *Green Chem.* 10 (2008) 1142–1145.
- [2] J. Fraga-Dubreuil, K. Bourahla, M. Rahmouni, J.P. Bazureau, J. Hamelin, Catalysed esterifications in room temperature ionic liquids with acidic counterion as recyclable reaction media, *Catal. Commun.* 3 (2002) 185–190.
- [3] B. Weyershausen, K. Hell, U. Hesse, Industrial application of ionic liquids as process aid, *Green Chem.* 7 (2005) 283–287.
- [4] C. Ye, W. Liu, Y. Chen, L. Yu, Room-temperature ionic liquids: a novel versatile lubricant, *Chem. Commun.* 21 (2001) 2244–2245.
- [5] B. Weyershausen, K. Lehmann, Industrial application of ionic liquids as performance additives, *Green Chem.* 7 (2005) 15–19.
- [6] P. Wasserscheid, W. Keim, Ionic liquids—new “solutions” for transition metal catalysis, *Angew. Chem., Int. Ed.* 39 (2000) 3772–3789.
- [7] J. Anthony, E. Maginn, J. Brennecke, Solubilities and thermodynamic properties of gases in the ionic liquid 1-n-butyl-3-methylimidazolium hexafluorophosphate, *J. Phys. Chem. B* 106 (2002) 7315–7320.
- [8] J.L. Anthony, S.N.V.K. Aki, E.J. Maginn, J.F. Brennecke, Feasibility of using ionic liquids for carbon dioxide capture, *Int. J. Environ. Technol. Manage.* 4 (2004) 105–115.
- [9] E. Bates, R. Mayton, I. Ntai, J. Davis, CO₂ capture by a task-specific ionic liquid, *J. Am. Chem. Soc.* 124 (2002) 926–927.
- [10] S. Zhang, Y. Chen, F. Li, X. Lu, W. Dai, R. Mori, Fixation and conversion of CO₂ using ionic liquids, *Catal. Today* 115 (2006) 61–69.
- [11] P.J. Carvalho, V.H. Álvarez, J.J.B. Machado, J. Pauly, J. Daridon, I.M. Marrucho, M. Aznar, J.A.P. Coutinho, High pressure phase behavior of carbon dioxide in 1-alkyl-3-methylimidazolium bis(trifluoromethylsulfonyl)imide ionic liquids, *J. Supercrit. Fluids* 48 (2009) 99–107.
- [12] P.J. Carvalho, V.H. Alvarez, B. Schröder, A.M. Gil, I.M. Marrucho, M. Aznar, L.M.N.B.F. Santos, J.A.P. Coutinho, Specific solvation interactions of CO₂ on acetate and trifluoroacetate imidazolium based ionic liquids at high pressures, *J. Phys. Chem. B* 113 (2009) 6803–6812.
- [13] S.N.V.K. Aki, B.R. Mellein, E.M. Sauer, J.F. Brennecke, High-pressure phase behavior of carbon dioxide with imidazolium-based ionic liquids, *J. Phys. Chem. B* 108 (2004) 20355–20365.
- [14] J.L. Anderson, J.K. Dixon, J.F. Brennecke, Solubility of CO₂, CH₄, C₂H₆, C₂H₄, O₂, and N₂ in 1-hexyl-3-methylpyridinium bis(trifluoromethylsulfonyl)imide: comparison to other ionic liquids, *Acc. Chem. Res.* 40 (2007) 1208–1216.
- [15] J. Anthony, J. Anderson, E. Maginn, J. Brennecke, Anion effects on gas solubility in ionic liquids, *J. Phys. Chem. B* 109 (2005) 6366–6374.
- [16] L. Blanchard, Z. Gu, J. Brennecke, High-pressure phase behavior of ionic liquid/CO₂ systems, *J. Phys. Chem. B* 105 (2001) 2437–2444.
- [17] A. Shariati, C.J. Peters, High-pressure phase behavior of systems with ionic liquids: part iii, the binary system carbon dioxide + 1-hexyl-3-methylimidazolium hexafluorophosphate, *J. Supercrit. Fluids* 30 (2004) 139–144.
- [18] A. Shariati, C.J. Peters, High-pressure phase equilibria of systems with ionic liquids, *J. Supercrit. Fluids* 34 (2005) 171–176.
- [19] X. Yuan, S. Zhang, Y. Chen, X. Lu, W. Dai, R. Mori, Solubilities of gases in 1,1,3,3-tetramethylguanidium lactate at elevated pressures, *J. Chem. Eng. Data* 51 (2006) 645–647.
- [20] X. Yuan, S. Zhang, J. Liu, X. Lu, Solubilities of CO₂ in hydroxyl ammonium ionic liquids at elevated pressures, *Fluid Phase Equilib.* 257 (2007) 195–200.
- [21] S. Zhang, Y. Chen, R. Ren, Y. Zhang, J. Zhang, X. Zhang, Solubility of CO₂ in sulfonate ionic liquids at high pressure, *J. Chem. Eng. Data* 50 (2005) 230–233.
- [22] J. Anderson, J. Dixon, E. Maginn, J. Brennecke, Measurement of SO₂ solubility in ionic liquids, *J. Phys. Chem. B* 110 (2006) 15059–15062.
- [23] L.E. Barrosse-Antle, C. Hardacre, R.G. Compton, SO₂ saturation of the room temperature ionic liquid [C₂mim][NTf₂] much reduces the activation energy for diffusion, *J. Phys. Chem. B* 113 (2009) 1007–1011.
- [24] J.E. Bara, C.J. Gabriel, S. Lessmann, T.K. Carlisle, A. Finotello, D.L. Gin, R.D. Noble, Enhanced CO₂ separation selectivity in oligo(ethylene glycol) functionalized room-temperature ionic liquids, *Ind. Eng. Chem. Res.* 46 (2007) 5380–5386.
- [25] J.E. Bara, T.K. Carlisle, C.J. Gabriel, D. Camper, A. Finotello, D.L. Gin, R.D. Noble, Guide to CO₂ separations in imidazolium-based room-temperature ionic liquids, *Ind. Eng. Chem. Res.* 48 (2009) 2739–2751.
- [26] M.B. Shiflett, D.J. Kasprzak, C.P. Junk, A. Yokozeki, Phase behavior of {carbon dioxide + [bmim][Ac]} mixtures, *J. Chem. Thermodyn.* 40 (2008) 25–31.
- [27] M.B. Shiflett, A. Yokozeki, Phase behavior of carbon dioxide in ionic liquids: [emim][acetate], [emim][trifluoroacetate], and [emim][acetate]+[emim][trifluoroacetate] mixtures, *J. Chem. Eng. Data* 54 (2009) 108–114.
- [28] L. Crowhurst, P.R. Mawdsley, J.M. Perez-Arlanidis, P.A. Salter, T. Welton, Solvent-solute interactions in ionic liquids, *Phys. Chem. Chem. Phys.* 5 (2003) 2790–2794.
- [29] H.W. Pennline, D.R. Luebke, K.L. Jones, C.R. Myers, B.I. Morsi, Y.J. Heintz, J.B. Ilconich, Progress in carbon dioxide capture and separation research for gasification-based power generation point sources, *Fuel Process. Technol.* 89 (2008) 897–907.
- [30] A. Yokozeki, M.B. Shiflett, C.P. Junk, L.M. Grieco, T. Foo, Physical and chemical absorptions of carbon dioxide in room-temperature ionic liquids, *J. Phys. Chem. B* 112 (2008) 16654–16663.
- [31] D.R. MacFarlane, J.M. Pringle, K.M. Johansson, S.A. Forsyth, M. Forsyth, Lewis base ionic liquids, *Chem. Commun.* 18 (2006) 1905–1917.
- [32] D. Peng, D.B. Robinson, A new two-constant equation of state, *Ind. Eng. Chem. Fundam.* 15 (1976) 59–64.
- [33] D.S.H. Wong, S.I. Sandler, A theoretically correct mixing rule for cubic equations of state, *AIChE J.* 38 (1992) 671–680.
- [34] D.S. Abrams, J.M. Prausnitz, Statistical thermodynamics of liquid mixtures: a new expression for the excess Gibbs energy of partly or completely miscible systems, *AIChE J.* 21 (1975) 116–128.
- [35] M.G. Freire, P.J. Carvalho, A.M. Fernandes, I.M. Marrucho, A.J. Queimada, J.A.P. Coutinho, Surface tensions of imidazolium based ionic liquids: anion, cation, temperature and water effect, *J. Colloid Interface Sci.* 314 (2007) 621–630.
- [36] K.R. Seddon, A. Stark, M. Torres, Influence of chloride, water, and organic solvents on the physical properties of ionic liquids, *Pure Appl. Chem.* 72 (2000) 2275–2287.
- [37] J.G. Huddleston, A.E. Visser, W.M. Reichert, H.D. Willauer, G.A. Broker, R.D. Rogers, Characterization and comparison of hydrophilic and hydrophobic room temperature ionic liquids incorporating the imidazolium cation, *Green Chem.* 3 (2001) 156–164.
- [38] R.L. Gardas, M.G. Freire, P.J. Carvalho, I.M. Marrucho, I.M.A. Fonseca, A.G.M. Ferreira, J.A.P. Coutinho, High pressure densities and derived thermodynamic properties of imidazolium based ionic liquids, *J. Chem. Eng. Data* 52 (2007) 80–88.
- [39] D. Fu, X. Sun, J. Pu, S. Zhao, Effect of water content on the solubility of CO₂ in the ionic liquid [Bmim][PF₆]_n, *J. Chem. Eng. Data* 51 (2006) 371–375.

- [40] S. Vitu, J.N. Jaubert, J. Pauly, J.L. Daridon, D. Barth, Phase equilibria measurements of CO_2 + methyl cyclopentane and CO_2 + isopropyl cyclohexane binary mixtures at elevated pressures, *J. Supercrit. Fluids* 44 (2008) 155–163.
- [41] J. Pauly, J. Coutinho, J.L. Daridon, High pressure phase equilibria in methane + waxy systems. 1. methane + heptadecane, *Fluid Phase Equilib.* 255 (2007) 193–199.
- [42] S.P.M. Ventura, J. Pauly, J.L. Daridon, J.A.L. da Silva, I.M. Marrucho, A.M.A. Dias, J.A.P. Coutinho, High pressure solubility data of carbon dioxide in tri-isobutyl(methyl)phosphonium tosylate–water systems, *J. Chem. Thermodyn.* 40 (2008) 1187–1192.
- [43] A.M.A. Dias, H. Carrier, J.L. Daridon, J.C. Pamies, L.F. Vega, J.A.P. Coutinho, I.M. Marrucho, Vapor-liquid equilibrium of carbon dioxide–perfluoroalkane mixtures: experimental data and saft modeling, *Ind. Eng. Chem. Res.* 45 (2006) 2341–2350.
- [44] S.P.M. Ventura, J. Pauly, J.L. Daridon, I.M. Marrucho, A.M.A. Dias, J.A.P. Coutinho, High-pressure solubility data of methane in aniline and aqueous aniline systems, *J. Chem. Eng. Data* 52 (2007) 1100–1102.
- [45] V.H. Alvarez, R. Larico, Y. Yanos, M. Aznar, Parameter estimation for VLE calculation by global minimization: genetic algorithm, *Braz. J. Chem. Eng.* 25 (2008) 409–418.
- [46] E. Shin, B. Lee, J.S. Lim, High-pressure solubilities of carbon dioxide in ionic liquids: 1-alkyl-3-methylimidazolium bis(trifluoromethylsulfonyl)imide, *J. Supercrit. Fluids* 45 (2008) 282–292.
- [47] T.M. Letcher, *Developments and Applications in Solubility*, Royal Society of Chemistry, 2007.
- [48] Public 1.2. The DIPPR Information and Data Evaluation Manager; 2000.
- [49] J. Valderrama, P. Robles, Critical properties, normal boiling temperatures, andacentric factors of fifty ionic liquids, *Ind. Eng. Chem. Res.* 46 (2007) 1338–1344.
- [50] V.H. Alvarez, M. Aznar, Thermodynamic modeling of vapor-liquid equilibrium of binary systems ionic liquid + supercritical $\{\text{CO}_2 \text{ or } \text{CHF}_3\}$ and ionic liquid + hydrocarbons using Peng–Robinson equation of state, *J. Chin. Inst. Chem. Eng.* 39 (2008) 353–360.

Artigo 4.11: Specific solvation interactions of CO₂ on acetate and trifluoroacetate imidazolium based ionic liquids at high pressures

J. Phys. Chem. B 2009, 113, 6803–6812

6803

Specific Solvation Interactions of CO₂ on Acetate and Trifluoroacetate Imidazolium Based Ionic Liquids at High Pressures

Pedro J. Carvalho,[†] Víctor H. Álvarez,[‡] Bernd Schröder,[†] Ana M. Gil,[†] Isabel M. Marrucho,[†] Martín Aznar,[‡] Luís M. N. B. F. Santos,[§] and João A. P. Coutinho^{*,†}

CICECO, Departamento de Química, Universidade de Aveiro, 3810-193 Aveiro, Portugal, Faculdade de Engenharia Química, Universidade Estadual de Campinas, 13083-970 Campinas, SP, Brasil, Centro de Investigação em Química, Faculdade de Ciências da Universidade do Porto, Universidade do Porto, R. Campo Alegre, 687 4169-007 Porto, Portugal

Received: February 11, 2009; Revised Manuscript Received: March 13, 2009

New classes of acidic or basic ionic liquids (ILs) are gaining special attention, since the efficiency of many processes can be enhanced by the judicious manipulation of these properties. The absorption of sour gases can be enhanced by the basic character of the IL. The fluorination of the cation or the anion can also contribute to enhance the gas solubility. In this work these two characteristics are evaluated through the study of the gas–liquid equilibrium of two ionic liquids based on similar anions, 1-butyl-3-methylimidazolium acetate ([C₄mim][Ac]) and 1-butyl-3-methylimidazolium trifluoroacetate ([C₄mim][TFA]), with carbon dioxide (CO₂) at temperatures up to 363 K and pressures up to 76 MPa. The data reported are shown to be thermodynamically consistent. Henry's constants estimated from the experimental data show the solubility of CO₂ on the [C₄mim][Ac] to be spontaneous unlike in [C₄mim][TFA] due to the differences in solvation enthalpies in these systems. Ab initio calculations were performed on simple intermolecular complexes of CO₂ with acetate and trifluoroacetate using MP2/6-31G(d) and the G3 and G3MP2 theoretical procedures to understand the interactions between CO₂ and the anions. The theoretical study indicates that although both anions exhibit a simultaneous interaction of the two oxygen of the carboxylate group with the CO₂, the acetate acts as a stronger Lewis base than the trifluoroacetate. ¹³C high-resolution and magic angle spinning (HRMAS) NMR spectra provide further evidence for the acid/base solvation mechanism and the stability of the acetate ion on these systems. Further similarities and differences observed between the two anions in what concerns the solvation of CO₂ are discussed.

Introduction

Ionic liquids (ILs) are a class of *neoteric* organic solvents that have been the object of an unprecedented burst of interest, both from academia and industry, in recent years. The large organic cations and asymmetrical organic or inorganic anions compel these molecules to remain liquid at or near room temperature, while presenting, among other relevant properties, negligible vapor pressures, high thermal stability, large liquidus range, nonflammability, and high solvation capacity.^{1–4} The tunable properties of ILs, through an endless combination of cations and anions, allow the design of solvents for the development of more efficient and sustainable processes and products. These compounds' aptness for fine-tuning of their properties catalogued them as *designer solvents*. However, the design of a task-specific compound requires the definition of target properties and of the characteristics that are behind them.

Among the several applications foreseeable for task-specific ionic liquids such as solvents for reactions involving gaseous reactants and products,⁵ catalysts for acid-catalyzed organic reactions,⁶ and chemical absorption,⁷ their use in processes with compressed gases for capture/sequestration of sour gases such

as CO₂, H₂S, and SO₂, in refinery, coal combustion, and cleaning of gas streams, is one of the most exciting.

A considerable amount of work, concerning the development of task-specific ionic liquids, has been carried out, addressing essentially the IL cation. Bates et al.⁸ reported amino-functionalized ILs, while Yuan et al.⁹ and Sun et al.¹⁰ used hydroxyl-functionalized ILs as a novel efficient catalyst for chemical fixation of CO₂. Yu et al.⁷ and Huang et al.⁵ proposed guanidinium-based ILs, where the electron-donating groups increased the strength of the donor–acceptor interactions on -NH₂ and consequently enhanced the interactions between -NH₂ and CO₂. Li et al.⁶ investigated the ability of switching the ILs basicity by repeatedly bubbling CO₂ and N₂, improving efficiency of the processes. Bara et al.¹¹ synthesized imidazolium-based ILs with one, two, or three oligo(ethylene glycol) substituents that, in spite of presenting CO₂ solubilities similar to that in [C_nmim][Tf₂N] analogues, present lower solubilities toward N₂ and CH₄ and therefore enhanced selectivities.

Acidic or basic ILs represent new classes of acids or bases. The study of the acidity/basicity of the ILs is of great importance, since the efficiency of many processes depends on the basicity of the media or can be controlled by it. Crowhurst et al.¹² reported that the hydrogen bond basicities of ILs are controlled by the anion, and the hydrogen bond donating behavior is also dominated by the hydrogen bond basicity of the anions, with a smaller contribution from the hydrogen bond acidity of the cation. Furthermore, for the imide ionic liquids

* To whom correspondence should be addressed. Tel.: +351 234 401 507. Fax: + 351 234 370 084. E-mail: jcoutinho@ua.pt.

[†] Universidade de Aveiro.

[‡] Universidade Estadual de Campinas.

[§] Universidade do Porto.

an increase of the hydrogen bond acidity with the cation change was found.¹² Nonetheless, changing to more basic anions leads to a dramatic drop in the acidity. Pennline et al.¹³ screened quaternary ammonium polyether ILs as potential solvents for CO₂ capture based in the Pearson's "hard and soft acid–base" principles, where the solvent should possess a Pearson "hard base" allowing a strong affinity toward CO₂. Maginn et al.¹⁴ and Shiflett et al.^{15–17} reported on imidazolium-based ionic liquid with the acetate and other carboxylate anions that seem to present an uncharacteristic behavior. The systems with the acetate-based IL present a low vapor pressure for mixtures up to about 20 mol %, indicating that CO₂ could have formed a nonvolatile or very low vapor pressure molecular complex with the ionic liquid. The solvation of CO₂ by these anions is, however, yet poorly understood.

The present study will explore the basicity of the anion as a means to enhance the absorption of sour gases by ionic liquids, along with another strategy to foster the gas solubility in an IL by the fluorination of its alkyl chains.^{18,19} In this work the two effects will be compared and evaluated in a wide range of pressures and temperatures aiming at a better understanding of the mechanisms of solvation of CO₂ on ILs with these characteristics. For that purpose the gas–liquid equilibrium (GLE) of the atypical and challenging binary systems, CO₂ + 1-butyl-3-methylimidazolium acetate ([C₄mim][Ac]), and CO₂ + 1-butyl-3-methylimidazolium trifluoroacetate ([C₄mim][TFA]) previously approached only by Shiflett et al.,^{15–17} will be here extended to higher pressures, temperatures, and concentrations. The comparison between these two systems will provide not only a better understanding of the anion acid/base interactions with the CO₂ but also the influence of the fluoroalkyl groups in the molecule behavior and consequently, in the CO₂ solubility. A thermodynamic consistency test developed for systems with incomplete *PTxy* data,^{20–23} is here used to evaluate the quality of the data reported through its thermodynamic consistency.

There is plenty of evidence in the literature for Lewis acid/Lewis base (A/B) interaction between CO₂ and the carbonyl group.^{24–26} Raveendran and Wallen²⁷ have studied the role of a cooperative C–H···O interaction as an additional stabilizing interaction between the CO₂ and the carbonyl group and their implications for the solvation of CO₂ on these compounds. The CO₂ acts as a LA where the acidic central carbon interacts with charged or uncharged Lewis bases.

To understand the interactions between CO₂ and the [Ac] and [TFA] anions, ab initio calculations were performed on simple intermolecular complexes using MP2/6-31G(d), and the G3 and G3MP2 theoretical procedures. A simultaneous interaction, of the two oxygens of the carboxylate group with the CO₂, is found in both anions, [Ac] and [TFA].

¹³C high-resolution and magic angle spinning (HRMAS) NMR spectra of the CO₂ + [C₄mim][Ac] are shown to further support the acid/base interaction mechanism behind the solvation of CO₂ at low pressures. They also provide further evidence to the stability of the acetate on these systems.

Experimental Section

Materials. Two ILs based on the 1-butyl-3-methylimidazolium cation, namely, 1-butyl-3-methylimidazolium trifluoroacetate [C₄mim][TFA] and 1-butyl-3-methylimidazolium acetate [C₄mim][Ac], were used on this study. The [C₄mim][TFA] was acquired from Solchemar with mass fraction purities > 99% and bromide impurity mass fraction < 10⁻⁴, while the [C₄mim][Ac] was synthesized by means of carbonate-based ionic liquid synthesis (CBILS) of proionic/Sigma-Aldrich.²⁸

1-Butyl-3-methylimidazolium hydrogencarbonate (the CBIL precursor as a 50.0% solution in H₂O) was treated with an exact stoichiometric amount of acetic acid (FIXANAL/Riedel-de Haën). After the evolution of CO₂ ceased, water and solvents were removed under vacuum. The purities stated by the supplier and those of the [C₄mim][Ac] IL, were checked by ¹H NMR, ¹³C NMR, and ¹⁹F NMR. For the [C₄mim][Ac] the ¹H NMR obtained presents the following(chloroform-d, δ /ppm relative to TMS): 10.56 (s, 1H), 7.47 (d, 2H), 4.08 (s, 6H).

It is well-established that IL physical properties are influenced by their water content.^{29–32} Blanchard et al.³³ reported that even minor amounts of water, dissolved in [C₄mim][PF₆]_n, lead to a reduction of 77% on the CO₂ solubility. More recently, in a systematic study on the influence of water on the solubility of CO₂ for the same compound, Fu et al.³⁴ reported a less pronounced, <15%, influence. Nonetheless, these reports clearly state the importance of implementing purifying procedures prior to the measurements. Thus, to reduce the content of water and volatile compounds to negligible values, vacuum (0.1 Pa), stirring and moderate temperature (353 K) were applied for a period of at least 48 h prior to the measurements to the ILs. The final water content was determined with a Metrohm 831 Karl Fischer coulometer, indicating a water mass fraction of 495 × 10⁻⁶ and 554 × 10⁻⁶ for [C₄mim][TFA] and [C₄mim][Ac], respectively.

The CO₂ used was from Air Liquide with a purity of ≥99.998% and H₂O, O₂, C_nH_m, N₂, and H₂ impurity volume fractions lower than 3 × 10⁻⁶, 2 × 10⁻⁶, 2 × 10⁻⁶, 8 × 10⁻⁶, and 0.5 × 10⁻⁶, respectively.

Experimental Measurements. The high-pressure equilibrium cell used in this work is based on the synthetic method and is sketched in Figure 1. The cell is based on the design of Daridon et al.^{35–39} and was previously found to be adequate to measure IL systems.^{35,39} It consists of a horizontal hollow stainless steel cylinder, closed at one end by a movable piston and at the other end by a sapphire window. This window, along with a second window on the cell wall through which an optical fiber lights the cell chamber, allows the operator to follow the behavior of the sample with pressure and temperature. The orthogonal positioning of the sapphire windows minimizes the parasitic reflections and improves the observation in comparison to axial lighting.

A small magnetic bar placed inside the cell allows the homogenization of the mixture by means of an external magnetic stirrer. The sapphire window on the cell wall limits the minimum internal volume of the cell to 8 cm³, while the maximum value is set to 30 cm³. The presence of the magnetic stirrer as well as the cell reduced volume helps to minimize the inertia and temperature gradients within the sample.

The cell is thermostatized by circulating a heat-carrier fluid through three flow lines directly managed into the cell. The heat-carrier fluid is thermoregulated with a temperature stability of ±0.01 K by means of a thermostat bath circulator (Julabo MC). The temperature is measured with a high precision thermometer, Model PN 5207 with an accuracy of 0.01 K connected to a calibrated platinum resistance inserted inside the cell close to the sample. The pressure is measured by a piezoresistive silicon pressure transducer (Kulite HEM 375) fixed directly inside the cell to reduce dead volumes, which was previously calibrated and certified by an independent laboratory with IPAC accreditation, following the EN 837-1 standard and with accuracy better than 0.2%.

A fixed amount of IL was introduced inside the cell; its exact mass was determined by weighting, using a high-weight/high-

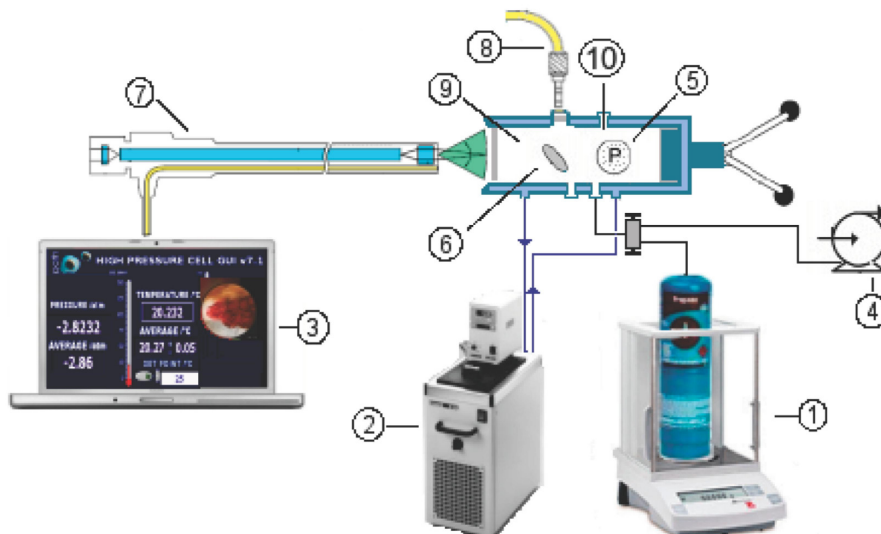


Figure 1. Schematic apparatus: 1, analytical balance (Sartorius LA200P); 2, thermostated bath circulator (Julabo MC); 3, computer for data and video acquisition; 4, vacuum pump (Edwards RV3); 5, piezo resistive pressure transducer (Kulite HEM 375); 6, magnetic bar; 7, endoscope plus a video camera; 8, light source with optical fiber cable; 9, high-pressure variable-volume cell; 10, temperature probe (K type thermocouple).

precision balance with an accuracy of 1 mg (Sartorius LA200P). To avoid any interference of atmospheric gases during the manipulation, after placing the IL inside the cell, this was kept under vacuum overnight, while stirring and heating at 353 K.

The CO₂ was introduced under pressure from an aluminum reservoir tank. Its quantity was measured on the precision balance and introduced into the measuring cell by means of a flexible high-pressure capillary.

After preparation of a mixture of known composition, it was allowed to reach the desired temperature at low pressure; the pressure was then slowly increased at constant temperature until the system becomes monophasic. The pressure at which the last bubble disappears represents the equilibrium pressure for the fixed temperature.

The purity of the IL is checked again by NMR at the end of the study to confirm that no degradation of the IL takes place during the measurements. The ¹H, ¹³C, and ¹⁹F NMR spectra were recorded using a Bruker Avance 300 at 300.13 MHz using deuterated water (D₂O) and/or deuterated chloroform (CDCl₃) as solvents (below the IL saturation limit and low enough to ensure complete dissociation in aqueous solution).

¹³C HRMAS spectra were recorded on a Bruker Avance DRX-500 spectrometer resonating at 125.8 MHz for carbon and using a HRMAS 4 mm double-bearing probe. The use of HRMAS technology allows higher resolution to be obtained for viscous liquids such as the ILs hereby studied. MAS rotors with a fixed bottom spacer and a sealable top spacer were employed, accommodating a total of 60 μ L of sample (50 μ L of ionic liquid and 10 μ L of 0.75% 3-(trimethylsilyl)propionate sodium salt (TSP) D₂O solution for chemical shift reference and lock purposes). Spectra were acquired at a 4 kHz spinning rate, with a 90° pulse of 5.3 μ s, a 2 s recycle delay, and 128 or 256 scans.

Thermodynamic Modeling and Consistency

Valderrama and Álvarez^{21–23} developed a thermodynamic consistency test for systems with incomplete PT_{xy} data, cataloging them as thermodynamic consistent (TC), thermodynamic inconsistent (TI), or not fully consistent (NFC). As in previous

works^{16,23,38} we have applied an extension of this approach to CO₂ + IL systems using a method based on the Gibbs–Duhem equation, using the Peng–Robinson equation of state (EoS),⁴⁰ with the Wong–Sandler mixing rule.⁴¹ A detailed description of that approach can be found in the Supporting Information. The equation of state was used to estimate the Henry's constants for the systems studied.¹⁶

Results and Discussion

Experimental Data. High-pressure gas–liquid data for mixtures of CO₂ and ILs are scarce, and important discrepancies among data from different authors^{19,42,43} can be found in the literature.

The solubility of carbon dioxide in the ILs studied in this work was measured for mole fractions from 0.2 to 0.8, in the temperature range from 293 to 363 K and pressures from 0.2 to 76 MPa, as reported in Tables 1 and 2 and depicted in Figure 2. The shape of the phase diagrams obtained for these systems is analogous to what was previously reported to binary mixtures of CO₂ and ionic liquids. At low CO₂ concentrations, the pressure increase with the CO₂ content is almost linear, while for CO₂ mole fractions higher than 0.4 for [C₄mim][Ac] and 0.55 for [C₄mim][TFA] a dramatic increase in pressure with concentration is observed. At temperatures below the CO₂ critical temperature a two-phase region is observed above these concentrations. The most surprising feature observed on these systems is the very large solubility of CO₂ in [C₄mim][Ac] up to a mole fraction of 0.3. This IL seems to be able to dissolve a very large amount of carbon dioxide at low pressure. This was also observed by Shifflet et al.^{15–17} In spite of this larger solubility at low pressures, as the CO₂ concentration increases, its solubility in [C₄mim][Ac] becomes inferior to the solubility in [C₄mim][TFA] as observed in Figure 3.

The results of the application of the thermodynamic consistency test to the binary systems containing ionic liquids is presented in Table 3 for the thermodynamically consistent data, and in the Supporting Information, for all the experimental data. In this table, NP is the number of data points, T is the

TABLE 1: Bubble Point Data of the System CO₂ (1) + [C₄mim][Ac]

x_1	T/K	p/MPa	x_1	T/K	p/MPa
0.201	323.05	0.230	0.402	323.57	5.272
0.201	333.07	0.355	0.402	333.35	6.580
0.201	343.18	0.652	0.402	343.16	8.060
0.201	353.10	0.971	0.402	353.24	9.850
0.251	313.09	0.498	0.450	313.09	5.730
0.251	322.96	0.830	0.450	323.00	7.394
0.251	333.30	1.275	0.450	333.27	9.564
0.251	343.05	1.695	0.450	343.06	12.188
0.251	353.20	2.235	0.450	353.18	15.281
0.300	313.04	1.398	0.500	322.98	13.478
0.300	323.22	1.923	0.500	333.06	18.051
0.300	333.33	2.515	0.500	343.10	22.985
0.300	343.10	3.205	0.500	353.13	28.055
0.300	352.98	3.980	0.550	313.31	27.965
0.351	313.04	2.589	0.550	323.40	34.865
0.351	322.83	3.360	0.550	333.37	41.807
0.351	333.42	4.288	0.550	343.25	48.107
0.351	343.22	5.265	0.550	353.05	53.904
0.351	353.22	6.430	0.599	313.10	67.371
0.402	313.07	4.090	0.599	323.09	75.526

TABLE 2: Bubble Point Data of the System CO₂ (1) + [C₄mim][TFA]

x_1	T/K	p/MPa	x_1	T/K	p/MPa
0.225	293.43	0.979	0.502	313.18	5.860
0.225	303.22	1.338	0.502	323.49	7.413
0.225	313.20	1.706	0.502	333.35	9.135
0.225	323.11	2.146	0.502	343.07	11.151
0.225	333.35	2.587	0.502	353.03	13.225
0.225	343.23	3.105	0.502	363.03	15.498
0.225	353.08	3.612	0.601	293.44	7.936
0.225	363.04	4.165	0.601	303.21	13.268
0.300	293.25	1.540	0.601	313.21	18.548
0.300	303.30	2.056	0.601	323.21	22.835
0.300	313.15	2.619	0.601	333.09	28.263
0.300	323.08	3.160	0.601	343.14	32.589
0.300	333.06	3.912	0.601	353.10	36.545
0.300	343.15	4.726	0.601	363.12	42.075
0.300	353.13	5.559	0.650	293.46	26.422
0.300	363.18	6.416	0.650	303.35	32.581
0.401	293.52	2.419	0.650	313.17	37.835
0.401	303.23	3.108	0.650	323.04	43.392
0.401	313.14	3.959	0.650	333.25	48.458
0.401	323.04	4.840	0.650	343.06	52.947
0.401	333.08	5.996	0.650	353.11	56.890
0.401	343.02	6.957	0.650	363.10	62.989
0.401	353.07	8.144	0.679	293.59	43.625
0.401	363.07	9.337	0.679	303.34	50.189
0.502	293.61	3.513	0.679	313.08	55.966
0.502	303.40	4.611	0.679	323.08	62.473

temperature, and k_{12} , α_{12} , $g_{12} - g_{22}$ and $g_{21} - g_{11}$ are the interaction parameters of the model, where 1 stands for the CO₂ and 2 for the ionic liquid. This table is divided into sections for each system studied. The CO₂ + [C₄mim][Ac] system determined by Shifflet et al.¹⁵ was also investigated. The parameters used in the thermodynamic model are reported in Table 4. The consistency test shows that, in general, the data measured in this work are thermodynamically consistent with the exception, in a few cases, of the mixtures richer in CO₂. The results obtained denote larger deviations in individual areas for the CO₂ + [C₄mim][Ac] system for $x_1 > 0.5$ isopleths and for the CO₂ + [C₄mim][TFA] system for the $x_1 > 0.65$ isopleths leading to not fully consistent isotherms. However, these data points at higher CO₂ concentrations must be considered with care, since they present a more complex phase behavior which could be

the cause for the apparent inconsistencies. The data for the CO₂ + [C₄mim][Ac] system here reported present a thermodynamic coherence superior to the data previously reported by Shifflet et al.,¹⁵ in particular at lower and higher temperatures for which the data present deviations larger than the established limit for the values of $\% \Delta p_i$ and thereafter, the test could not be applied, denoting inaccuracies in the experimental data measurements.

As depicted in Figure 4, the equation of state used provides a good description of the experimental data.

Henry's Constants. Henry's law relates the fugacity of a gas dissolved in a liquid with its concentration and can be described as

$$H_{12}(T, P) = \lim_{x_1 \rightarrow 0} \left(\frac{f_i^L}{x_1} \right) \quad (1)$$

where $H_{12}(T, P)$ is the Henry's constant, x_1 is the mole fraction of gas dissolved in the liquid phase, and f_i^L is the fugacity of gas in the liquid phase. As shown, eq 1 is only rigorously valid in the diluted region limit. Given the good description of the experimental data provided by the equation of state used, the Henry constants for the CO₂ in the ILs studied in this work were estimated by extrapolating the equation of state description of the experimental data to the dilute region.¹⁶ Although this approach introduces some uncertainty on the estimated Henry's constants, they are different enough to allow a discussion of the interactions between the CO₂ and the ionic liquid based on these values. The estimated Henry's constants are reported in Table 3. The results indicate that the Henry's constant decreases slightly (i.e., CO₂ solubility increases) as the temperature decreases. Nonetheless, Henry's constant for the [C₄mim][TFA] presents a larger temperature dependence than the one of [C₄mim][Ac].

The results for the Henry's constant of CO₂ in [C₄mim][Ac] and CO₂ in [C₄mim][TFA] were correlated as a function of temperature by an empirical equation of the type

$$\ln(H_{12}) = A\left(\frac{1}{T}\right) + B \quad (2)$$

where coefficients A and B obtained are listed in Table 5, together with the Henry's constant average absolute deviations, $|\Delta H_{12}|$, obtained for each ionic liquid.

The effect of temperature on the CO₂ solubility can be related to the Gibbs energy of solvation, the partial molar entropy, and the partial molar enthalpy of solvation⁴⁴ that can be calculated from an appropriate correlation of Henry's constant:

$$\Delta_{\text{solv}} G^\circ = RT(\ln(H_{12}))_p \quad (3)$$

$$\Delta_{\text{solv}} H^\circ = -T^2 \left(\frac{\partial \Delta_{\text{solv}} G^\circ}{\partial T} \right)_T = -RT^2 \left(\frac{\partial \ln H_{12}}{\partial T} \right)_p \quad (4)$$

$$\Delta_{\text{solv}} S^\circ = \frac{\Delta_{\text{solv}} H^\circ - \Delta_{\text{solv}} G^\circ}{T} = -RT \left(\frac{\partial \ln H_{12}}{\partial T} \right)_p - R \ln(H_{12})_p \quad (5)$$

The partial molar enthalpy of gas solvation gives an indication of the strength of interactions between the gas and IL, while the partial molar entropy illustrates the amount of ordering present in the gas/IL mixture.

The results in Table 5 show that the partial molar entropies in both fluids are essentially identical, indicating a similar structural solvation interaction. The partial molar enthalpy of solvation of the CO₂ in [C₄mim][Ac] is lower than in [C₄mim][TFA], indicating a stronger interaction between the

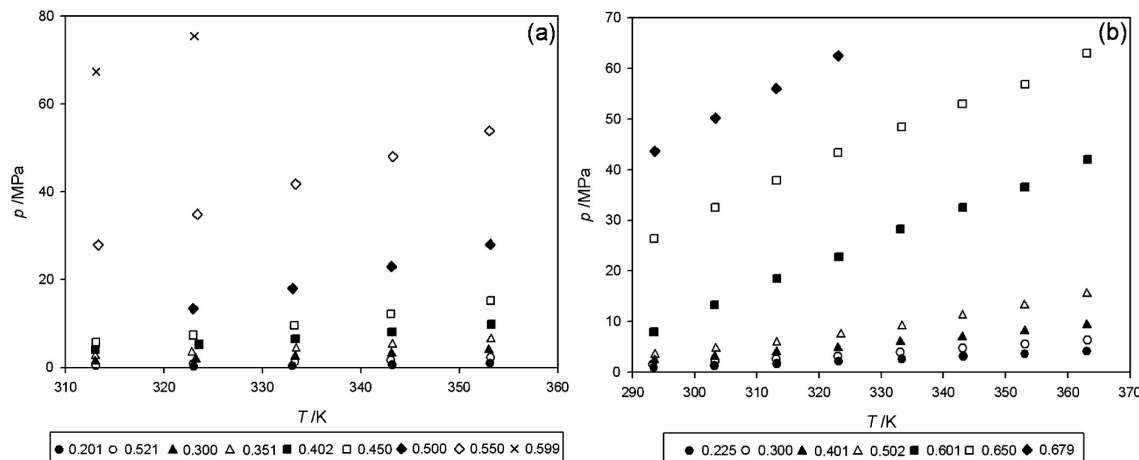


Figure 2. Pressure-temperature diagram of the binary systems (a) CO₂ + [C₄mim][Ac] and (b) CO₂ + [C₄mim][TFA].

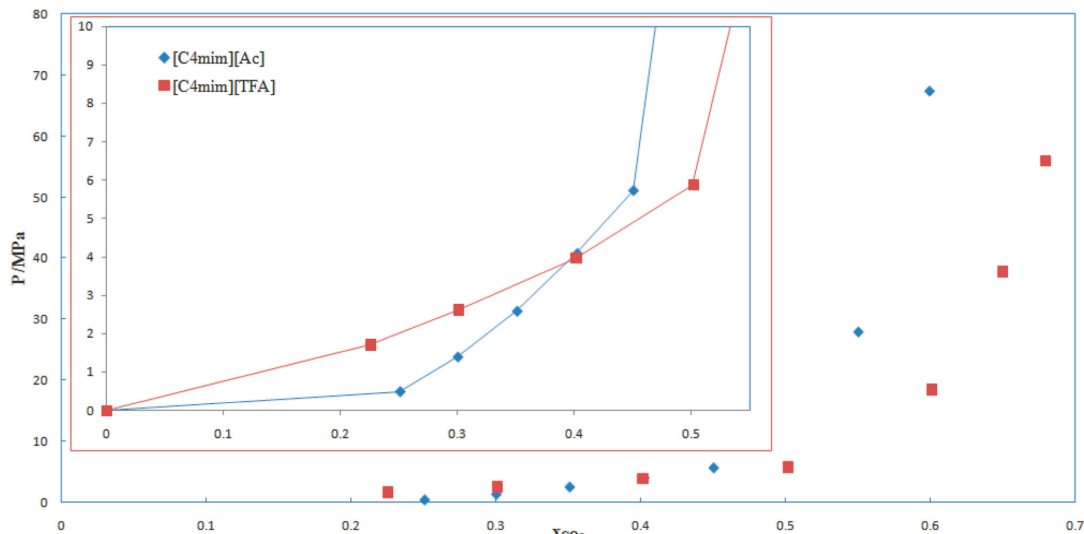


Figure 3. Pressure-composition diagram of the binary systems CO₂ + [C₄mim][Ac] and CO₂ + [C₄mim][TFA] at 313 K.

CO₂ and the [C₄mim][Ac] when compared with the [C₄mim][TFA]. The differences between the enthalpies and entropies of solvation contribution observed make the solubility of CO₂ in [C₄mim][Ac] spontaneous, unlike for [C₄mim][TFA], which explains the large solubility observed at low pressures.

To obtain further information about the interaction CO₂/[C₄mim][Ac], which seems to be responsible for the enhanced solubility of CO₂ in this IL at low pressures, ¹³C HRMAS NMR spectra of the pure and CO₂-saturated IL at atmospheric pressure were acquired and reported in Figure 5. The comparison between the two spectra shows an important downfield shift of the carboxylate carbon (11) (from 179 to 183 ppm) due to the presence of CO₂ and indicating the Lewis acid/base interaction to be responsible for the enhanced solubility of CO₂ in this solvent. The upfield shift in carbon (12), the other anion carbon, results also from this acid/base interaction with CO₂. The other major difference observed on these spectra is related to the cation carbon (2), which is connected to an acid hydrogen. In the absence of CO₂ (Figure 5a), this resonance is significantly broadened and so are, to a lesser extent, ring resonances C(4)

and C(5). This is expected due the proximity to the quadrupolar nuclei of the neighboring ¹⁴N atoms, in case molecular motion is relatively slow and unable to average out ¹³C/¹⁴N interactions. The introduction of CO₂ in the system will shift the interaction of the acetate from the imidazolium ring, and particularly C(2), toward the gas, increasing the mobility of the imidazolium ring with a noticeable effect on the peaks of the carbon at the imidazolium ring, most spectacularly C(2). Interestingly, in both systems resonances C(6) and C(10) are also broadened due to nitrogen proximity. These spectra also confirm that, even in the presence of CO₂, there is no formation of acetic acid in the system as suggested by some authors.^{14,15} The fact that a CO₂ peak is not observed (possibly at about 120–130 ppm) can only be attributed to the high mobility of this molecule in solution. Its strong interaction with the acetate does not bind it to the carboxylate group but instead the CO₂ must be quickly changing among neighbor carboxylates.

Solubility measurements,^{43,45} spectroscopic studies,⁴⁶ and molecular simulations⁴⁵ indicated that CO₂ solubility in ILs depends primarily on the strength of interaction of the CO₂ with

TABLE 3: Estimated Interaction Parameters, for the Thermodynamically Consistent Data, and Henry Constant Predicted for the CO₂ (1) + ILs (2) Systems at Different Temperatures

ref	NP	T/K	k_{ij}	α_{12}	$g_{12}-g_{22}/(J/mol)$	$g_{21}-g_{11}/(J/mol)$	$ \Delta p /\%$	$ \Delta A /\%$	H/MPa
CO ₂ + [C ₄ mim][Ac]									
15	8	298.10	-0.6470	0.2166	-32855.6133	5999.5654	2.5	6.1	
	7	323.10	1.0000	0.3244	-11206.7412	2763.3943	3.4	7.3	
this work	5	313.10	-0.0146	0.2979	-29707.8203	7932.1289	1.3	3.8	0.056
	7	323.09	-0.3497	0.2482	-50410.7500	-1595.7640	1.0	4.6	0.086
	7	333.00	0.2981	0.3177	-40720.8945	-2724.8025	2.6	9.4	0.121
	7	343.00	-0.8572	0.3043	-44254.0312	89950.4766	4.2	10.8	0.137
	6	348.00	0.7969	0.4229	-32920.5625	-3534.8833	1.2	2.7	0.203
	6	352.98	0.9949	0.4392	-33570.1133	-4218.7607	0.8	3.7	0.253
	CO ₂ + [C ₄ mim][TFA]								
this work	5	294.00	0.2188	0.2045	34112.2930	-2444.4580	5.8	4.3	3.40
	5	298.00	0.2236	0.2059	34037.5859	-2354.5664	6.2	4.7	3.85
	5	303.00	0.2422	0.2027	34804.6875	-2620.2393	3.1	7.1	4.03
	4	313.00	0.0625	0.2132	35599.7812	-1764.0344	0.6	4.2	5.93
	4	323.00	0.2745	0.2497	33887.6523	-1097.2380	0.8	4.4	7.45
	5	333.00	-0.0063	0.2001	42388.7930	-1258.0310	0.7	15.3	8.97
	5	343.00	0.0801	0.2000	45219.8125	-781.5312	1.2	11.7	11.74
	5	348.00	-0.0001	0.2008	46516.1133	-791.0156	1.5	9.3	11.94
	5	353.00	0.1250	0.2006	47268.5469	-702.7494	1.9	12.5	13.50
	4	363.00	0.1601	0.2026	46758.0273	-1230.8120	6.0	4.4	13.57

TABLE 4: Properties of the Substances Used in the Modeling

compound	T_c/K	p_c/MPa	ω
CO ₂	304.21 ^a	7.38 ^a	0.2236 ^a
[C ₄ mim][TFA]	826.72 ^b	2.09 ^b	0.6891 ^b
[C ₄ mim][Ac]	847.31 ^b	2.44 ^b	0.6681 ^b

^a Reference 57. ^b Calculated with ref 23.

the anion. Furthermore, Crowhurst et al.¹² reported that in terms of solvation the ionic liquid hydrogen bond donor behavior was dominated by the hydrogen bond basicity of the anions, with a low contribution from the hydrogen bond acidity of the cation. Thus, the presence of fluoroalkyl groups in the basic trifluoroacetate anion based ILs⁴⁷ makes them “CO₂-philic”, meaning that they present higher CO₂ solubilities than other ILs, resulting in lower equilibrium pressures. This behavior, not yet fully understood, seems to be related to the interaction between the negative fluorine atoms and the positive charge on the carbon of the CO₂ molecule.^{19,48–51} Anderson et al.⁵² suggests that the Tf₂N anion is the anion displaying the most significant influence in the hydrogen bond donor ability of the IL. In fact, Anderson’s statement reflects well the behavior of the [C₄mim][Tf₂N] and [C₄mim][TFA] ILs, since both present higher solubility, than other ILs, for a wider range of CO₂ mole fractions.^{39,53}

The comparison between the solubilities of CO₂ in [C₄mim][Ac] and [C₄mim][TFA] reveals a curious behavior. For low CO₂ molar fractions (<30%) the [C₄mim][Ac] presents higher CO₂ solubility than any IL previously studied¹⁵ but, as the CO₂ molar fraction increases, the solubility in [C₄mim][Ac] quickly drops below the solubility in [C₄mim][TFA] as shown in Figure 3. This behavior could be explained by a chemisorption taking place in [C₄mim][Ac] at low CO₂ pressure, but as the chemical solvation sites become saturated and the physisorption dominates, the solvation capacity of the fluorinated acetate becomes dominant. The fluorination of the acetate seems however to reduce its chemical solvation capacity. For a deeper understanding of these interactions we resorted to ab initio calculations to analyze the interactions between the fluorinated and non-fluorinated acetate and the CO₂.

Ab Initio Calculations. Ab initio calculations on the CO₂/[Ac] and CO₂/[TFA] interactions were performed using the

Gaussian 03 program.⁵⁴ Geometry optimizations were performed at the second-order Møller–Plesset (MP2) level using the 6-31+G(d) basis set to include the effects of electron correlation. The vibrational frequencies were also calculated to confirm that the structures were at the real potential energy minimum. The optimized geometries are shown in Figures 6 and 7 for the CO₂ complex with the acetate and trifluoroacetate, respectively. The CO₂ is interacting as Lewis acid with the acetate group, which acts as Lewis base. The CO₂ molecule is significantly distorted from linearity. The shorter C(carboxylate) to C(CO₂) distance and the larger CO₂ distortion angle in the CO₂ complex with the acetate is a structural indication that the CO₂/[Ac] interaction is stronger than CO₂/[TFA].

Conformation “B”, depicted in Figure 8, represents the complex formation of the CO₂ with the oxygen of the carboxylate that was found to have a local energy minimum with a MP2/6-31+G(d).

The Gaussian-3 (G3)⁵⁵ and (G3MP2)⁵⁶ theoretical procedures were used to evaluate the interaction enthalpies of the complexes between the acetate Lewis base (B) and the CO₂ Lewis acid (A) according the following equation:

$$\Delta H = H_{AB} - (H_A + H_B) \quad (6)$$

where H_{AB} is the G3 or G3MP2 enthalpy of the CO₂ complex with acetate or trifluoroacetate and the H_A and H_B represent the G3 or G3MP2 enthalpies of the monomers. Gaussian-3 (G3) theory is based on the 6-31G(d,p) basis set and several basis extensions, including the G3 large basis set. Geometries are calculated at the MP2(full)/6-31G(d) level, and scaled (0.8929) HF/6-31G(d) zero point energies (ZPEs) are included in the final energies. Treatment of electron correlation is done by Møller–Plesset (MP) perturbation theory and quadratic configuration interaction, and the final energies are effectively performed at the QCISD(T)/G3 large level. Gaussian-3 (G3MP2) theory represents a simplification of the G3 theory with a reduced MP order, thus eliminating the MP4 calculation.

The enthalpic interactions were also evaluated directly using the MP2/6-31+G(d) energies. ZPEs and the enthalpic correction to 298 K were included in the interaction using the MP2 frequencies scaled by 0.95 for the calculation of ZPEs and the enthalpies correction to 298 K. The basis set superposition errors (BSSE) for the MP2/6-31+G(d) interaction was also evaluated

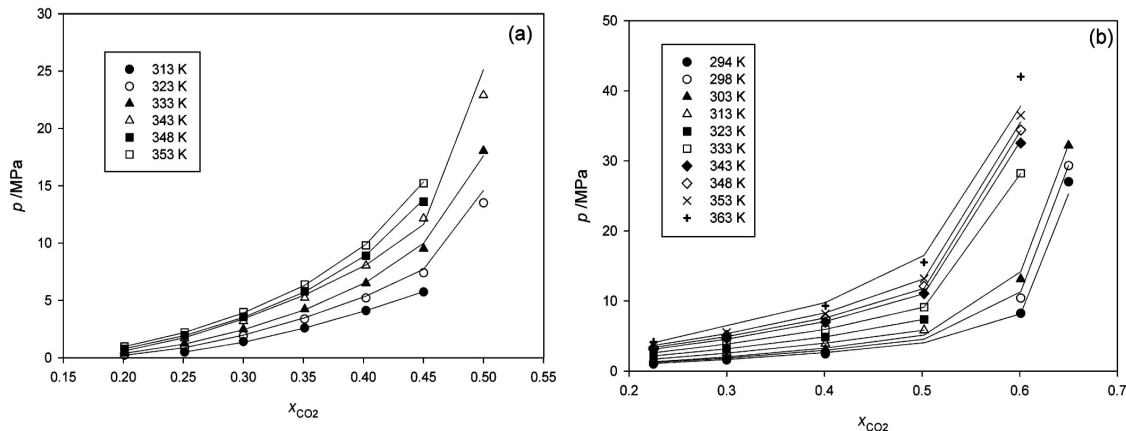


Figure 4. PTx diagram and modeling for the systems $\text{CO}_2 + [\text{C}_4\text{mim}][\text{Ac}]$ (a) and $\text{CO}_2 + [\text{C}_4\text{mim}][\text{TFA}]$ (b). The solid lines represent the calculations from PR-WS/NRTL EoS.

TABLE 5: Coefficients A and B, Partial Molar Enthalpy, and Partial Molar Entropy Obtained for CO₂ (1) + ILs (2)

ionic liquid	A/K	B	$ \Delta H_{12} /\text{kcal/mol}$	$\Delta_{\text{sol}}H^{\circ}/(\text{kJ mol}^{-1})$	$\Delta_{\text{sol}}S^{\circ}/(\text{J K}^{-1} \text{mol}^{-1})$	$-T\Delta_{\text{sol}}S^{\circ}_{T=298\text{K}}/(\text{kJ mol}^{-1})$
[C ₄ mim][Ac]	-3892 ± 365	11.84 ± 1.09	0.45	-32.4 ± 3.0	-98.5 ± 9.1	29.4 ± 2.7
[C ₄ mim][TFA]	-2325 ± 106	11.44 ± 0.33	0.22	-19.3 ± 0.9	-95.2 ± 2.7	28.4 ± 0.8

^a Standard enthalpy. ^b Standard ($P_0 = 0.1$ MPa) molar entropy.

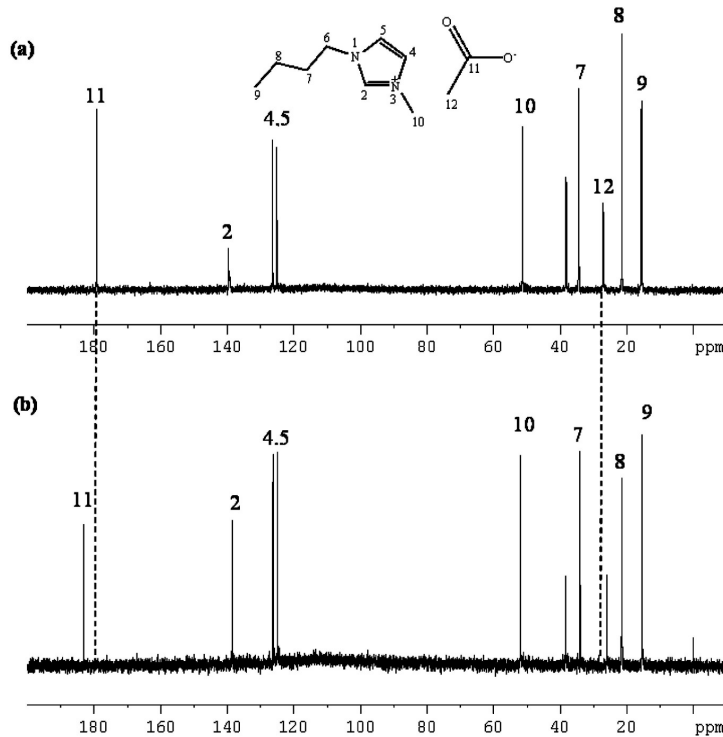


Figure 5. ^{13}C HRMAS NMR spectra for pure [C₄mim][Ac], 128 scans (a), and [C₄mim][Ac] saturated with CO₂, 256 scans (b).

and found to be negligible, taking into account the large energy interaction. The binding enthalpies at the different levels of theory are listed in Table 6. It is interesting to observe that the difference between the enthalpic interactions (acetate and trifluoroacetate) obtained by ab initio in gas phase (7–10 kJ mol⁻¹) present a good agreement with the experimental differ-

ence between the enthalpy of solvation of the CO₂ in the [C₄mim][Ac] and in [C₄mim][TFA] (13.1 ± 3.1 kJ mol⁻¹).

The calculated interactions support the idea of a chemisorption of CO₂ in [C₄mim][Ac] but seem to fail in explaining the low, and nonspontaneous nature, of CO₂ solubility in [C₄mim][TFA] as both interactions seem to be similar with a difference of just

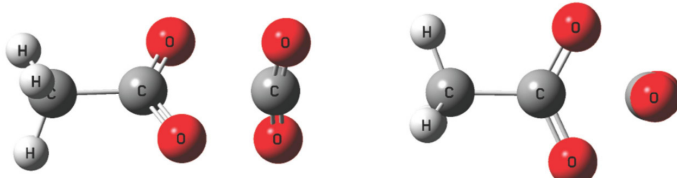


Figure 6. Geometry optimizations of the CO_2 -acetate complex (conformation A) at MP2/6-31+G(d) level of theory: carbon to carbon distance C(carboxylate)-C(CO_2), 2.963 Å; CO_2 , O-C-O angle, 169.0°.

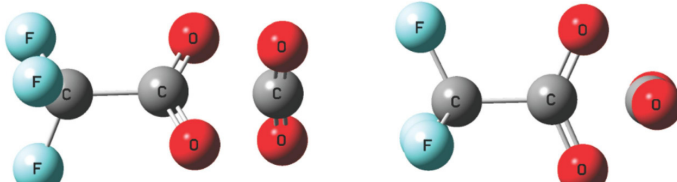


Figure 7. Geometry optimization of the CO_2 -trifluoroacetate complex at the MP2/6-31+G(d) level of theory: carbon to carbon distance C(carboxylate)-C(CO_2), 3.059 Å; CO_2 , O-C-O angle, 172.9°.

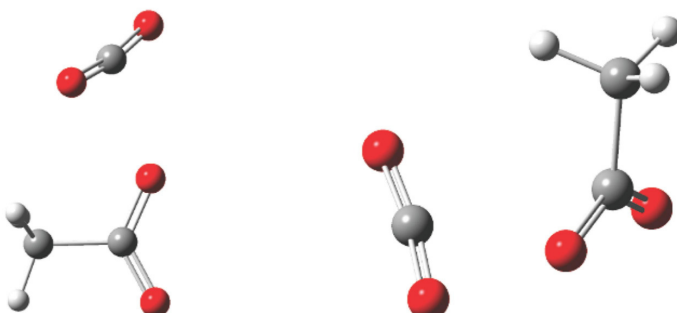


Figure 8. Geometry optimization of the CO_2 -acetate complex (conformation B) at the MP2/6-31+G(d) level of theory: carbon to carbon distance O(carboxylate)-C(CO_2), 2.466 Å; CO_2 , O-C-O angle, 169.5°.

TABLE 6: Enthalpies of Complex Formation between the Acetate/Trifluoroacetate with the CO_2 in Gas Phase Derived by ab Initio Calculation at Different Levels of Theory (Values in kilojoules per mole)

	$\Delta H(\text{Ac}:\text{CO}_2)$ acetate $\cdots\text{CO}_2$	$\Delta H(\text{TFA}:\text{CO}_2)$ trifluoroacetate $\cdots\text{CO}_2$	diff ^b
Gaussian G3 (conformation "A")	-41.4	-33.7	+7.7
Gaussian G3(MP2) (conformation "A")	-39.5	-32.2	+7.3
MP2/6-31+G(d) ^a (conformation "A")	-42.0	-31.8	+10.2
MP2/6-31+G(d) ^a (conformation "B")	-29.7		

^a Zero point energies and enthalpy correction were performed using the values of harmonic frequencies scaled by 0.95. ^b Diff = $\Delta H(\text{TFA}:\text{CO}_2) - \Delta H(\text{Ac}:\text{CO}_2)$.

13 kJ mol⁻¹ between the two. Yet this small difference does make all the difference and is indeed enough to explain the differences observed between the two ILs. Since, as shown before, the entropies of solvation are identical in the two ionic liquids, the differences in the Gibbs energy of solvation arise essentially from the differences in the enthalpies of solvation. If eq 3 is used to estimate the differences in the Gibbs energies of solvation between the two fluids in the temperature range of 313–353 K, these values range between 11.6 and 12.1 kJ mol⁻¹. The differences in solubility between the two fluids result essentially from their solvation enthalpy differences and a value of 11–12 kJ mol⁻¹ is enough to explain the observed solubility difference. The “chemisorption” observed is nothing more than the expression of the spontaneous solubility of CO_2 on the ionic liquid due to an enthalpy of solvation larger than the corresponding entropy of solvation. We postulate that all ionic liquids with an enthalpy of solvation contribution superior to their

entropy of solvation contribution to the Gibbs free energy of solvation, and thus to the solubility, will present a behavior similar to what is presented by [C₄mim][Ac], while the others will behave as [C₄mim][TFA]. This could explain the differences observed between ionic liquids with carboxylate anions studied by Yokozeki et al.,¹⁶ where some do have a “chemisorption-like” behavior while others do not. More studies are however required to provide support for this hypothesis.

Conclusions

Gas solubility of CO_2 in two ionic liquids, namely, 1-butyl-3-methylimidazolium acetate and 1-butyl-3-methylimidazolium trifluoroacetate, has been investigated in a wide range of temperatures, pressures and CO_2 mole fractions, aiming at understanding the effect of the basicity and the fluorination of the anion on the gas solubility in the ionic liquids.

The two systems studied present interesting contrasting behaviors. The binary system 1-butyl-3-methylimidazolium acetate + CO₂ at low pressures presents a high CO₂ solubility, larger than those observed for the other ILs at these pressures, but as the CO₂ molar fraction increases, the solubility decreases exponentially and the solubilities become more important on [C₄mim][TFA] at high pressures.

The data are shown to be thermodynamically consistent, and the Peng–Robinson EoS with the Wong–Sandler/NRTL mixing rule allows a good description of the experimental data and the estimation of the Henry constants for these systems. The partial Gibbs energy, enthalpies, and entropies of solvation estimated from the Henry's constants show the solubility of CO₂ in [C₄mim][Ac] to be spontaneous at the standard pressure (0.1 MPa), while the entropies of solvation in the two systems are essentially identical, making the solubility on these systems controlled by the solvation enthalpies.

¹³C HRMAS NMR spectra and ab initio calculations indicate that the preferential interaction of the CO₂ with [C₄mim][Ac] results from an acid/base interaction between the carboxylate and the acid carbon in the CO₂ molecule. A good agreement between the measured and calculated differences in the interactions between the CO₂ and the anion in the two systems were obtained, and it is shown that, in the diluted region, a difference in the order of 10 kJ mol⁻¹ in the interaction energy is enough to explain the solubility differences observed between the two systems.

Acknowledgment. This work was supported by Fundação para a Ciência e a Tecnologia (Project POCI/EQU/58152/2004). P.J.C. and B.S. acknowledge the financial support from Fundação para a Ciência e a Tecnologia through, respectively, their Ph.D. (Grant SFRH/BD/41562/2007) and postdoctoral scholarships (Grant SFRH/BPD/38637/2007). We acknowledge FAPESP (Fundação de Amparo à Pesquisa do Estado de São Paulo), Process No. 2006/03711-1. We are also grateful to Catarina M. S. S. Neves and Prof. Artur M. Silva for the help with the NMR spectra.

Supporting Information Available: Text describing the thermodynamic modeling and consistency with supporting references and tables listing consistency test results, interpolated VLE data, and detailed results of the studied systems. This material is available free of charge via the Internet at <http://pubs.acs.org>.

References and Notes

- (1) Rogers, R. D.; Seddon, K. R. *Science* **2003**, *302*, 792–793.
- (2) Marsh, K. N.; Boxall, J. A.; Lichtenhaler, R. *Fluid Phase Equilib.* **2004**, *219*, 93–98.
- (3) Chiappe, C.; Pieraccini, D. *J. Phys. Org. Chem.* **2005**, *18*, 275–297.
- (4) Earle, M. J.; Esperanca, J. M. S. S.; Gilea, M. A.; Canongia Lopes, J. N.; Rebelo, L. P. N.; Magee, J. W.; Seddon, K. R.; Widgren, J. A. *Nature (London)* **2006**, *439*, 831–834.
- (5) Huang, J.; Riisager, A.; Berg, R. W.; Fehrmann, R. *J. Mol. Catal. A: Chem.* **2008**, *279*, 170–176.
- (6) Li, W.; Zhang, Z.; Han, B.; Hu, S.; Song, J.; Xie, Y.; Zhou, X. *Green Chem.* **2008**, *10*, 1142–1145.
- (7) Yu, G.; Zhang, S.; Yao, X.; Zhang, J.; Dong, K.; Dai, W.; Mori, R. *Ind. Eng. Chem. Res.* **2006**, *45*, 2875–2880.
- (8) Bates, E.; Mayton, R.; Ntai, I.; Davis, J. *J. Am. Chem. Soc.* **2002**, *124*, 926–927.
- (9) Yuan, X.; Zhang, S.; Liu, J.; Lu, X. *Fluid Phase Equilib.* **2007**, *257*, 195–200.
- (10) Sun, J.; Zhang, S.; Cheng, W.; Ren, J. *Tetrahedron Lett.* **2008**, *49*, 3588–3591.
- (11) Bara, J. E.; Gabriel, C. J.; Lessmann, S.; Carlisle, T. K.; Finotello, A.; Gin, D. L.; Noble, R. D. *Ind. Eng. Chem. Res.* **2007**, *46*, 5380–5386.
- (12) Crowhurst, L.; Mawdsley, P. R.; Perez-Arlandis, J. M.; Salter, P. A.; Welton, T. *Phys. Chem. Chem. Phys.* **2003**, *5*, 2790–2794.
- (13) Pennline, H. W.; Luebke, D. R.; Jones, K. L.; Myers, C. R.; Morsi, B. I.; Heintz, Y. J.; Ilconich, J. B. *Fuel Process. Technol.* **2008**, *89*, 897–907.
- (14) Maginn, E. J. *Quarterly Technical Report to DOE*, DOE Award No. DE-FG26-04NT42122, May 31, 2005.
- (15) Shiflett, M. B.; Kasprzak, D. J.; Junk, C. P.; Yokozeki, A. *J. Chem. Thermodyn.* **2008**, *40*, 25–31.
- (16) Yokozeki, A.; Shiflett, M. B.; Junk, C. P.; Grieco, L. M.; Foo, T. *J. Phys. Chem. B* **2008**, *112*, 16654–16663.
- (17) Shiflett, M. B.; Yokozeki, A. *J. Chem. Eng. Data* **2009**, *54*, 108–114.
- (18) Muldoon, M.; Aki, S.; Anderson, J.; Dixon, J.; Brennecke, J. F. *Phys. Chem. B* **2007**, *111*, 9001–9009.
- (19) Aki, S. N. V. K.; Mellein, B. R.; Saurer, E. M.; Brennecke, J. F. *J. Phys. Chem. B* **2004**, *108*, 20355–20365.
- (20) Alvarez, V. H.; Aznar, M. *J. Chin. Inst. Chem. Eng.* **2008**, *39*, 353–360.
- (21) Valderrama, J. O.; Alvarez, V. H. *Fluid Phase Equilib.* **2004**, *226*, 149–159.
- (22) Alvarez, V. H.; Aznar, M. *Open Thermodyn. J.* **2008**, *2*, 25–38.
- (23) Valderrama, J. O.; Reategui, A.; Sanga, W. W. *Ind. Eng. Chem. Res.* **2008**, *47*, 8416–8422.
- (24) Cabaço, M. I.; Dantén, Y.; Tassaing, T.; Longelin, S.; Besnard, M. *Chem. Phys. Lett.* **2005**, *413*, 258–262.
- (25) Nelson, M. R.; Borkman, R. F. *J. Phys. Chem. A* **1998**, *102*, 7860–7863.
- (26) Kazarian, S. G.; Vincent, M. F.; Bright, F. V.; Liotta, C. L.; Eckert, C. A. *J. Am. Chem. Soc.* **1996**, *118*, 1729–1736.
- (27) Raveendran, P.; Wallen, S. L. *J. Am. Chem. Soc.* **2002**, *124*, 12590–12599.
- (28) Sigma-Aldrich CBILS Chemical Synthesis: http://www.sigmaplaldrich.com/Area_of_Interest/Chemistry/Chemical_Synthesis/Product_Highlights/CBILS.html.
- (29) Freire, M. G.; Carvalho, P. J.; Fernandes, A. M.; Marrucho, I. M.; Queimada, A. J.; Coutinho, J. A. *J. Colloid Interface Sci.* **2007**, *314*, 621–630.
- (30) Seddon, K. R.; Stark, A.; Torres, M. *Pure Appl. Chem.* **2000**, *72*, 2275–2287.
- (31) Huddleston, J. G.; Visser, A. E.; Reichert, W. M.; Willauer, H. D.; Broker, G. A.; Rogers, R. D. *Green Chem.* **2001**, *3*, 156–164.
- (32) Gardas, R. L.; Freire, M. G.; Carvalho, P. J.; Marrucho, I. M.; Fonseca, I. M. A.; Ferreira, A. G. M.; Coutinho, J. A. P. *J. Chem. Eng. Data* **2007**, *52*, 80–88.
- (33) Blanchard, L.; Gu, Z.; Brennecke, J. *J. Phys. Chem. B* **2001**, *105*, 2437–2444.
- (34) Fu, D.; Sun, X.; Pu, J.; Zhao, S. *J. Chem. Eng. Data* **2006**, *51*, 371–375.
- (35) Vitu, S.; Jaubert, J. N.; Pauly, J.; Daridon, J. L.; Barth, D. *J. Supercrit. Fluids* **2008**, *44*, 155–163.
- (36) Pauly, J.; Coutinho, J.; Daridon, J. L. *Fluid Phase Equilib.* **2007**, *255*, 193–199.
- (37) Dias, A. M. A.; Carrier, H.; Daridon, J. L.; Pamies, J. C.; Vega, L. F.; Coutinho, J. A. P.; Marrucho, I. M. *Ind. Eng. Chem. Res.* **2006**, *45*, 2341–2350.
- (38) Ventura, S. P. M.; Pauly, J.; Daridon, J. L.; Marrucho, I. M.; Dias, A. M. A.; Coutinho, J. A. P. *J. Chem. Eng. Data* **2007**, *52*, 1100–1102.
- (39) Carvalho, P. J.; Alvarez, V. H.; Machado, J. J. B.; Pauly, J.; Daridon, J.; Marrucho, I. M.; Aznar, M.; Coutinho, J. A. P. *J. Supercrit. Fluids* **2009**, *49*, 99–107.
- (40) Peng, D.; Robinson, D. B. *Ind. Eng. Chem. Fund.* **1976**, *15*, 59–64.
- (41) Wong, D. S. H.; Sandler, S. I. *AIChE J.* **1992**, *38*, 671–680.
- (42) Shin, E.; Lee, B.; Lim, J. S. *J. Supercrit. Fluids* **2008**, *45*, 282–292.
- (43) Anthony, J.; Anderson, J.; Maginn, E.; Brennecke, J. *J. Phys. Chem. B* **2005**, *109*, 6366–6374.
- (44) Letcher, T. M. *Developments and Applications in Solubility*; Royal Society of Chemistry: London, 2007.
- (45) Cadena, C.; Anthony, J.; Shah, J.; Morrow, T.; Brennecke, J.; Maginn, E. *J. Am. Chem. Soc.* **2004**, *126*, 5300–5308.
- (46) Kazarian, S. G.; Briscoe, B. J.; Welton, T. *Chem. Commun. (Cambridge)* **2000**, 2047–2048.
- (47) Freire, M. G.; Carvalho, P. J.; Silva, A. M. S.; Santos, L. M. N. B. F.; Rebelo, L. P. N.; Marrucho, I. M.; Coutinho, J. A. P. *J. Chem. Phys. B* **2008**, *113*, 202–211.
- (48) Diep, P.; Jordan, K.; Johnson, J.; Beckman, E. *J. Phys. Chem. A* **1998**, *102*, 2231–2236.
- (49) Yonker, C.; Palmer, B. *J. Phys. Chem. A* **2001**, *105*, 308–314.
- (50) Costa Gomes, M. F.; Padua, A. A. H. *J. Phys. Chem. B* **2003**, *107*, 14020–14024.

- (51) Anderson, J. L.; Dixon, J. K.; Brennecke, J. F. *Acc. Chem. Res.* **2007**, *40*, 1208–1216.
- (52) Anderson, J.; Ding, J.; Welton, T.; Armstrong, D. *J. Am. Chem. Soc.* **2002**, *124*, 14247–14254.
- (53) Carvalho, P. J.; Alvarez, V. H.; Marrucho, I. M.; Aznar, M.; Coutinho, J. A. P. *Ind. Eng. Chem. Res.*, submitted for publication.
- (54) Frisch, M. J.; Trucks, G. W.; Schlegel, H. B.; Scuseria, G. E.; Robb, M. A.; Cheeseman, J. R.; Montgomery, J. A., Jr.; Vreven, T.; Kudin, K. N.; Burant, J. C.; Millam, J. M.; Iyengar, S. S.; Tomasi, J.; Barone, V.; Mennucci, B.; Cossi, M.; Scalmani, G.; Rega, N.; Petersson, G. A.; Nakatsuji, H.; Hada, M.; Ehara, M.; Toyota, K.; Fukuda, R.; Hasegawa, J.; Ishida, M.; Nakajima, T.; Honda, Y.; Kitao, O.; Nakai, H.; Klene, M.; Li, X.; Knox, J. E.; Hratchian, H. P.; Cross, J. B.; Bakken, V.; Adamo, C.; Jaramillo, J.; Gomperts, R.; Stratmann, R. E.; Yazyev, O.; Austin, A. J.; Cammi, R.; Pomelli, C.; Ochterski, J. W.; Ayala, P. Y.; Morokuma, K.; Voth, G. A.; Salvador, P.; Dannenberg, J. J.; Zakrzewski, V. G.; Dapprich, S.; Daniels, A. D.; Strain, M. C.; Farkas, O.; Malick, D. K.; Rabuck, A. D.; Raghavachari, K.; Foresman, J. B.; Ortiz, J. V.; Cui, Q.; Baboul, A. G.; Clifford, S.; Cioslowski, J.; Stefanov, B. B.; Liu, G.; Liashenko, A.; Piskorz, P.; Komaromi, I.; Martin, R. L.; Fox, D. J.; Keith, T.; Al-Laham, M. A.; Peng, C. Y.; Nanayakkara, A.; Challacombe, M.; Gill, P. M. W.; Johnson, B.; Chen, W.; Wong, M. W.; Gonzalez, C.; Pople, J. A. *Gaussian 03*, Revision C.02; Gaussian: Wallingford, CT, 2004.
- (55) Curtiss, L. A.; Raghavachari, K.; Redfern, P. C.; Rassolov, V.; Pople, J. A. *J. Chem. Phys.* **1998**, *109*, 7764–7776.
- (56) Curtiss, L. A.; Redfern, P. C.; Raghavachari, K.; Rassolov, V.; Pople, J. A. *J. Chem. Phys.* **1999**, *110*, 4703–4709.
- (57) Diadem Public 1.2. The DIPPR Information and Data Evaluation Manager, 2000.

JP901275B

Artigo 4.12: High carbon dioxide solubilities in trihexyltetradecylphosphonium-based ionic liquids

J. of Supercritical Fluids 52 (2010) 258–265



Contents lists available at ScienceDirect

The Journal of Supercritical Fluids

journal homepage: www.elsevier.com/locate/supflu



High carbon dioxide solubilities in trihexyltetradecylphosphonium-based ionic liquids

Pedro J. Carvalho^a, Víctor H. Álvarez^b, Isabel M. Marrucho^a, Martín Aznar^b, João A.P. Coutinho^{a,*}

^a CICECO, Departamento de Química, Universidade de Aveiro, 3810-193 Aveiro, Portugal

^b Faculdade de Engenharia Química, Universidade Estadual de Campinas, 13083-970, Campinas-SP, Brazil

ARTICLE INFO

Article history:

Received 17 November 2009

Received in revised form 29 January 2010

Accepted 1 February 2010

Keywords:

Trihexyltetradecylphosphonium

bis(trifluoromethylsulfonyl)imide

Trihexyltetradecylphosphonium chloride

Carbon dioxide

Phase behavior

Supercritical

Experimental

High pressure

Henry's constant

ABSTRACT

Due to the potential of ionic liquids for industrial application in CO₂ capture and gas separation processes, solubility of near or supercritical CO₂ in ionic liquids has been object of extensive research during the last few years. This work studies the solubility of CO₂ in phosphonium-based ionic liquids that, unlike imidazolium-based ILs, have received little attention in spite of their interesting characteristics. This work addresses the study of the gas–liquid equilibrium of two ionic liquids, trihexyltetradecylphosphonium bis(trifluoromethylsulfonyl)imide and trihexyltetradecylphosphonium chloride, in a wide range of temperatures, pressures, showing that phosphonium ionic liquids can dissolve even larger amounts of CO₂ (on a molar fraction basis) than the corresponding imidazolium-based ILs. In particular trihexyltetradecylphosphonium bis(trifluoromethylsulfonyl)imide seems to be the IL with the largest CO₂ sorption capacity reported up to present, revealing the potential of phosphonium-based ILs for CO₂ capture.

A thermodynamic model based on the Peng–Robinson equation of state with the Wong–Sandler mixing rule, using the UNIQUAC model for the activity coefficients, was here adopted to describe the experimental data and for the estimation of the Henry's constants. A universal correlation, for the description of the solubility of CO₂ in ILs previously proposed by us was also applied to the description of the data here measured showing a good agreement with the experimental data.

© 2010 Elsevier B.V. All rights reserved.

1. Introduction

The high solubility of CO₂ in ionic liquids has been the object of extensive research during the last few years. Aiming at enhancing sour gases solubility and ultimately replace the hazard volatile organic compounds (VOCs), many researchers have judiciously tailored ionic liquids (ILs) to accomplish such task either through the introduction of fluorinated groups on the IL ions, or by adding basic groups such as amines or acetates [1–15]. With the exception of this last type of ILs, where chemical interactions dominate the sorption mechanism, in most ionic liquids the gas solubility is simply driven by a physical absorption mechanism [11,16,17]. Among the ILs previously reported in the literature the imidazolium-based ionic liquids, especially those with fluorinated anions such as the bis(trifluoromethylsulfonyl)imide, NTF₂, and bis(pentafluoroethyl)trifluorophosphate, pFAP, are the ones with the highest CO₂ solubilities reported [9,15,18].

Despite their attractive characteristics, such as negligible vapor pressures, high thermal stability, large liquidus range, nonflammability, high solvation capacity, compatibility with strong alkaline solutes, stabilizing effect on palladium catalysts, effective media for Heck and Suzuki reactions and their low cost, the phosphonium-based ionic liquids have received surprisingly little attention in the last few years from academia [8,19–26]. Some authors have focused their study on the solubility of alcohols [27], alkanes and alkenes [25,26,28–32], or even on methane [30,31], carbon monoxide [32] or oxygen [30] in phosphonium ILs but few have reported solubilities of carbon dioxide in these ILs [19,24–26,29]. Furthermore, among those only a couple reported CO₂ solubilities under high pressure [19,29]. Ferguson and Scovazzo [25] have shown that imidazolium and phosphonium-based ILs have similar solubilities for several gases, while Anthony and coworkers [26] suggested that the nature of the anion has the most significant influence on the gas solubility. Hutchings et al. [8] have reported that, at subcritical temperatures, several phosphonium ionic liquids would completely dissolve as soon as all the CO₂ condensed and that the isopleths for these systems follow the vapor pressure curve of the pure CO₂.

Disregarding academia lack of interest, their properties and low cost have attracted the industry attention [33]. Central Glass Co. Ltd., from Japan, developed pharmaceutical intermediates using phosphonium ionic liquids [33], while Texaco used a “ruthenium melt catalyst” dispersed in phosphonium or quaternary ammonium ILs to convert syngas into acetic acid, esters, alcohols and glycol

* Corresponding author. Tel.: +351 234 401 507; fax: +351 234 370 084.
E-mail address: jcoutinho@ua.pt (J.A.P. Coutinho).

[34]. Rhone-Poulenc, by other hand, used a tetrabutylphosphonium chloride to stabilize zero-valent palladium catalysts for carbonylation [34] and Eastman Chemical Company used a Lewis basic phosphonium iodide ionic liquid along with a Lewis acid catalyst for the isomerization of 3,4-epoxybut-1-ene to 2,5-dihydrofuran [33].

In the wake of previous works [11,17,18,35], the purpose of the present study is to identify ILs with large CO₂ solubilities and to further explore the mechanism behind the absorption of carbon dioxide by the ionic liquids. For that purpose, trihexyltetradecylphosphonium chloride, [THTDP][Cl], and trihexyltetradecylphosphonium bis(trifluoromethylsulfonyl)imide, [THTDP][NTf₂], ionic liquids were chosen. The structure of the phosphonium cation minimizes any specific interactions between the IL cation and the carbon dioxide. Furthermore, the chloride anion of the [THTDP][Cl] allows also to minimize any anion interaction with the CO₂.

The Peng–Robinson equation of state [36] with the Wong–Sandler/UNIQUAC mixing rule [37], using the UNIQUAC model [38] for the activity coefficients, was used to model the experimental data measured in this work and to estimate the Henry's constants from which the enthalpies and entropies of solvation are derived and used to assess the CO₂ IL interactions.

2. Experimental

2.1. Materials

Two ILs based on the trihexyltetradecylphosphonium cation, trihexyltetradecylphosphonium bis(trifluoromethylsulfonyl)imide, [THTDP][NTf₂] and trihexyltetradecylphosphonium chloride, [THTDP][Cl], were used in this study. All compounds were obtained from Cytec with mass fraction purities higher than 97%. The chloride impurity for [THTDP][NTf₂] was inferior to 0.1%. The purities stated by the supplier, of each ionic liquid, were checked by ¹H NMR, ¹³C NMR and ¹⁹F NMR.

The ILs were further purified by washing them with ultra pure water followed by drying under high vacuum (1×10^{-3} Pa) and moderate temperature (353 K) for a period of 48 h. The water used was double-distilled, passed through a reverse osmosis system, and further treated with a MilliQ plus 185 water purification apparatus. It has a resistivity of 18.2 MΩ cm, a TOC smaller than 5 µg L⁻¹, and it is free of particles greater than 0.22 µm. The purities of each ionic liquid were checked by ¹H NMR, ¹³C NMR and ¹⁹F NMR after each purification step and the purification was repeated until no impurities were observed in the ILs by NMR analysis. The final purity is estimated to be better than 99%. The final IL water content was determined with a Metrohm 831 Karl Fischer coulometer, indicating a water mass fraction of $(67 \text{ and } 97) \times 10^{-6}$ for [THTDP][NTf₂] and [THTDP][Cl], respectively.

The carbon dioxide (CO₂) was acquired from Air Liquide with a purity of ≥99.998% and H₂O, O₂, C_nH_m, N₂ and H₂ impurities volume fractions lower than $(3, 2, 2, 8 \text{ and } 0.5) \times 10^{-6}$, respectively.

2.2. Experimental equipment

The high pressure equilibrium cell used in this work is based on a cell designed by Daridon et al. [19,39–42] using the synthetic method. Both the apparatus and the methodology here followed were fully described in previous works [11,18,35], and shown to be adequate to accurately measure vapor–liquid phase equilibrium in a wide range of pressures and temperatures [11,18,19,35,39–42]. The high pressure equilibrium cell, that can operate up to pressures of 1000 bar and in the (283–373) K temperature range, consists of a horizontal hollow stainless-steel cylinder, closed at one end by a movable piston and at the other end by a sapphire window. This window, along with a second window on the

cell wall, through which an optical fiber lights the cell chamber, allows the operator to follow the behavior of the sample with pressure and temperature. The orthogonal positioning of both sapphire windows minimizes the parasitic reflections and improves the observation in comparison to axial lighting. A small magnetic bar placed inside the cell allows the homogenization of the mixture by means of an external magnetic stirrer. The presence of the magnetic stirrer, as well as the cell reduced volume, help to minimize the inertia and temperature gradients within the sample. The cell is thermostated by circulating a heat-carrier fluid through three flow lines directly connected to the cell. The heat-carrier fluid is thermo-regulated with a temperature stability of ±0.01 K by means of a thermostat bath circulator (Julabo MC). The temperature is measured with a high precision thermometer, Model PN 5207 with an accuracy of 0.01 K, connected to a calibrated platinum resistance inserted inside the cell close to the sample. The pressure is measured by a piezoresistive silicon pressure transducer (Kulite) fixed directly inside the cell to reduce dead volumes, that was previously calibrated and certified by an independent laboratory with IPAC accreditation, following the EN 837-1 standard and with accuracy better than 0.2%.

A fixed amount of IL was introduced inside the cell; its exact mass was determined by weighting, using a high weight/high precision balance with an accuracy of 1 mg (Sartorius). In order to avoid any interference of atmospheric gases during the manipulation, after placing the IL inside the cell, it was kept under vacuum overnight while stirring and heating at 353 K.

The CO₂ was introduced under pressure from an aluminum reservoir tank. Its mass was measured with a precision balance and introduced into the measuring cell by means of a flexible high pressure capillary.

After preparation of a mixture of known composition and the desired temperature at low pressure was reached, the pressure was then slowly increased at constant temperature until the system becomes monophasic. The pressure at which the last bubble disappears represents the equilibrium pressure for the fixed temperature.

The purity of the IL is checked again by NMR at the end of the study to confirm that no degradation takes place during the measurements.

2.3. Thermodynamic modeling

To describe the experimental data measured, the Peng–Robinson equation of state [36] was used in this work,

$$P = \frac{RT}{V - b_m} + \frac{a_m}{V(V + b_m) + b_m(V - b_m)} \quad (1)$$

with the Wong–Sandler mixing rule [37]

$$\begin{aligned} b_m &= \frac{\sum \sum x_i x_j (b - a/RT)_{ij}}{1 - \sum x_i a_i / b_i RT - A_\infty^E(x) / \Omega RT} \left(b - \frac{a}{RT} \right)_{ij} \\ &= \frac{1}{2} [b_i + b_j] - \frac{\sqrt{a_i a_j}}{RT} (1 - k_{ij}) \end{aligned} \quad (2)$$

$$a_m = b_m \left(\sum x_i \left[\frac{a_i}{a_j} \right] + \frac{A_\infty^E(x)}{\Omega} \right) \quad (3)$$

where a_m and b_m are the equation of state constants, $\Omega = 0.34657$ for the Peng–Robinson equation, and $A_\infty^E(x)$ is calculated using the UNIQUAC model and assuming that $A_\infty^E(x) \approx A_0^E(x) \approx C_0^E(x)$, being $G_0^E(x)$ the excess Gibbs free energy at low pressure described

Table 1
Bubble point data of the system CO₂ (1)+[THTDP][NTf₂] (2).

x ₁	T/K	p/MPa												
0.169	293.26	0.106	0.205	293.34	0.252	0.308	293.20	0.612	0.421	293.30	1.145	0.504	293.37	1.584
0.169	303.25	0.226	0.205	303.22	0.399	0.308	303.15	0.806	0.421	303.22	1.425	0.504	303.58	1.966
0.169	313.20	0.355	0.205	313.10	0.555	0.308	313.16	1.023	0.421	313.24	1.748	0.504	313.05	2.378
0.169	323.26	0.471	0.205	323.11	0.716	0.308	323.25	1.266	0.421	323.22	2.079	0.504	323.24	2.823
0.169	333.25	0.609	0.205	333.15	0.887	0.308	333.13	1.492	0.421	333.38	2.439	0.504	333.21	3.267
0.169	343.22	0.760	0.205	343.20	1.055	0.308	343.13	1.739	0.421	343.19	2.786	0.504	343.27	3.737
0.169	353.21	0.909	0.205	353.21	1.235	0.308	353.11	1.993	0.421	353.21	3.154	0.504	353.26	4.216
0.169	363.24	1.066	0.205	363.40	1.425	0.308	363.29	2.246	0.421	363.34	3.535	0.504	363.45	4.702
0.601	292.88	2.275	0.702	293.14	3.305	0.806	293.17	4.817	0.822	293.15	5.510	0.830	293.20	7.546
0.601	303.27	2.845	0.702	303.11	4.197	0.806	303.31	6.208	0.822	303.20	7.450	0.830	303.20	9.480
0.601	313.10	3.427	0.702	313.11	4.975	0.806	313.39	7.948	0.822	313.19	9.634	0.830	313.23	11.584
0.601	323.24	4.020	0.702	323.15	5.921	0.806	323.28	10.007	0.822	323.31	12.009	0.830	323.23	13.838
0.601	333.22	4.657	0.702	333.27	6.912	0.806	333.29	12.119	0.822	333.24	14.307	0.830	333.28	16.063
0.601	343.20	5.342	0.702	343.38	7.946	0.806	343.40	14.180	0.822	343.10	16.481	0.830	343.28	18.182
0.601	353.23	5.995	0.702	353.33	8.996	0.806	353.23	16.095	0.822	353.20	18.493	0.830	353.41	20.290
0.601	363.31	6.675	0.702	363.53	10.078	0.806	363.28	17.975	0.822	363.21	20.420	0.830	363.45	22.264
0.840	293.20	12.025	0.850	293.33	18.870	0.860	293.30	26.885	0.870	293.26	44.564	0.879	296.58	72.185
0.840	303.18	12.808	0.850	303.10	18.188	0.860	303.02	24.711	0.870	302.95	34.630	0.879	303.08	49.350
0.840	313.29	14.587	0.850	313.21	18.747	0.860	313.18	23.840	0.870	313.10	30.585	0.879	313.35	39.536
0.840	323.19	16.420	0.850	323.22	20.190	0.860	323.34	24.304	0.870	323.24	29.743	0.879	323.35	36.280
0.840	333.23	18.457	0.850	333.26	21.719	0.860	333.19	25.423	0.870	333.20	30.253	0.879	333.38	35.408
0.840	343.18	20.490	0.850	343.12	23.608	0.860	343.19	26.972	0.870	343.12	31.183	0.879	343.23	35.732
0.840	353.26	22.557	0.850	353.01	25.482	0.860	353.26	28.426	0.870	353.25	32.463	0.879	353.06	36.563
0.840	363.14	24.401	0.850	363.14	27.163	0.860	363.28	30.227	0.870	363.35	33.815	0.879	361.67	37.445

as

$$\frac{G^E}{RT} = \sum_{i=1}^n x_i \ln \left(\frac{\Phi_i}{x_i} \right) + \frac{Z}{2} \sum_{i=1}^n q_i x_i \ln \frac{\theta_i}{\Phi_i}$$

$$- \sum_{i=1}^n x_i q_i \ln \left[\sum_{j=1}^n \theta_j \exp \left(-\frac{\lambda_{ij} - \lambda_{ii}}{q_i RT} \right) \right] \quad (4)$$

with

$$\Phi_i = \frac{x_i r_i}{\sum_j x_j r_j} \quad \text{and} \quad \theta_i = \frac{x_i q_i}{\sum_j x_j q_j} \quad (5)$$

The correlation of the experimental data was carried by the minimization of the objective function, OF, for

$$OF = \sum_{i=1}^N \left[\frac{P_{i,cal} - P_{i,exp}}{\sigma_P} \right]^2 \quad (6)$$

where N is the number of data points, P is the pressure, the superscripts "exp" and "cal" refers to the experimental and calculated values, respectively, and σ_P is the standard deviation of pressure. The experimental uncertainties in the pressure data were used for

σ_P. The minimization method was performed using a genetic algorithm code, implemented and fully explained in Álvarez et al. [43]. The difference between experimental and calculated values was calculated as the average percent deviation, expressed in absolute form, as follows:

$$|\Delta P| = \frac{100}{N} \sum_{i=1}^N \left[\frac{|P_{i,cal} - P_{i,exp}|}{P_{i,exp}} \right] \quad (7)$$

Furthermore the proposed model was applied, in the diluted region limit, to determine the Henry's constant for the studied systems.

3. Results and discussion

The solubility of carbon dioxide in the studied ILs was measured for mole fractions ranging from 0.2 to 0.9, in the temperature range 293–363 K and pressures from 0.1 to 72 MPa, as reported in Tables 1 and 2 and depicted in Fig. 1. The temperature increase leads to an increase in the equilibrium pressures and by increasing CO₂ concentration, the equilibrium pressures increase gradually at first, and then rapidly for higher CO₂ contents as a liquid–liquid like region is reached, as also observed previously for other ILs

Table 2
Bubble point data of the system CO₂ (1)+[THTDP][Cl] (2).

x ₁	T/K	p/MPa	x ₁	T/K	p/MPa	x ₁	T/K	p/MPa	x ₁	T/K	p/MPa	x ₁	T/K	p/MPa
0.119	313.16	0.168	0.164	303.35	0.225	0.200	303.42	0.357	0.305	303.40	0.820	0.400	303.27	2.311
0.119	323.16	0.274	0.164	313.03	0.371	0.200	313.27	0.517	0.305	313.54	1.120	0.400	313.56	2.850
0.119	333.46	0.453	0.164	323.30	0.523	0.200	323.40	0.682	0.305	323.66	1.355	0.400	323.57	3.357
0.119	343.37	0.546	0.164	333.30	0.641	0.200	333.50	0.849	0.305	333.59	1.605	0.400	333.63	3.924
0.119	353.30	0.690	0.164	343.00	0.784	0.200	343.68	1.033	0.305	343.52	1.873	0.400	343.55	4.495
0.119	363.22	0.770	0.164	353.16	0.943	0.200	353.75	1.220	0.305	353.66	2.160	0.400	353.46	5.092
			0.164	363.20	1.089	0.200	363.66	1.397	0.305	363.54	2.440	0.400	363.58	5.692
0.503	303.32	2.311	0.603	303.33	3.417	0.701	303.36	4.987	0.752	303.42	5.998	0.800	302.55	14.995
0.503	313.47	2.850	0.603	313.28	4.135	0.701	313.70	6.130	0.752	313.38	7.503	0.800	313.44	16.310
0.503	323.43	3.357	0.603	323.47	4.924	0.701	323.56	7.314	0.752	323.45	9.328	0.800	323.83	17.595
0.503	333.47	3.924	0.603	333.69	5.760	0.701	333.54	8.658	0.752	333.58	11.307	0.800	333.78	19.295
0.503	343.55	4.495	0.603	343.64	6.586	0.701	343.48	10.018	0.752	343.46	13.226	0.800	343.72	21.108
0.503	353.64	5.092	0.603	353.69	7.457	0.701	353.77	11.461	0.752	353.58	15.138	0.800	353.66	22.815
0.503	363.67	5.692	0.603	363.53	8.330	0.701	363.68	12.821	0.752	363.67	16.927	0.800	363.65	24.570

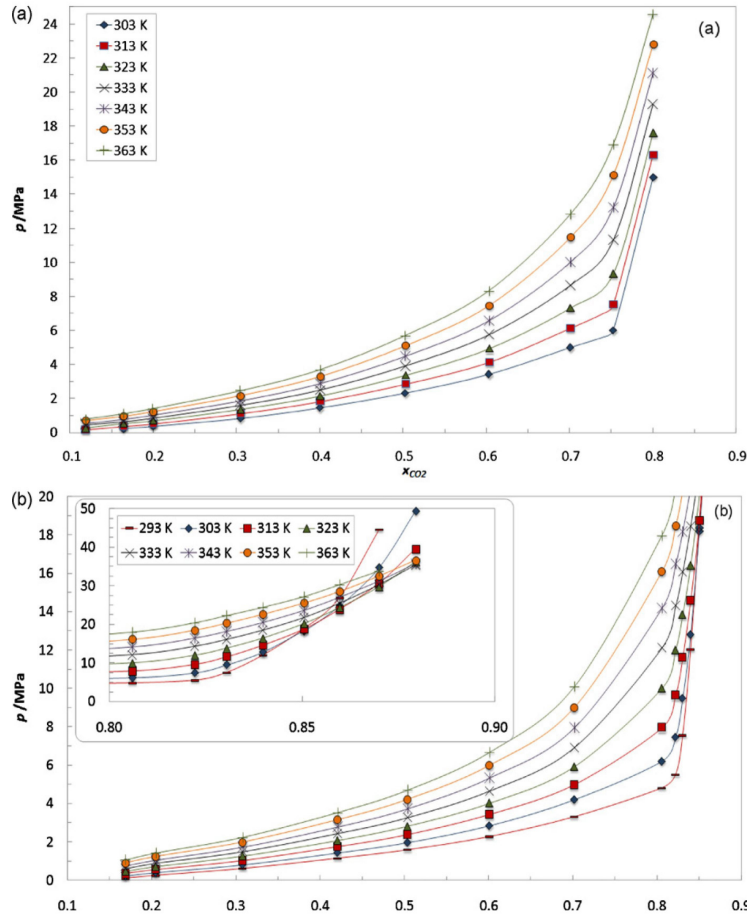


Fig. 1. Pressure–composition diagram of the binary systems: (a) $CO_2 + [THTDP][Cl]$ and (b) $CO_2 + [THTDP][NTf_2]$. The solid curves are guides for the eye.

[11,18,35]. A singular phenomenon was observed for the system $[THTDP][NTf_2] + CO_2$ at CO_2 concentrations higher than 0.8. At these conditions the equilibrium pressure changes its behavior and starts to decrease with the temperature increase, as depicted in Figs. 1(b) and 2(b). This unusual behavior, previously observed for the solubility of CO_2 in aqueous solutions of phosphonium-based ILs is related to the liquid–liquid region, as previously noticed [19], and to a change in the relative densities of the phases. At low pressures the IL phase is denser than the CO_2 and dP/dT is positive. At high pressures the CO_2 phase becomes denser than the IL phase and then, as predicted by the Clausius–Clapeyron equation, the dP/dT becomes negative and the solubility increases with temperature.

The solubilities of CO_2 in the ILs studied in this work are among the highest measured up to present. These ILs present identical or higher CO_2 solubilities than those reported for imidazolium-based ILs, with fluorinated anions like the NTf_2 [9,15,44,45] or pFAP [9,15], for which several authors justify the high solubilities as a result of special interactions between the CO_2 and the IL ions. A comparison between the CO_2 solubility in these ILs and in the ILs studied in this work is depicted in Fig. 3.

Hutchings et al. [8] found that for subcritical temperatures several phosphonium ionic liquids, including the $[THTDP][Cl]$ here studied, would completely dissolve in CO_2 as soon as all the CO_2 condensed and that the isopleths for these systems follow the vapor pressure curve of the pure CO_2 . In this work we have tried to

reproduce the results from Hutchings et al. [8] without success. No significant solubility of phosphonium ionic liquids in near or supercritical CO_2 was observed.

The results of the application of the equation of state to the modeling of the binary systems containing ionic liquids studied in this work are presented in Table 3 for all the experimental data. In the table, NP is the number of data points, T is the temperature, k_{12} , A_{12} and A_{21} are the interaction parameters of the model, where ‘1’

Table 3

Temperature-independent interaction parameters and predicted Henry's constant for the studied systems.

$[THTDP][NTf_2] + CO_2^a$		$[THTDP][Cl] + CO_2^b$	
T/K	H_{12}/MPa	T/K	H_{12}/MPa
293.44	1.98		
303.18	2.30	303.27	1.89
313.19	2.64	313.36	2.40
323.24	3.00	323.48	2.99
333.25	3.38	333.55	3.67
343.21	3.76	343.50	4.41
353.22	4.14	353.57	5.21
363.21	4.54	363.54	6.08

^a $K_H = 0.001116T - 0.2307$, $A_{12} = -2.534T + 1867.153$, $A_{21} = 2.490T + 351.268$, $|Δp|(\%) = 9.2$.

^b $K_H = 0.00574T - 3.0269$, $A_{12} = 14.331T - 3908.572$, $A_{21} = 2.298T + 570.848$, $|Δp|(\%) = 9.4$.

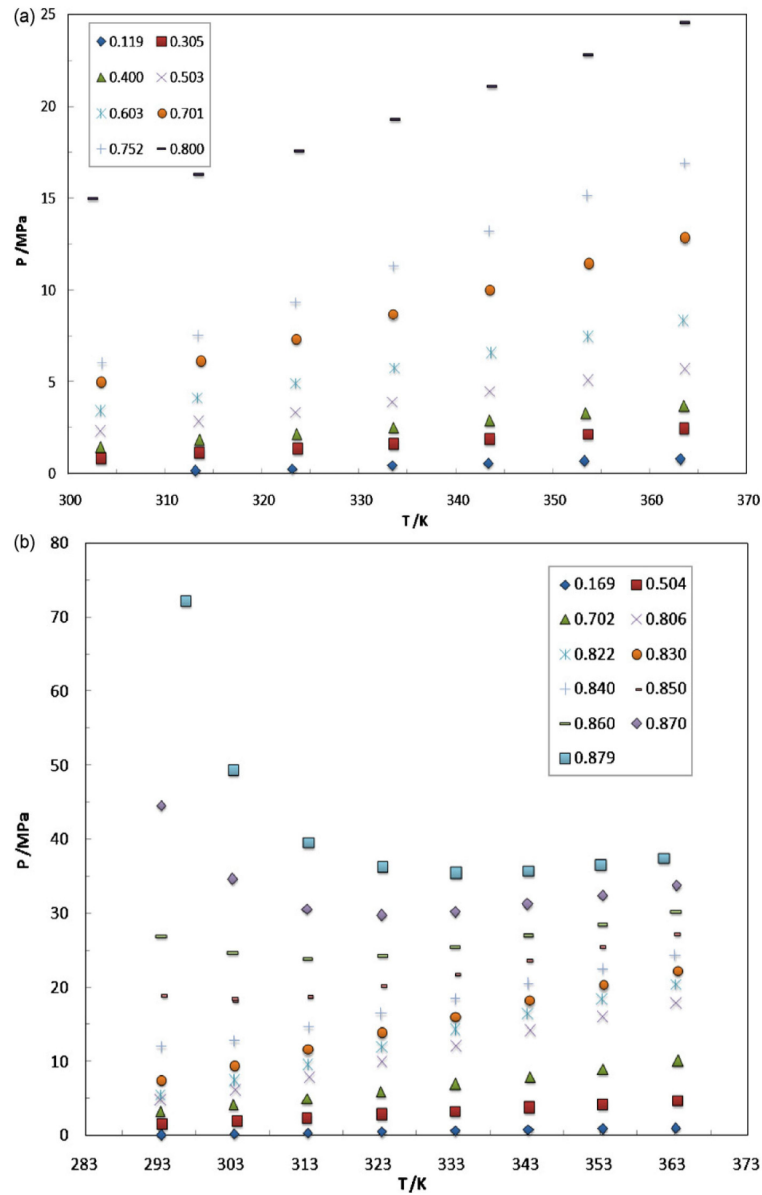


Fig. 2. Pressure–temperature diagram, as function of CO_2 mole fractions, of the binary systems: (a) $\text{CO}_2 + [\text{THTDP}][\text{Cl}]$ and (b) $\text{CO}_2 + [\text{THTDP}][\text{NTf}_2]$.

refers to the CO_2 and '2' for the ionic liquid. This table is divided in sections for each system studied. The properties of the compounds used in the modeling are reported in Table 4. As depicted in Fig. 4, the model provides a good description of the experimental data. The

equation of state was then used to estimate the Henry's constant for the studied systems.

The Henry's law relates the amount of gas dissolved in a liquid, at a constant temperature and pressure, to the fugacity of that gas and can be described as

$$H_{12}(T, P) = \lim_{x_1 \rightarrow 0} \frac{f_1^L}{x_1} \quad (8)$$

where $H_{12}(T, P)$ is the Henry's constant, x_1 is the mole fraction of gas dissolved in the liquid phase, and f_1^L is the fugacity of the gas in the liquid phase. Eq. (8) is only rigorously valid in the diluted region limit. The Henry's constants for CO_2 in the investigated ILs were estimated by fitting the PR-WS/UNIQUAC model to the experimental data and calculating the limiting slope defined in Eq. (8) as the solubility approaches zero. This approach introduces some uncer-

Table 4
Properties of the substances used in the modeling.

Compound	T_c/K	P_c/MPa	ω	r	q
CO_2	304.21 ^a	7.38 ^a	0.2236 ^a	3.26 ^c	2.38 ^c
$[\text{THTDP}][\text{NTf}_2]$	1588.22 ^b	8.51 ^b	0.8801 ^b	82.08 ^c	52.97 ^c
$[\text{THTDP}][\text{Cl}]$	1225.80 ^b	7.95 ^b	0.7698 ^b	69.29 ^c	44.07 ^c

^a Ref. [47].

^b Calculated with [48].

^c Calculated with [49].

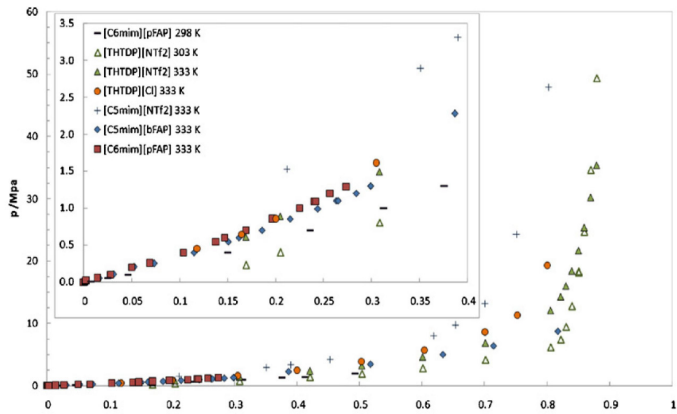


Fig. 3. Pressure–composition diagram of the binary systems: (○) $\text{CO}_2 + [\text{THTDP}][\text{Cl}]$ 298 K, (\triangle , Δ) $\text{CO}_2 + [\text{THTDP}][\text{NTf}_2]$, (\blacksquare , \blacksquare) $\text{CO}_2 + [\text{C}_6\text{mim}][\text{pFAP}]$ [9,15], (\diamond) $\text{CO}_2 + [\text{C}_5\text{mim}][\text{pFAP}]$ [9], and (+) $\text{CO}_2 + [\text{C}_5\text{mim}][\text{NTf}_2]$ [18].

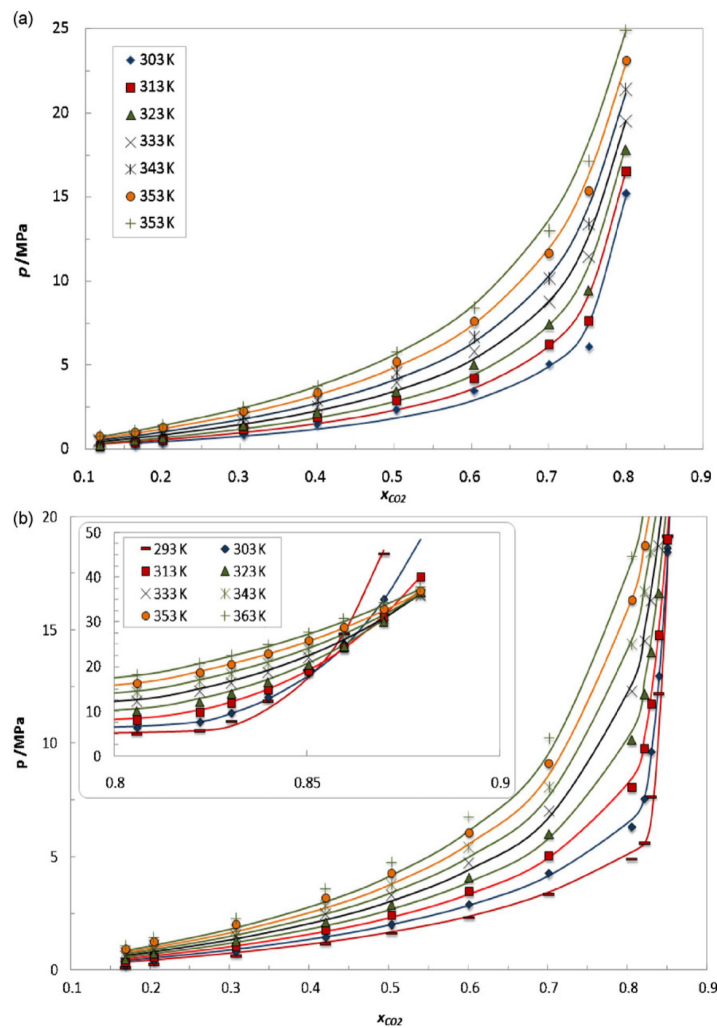
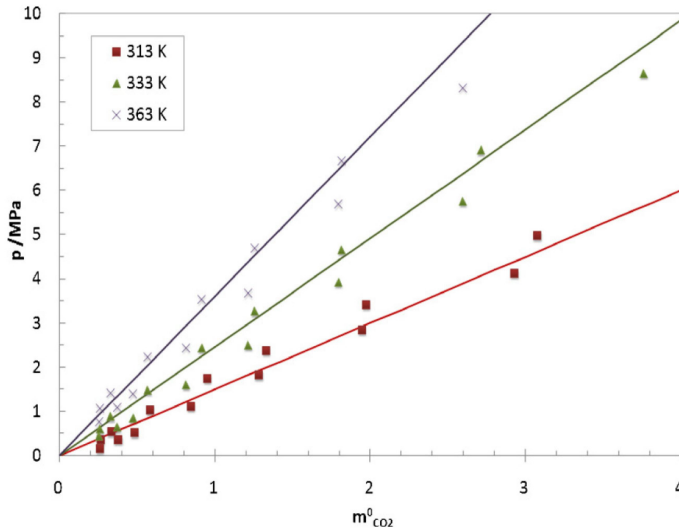


Fig. 4. PTx diagram and modeling for the systems: $\text{CO}_2 + [\text{THTDP}][\text{Cl}]$ (a) and $\text{CO}_2 + [\text{THTDP}][\text{NTf}_2]$ (b). The solid lines represent the calculations with PR-WS/UNIQUAC EoS.

Table 5Coefficients A and B in Eq. (4) and partial molar enthalpy and partial molar entropy of solvation obtained for CO₂ + ILs systems.

Ionic liquid	A	B	ΔH ₁₂ (%)	Δ _{solv} H (kJ mol ⁻¹)	Δ _{solv} S (J mol ⁻¹ K ⁻¹)	-T·Δ _{solv} S _{T=298K} (kJ mol ⁻¹)
[THTDP][NTf ₂]	-1268.272	5.015	0.65	-10.54	-32.31	9.63
[THTDP][Cl]	-2147.851	7.737	0.84	-17.86	-53.86	16.06

Fig. 5. PTm⁰ diagram for the systems CO₂ + ILs. The solid lines represent the universal correlation previously proposed [17].

tainty on the estimated Henry's constants but the values of these constants for the two studied ILs are different enough to allow a discussion of the CO₂ solubility in the two ionic liquids based on these values. The estimated Henry's constants results, reported in Table 3, indicate that Henry's constant slightly decreases (i.e., CO₂ solubility increases) with the temperature.

The results for the Henry's constant of CO₂ in [THTDP][NTf₂] and in [THTDP][Cl] were correlated as a function of temperature by an empirical equation of the type:

$$\ln(H_{12}) = A \left(\frac{1}{T} \right) + B \quad (9)$$

where the coefficients A and B are listed in Table 5, together with the Henry's constant average absolute deviations, |ΔH₁₂|, obtained for each ionic liquid.

The effect of temperature on CO₂ solubility can be related to the Gibbs energy, the partial molar entropy and partial molar enthalpy of solvation [46] and can be calculated from an appropriate correlation of Henry's constant:

$$\Delta_{solv}G^\circ = R \cdot T \cdot (\ln(H_{12}))_p \quad (10)$$

$$\Delta_{solv}H^\circ = -T^2 \left(\frac{\partial \Delta_{solv}G^\circ}{\partial T} \right) = -R \cdot T^2 \left(\frac{\partial \ln H_{12}}{\partial T} \right)_p \quad (11)$$

$$\Delta_{solv}S^\circ = \frac{\Delta_{solv}H^\circ - \Delta_{solv}G^\circ}{T} = R \cdot T^2 \left(\frac{\partial \ln H_{12}}{\partial T} \right)_p = -R \cdot \ln(H_{12})_p \quad (12)$$

The partial molar enthalpy of solvation gives an indication of the strength of interactions between the gas and the IL, while the partial molar entropy illustrates the amount of ordering present in the gas/IL mixture. The results presented in Table 5 show that the partial molar entropy of CO₂ in [THTDP][Cl] is somewhat higher

than in [THTDP][NTf₂], indicating a stronger structural solvation interaction for the CO₂/[THTDP][Cl] system. The partial molar enthalpy of solvation of the CO₂ in [THTDP][NTf₂] is higher than in [THTDP][Cl], indicating a stronger interaction between the CO₂ and the [THTDP][Cl]. The partial molar enthalpies of solvation observed for these ILs are however similar to those previously reported by us for the imidazolium-based ionic liquids [C₄mim][Trifluoroacetate], [C₄mim][Dicyanamide] and [C₄mim][NTf₂] [11,18,35] showing that solvation of CO₂ on phosphonium ILs is similar to what is observed in imidazolium ILs, and driven mainly by entropic effects [17]. Based on this idea, we have proposed a universal correlation for the solubility of CO₂ in ionic liquids [17] that can be described by Eq. (13)

$$p = m_i^0 e^{(6.8591(-2004.3/T))} \quad (13)$$

where m_i^0 is the carbon dioxide concentration in molality.

In Fig. 5, the predictions obtained are compared to the experimental data measured in this work. As can be seen a good prediction (~7% and 20% for the [THTDP][NTf₂] and [THTDP][Cl], respectively) of the experimental data can be obtained using this approach.

4. Conclusions

CO₂ solubility in, trihexyltetradecylphosphonium bis(trifluoromethylsulfonyl)imide and trihexyltetradecylphosphonium chloride was studied in a wide range of temperatures and pressures. It is shown that phosphonium ionic liquids can dissolve even larger amounts of CO₂ (on a molar fraction basis) than the imidazolium-based ILs with the same anion. The solubilities here reported are the largest observed for ionic liquids in absence of chemical interactions. Moreover, an interesting increase of the CO₂ solubility with temperature was observed for these ILs at very high pressures.

A thermodynamic model based on the Peng–Robinson EoS with the Wong–Sandler/UNIQUAC mixing rule was used with success

in the correlation of the measured data. The model provides a good description of the experimental data and the estimation of the Henry's constants for these systems. The enthalpies of solvation derived from the Henry's constants show a lower interaction between the CO₂ and the ILs than previously observed for the imidazolium ionic liquids. A correlation for the solubility of CO₂ in ILs previously proposed by us was applied to the description of the data here measured showing a good agreement with the experimental data measured.

Acknowledgments

The authors are thankful for financial support from Fundação para a Ciência e a Tecnologia (Project PTDC/EQU-FTT/102166/2008) and PhD grant (SFRH/BD/41562/2007) of Pedro J. Carvalho.

The authors would like to acknowledge FAPESP (Fundação de Amparo à Pesquisa do Estado de São Paulo), process #2006/03711-1.

M. Aznar is the recipient of a CNPq fellowship.

The authors are thankful for the ionic liquid samples supplied by Cytec.

References

- [1] J.L. Anthony, S.N.V.K. Aki, E.J. Maginn, J.F. Brennecke, Feasibility of using ionic liquids for carbon dioxide capture, *Int. J. Environ. Technol. Manage.* 4 (2004) 105–115.
- [2] J.E. Bara, C.J. Gabriel, S. Lessmann, T.K. Carlisle, A. Finotello, D.L. Gin, R.D. Noble, Enhanced CO₂ separation selectivity in oligo(ethylene glycol) functionalized room-temperature ionic liquids, *Ind. Eng. Chem. Res.* 46 (2007) 5380–5386.
- [3] U. Domanska, A. Marciniak, M. Krolkowski, Phase equilibria and modeling of ammonium ionic liquid, C₂N₂F₂, solutions, *J. Phys. Chem. B* 112 (2008) 1218–1225.
- [4] A. Finotello, J. Bara, D. Camper, R. Noble, Room-temperature ionic liquids: temperature dependence of gas solubility selectivity, *Ind. Eng. Chem. Res.* 47 (2007) 3453–3459.
- [5] A. Heintz, Recent developments in thermodynamics and thermophysics of non-aqueous mixtures containing ionic liquids. A review, *J. Chem. Thermodyn.* 37 (2005) 525–535.
- [6] G. Hong, J. Jacquemin, M. Deetlefs, C. Hardacre, P. Husson, M. Costa Gomes, Solubility of carbon dioxide and ethane in three ionic liquids based on the bis((trifluoromethyl)sulfonyl)imide anion, *Fluid Phase Equilibr.* 257 (2007) 27–34.
- [7] J. Huang, A. Riisager, R.W. Berg, R. Fehrmann, Tuning ionic liquids for high gas solubility and reversible gas sorption, *J. Mol. Catal. A: Chem.* 279 (2008) 170–176.
- [8] J.W. Hutchings, K.L. Fuller, M.P. Heitz, M.M. Hoffmann, Surprisingly high solubility of the ionic liquid trihexyltetradecylphosphonium chloride in dense carbon dioxide, *Green Chem.* 7 (2005) 475–478.
- [9] M. Muldoon, S. Aki, J. Anderson, J. Dixon, J. Brennecke, Improving carbon dioxide solubility in ionic liquids, *J. Phys. Chem. B* 111 (2007) 9001–9009.
- [10] M.B. Shiflett, D.J. Kasprzak, C.P. Junk, A. Yokozeiki, Phase behavior of (carbon dioxide + [bmim][ac]) mixtures, *J. Chem. Thermodyn.* 40 (2008) 25–31.
- [11] P.J. Carvalho, V.H. Álvarez, B. Schröder, A.M. Gil, I.M. Marrucho, M. Aznar, L.M.N.B.F. Santos, J.A.P. Coutinho, Specific solvation interactions of CO₂ on acetate and trifluoroacetate imidazolium based ionic liquids at high pressures, *J. Phys. Chem. B* 113 (2009) 6803–6812.
- [12] E. Bates, R. Mayton, I. Ntai, J. Davis, CO₂ capture by a task-specific ionic liquid, *J. Am. Chem. Soc.* 124 (2002) 926–927.
- [13] X. Yuan, S. Zhang, J. Liu, X. Lu, Solubilities of CO₂ in hydroxyl ammonium ionic liquids at elevated pressures, *Fluid Phase Equilibr.* 257 (2007) 195–200.
- [14] J. Sun, S. Zhang, W. Cheng, J. Ren, Hydroxyl-functionalized ionic liquid: a novel efficient catalyst for chemical fixation of CO₂ to cyclic carbonate, *Tetrahedron Lett.* 49 (2008) 3588–3591.
- [15] M.B. Shiflett, A. Yokozeiki, Phase behavior of carbon dioxide in ionic liquids: [emim][acetate], [emim][trifluoroacetate], and [emim][acetate] + [emim][trifluoroacetate] mixtures, *J. Chem. Eng. Data* 54 (2009) 108–114.
- [16] A. Yokozeiki, M.B. Shiflett, C.P. Junk, L.M. Grieco, T. Foo, Physical and chemical absorptions of carbon dioxide in room-temperature ionic liquids, *J. Phys. Chem. B* 112 (2008) 16654–16663.
- [17] P.J. Carvalho, J.A.P. Coutinho, On the non ideality of CO₂ solutions in ionic liquids and other low volatile solvents, *J. Phys. Chem. Lett.* (2010), doi:10.1021/jz100009c.
- [18] P.J. Carvalho, V.H. Álvarez, J.J.B. Machado, J. Pauly, J. Daridon, I.M. Marrucho, M. Aznar, J.A.P. Coutinho, High pressure phase behavior of carbon dioxide in 1-alkyl-3-methylimidazolium bis(trifluoromethylsulfonyl)imide ionic liquids, *J. Supercrit. Fluids* 48 (2009) 99–107.
- [19] S.P.M. Ventura, J. Pauly, J.L. Daridon, J.A.L. da Silva, I.M. Marrucho, A.M.A. Dias, J.A.P. Coutinho, High pressure solubility data of carbon dioxide in tri-
- iso-butyl(methyl)phosphonium tosylate–water systems, *J. Chem. Thermodyn.* 40 (2008) 1187–1192.
- [20] R.D. Rogers, K.R. Seddon, Ionic liquids—solvents of the future? *Science* 302 (2003) 792–793.
- [21] K.N. Marsh, J.A. Boxall, R. Lichtenthaler, Room temperature ionic liquids and their mixtures – a review, *Fluid Phase Equilibr.* 219 (2004) 93–98.
- [22] C.Chiappe, D. Pieraccini, Ionic liquids: solvent properties and organic reactivity, *J. Phys. Org. Chem.* 18 (2005) 275–297.
- [23] M.J. Earle, J.M.S. Esperanca, M.A. Gilea, J.N. Canongia Lopes, L.P.N. Rebelo, J.W. Magee, K.R. Seddon, J.A. Widgren, The distillation and volatility of ionic liquids, *Nature* 439 (2006) 831–834.
- [24] S. Zhang, Y. Chen, R. Ren, Y. Zhang, J. Zhang, X. Zhang, Solubility of CO₂ in sulfonate ionic liquids at high pressure, *J. Chem. Eng. Data* 50 (2005) 230–233.
- [25] L. Ferguson, P. Scovazzo, Solubility, diffusivity, and permeability of gases in phosphonium-based room temperature ionic liquids: data and correlations, *Ind. Eng. Chem. Res.* 46 (2007) 1369–1374.
- [26] J. Anthony, J. Anderson, E. Maginn, J. Brennecke, Anion effects on gas solubility in ionic liquids, *J. Phys. Chem. B* 109 (2005) 6366–6374.
- [27] U. Domanska, K. Paduszynski, Phase equilibria study in binary systems (tetra-n-butylphosphonium selective ionic liquid + 1-alcohol, or benzene, or n-alkylbenzene), *J. Phys. Chem. B* 112 (2008) 11054–11059.
- [28] Solubility of adamantane in phosphonium-based ionic liquids, *J. Chem. Eng. Data*, 55(2010)662–665.
- [29] T. Wang, C. Peng, H. Liu, Y. Hu, Description of the PVT behavior of ionic liquids and the solubility of gases in ionic liquids using an equation of state, *Fluid Phase Equilibr.* 250 (2006) 150–157.
- [30] R. Condamin, P. Scovazzo, Gas permeabilities, solubilities, diffusivities, and diffusivity correlations for ammonium-based room temperature ionic liquids with comparison to imidazolium and phosphonium RTIL data, *Chem. Eng. J.* 147 (2009) 51–57.
- [31] D. Morgan, L. Ferguson, P. Scovazzo, Diffusivities of gases in room-temperature ionic liquids: data and correlations obtained using a lag-time technique, *Ind. Eng. Chem. Res.* 44 (2005) 4815–4823.
- [32] J. Anthony, E. Maginn, J. Brennecke, Solubilities and thermodynamic properties of gases in the ionic liquid 1-n-butyl-3-methylimidazolium hexafluorophosphate, *J. Phys. Chem. B* 106 (2002) 7315–7320.
- [33] N.V. Plechkova, K.R. Seddon, Applications of ionic liquids in the chemical industry, *Chem. Soc. Rev.* 37 (2008) 123–150.
- [34] J.F. Jenck, F. Agterberg, M.J. Droscher, Products and processes for a sustainable chemical industry: a review of achievements and prospects, *Green Chem.* 6 (2004) 544–556.
- [35] P.J. Carvalho, V.H. Álvarez, I.M. Marrucho, M. Aznar, J.A.P. Coutinho, High pressure phase behavior of carbon dioxide in 1-butyl-3-methylimidazolium bis(trifluoromethylsulfonyl)imide and 1-butyl-3-methylimidazolium dicyanamide ionic liquids, *J. Supercrit. Fluids* 50 (2009) 105–111.
- [36] D. Peng, D.B. Robinson, A new two-constant equation of state, *Ind. Eng. Chem. Fund.* 15 (1976) 59–64.
- [37] D.S.H. Wong, S.I. Sandler, A theoretically correct mixing rule for cubic equations of state, *AIChE J.* 38 (1992) 671–680.
- [38] D.S. Abrams, J.M. Prausnitz, Statistical thermodynamics of liquid mixtures: a new expression for the excess Gibbs energy of partly or completely miscible systems, *AIChE J.* 21 (1975) 116–128.
- [39] S. Vitu, J.N. Jaubert, J. Pauly, J.L. Daridon, D. Barth, Phase equilibria measurements of CO₂ + methyl cyclopentane and CO₂ + isopropyl cyclohexane binary mixtures at elevated pressures, *J. Supercrit. Fluids* 44 (2008) 155–163.
- [40] J. Pauly, J. Coutinho, J.L. Daridon, High pressure phase equilibria in methane + waxy systems. 1. Methane + heptadecane, *Fluid Phase Equilibr.* 255 (2007) 193–199.
- [41] A.M.A. Dias, H. Carrier, J.L. Daridon, J.C. Pamies, L.F. Vega, J.A.P. Coutinho, I.M. Marrucho, Vapor–liquid equilibrium of carbon dioxide–perfluoroalkane mixtures: experimental data and saft modeling, *Ind. Eng. Chem. Res.* 45 (2006) 2341–2350.
- [42] S.P.M. Ventura, J. Pauly, J.L. Daridon, I.M. Marrucho, A.M.A. Dias, J.A.P. Coutinho, High-pressure solubility data of methane in aniline and aqueous aniline systems, *J. Chem. Eng. Data* 52 (2007) 1100–1102.
- [43] V.H. Alvarez, R. Larico, Y. Yanos, M. Aznar, Parameter estimation for VLE calculation by global minimization: genetic algorithm, *Braz. J. Chem. Eng.* 25 (2008) 409–418.
- [44] S. Raeissi, C.J. Peters, Carbon dioxide solubility in the homologous 1-alkyl-3-methylimidazolium bis(trifluoromethylsulfonyl)imide family, *J. Chem. Eng. Data* 54 (2009) 382–386.
- [45] J. Kumelán, Á.P. Kamps, D. Tuma, G. Maurer, Solubility of CO₂ in the ionic liquid [hmim][NTf₂], *J. Chem. Thermodyn.* 38 (2006) 1396–1401.
- [46] T.M. Letcher, Developments and Applications in Solubility, Royal Society of Chemistry, 2007.
- [47] Diadem Public 1.2, The DIPPR Information and Data Evaluation Manager, 2000.
- [48] J. Valderrama, P. Robles, Critical properties, normal boiling temperatures, and acentric factors of fifty ionic liquids, *Ind. Eng. Chem. Res.* 46 (2007) 1338–1344.
- [49] V.H. Álvarez, M. Aznar, Thermodynamic modeling of vapor–liquid equilibrium of binary systems ionic liquid + supercritical [CO₂ or CHF₃] and ionic liquid + hydrocarbons using Peng–Robinson equation of state, *J. Chin. Inst. Chem. Eng.* 39 (2008) 353–360.

Artigo 4.13: High Pressure CO₂ Solubility in N-methyl-2-hydroxyethylammonium Protic Ionic Liquids

Silvana Mattedi¹, Pedro J. Carvalho², João A.P. Coutinho², Víctor H. Alvarez³ and Miguel*

Iglesias^{1,4}

¹Programa de Pós Graduação em Engenharia Química, Escola Politécnica, Universidade Federal da Bahia (UFBA), R. Aristides Novis 2 Federação 40210-630 Salvador-Bahia, Brasil

²Departamento de Química, CICECO, Universidade de Aveiro, Campus Universitário de Santiago, 3810-193, Aveiro, Portugal

³Faculdade de Engenharia Química, Universidade Estadual de Campinas (UNICAMP), Cidade Universitária "Zeferino Vaz" Av. Albert Einstein, 500 - CEP 13083-852 - Campinas - SP - Brasil

⁴Departamento de Ingenería Química – ETSE, Universidade de Santiago de Compostela (USC), Rúa Lope Gómez de Marzoa s/n, Campus Sur, 15782 Santiago de Compostela, Spain.

Abstract:

The use of ionic liquids for CO₂ capture and natural gas sweetening is being object of intense research. Within the enormous group of existing ionic liquids, those based on conjugate bases of carboxylic acids seem to be particularly promising. This work addresses the study of the high pressure CO₂ solubility (up to 80 MPa) in two protic ionic liquids, N-methyl-2-hydroxyethylammonium formate and N-methyl-2-hydroxyethylammonium acetate, in a wide range of temperatures (293 K to 353 K). A thermodynamic model based on the Peng–Robinson equation of state with the Wong–Sandler mixing rule, using the NRTL model for the activity coefficients, was here adopted to describe and evaluate the thermodynamic consistency of the experimental data. Furthermore, the study of a ternary mixture of CO₂ + CH₄ + N-methyl-2-hydroxyethylammonium acetate was investigated showing a high selectivity from the IL towards these solutes.

Keywords: Brønsted ionic liquids, protic ionic liquids, carbon dioxide, supercritical, N-methyl-2-

* To whom all correspondence should be addressed. E-mail: silvana@ufba.br. Fax:+55 71 32839810. Phone: +55 71 32839813

hydroxyethylammonium acetate, N-methyl-2-hydroxyethylammonium formate, solubility.

1. Introduction

Ionic liquids (ILs) are a new class of solvents composed only of ions but whose size and shape differences allow them to remain liquid at temperatures below 100°C. Among other interesting properties they present negligible vapor pressures, high thermal stabilities, large liquid phase range, no flammability and high solvation capacity. The possibilities of fine tune the ILs properties, through an endless combination of cations and anions, allow the design of solvents for task specific applications leading to more efficient and sustainable processes and products.

Until now, studies concerning ionic liquids have been based on the imidazolium cation and, to a lesser extent, on the alkyl pyridiniums and trialkylamines [1]. Protic ionic liquids (PILs) have, however, received limited attention from the academia. The first PIL reported, ethanolammonium nitrate, was reported by Gabriel and Weiner in 1888 [2], followed by ethylammonium nitrate (EAN), in 1914, synthesized by Walden [3]. These PILs were produced by a stoichiometric acid-base Brønsted reaction and their main difference, compared to aprotic ILs (AILs), is the presence of at least a proton, which is/are able to promote extensive hydrogen bonding [4]. These liquids present some characteristics, such as a slightly lower conductivity and stability, which may reduce, at first, their interest for a number of applications. However, their low cost, simple synthesis and purification methods, low toxicity and high biodegradation character, among other set of appealing characteristics, overcomes those limitations for many different purposes.

Recently, some work has been reported on the synthesis, physicochemical and structural characterization of PILs. Bicak [5] synthesized the 2-hydroxyethylammonium formate (2-HEAF), an ionic liquid formed by the neutralization of monoethanolamine with formic acid. Greaves *et al.* [6] proposed different protic ionic liquids from primary amines and organic and inorganic acids. Cota *et al.* [7], Kurnia *et al.* [8] and Alvarez *et al.* [9] synthesized a family of these ILs by

modifying the aliphatic chain of the organic acid and/or using secondary and tertiary hydroxyamines. There were also studies that use PILs in catalytic reactions [7] and on the interaction with hydroxilic solvents (like water and alcohols), showing that 2-HEAF is soluble in water, ethanol and methanol in all the concentration range [10]. Moreover, a relevant aspect, considering the interest in these substances as more environmentally sustainable solvents, is their potential toxicity. This issue has not been sufficiently studied until now, especially taking into account the need of this information to fulfill the REACH (Registration, Evaluation, Authorization and Restriction of Chemical Substances) requirements (UE) and so, allowing the assessment of hygiene and safety issues derived from their manufacture, use, and transport in the industrial sectors in which these substances will be applied. In what is referred to PIL's, the first results highlight that total biodegradation and low toxicity are intrinsic characteristics of these kind of ionic liquids [11, 12]

The presence of an anion with a strong basic character suggests that PILs could be an interesting alternative to be applied to processes with supercritical gases for capture of acid gases, such as CO₂, H₂S and SO₂ [13-15]. In order to study the viability of such alternative, vapor-liquid equilibria data at high and moderate pressures are necessary. Thus, in the wake of previous studies [16-19], this work investigates gas-liquid equilibrium of binary CO₂ + N-methyl-2-hydroxy ethylammonium-based ILs systems, in temperatures up to 363.15K and pressures up to 80 MPa. Furthermore, the study of a ternary mixture of CO₂ + CH₄ + N-methyl-2-hydroxyethylammonium acetate was also investigated, showing a high selectivity from the IL towards these solutes.

The Peng–Robinson equation of state with the Wong–Sandler/NRTL mixing rule, using the NRTL model for the activity coefficients, was used to model the experimental data measured in this work.

2. Experimental Section

2.1. Materials

Two protic ionic liquids, N-methyl-2-hydroxy ethylammonium acetate, m-2-HEAA, and N-methyl-2-hydroxy ethylammonium formate, m-2-HEAF, were used in this study. Both ionic liquids were synthesized, at our laboratories, by reacting equimolar amounts of amine and organic acid. The amine was placed in a three necked glass flask, mounted in a thermal bath at 283.15 K, equipped with a reflux condenser, a PT-100 temperature probe for controlling temperature and a dropping funnel. Strong agitation (ca. 450 rpm) was applied in order to improve the contact between the reactants allowing the reaction to be completed. The organic acid was added drop wise to the flask under stirring with a magnetic bar. Stirring was continued for 24 h at laboratory temperature, in order to obtain a final viscous liquid. Then, agitation, slight heating (temperature up to 293.15 K for m-2-HEAF and up to 323.15 K for m-2-HEAA) and moderate vacuum (20 KPa) for the vaporization of residual non reactants were applied for at least 48 h. During the purification step and storage the m-2-HEAF was light protected in order to prevent any degradation. More details about the synthesis can be found in Alvarez *et al.* [9]. The ionic liquids were dried under high vacuum (10^{-4} Pa), for a period never smaller than 48 h, and the structure and purity checked by ^1H NMR and ^{13}C NMR both before and after the measurements. These spectra have shown purity better than 95% (w/w). The adopted purification procedure assures that water and volatile compounds are removed and consequently the influence of these impurities on the thermophysical properties of ILs minimized [20-22].

The final water content was determined with a Metrohm 831 Karl Fischer coulometer, indicating a water mass fraction of $(184 \text{ and } 60) \cdot 10^{-6}$ for m-2-HEAA and m-2-HEAF, respectively.

The carbon dioxide (CO_2) and methane (CH_4) were acquired from Air Liquide. The CO_2 presents a purity of $\geq 99.998\%$ and H_2O , O_2 , C_nH_m , N_2 and H_2 impurities volume fractions lower than $(3, 2, 2, 8 \text{ and } 0.5) \cdot 10^{-6}$, respectively, while the methane presents a purity of $\geq 99.9\%$ and H_2O , O_2 , CO_2 , C_nH_m , N_2 , H_2 and C_2H_6 impurities volume fractions lower than $(20, 50, 10, 80, 500, 40 \text{ and } 400) \cdot 10^{-6}$, respectively.

2.2. Experimental equipment

The high pressure equilibrium cell used in this work is based on a cell designed by Daridon *et al.* [23-27] using the synthetic method. Both the apparatus and the methodology here followed were fully described in previous works [16-19], and shown to be adequate to accurately measure vapour–liquid phase equilibrium in a wide range of pressures and temperatures. The temperature is measured with a high precision thermometer, model PN 5207 with an accuracy of 0.01 K, connected to a calibrated platinum resistance inserted inside the cell close to the sample. The pressure is measured by a piezoresistive silicon pressure transducer (Kulite) fixed directly inside the cell to reduce dead volumes, that was previously calibrated and certified by an independent laboratory with IPAC accreditation, following the EN 837-1 standard and with accuracy better than 0.2%. The accuracy for the measured mole fraction of gas dissolved in the liquid phase was better than 0.003.

The purity of the IL is checked again by NMR at the end of the study to confirm that no degradation takes place during the measurements.

2.3 Thermodynamic Modeling

The well known Peng-Robinson equation of state [28],

$$P = \frac{RT}{V - b} - \frac{a}{V(V + b) + b(V - b)} \quad (1)$$

where the constants a_m and b_m are expressed as functions of concentration of the different components in the mixture through the Wong and Sandler mixing rule [29] using the NRTL model [30] for the activity coefficient was applied to the modeling of the experimental data and the thermodynamic consistency was studied with the method of Alvarez and Aznar [31, 32].

$$b_m = \frac{\sum_i \sum_j x_i x_j \left(b - \frac{a}{RT} \right)_{ij}}{1 - \sum_i \frac{x_i a_{ii}}{b_i RT} - \frac{A_\infty^E}{\Omega RT}} \quad (2)$$

$$a_m = b_m \left[\sum_i \frac{x_i a_{ii}}{b_{ii}} + \frac{A_\infty^E}{\Omega} \right] \quad (3)$$

$$\left(b - \frac{a}{RT} \right)_{ij} = \frac{(b_{ii} + b_{jj})}{2} - \frac{(1 - k_{ij})\sqrt{a_{ii}a_{jj}}}{RT} \quad (4)$$

in these equations, a_m and b_m are the EoS constants, $\Omega = 0.34657$, and A_∞^E , the excess Helmholtz free energy at the limit of infinite pressure, that is calculated assuming that $A_\infty^E = A_\infty^G$, where G_∞^E is the excess Gibbs free energy at the limit of zero pressure here calculated using the NRTL model [30]. The equations for the NRTL model to calculate the activity coefficient in multicomponent systems are:

$$\frac{G^E}{RT} = \sum_{i=1}^N x_i \ln \frac{\sum_{j=1}^N G_{ji} \tau_{ji} x_j}{\sum_{k=1}^N G_{ki} x_k} \quad (5)$$

$$\tau_{ij} = \frac{A_{ij}}{RT} \quad (\tau_{ij} \neq \tau_{ji}), \quad G_{ij} = \exp(-\alpha_{ij} \tau_{ij}) \quad (\alpha_{ij} = \alpha_{ji}) \quad (6)$$

where A_{ij} and A_{ji} represent the interaction energy between molecules i and j , R is the universal constant of gases, T is the temperature, and α_{ji} is the non-randomness parameter.

Furthermore, the proposed model was applied, in the diluted region limit, to determine the Henry's constant for the studied systems. The Henry's law relates the amount of a given gas dissolved in a given type and volume of liquid, at a constant temperature, to the fugacity of that gas in equilibrium with that liquid and can be described as

$$H_{12}(T, P) = \lim_{x_1 \rightarrow 0} \frac{f_i^L}{x_1} \quad (7)$$

where $H_{12}(T, p)$ is the Henry's constant, x_1 is the mole fraction of gas dissolved in the liquid phase, and f_i^L is the fugacity of the gas in the liquid phase. Furthermore the proposed model was applied, in the diluted region limit, to determine the Henry's constant for the studied systems.

The results for the Henry's constant of CO₂ in m-2-HEAF and in m-2-HEAA were correlated as a function of temperature by an empirical equation of the type:

$$\ln(H_{12}) = A\left(\frac{1}{T}\right) + B \quad (8)$$

The correlation of the experimental data was carried by the minimization of the objective function, *OF*, for

$$OF = \sum_{i=1}^N \left[\frac{P^{cal} - P^{exp}}{\sigma_p^{exp}} \right]^2_i \quad (9)$$

where *N* is the number of data points, *p* is the pressure, the superscripts "exp" and "cal" refers to the experimental and calculated values respectively, and σ_p is the standard deviation of pressure. The experimental uncertainties in the pressure data were used for σ_p . The minimization method was performed using a genetic algorithm code, implemented and fully explained in Alvarez et al. [33]. The difference between experimental and calculated values was calculated as the average percent deviation, expressed in absolute form, as follows:

$$|\Delta p| = \frac{100}{N} \sum_{i=1}^N \left[\frac{P^{cal} - P^{exp}}{P^{exp}} \right]_i \quad (10)$$

Results and Discussion

The solubility of carbon dioxide and methane in the studied ILs was measured for concentrations from (0.2 to 0.9), in the temperature range (293 to 363) K and pressures from (0.1 to 80) MPa. The solubility data is reported in Tables 1 through 3 and plotted in Figures 1a, 1b and 2. It follows the typical solubility behavior decreasing with temperature and increasing with pressure as observed previously for other ILs [16-19].

Table 1. Bubble point data of the system CO₂ (1) + m-2-HEAF (2).

<i>x₁</i>	T /K	p /MPa												
0.057	293.22	0.494	0.119	293.21	1.194	0.172	293.30	1.835	0.231	293.26	2.482	0.281	293.37	3.108
0.057	303.07	0.666	0.119	303.12	1.563	0.172	303.22	2.317	0.231	303.15	3.155	0.281	303.27	3.959
0.057	313.25	0.889	0.119	313.16	1.912	0.172	313.16	2.843	0.231	313.26	3.895	0.281	313.33	4.940
0.057	323.28	1.105	0.119	323.28	2.284	0.172	323.18	3.435	0.231	323.22	4.746	0.281	323.13	5.985
0.057	333.31	1.354	0.119	333.30	2.710	0.172	333.25	4.078	0.231	333.21	5.622	0.281	333.15	7.176
0.057	343.42	1.662	0.119	343.18	3.133	0.172	343.27	4.742	0.231	343.29	6.576	0.281	343.19	8.456
0.057	353.26	1.950	0.119	353.19	3.612	0.172	353.18	5.414	0.231	353.20	7.572	0.281	353.24	9.764
0.057	363.21	2.280	0.119	363.27	4.071	0.172	363.23	6.112	0.231	363.31	8.549	0.281	363.42	11.138
<i>x₁</i>	T /K	p /MPa												
0.336	293.27	3.808	0.381	293.30	4.417	0.429	293.32	5.116	0.483	293.29	12.094	0.534	293.32	26.849
0.336	303.18	4.885	0.381	303.23	5.746	0.429	303.14	6.950	0.483	303.20	17.625	0.534	303.37	32.578
0.336	313.12	6.150	0.381	313.10	7.366	0.429	313.31	11.215	0.483	313.30	22.384	0.534	313.32	37.662
0.336	323.23	7.632	0.381	323.11	9.467	0.429	323.28	15.098	0.483	323.29	26.654	0.534	323.17	42.016
0.336	333.17	9.293	0.381	333.25	12.078	0.429	333.33	18.618	0.483	333.25	30.414	0.534	333.27	45.617
0.336	343.23	11.098	0.381	343.23	14.687	0.429	343.21	21.819	0.483	343.23	33.635	0.534	343.28	48.511
0.336	353.28	12.966	0.381	353.50	17.347	0.429	353.23	24.718	0.483	353.21	36.359	0.534	353.22	50.852
0.336	363.17	14.818	0.381	363.31	19.623	0.429	363.15	27.090	0.483	363.25	38.678	0.534	363.28	52.910

Table 2. Bubble point data of the system CO₂ (1) + m-2-HEAA (2).

<i>x₁</i>	T /K	p /MPa									
0.157	313.27	0.840	0.208	313.12	1.732	0.249	312.93	2.790	0.299	313.28	3.903
0.157	323.40	1.230	0.208	323.33	2.194	0.249	323.22	3.571	0.299	323.37	4.865
0.157	333.60	1.680	0.208	333.36	2.774	0.249	333.16	4.225	0.299	333.59	6.070
0.157	343.42	2.151	0.208	343.37	3.438	0.249	343.06	5.027	0.299	343.37	7.421
0.157	353.25	2.682	0.208	353.28	4.187	0.249	353.31	6.235	0.299	353.44	8.923
0.157	363.20	3.357	0.208	362.62	4.910	0.249	363.48	7.794	0.299	363.27	10.516
<i>x₁</i>	T /K	p /MPa									
0.402	313.26	7.498	0.452	313.02	19.475	0.500	313.09	46.587			
0.402	323.21	10.590	0.452	323.16	26.393	0.500	323.23	55.198			
0.402	333.23	14.872	0.452	333.33	33.002	0.500	333.33	62.754			
0.402	343.25	19.405	0.452	343.31	38.887	0.500	343.36	69.597			
0.402	353.19	24.254	0.452	353.48	44.317	0.500	353.38	75.591			
0.402	363.25	28.545	0.452	363.61	49.244	0.500	363.35	80.500			

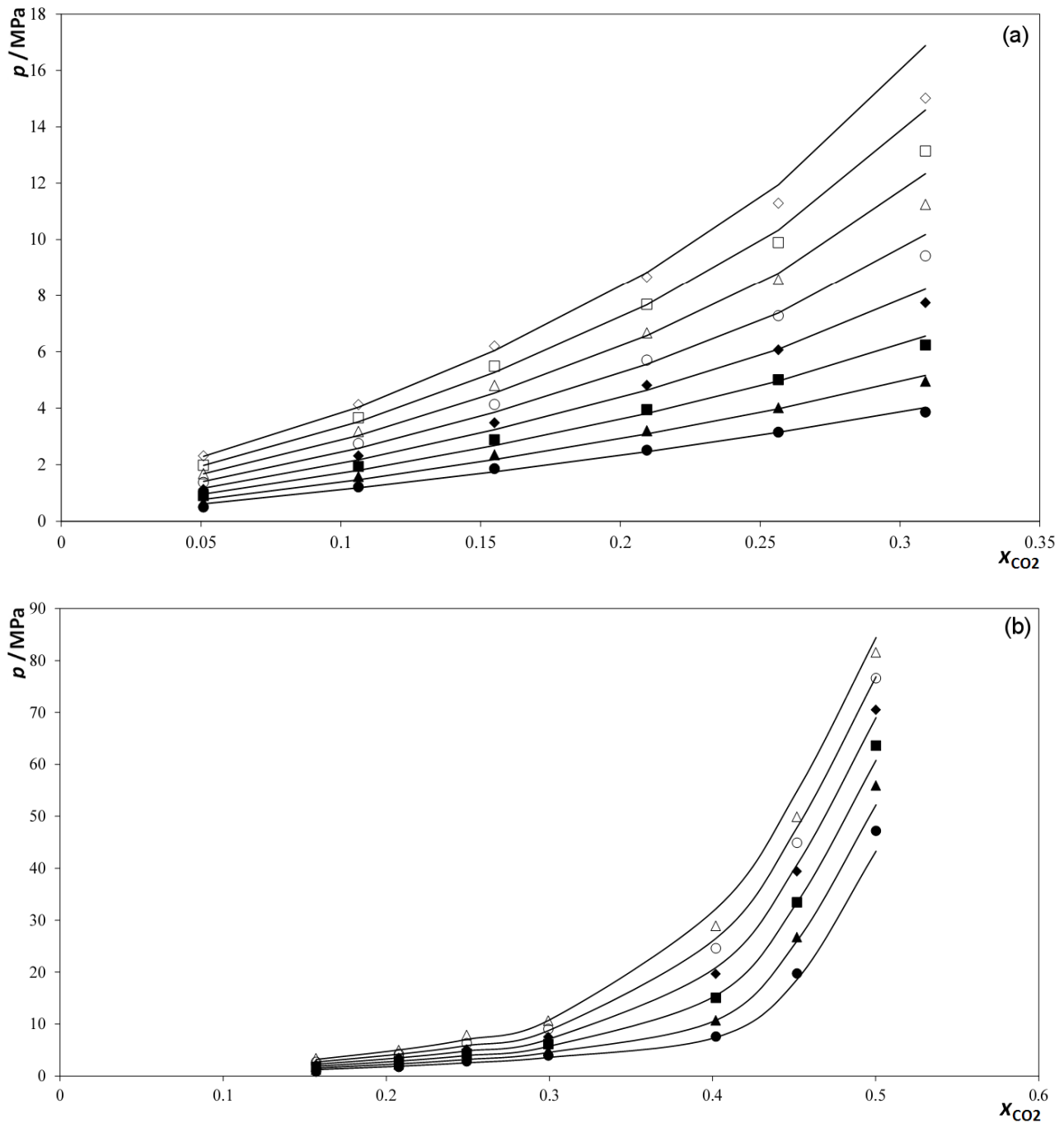


Figure 1. PTx diagram and modeling for the systems $\text{CO}_2 + \text{m-2-HEAF}$, 293.15(\bullet), 303.15(\blacktriangle), 313.15(\blacksquare), 323.15(\blacklozenge), 333.15(\circ), 343.15(\triangle), 353.15(\square), 363.15(\diamond) (a) and $\text{CO}_2 + \text{m-2-HEAA}$, 313.15(\bullet), 323.15(\blacktriangle), 333.15(\blacksquare), 343.15(\blacklozenge), 353.15(\circ), 363.15(\triangle), (b). The solid line represents the calculations from PR-WS/NRTL EoS.

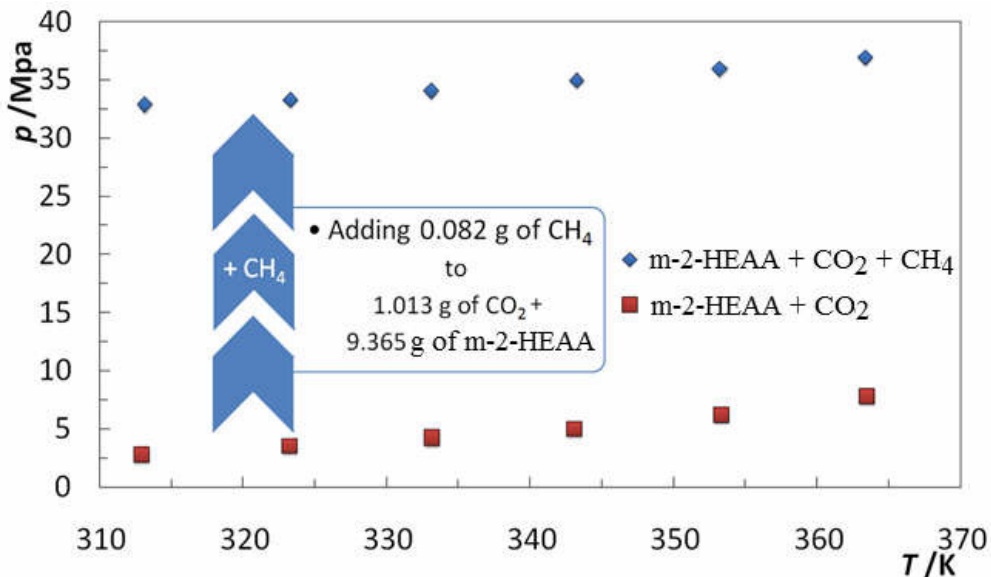


Figure 2. Pressure–temperature diagram of the systems CO_2 ($x_{\text{CO}_2}=0.25$) + m-2-HEAA ($x_{\text{IL}}=0.75$) and CO_2 ($x_{\text{CO}_2}=0.24$) + CH_4 ($x_{\text{CH}_4}=0.05$) + m-2-HEAA ($x_{\text{IL}}=0.71$). Na figura concertar as siglas dos LIIs.

Table 3. Bubble point data of the system CO_2 (1) + CH_4 (2) + m-2-HEAA (3).

x_1	x_2	T / K	p / MPa
0.236	0.052	313.13	32.85
0.236	0.052	323.30	33.29
0.236	0.052	333.11	34.02
0.236	0.052	343.23	34.96
0.236	0.052	353.25	35.95
0.236	0.052	363.37	36.92

The carbon dioxide solubility in the m-2-HEAF and m-2-HEAA ILs, at 313 K, is compared with the CO_2 solubility in the 2-HEAF and 2-hydroxy ethylammonium acetate (2-HEAA) reported by Yuan *et al.* [14] as depicted in Figure 3. The inclusion of a methyl group on the cation leads to an increase of the CO_2 solubility which is in agreement with the conclusions of our previous work showing that the physical sorption of CO_2 increases with the molecular weight of the compound when the concentration is expressed in mole fractions [34]. Furthermore, while the addition of a methyl group produces a slight increase of the CO_2 solubility in the formate-based ionic liquid (m-2-HEAF and 2-HEAF have similar solubility values at ca. 2 MPa) for the acetate-

based ILs it leads to a higher increase. The m-2-HEAA phase behavior suggests that, for low CO₂ mole fractions exists chemical interaction between the CO₂ and the IL. The formation of electron donor acceptor (EDA) complexes between CO₂ and acetate anions was previously observed by ¹³C HRMAS NMR spectra for the CO₂ + 1-butyl-3-methylimidazolium acetate, [C₄mim][Ac], system [17]. The formation of the EDA complex is here confirmed since, as previously observed [34] for the CO₂ + [C₄mim][Ac] system, the CO₂ + m-2-HEAA system, unlike CO₂ + m-2-HEAF system, does not follow the universal correlation previously proposed [34], as depicted in Figure 4. Moreover, the chemisorption present at low CO₂ mole fractions, leads in the m-2-HEAA system to solubilities higher than those observed for ammonium-based ILs with similar molecular weight [14] for pressures up to ca. 4 MPa. For higher pressures the solubility becomes slightly lower and the equilibria pressure increases exponentially. This can be explained considering that m-2-HEAA forms the EDA complexes with carbon dioxide in the low pressure region where the chemical absorption is the predominant phenomena. Upon saturation the physical dissolution becomes predominant with small solubility changes induced by large pressure variations. This trend was also observed with another acetate based IL where chemical followed by physical absorption takes place [17].

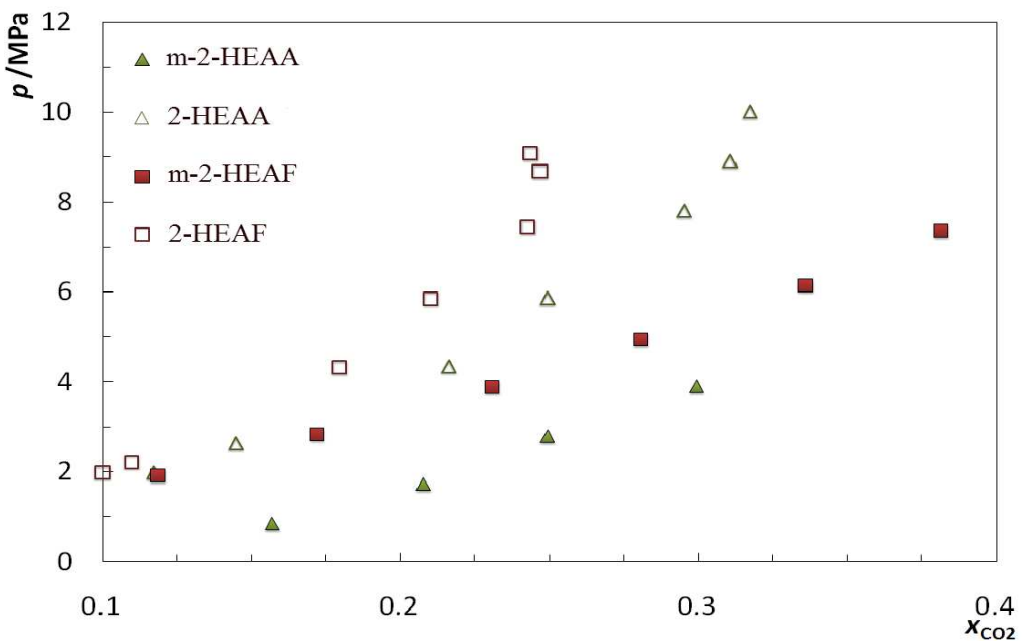


Figure 3. Comparison between the CO_2 solubility, at 313 K, in m-2-HEAF and m-2-HEAA and that in 2-HEAF and 2-HEAA previously reported by Yuan et al. [12].

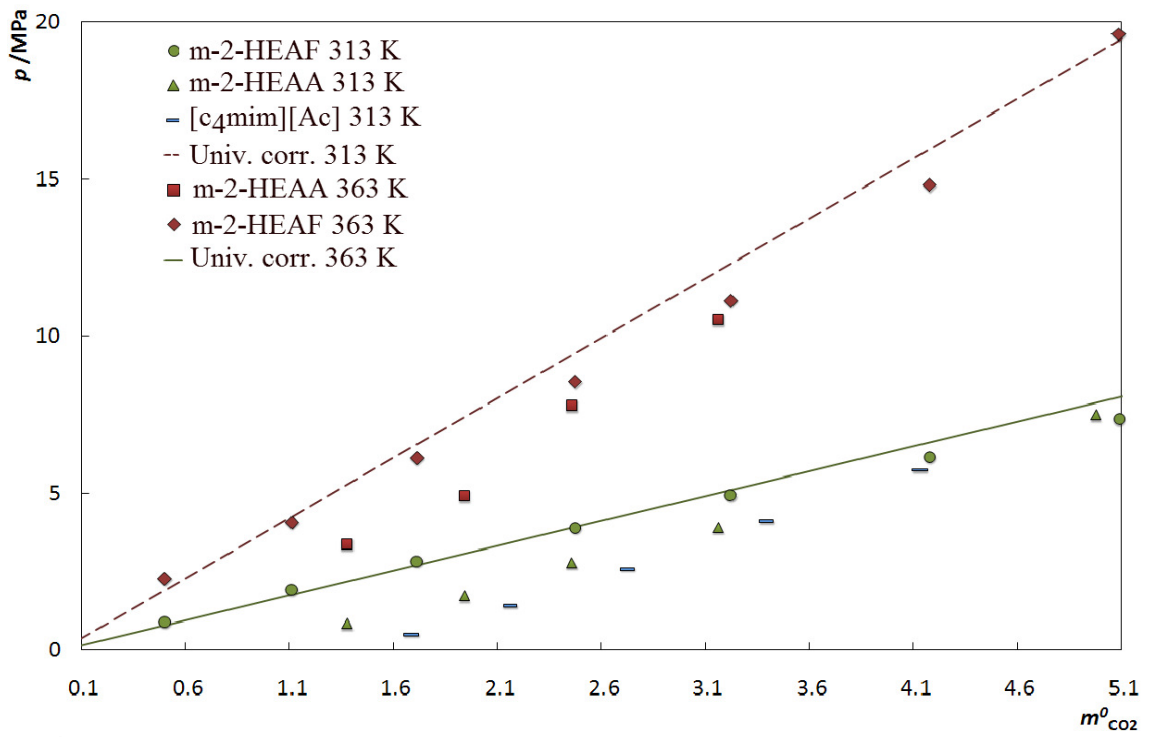


Figure 4. Pressure–molality diagram of the systems $\text{CO}_2 + \text{m-2-HEAF}$ and $\text{CO}_2 + \text{m-2-HEAA}$. The solid and dashed line represents the universal correlation for 313 K and 363 K, respectively [34].

The results of the application of the thermodynamic consistency test to the binary systems

are presented in Table 4, the properties of the substances used in the modeling in Table 5. They show that the data from $\text{CO}_2 + \text{m-2-HEAF}$ binary system is thermodynamically consistent (TC), while the $\text{CO}_2 + \text{m-2-HEAA}$ binary system is not fully consistent (NFC). Nonetheless, the elimination of the data points with individual area deviations greater than 20% leads to consistent data for the remaining points. The $\text{CO}_2 + \text{m-2-HEAA}$ system presents high deviations for the isopleths at $x_1 = 0.5$, for temperatures lower than 343 K, and $x_1 = 0.157$, for temperatures over 343 K. Therefore, the isotherms with these compositions are not fully consistent. Nonetheless, the model provides a very good description of the experimental data, as depicted in Figures 1a and 1b. Also, Table 4 shows the calculated coefficients A and B for the equation (8) together with the Henry's constant average absolute deviations, $|\Delta H_{12}|$, obtained for each ionic liquid.

Table 4. Results of the consistency test using PR+WS/NRTL, with estimated k_{ij} , α , A_{12} and A_{21} parameters, and Henry constant predicted

NP	T (K)	k_{ij}	α	A_{12} KJ/Kmol	A_{21} KJ/Kmol	$ \Delta P (\%)$	Result	H_{12} MPa
$\text{CO}_2 + \text{m-2-HEAF}, \ln H_{12} = -2163.8783/T + 9.7305, \%\Delta H_{12} =2.2$								
6	293.15	-0.9995	0.5500	-41071.4023	18683.8926	5.5	TC	9.91
6	303.15	-0.0852	0.4706	7901.9165	56426.9609	1.9	TC	13.95
6	313.15	-0.2812	0.3850	9843.7500	-65.5746	0.3	TC	17.06
6	323.15	-0.1106	0.4493	7648.2334	33752.0586	0.2	TC	20.96
6	333.15	0.4536	0.3253	1926.8668	46596.8359	0.3	TC	25.55
6	343.15	0.4073	0.5391	2646.3318	24960.9375	0.4	TC	31.17
6	353.15	0.5625	0.3613	1859.4362	39505.7617	0.4	TC	36.42
6	363.15	0.6750	0.4489	1569.2855	30238.8379	0.4	TC	42.42
$\text{CO}_2 + \text{m-2-HEAA}, \ln H_{12} = -3304.5677/T + 12.2156, \%\Delta H_{12} =2.6$								
7	313.15	-0.9980	0.2527	-71728.2344	-3126.9836	9.6	NFC/TC	5.12
7	323.15	0.1860	0.3805	-49838.1055	-3911.3367	11.1	NFC/TC	7.52
7	333.15	-0.9780	0.2724	-78574.2422	-3889.1602	1.9	NFC/TC	10.15
7	343.15	1.0000	0.3721	-89949.1953	-8085.9268	7.6	NFC/TC	12.85
7	353.15	0.1937	0.2000	31291.0371	-3864.1941	6.6	NFC/TC	18.21
7	363.15	0.2360	0.2000	29020.3438	-4191.6221	5.4	NFC/TC	21.86

TC: thermodynamically consistent; NFC: Not fully consistent

Table 5. Properties of the substances used in the modeling.

Compound	T _b /K	T _c /K	P _c /MPa	ω
CO ₂		304.21 ^a	7.38 ^a	0.2236 ^a
m-2-HEAF	514.55 ^c	698.95 ^b	4.14 ^b	0.9359 ^d
m-2-HEAA	538.13 ^c	715.66 ^b	3.33 ^b	0.9836 ^d

^aref, [35]; ^bCalculated with [36]; ^cCalculated with [37]; ^dCalculated with [38]

The introduction of methane, CH₄ ($m_{CH_4}=0.082$ g), in the binary system m-2-HEAA + CO₂ ($x_{CO_2}=0.249$) leads to a strong increase on the equilibrium pressure as shown in Figure 2. This indicates that methane, unlike the carbon dioxide, is poorly soluble on this PIL and suggests that the 2mHEAA could be used to selectively separate the carbon dioxide from methane.

Conclusions

Gas solubilities of carbon dioxide in two protic ionic liquids, namely N-methyl-2-hydroxy ethylammonium acetate and N-methyl-2-hydroxy ethylammonium formate, was presented for temperatures from (293 to 353) K and pressures up to 80 MPa.

Comparison with other similar fluids indicates that while the m-2-HEAF presents no specific interaction towards the CO₂ whereas the m-2-HEAA asymmetric and nonideal phase diagram suggests that this ionic liquid interact chemically with the carbon dioxide at low CO₂ molar concentrations.

The data here reported were well correlated by the PR EoS and found to be thermodynamically consistent for the m-2-HEAF + CO₂ system and not fully consistent for the m-2-HEAA + CO₂ system.

The high solubility pressures exhibited by the ternary mixture CO₂ + CH₄ + m-2-HEAA indicate the m-2-HEAA could be used to selectively separate carbon dioxide from methane mixture.

Acknowledgments:

The authors are thankful for financial support from Fundação para a Ciência e a Tecnologia (Project PTDC/EQU-FTT/102166/2008) and Ph.D. grant (SFRH/BD/41562/2007) of Pedro J. Carvalho. The authors would like to acknowledge FAPESP (Fundação de Amparo à Pesquisa do Estado de São Paulo), for a D.Sc. grant (process #2006/03711-1) of Victor H. Alvarez. Silvana Mattedi would like to thank the support of Universidade de Santiago de Compostela, during her stay in Santiago de Compostela, Spain. Additionally financial support from CNPq [Process PDE 201764/2008-3] is gratefully acknowledged. Miguel Iglesias would like to acknowledge to the Fundacion Ibercaja (Programa de Excelencia en Investigacion 2009) for its support in developing this research.

References

- [1] K.N. Marsh, J.A. Boxall, R. Lichtenthaler, Room temperature ionic liquids and their mixtures – a review, *Fluid Phase Equilib.* 219 (2004) 93-98
- [2] S. Gabriel, J. Weiner, Ueber einige Abkömmlinge des Propylamins, *Ber.* 21 (1888) 2669-2679
- [3] P. Walden, *Bull. Acad. Sci. St. Petersburg* (1914) 405-422
- [4] D.F. Kennedy, C.J. Drummond, Large aggregated ions found in some protic ionic liquids, *J. Phys. Chem. B* 113 (2009) 5690-5693
- [5] N. Bicak, A new ionic liquid: 2-hydroxy ethylammonium formate, *J. Mol. Liq.* 116 (2005) 15-18
- [6] T.L. Greaves, A. Weerawardena, C. Fong, I. Krodkiewska, C.J. Drummond, Protic ionic liquids: solvents with tunable phase behavior and physicochemical properties, *J. Phys. Chem. B* 110 (2006) 22479-22489

- [7] I. Cota, R. Gonzalez-Olmos, M. Iglesias, F. Medina, New short aliphatic chain ionic liquids: synthesis, physical properties, and catalytic activity in aldol condensations, *J. Phys. Chem. B* 111 (2007) 12468-12477
- [8] K. Kurnia, C. Wilfred, T. Murugesan, Thermophysical properties of hydroxyl ammonium ionic liquids, *J. Chem. Thermodyn.* 41 (2009) 517-521
- [9] V.H. Alvarez, N. Dosil, R. Gonzalez-Cabaleiro, S. Mattedi, M. Martin-Pastor, M. Iglesias, J.M. Navaza, Brønsted Ionic Liquids for Sustainable Processes: Synthesis and Physical Properties, *J. Chem. Eng. Data*, 55 (2010) 625-632
- [10] M. Iglesias, A. Torres, R. Gonzalez-Olmos, D. Salvatierra, Effect of temperature on mixing thermodynamics of a new ionic liquid: {2-Hydroxy ethylammonium formate (2-HEAF) + short hydroxylic solvents}, *J. Chem. Thermodyn.* 40 (2008) 119-133
- [11] D. J. Couling, R. J. Bernot, K. M. Docherty, J. K. Dixon, E. J. Maginn, Assessing the factors responsible for ionic liquid toxicity to aquatic organisms via quantitative structure-property relationship modeling, *Green Chem.* 8 (2006) 82-90
- [12] M. Anouti, M. Caillon-Caravanier, C. Le Floch, D. Lemordant, Alkylammonium-Based protic ionic liquids part I: Preparation and physicochemical characterization, *J. Phys. Chem. B* 112 (2008) 9406-9411
- [13] V.H. Alvarez, D. Gómez-Díaz, D. Díaz, A. Figueiras, M. Martin-Pastor, S. Mattedi, M. Aznar, M. Iglesias, J.M. Navaza, *Braz. J. Chem. Eng.* (2010) submitted
- [14] X. Yuan, S. Zhang, J. Liu, X. Lu, Solubilities of CO₂ in hydroxyl ammonium ionic liquids at elevated pressures, *Fluid Phase Equilib.* 257 (2007) 195-200
- [15] X. Yuan, S. Zhang, X. Lu, Hydroxyl ammonium ionic liquids: synthesis, properties, and solubility of SO₂, *J. Chem. Eng. Data* 52 (2007) 596-599
- [16] P.J. Carvalho, V.H. Alvarez, J.J.B. Machado, J. Pauly, J. Daridon, I.M. Marrucho, M. Aznar, J.A.P. Coutinho, High pressure phase behavior of carbon dioxide in 1-alkyl-3-methylimidazolium bis(trifluoromethylsulfonyl)imide ionic liquids, *J. Supercrit. Fluids* 48 (2009) 99-107
- [17] P.J. Carvalho, V.H. Alvarez, B. Schröder, A.M. Gil, I.M. Marrucho, M. Aznar, L.M.N.B.F. Santos, J.A.P. Coutinho, Specific solvation interactions of CO₂ on acetate and trifluoroacetate

imidazolium based ionic liquids at high pressures, *J. Phys. Chem. B* 113 (2009) 6803-6812

- [18] P.J. Carvalho, V.H. Alvarez, I.M. Marrucho, M. Aznar, J.A.P. Coutinho, High pressure phase behavior of carbon dioxide in 1-butyl-3-methylimidazolium bis(trifluoromethylsulfonyl)imide and 1-butyl-3-methylimidazolium dicyanamide ionic liquids, *J. Supercrit. Fluids* 50 (2009) 105-111
- [19] P.J. Carvalho, V.H. Alvarez, I.M. Marrucho, M. Aznar, J.A.P. Coutinho, High carbon dioxide solubilities in trihexyltetradecylphosphonium-based ionic liquids, *J. Supercrit. Fluids* 52 (2010) 258-265
- [20] M.G. Freire, P.J. Carvalho, A.M. Fernandes, I.M. Marrucho, A.J. Queimada, J.A.P. Coutinho, Surface tensions of imidazolium based ionic liquids: anion, cation, temperature and water effect, *J. Colloid Interface Sci.* 314 (2007) 621-630
- [21] K.R. Seddon, A. Stark, M. Torres, Influence of chloride, water, and organic solvents on the physical properties of ionic liquids, *Pure Appl. Chem.* 72 (2000) 2275-2287
- [22] J.G. Huddleston, A.E. Visser, W.M. Reichert, H.D. Willauer, G.A. Broker, R.D. Rogers, Characterization and comparison of hydrophilic and hydrophobic room temperature ionic liquids incorporating the imidazolium cation, *Green Chem.* 3 (2001) 156-164
- [23] S. Vitu, J.N. Jaubert, J. Pauly, J.L. Daridon, D. Barth, Phase equilibria measurements of CO₂ + methyl cyclopentane and CO₂ + isopropyl cyclohexane binary mixtures at elevated pressures, *J. Supercrit. Fluids* 44 (2008) 155-163
- [24] J. Pauly, J. Coutinho, J.L. Daridon, High pressure phase equilibria in methane + waxy systems: 1. methane + heptadecane, *Fluid Phase Equilib.* 255 (2007) 193-199
- [25] S.P.M. Ventura, J. Pauly, J.L. Daridon, J.A.L. da Silva, I.M. Marrucho, A.M.A. Dias, J.A.P. Coutinho, High pressure solubility data of carbon dioxide in tri-iso-butyl(methyl)phosphonium tosylate - water systems, *J. Chem. Thermodyn.* 40 (2008) 1187-1192
- [26] A.M.A. Dias, H. Carrier, J.L. Daridon, J.C. Pamies, L.F. Vega, J.A.P. Coutinho, I.M. Marrucho, Vapor-liquid equilibrium of carbon dioxide-perfluoroalkane mixtures: experimental data and saft modeling, *Ind. Eng. Chem. Res.* 45 (2006) 2341-2350
- [27] S.P.M. Ventura, J. Pauly, J.L. Daridon, I.M. Marrucho, A.M.A. Dias, J.A.P. Coutinho, High-pressure solubility data of methane in aniline and aqueous aniline systems, *J. Chem. Eng.*

Data 52 (2007) 1100-1102

- [28] D. Peng, D.B. Robinson, A new two-constant equation of state, *Ind. Eng. Chem. Fund.* 15 (1976) 59-64
- [29] D.S.H. Wong, S.I. Sandler, A theoretically correct mixing rule for cubic equations of state, *AIChE J.* 38 (1992) 671-680
- [30] H. Renon, J.M. Prausnitz, Local compositions in thermodynamic excess functions for liquid mixtures, *AIChE J.* 14 (1968) 135-144
- [31] V.H. Alvarez, M. Aznar, Application of a thermodynamic consistency test to binary mixtures containing an ionic liquid, *Open Thermodyn. J.* 2 (2008) 25-38
- [32] V.H. Alvarez, M. Aznar, An efficient approach to optimal interpolation of experimental data, *J. Taiwan Inst. Chem. E.* 41 (2010) 184-189
- [33] V.H. Alvarez, R. Larico, Y. Ianos, M. Aznar, Parameter estimation for vle calculation by global minimization: genetic algorithm, *Braz. J. Chem. Eng.* 25 (2008) 409-418
- [34] P.J. Carvalho, J.A.P. Coutinho, On the nonideality of CO₂ solutions in ionic liquids and other low volatile solvents, *J. Phys. Chem. Lett.* 1 (2010) 774-780
- [35] Diadem Public 1.2. The DIPPR Information and Data Evaluation Manager, 2000.
- [36] J.O. Valderrama, V.H. Alvarez, A versatile thermodynamic consistency test for incomplete phase equilibrium data of high-pressure gas-liquid mixtures, *Fluid Phase Equilib.* 226 (2004) 149-159
- [37] K.K. Joback, R. Reid, Estimation of pure component properties from group contribution, *Chem. Eng. Commun.* 57 (1987) 233-247
- [38] J.O. Valderrama, P. Robles, Critical properties, normal boiling temperatures, and acentric factors of fifty ionic liquids, *Ind. Eng. Chem. Res.* 46 (2007) 1338-1344

4.2.2.4 Equilíbrio líquido-líquido

A metodologia experimental utilizada foi validada em trabalhos anteriores (Oliveira, 2009) e foi utilizada para determinar o ELL para o sistema ternário butirato de N-metil-2-hidroxietilamônio + dibenzotifeno + n-dodecano a 298,15 K à pressão atmosférica (≈ 95 kPa). O líquido iônico foi sintetizado e purificado como descrito nas seções anteriores e os outros compostos foram utilizados sem purificação adicional.

Como descrito na seção anterior a curva binodal foi obtida por pontos de névoa. Logo, os dados de pontos de névoa foram utilizados para obter as curvas de calibração:

$$n_D^{25} = 1,6619 + 0,2073w_{LI} \quad 4.1$$

$$n_D^{25} = 1,4559 + 0,2115w_{DBT} \quad 4.2$$

Como o líquido iônico não é solúvel no n-dodecano, temos um sistema binário na fase alifática, a solução dibenzotifeno + n-dodecano. A curva de calibração para este sistema foi obtido de Oliveira (2009).

$$n_D^{25} = 1,4196 + 0,1732w_{DBT} \quad 4.3$$

Os resultados foram analisados no artigo apresentado por Oliveira et al (2010)

Artigo publicado:

O seguinte artigo contém os dados experimentais e a modelagem do sistema ternário m-2-HEAB + benzotifeno + n-dodecano.

OLIVEIRA, L. H.; ALVAREZ, V.H.; AZNAR, M. Liquid-liquid Equilibrium for n-dodecane + DBT + n-methyl-2-hydroxyethylammonium butyrate at 25°C and 95 kPa, aceito no XVIII Congresso Brasileiro de Engenharia Química, COBEQ 2010, Foz do Iguaçu, 2010.

Artigo 4.14: Liquid-liquid equilibrium for n-dodecane + DBT + n-methyl-2-hydroxyethylammonium butyrate at 25°C and 95 kPa

L. H. de OLIVEIRA, V. H. ÁLVAREZ and M. AZNAR*

Universidade Estadual de Campinas, Faculdade de Engenharia Química

*e-mail: maznar@feq.unicamp.br

ABSTRACT – In this work, liquid-liquid equilibrium (LLE) data for n-dodecane + dibenzothiophene (DBT) + n-methyl-2-hydroxyethyl butyrate (m-2-HEAB) at 25 °C and atmospheric pressure (\approx 95 kPa) were determined by refractometry and compared with data for [emim][EtSO₄] and [emim][DEtPO₄]. DBT and its derivatives represent the most difficult diesel sulfur pollutants to remove by the conventional process of hydrodesulfurization (HDS). This system presents a small liquid-liquid equilibrium region at the bottom of ternary diagram. The LLE data were used to analyze the DBT extraction from n-dodecane as model diesel oil. DBT distribution coefficient, solvent selectivity and extraction data indicate that m-2-HEAB is not as good solvent for DBT extractive desulfurization (EDS) from dodecane as [emim][EtSO₄] or [emim][DEtPO₄]. Hand and Othmer-Tobias correlations present $R^2 > 0.99$. NRTL model was used to correlate LLE data and shows mean square deviations $< 0.02\%$.

KEYWORDS: ionic liquids, extractive desulfurization, dibenzothiophene.

1. INTRODUCTION

It is well known that the sulfur present in fuels pollutes the atmosphere in the form of SO_X. Moreover, this compound inhibits the control pollution equipment performance (Araújo et al., 2010). Brazil follows the tendencies of USA (limit to 15 ppm since 2006), Japan and the Europe (10 ppm since 2009), to reduce the maximum sulfur content in diesel oil from 5000-2000 ppm to 50 ppm in 2009 (Babich & Moulijn, 2003). In order to achieve these environmental laws, liquid extraction with ionic liquids as a complementary process to the usual hydrodesulfurization has received academic attention in the last decade (Zhang et al., 2004; Eßer et al, 2004; Alonso et al., 2008), since HDS requires hard conditions to operate ($>300^\circ\text{C}$, >30 bar, H₂ large amounts, expensive catalysts, etc) [5], it is not effective to remove some sulfur compounds, such as the sterically hindered dibenzothiophenes by DBT itself, 4-methyl-dibenzothiophene (4-MDBT) and 4,6-dimethyl-dibenzothiophene (4,6-DMDBT) (Kwak et al, 2000).

Diesel EDS process involves separation of DBT derivatives from fuel by utilizing a liquid extracting agent that is not miscible with diesel. EDS can be performed at mild operation conditions (low pressure and temperature). Literature data for EDS involving ionic liquids as extracting solvents, DBT derivatives as solute sulfur species, and C₁₂-C₁₆ as model diesel oil,

consists solely in extraction curves data (Zhang et al., 2004; Eßer et al, 2004). However, phase equilibrium involving an ionic liquid + a non aromatic sulfur compound + an alkane with aim in diesel and gasoline desulfurization had been recently reported (Alonso et al., 2008).

In this work, LLE data were determined for n-metil-2-hidroxiethyl butyrate + DBT + n-dodecane as model diesel oil, at 25°C and atmospheric pressure (\approx 95 kPa).

2. EXPERIMENTAL

2.1. Materials: The properties of chemicals used are listed in Table 1.

Table 1 – Properties of the pure components

Chemical	MM (g/mol)	n_D (25°C)	
		Exp.	Lit.
m-2-HEAB	163.21	1.4563	1.4549 ^a
DBT	184.26	-	-
n-dodecane	170.33	1.4196	1.42011 ^b

^a Álvarez et al. (2010), ^b Alonso et al., 2008

The m-2-HEAB ionic liquid were synthesized in our laboratories as shown in Álvarez et al. (2010). The difference in refractive indexes can be explained by humidity content. Removal of residual volatile compounds and moisture from ionic liquids was carried out under vacuum (8 kPa) and magnetic stirring at 50°C for 24 h. After, ionic liquids were stored under nitrogen atmosphere. Water content below 500 ppm was achieved. Other chemicals were used as received and purchased from Fluka.

2.2. Procedure: Experiments were carried out in equilibrium cells, such as suggested by Sandler (2006) and described by Oliveira (2009). The cell temperature was regulated by a Tecnal TE-184 thermostatic bath, accurate to $\pm 0.1^\circ\text{C}$.

The cloud point method of Letcher and Siswana (1992) was utilized for determination of binodal curves in the ionic liquid rich phase, by titration of known binary mixtures of aromatic sulfur + ionic liquid with n-dodecane until constant turbidity. Then, the refractive index (n_D) of each point was measure in triplicate with a Mettler-Toledo RE 40D refractometer for determination of calibration curves. The n_D of known binary (n-dodecane + DBT) binodal curves was measured by Oliveira (2009).

In phase equilibrium experiments, ternary mixtures of known composition within the immiscibility gap were prepared by weighing the components within the cell using a Shimadzu AX200 analytical balance, accurate to $\pm 1 \times 10^{-4}$ g. The mixtures were hardly agitated with a Fisatom 752 magnetic stirrer for 12 h in order to allow an intimate interaction between the phases, and decanted for 24 h until equilibrium phases settle down. The system separate in two clean liquid phases. For binary SLE, pure DBT precipitates in equilibrium with a saturated

mixture of n-dodecane + DBT (Oliveira, 2009). For each liquid phase of unknown composition the refractive index was measured in triplicate and the average used for composition determination.

3. RESULTS AND DISCUSSION

3.1. Cloud Points and Calibration Curves: the mass fractions (w), refractive indices and standard deviation (σ) of cloud points determined are shown Table 2. Applying linear regression on these data, the equations of calibration curves obtained for m-2-HEAB rich phase are:

$$n_D^{25} = 1.6619 - 0.2073 w_1 \quad (1)$$

$$n_D^{25} = 1.4559 + 0.2115 w_2 \quad (2)$$

Table 2 – Mass fraction (w), refractive index (n_D) and standard deviation (σ) of cloud points for m-2-HEAB (1) + DBT (2) + n-dodecane (3) at 25°C.

w ₁	w ₂	n _D	10 ⁴ σ
0.9933	0.0000	1.4560	0.58
0.9892	0.0049	1.4569	0.58
0.9834	0.0095	1.4579	0.00
0.9783	0.0151	1.4591	0.58

The binary n-dodecane + DBT calibration curve points are reported elsewhere (Oliveira, 2009).

3.2. Experimental equilibrium data: LLE data (mole fractions) for m-2-HEAB + DBT + n-dodecane at 25°C and atmospheric pressure (≈ 95 kPa), are reported in Table 3. The Nersnt distribution coefficient and the selectivity of the solvent was calculated by Equations 3 and 4.

$$K_N = \frac{x_2^{\text{ilp}}}{x_2^{\text{ap}}} \quad (3)$$

$$S = \frac{x_2^{\text{ilp}}}{\sum_{i=1}^3 x_i^{\text{ilp}}} \quad (4)$$

In Eqs. 3 and 4, “2” refers to DBT and “3” to n-dodecane; the superscripts “ilp” and “ap” refer to ionic liquid and alcane phase, respectively.

Rectangular and triangular diagrams representing the LLE data are shown in Figure 1. As visualized in triangular diagram, the LLE region is at the bottom, as noted by Eber et al. (2004).

Inclination of tie-lines in Figure 1 and the distribution of DBT in both phases (Figure 2) shown that the solute stabilizes preferably in n-dodecane. Selectivity values above 70 (Figure 3), leads to the fact that m-2-HEAB shows a similar behavior of [emim][EtSO₄], and presents lower values of selectivity than [emim][DEtPO₄].

Table 3 – Equilibrium data for m-2-HEAB (1) + DBT (2) + n-dodecane (3) at 25°C.

x ₁	x ₂	n _D	10 ⁴ σ
<i>N-dodecane rich phase</i>			
0.0000	0.0128	1.4220	1.00
0.0000	0.0247	1.4242	0.58
0.0000	0.0353	1.4262	0.00
<i>Ionic liquid rich phase</i>			
0.9876	0.0063	1.4574	0.00
0.9824	0.0113	1.4586	0.00
0.9772	0.0164	1.4598	0.00
<i>Feed</i>			
0.3787	0.0094		
0.3762	0.0189		
0.3749	0.0272		

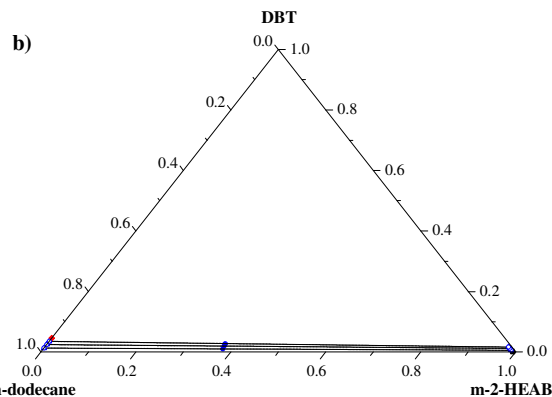
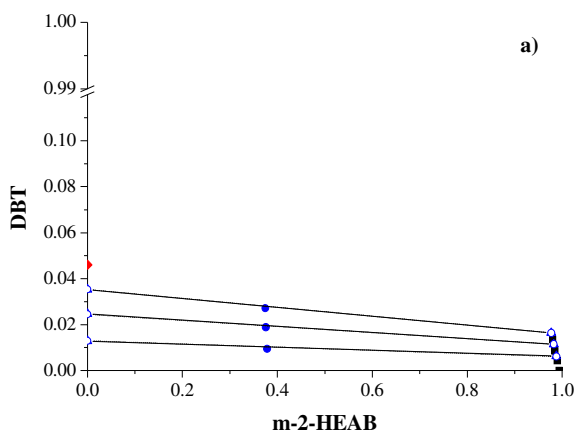


Figure 1 – Experimental and calculated LLE data for m-2-HEAB + DBT + n-dodecane at 25°C.
 a) Rectangle diagram; b) Triangular diagram. Cloud points (■), feed points (●), tie-lines (▲, solid line), DBT saturation in n-dodecane (♦), NRTL correlation (○, dotted line).

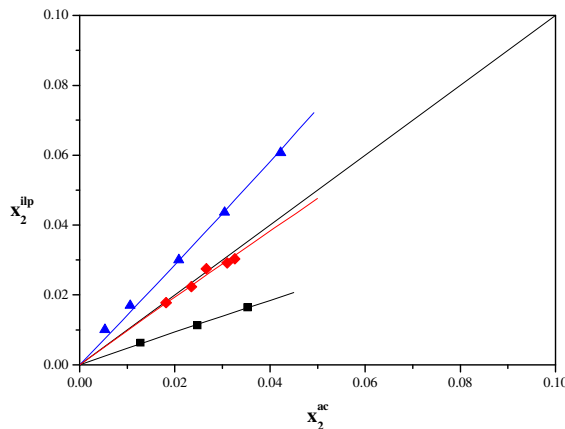


Figure 2 – Distribution of DBT between IL and n-dodecane rich phase: m-2-HEAB (■); [emim][EtSO₄] (♦), [emim][DEtPO₄] (▲); lines are calculated by NRTL.

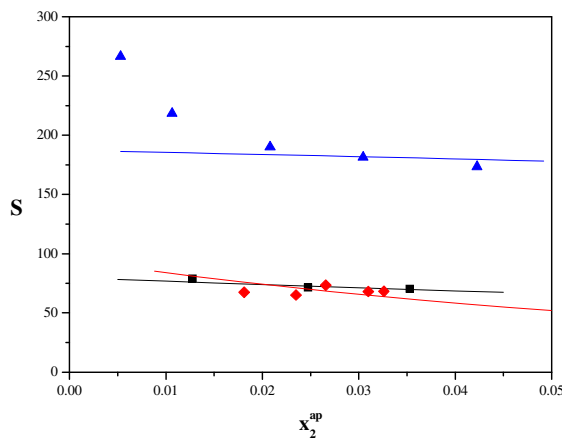


Figure 3 – Selectivity of ionic liquids at 25°C: m-2-HEAB (■); [emim][EtSO₄] (♦), [emim][DEtPO₄] (▲); lines are calculated by NRTL.

The quality of the LLE data is verified with two factors: a) Tie lines agree very well with the cloud points and are very closer to the feed points, indicating low experimental error by loss of mass or analysis; b) the LLE data were tested with Hand (Hand, 1930) and Othmer-Tobias (Othmer & Tobias, 1942) correlations in molar fractions, Equations 5 and 6, respectively.

$$\log \left(\frac{x_2^{lp}}{x_2^{ap}} \right) = k_H \log \left(\frac{x_2^{lp}}{x_3^{ap}} \right) + \text{const}_H \quad (5)$$

$$\log\left(\frac{1-x_1^{\text{ip}}}{x_1^{\text{ip}}}\right) = k_H \log\left(\frac{1-x_3^{\text{ap}}}{x_3^{\text{ap}}}\right) + \text{const}_H \quad (6)$$

In Eqs. 4 and 5, k_H and k_{OT} are the angular coefficients of Hand and Othmer-Tobias correlations respectively; const_H and const_{OT} are the linear coefficients for the same correlations. $R^2 > 0.99$ was obtained for both correlations, as shown in Figures 4 and 5.

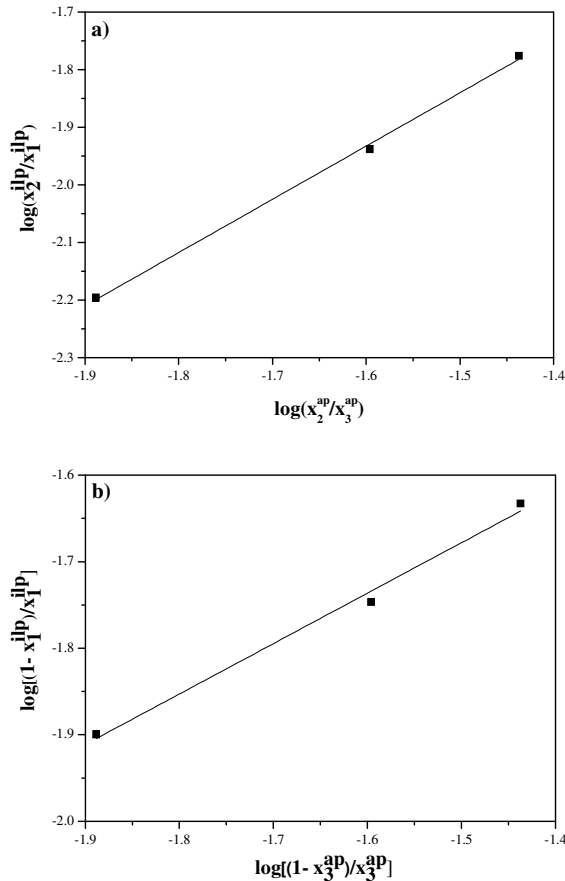


Figure 4 – Hand (a) and Othmer-Tobias (b) correlations for LLE data determined.

3.3. Removal of DBT: the analysis for DBT extraction use the Equations 7-9 and the liquid-liquid equilibrium data present in Table 3.

$$\% \text{ Removal} = \frac{C_0 - C}{C_0} \quad (7)$$

$$C_0 = \left(\frac{w_2}{w_2 + w_3} \right)_{\text{feed}} \quad (8)$$

$$C_f = \left(\frac{w_2}{w_2 + w_3} \right)_{\text{alkane phase}} \quad (9)$$

where, C_0 and C_f are the mass fractions of DBT in n-dodecane before and after reach equilibrium, respectively. The results for an ionic liquid / n-dodecane mass ratio = 0.6 is shown in Table 4 and Figure 5.

Table 4 – Percent of DBT removal from model oil.

C_0	% Removal
0.0164	15.67
0.0326	18.19
0.0469	18.87

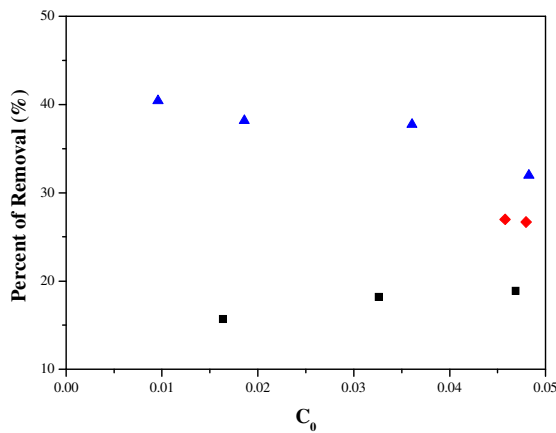


Figure 5 – Percent of DBT removal from model oil at 25°C: m-2-HEAB (■); [emim][EtSO₄] (◆), [emim][DEtPO₄] (▲).

For systems with m-2-HEAB, the percent of DBT extraction were below 20%; otherwise, 24-30% was reached with [emim][EtSO₄] and 34-40% for [emim][DEtPO₄].

3.4. Thermodynamic modeling: The non-random two-liquid model (NRTL) (Renon & Prausnitz, 1968), based on the local composition concept, was used for correlate the experimental data. The NRTL equations are given Equations 10-12:

$$\ln \gamma_i = \frac{\sum_j \tau_{ji} G_{ji} x_j}{\sum_k G_{ki} x_k} + \sum_j \frac{x_j G_{ij}}{\sum_k G_{kj} x_k} \left[\tau_{ij} - \frac{\sum_k x_k \tau_{kj} G_{ki}}{\sum_k G_{kj} x_k} \right] \quad (10)$$

$$\tau_{ij} = \frac{\Delta g_{ij}}{RT} = A_{ij} + \frac{B_{ij}}{T} \quad (\tau_{ij} \neq \tau_{ji}) \quad (11)$$

$$G_{ij} = \exp(-\alpha_{ij} \tau_{ij}) \quad (\alpha_{ij} = \alpha_{ji}) \quad (12)$$

where, γ , is the activity coefficient; τ , NRTL parameter; x , mole fraction; G , NRTL term; Δg , Gibbs excess energy; R , gases constant; T , temperature in K; A_{ij} , binary parameter; B_{ij} ,

temperature dependent binary parameter; α_{ij} , non randomicity parameter; and the subscripts i, j, k refer to component.

New energy interaction parameters were estimated by using the Fortran code TML-LLE 2.0 (Stragevich, 1997); the procedure is based on the Modified Simplex Method (Nelder & Mead, 1965) and consists in the minimization of a concentration-based objective function, F (Sørensen et al., 1979):

$$F = \sum_k^D \sum_j^M \sum_i^N \left\{ (x_{ijk}^{I,exp} - x_{ijk}^{I,calc})^2 + (x_{ijk}^{II,exp} - x_{ijk}^{II,calc})^2 \right\} \quad (13)$$

Here, D is the number of temperature sets, N and M are the number of components and tie lines in each data set and superscripts I and II refer to the two liquid phases, while superscripts exp and $calc$ refer to the experimental and calculated concentration. Calculated compositions can be compared with the experimental ones through root mean square deviations, also shown in Table 6, given by:

$$\delta x = 100 \sqrt{\frac{\sum_i^M \sum_j^N (x_{ij}^{I,exp} - x_{ij}^{I,calc})^2 + (x_{ij}^{II,exp} - x_{ij}^{II,calc})^2}{2MN}} \quad (14)$$

The estimated NRTL parameters are shown in Table 5, and the calculated tie lines are in Figure 1. The calculated distribution and selectivities are in Figures 2 and 3. In Figure 3, the NRTL model gave good approximations for selectivities lower than 150. Above this value, i. e., for desulfurization of diluted solutions of DBT in n-dodecane, NRTL does not give a good representation of experimental selectivity.

Table 5 – Estimated NRTL parameters and deviations for m-HEAB (1) + DBT (2) + n-dodecane (3) system at 25°C.

i	j	A_{ij}	A_{ji}	α_{ij}
1	2	-1691.8	-227.9	0.28
1	3	1240.1	3598.3	0.20
2	3	1235.7	-2741.3	0.20

4. CONCLUSIONS

Phase diagrams showing LLE experimental data were obtained m-2-HEAB + DBT + n-dodecane systems at 25 °C, and ≈95 kPa. From these data, and from values of distribution, selectivity and removal percent, it is observed that m-2-HEAB is not as good solvent than [emim][EtSO₄] or [emim][DEtPO₄], which is the better solvent for extraction of DBT from n-dodecane tested in our laboratories. m-2-HEAB extracts below 20% of DBT initially inserted in n-dodecane; the other ionic liquids show results greater than 30%. The m-2-HEAB, as like the other two ionic liquids, did not dissolve in n-dodecane, but n-dodecane is present as small

amounts in ionic liquid rich phase. The LLE data were correlated with the NRTL model, with estimation of new energy interaction parameters. The deviations between experimental and calculated compositions was always below 0.02%.

5. ACKNOWLEDGEMENTS

The financial support from FAPESP (grants 07/53024-3 and 07/52032-2) is gratefully acknowledged. M. Aznar is the recipient of a CNPq fellowship.

6. REFERENCES

- ALONSO, L.; ARCE, A.; FRANCISCO, M.; SOTO, A. Thiophene separation from aliphatic hydrocarbons using the 1-ethyl-3-methylimidazolium ethylsulfate ionic liquid. *Fluid Phase Equilib.* v. 270, p. 97–102, 2008.
- ÁLVAREZ, V.H.; DOSIL, N.; GONZALEZ-CABALEIRO, R.; MATTEDI, S., MARTIN-PASTOR, M.; IGLESIAS, M.; NAVAZA, J. M. Brønsted Ionic Liquids for Sustainable Processes: Synthesis and Physical Properties, *J. Chem. Eng. Data*, v.55, p. 625–632, 2010.
- ARAÚJO, J. A.; SANTOS, F. K. G.; BARBOSA, C. M. B. M.; CARVALHO, M. W. N. C. Dessulfurização da mistura combustível ciclohexeno-propanotiol utilizando adsorventes do tipo ME/ALPO'S. *4º Congresso Brasileiro de P&D em Petróleo e Gás*. Campinas, 2007.
- BABICH, I. V.; MOULIJN, J. A. Science and technology of novel processes for deep desulfurization of oil refinery streams: a review. *Fuel*, v. 82, p. 607-631. 2003.
- EßER, J.; WASSERSCHEID, P.; JESS, A. Deep desulfurization of oil refinery streams by extraction with ionic liquids. *Green Chem.* v. 6, p. 316-322. 2004.
- HAND, D. B. Dimeric distribution. *J. Phys. Chem.* v. 34, p. 1961–2000, 1930.
- KWAK, C.; LEE, J. J.; BAE, J. S.; CHOI, K.; MOON, S. H. Hydrodesulfurization of DBT, 4-MDBT, and 4,6-DMDBT on fluorinated CoMoS/Al₂O₃ catalysts. *Appl. Catal. A*. v. 200, p. 233–242, 2000.
- LETCHER, T. M.; SISWANA, P. M. Liquid-liquid equilibria of mixtures of an alkanol + water + a methyl substituted benzene at 25°C. *Fluid Phase Equilib.* v. 74, p. 203–217, 1992.
- NELDER, J. A.; MEAD, R. A simplex method for function minimization. *Computer J.* v. 7, p. 308–313, 1965.
- OLIVEIRA, L. H. *Thermodynamic study of liquid-liquid equilibrium aiming sulfur removal by using ionic liquids*, M. Sc. Dissertation, School of Chemical Engineering, State University of Campinas, Campinas, 2009.

OTHMER, D. F.; TOBIAS, P. E. Tie-line correlation. *Ind. Eng. Chem.* v. 34, p. 693–696, 1942.

RENON, H.; PRAUSNITZ, J. M. Local compositions in thermodynamic excess functions for liquid mixtures. *AICHE J.* v. 14, p. 135–144, 1968.

SANDLER, S. I. *Chemical, Biochemical, and Engineering Thermodynamics*; John Wiley & Sons: Hoboken, 2006.

SØRENSEN, J. M.; MAGNUSEN, T.; RASMUSSEN, P.; FREDENSLUND, A. Liquid-liquid equilibrium data: their retrieval, correlation and prediction. Part II: correlation. *Fluid Phase Equilib.* v. 3, p. 47–82, 1979.

STRAGEVICH, L. *Liquid-liquid Equilibrium in Non-electrolyte Systems*, D. Sc. Thesis, School of Chemical Engineering, State University of Campinas, Campinas, 1997.

ZHANG, S.; ZHANG, Q.; ZHANG, Z. C. Extractive desulfurization and denitrogenation of fuels using ionic liquids. *Ind. Eng. Chem. Res.* v. 43, p. 612–622. 2004.

4.3. ALGUMAS APLICAÇÕES DOS LÍQUIDOS IÔNICOS

Os resultados são apresentados como artigos publicados.

4.3.1 Separação do azeótropo etanol + água

ÁLVAREZ, V.H.; FERREIRA, C.; AZNAR, M.; MATTEDEI, S. Use of Ionic Liquid 2-Hydroxy Ethylammonium Formate As Entrainer For Anhydrous Ethanol Production, XVII Congresso Brasileiro de Engenharia Química, COBEQ 2008, Recife, 2008.

ÁLVAREZ, V. H.; ALIJO, P.; SERRÃO, D.; MACIEL FILHO, R.; AZNAR, M.; MATTEDEI, S. Production of Anhydrous Ethanol by Extractive Distillation of Diluted Alcoholic Solutions with Ionic Liquids, 10th International Symposium on Process Systems Engineering, ELSEVIER, v. 27, p. 1137-1142, 2009.

ÁLVAREZ, V.H.; FERREIRA, C.; AZNAR, M.; MATTEDEI, S. An Evaluation and Industrial Application of Ionic Liquid as Separation Agent for Separation of Diluted Ethanol-Water Mixtures, Fenomenos de Transferencia, v4, p. 8-12, 2008.

Artigo 4.15: Use of ionic liquid 2-hydroxy ethylammonium formate as entrainer for anhydrous ethanol production

V.H. Álvarez¹; C. Ferreira²; M. Aznar¹; S. Mattedi²

¹School of Chemical Engineering, State University of Campinas,
UNICAMP.

P.O.Box 6066 – CEP 13083-970 – Campinas – SP – Brazil
Phone: (xx-19) 3521-3962 – Fax: (xx-19) 3521-3910 – Email:
valvarez@feq.unicamp.br

²Department of Chemical Engineering, Polytechnic School, Federal
University of Bahia. 40210-630, Salvador – BA – Brazil – Email:
silvana@ufba.com.br

RESUMO – O equilíbrio líquido vapor (ELV) para o sistema etanol + água contendo o líquido iônico (LI) formiato de 2-hidroxi etil amônia foi medido, a pressão atmosférica (101,32 kPa), em um ebuliômetro tipo Othmer com recirculação em ambas as fases. Os resultados mostram que a adição do LI desloca o ponto azeotrópico. Todas as misturas estudadas, desde 6% até 24% em massa de LI, mostraram o deslocamento do ponto azeotrópico para um ponto de menor temperatura de ebulição do que o do sistema livre de líquido iônico, com mudança na volatilidade relativa do etanol.

PALAVRAS-CHAVE: equilíbrio líquido-vapor; ebuliômetro Othmer; azeótropo etanol-água.

ABSTRACT – Vapor–liquid equilibrium (VLE) data for ethanol + water system containing the ionic liquid (IL) 2-hydroxy ethylammonium formate at atmospheric pressure (101.32 kPa) was measured with an Othmer-type still with recirculation of both phases. The results showed that the addition of IL shifted the azeotropic point. All studied mixtures, from 6 up to 24 weight% of IL, showed the shifting of the azeotropic point to a lower boiling temperature than the IL-free system, which change in the relative volatility of ethanol.

KEYWORDS: vapor liquid equilibrium; Othmer still, ethanol-water azeotrope.

1. INTRODUCTION.

Brazil is world-wide known by the pioneering work of the insertion of ethanol in its energetic matrix. The three most important routes for the ethanol production are direct ethylene hydration, indirect ethylene hydration and fermentation. Currently, the Brazilian ethanol industry produces both hydrated and anhydrous ethanol. Anhydrous ethanol is used as oxidant agent for the gasoline and, more recently, as reactant at transesterification process by basic catalysis for biodiesel production. The blending ratio of anhydrous ethanol with gasoline (20-25%) completely substituted older toxic oxidant additives, such as lead, MTBE or benzene.

The growing demand for anhydrous ethanol and the preservation of the environment need a safe, inexpensive and green process. There are some industrial techniques used for the separation of ethanol/water azeotropic mixture, such as crystallization, liquid-liquid extraction, adsorption and azeotropic or extractive distillation, where the latter is the most largely used in the production of anhydrous ethanol (Huang et al., 2008).

Usually, for the anhydrous ethanol production by extractive distillation, the liquid agent for the separation (the entrainer) is the benzene. This operation is energetically favorable, but it has poor health conditions and operating unstable control. Other liquid agents in the extractive distillation, such as furfural, pentane, diethyl ether, ethylene glycol and toluene, have been restricted by environmental legislation (Ligero and Ravagnani, 2003).

Another variant of extractive distillation is the use of a saline entrainer (a non volatile salt), such as calcium chloride and potassium acetate, which is introduced into the upper distillation plate, step down through the plates and removed with the bottom products.

Recently, the crescent research appointed to evaluation and application of ionic liquids as separation agents. Ionic liquids (ILs) are organic salts which are liquid at room temperature, with melting points below 373 K (Marsh et al., 2004).

These substances present a wide range of applications, as in catalytic reactions, separation of gases and liquids, electrolytic cells, heat transfer fluids and lubricants. Ionic liquids have emerged as possible "green" solvents because they are not volatile and, therefore, do not have pollutant gas emissions.

A IL might be used as a suitable entrainer in the extractive distillation process, and might be superior to the commonly used entrainer due to its non-volatility. Furthermore, thermodynamic data for IL-containing systems are essential for a better understanding of thermodynamic behaviors for separation design purpose and for the development of thermodynamic models. Bicak (2005) synthesized 2-hydroxy ethylammonium formate (2-HEAF) by the reaction of monoethanolamine with formic acid. Then, Iglesias et al. (2008) synthesized a family of ILs by modified aliphatic chain reagents. Since these ILs have a lower cost, it could be feasible to use them as entrainers in anhydrous ethanol production. In this work, isobaric VLE data for ethanol-water systems containing the IL 2-HEAF were determined at atmospheric pressure (101.32 kPa), and the effect of 2-HEAF on the VLE of the ethanol + water system is discussed. The structure of 2-HEAF is:

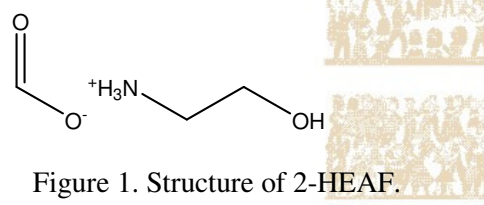


Figure 1. Structure of 2-HEAF.

2. EXPERIMENTAL.

2.1 Materials

The chemical reagents used were ethanol, redistilled water and 2-HEAF. HPLC grade ethanol with purity of 99.8% was purchased from Sigma-Aldrich Company. The purity of reagents was checked by a gas chromatography (Varian Star 3400 CX, USA). 2-HEAF was kindly supplied by Prof. M. Iglesias (Universitat Rovira i Virgili, Spain), as part of a cooperative research on ILs.

2.2 Procedure

The VLE data were measured by using a modified Othmer-type vapor-liquid equilibrium still with recirculation in both phases (Ocón and Espantoso, 1958, Resa et al., 2004). Figure 2 shows the modified Othmer still.



Figure 2. Modified Othmer still.

A Yokogawa model 7563 thermometer and Pt100 platinum sensor was used to measure the temperature cell, with an uncertainty of ± 0.07 K. The thermometer and sensor were standardized by the Laboratory of Metrology of the Federal University of Bahia, certified by National Institute for Metrology, Normalization and Industrial Quality (INMETRO). For the pressure measurement, a differential U-tube glycerol manometer was used, with an uncertainty of ± 0.01 kPa. Nitrogen was injected into the still to maintain a constant pressure of 101.32 kPa, in agreement with the laboratory local pressure. The local pressure was calculated by altitude difference with the meteorological station located at Salvador International Airport. The altitude with respect to mean sea level was measured with an uncertainty

of 1.0 mm by the geo-reference method. The total volume of the still was about 720 cm³, of which about 360 cm³ were occupied by the liquid solution. The still was heated through a resistance coil controlled by a Variac voltage transformer. During the operation, a liquid solution was put into the boiling chamber and heated. The mixture of vapor and liquid in the boiling chamber was carried upward to the equilibrium chamber, where the vapor and liquid phases were separated after flowing directly along the thermometer stem. The vapor was condensed in the condenser and went to the mixing chamber. The equilibrium was usually reached in about 30-60 minutes, as indicated by the constant boiling temperature. The system was maintained in equilibrium for about 1 h, and then samples of the vapor and liquid were taken out.

2.3 Samples analysis

The compositions of the vapor and liquid phases were determined by densimetry analysis. The density of both phases was measured at 298.15 K and the results were compared with those from mixtures of known composition, through an inverse interpolation. The densities of the pure liquids and mixtures were measured using an Anton Paar DSA-5000 digital vibrating tube densimeter. The uncertainty is $\pm 2 \cdot 10^{-6}$ g.cm⁻³ for the density measurement, and ± 0.01 m.s⁻¹ for the speed of sound measurements. In Table 1, the experimental density and speed of sound of the pure components are compared with literature data. The accuracy of the measured vapor and liquid phase compositions is estimated to be ± 0.001 in mole fraction. The IL content in liquid phase is determined through a mass balance by measuring the mass difference of vapor sample.

Table 1. Experimental and literature data for pure components at 298.15 K.

Reagents	density (g.cm ⁻³)		speed of sound (m.s ⁻¹)	
	exp	lit	exp	lit
ethanol	0.78533	0.7854 ^a	1147.86	1142 ^b
water	0.99705	0.9971 ^c	1496.91	1498 ^d
2-HEAF	1.16597	1.1771 ^e	1730.7	1719.6 ^e

^aNikam et al. (1995), ^bOrge et al. (1997), ^cKapadi et al. (2000), ^dGeorge et al. (2003), ^eIglesias et al. (2008).

3. RELIABILITY ASSESSMENT.

In order to check the reliability of the experimental set-up, isobaric VLE data for the ethanol-water system at atmospheric pressure (101.32 kPa) were measured and compared with data from Kojima et al. (1968). It can be seen from Figure 3 that the measured data were in good agreement with those from Kojima et al. (1968). Hence the set-up can be used to investigate the effect of IL on the VLE of the ethanol-water system at atmospheric pressure. The experimental isobaric VLE data for the ethanol-water binary system at atmospheric pressure (101.32 kPa) were listed in Table 2.

Table 2. Experimental isobaric VLE data for the ethanol (1) + water (2) binary system.

T (K)	x ₁	y ₁
360.68	0.0714	0.3762
359.60	0.0849	0.4145
357.55	0.1164	0.4865
355.51	0.1771	0.5238
354.37	0.2250	0.5686
353.85	0.2915	0.5955
352.18	0.8683	0.8714
352.85	0.4864	0.6628
354.84	0.2672	0.5830
351.44	0.9891	0.9873

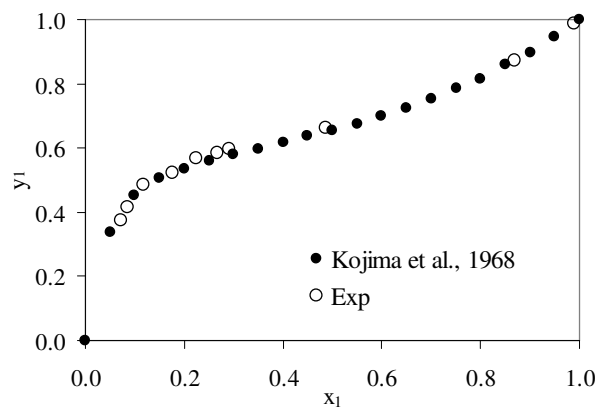


Figure 3: Isobaric VLE diagram for ethanol (1) + water (2) at atmospheric pressure (101.32 kPa).

4. VLE FOR THE IL-CONTAINING TERNARY SYSTEM.

Table 3. VLE data for ethanol(1) + water(2) + 2-HEAF(3) at different IL weight %.

IL wt %	T (K)	x ₁	x ₂	y ₁	y ₂	α_{12}
6.291	351.42	0.9653	0.0049	0.9812	0.0188	0.27
6.291	351.35	0.8266	0.1459	0.8352	0.1648	0.89
6.290	351.58	0.7016	0.2733	0.7711	0.2289	1.31
6.291	352.04	0.5989	0.3779	0.7160	0.2840	1.59
6.285	352.57	0.5100	0.4684	0.6698	0.3302	1.86
6.272	353.08	0.4337	0.5463	0.6405	0.3595	2.24
6.270	353.32	0.3754	0.6057	0.6276	0.3724	2.72
6.271	353.95	0.3244	0.6577	0.5890	0.4110	2.91
10.040	351.31	0.9416	0.0063	0.9639	0.0361	0.18
10.038	351.23	0.8705	0.0798	0.8868	0.1132	0.72
10.036	351.18	0.8571	0.0935	0.8778	0.1222	0.78
10.040	351.16	0.8520	0.0989	0.8818	0.1182	0.87
10.670	351.35	0.8434	0.1110	0.8615	0.1385	0.82
10.579	351.53	0.7029	0.2536	0.7719	0.2281	1.22
10.572	351.80	0.5416	0.4221	0.7255	0.2745	2.06
10.573	352.31	0.4720	0.4937	0.6792	0.3208	2.21
24.138	350.73	0.8710	0.0000	0.9639	0.0361	0.00
24.129	350.82	0.8702	0.0010	0.9011	0.0989	0.01
24.133	350.98	0.7331	0.1497	0.8199	0.1801	0.93
24.125	351.38	0.6190	0.2737	0.7735	0.2265	1.51
24.111	351.55	0.5243	0.3773	0.7244	0.2756	1.89

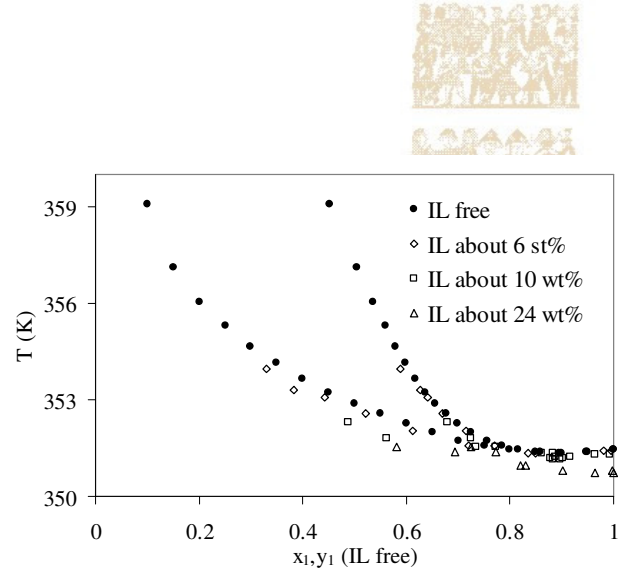


Figure 4: T-x-y diagram for ethanol (1) + water (2) + 2-HEAF (3) at 101.32 kPa.

The isobaric VLE data for the ethanol-water system containing 2-HEAF at different IL contents (from about 6 to 24 wt.%) were measured and listed in Table 3; these data are also plotted as Txy diagrams in Figure 4 and as xy diagrams in Figure 5. It should be noted that the mole fraction of liquid component shown in the tables and figures is on an IL-free basis.

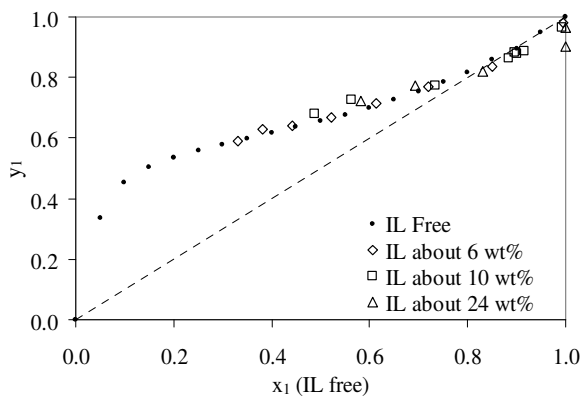


Figure 5. Isobaric VLE diagram for the ethanol (1) + water (2) + 2HEAF (3) system at atmospheric pressure (101.32 kPa).

In addition, the relative volatility of ethanol was also calculated as:

$$\alpha_i = \frac{y_1/x_1}{y_2/x_2} \quad (1)$$

where x_1 and x_2 are mole fraction of ethanol and water, respectively, on IL-free basis. The relative volatilities are also listed in Table 3.

As can be seen from Figure 4, the addition of 2-HEAF modified the relative volatility of ethanol, causing a shifting of the azeotropic point.

Figure 5 and Table 3 indicate the effect of the addition of 2-HEAF on the VLE of the ethanol-water system. In the ethanol rich region, the relative volatility of ethanol decreases with the IL content, while an opposite trend is obtained in the water rich region. The IL effect on the VLE of ethanol–water system can be ascribed to the

affinity difference between its ions and water-ethanol molecules. Specifically, the ions dissociated from IL have a stronger attraction to ethanol than to water due to the polar similarity. In the water-rich region, water molecules are preferentially bonded by ions; however, with the increasing of IL content, from 6 to 24 wt%, the ethanol molecules are also bonded. As the number of ethanol molecules is relatively small, the relative volatility of ethanol is accordingly decreased.

5. THERMODYNAMIC MODEL.

The Peng-Robinson (1976) EoS with the Wong-Sandler (1992) mixing rule, coupled with the NRTL model (Renon and Prausnitz, 1968) for the excess Gibbs free energy, is used as the standard thermodynamic model in a bubble point calculation:

$$P = \frac{RT}{V - b} - \frac{a}{V(V + b) + b(V - b)} \quad (2)$$

$$a = a_c \alpha(T) \quad (3)$$

$$a_c = 0.457235(RT_c/P_c)^2 \quad (4)$$

$$b = 0.077796(RT_c/P_c) \quad (5)$$

$$\alpha(T) = \left[1 + F(1 - T_r^{0.5}) \right]^2 \quad (6)$$

$$F = 0.37464 + 1.54226\omega - 0.26992\omega^2 \quad (7)$$

where T_r is the reduced temperature, T_c is the critical temperature, P_c is the critical pressure, R is the gas constant, and ω is the acentric factor. For mixtures:

$$P = \frac{RT}{V - b_m} - \frac{a_m}{V(V + b_m) + b_m(V - b_m)} \quad (8)$$

The mixture constants a_m and b_m are expressed by the Wong-Sandler mixing rules:

$$b_m = \frac{\sum_i \sum_j x_i x_j \left(b - \frac{a}{RT} \right)_{ij}}{1 - \sum_i \frac{x_i a_i}{b_i RT} - \frac{A_\infty^E}{\Omega RT}} \quad (9)$$

$$a_m = b_m \left[\sum_i \frac{x_i a_i}{b_i} + \frac{A_\infty^E}{\Omega} \right] \quad (10)$$

$$\left(b - \frac{a}{RT} \right)_{ij} = \frac{(b_i + b_j)}{2} - \frac{(1 - k_{ij}) \sqrt{a_i a_j}}{RT} \quad (11)$$

where $\Omega = \ln(\sqrt{2}-1)/\sqrt{2}$ for PR EoS, x is the molar fraction, A_∞^E is the excess Helmholtz energy at infinite pressure and k_{ij} is a binary interaction parameter. The excess Helmholtz energy at infinite pressure can be approximated by the excess Gibbs energy at zero pressure (Mollerup, 1986), and the latter can be expressed by the NRTL model (Renon and Prausnitz, 1968) as:

$$\frac{G^E}{RT} = \sum_i x_i \ln \frac{\sum_j G_{ji} \tau_{ji} x_j}{\sum_k G_{ki} x_k} \quad (12)$$

$$\tau_{ij} = U_{ij} / (RT) \quad (13)$$

$$G_{ij} = \exp(-\alpha_{ij} \tau_{ij}) \quad (14)$$

$$\alpha_{ij} = \alpha_{ji} \quad (15)$$

where U_{ij} and U_{ji} represent the interaction energy difference between i-j and j-j pair molecules and between j-i and i-i pair molecules, respectively; R is the universal constant of gases; T is the temperature; and α_{ji} is the non-randomness parameter.

Table 4 presents some properties of the components used in this work. 2-HEAF data was calculated by the Alvarez and Valderrama (2004) method.

Table 4. Critical properties.

Compound	MM	P_c (MPa)	T_c (K)	Z_c	ω
water	18.01	22.1	647.1	0.229	0.344
ethanol	46.07	6.1	513.9	0.240	0.644
2-HEAF	107.11	54.0	683.2	0.271	0.898

Table 5 shows the interaction independent-concentration parameters calculated from VLE data. The interaction parameters for ethanol-water were obtained from the ethanol + water binary system (Table 2). The other interactions were calculated from the ethanol + water + IL ternary system (Table 3). The calculated VLE for IL free system is shown in Figure 6.

Table 5. Estimated NRTL parameters.

i	j	k_{ij}	α_{ij}	U_{ij} (J mol ⁻¹)	U_{ji} (J mol ⁻¹)
ethanol	water	0.4858	0.20	2292.84	-1076.5
ethanol	2-HEAF	0.4125	0.39	$1.64 \cdot 10^4$	-5190.3
water	2-HEAF	0.6416	0.39	$1.57 \cdot 10^4$	-7819.4

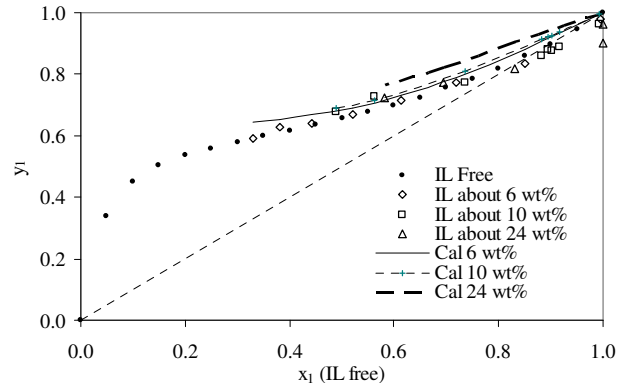


Figure 6. Experimental and calculated VLE for the ethanol (1) + water (2) + 2-HEAF (3) system.

The goodness of the fit was evaluated with the relative deviations in the temperature and ethanol concentration in the vapor phase for data point “i”, defined as:

$$\% \Delta T_i = 100(T_i^{\text{cal}} - T_i^{\text{exp}}) / T_i^{\text{exp}} \quad (16)$$

$$\% \Delta y_i = 100[(y_i^{\text{cal}} - y_i^{\text{exp}}) / y_i^{\text{exp}}]_i \quad (17)$$

Table 6 shows these relative deviations for temperature and ethanol concentration in vapor phase, as well as the predicted values of ionic liquid concentration in vapor phase (y_3^{cal}), for different IL concentrations. The global temperature mean relative deviation is 0.05% and the global ethanol concentration mean relative deviation is 5.3%; the global predicted mole fraction of ionic liquid in vapor phase was 0.0002. Then, the thermodynamic model was able to predict the low ionic liquid concentrations in the vapor phase; however, the ethanol concentration in vapor phase was not so successfully predicted.

Table 6. Mean relative deviations for temperature and ethanol concentration and the calculated ionic liquid concentration in vapor phase

IL wt %	% ΔT	% Δy_1	y_3^{cal}
6.3	0.07	3.7	0.0001
10.3	0.07	4.8	0.0002
24.1	0.03	7.3	0.0002
global	0.05	5.3	0.0002

6. CONCLUSIONS.

Isobaric VLE data for the ethanol-water systems containing the ionic liquid 2-HEAF were measured at atmospheric pressure (101.32 kPa). The results indicated that 2-HEAF did not show a salting-out effect; however, a new azeotropic phenomenon was observed: the azeotropic point was shifted towards a lower ethanol concentration. The experimental data were correlated with the Peng-Robinson equation of state, coupled with the Wong-Sandler/NRTL mixing rule. The model was able to correlate the temperature with a low deviation, as well as to predict the ionic liquid concentration in the vapor phase; however, the results for the ethanol concentration in vapor phase were not fully satisfactory.

7. ACKNOWLEDGEMENTS.

The authors are grateful to Dr. Artur Brandão (Federal University of Bahia) who measured the altitude, and to the meteorology service of the Salvador International Airport for temperature and barometric data. This work was supported by

Conselho Nacional de Desenvolvimento Científico e Tecnológico (CNPq) and Fundação de Amparo à Pesquisa do Estado de São Paulo (FAPESP).

8. REFERENCES

- ALVAREZ, V.H.; VALDERRAMA, J.O. A modified Lydersen-Joback-Reid method to estimate the critical properties of biomolecules. *Alimentaria*, 354, 55-66, 2004.
- BICAK, N. A new ionic liquid: 2-hydroxy ethylammonium formate. *J. Mol. Liq.*, 116, 15-18, 2005.
- GEORGE, J.; SASTRY, N.V. Densities, dynamic viscosities, speeds of sound, and relative permittivities for water + alkanediols (propane-1,2- and -1,3-diol and butane-1,2-, -1,3-, -1,4-, and -2,3-diol) at different temperatures. *J. Chem. Eng. Data*, 48, 1529-1539, 2003.
- HUANG, H.J.; RAMASWAMY, S.; TSCHIRNER, U.W.; RAMARAO, B.V. A review of separation technologies in current and future biorefineries. *Separ. Purif. Tech.*, 62, 1-21, 2008.
- IGLESIAS, M.; TORRES, A.; GONZALEZ-OLMOS, R.; SALVATIERRA, D. Effect of temperature on thermodynamics of a new ionic liquid: 2-hydroxy ethylammonium formate (2-HEAF) + short hydroxylic solvents. *J. Chem. Therm.*, 40, 119-133, 2008.
- IGLESIAS, M.; GARCIA-MUÑOZ, R.; GONZALEZ-OLMOS, R.; SALVATIERRA, D.; MATTEDEI, S. Synthesis of new short aliphatic chain ionic liquids and influence of temperature on thermodynamic properties. *J. Mol. Liq.*, submitted, 2008.
- KAPADI, U.R.; HUNDIWALE, D.G.; PATIL, N.B.; PATIL, P.R.; LANDE, M.K. Densities, excess molar volumes, viscosities of binary mixtures of ethanediol with water at various temperatures. *J. Ind. Chem. Soc.*, 77, 319-321, 2000.
- KOJIMA, K.; TOCHIGI, K.; SEKI, H.; WATASE, K. Determination of vapor-liquid

equilibrium from boiling point curve. *Kagaku Kogaku*, 32, 149–150, 1968.

LIGERO, E.L., RAVAGNANI, T.M. Dehydration of ethanol with salt extractive distillation – a comparative analysis between process with salt recovery. *Chem. Eng. Process*, 42, 543-552, 2003.

MARSH, K.N.; BOXALL, J.A.; LICHTENTHALER., R. Room temperature ionic liquids and their mixtures – a review. *Fluid Phase Equilib.*, 219, 93-98, 2004.

MOLLERUP, J. A note on the derivation of mixing rules from excess Gibbs energy models. *Fluid Phase Equilib.*, 25 , 323-327, 1986.

NIKAM, P.; JADHAV, M.C.; HASAN, M. Density and viscosity of mixtures of nitrobenzene with methanol, ethanol, propan-1-ol, propan-2-ol, butan-1-ol, 2-methylpropan-1-ol, and 2-methylpropan-2-ol at 298.15 and 303.15 K. *J. Chem. Eng. Data*, 40, 931-934, 1995.

OCÓN, J.; ESPANTOSO, J. Vapor-liquid equilibria III. Study of a new VLE ebulliometer. Methanol-carbon tetrachloride system. *An. Quim.*, 54B, 413-420, 1958.

ORGE, B.; IGLESIAS, M.; RODRIGUEZ, A.; CANOSA, J.M.; TOJO, J. Mixing properties of (methanol, ethanol, or 1-propanol) with (n-pentane, n-hexane, n-heptane and n-octane) at 298.15 K. *Fluid Phase Equilib.*, 133, 213-217, 1997.

PENG, D.Y.; D.B. ROBINSON, A new two-constant equation of state. *Ind. Eng. Chem. Fund.*, 15, 59-64, 1976.

RENON, H.; PRAUSNITZ, J.M. Local compositions in thermodynamics excess functions for liquid mixtures. *AIChE J.*, 14, 135-142, 1968.

RESA, J.M.; GONZÁLEZ, C.; GOENAGA, J.M.; IGLESIAS, M. Density, refractive index, speed of sound at 298.15 K and vapor-liquid equilibria at 101.3 kPa for binary mixtures of ethyl acetate + 1-pentanol and ethanol + 2-methyl-1-propanol. *J. Chem. Eng. Data*, 49, 804-808, 2004.

WONG, D.H.S.; SANDLER, S.I. A theoretically correct mixing rule for cubic equations of state. *AIChE J.*, 38, 671-680, 1992.

Artigo 4.16: Production of Anhydrous Ethanol by Extractive Distillation of Diluted Alcoholic Solutions with Ionic Liquids

Víctor H. Álvarez¹, Pedro Alijó², Diego Serrão², Rubens Maciel Filho¹, Martín Aznar¹ and Silvana Mattedi²

¹*School of Chemical Engineering, State University of Campinas (UNICAMP)*

P.O. Box 6066, 13083-970, Campinas-SP, Brazil

²*Chemical Engineering Department, Polytechnic School, Federal University of Bahia (UFBA), R. Aristides Novis 2, Federação, 40210-630 Salvador-BA, Brazil*

Abstract

In this work, the use of the ionic liquid 1-methyl-3-methylimidazolium dimethylphosphate or ethylene glycol as an separation agent was evaluated in a two-column or three-column configuration extractive distillation for the production of anhydrous ethanol (99.8% weight, 99.5% mol) from diluted solutions (11% weight). The extractive distillation process was simulated and optimized with the HYSYS® software. The vapor liquid equilibrium for the system was calculated by the NRTL thermodynamic model, whose interactions parameters were previously published. Experimental design was used in combination with modeling and simulation to determine the operational conditions that minimize reboiler duty. Simulation results showed that both separating agents present similar reboiler duty to produce high-purity ethanol.

Keywords: anhydrous ethanol, ionic liquids, extractive distillation, simulation.

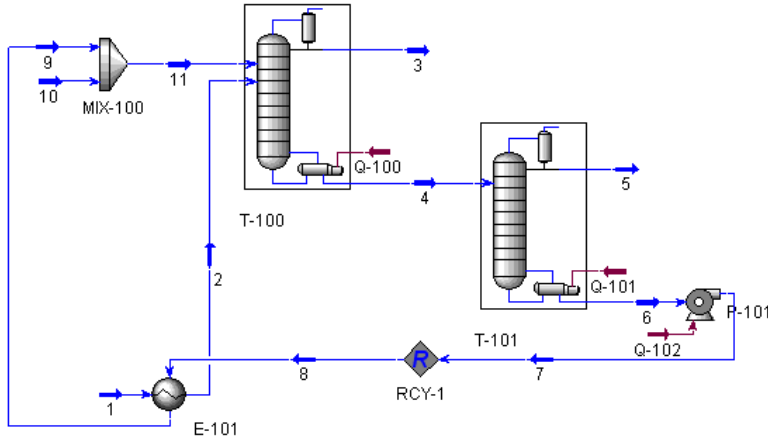
1. Introduction

The growing demand for anhydrous ethanol and the preservation of the environment need a safe, inexpensive and green process. Many industrial techniques have been proposed to separate of ethanol/water azeotropic mixture, such as crystallization, liquid-liquid extraction, adsorption and azeotropic or extractive distillation (Huang et al. 2008). We have focused our attention on the extractive distillation. Extractive distillation is a partial vaporization process, in the presence of a non-volatile and high boiling point compound, usually called solvent or separating agent, which is added to prevent the azeotrope formation (Perry et al., 1992). In most commercial extractive distillation process, there are three-column or two-column configurations to obtain pure ethanol from a dilute aqueous ethanol solution. The separating agent is fed in the upper part of the extractive column, above the feed stream (Pinto et al., 2000; Ligero and Ravagnani, 2003). In the three-column configuration, the concentrator and stripper are in different columns. In the two-column configuration, both columns could be joined together and the last column is used to recuperate the separation agent, recycling it to the extractive column. Usually, the separating agent is the benzene, but this compound is toxic and shows operating unstable control. Another solvent, as reported by Meirelles et al. (1992), is the ethylene glycol (EG). On other hand, ionic liquids have emerged as possible "green" solvents because they are not volatile and, therefore, do not have pollutant gas emissions. Ionic liquids are organic salts which are liquid at room temperature, with melting points below 373 K (Marsh et al., 2004). Zhao et al. (2006) reported vapor pressure data for the ionic liquids 1-methyl-3-methylimidazolium dimethylphosphate ([mmim][DMP]) in systems containing ethanol/water at several temperatures and compositions. The main objective of this work is to model and optimize the two-column and three-column configurations using EG or [mmim][DMP] in order to produce 99.8% weight ethanol from an 11% weight ethanol solution. The results are compared in terms of heat duties and impurities contained in the ethanol product stream.

2. Methodology

The flowsheet of the extractive distillation process for modeling and optimization can be seen in Figure 1. This figures show the recycle point for the simulation (RCY-1).

(a)



(b)

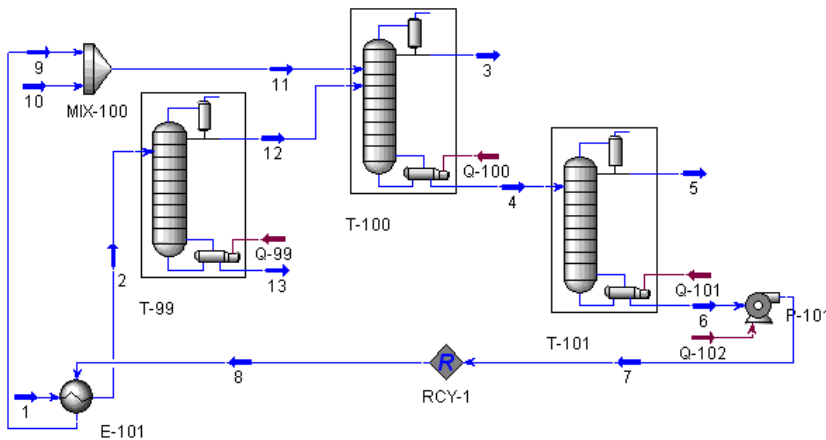


Figure 1. (a) Two-column configuration. (b) Three-column configuration.

2.1. Thermodynamic Model

The ionic liquid was created as a hypothetical component in the HYSYS® software using the liquid density from NIST (2008), pseudo critical properties calculated with the method of Valderrama and Robles (2007) and other properties estimated within HYSYS®. The activity coefficient was described using the NRTL (Renon and Prausnitz, 1968) thermodynamic model. The binary interaction parameters were taken from Zhao et al. (2006) for [mmim][DMP] systems, and from Meirelles et al. (1992) for EG systems. Table 1 displays these NRTL binary interaction parameters. Activity coefficient calculations for the mixture were validated with experimental data reported in previous works (Zhao et al., 2006; Meirelles et al., 1992) using HYSYS® simulator.

Table 1: NRTL binary interaction parameters.

Compound (1) + (2)	α_{12}	Δg_{12o} (J/mol)	Δg_{12t} (J/molK)	Δg_{21o} (J/mol)	Δg_{21t} (J/molK)
water + [mmim][DMP]	0.4116	5065.44	-	-9565.9	-
ethanol + [mmim][DMP]	0.5927	13172.16	-	-6426.83	-
water + EG	0.1859	1383.43	8.0409	-1445.97	-9.1506
ethanol + EG	0.3704	13527.42	-92.7391	-4351.97	53.3769
ethanol + water	0.3008	5612.08	-	-510.81	-

$$\Delta g_{12} = \Delta g_{12o} + T \Delta g_{12t}$$

2.2. Experimental design

In distillation process with new chemical components, the first step is to know the main operational variables. The second step is selecting the correct interval of work of these main operational variables and, finally their optimization. The software Statistica (Statsoft, v. 7.0) was used to analyze the results for all experimental design.

2.2.1. Finding the main operational variables

Experiments are very time-consuming when many factors have to be considered. In contrast, Plackett–Burman designs (Plackett and Burman, 1946) are very useful for picking up the most important factors from a long list of factors (operational variables) with the less number of experimental trials. In order to perform these steps, the EG separating agent was arbitrarily selected. There were considered as the most important variables those listed in Table 2. Then, the influences of these variables on separation agent loss (X) and energy consumption (Y) was investigated.

2.2.2. Selecting the correct interval of operational variables

In order to select the interval of operational variables, a sensibility analysis was performed, where the column theoretical stage, the separation agent molar flow, and the separation agent feed stage were analyzed. Also, several variables are maintained constants, such as the fermentation broth temperature feed (298 K), the operational pressure of concentrator and extractive column (101.3 kPa), the ethanol molar fraction in the concentrator or extractive column bottom (10^{-6}), the ethanol molar fraction in distillate extractive column (0.995), the water molar fraction in the recovery column bottom (10^{-6}), and the separation agent molar fraction in the distillate recovery column (10^{-6}). Then, the analyzed variables were varied up to obtain constant values of reboiler duty or ethanol molar fraction. The optimal stage for the stream feeds are into the coalescence between the rectification and stripping sections of the distillation column (Walas, 1990). Then, the feed stage was selected as the lowest reboiler duty was obtained for a column.

2.2.3. Optimization of the operational variables:

This step found the operational variables optimal value for the lowest energy consumption (Y). The operational variables selected by Plackett–Burman analysis with limits chosen by the sensibility analysis and the other factor used as constants are the input variables in this optimization. The optimization can be done by using either complex or gradient methods to solve the mathematical model or by direct variation of variables by the Taguchi method (Taguchi et al., 1990). In this work, the Taguchi method was used because give a fast and reliable solution. Once the interval values of relevant variables were selected, experiments were designed by the Taguchi method with energy consumption as response. The L₉ orthogonal array was selected in the Taguchi method to analyze the variables at different levels.

3. Results

Since the value range of the variables is unknown, a sensibility analysis was performed to estimate it. Thereby, (1) the reboiler duty is maintained constant over 40, 30 and 12 theoretical stages for the concentrator, extractive and recovery columns, respectively, (2) the separation agent molar flow should be over 3 kmol/h to obtain 0.998% w ethanol, (3) lower separation agent molar flow results in a lower reboiler duty, (4) in order to prevent contamination of the distillate, the separation agent feed stage should be 2 and 5 for [mmim][DMP] and EG, respectively, (5) the separating agent temperature feed can be equal to the boiling point of ethanol. In order to know the main operational variables in the process, each operational variable was tested at two levels, as shown in Table 2. The interval values used are in agreement with the previously sensibility analysis.

Table 2. Variables process using ethylene glycol.

N	Variable name	-1	+1
Two-column configuration			
1	Molar flow of separation agent (kmol/h)	3.00	9.00
2	Number of theoretical stages in extractive column	35.00	55.00
3	Separation agent feed stage	2.00	5.00
4	Pressure in recovery column (kPa)	20.26	101.3
5	Number of theoretical stages in recovery column	15.00	30.00
6	Separation agent temperature (K)	341.44	361.44
Three-column configuration			
1	Molar flow of separation agent (kmol/h)	3.00	9.00
2	Number of theoretical stages in concentrator column	25.00	50.00
3	Ethanol molar fraction in distillate of concentrator column	0.50	0.90
4	Number of theoretical stages in extractive column	25.00	45.00
5	Separation agent feed stage	2.00	5.00
6	Pressure in recovery column (kPa)	20.26	101.3
7	Number of theoretical stages in recovery column	15.00	30.00
8	Separation agent temperature (K)	341.44	361.44

The Plackett–Burman results are shown as Pareto charts of effects on separation agent lost in distilled (X) and energy consumption (Y) at 95% confidence level. The variables near to the statistical p-value equal 0.05 are significant. The results for the two-column configuration are shown in Figure 2. The energy consumption was mainly affected by the separation agent molar flow (N1), the separation agent feed stage (N3), and the pressure in recovery column (N4), while for solvent loss, the separation agent molar flow (N1), and the separation agent feed stage (N5) are the significant variables.

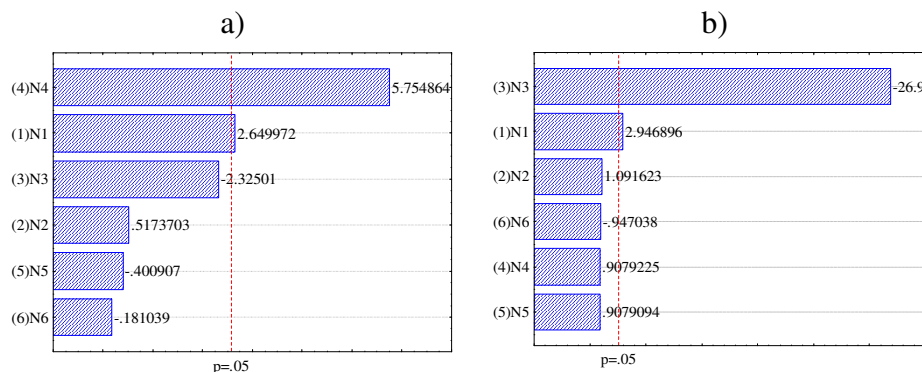


Figure 2. Pareto chart of variables effects at 95% of confidence level for two-column configuration. a) energy consumption, b) agent separation loss.

The results for the three-column configuration are shown in Figure 3. The energy consumption was mainly affected by the separation agent molar flow (N1), the number of theoretical stages in concentrator column (N2), the ethanol molar fraction in distillate concentrator column (N3), the separation agent feed stage (N5), and the separation agent temperature (N8), while for solvent loss, the separation agent molar flow (N1), the number of theoretical stages in concentrator column (N2) and the separation agent feed stage (N5) are the significant variables.

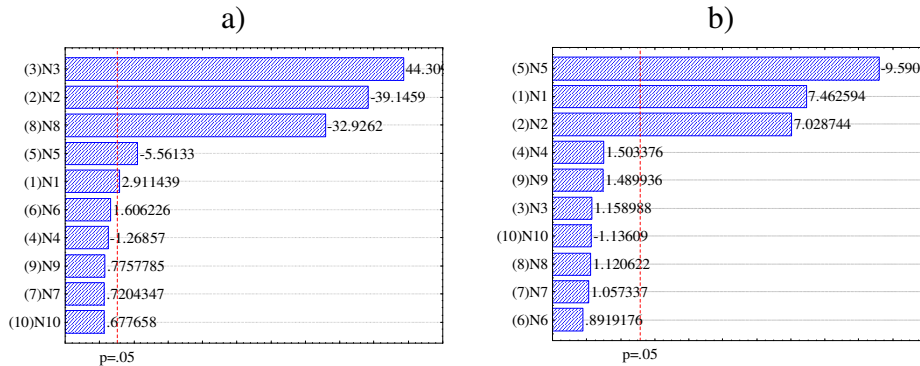


Figure 3. Pareto chart of variables effects at 95% of confidence level for three-column configuration. a) energy consumption, b) agent separation loss.

According the results, the two-column configuration does not need variable optimization, because all variables can be fixed using values from sensibility analysis. The pressure in recovery column and the separation agent molar flow should be the lowest in order to obtain the lowest reboiler duty, 20.26 kPa and 3 kmol/h, respectively. The optimal values for the two-column configuration are displayed in Table 3.

Table 3. Optimum conditions and performance for the two-column configuration.

Separation agent	N1	N2	N3	N4	N5	N6	Energy consumption (kJ/kg ethanol)	Separation agent loss (kmol/h)
[mmim][DMP]	3	40	2	20.26	12	351.44	25819.5	$9 \cdot 10^{-11}$
EG	3	40	5	20.26	18	351.44	25515.5	$1 \cdot 10^{-4}$

The Taguchi method was applied for the three-column configuration variables with significant effect. The factors not marked as statistically important by the Plackett–Burman analysis were fixed as constant (N4=35, N5=5, N6=20.26, N7=18 for EG and N4=35, N5=2, N6=20.26, N7=12 for [mmim][DMP]). Table 4 shows the factors and levels, while the optimal values for operational variables are displayed in Table 5.

Table 4. Factors and their levels for the three-columns configuration.

Level	N1	N2	N3	N8
1	3	25	0.7	341.44
2	6	40	0.8	351.44
3	9	55	0.9	361.44

Table 5. Optimal conditions and performance for the three-column configuration

Separation agent	N1	N2	N3	N8	Energy consumption (kJ/kg ethanol)	Separation agent loss (kmol/h)
[mmim][DMP]	3	55	0.8	361.44	6987.2	$1 \cdot 10^{-6}$
EG	3	55	0.8	361.44	6909.0	$3 \cdot 10^{-5}$

Table 5 shows simulation results with variables by Taguchi method that, for an efficient use of the energy, the concentrator column should produce an ethanol molar fraction equal to 0.8, a variable not well studied in dehydration ethanol works. The ionic liquid is the separating agent with less contamination of the distillated ethanol.

4. Conclusions

The energy consumption of dehydration of aqueous ethanol by an extractive distillation method was compared for two different configurations and two different separating agents. The calculated results showed that ethylene glycol is more contaminant than [mmim][DMP], but the energy consumption is similar. On the other hand, the three-column configuration process has lower energy consumption than the two-column configuration process.

Acknowledgements

The financial support by FAPESP is gratefully acknowledged. M. Aznar and R. Maciel Filho are recipients of a CNPq fellowship.

References

- H.J. Huang, S. Ramaswamy, U.W. Tschirner, B. Ramarao, 2008, *Separ. Purif. Tech*, 62, 1-21.
E. Ligero, T.M. Ravagnani, 2003, *Chem. Eng. and Process*, 42, 543-552.
A. Meirelles, S. Weiss, H. Herfurth, 1992, *J. Chem. Tech. Biotechnol.*, 53, 181-188.
K. Marsh, J.A. Boxall, R. Lichtenthaler, 2004, *Fluid Phase Equilib.*, 219, 93-98.
NIST, Ionic Liquids Database-ILThermo, <http://ilthermo.boulder.nist.gov/IL> (accessed on 2008).
R. Perry, D. Green, J. Maloney, 1997, *Perry's Chemical Engineer's Handbook*, 7th ed., McGraw-Hill, New York.
R. Plackett, J.P. Burman, 1946, *Biometrika*, 33, 305-25.
R. Pinto, M.R. Wolf Maciel, L. Lintomen, 2000, *Comput. Chem. Eng.*, 24, 1689-1694.
H. Renon, J.M. Prausnitz, 1968, *AIChE J.*, 14, 135-144.
G. Taguchi, E.A. Elsayed, T.C. Hsiang, 1990, *Engenharia da Qualidade em Sistemas de Produção*, McGraw-Hill, São Paulo.
J. Valderrama, P.A. Robles, 2007, *Ind. Eng. Chem. Res.*, 46, 1338-1344.
S. Walas, 1990, *Chemical Process Equipment*. Butterworth-Heinemann, Newton, MA.
J. Zhao, X.C. Jiang, C.X. Li, Z.H. Wang, 2006, *Fluid Phase Equilib.*, 247, 190-198.

Artigo 4.17: An Evaluation and Industrial Application of Ionic Liquid as Separation Agent for Separation of Diluted Ethanol-Water Mixtures



An evaluation and industrial application of ionic liquid as separation agent for separation of diluted ethanol-water mixtures

Víctor H. Álvarez A.^{1,2,*}, R. Maciel Filho², Martín Aznar² and Silvana Mattedi¹

¹Chemical Engineering Department, Polytechnic School, Federal University of Bahia

²School of Chemical Engineering, State University of Campinas, UNICAMP

Abstract

In this work, the use of the ionic liquid 1-methyl-3-methylimidazolium dimethylphosphate as an separation agent in an extractive distillation column for the production of anhydrous ethanol was evaluated, with a concentration over 99.7% weight. The extractive column distillation was simulated and optimized with the HYSYS® software platform. The vapor liquid equilibrium for the system was calculated by the UNIQUAC thermodynamic models, whose interactions parameters were previously published. Response surface analysis was used in combination with modelling and simulation to determine the operational conditions that minimize reboiler duty. Simulation results showed that it is possible to produce high-purity ethanol from diluted ethanol-water mixtures. Also, the distillation column specified for this separation can operate with a smaller number of plates and a smaller reflux ratio than a typical saline extractive distillation process. Finally, a comparative study using ionic liquid extractive distillation process and the saline extractive distillation was carried out.

Keywords: anhydrous ethanol distillation, ionic liquids, extractive distillation, simulation

Resumen

En este trabajo se usa líquido iónico dimetilfosfato de 1-metil-3-metilimidazolio como agente de separación en una columna de destilación extractiva para producir etanol deshidratado con una concentración mayor a 99.7% en masa. La columna de destilación extractiva fué simulada y optimizada con el paquete HYSYS®. El equilibrio líquido vapor para este sistema fue calculado con el modelo UNIQUAC, cuyos parámetros ya están publicados. El análisis de superficie de respuesta junto con el modelado y simulación fué utilizado para determinar las condiciones de operación que minimizan el consumo de la caldera. Los resultados de La simulación muestran la factibilidad de producir etanol de alta pureza desde mezclas diluidas de etanol en agua. Tambien, el nuevo diseño de la columna de destilación puede operar con un numero menor de platos y una menor razón de reflujo comparada con la típica columna de destilación salina. Finalmente, se realizo um estudio comparativo de la destilación extractiva utilizando el líquidos iónico y sal.

Palabras clave: destilación de etanol deshidratado, líquidos iónicos, destilación extractiva, simulación

1. INTRODUCTION

The growing demand for anhydrous ethanol and the preservation of the environment need a safe, inexpensive and green process. There are some industrial techniques used for the separation of ethanol/water azeotropic mixture, such as crystallization, liquid-liquid extraction, adsorption and azeotropic or extractive distillation^(1; 2).

Usually, for the anhydrous ethanol production by extractive distillation, the liquid agent for the separation is the benzene. This operation is energetically favorable, but it has poor health conditions and operating unstable control. Other liquid agents in the extractive distillation, such as furfural, pentane, diethyl ether, ethylene glycol and toluene, have been restricted by environmental legislation. Another variant of extractive distillation is the use of saline agents, where a non volatile salt is introduced into the upper distillation plate,

after step down between the plates and removed with the bottom products⁽³⁾.

Among these methods to obtain a pure ethanol, we have focused our attention on the extractive distillation process, because Pinto and co-workers⁽⁴⁾ related that saline distillation is the best option for anhydrous ethanol production, where the process required lesser energy consumption.

In most commercial extractive distillation process, there are three-column configuration and two-column configuration^(4, 3). In the three-column configuration, the concentrator and stripper are in different columns. Therefore, this configuration can be modified into a one column configuration by combining the concentrator and the stripper obtaining a two column configuration. The last column is used to recuperate the separation agent to use

again in the extractive column. Then, the extractive column in the process determined the successful of the separation.

For other hand, Ionic liquids have emerged as possible "green" solvents because they are not volatile and, therefore, do not have pollutant gas emissions. Ionic liquids are organic salts which are liquid at room temperature, with melting points below 373 K^(5; 6). These substances present a wide range of applications, as in catalytic reactions, separation of gases and liquids, electrolytic cells, heat transfer fluids and lubricants.

The work of Zhao⁽⁷⁾ reported vapor pressure data for nine binary systems containing ethanol/water plus ionic liquid at several temperatures and compositions, where the ionic liquids 1-methyl-3-methylimidazolium dimethylphosphate ([mmim][DMP]), 1-ethyl-3-methylimidazolium diethylphosphate ([emim][DEP]), and 1-butyl-3-methylimidazolium dibutylphosphate ([bmim][DMP]) were used. The authors claim that the equilibrium data can be correlated using the NRTL model⁽⁸⁾, and the binary parameters obtained can be applied to prediction of the vapor pressure of ethanol + water + ionic liquid with good agreement.

Therefore, the main objective of this work is to evaluate the use of ([mmim][DMP]) as an separation agent in an extractive column in order to produce 99.7% weight anhydrous ethanol from a solution with 24% weight ethanol.

2. METHODOLOGY

In this work, the extractive distillation column was simulated, with 1-methyl-3-methylimidazolium dimethylphosphate as separation agent. The flowsheet of the extractive distillation process was based on the work of Pinto⁽⁴⁾, and it can be seen in Figure 1.

2.1. Property package for HYSYS

The phase equilibrium of the water-ethanol-ionic liquid mixtures were described using UNIQUAC⁽⁹⁾ thermodynamic model. The binary interaction parameters of the ionic liquid were obtained from Kato and Gmehling⁽¹⁰⁾, while the ions of ethanol-water were from Hyprotech Internal Database. Table 1 displayed the binary interaction parameters for UNIQUAC model of these ternary systems. The simulations were performed with the HYSYS® software⁽¹¹⁾.

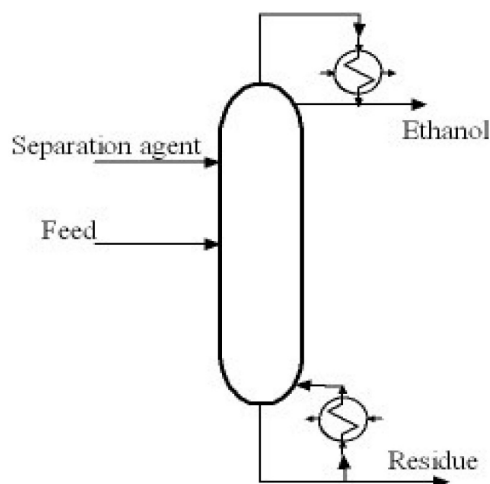


Figure 1. Extractive distillation flowsheet using salt as separation agent.

Table 1. Binary interaction parameters for UNIQUAC model

Compound (1) + (2)	UNIQUAC ^a (J/mol)	
	$\Delta\gamma_{21}$	$\Delta\gamma_{12}$
water + [mmim][DMP]	-2949.4	-3130.2
ethanol + [mmim][DMP]	-586.61	-2027.6
ethanol + water	970.75	212.91

^aTaken from reference (10)

The ionic liquid was create as hypothetical component in the HYSYS® software using the liquid density from NIST⁽¹²⁾, pseudo critical properties calculated with the method of Valderrama and Robles⁽¹³⁾ and the other properties estimated with HYSYS® software. Table 2 presents some properties for the pure compound of the ternary mixtures included in this work.

Table 2. Properties for the pure compound.

Compound	$\rho^{298\text{ K}}$ (g/cm ³)	T_b (K)	P_c (bar)	T_c (K)	V_c (cm ³ /mol)	ω
water	0.9947	373.2	221	647.1	55.95	0.344
ethanol	0.7859	351.4	61.4	513.9	168.0	0.644
[mmim][DMP]	1.253	623.0	28.6	880.4	598.4	0.506

2.2. Simulation data

Table 3 shows the simulation results obtained with the same parameters for the column used for Pinto⁽⁴⁾.

Table 3. Simulation results with the same input data of Pinto⁽⁴⁾ using [mmim][DMP] as separation agent

Parameter	Units	Value
Input data		
Feed flow rate	kmol/h	100
Temperature feed	K	298.15
Salt feed flow rate	kmol/h	1.5
Temperature salt feed	K	298.15
Feed ethanol composition	molar %	11
Feed water composition	molar %	89
Specified design and operating parameters		
Theoretical stage number	-	30
Operating pressure	atm.	1
Distillate flow rate	kmol/h	11
Reflux ratio	-	2.6
Feed stage number	-	20
Ionic liquid feed stage number	-	2
Simulation results for distillate and reboiler		
Ethanol flow rate	kmol/h	10.83
Water flow rate	kmol/h	0.17
Ethanol weight fraction	%	99.39
Water weight fraction	%	0.61
Reboiler duty	kJ/kg ethanol	4278.0

where, the ethanol weight fraction and reboiler duty are the more important simulation results. This simulation results show that, it was not feasible to produce ethanol with more than 99.7 weight%. Then, the operational variables would be optimized to carry out the desired concentration of ethanol.

2.3. Process optimization

The extractive distillation process may be optimized using response surface methodology, which is a procedure that does not require model simplifications and the explicit formulation of an objective function. The input variables considered for the optimization were the ones whose influence on the optimal operational conditions that minimize reboiler duty, with high ethanol concentration as constraint.

The work of Medrado⁽¹⁴⁾ explain that the feed stage number, reflux ratio, theoretical stage number, separation agent feed flow rate and separation agent feed stage number are determined are relevant variables for the extractive column. A factorial design 3^5 configuration was performed to determine two quadratic models with feed stage number (FSN), reflux ratio (RR), theoretical stage number (TSN), separation agent feed flow rate (EFR) and separation agent feed stage

number (ESN) as independent variables and ethanol weight fraction and reboiler duty as dependent variables. In the following simulations the other parameters were considered constants and equals for the values presents by Pinto⁽⁴⁾.

Where, each operational variables were tested at two levels, a high (+1) and a low (-1) level, as shown in Table 4. This Table shows the coded factor levels and the real values for the input variables. The interval values are in agreement with values used by Pinto⁽⁴⁾.

Table 4. Coded factor levels and real values for factorial design

Variables	Level (-1)	Central point(0)	Level (+1)
Feed stage number (FSN)	10	15	20
Reflux ratio (RR)	1.0	2	3
Theoretical stage number (TSN)	20	25	30
Separation agent feed flow (EFR)	1.5	3	5
Separation agent feed stage number (ESN)	1.0	3	5

The HYSYS® software was used to simulate the extractive distillation process. The software Statistica (Statsoft, v. 7.0) was used to analyze the results of the factorial experiment. The quadratic models obtained for %weight ethanol and reboiler duty as a function of the more significant variables at 95% were:

$$\text{Ethanol weight fraction } (\%) = 100.1919 - 0.4664 \text{ FSN} - 1.1003 \text{ FSN}^2 + 1.4595 \text{ RR} - 1.3491 \text{ RR}^2 + 0.8657 \text{ TSN} - 0.8808 \text{ TSN}^2 + 0.9295 \text{ EFR} - 0.3586 \text{ ESN} + 0.6540 \text{ (FSN)(RR)} + 1.3072 \text{ (FSN)(TSN)} + -0.4534 \text{ (RR)(TSN)} - 0.4946 \text{ (RR)(EFR)} \quad (1)$$

$$\text{Reboiler duty } (\text{kJ/kg ethanol}) = 3818.126 + 21.697 \text{ FSN} + 58.592 \text{ FSN}^2 + 787.227 \text{ RR} + 54.191 \text{ RR}^2 + -44.471 \text{ TSN} + 45.412 \text{ TSN}^2 + 39.696 \text{ EFR} - 29.359 \text{ (FSN)(RR)} - 67.849 \text{ (FSN)(TSN)} + 20.484 \text{ (FSN)(EFR)} \quad (2)$$

Both responses present a high correlation coefficient and the models can be considered statistically significant according to the F-test with 95% of confidence. The equations (1) and (2) were applied as a problem to minimize the reboiler duty with the constraint of ethanol weight fraction equal than 99.7 %. The variable optimization for these equations were performed using a genetic algorithm code, this code is implemented and fully explained in the work of Álvarez⁽¹⁵⁾.

3. RESULTS

The solution of equations 1 and 2 are the coded factor levels and the real values for the input variables are show in Table 5.

Table 5. Coded factor levels and real values for optimal distillation process

Variables	Code factor level	Variable value
Feed stage number (FSN)	-0.205	14.00
Reflux ratio (RR)	-0.988	1.01
Theoretical stage number (TSN)	0.543	27.71
Separation agent feed flow (EFR)	1.000	5.00
Separation agent feed stage number (ESN)	-1.000	1.00

Table 6. Input data, simulation results and parameters for a new column with [mmim][DMP]

Parameter	Units	Value
Input data		
Feed flow rate	kmol/h	100
Temperature feed	K	298.15
Ionic liquid feed flow rate	kmol/h	5
Temperature ionic liquid	K	298.15
Feed ethanol composition	molar %	11
Feed water composition	molar %	89
Specified design and operating parameters		
Theoretical stage number	-	30
Operating pressure	atm.	1
Distillate flow rate	kmol/h	11
Reflux ratio	-	2.6
Feed stage number	-	20
Ionic liquid feed stage number	-	2
Simulation results for distillate and reboiler		
Ethanol flow rate	kmol/h	10.998
Water flow rate	kmol/h	0.002
Ethanol weight fraction	%	99.99
Water weight fraction	%	0.01
Reboiler duty	kJ/kg ethanol	2974.8

The optimal parameters in Table 5 designed a new the extractive column distillation using [mmim][DMP] as separation agent. In this Table the feed stage number have been rounded to the closest integer. The input data and simulation results for the new extractive column are presented in Table 6.

The comparison of reboiler duties from Tables 6 and 7 with the feed temperature of 298 K show a difference less than 5.5%. This value shows a similar operational cost with both processes.

The results in Table 7 show that the desired separation was possible by a new distillation column with a lesser number of plates and lesser reflux molar ratio than the distillation column used by Pinto⁽⁴⁾.

Table 7. Input data, simulation results and parameters for the column using NaCl⁽⁴⁾.

Parameter	Units	Value
Input data		
Feed flow rate	kmol/h	100
Salt feed flow rate	kmol/h	1.5
Feed ethanol composition	molar %	11
Feed water composition	molar %	89
Specified design and operating parameters		
Theoretical stage number	-	30
Operating pressure	atm.	1
Distillate flow rate	kmol/h	11
Reflux ratio	-	2.6
Feed stage number	-	20
Ionic liquid feed stage number	-	2
Simulation results for distillate and reboiler		
Ethanol flow rate	kmol/h	10.998
Water flow rate	kmol/h	0.002
Ethanol weight fraction	%	99.99
Water weight fraction	%	0.01
Reboiler duty	kJ/kg ethanol	2974.8

4. CONCLUSIONS

The use of the ionic liquid 1-methyl-3-methylimidazolium dimethylphosphate as a separation agent in an extractive distillation process for the production of anhydrous ethanol over 99.7% weight from diluted mixtures of ethanol + water was studied. The simulation results show technical and economical advantages for the production of anhydrous ethanol using ionic liquid, since the distillation column for this process uses less stages and less reflux molar ratio compared with the classic saline extractive distillation. The UNIQUAC models were applicable to the correlation of the phase equilibria of ethanol + water + ionic liquid.

NOMENCLATURE

[mmim][DMP]	1-methyl-3-methylimidazolium dimethylphosphate
$\Delta g_{12}, \Delta g_{21}$	UNIQUAC parameters for interaction energy between molecules 1 and 2
ρ	density
T_b	normal boiling point
P_c	critical pressure
T_c	critical temperature
V_c	critical volume
ω	acentric factor

REFERENCES

- 1) Furter W.F., R.A. Cook, *Salt effect in distillation: a literature review*, Int. J. Heat Mass Transfer, 10 (1967) 23-36.
- 2) Huang H.J., S. Ramaswamy, U.W. Tschirner, B.V. Ramarao, *A review of separation technologies in current and future biorefineries*, Separ. Purif. Tech., 62 (2008) 1-21.
- 3) Ligero E.L., T.M. Ravagnani, *Dehydration of ethanol with salt extractive distillation – a comparative analysis between process with salt recovery*, Chem. Eng. and Process, 42 (2003) 543-552.
- 4) Pinto R.T., M.R. Wolf Maciel, L. Lintomen, *Saline extractive distillation process for ethanol purification*, Comput. Chem. Eng., 24 (2000) 1689-694.
- 5) Marsh K.N., J.A. Boxall, R. Lichtenthaler, *Room temperature ionic liquids and their mixtures – a review*, Fluid Phase Equilib., 219 (2004) 93-98.
- 6) Kato R., J. Gmehling, *Activity coefficients at infinite dilution of various solutes in the ionic liquids [MMIM]⁺[CH₃SO₄]⁻, [MMIM]⁺[CH₃OC₂H₄SO₄]⁻, [MMIM]⁺[(CH₃)₂PO₄]⁻ and [C₅H₅NC₂H₅]⁺[(CF₃SO₂)₂N]⁻, [C₅H₅NH]⁺ [C₂H₅OC₂H₄OSO₃]⁻*, Fluid Phase Equilib., 226 (2004) 37-44.
- 7) Zhao J., X.C. Jiang, C.X. Li, Z.H. Wang, *Vapor pressure measurement for binary and ternary systems containing a phosphoric ionic liquid*, Fluid Phase Equilib., 247 (2006) 190-198.
- 8) Renon H., J.M. Prausnitz, *Local compositions in thermodynamic excess functions for liquid mixtures*, AIChE J., 14 (1968) 135-144.
- 9) Abrams D.S., J.M. Prausnitz, *Statistical thermodynamics of liquid mixtures: a new expression for the excess Gibbs energy of partly or completely miscible systems*, AIChE J., 21 (1975) 116-128.
- 10) Kato R., J. Gmehling, *Measurement and correlation of vapor-liquid equilibria of binary systems containing the ionic liquids [EMIM]⁺[(CF₃SO₂)₂N]⁻, [BMIM]⁺[(CF₃SO₂)₂N]⁻, [MMIM]⁺[(CH₃)₂PO₄]⁻, and oxygenated organic compounds respectively water*, Fluid Phase Equilib., 231 (2005) 38-43.
- 11) Hyprotech, <http://www.hyprotech.com>, (2008).
- 12) NIST (National Institute of Standards and Technology), *Ionic Liquids Database-IL Thermo*, <http://ilthermo.boulder.nist.gov/IL> and *Thermo/ mainmenu.uix* (accessed on July 2008).
- 13) Valderrama J. O., P. A. Robles, *Critical properties, normal boiling temperatures, and acentric factors of fifty ionic liquids*, Ind. Eng. Chem. Res., 46 (2007) 1338-1344..
- 14) Medrado, C. D. B., V.H. Álvarez, M. Aznar, S. Mattedi, *Use of ionic liquid as entrainer for production of anhydrous ethanol by extractive distillation*. CHISA 2008, Prague – Czech Republic – 2008.
- 15) Álvarez, V.H., R. Larico, Y. Yano, M. Aznar, *Parameter estimation for VLE calculation by global minimization: genetic algorithm*, Braz. J. Chem. Eng., 25 (2008) 409-418.

Recibido: Agosto 28 del 2009

Aceptado: Octubre 25 del 2009

* Part of this work was presented at the I Congreso Nacional de Fenómenos de Transferencia, Chiclayo (2008).

* CORRESPONDING AUTHOR:

Álvarez (alvarez.a.v.h@gmail.com)

Mattedi (silvana@ufba.br)

R. Aristides Novis 2, Federação, 40210-630
Salvador-BA, Brazil

Aznar (maznar@feq.unicamp.br)

P.O. Box 6066, 13083-970, Campinas-SP, Brazil

4.3.2 Absorção de gases usando líquidos iônicos

ÁLVAREZ, V.H.; GÓMEZ-DÍAZ, D.; DÍAZ, D.; FIGUEIRAS, A.; MARTIN-PASTOR, M.; MATTEDI, S.; AZNAR, M.; IGLESIAS, M.; NAVAZA, J. M. CO₂ absorption into amine-based ionic liquids, *Brazilian Journal of Chemical Engineering.*, submetido, 2010.

Artigo 4.18: CO₂ absorption into amine-based ionic liquids

V.H. Álvarez^{2,2}, D. Gómez-Díaz², D. Díaz², A. Figueiras², M. Martín-Pastor³, S. Mattedi⁴, M. Aznar¹, M. Iglesias² and J.M. Navaza²

¹*School of Chemical Engineering, State University of Campinas, Campinas-SP, Brazil*

²*Chemical Engineering Department – ETSE, University of Santiago de Compostela, Santiago de Compostela, Spain*

³*Unidade de Resonancia Magnética, RIAIDT, edif. CACTUS. University of Santiago de Compostela, Santiago de Compostela, Spain*

⁴*Chemical Engineering Department, Polytechnic School, Federal University of Bahia, Salvador-BA, Brazil*

Abstract: This work determines the CO₂ absorption into two amine-based ionic liquids using a semi-continuous bubble column at 288.2 K, 298.2 K and 308.2 K. Chemical reactions between carbon dioxide and ionic liquids have been observed. The CO₂ absorption and desorption are reversible in the ionic liquids, so the absorbed CO₂ can be reversibly released and recovered as a carbon dioxide resource. The influence of gas flow-rate and temperature has also been analyzed. The results show the temperature of the system as the more important limitation in this process.

Keywords: ionic liquids, carbon dioxide, absorption, NMR spectra

INTRODUCTION

One of the most serious environmental problems is the greenhouse effect, due mainly to the presence of CO₂. Then, CO₂ capture is an important issue within commercial and environmental desirable process. The most used technique for the separation of a target compound from a mixture of gases in a gas stream is selective absorption into a liquid. Interactions between gases and pure liquids or solutions are the basis for numerous gas separation technologies, including commercial systems for the removal of CO₂ from natural gas. Several of these processes use a chemical reaction of the target gas with a solute in the liquid phase. In the case of large-scale CO₂ capture, aqueous amines are commonly used to chemically trap the CO₂ by forming ammonium carbamate (Bates et al., 2002). Although these aqueous alkanolamine solutions are industrially

Address correspondence to Víctor H. Álvarez, School of Chemical Engineering, State University of Campinas (UNICAMP), P.O. Box 6066, 13083-970, Campinas-SP, Brazil. Email: valvarez@feq.unicamp.br

effective for capturing CO₂, there are several serious drawbacks inherently connected to them: 1) the loss of the sequestering agent, a volatile amine, into the gas stream, 2) the uptake of water into the gas stream cause intensive energy consumption, cost increases, and corrosion problems. In order to solve these difficulties, is absolutely necessary to seek a new kind of sequestering agent, such as ionic liquids, which present characteristics such as a very low vapor pressure and thermal stability.

Ionic liquids are organic salts with melting point below 100 °C. Due to their unique properties, such as negligible vapor pressure, high thermal stability, nonflammability, design with tailored properties, and others (Bates et al., 2002; Rogers and Seddon, 2002), ionic liquids have been recognized as a versatile alternative to conventional organic solvents in reactions, separations, material engineering, and other fields.

The solubility and phase behavior of CO₂ in common ionic liquids, such as imidazolium-based (Cadena et al., 2004; Shiflett and Yokozeki, 2005; Blanchard et al., 2001; Carvalho et al., 2009ab), phosphonium-based (Zhang et al., 2005) and pyridinium-based (Blanchard et al., 2001) ones have been extensively studied experimentally. These works obtained absorption values of about 0.02 mol CO₂/mol ionic liquid (Scovazzo et al., 2004) showing only physical absorption of CO₂ at room temperature and atmospheric pressure. This value can be increased up to about 1.78 mol CO₂/mol ionic liquid (Carvalho et al., 2009c) through chemical absorption of CO₂.

Comparing the numerous studies on the solubility and phase equilibria of CO₂ in common ionic liquids, there is little research on the capturing of CO₂ from a gas stream. Bates et al. (2002) reported for the first time an effectively chemical capture of CO₂ by an ionic liquid with -NH₂ group, the 1-n-propylamine-3-butylimidazolium tetrafluoroborate. Unexpectedly, other works showed low equilibrium concentrations of CO₂; for example, Zhang et al. (2005) found 0.01 mol CO₂/mol 1,1,3,3-tetramethylguanidium lactate at room temperature and atmospheric pressure. Some works have proposed that ammonium-based ionic liquids should be more effective to capture CO₂ through chemical absorption (Yu et al., 2006), and, in addition, such ionic liquids are less toxic than imidazolium-based ones (Sierra et al., 2008). The solubility of CO₂ in ammonium-based ionic liquids was studied at high pressure conditions (Yuan et al., 2007).

In this work, an experimental investigation is carried out in order to evaluate the ability of two amine-based ionic liquids, 2-hydroxyethylammonium formate (2-HEAF) and N-methyl-2-hydroxyethylammonium formate (m-2-HEAF) for the absorption of CO₂. The ionic liquids were

synthesized from the correspondent amines and formic acid. The absorption studies were carried out in a semi-continuous gas-liquid column. The results show that these ionic liquids can be alternative sequestering agents for the recovery of CO₂ from a gas stream.

EXPERIMENTAL PROCEDURE

Materials

N-Methylethanolamine and ethanolamine were obtained from Aldrich (99% wt) and formic acid was obtained from Sigma (> 99.5% wt). These components were used as received. During the course of the experiments, the purity of solvents was monitored by density and the speed of sound measurements.

Synthesis of Ionic Liquids

N-Methylethanolamine or ethanolamine was placed in a three-necked flask made entirely of glass, equipped with a reflux condenser, a PT-100 temperature sensor for controlling temperature, and a dropping funnel. The flask was mounted in a thermostatic bath. The formic acid was slowly added to the flask with stirring with a magnetic bar. The reaction is a simple acid-base neutralization, producing an ester and a salt, and should be expressed as in Figure 1.

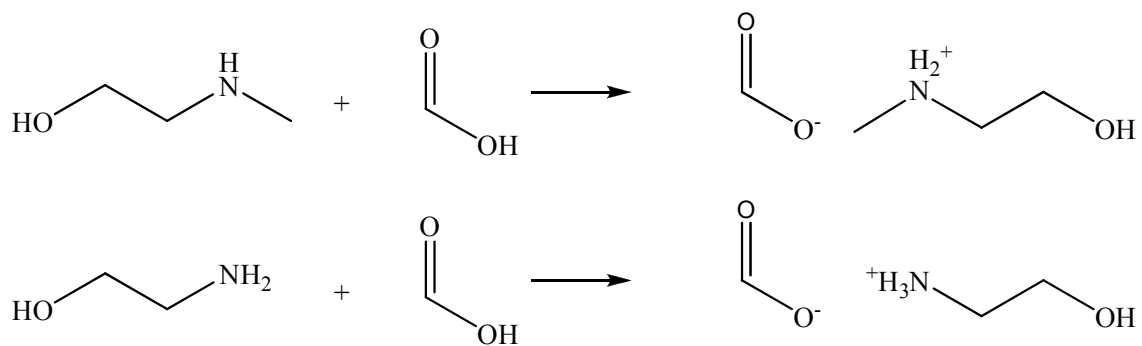


Figure 1. Ionic liquids produced by acid-base neutralization.

These reactions are highly exothermic, so an adequate control of temperature is essential throughout the reaction; otherwise heat generation may produce the dehydration of the salt to the corresponding amide, as in the case for nylon salts (salts of diamines with dicarboxylic acids).

The color varied in each case from transparent to dark yellow when the reaction process and purification (strong agitation and slight heating for the vaporization of residual acid for at least 48 h) were completed. In order to decrease the water content as much as possible, the ionic liquid was dried for 48 hours at ambient temperature and under vacuum of 20 kPa, with stirring, before each use.

FT-IR Spectroscopy

The FT-IR spectra were obtained with a Varian FT-IR 670 set at medium and high frequency spectrum ($7.900\text{-}20\text{ cm}^{-1}$), using the ATR method. The device has a resolution of 0.10 cm^{-1} and a relation signal-noise of 5 s. of 12.000:1 with 75% of light attenuation.

NMR spectroscopy

All the NMR analysis were performed at 298.2 K in an 11.7 T Varian Inova-750 spectrometer (operating at 750 MHz proton frequency). The spectra were processed with Mestre-C software (Cobas and Sardina, 2003).

Samples of 2-HEAF and m-2-HEAF were studied by NMR. Sample preparation required only the transfer to a 5 mm NMR tube. An external reference standard capillary was introduced coaxially in the tube containing deuterated 3-(trimethylsilyl)-propionic-D4 acid (TSP) 0.1 M in DMSO. The TSP signal at ≈ 0 ppm was used to determine absolute concentrations in the 1D proton spectrum and the DMSO was used for deuterium lock. The integral of the $^1\text{H-NMR}$ signal of TSP in the capillary was calibrated respect to a sample of 0.2 M of sucrose dissolved in D_2O prepared in a 5 mm NMR. The anomeric glucose proton appearing at ≈ 5.2 ppm was chosen for the calibration.

A 1D- ^1H NMR quantitative experiment was acquired with a 33° pulse and a conveniently long interscan relaxation time (d_1 10 s). These conditions were used to assure the exactness of the signal integration. NMR spectra 1D ^{13}C , 1D ^{15}N , were acquired using standard methodology.

Apparatus

The apparatus of absorption of CO_2 in these ionic liquids is showed in Figure 2, and consisted mainly of a jacketed glass vessel maintained at the desired temperature through circulating water. The water temperature was controlled by a thermostatic bath with a temperature accuracy of ± 0.1 K. A PT100 sensor (Senso term II, J.P. Selecta) with an uncertainty of ± 0.1 K was used to

determine the temperature of the system. CO_2 gas was bubbled through predetermined amounts of ionic liquids (95 ml) loaded in the glass vessel. There are valves in the inlet and outlet lines of gas. The inlet gas flow rate was measured with a Control Electronics 0154 device (Brooks Instruments) with an uncertainty of $\pm 0.01 \text{ ml CO}_2 \text{ min}^{-1}$ and the outlet gas flow rate was measured with an ADM 2000 device (Agilent) with an uncertainty of $\pm 0.1 \text{ ml CO}_2 \text{ min}^{-1}$. The absorption concentration of CO_2 in ionic liquids versus time was determined at 288.2 K, 298.2 and 308.2 K at ambient pressure ($\approx 100 \text{ kPa}$), and at two flow rates (149 and 199 ml min^{-1}). This apparatus was used in previous works (Gonzalez-Olmos and Iglesias, 2009) with the operational procedure adapted using the work of Vasques et al. (1997).

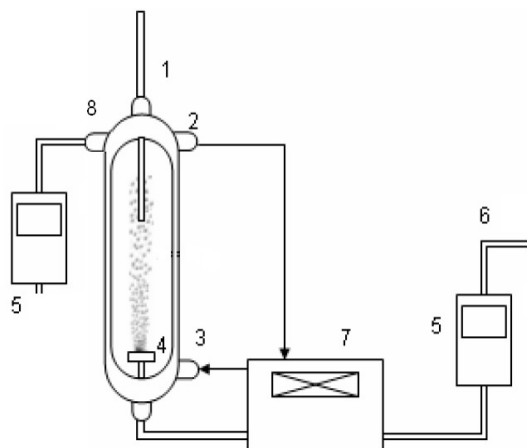


Figure 2. Absorption column: (1) PT100 sensor; (2) thermostatic water outlet; (3). thermostatic water inlet; (4) fritted glass; (5) gas flowmeters; 6) (CO_2 inlet; (7) thermostatic bath; (8) CO_2 outlet.

RESULTS AND DISCUSSION

Synthesis and Characterization

The two hydroxyl ammonium ionic liquids were synthesized and characterized. The results of the FT-IR analyses were very similar for both ionic liquids. The spectra showed a broad band in the 3500-2400 cm^{-1} range, which is characteristic of the ammonium structure. The OH stretching vibration is embedded in this band. The FT-IR spectrum for the m-2-HEAF is shown in Figure 3. NMR provided further insight in the chemical composition of the ionic liquids. The chemical composition was determined by combination of 1D 1H, 1D 13C, 1D 15N, 2D-TOCSY, and 2D-HMBC. The 2D experiments provided H-H or H-C through-bond correlations that assisted the

NMR signal assignment and confirmed the structure synthesized. The 1D proton NMR spectrum of 2-hydroxyethylammonium formate is in good agreement with that reported by Bicak (2005). For instance, in Figure 4 is shown the 2D TOCSY spectrum of m-2-HEAF.

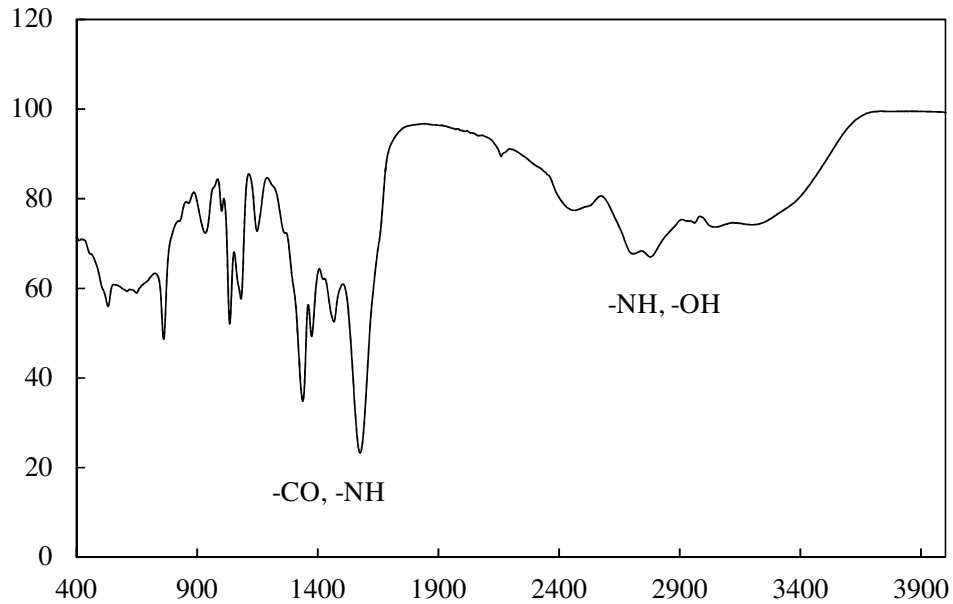


Figure 3. FT-IR spectrum for m-2-HEAF.

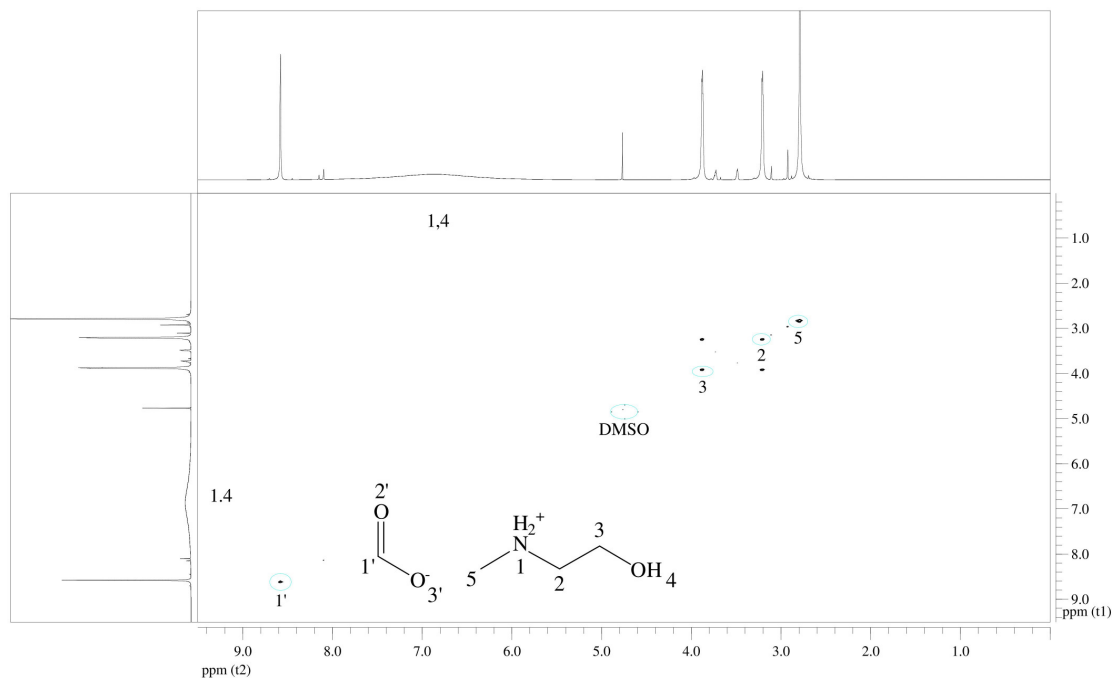


Figure 4. TOCSY spectrum for the m-2-HEAF. The vertical and horizontal traces shown correspond to the 1D proton spectrum.

Physical properties of the synthesized ionic liquids are presented in Table 1. The density and sound velocity are in good agreement with those reported by Bicak (2005) and Alvarez et al. (2010). From Table 1, it can be seen that the density and viscosity for the m-2-HEAF are lower, which makes it potentially applicable for industrial use.

Table 1. Pure component properties at 298.15 K.

Property	2-HEAF		m-2-HEAF	
	Lit.	Exp.	Lit.	Exp.
$\rho \text{ g cm}^{-3}$	1.204 ^(a)	1.20341	1.12825 ^(c)	1.12842
$u \text{ m s}^{-1}$	1798.54 ^(b)	1799.46	1815.30 ^(c)	1815.78
$\eta \text{ mPa s}$	105.00 ^(a)	119.25	20.27 ^(c)	21.45

^(a)Bicak (2005), ^(b)Cota et al. (2007), ^(c)Alvarez et al. (2010)

Absorption of CO₂ in Ionic Liquids

Each experiment was done on triplicate with a standard deviation of $\pm 1.5 \text{ ml min}^{-1}$ of the CO₂ flow rate. The flow rate has noise data, so a polynomial fit was applied to the data and the mean results are presented in Figures 5 to 7. The equilibrium absorption was not reached and after several hours the experiment was finished. For example, with four hours of absorption at 149 ml CO₂ min⁻¹ and 308.2 K, the CO₂ absorbed for one mol of 2-HEAF or m-2-HEAF were ≈ 0.04 moles and ≈ 0.06 moles, respectively. The absorption rate of CO₂ in both synthesized ionic liquids can be seen in Figures 6 to 7. Also, the CO₂ absorbed during 7200 s are shown in Table 2. Figures 6 to 7 and Table 2 show that the absorption rate of CO₂ in both ionic liquids decrease sharply when the flow rate of CO₂ and temperature decreases. For example, in Figure 5 at 5000 s and 149 ml CO₂ min⁻¹, the quantity of CO₂ absorbed in m-2-HEAF at 308.2 K is greater than at 298.2 K. Besides, experimental viscosity of pure ionic liquids increases as temperature decreases (Shiflett and Yokozeki, 2005). Also, from Figures 5 to 7, it can be seen that the effect of cation on the solubilities of CO₂ follow the sequence the N-methyl-2-hydroxyethylammonium > 2-hydroxyethylammonium. In addition, the viscosity of the 2-hydroxyethylammonium formate is greater than that of N-methyl-2-hydroxyethylammonium formate.

Table 2. CO₂ absorbed into the ionic liquids during 7200 s.

T (K)	Flow rate input ml CO ₂ ·min ⁻¹	2-HEAF		m-2-HEAF	
		mol CO ₂ ·(l IL) ⁻¹	mol CO ₂ ·(mol IL) ⁻¹	mol CO ₂ ·(l IL) ⁻¹	mol CO ₂ ·(mol IL) ⁻¹
308.15	149	0.283	0.026	0.397	0.043
298.15	149	0.216	0.019	0.355	0.038
288.15	149	0.156	0.009	0.276	0.029
298.15	149, x _{water} =0.1	0.257	0.021	0.325	0.032
308.15	199	0.300	0.028	0.361	0.039
298.15	199	0.263	0.023	0.344	0.037
288.15	199	0.301	0.027	0.323	0.034

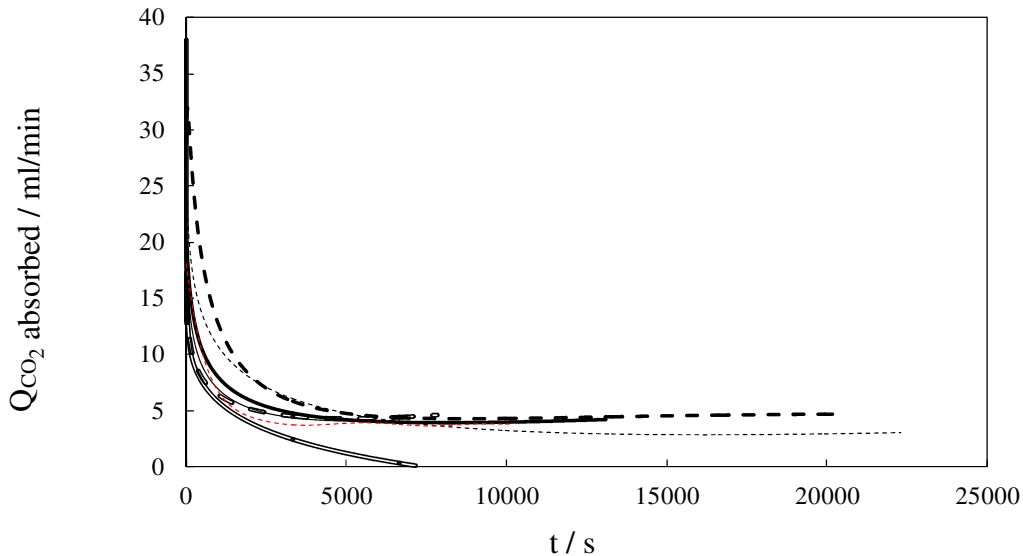


Figure 5. CO₂ absorbed into ionic liquid against the absorption time with CO₂ flow rate of 149 ml/min, at (—) 308.2 K, (—) 298.2 K, (==) 288.2 K for 2-HEAF and (----) 308.2 K, (--) 298.2 K, (==) 288.2 K for m-2-HEAF. The red symbols are a mixture of 2-HEAF with 0.1 molar fraction of water at 298.2 K.

The effect of the water into these systems was also studied, as can be seen in Figure 5 and Table 2. This data shows that 0.1 molar fraction of water decrease slowly the CO₂ absorbed, but a whole range of dissolution should be studied to fully understand these behaviors. Table 2 shows the CO₂ absorbed is greater than other ILs used in the open literature (Scovazzo et al., 2004; Carvalho et al., 2009c; Zhang et al., 2005), so far with the addition of water into these ILs.

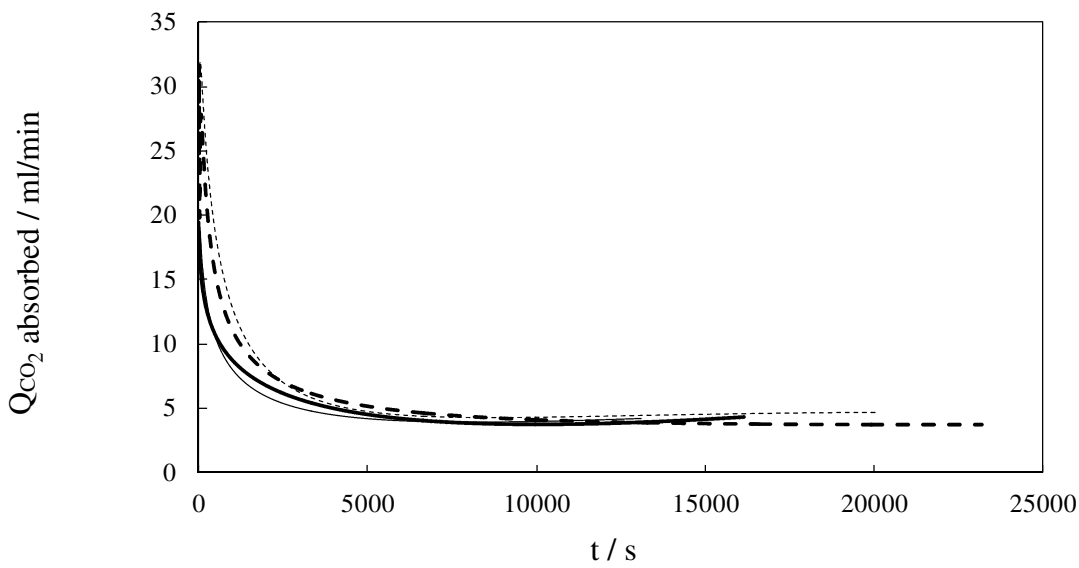


Figure 6. CO_2 absorbed into ionic liquid against the absorption time at 308.2 K. The CO_2 flow rates were: (—) 199 $\text{ml}\cdot\text{min}^{-1}$ and (—) 149 $\text{ml}\cdot\text{min}^{-1}$ for 2-HEAF and (— —) 199 $\text{ml}\cdot\text{min}^{-1}$ and (--) 149 $\text{ml}\cdot\text{min}^{-1}$ for m-2-HEAF.

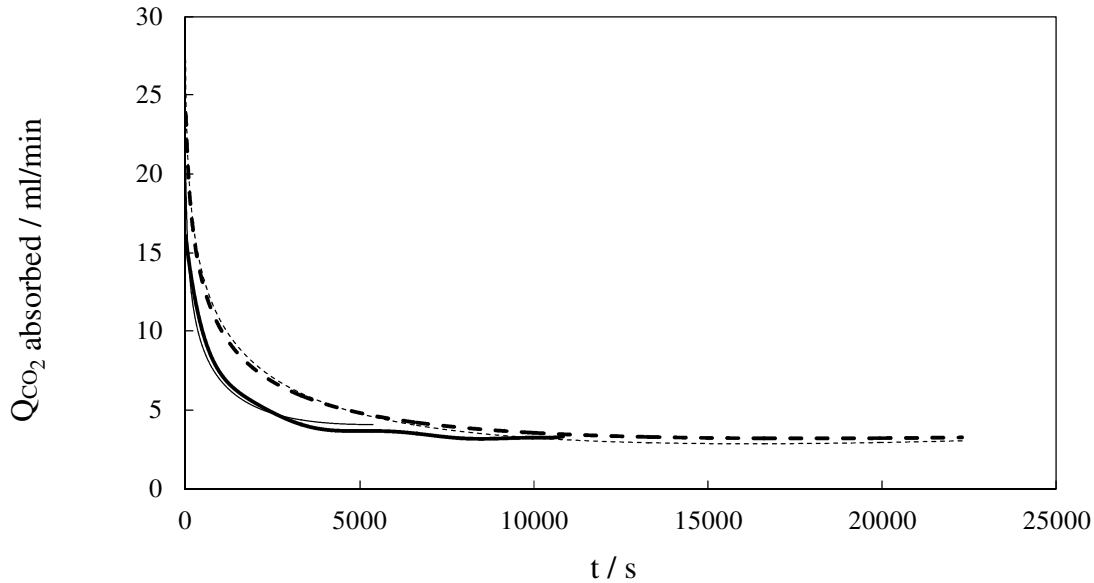


Figure 7. CO_2 absorbed into ionic liquid against the absorption time at 298.2 K. The CO_2 flow rates were (—) 199 $\text{ml}\cdot\text{min}^{-1}$ and (—) 149 $\text{ml}\cdot\text{min}^{-1}$ for 2-HEAF and (— —) 199 $\text{ml}\cdot\text{min}^{-1}$ and (--) 149 $\text{ml}\cdot\text{min}^{-1}$ for m-2-HEAF.

The absorption and desorption cycles were conducted to study the recovery of CO_2 and recycle for the IL with high absorption, the m-2-HEAF. The mixtures were slowly heated with a 3 K increase per 30 min with stirring at 20 kPa until constant weight. These recycling experiments were repeated for three times at 298.2 K during 5000 s for the m-2-HEAF. The results are shown

in Figure 8, which shows a very little decrease of the absorption ability of CO₂, as ≈98 %, ≈94 %, and ≈89 %, respectively.

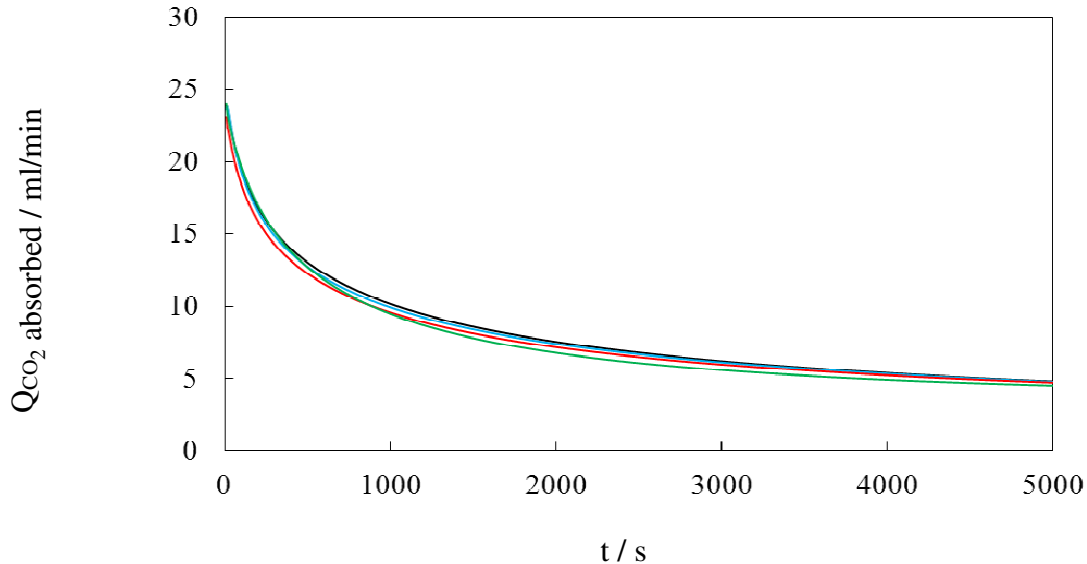


Figure 8. CO₂ absorbed into m-2-HEAF against the absorption time at 298.2 K and CO₂ flow rate of 199 ml·min⁻¹: (—) original, (—) first time recycled, (—) second time recycled, and (—) third time recycled.

The procedure to determine the volumetric mass transfer coefficient is based on the measurement of the amount of gas absorbed per time unit and volume unit according to the following equation (Vázquez et al., 1997):

$$\frac{dC}{dt} = k_L a(C^* - C) \quad (1)$$

where C^* is the interfacial concentration of gas compound in the liquid phase at equilibrium (i.e. the solubility of the gas in the liquid phase) and C is the concentration of carbon dioxide in the bulk liquid, that is calculated from the experimental absorption rate data. This gives:

$$\ln\left(\frac{C^*}{C^* - C}\right) = k_L at \quad (2)$$

Then, k_{La} could be calculated from values of concentration as time function. The values for the interfacial concentration of gas compound in the liquid phase at equilibrium was approximated by the concentration of CO₂ into the ionic liquid after several hours, when the absorption of the CO₂ was negligible (see Figures 5 to 7).

The CO₂ concentration in the bulk of the ionic liquid increases with time until the liquid phase is saturated. The experimental results show that for the ionic liquid, an increase of the viscosity (decrease of the temperature) produces an increase of the volumetric mass transfer coefficient (Table 3). Probably, this behavior was achieved by exothermic nature of this kind of absorption (Mattedi et al., 2010). Finally, the temperature is more influent in the absorption than the viscosity.

Table 3. Volumetric mass transfer coefficient as function of viscosity

Flow rate input mL CO ₂ min ⁻¹	2-HEAF			m-2-HEAF	
	T / K	η / mPa·s ^a	$10^4 \times k_{La} \cdot s^{-1}$	η / mPa·s ^b	$10^4 \times k_{La} \cdot s^{-1}$
149	288.2	41.8	4.816	34.20	2.282
	298.2	32.7	3.845	20.27	1.014
	308.2	21.6	1.557	13.73	0.955
199	288.2	41.8	2.182	34.20	2.170
	298.2	32.7	1.933	20.27	1.003
	308.2	21.6	1.182	13.73	0.878

^aIglesias et al. (2009); ^bAlvarez et al. (2010)

Evidence of Chemical Absorption

FTIR spectra of CO₂-absorbed ionic liquids were compared with pure ionic liquids. The results of the FT-IR analyses were very similar for both cases: the spectrum of the CO₂ treated material manifests a new absorption at 1668 cm⁻¹, consistent with a carbamate C=O stretch.

The NMR results in Figure 9 shows the 1D proton spectrum of CO₂ into 2-HEAF. The small peaks observed in this spectrum correspond to protons of the neutral species produced by the chemical absorption of CO₂. For each ionic liquid studied, the ratio cation:anion obtained from the quantitative analysis of the non-exchangeable signals in the ¹D proton spectra is ca. 1 ± 0.07, which is in agreement with the expected for each ionic liquid. Another observation in the Figure 9 is the peak of two broad signals of NH₃⁺ and NH centered at ≈6.4 ppm and ≈4.6 ppm, respectively. The number of protons determined for the NH₃⁺ labile protons are apparent values,

since the signal is affected by fast exchange with other labile protons, in particular with H₂O traces due to sample inherent hygroscopicity and possibly with OH-4, OH-4' protons.

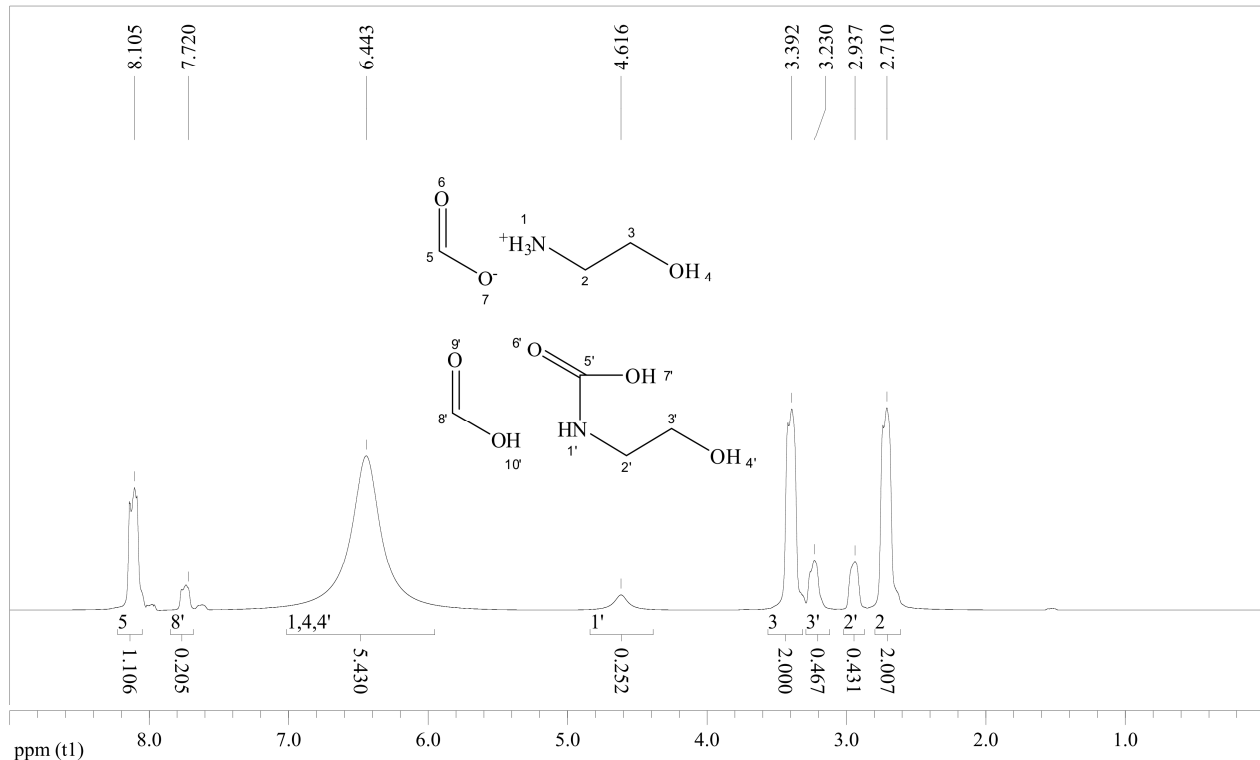


Figure 9. 1D proton spectrum for 2-HEAF and neutral species after the reaction with CO₂.

Figure 10 shows the ¹³C NMR spectrum of the CO₂ into 2-HEAF. It shows the ionic liquid ammonium carbamate formation. This new resonance is observed at δ 166.20 ppm, attributed to a carbamate carbonyl carbon. Also new are the peaks at 62.31 ppm and 42.78 ppm, consistent with a methylene carbon into the new neutral species. The other features of the spectrum generally consist of peaks near those of the starting pure ionic liquid. These previous evidence of new species can be explained with the reversible reactions of 2-HEAF with CO₂ expressed in Figure 11.

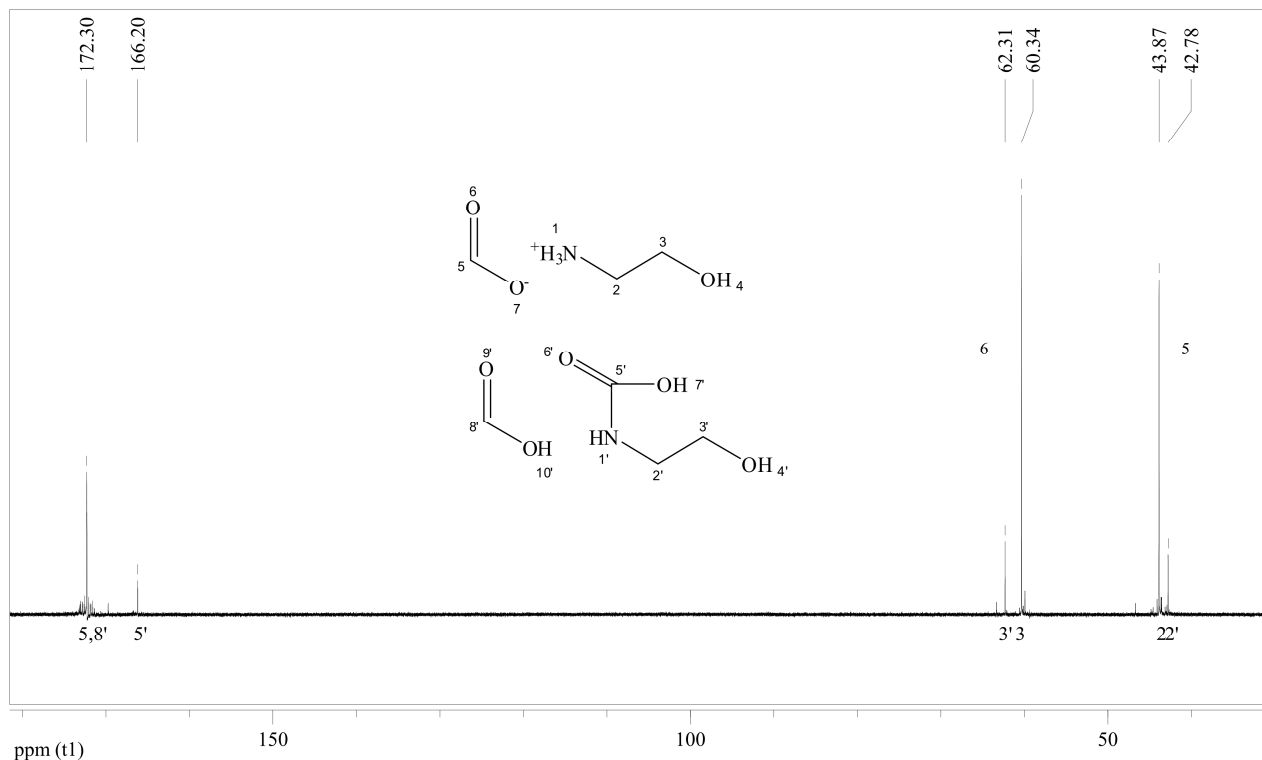


Figure 10. 1D ^{13}C spectrum for 2-HEAF and neutral species after the reaction with CO_2 .

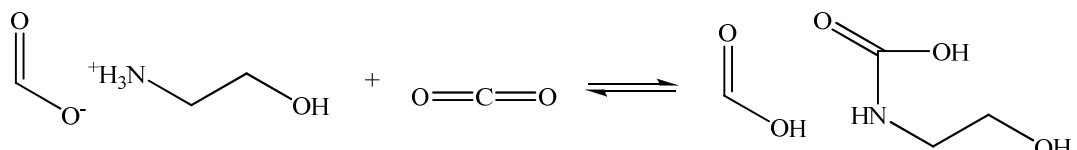


Figure 11. Proposed reaction between 2-HEAF and CO_2 .

CONCLUSIONS

Two hydroxylammonium ionic liquids were synthesized with the formate anion. The CO_2 molecule attacks the group of -NH in the cation of the ionic liquids more easily, and the increase of the absorption was influenced for the high flow of CO_2 . After three recycle times using vacuum and heat, the recycled ionic liquids show stable capability in the absorption of CO_2 . Besides, m-2-HEAF shows potential as alternative sequestering agent for the recovery of CO_2 in industrial process and an appealing subject of research.

ACKNOWLEDGMENTS

V.H. Álvarez acknowledges the Mobilidade Internacional Santander scholarship and the financial support from FAPESP (Fundação de Amparo à Pesquisa do Estado de São Paulo), process # 2006/03711-1. S. Mattedi thanks the financial support for her postdoctoral leave from CNPq (Brazil). Both also thank the support of the PF&PT research team (USC) during their stay in Santiago de Compostela. M. Iglesias thanks the support of the Dirección Xeral de Investigación, Desenvolvimento e Innovación, Conselleria de Innovación e Industria (Xunta de Galicia, Spain). M. Aznar is the recipient of a CNPq (Brazil) fellowship.

REFERENCES

- Álvarez, V. H., Dosil, N., Gonzalez-Cabaleiro, R., Mattedi, S., Martin-Pastor, M., Iglesias, M., Navaza, J. M. Brønsted ionic liquids for sustainable processes: Synthesis and physical properties, *J. Chem. Eng. Data*, 55, 625 (2010).
- Bates, E. D., Mayton, R. D., Ntai, I.; Davis, Jr. J. H. CO₂ capture by a task-specific ionic liquid, *J. Am. Chem. Soc.*, 124, 926 (2002).
- Bicak, N. A new ionic liquid: 2-hydroxy ethylammonium formate, *J. Mol. Liq.*, 116, 15 (2005).
- Blanchard, L. A., Gu, Z. Y., Brennecke, J. F. High-pressure phase behavior of ionic liquid/CO₂ systems, *J. Phys. Chem. B*, 105, 2437 (2001).
- Cadena, C., Anthony, J. L., Shah, J. K., Morrow, T. I., Brennecke, J. F., Maginn, E. J. Why is CO₂ so soluble in imidazolium-based ionic liquids? *J. Am. Chem. Soc.*, 126, 5300 (2004).
- Carvalho, P. J., Álvarez, V. H., Machado, J. J. B., Pauly, J., Daridon, J., Marrucho, I. M., Aznar, M., Coutinho, J. A. P. High pressure phase behavior of carbon dioxide in 1-alkyl-3-methylimidazolium bis(trifluoromethylsulfonyl)imide ionic liquids, *J. Supercrit. Fluids*, 48, 99 (2009a).
- Carvalho, P. J., Álvarez, V. H., Marrucho, I. M., Aznar, M., Coutinho, J. A. P. High pressure phase behavior of carbon dioxide in 1-butyl-3-methylimidazolium bis(trifluoromethylsulfonyl)imide and 1-butyl-3-methylimidazolium dicyanamide ionic liquid, *J. Supercrit. Fluids*, 50, 105 (2009b).
- Carvalho, P. J., Álvarez, V. H., Schröder, B., Gil, A. M., Marrucho, I. M., Aznar, M., Santos, L. M. N. B. F., Coutinho, J. A. P. Specific solvation interactions of CO₂ on acetate and trifluoroacetate imidazolium based ionic liquids at high pressures, *J. Phys. Chem. B*, 113, 6803 (2009c).
- Cobas, J. C., Sardina, F. J. Nuclear magnetic resonance data processing: MestRe-C, a software package for desktop computers, *Concepts Magn. Reson.*, 19, 80 (2003).

- Cota, I., Gonzalez-Olmos, R., Iglesias, M., Medina, F. New short aliphatic chain ionic liquids: synthesis, physical properties, and catalytic activity in aldol condensations, *J. Phys. Chem. B*, 111, 12468 (2007).
- Gonzalez-Olmos, R., Iglesias, M. Thermodynamics of water-air transfer of fuel oxygenates by the dynamic method of batch air stripping: experimental study of temperature and cosolvency effects, *Sep. Sci. Tech.*, 44, 3615 (2009).
- Iglesias M., Oliveira E.N., Ferreira C.M., Guerra I.R., Serra J.S., Mattedi S. Viscosities of protic ionic liquids: 2-hydroxy ethylammonium formate, 2-hydroxy ethylammonium acetate and 2-hydroxy diethylammonium acetate, 24th ESAT, European symposium on applied thermodynamics, Santiago de Compostela, Spain, june. (2009).
- Mattedi, S., Carvalho, P. J., Coutinho, J. A.P., Álvarez, V.H., Iglesias, M. Vapor-liquid equilibria of a Brønsted ionic liquid and CO₂, II Iberoamerican Conference on Supercritical Fluids, PROSCIBA 2010, Natal, Brazil, april (2010).
- Rogers, R. D., Seddon, K. R. Eds. Ionic Liquids: Industrial Applications to Green Chemistry, Oxford University Press: Washington, D.C. (2002).
- Scovazzo, P., Camper, D., Kieft, J., Poschusta, J., Koval, C., Noble, R. Regular solution theory and CO₂ gas solubility in room-temperature ionic liquids, *Ind. Eng. Chem. Res.*, 43, 6855 (2004).
- Shiflett, M. B., Yokozeki, A. Solubilities and diffusivities of carbon dioxide in ionic liquids: [bmim][PF₆] and [bmim][BF₄]. *Ind. Eng. Chem. Res.*, 44, 4453 (2005).
- Sierra, J., Martí, E., Mengíbar, A., González-Olmos, R., Iglesias, M., Cruañas, R., Garau, M.A. Effect of new ammonium based ionic liquids on soil microbial activity, 5^o Society of Environmental Toxicology and Chemistry Congress, Sydney. (2008).
- Vázquez, G., Cancela, MA, Varela, R., Alvarez, E., Navaza, JM. Influence of surfactants on absorption of CO₂ in a stirred tank with and without bubbling, *Chem. Eng. J.* 67, 131 (1997).
- Yu, G., Zhang, S., Yao, X., Zhang, J., Dong, K., Dai, W., Mori, R. Design of task-specific ionic liquids for capturing CO₂: a molecular orbital study, *Ind. Eng. Chem. Res.*, 45, 2875 (2006).
- Yuan, X., Zhang, S., Liua, J., Lu, X. Solubilities of CO₂ in hydroxyl ammonium ionic liquids at elevated pressures, *Fluid Phase Equilib.*, 257, 195 (2007).
- Zhang, S. J., Chen, Y. H., Ren, R. X. F., Zhang, Y. Q., Zhang, J. M., Zhang, X. P. Solubility of CO₂ in sulfonate ionic liquids at high pressure, *J. Chem. Eng. Data*, 50, 230 (2005).
- Zhang, S., Yuan, X., Chen, Yu., Zhang, X. Solubilities of CO₂ in 1-butyl-3-methylimidazolium hexafluorophosphate and 1,1,3,3-tetramethylguanidium lactate at elevated pressures, *J. Chem. Eng. Data*, 50, 1582 (2005).

4.3.3 Dessulfurização do petróleo

O ELL obtido no capítulo anterior permitiu observar a capacidade dos líquidos iônicos sintetizados para a remoção do DBT contido no óleo diesel modelo. Assim, foram feitos testes com o m-2-HEAA obtendo uma baixa remoção. Sendo que a única diferença entre os m-2-HEAA e m-2-HEAB foram dois carbonos na cadeia do ânion. Poderia-se considerar que a adição de carbonos na cadeia alquilica do ânion permitiria uma maior remoção do DBT. Isso foi verificado com o ELL para o sistema ternário m-2-HEAH + DBT + n-dodecano, Os resultados do ELL são comparados com dados dos líquidos iônicos $[\text{emim}]^+[\text{EtSO}_4]^-$ e $[\text{emim}]^+[\text{DEtPO}_4]^-$, obtidos de Oliveira (2009). Estes resultados são apresentados, a saber, com a distribuição do DBT nas fases, na Figura 4.10, a seletividade no líquido iônico na Figura 4.11 e a remoção de DBT obtida na Figura 4.12.

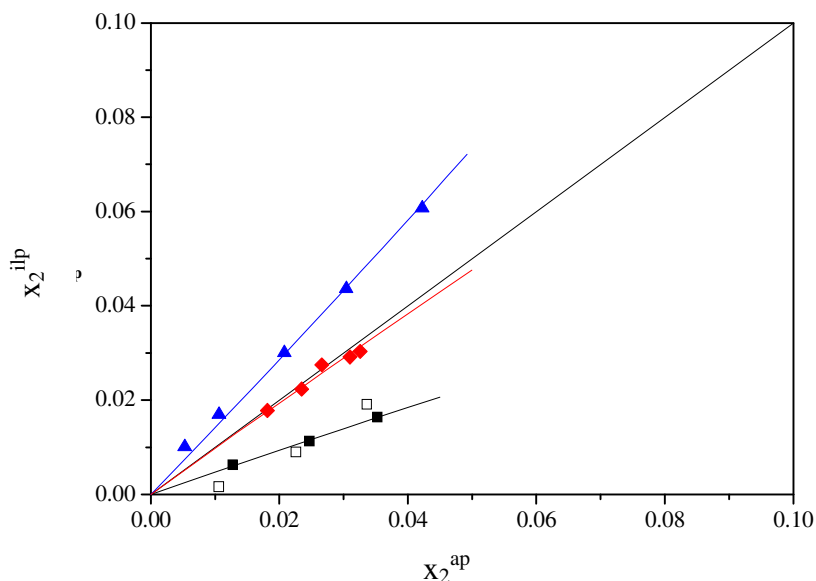


Figura 4.10. Distribuição do DBT entre o líquido iônico e o n-dodecano a 298,15 K. Utilizando, m-2-HEAB (■); m-2-HEAH (□); $[\text{emim}]^+[\text{EtSO}_4]^-$ (◆), $[\text{emim}]^+[\text{DEtPO}_4]^-$ (▲); linhas calculadas pelo modelo NRTL.

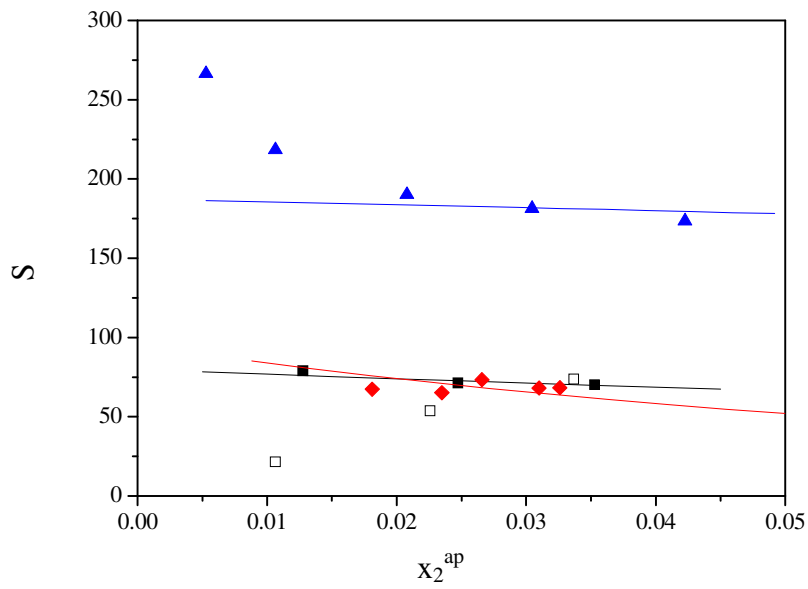


Figura 4.11. Seletividade do líquido iônico a 298,15 K. Utilizando-se, m-2-HEAB (■); m-2-HEAH (□); $[\text{emim}]^+[\text{EtSO}_4]^-$ (◆), $[\text{emim}]^+[\text{DEtPO}_4]^-$ (▲); linhas calculadas pelo modelo NRTL.

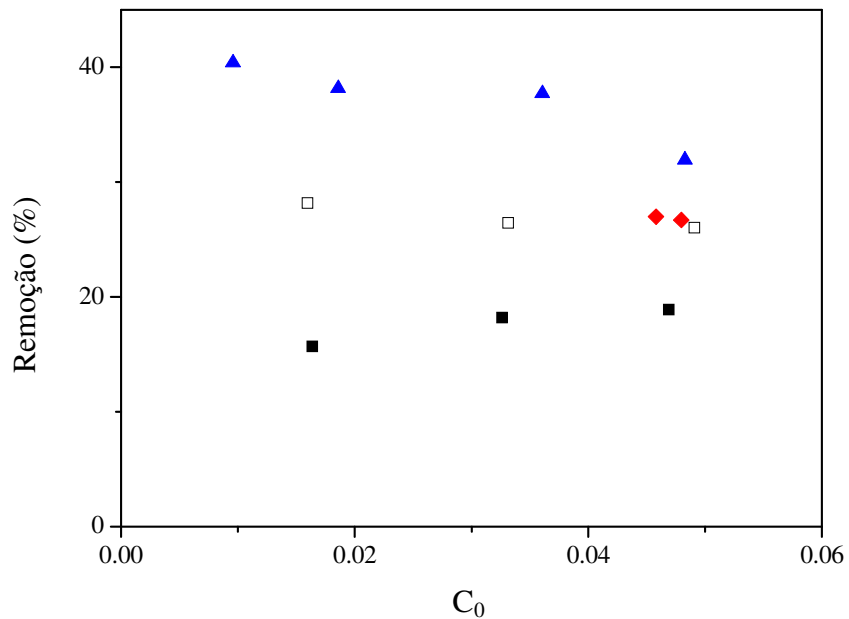


Figura 4.12. Porcentagem do DBT removido do óleo modelo, a 298,15 K. Utilizando-se, m-2-HEAB (■); m-2-HEAH (□); $[\text{emim}]^+[\text{EtSO}_4]^-$ (◆), $[\text{emim}]^+[\text{DEtPO}_4]^-$ (▲).

Segundo os dados do ELL e dos valores de distribuição, seletividade e porcentagem de remoção, observa-se que o m-2-HEAH é melhor solvente que o m-2-HEAB, similar ao $[\text{emim}]^+[\text{EtSO}_4]^-$, mas de menor qualidade que $[\text{emim}]^+[\text{DEtPO}_4]^-$, o qual é melhor solvente para extração de DBT neste estudo. Adicionalmente, temos que considerar a natureza biodegradável dos líquidos iônicos m-2-HEAB e m-2-HEAH, que permite um processo ecológico. O líquido iônico m-2-

HEAH extrai aproximadamente 30% do DBT inicialmente inserido no n-dodecano e o m-2-HEAH, como os outros líquidos iônicos, não se dissolve em n-dodecano, mas n-dodecano é presente em baixas quantidades na fase rica em líquido iônico. Finalmente, a vantagem do m-2-HEAH frente ao $[\text{emim}]^+[\text{EtSO}_4]^-$ é sua síntese ecológica (não precisa solventes), baixo custo de síntese, e apresenta uma estrutura mais simples de ser degradada no meio ambiente.

As modificações na estrutura do cátion foram analisadas com os líquidos iônicos 2-HE2AB e N-(2-HE)edAB, modificações do líquido iônico m-2-HEAB, como observado na Figura 4.13.

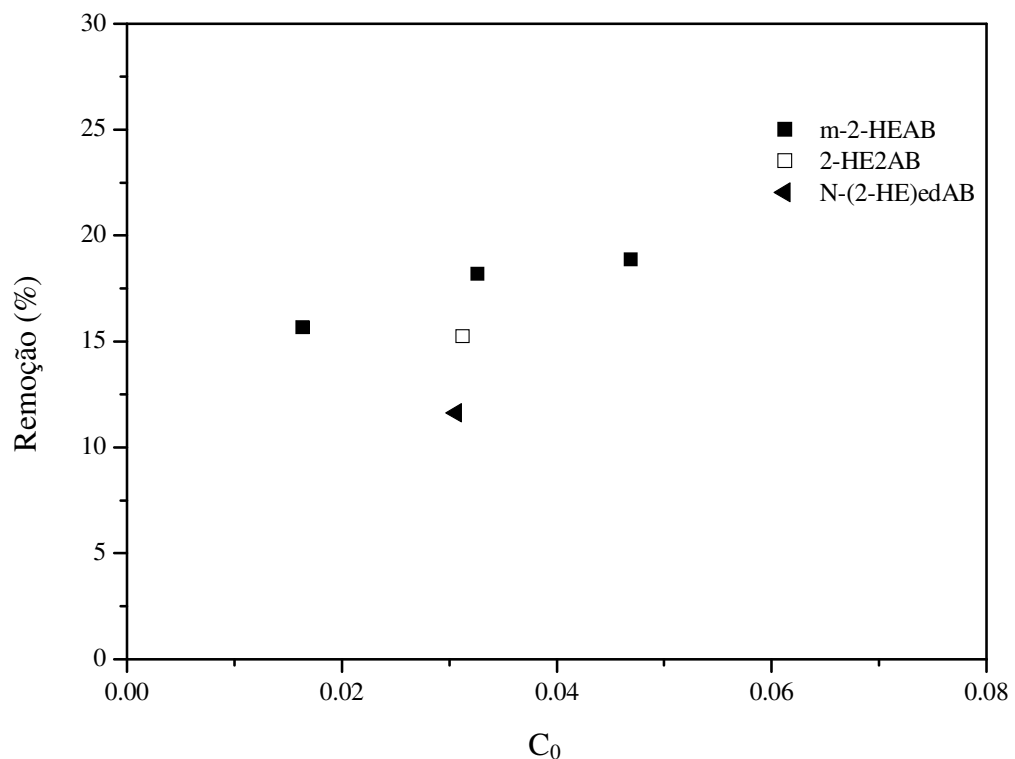


Figura 4.13. Porcentagem do DBT removido do óleo modelo, a 298,15 K. Utilizando-se, m-2-HEAB (■); 2-HE2AB (□); N-(2-HE)edAB (◀).

A Figura 4.13 sugere que as modificações no cátion diminuem a remoção de DBT. Isto pode ser explicado pela maior viscosidade dos dois líquidos iônicos: 2-HE2AB e N-(2-HE)edAB.

5. CONCLUSÕES E SUGESTÕES FUTURAS

5.1. CONCLUSÕES

Síntese e caracterização de líquidos iônicos

Foram sintetizados onze novos líquidos iônicos próticos baseados no cátion amônio, através de uma reação estequiométrica entre ácido e base de Brønsted, e foi verificada a presença de pelo menos um próton instável, o qual é capaz de promover uma extensa rede com ligações de hidrogênio. Os líquidos iônicos próticos foram estudados principalmente com variações no comprimento da cadeia alquílica no ânion. Na caracterização estrutural, foi confirmada a formação de agregados nessa família de líquidos iônicos. Observou-se que o comprimento da cadeia alquílica no ânion modifica as características químicas e físicas do líquido iônico. Por exemplo, o comprimento da cadeia alquílica do ânion influí na formação de agregados no líquido iônico e na solubilidade em ésteres.

Foi desenvolvida uma metodologia de desidratação do líquido iônico, consistindo na desidratação à vácuo e armazenamento em atmosfera de nitrogênio. Os resultados mostram a importância da utilização do nitrogênio para a armazenagem do líquido iônico e que uma umidade aceitável ($<1000 \pm 200$ ppm) pode ser obtida, depois de 35 horas. As curvas de desidratação à vácuo em função do tempo para o líquido iônico aprótico e prótico foram de uma umidade final de 100 ppm e 1000 ppm, respectivamente.

Para evitar a captura de água durante a preparação das misturas binárias foi projetada, construída e implementada uma caixa de acrílico. A caixa serve para manter uma atmosfera inerte e seca durante a manipulação do líquido iônico.

Soluções contendo líquidos iônicos - propriedades físico-químicas

A agregação, o comportamento dinâmico e a ligação do hidrogênio na rede nas soluções binárias 2-HEAA + (água ou metanol ou etanol) foram estudadas através de propriedades termo-acústicas, raios-X e RMN. Os resultados indicam uma leve perturbação da estrutura do líquido iônico nas regiões apolares pela presença de solventes hidroxílicos; a formação de uma estrutura em torno do grupo amônio foi observada em diferentes composições da água.

O estudo das propriedades físicas dos compostos puros permite observar a baixa viscosidade que podem ter os líquidos iônicos com cátion amônio e que o acréscimo da cadeia alquílica no ânion permite obter propriedades de cristal líquido. As propriedades das soluções binárias permitem observar que esses líquidos iônicos apresentam uma concentração crítica de formação de agregados. Além disso, as propriedades de empacotamento estrutural como o índice de refração ou compressibilidade isotérmica em função da molalidade, fornecem evidência de formação de agregados.

No estudo das misturas com solventes hidroxílicos, mostra-se que esses líquidos iônicos próticos, ainda com cadeias alquílicas de 18 carbonos no ânion, são parcialmente solúveis em água, e completamente solúveis em etanol e metanol em todo o intervalo de concentração. Os líquidos iônicos com cadeia alquílica maior que seis carbonos favorece a solubilidade total em ésteres e, em misturas com aldeídos, produz uma mistura exotérmica, seguida de uma separação de duas fases.

A solubilidade dos líquidos iônicos nos ésteres é fortemente influenciada pela mudança do cátion e a solubilidade pode ser aumentada por cadeias alquilicas maiores no ânion. A mudança no cátion do líquido iônico contendo o anion butirato mostrara que a adição de grupos hidroxilos diminui a solubilidade nos ésteres, e um líquido iônico dibutirato é solúvel só no acetato de metila.

Nas misturas de líquidos iônicos próticos (m-2-HEAB, m-2-HEAH) verificou-se a alta mobilidade do próton livre, pela mistura exotérmica com aldeídos, o que não acontece com líquidos iônicos apróticos ($[emim]^+ [EtSO_4]^-$).

A densidade das soluções pode ser predita com o modelo PR+WS/COSMO-SAC com desvios menores a 2,3%.

Em todas as soluções, a estrutura mais compacta é obtida com os solventes que contêm cadeias alquílicas maiores. Esta propriedade pode ser explicada pela maior similaridade entre os compostos. O perfil sigma do modelo COSMO-SAC pode ser utilizado a priori como método qualitativo na detecção de misturas mais compactas.

Soluções contendo líquidos iônicos - equilíbrio líquidor-vapor a baixas pressões

Os líquidos iônicos baseados no cátion imidazólio apresentaram solubilidade nos aldeídos propanal e pentanal, enquanto os líquidos iônicos baseados no cátion amônio mostraram solubilidade nos ésteres acetato de metila, acetato de etila e acetato de propila. Foi projetado e sintetizado um líquido iônico específico para ser solúvel nestes ésteres, com base no comprimento da cadeia alquílica do ânion. Apenas as misturas totalmente solúveis foram usadas posteriormente para a determinação dos dados de equilíbrio líquido-vapor a baixas pressões.

Os dados de ELV a baixa pressão mostram que o acréscimo da cadeia alquílica no líquido iônico aumenta a temperatura de ebulição da solução, e o líquido iônico dication, tem pouca influencia no ponto de ebulição do sistema. Conseguiram-se medidas para frações molares do líquido iônico menores que 0,7. Essa composição é próxima ao máximo empacotamento estrutural das soluções binárias contendo ésteres ou aldeídos. Para maiores concentrações de líquido iônico, as moléculas deixam de estar solvatadas para iniciar a formação de agregados e dificultam a adequada ebulição do sistema no ebulíometro.

Na modelagem dos sistemas, o modelo termodinâmico utiliza a equação de estado de Peng-Robinson com a regra de mistura de Wong-Sandler. Essa regra de mistura utilizou os modelos de UNIQUAC e NRTL para correlacionar os ELV, e o modelo COSMO-SAC para predizer os dados do ELV e a densidade das soluções. Os resultados da correlação e predição mostram uma adequada tendência dos dados experimentais. Adicionalmente, a fase vapor é adequadamente modelada, sem concentrações de líquido iônico.

Soluções contendo líquidos iônicos - Equilíbrio líquido-vapor a altas pressões

O método de consistência termodinâmica mostra-se como uma ferramenta útil para determinar os dados experimentais que apresentam erros maiores aos aceitáveis no conjunto de dados. Mostra-se que líquidos iônicos próticos de estrutura simples, biodegradáveis e de baixa toxicidade podem conseguir solubilidades superiores de CO₂ que os clássicos líquidos iônicos apróticos. Determinou-se que a estrutura molecular do ânion acetato determina uma maior afinidade química no líquido iônico para aumentar a solubilidade do CO₂.

Os dados do ELV a altas pressões mostram que o CO₂ é absorvido pelos líquidos iônicos apróticos, principalmente pelas interações físicas entre as moléculas de um soluto pequeno e moléculas grandes do solvente. Mas, no caso da presença de grupos funcionais que polarizem a molécula do líquido iônico, como para os grupos éster ou amina, forma-se uma interação química com o CO₂. Essa interação permite maior absorção do CO₂ no líquido iônico, formando um carbamato, ligação que pode ser quebrada pela adição de calor à mistura, reutilizando o líquido iônico.

Misturas contendo líquidos iônicos – Equilíbrio líquido-líquido

Foram determinados dados de ELL para sistemas envolvendo a extração do componente aromático sulfuroso dibenzotiofeno. Verificou-se a extração de dibenzotiofeno com líquidos iônicos próticos de estruturas simples.

Os dados do ELL mostram que a polarização mais acentuada na molécula do líquido iônico prótico tem uma extração de solutos sulfurosos similar ao líquido iônico com estrutura mais complexa e massa molecular maior. Observou-se também que o simples acréscimo da cadeia alquílica no ânion do líquido iônico prótico pode originar um líquido iônico com maior poder de dessulfurização.

Considerações

Com as experiências anteriormente citadas, podem ser escolhidos diferentes íons para criar uma vasta gama de líquidos iônicos próticos; o ânion deve ser escolhido para controlar a afinidade química ou física, e o cátion deve ser escolhido para um maior afinamento das propriedades físicas segundo necessidades dos engenheiros.

Além disso, foram feitos os estudos para oito sistemas binários no equilíbrio líquido-vapor e um sistema ternário no equilíbrio líquido-líquido. Nos experimentos do equilíbrio líquido-vapor e líquido-líquido, observa-se que existe uma interação eletrostática entre o líquido iônico e o soluto. Isto é confirmado pelas moléculas maiores do líquido iônico que podem absorver mais CO₂ ou DBT. Mas se algum átomo no líquido iônico tiver afinidade química com o soluto, a absorção de CO₂ ou extração de DBT é aumentada substancialmente. Isto é observado na simples

estrutura molecular dos líquidos iônicos próticos comparada com a maior estrutura dos líquidos iônicos baseados em imidazólio.

Além disso, um aspecto relevante, algumas vezes desconsiderado em relação à aplicação de líquidos iônicos e o meio ambiente, é sua potencial toxicidade. Questão insuficientemente estudada até o momento, especialmente tendo em conta a tendência mundial que origina a necessidade de informações para o cumprimento do registro REACH da UE (do inglês *Registration, Evaluation, Authorization and Restriction of Chemical Substances*). No que se refere aos líquidos iônicos sintetizados nesse trabalho, são de baixo custo econômico, não utilizam-se solventes adicionais na síntese, tem baixa pressão de vapor e os primeiros resultados destacam a biodegradação total e baixa toxicidade como características intrínsecas dessa família de líquidos iônicos.

5.2. PROPOSTAS DE PESQUISAS FUTURAS

Sintetizar e caracterizar líquidos iônicos com mais de um cátion ou ânion, com a finalidade de estudar a influência da nova estrutura nas propriedades físico-químicas, mas mantendo características de baixa toxicidade e alta biodegradabilidade.

Sintetizar líquidos iônicos contendo átomos metálicos.

Estudar a estrutura dos líquidos iônicos com espalhamento de raios X em baixo ângulo para conseguir medir os agregados formados e caracterizar seu tamanho e forma (micela ou lamela).

Projetar líquidos iônicos com o cátion amônio solúveis em aldeídos.

Reparametrizar o modelo COSMO-SAC para obter melhores previsões do ELV ou ELL contendo líquidos iônicos.

REFERÊNCIAS

- ABRAMS, D.S.; PRAUSNITZ, J.M. Statistical thermodynamics of liquid-mixtures - new expression for excess Gibbs energy of partly or completely miscible systems, *AIChe Journal*, v. 21, n. 1, p. 116-128, 1975.
- ANASTAS, P.T.; WARNER, J.C. *Green chemistry theory and practice*, New York, Oxford: University Press, 2000.
- ANGELL, C. A.; BYRNE, N.; BELIERES J-P. Parallel developments in aprotic and protic ionic liquids: Physical chemistry and applications, *Accounts of Chemical Research*, v. 40, p. 1228–1236, 2007.
- ALONSO, L.; ARCE, A.; FRANCISCO, M.; SOTO, A. Thiophene separation from aliphatic hydrocarbons using the 1-ethyl-3-methylimidazolium ethylsulfate ionic liquid. *Fluid Phase Equilibria*, v. 270, p. 97-102, 2008.
- ALONSO, L.; ARCE, A.; FRANCISCO, M.; SOTO, A. Solvent extraction of thiophene from n-alkanes (C7, C12, and C16) using the ionic liquid [c₈mim][BF₄], *The Journal of Chemical Thermodynamics*, v. 40, p. 966-972, 2008.
- ÁLVAREZ V.H.; AZNAR M. Application of a thermodynamic consistency test to binary mixtures containing an ionic liquid, *The Open Thermodynamics Journal*, v. 2, p. 25-38, 2008a.
- ÁLVAREZ V.H.; AZNAR M. Thermodynamic modeling of vapor–liquid equilibrium of binary systems ionic liquid + supercritical {CO₂ or CHF₃} and ionic liquid + hydrocarbons using Peng-Robinson equation of state, *Journal of the Chinese Institute Of Chemical Engineers*, v. 39, p. 353-360, 2008b.
- ÁLVAREZ V.H.; AZNAR M. An efficient approach to optimal interpolation of experimental data, *Journal of the Taiwan Institute of Chemical Engineers*, v. 41, p. 184-189, 2010.
- ÁLVAREZ, V.H.; LARICO, R.; YANOS, Y.; AZNAR, M. Parameter Estimation for VLE calculation by global minimization: genetic algorithm, *Brazilian Journal of Chemical Engineering*, v. 25, p. 409-418, 2008.
- ÁLVAREZ, V.H.; DOSIL, N.; GONZALEZ-CABALEIRO, R.; MATTEDEI, S., MARTIN-PASTOR, M.; IGLESIAS, M.; NAVAZA, J. M. Brønsted ionic liquids for sustainable processes: synthesis and physical properties, *Journal of Chemical & Engineering Data*, v.55, p. 625–632, 2010a.
- ÁLVAREZ ,V.H.; MATTEDEI, S.; AZNAR, M. Vapor-liquid equilibrium data from modified othmer still: optimization of standard operating procedure, *Chemical Engineering and Processing*, submetido, 2010b.
- ÁLVAREZ V. H., MATTEDEI S.; AZNAR M. Density, refractive index and vapor-liquid equilibria of n-methyl-2-hydroxyethylammonium butyrate plus (methyl acetate or ethyl acetate or propyl acetate) at several temperatures, aceito no XVIII Congresso Brasileiro de Engenharia Química, COBEQ 2010, Foz do Iguaçu, 2010c.

- ANGELL, C.A.; BYRNE, N.; BELIERES J-P. Parallel developments in aprotic and protic ionic liquids: Physical chemistry and applications, *Accounts of Chemical Research*, v. 40, n. 11, p. 1228–1236, 2007.
- ANOUTI, M.; JONES, J.; BOISSET, A.; JACQUEMIN, J.; CAILLON-CARAVANIER, M.; LEMORDANT, D. Aggregation behavior in water of new imidazolium and pyrrolidinium alkylcarboxylates protic ionic liquids, *Journal of Colloid and Interface Science*, v. 340, p. 104–111, 2009.
- ANSARI, I. A.; GREE, R. TEMPO-Catalyzed aerobic oxidation of alcohols to aldehydes and ketones in ionic liquid [bmim][PF₆], *Organic Letter*, v. 4, n. 9, p. 1507-1509, 2002.
- ANTHONY J. L.; ANDERSON J. L.; MAGINN E. J.; BRENNCKE J. F. Anion effects on gas solubility in ionic liquids, *The Journal of Physical Chemistry B*, v. 109, p. 6366-6374, 2005.
- APARÍCIO, S.; ALCALDE R.; DÁVILA M.J.; GARCIA B.; LEAL J.M. Properties and structure of aromatic ester solvents, *The Journal of Physical Chemistry B*, v. 111, p. 4417-4431, 2007.
- ARLT, W.; SPUHL O.; KLAMT A. Challenges in thermodynamics, *Chemical Engineering and Processing*, v. 43, p. 221–238, 2004
- ASSELINÉAU, L.; BOGDANIC, G.; VIDAL, J. Calculation of thermodynamic properties and vapor-liquid equilibria of refrigerants, *Chemical Engineering Science*, v. 33, n. 9, p. 1269-1276, 1978.
- ATKINS, M.P.; DAVEY, P.; FITZWATER, G.; ROUHER, O.; SEDDON, K.R.; SWINDALL, J. *Ionic liquids: A map for industrial innovation*, Report Q001, QUILL, Belfast, 2004.
- AWAD, W. H.; GILMAN, J. W.; NYDEN, M.; HARRIS, R. H.; SUTTO, T. E.; CALLAHAN, J.; TRULOVE, P. C.; DELONG, H. C.; FOX, D. M. Thermal degradation studies of alkyl-imidazolium salts and their application in nanocomposites, *Thermochimica Acta*, v. 409, p. 3-11, 2004.
- BANERJEE, T.; VERMA K.K.; KHANNA A. Liquid-liquid equilibrium for ionic liquid systems using COSMO-RS: Effect of cation and anion dissociation, *AICHE Journal*, v. 54, p. 1874-1885, 2008.
- BATES, E. D.; MAYTON, R. D.; NTAI, I.; DAVIS, JR. J. H. CO₂ capture by a task-specific ionic liquid, *Journal of the American Chemical Society*, v. 124, p. 926-927, 2002
- BELIERES, J.-P.; ANGELL, C. A. Protic ionic liquids: preparation, characterization, and proton free energy level representation, *The Journal of Physical Chemistry B*, v. 111, p. 4926-4937, 2007.
- BICAK, N. A new ionic liquid: 2-hydroxyethylammonium formate, *Journal of Molecular Liquids*, v. 116, p. 15–18, 2005.
- BINNEMANS, K. Ionic liquid crystals, *Chemical Reviews*, v. 105, p. 4148-4204, 2005.
- BONDI, A., van der Waals Volumes and Radii, *Journal of Physical Chemistry*, 68, 441-451, 1964.
- BLANCHARD, L. A.; HANCU, D.; BECKMAN, E.J; BRENNCKE, J.F. Green processing using ionic liquids and CO₂ , *Nature*, v. 399, n. 6731, p. 28-29, 1999.

- BRINGGS, S.W.; COMINGS, E.W. Effect of temperature on liquidliquid equilibrium, *Industrial & Engineering Chemistry Research*, v. 35, p. 411-417, 1943.
- CALVAR, N.; GONZÁLEZ, B.; GÓMEZ, E.; DOMINGUEZ, Á. Vapor–liquid equilibria for the ternary system ethanol + water +1-ethyl-3-methylimidazolium ethylsulfate and the corresponding binary systems containing the ionic liquid at 101.3 kPa, *Journal of Chemical & Engineering Data*, v. 53, p. 820-825, 2008
- CARVALHO, P.J.; ÁLVAREZ, V.H.; MACHADO, J.J.B.; PAULY, J.; DARIDON, J-L.; MARRUCHO, I.M.; AZNAR, M.; COUTINHO, J.A.P. High pressure phase behavior of carbon dioxide in 1-alkyl-3-methylimidazolium bis(trifluoromethylsulfonyl)imide ionic liquids, *The Journal of Supercritical Fluids*, v. 48, p. 99–107, 2009a.
- CARVALHO, P.J.; ÁLVAREZ, V.H.; SCHRÖDER, B.; GIL, A.M., MARRUCHO, I.M.; AZNAR, M., SANTOS, L.M.N.B.F.; COUTINHO, J.A. P. Specific solvation interactions of CO₂ on acetate and trifluoroacetate imidazolium based ionic liquids at high pressures, *The Journal of Physical Chemistry B*, v. 113, p. 6803-6812, 2009b.
- CEPAGRI, Centro de Pesquisas Meteorológicas e Climáticas Aplicadas à Agricultura, <http://www.cpa.unicamp.br/>, acessado em março de 2010.
- CHANDRASEKHAR, S. *Liquid crystals*, segunda edição, USA: Cambridge University Press, 1994.
- CHAUMONT, A.; SCHURHAMMER, R.; WIPFF, G. Aqueous interfaces with hydrophobic room-temperature ionic liquids: A molecular dynamics study, *The Journal of Physical Chemistry B*, v. 109, p. 18964-18973, 2005
- COBAS, J.C.; SARDINA, F.J. Nuclear magnetic resonance data processing. MestRe-C: A software Sardina package for desktop computers, *Concepts in Magnetic Resonance*, v. 19A, p. 80-96, 2003
- COTA, I.; GONZALEZ-OLMOS, R.; IGLESIAS, M.; MEDINA, F. New short aliphatic chain ionic liquids: synthesis, physical properties, and catalytic activity in aldol condensations, *The Journal of Physical Chemistry B*, v. 111, p. 12468-12477, 2007
- COULING, D. J.; BERNOT, R.J.; DOCHERTY, K. M.; DIXON, J. K.; MAGINN, E. J. Assessing the factors responsible for ionic liquid toxicity to aquatic organisms via quantitative structure–property relationship modeling, *Green Chemistry*, v. 8, p. 82–90, 2006.
- CUADRADO-PRADOA, S.; DOMÍNGUEZ-PÉREZA, M.; RILOA, E.; GARCÍA-GARABALA, S.; SEGADEA, L.; FRANJOA C.; CABEZA, O. Experimental measurement of the hygroscopic grade on eight imidazolium based ionic liquids, *Fluid Phase Equilibria*, v. 278, n. 1-2, p. 36-40, 2009.
- CHRISTIE S.; DUBOIS, R.H.; ROGERS, R.D.; WHITE, P.S.; ZAWOROTKO, M.J. Air stable liquid clathrates: Solid state structure and hydrocarbon solubility of organic cation triiodide salts, *Journal of Inclusion Phenomena and Molecular Recognition in Chemistry*, v. 11, n. 2, p. 103-114, 1991.
- CHRISTENSEN, J.J.; HANKS, R.W.; IZATT, R.M. *Handbook of heats of mixing*, New York: John Wiley, 1982

- DAVIS, J.H.; FOX, P.A. From curiosities to commodities: ionic liquids begin the transition, *Chemical Communications*, v. 11, p. 1209-1212, 2003
- DOCHERTY, K.M.; DIXON, J.K.; KULPA, C.F. Biodegradability of imidazolium and pyridinium ionic liquids by an activated sludge microbial community, *Biodegradation*, v. 18, p. 481–493, 2007.
- DOMAŃSKA, U.; BOGEL-ŁUKASIK, E.; BOGEL-ŁUKASIK, R. 1-Octanol/Water Partition Coefficients of 1-Alkyl-3-methylimidazolium Chloride⁺, *Chemistry – A European Journal*, v. 9, p. 3033 - 3041, 2003.
- DUPONT, J. On the solid, liquid and solution structural organization of imidazolium ionic liquids. *Journal of Brazilian Chemical Society*, v. 15, p. 341-350, 2004,
- EARLE, M.J.; KATDARE, S.P.; SEDDON, K.R. Paradigm confirmed: The first use of ionic liquids to dramatically influence the outcome of chemical reactions, *Organic Letters*, v. 6, p. 707-710, 2004.
- EGOROVA, M.; PRINS, R. Hydrodesulfurization of dibenzothiophene and 4,6-dimethylbenzothiophene over sulfided NiMo/γ-Al₂O₃, CoMo/γ-Al₂O₃, and Mo/γ-Al₂O₃ catalysts, *Journal of Catalysis*, v. 225, p. 417-427, 2004.
- ERBELLINGER M.; MESIANO, A.J.; RUSSEL, A.J. Enzymatic catalysis of formation of Z-aspartame in ionic liquid – an alternative to enzymatic catalysis in organic solvents. *Biotechnology Progress*, v. 16, p. 1129–1131, 2000
- FRANCISCO, M.; ARCE, A.; SOTO, A. Ionic liquids on desulfurization of fuel oils, *Fluid Phase Equilibria*, no prelo, 2010.
- FREDLAKE, C.P.; CROSTHWAITE, J. M.; HERT, D. G.; AKI, S. N. V. K.; BRENNECKE, J. F. Thermophysical properties of imidazolium-based ionic liquids, *Journal of Chemical & Engineering Data*, v. 49, p. 954-964, 2004
- FREDENSLUND, A.; JONES, R.L.; PRAUSNITZ, J.M. Group-contribution estimation of activity-coefficients in nonideal liquid-mixtures, *AIChE Journal*, v. 21, p. 1086-1099, 1975
- FREIRE, M.G.; VENTURA, S.P.M.; SANTOS, L.M.N.B.F.; MARRUCHO, I.M.; COUTINHO, J.A.P. Evaluation of COSMO-RS for the prediction of LLE and VLE of water and ionic liquids binary systems, *Fluid Phase Equilibria*, v. 268, p. 74-84, 2008
- GABRIEL, S.; WEINER, J. Ueber einige Abkömmlinge des Propylamins, *Berichte Der Deutschen Chemischen Gesellschaft*, v. 21, p. 2669–2679, 1888.
- GATHERGOOD, N.; SCAMMELLS, P. J. Design and preparation of room-temperature ionic liquids containing biodegradable side chains, *Australian Journal of Chemistry*, 55, 557-560, 2002.
- GAO, H.; XING, J.; LI, Y.; LI, W.; LIU, Q.; LIU, H. Desulfurization of diesel fuel by extraction with lewis-acidic ionic liquid, *Separation Science and Technology*, v. 44, p. 971-982, 2009
- GMEHLING, J.; LI, J.D.; SCHILLER, M. A modified UNIFAC model. 2. Present parameter matrix and results for different thermodynamic properties, *Industrial & Engineering Chemistry Research*, v. 32, p. 178-193, 1993.

- GIERNOTH, R.; BANKMANN, D.; SCHLÖRER, N. High performance NMR in ionic liquids. *Green Chemistry*, v.7, p.279–282, 2005.
- GOMIS, V.; RUIZ, F.; ASENSI, J.C. The application of ultrasound in the determination of isobaric vapour–liquid–liquid equilibrium data, *Fluid Phase Equilibria*, v. 172, p. 245-259, 2000
- GORDON, C. M.; HOLBREY, J. D.; KENNEDY, A. R.; SEDDON, K. R., Ionic liquid crystals: Hexafluorophosphate salts, *Journal of Materials Chemistry*, v. 8, p. 2627-2636, 1998
- GRABOSKI, M. S.; DAUBERT, T. E. A. Modified soave equation of state for phase equilibrium calculations, *Industrial and Engineering Chemistry Process Design and Development*, v. 17, n. 4, p. 443-454, 1978.
- GREAVES, T. L.; WEERAWARDENA, A.; FONG, C.; KRODKIEWSKA, I.; DRUMMOND, C. J. Protic ionic liquids: Solvents with tunable phase behavior and physicochemical properties, *The Journal of Physical Chemistry B*, v. 110, p. 22479-22487, 2006.
- GROS, H.P.; BOTTINI, S.; BRIGNOLE, E.A. A group contribution equation of state for associating mixtures, *Fluid Phase Equilibria*, v. 116, p. 537-544, 1996.
- GUTMANN, V. Solvent effects on the reactivities of organometallic compounds, *Coordination Chemistry Reviews*, v. 18, p. 225-255, 1976.
- HÁLA E.; PICK, J.; FRIED, V.; VILIM, O. *Vapor liquid equilibrium*, Oxford: Pergamon Press, 1967.
- HILDEBRAND, J. H.; PRAUSNITZ, J.M.; SCOTT, R. L. *Regular and related solutions*, New York: Van Nostrand Reinhold, 1970.
- HOLBREY, J. D.; REICHERT, W. M.; REDDY, R. G.; ROGERS, R. D. Heat capacities of ionic liquids and their applications as thermal fluids. In *Ionic liquids as green solvents*; Seddon, K. R., Rogers, R. D., Eds.; ACS Symposium Series 856; American Chemical Society: Washington, D. C., p. 121-133, 2003.
- HOLBREY, J. D.; SEDDON, K. R. The phase behaviour of 1-alkyl-3-methylimidazolium tetrafluoroborates; ionic liquids and ionic liquid crystals, *Journal of the Chemical Society Dalton Transactions*, p. 2133-2139, 1999.
- HOLDERBAUM, T.; GMEHLING, J. PSRK: A group-contribution equation of state based on UNIFAC, *Fluid Phase Equilibria*, v. 70, p. 251-265, 1991
- HUANG, J.; RIISAGER, A.; BERG, R.W.; FEHRMANN, R. Tuning ionic liquids for high gas solubility and reversible gas sorption, *Journal of Molecular Catalysis A: Chemical*, v. 279, p. 170–176, 2008
- HUDDLESTON, J.G.; WILLAUER, H.D.; SWATLOSKI, R.P.; VISSER, A.E.; ROGERS, R.D. Room temperature ionic liquids as novel media for ‘clean’ liquid-liquid extraction, *Chemical Communication*, n. 16, p. 1765-1766, 1998.
- HUDDLESTON, J. G.; VISSER, A. E.; REICHERT, W. M.; WILLAUER, H. D.; BROKER G. A.; Rogers, R. D. Characterization and comparison of hydrophilic and hydrophobic room temperature ionic liquids incorporating the imidazolium cation, *Green Chemistry*, v. 3, p. 156–164, 2001.

- HURON, M. J.; DUFOUR, G. N.; VIDAL, J. Vapour -liquid equilibrium and critical locus curve calculations with the soave equation for hydrocarbon systems with carbon dioxide and hydrogen sulfide, *Fluid Phase Equilibria*, v. 1, n. 4, p. 247-265, 1978.
- HURLEY, F.H. Electrodeposition of aluminium. US. Patent. U. p. office, 4,446,331., 1948.
- IGLESIAS, M.; TORRES, A.; GONZALEZ-OLMOS, R.; SALVATIERRA, D. Effect of temperature on mixing thermodynamics of a new ionic liquid: {2-hydroxyethylammonium formate (2-HEAF) + short hydroxylic solvents}, *The Journal of Chemical Thermodynamics*, v. 40, p. 119-133, 2008
- IGLESIAS, M.; OLIVEIRA, E.N.; FERREIRA, C.M.; GUERRA, I.R.; SERRA, J.S.; MATTEDE, S. Viscosities of protic ionic liquids: 2-hydroxy ethylammonium formate, 2-hydroxy ethylammonium acetate and 2-hydroxy diethylammonium acetate, 24th ESAT, European symposium on applied thermodynamics, Santiago de Compostela, Spain, 2009.
- ILOUKHANI, H.; ROSTAMI, Z. Densities, Viscosities, Speeds of Sound, and Refractive Indices for Binary Mixtures of Diethylcarbonate, Acetophenone, and 1-Hexanol at (293.15, 303.15, 313.15, and 323.15) K for the Liquid Region and at Ambient Pressure, *Journal of Chemical & Engineering Data*, v. 52, p. 921-928, 2007.
- ISI WEB OF KNOWLEDGE, <http://isiwebofknowledge.com>, acessado em janeiro de 2010.
- JOHNSON, K.E. What's an Ionic Liquid?, *The Electrochemical Society Interface*, v.16, n. 1, p. 38-41, 2007.
- JACOBSON, B. Intermolecular free lengths in the liquid state. I. Adiabatic and isothermal compressibilities, *Acta Chemica Scandinavica*, v. 6, p. 1485-1498, 1952
- JIANG, X.; NIE, Y.; LI, C.; WANG, Z. Imidazolium-based alkylphosphate ionic liquids - A potential solvent for extractive desulfurization of fuel, *Fuel*, v. 87, p. 79-84, 2008
- KATO, R.; GMEHLING, J. Systems with ionic liquids: Measurement of VLE and gamma(infinity) data and prediction of their thermodynamic behavior using original UNIFAC, mod. UNIFAC(Do) and COSMO-RS(O1), *Journal of Chemical Thermodynamics*, v. 37, p. 603-619, 2005.
- KLAMT, A. Conductor-like screening model for real solvents - a new approach to the quantitative calculation of solvation phenomena, *The Journal of Physical Chemistry*, v. 99, p. 2224-2235, 1995
- KLAMT, A.; ECKERT F. COSMO-RS: A novel and efficient method for the a priori prediction of thermophysical data of liquids, *Fluid Phase Equilibria*, v. 172, p. 43-72, 2000
- KUMAR, J. Estimates of internal pressure and molar refraction of imidazolium based ionic liquids as a function of temperature, *Journal of Solution Chemistry*, v. 37, p. 203-214, 2008
- KUMAR, A.A.P.; BANERJEE, T. Thiophene separation with ionic liquids for desulphurization: A quantum chemical approach, *Fluid Phase Equilibria*, v. 278, p. 1-8, 2009
- LARSEN, B.L.; RASMUSSEN, P.; FREDENSLUND, A. A modified UNIFAC group-contribution model for prediction of phase-equilibria and heats of mixing, *Industrial & Engineering Chemistry Research*, v. 26, p. 2274-2286, 1987

- LAU, R.M.; VAN-RANTWIJK, F.; SEDDON, K.R.; SHELDON, R.A. Lipase-catalyzed reactions in ionic liquids, *Organic Letters*, v. 2, p. 4189–4191, 2000
- LOWERY, T.H.; RICHARDSON, K.S. *Mechanism and theory in organic chemistry*, Harper Collins Publishers, terceira edição, 1987.
- LE THI, C.; TAMOUZA, S.; PASSARELLO, J.P.; TOBALY, P.; HEMPTINNE, J.C. Modeling phase equilibrium of $H_2 + n\text{-Alkane}$ and $CO_2 + n\text{-alkane}$ binary mixtures using a group contribution statistical association fluid theory equation of state (GC-SAFT-EOS) with a kij group contribution method, *Industrial & Engineering Chemistry Research*, v. 45, p. 6803-6810, 2006
- LEE, S.Y.; TSUI, Y.P. Succeed at gas/liquid contacting, *Chemical Engineering Progress*, v. 95, p. 23–49, 1999.
- LEE, B.; RICHARDS, F. M. The Interpretation of Protein Structures: Estimation of Static Accessibility, *Journal of Molecular Biology*, v. 55, n. 3, p. 379-400, 1971.
- LEAL, J. P.; J. ESPERANÇA, J.M. S. S.; MINAS DA PIEDADE, M. E.; CANONGIA LOPES, J. N.; REBELO, L. P. N.; SEDDON, K. R. The nature of ionic liquids in the gas phase, *The Journal of Physical Chemistry A*, v. 111, p. 6176-6182, 2007.
- LENG, Y.; WANG, J.; ZHU, D.; REN, X.; GE, H.; SHEN, L. Heteropolyanion-Based Ionic Liquids: Reaction-Induced Self-Separation Catalysts for Esterification, *Angew. Chem. Int. Ed.*, v. 48, p. 168 –171, 2009.
- LETCHER, T. M.; SISWANA, P. M. Liquid-liquid equilibria of mixtures of an alkanol + water + a methyl substituted benzene at 25°C. *Fluid Phase Equilibria*, v. 74, p. 203–217, 1992.
- LETCHER, T. M. *Developments and application in solubility*, Cambridge, UK: The Royal Society of Chemistry, 2007
- LIKHANOVA, N.V.; PALOU, R.M.; PALOMEQUE, J.F. Desulfurization of hydrocarbons by ionic liquids and preparation of ionic liquids, US Patent Application Publication, US 2009/0288992 A1, 2009.
- LIN, S.-T.; SANDLER, S.I. A priori phase equilibrium prediction from a segment contribution solvation model, *Industrial & Engineering Chemistry Research*, v. 41, p. 899-913, 2002
- LIN, S.-T.; SANDLER, S.I. A priori phase equilibrium prediction from a segment contribution solvation model (v. 41, p. 903, 2004)- Additions and Corrections, *Industrial & Engineering Chemistry Research*, v. 43, p. 1322-1322, 2004.
- LOWRY T. H.; RICHARDSON K. S. *Mechanism and Theory in Organic Chemistry*, 3rd Edition, Benjamin-Cummings Publishing Company; New York, 1987.
- LUO, S.; MI, X.; ZHANG, L.; LIU, S.; XU, H.; CHENG, J-P. Functionalized ionic liquids catalyzed direct aldol reactions, *Tetrahedron*, v. 63, p. 1923–1930, 2007.
- MADURO, R.M., Equilíbrio líquido-líquido em sistemas contendo hidrocarbonetos aromáticos + hidrocarbonetos alifáticos + líquidos iônicos, Tese de doutorado, FEQ/UNICAMP, 2009.
- MAGEE, J. *Heat capacity and enthalpy of fusion for 1-butyl-3-methyl-imidazolium hexafluorophosphate*, Rostock, Germany: 17th IUPAC Conference on Chemical Thermodynamics (ICCT 2002), 2002.

- MARSH, K.N.; BOXALL, J.A.; LICHTENTHALER, R. Room temperature ionic liquids and their mixtures - A review, *Fluid Phase Equilibria*, v. 219, p. 93-98, 2004.
- MULLINS, E.; OLDDLAND, R.; LIU,Y. A.; WANG,S.; SANDLER, S.I.; CHEN,C-C.; ZWOLAK, M.; SEAVEY, K. C. Sigma-Profile Database for Using COSMO-Based Thermodynamic Methods, *Industrial & Engineering Chemistry Research*, v. 45, p. 4389-4415, 2006.
- NAMBOODIRI, V. V.; VARMA, R. S. Solvent-free sonochemical preparation of ionic liquids, *Organic Letters*, v. 4, n. 18, p. 3161-3163, 2002.
- NEBIG, S.; BÖLTS, R.; GMEHLING, J. Measurement of vapor-liquid equilibria (VLE) and excess enthalpies (H^E) of binary systems with 1-alkyl-3-methylimidazolium bis(trifluoromethylsulfonyl)imide and prediction of these properties and γ^∞ using modified UNIFAC (Dortmund), *Fluid Phase Equilibria*, v. 258, p. 168-178, 2007.
- NEBIG, S., LIEBERT, V., GMEHLING, J. Measurement and prediction of activity coefficients at infinite dilution (γ^∞) vapor-liquid equilibria (VLE) and excess enthalpies (H^E) of binary systems with 1,1-dialkyl-pyrrolidinium bis(trifluoromethylsulfonyl)imide using mod. UNIFAC (Dortmund), *Fluid Phase Equilibria*, v. 277, p. 61-67, 2009.
- NEBIG, S.; GMEHLING, J. Measurements of different thermodynamic properties of systems containing ionic liquids and correlation of these properties using modified UNIFAC (Dortmund), *Fluid Phase Equilibria*, v. 294, p. 206-212, 2010.
- NGO, H. L.; LECOMPTE, K.; HARGENS, L.; MCEWEN, A. B. Thermal properties of imidazolium ionic liquids. *Thermochimica Acta*, v. 357, p. 97-102, 2000.
- OCÓN, J.; ESPANTOSO, J. Vapor-liquid equilibria III. Study of a new VLE ebulliometer. Methanol-carbon tetrachloride system. *Anales de Química*, 54B, 413-420, 1958.
- OHNO, H.; FUKUMOTO, K. Amino acid ionic liquids, *Accounts of Chemical Research*, v. 40, p. 1122-1129, 2007
- OLIVEIRA, L. H.; ÁLVAREZ, V. H., AZNAR, M. Liquid-liquid equilibrium for n-dodecane + DBT + n-methyl-2-hydroxyethylammonium butyrate at 25°C and 95 kPa, aceito no XVIII Congresso Brasileiro de Engenharia Química, COBEQ 2010, Foz do Iguaçu, 2010
- OLIVEIRA, L. H. Thermodynamic study of liquid-liquid equilibrium aiming sulfur removal by using ionic liquids, M. Sc. Dissertation, School of Chemical Engineering, State University of Campinas, Campinas, 2009.
- PANDEY, J. D.; DEY, R.; BHATT, B.D. Applicability of thermoacoustical parameters for the computation of available volume in liquid systems, *PhysChemComm*, v. 5, p. 37-39, 2002
- PARICAUD, P. A general perturbation approach for equation of state development: Applications to simple fluids, ab initio potentials, and fullerenes, *Journal of Chemical Physics*, v. 124, p. 154505-154522, 2006
- PENG, D.Y.; ROBINSON, D.B. A New two-constant equation of state, *Industrial and Engineering Chemistry Fundamentals*, v. 15, p. 59-64, 1976.

- PEREIRO, A.B.; VERDÍA, P.; TOJO, E.; RODRÍGUEZ A. Physical Properties of 1-Butyl-3-methylimidazolium Methyl Sulfate as a Function of Temperature, *Journal of Chemical & Engineering Data*, v. 52, p. 377-380, 2007.
- PERIC, B.; SIERRA, J.; MARTI, E.; GONZALEZ-OLMOS, R.; IGLESIAS, M.; CRUAÑAS, R.; GARAU, M.A. 20th Society of Environmental Toxicology and Chemistry Congress, SETAC Europe Annual Meeting, Science and Technology for Environmental Protection, Sevilla (Spain). May, 2010.
- PERNAK, J.; SOBASZKIEWICZ K.; MIRSKA I. Anti-microbial activities of ionic liquids, *Green Chemistry*, v. 5, p. 52-56, 2003.
- PERRY, R. H.; GREEN, D. Chemical engineering handbook, 7^{ma} edição, New York: McGraw-Hill, 1999.
- PHAM, T.P.T.; CHO, C.-W.; YUN, Y.-S. Environmental fate and toxicity of ionic liquids: A review, *Water Research*, v. 44, p. 352-372, 2010
- Pollution Prevention Act of 1990, disponível em: <http://www.epa.gov/p2/pubs/p2policy/act1990.htm>, acessado em janeiro de 2010.
- PRAUSNITZ, J.M.; TAVARES, F.W. Thermodynamics of fluid-phase equilibria for standard chemical engineering, *AIChE Journal*, v. 50, p. 739-761, 2004.
- RANKE, J.; MÖLTER, K.; STOCK, F.; BOTTIN-WEBER, U.; POCZOBUTT, J.; HOFFMANN, J.; ONDRUSCHKA, B.; FILSER, J.; JASTORFF, B. Biological effects of imidazolium ionic liquids with varying chain lengths in acute *Vibrio fischeri* and WST-1 cell viability assays, *Ecotoxicology and Environmental Safety*, v. 58, p. 396-404, 2004.
- RENNER, R., Ionic liquids: an industrial cleanup solution. *Environmental Science & Technology*, v. 35, p. 410A-413A, 2001.
- RENON, H.; PRAUSNITZ, J. M. Local composition in thermodynamic excess functions for liquid mixtures, *AIChE Journal*, v. 14, p. 135-144, 1968.
- RENUNCIO J.A.R.; COTO, B.; CABANAS, A.; MENDUIÑA, C.; RUBIO, R.G.; PANDO, C. Excess enthalpies, and vapor-liquid equilibrium and surface properties of the highly non-ideal associated mixtures formed by an alcohol and propanal, *Fluid Phase Equilibria*, v. 126, p. 177-194, 1996.
- RESA, J.M.; GONZÁLEZ, C.; GOENAGA, J.M.; IGLESIAS, M. Density, refractive index, speed of sound at 298.15 K and vapor-liquid equilibria at 101.3 kPa for binary mixtures of ethyl acetate + 1-pentanol and ethanol + 2-methyl-1-propanol. *Journal of Chemical & Engineering Data*, 49, 804-808, 2004.
- RIDDICK, J.A.; BUNGER, W.B.; SAKANO, T.K. Organic Solvents, physical properties and methods of purification, 4th ed., Wiley Interscience, New York, 1986.
- SANDLER, S.I. *Chemical and Engineering Thermodynamics*, New York : J. Wiley, 1999.
- SARKARA L.; ROY M. N., Studies on liquid-liquid interactions of some ternary mixtures by density, viscosity, ultrasonic speed and refractive index measurements, *Thermochimica Acta*, v. 496, p. 124-128, 2009

- SCURTO, A.; AKI, S.; BRENNCKE, J. CO₂ as a separation switch for ionic liquid/organic mixtures, *Journal of the American Chemical Society*, v. 124, p. 10276–10277, 2002
- SCURTO, A.M.; AKI, S.N.V.K.; BRENNCKE, J.F. Carbon dioxide induced separation of ionic liquids and water, *Chemical Communications*, p. 572–573, 2003
- SEDDON, K.R. Ionic liquids for clean technology, *Journal of Chemical Technology and Biotechnology*, v. 68, 351-356, 1997
- SEDDON, K.R.; STARK, A.; TORRES, M.J. *Viscosity and density of 1-alkyl-3-methylimidazolium ionic liquids*, in *Clean Solvents: Alternative Media for Chemical Reactions and Processing*, Eds. M. Abraham and L. Moens, Washington D.C.: American Chemical Society Symposium Series, v. 819, p. 34-49, 2002
- SEDDON, K. R. Ionic liquids: A taste of the future, *Nature Materials*, v. 2, p. 363 – 365, 2003.
- SEDDON, K. R.; PLECHKOVA, N. V.; EARLE, M. J. Production of Bio-Diesel, patente de invenção, IPC8 Class: AC10L118FI, USPC Class: 44308, 2009. Disponível em: <http://www.faqs.org/patents/app/20090235574>.
- SHARIATI, A.; PETERS, C.J. High-Pressure Phase Behavior of Systems with Ionic Liquids: Measurements and Modeling of the Binary System Fluoroform + 1-Ethyl-3-methylimidazolium Hexafluorophosphate, *Journal of Supercritical Fluids*, v. 25, p. 109-117, 2003.
- SHELDON, R. The E factor: fifteen years on, *Green Chemistry*, v. 9, p. 1273 - 1283, 2007
- SHIMIZU, K.; COSTA GOMES, M.F.; PÁDUA, A.A.H.; REBELO, L.P.N.; CANONGIA LOPES, J.N. On the role of the dipole and quadrupole moments of aromatic compounds in the solvation by ionic liquids, *The Journal of Physical Chemistry B*, v. 113, p. 9894-9900, 2009
- SIERRA, J.; MARTÍ, E.; MENGÍBAR, A.; GONZÁLEZ-OLMOS, R.; IGLESIAS, M.; CRUAÑAS, R.; GARAU, M. A. Effect of new ammonium based ionic liquids on soil microbial activity. Presentado em: the 5th Society of Environmental Toxicology and Chemistry World Congress, SETAC2008, Sydney, Australia, Agosto, 2008,
- SIGMA-ALDRICH, <http://www.sigmaaldrich.com/>, acessado em janeiro do 2010.
- SKJØLD-JORGENSEN, S. Group contribution equation of state (GC-EOS): a predictive method for phase equilibrium computations over wide ranges of temperatures and pressures up to 30 MPa, *Industrial & Engineering Chemistry Research*, v. 27, p. 110-118, 1988
- SOAVE, G. Improvement of the van der Waals equation of state, *Chemical Engineering Science*, v. 39, p. 357-369, 1984.
- SUAREZ, P.A.Z.; DULLIUS, J.E.L.; EINLOFT, S.; DE SOUZA, R.F.; DUPONT, J. The use of new ionic liquids in two-phase catalytic hydrogenation reaction by rhodium complexes, *Polyhedron*, vol 15, n. 7, p. 1217-1219, 1996.
- SUN, J.; ZHANG, S.; CHENG, W.; REN, J. Hydroxyl-functionalized ionic liquid: a novel efficient catalyst for chemical fixation of CO₂ to cyclic carbonate, *Tetrahedron Letters*, v. 49, p. 3588–3591, 2008

- STEPNOWSKI, P.; ZALESKA, A. Comparison of different advanced oxidation processes for the degradation of room temperature ionic liquids, *Journal of Photochemistry and Photobiology A: Chemistry*, v. 170, p. 45-50, 2005.
- STOCK, F.; HOFFMANN, J.; RANKE, J.; STÖRMANN, R.; ONDRUSCHKA, B.; JASTORFF, B. Effects of ionic liquids on the acetylcholinesterase – a structure – activity relationship consideration, *Green Chemistry*, v. 6 , p. 286 – 290, 2004.
- STRAGEVITCH, L. Liquid-Liquid Equilibrium in nonelectrolyte mixtures (in Portuguese), Tese de doutorado, FEQ/UNICAMP, Campinas, 1997.
- SWATLOSKI, R. P.; SPEAR, S. K.; HOLBREY, J. D.; ROGERS, R. D. Dissolution of cellulose with ionic liquids. *Journal of the American Chemical Society*, v. 124, p. 4974–4975, 2002.
- TARAKAD, R.R.; SCHELLER, W.A., Isothermal vapor-liquid equilibrium data for the system n-heptane-n-valeraldehyde at 75 and 90 °C, *Journal of Chemical & Engineering Data*, v. 24, p. 119-120, 1979
- TINDALE, J. J.; RAGOGNA, P. J. Highly fluorinated phosphonium ionic liquids: novel media for the generation of superhydrophobic coatings, *Chemical Communications*, p. 1831 – 1833, 2009
- TRULOVE, P. C.; MANTZ, R. A., Electrochemical properties of ionic liquids, in Ionic liquids in synthesis, edited by Peter Wasserscheid, Thomas Welton, Wiley-VCH Verlag GmbH & Co. KGaA, Weinheim, Federal Republic of Germany, 2002.
- TSAVAS, P.; VOUTSAS, E.; MAGOULAS, K.; TASSIOS, D. Phase equilibrium calculations in aqueous and nonaqueous mixtures of sugars and sugar derivatives with a group-contribution model, *Industrial & Engineering Chemistry Research*, v. 43, p. 8391-8399, 2004.
- TUNDO, P.; ANASTAS, P.; BLACK, D.S.; BREEN, J.; COLLINS,T.; MEMOLI, S.; MIYAMOTO, J.; POLYAKOFF, M.; TUMAS,W. Synthetic pathways and processes in green chemistry. Introductory overview, *Pure and Applied Chemistry*, v. 72, n. 7, p. 1207–1228, 2000.
- VÁZQUEZ, G.; CANCELA, M.A.; VARELA, R.; ALVAREZ, E.; NAVAZA, J.M. Influence of surfactant on absorption of CO₂ in a stirred tank with and without bubbling, *Chemical Engineering Journal*, v. 67, p. 131-137, 1997
- VISSER, A. E.; SWATLOSKI, R. P.; REICHERT, W. M.; MAYTON, R.; SHEFF, S.; WIERZBICKI, A.; DAVIS, JR.J. H.; ROGERS, R. D. Task-specific ionic liquids incorporating novel cations for the coordination and extraction of Hg₂⁺ and Cd₂⁺: synthesis, characterization, and extraction studies, *Environmental Science & Technology*, v.36, p. 2523-2529, 2002
- VITU, S.; JAUBERT, J.N.; PAULY, J.; DARIDON, J.L.; BARTH, D. Phase equilibria measurements of CO₂ + methyl cyclopentane and CO₂ + isopropyl cyclohexane binary mixtures at elevated pressures, *The Journal of Supercritical Fluids*, v. 44, p. 155–163, 2008
- WALDEN, P. Ueber die Molekulargrösse und elektrische Leitfähigkeit einiger geschmolzener Salze (Molecular weights and electrical conductivity of several fused salts), *Bulletin de l'Academie Imperiale des Sciences de Saint-Pétersbourg*, v. 8, p. 405-422, 1914.

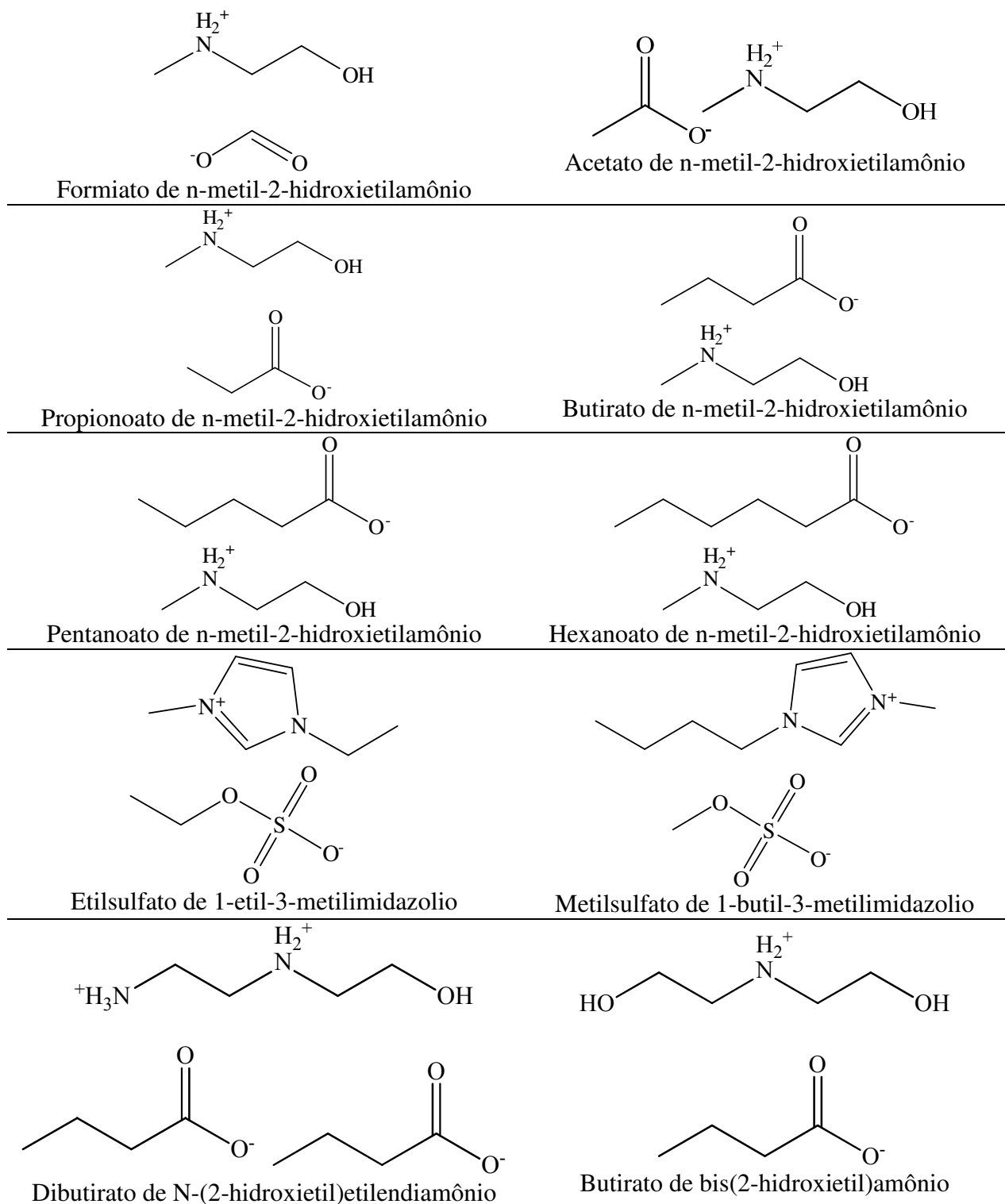
- WELTON, T. Room-Temperature Ionic Liquids. Solvents for Synthesis and Catalysis, *Chemical Reviews*, v. 99, p. 2071-2084, 1999
- WILKES, J.S.; ZAWOROTKO, M.J. Air and water stable 1-methyl-3-ethylimidazolium based ionic liquids. *Journal of the Chemical Society, Chemical Communications*, p. 965-967, 1992
- WILKES, J. S. Introduction, in Ionic liquids in synthesis, edited by Peter Wasserscheid, Thomas Welton, Wiley-VCH Verlag GmbH & Co. KGaA, Weinheim, Federal Republic of Germany, 2002.
- WILSON, G.M. Vapor-Liquid Equilibrium .11. New expression for excess free energy of mixing, *Journal of the American Chemical Society*, v. 86, n. 2, p. 127, 1964.
- WONG, D.S.H.; SANDLER, S.I. A Theoretically Correct mixing rule for cubic equations of state, *AICHE Journal*, v. 38, p. 671-680, 1992.
- XING, H.; WANG, T.; ZHOU, Z.; DAI, Y. Novel Brønsted-acidic ionic liquids for esterifications, *Industrial & Engineering Chemistry Research*, v. 44, p 4147–4150, 2005
- YANG, Q.; DIONYSIOU, D.D. Photolytic degradation of chlorinated phenols in room temperature ionic liquids. *Journal of Photochemistry and Photobiology, A: Chemistry*, v. 165, p. 229-240, 2004
- YUAN, X.; ZHANG, S.; LIU, J.; LU, X. Solubilities of CO₂ in hydroxyl ammonium ionic liquids at elevated pressures, *Fluid Phase Equilibria*, v. 257, p. 195–200, 2007
- YU, G.; ZHANG, S.; YAO, X.; ZHANG, J.; DONG, K.; DAI, W.; MORI, R. Design of task-specific ionic liquids for capturing CO₂ : a molecular orbital study, *Industrial & Engineering Chemistry Research*, v. 45, p. 2875–2880, 2006.

Synthesis and Purification of Ionic Liquids

James H. Davis, Jr., Charles M. Gordon, Claus Hilgers, and Peter Wasserscheid

ANEXO

A. Estrutura de alguns líquidos iônicos citados na tese



B. Os 12 princípios da química verde (Anastas e Warner, 2000)

- 1 É melhor prevenir do que tratar os resíduos, depois que são produzidos.
- 2 Métodos de síntese devem ser projetados para maximizar o uso de todos os materiais preparados durante o processo.
- 3 Sempre deverá ser viável a metodologia de síntese projetada para uso e geração de substâncias que possuam pouca ou nenhuma toxicidade para a saúde humana e ambiente.
- 4 Produtos químicos devem ser obtidos para preservar a eficácia da sua função, reduzindo a toxicidade.
- 5 O uso de substâncias auxiliares (por exemplo, solventes, agentes de separação, etc) deve ser desnecessário no processo sempre que for possível, ou inócuo, quando utilizado.
- 6 A demanda de energia deve ser calculada pelo seu impacto econômico e ambiental e deve ser minimizado. Métodos de síntese devem ser conduzidos à temperatura e pressão ambiente.
- 7 A matéria-prima fornecida deve ser renovável sempre que seja técnica e economicamente viável.
- 8 Derivatização desnecessária (modificação temporária de processos físico-químicos ou de substâncias) deve ser evitado sempre que possível.
- 9 Reagentes catalíticos (tão seletivos quanto possível) são superiores aos reagentes estequiométricos.
- 10 Os produtos químicos devem ser projetados de modo que no final de sua função, não persistam no ambiente para se decompor em produtos de degradação inócuos.
- 11 Metodologias de análise precisam ser desenvolvidas para monitorar e controlar em tempo real os processos, antes da formação de substâncias perigosas.
- 12 Substâncias e reagentes utilizados em um processo químico devem ser escolhidos de forma a minimizar o potencial para acidentes químicos, incluindo vazamentos, explosões e incêndios.

C. Literatura produzida nesta pesquisa

Artigos em periódicos indexados

1. ÁLVAREZ, V.H.; MATTEDI, S.; MARTIN-PASTOR, M.; AZNAR, M.; IGLESIAS, M. Thermophysical properties of binary mixtures of ionic liquid 2-hydroxy ethylammonium acetate + (water, methanol or ethanol). *Journal of Chemical Thermodynamics*, submetido, 2010.
2. ÁLVAREZ V.H.; MATTEDI S.; AZNAR M. Density, Refractive Index and Vapor-Liquid Equilibria of N-Methyl-2-Hydroxyethylammonium Butyrate plus (Methyl Acetate or Ethyl Acetate or Propyl Acetate) at Several Temperatures, em preparação.
3. ÁLVAREZ V.H.; MATTEDI S.; AZNAR M. Density, Refractive Index and Vapor-Liquid Equilibria of N-Methyl-2-Hydroxyethylammonium Hexanoate plus (Methyl Acetate or Ethyl Acetate or Propyl Acetate) at Several Temperatures, em preparação.
4. ÁLVAREZ V. H.; MATTEDI S.; AZNAR M. Isobaric Vapor-Liquid Equilibria of 1-Ethyl-3-Methylimidazolium Ethylsulfate Plus (Propionaldehyde or Valeraldehyde): Experimental Data and Prediction, *Journal of Chemical Thermodynamics*, submetido, 2010.
5. MATTEDI, S.; CARVALHO, P.J.; COUTINHO, J.A.P.; ÁLVAREZ, V.H.; IGLESIAS, M. Vapor-liquid Equilibria of a Brønsted Ionic Liquid and CO₂. *The Journal of Supercritical Fluids*, submetido, 2010.
6. ÁLVAREZ, V.H.; GÓMEZ-DÍAZ, D.; DÍAZ, D.; FIGUEIRAS, A.; MARTIN-PASTOR, M.; MATTEDI, S.; AZNAR, M.; IGLESIAS, M.; NAVAZA, J. M. CO₂ Absorption Into Amine-Based Ionic Liquids, *Brazilian Journal of Chemical Engineering*, submetido, 2010.
7. ÁLVAREZ, V.H.; MATTEDI, S.; MARTIN-PASTOR, M.; AZNAR, M; IGLESIAS, M. Synthesis and Thermophysical Properties of New Protic Long-chain Ionic Liquids with Oleate Anion. *Fluid Phase Equilibria*, doi:10.1016/j.fluid.2010.08.022, 2010.
8. CARVALHO, P.J.; ÁLVAREZ, V.H.; MARRUCHO, I.M.; AZNAR, M.; COUTINHO, J.A.P. High Carbon Dioxide Solubilities in Trihexyltetradecylphosphonium-based Ionic Liquids, *The Journal of Supercritical Fluids*. 52, 258-265, 2010.
9. ALVAREZ, V.H.; AZNAR, M. An Efficient Approach to Optimal Interpolation of Experimental Data. *Journal of the Taiwan Institute of Chemical Engineers*, 41, 184-189, 2010.
10. ALVAREZ, V.H.; MATTEDI, S.; IGLESIAS, M.; GONZALEZ-OLMOS, R; REZA, J.M. Phase Equilibria of Binary Mixtures Containing Methyl Acetate, Water, Methanol or Ethanol at 101.3 kPa. *Physics and Chemistry of Liquids*, 2010, accepted.
11. ALVAREZ, V.H.; DOSIL, N.; GONZALEZ-CABALEIRO, R.; MATTEDI, S.; MARTIN-PASTOR, M.; IGLESIAS, M.; NAVAZA, J.M. Brønsted Ionic Liquids for Sustainable Processes: Synthesis and Physical Properties. *Journal of Chemical and Engineering Data*, 55, 625-632, 2010.
12. CARVALHO, P.J.; ALVAREZ, V.H.; MACHADO, J.J.B.; PAULY, J.; DARIDON, J.-L.; MARRUCHO, I.M.; AZNAR, M.; COUTINHO, J.A.P. High Pressure Phase Behavior of Carbon Dioxide in 1-Alkyl-3-Methylimidazolium Bis(Trifluoromethylsulfonyl)Imide Ionic Liquids. *The Journal of Supercritical Fluids*, 48, 99-107, 2009.

13. CARVALHO, P.J.; ALVAREZ, V.H.; SCHRÖDER, B.; GIL, A.M.; MARRUCHO, I.M.; AZNAR, M.; SANTOS, L.M.N. B. F.; COUTINHO, J.A.P. Specific Solvation Interactions of CO₂ on Acetate and Trifluoroacetate Imidazolium Based Ionic Liquids at High Pressures. *Journal of Physical Chemistry B*, 113, 6803-6812, 2009.
14. CARVALHO, P.J.; ÁLVAREZ, V.H.; MARRUCHO, I.M.; AZNAR, M.; COUTINHO, J.A.P. High Pressure Phase Behavior of Carbon Dioxide In 1-Butyl-3-Methylimidazolium Bis(Trifluoromethylsulfonyl)Imide and 1-Butyl-3-Methylimidazolium Dicyanamide Ionic Liquids. *The Journal of Supercritical Fluids*, 50, 105-111, 2009.
15. ALVAREZ, V. H.; MACIEL FILHO, R.; AZNAR, M.; MATTEDEI, S. An Evaluation and Industrial Application of Ionic Liquid as Separation Agent for Separation of Diluted Ethanol-Water Mixtures. *Fenómenos de Transferencia*, 4, 8-12, 2009.
16. ALVAREZ, V.H.; AZNAR, M. Application of a Thermodynamic Consistency Test to Binary Mixtures Containing an Ionic Liquid. *The Open Thermodynamics Journal*, 2, 25-38, 2008.
17. ALVAREZ, V.H.; CCOPA-RIVERA, E. A.; COSTA, A.C.; MACIEL FILHO, R.; WOLF-MACIE, M.R.; AZNAR, M. Bioethanol Production Optimization: A Thermodynamic Analysis. *Applied Biochemistry and Biotechnology*, 148, 141-149, 2007.

Artigos publicados em anais de congressos

1. ALVAREZ, V.H.; MATTEDEI, S.; AZNAR, M. Density, refractive index and vapor-liquid equilibria of n-methyl-2-hydroxyethylammonium butyrate plus (methyl acetate or ethyl acetate or propyl acetate) at several temperatures. In: XVIII Congresso Brasileiro de Engenharia Química, Foz do Iguaçu, 2010.
2. OLIVEIRA, L.H.; ÁLVAREZ, V.H.; AZNAR, M. Liquid-liquid equilibrium for n-dodecane + dbt + n-methyl-2-hydroxyethylammonium butyrate at 25 °C and 95 kPa. In: XVIII Congresso Brasileiro de Engenharia Química, Foz do Iguaçu, 2010.
3. ALVAREZ, V.H.; ALIJO, P.; SERRÃO, D.; MACIEL FILHO, R.; AZNAR, M.; MATTEDEI, S. Production of Anhydrous Ethanol by Extractive Distillation of Diluted Alcoholic Solutions with Ionic Liquids. In: 10th International Symposium on Process Systems Engineering, PSE09, Salvador, 2009.
4. ALVAREZ, V. H.; MATTEDEI, S.; AZNAR, M.; MARTIN-PASTOR, M.; NAVAZA, J.M.; IGLESIAS, M. Synthesis and Thermophysical Properties of New Protic Long-chain Ionic Liquids with Oleate Anion. In: VIII Iberoamerican Conference on Phase Equilibria and Fluid Properties for Process Design, Praia da Rocha, 2009.
5. MEDRADO, C.D.B.; ALVAREZ, V.H.; AZNAR, M.; MATTEDEI, S. Use of ionic liquid as entrainer for production of anhydrous ethanol by extractive distillation. In: 18th International Congress of Chemical and Process Engineering - CHISA2008, Praga, 2008.
6. ALVAREZ, V.H.; MARTINS, C.F.; AZNAR, M.; MATTEDEI, S. Use of Ionic Liquid 2-Hydroxy Ethylammonium Formate as Entrainer for Anhydrous Ethanol Production. In: XVII Congresso Brasileiro de Engenharia Química, Recife, 2008.
7. ALVAREZ, V.H.; AZNAR, M. An Efficient Approach to Optimal Interpolation of Experimental Data. In: XVII Congresso Brasileiro de Engenharia Química, Recife, 2008.

8. ALVAREZ, V.H.; MADURO, R.M.; AZNAR, M. Robust and Efficient Implementation of Strategies for Chemical Engineering Regression Problems. In: 18th European Symposium on Computer Aided Process Engineering - ESCAPE18, Lyon, 2008.
9. ÁLVAREZ, V.H.; GOMEZ-DIAZ, D.; AZNAR, M.; MATTEDI, S.; IGLESIAS, M. CO₂ absorption into amine-based ionic liquid media. In: First Iberian Meeting on Ionic Liquids, 2009, Aveiro, 2009.
10. ALVAREZ, V.H.; CCOPA-RIVERA, E.A.; AZNAR, M.; COSTA, A.C.; WOLF-MACIEL, M.R.; MACIEL FILHO, R. Bioethanol Production Optimization: A Thermodynamic Analysis. In: 29th Symposium on Biotechnology for Fuels and Chemicals, Denver, 2008.
11. CCOPA-RIVERA, E.A.; ALVAREZ, V.H.; GONZAGA, J.C.; AZNAR, M.; MACIEL FILHO, R. A Kinetic Study of Poly(Ethylene Terephthalate) Synthesis in a Industrial-Scale Esterification Reactor. In: 20th International Symposium on Chemical Reaction Engineering-ISCRE 20, Kyoto, 2008.